Sandstone remobilisation in the Eocene to Miocene of the Central and Northern North Sea

by

Stephen Jon Martin Molyneux

A thesis submitted for the Degree of Doctor of Philosophy of the University of London and for the Diploma of Imperial College

University of London
T.H.Huxley School of the Environment, Earth Sciences and Engineering
Imperial College of Science, Technology and Medicine

March 2001

To my family, friends and Birkbeck College Cricket Club

"They think its all over...

(see page 348)

ABSTRACT

Sandstone remobilisation syn to post deposition of sedimentation requires:

(i) encasement of the sand fraction within an impermeable (generally clay prone) sediment

(ii) build up of overpressure within the sand body

(iii) release of overpressure (often causing sandstone intrusions)

This thesis studied Palaeocene/Eocene to Mio-Pliocene sediments of the Central and Northern North Sea containing deepwater sediments within interpreted submarine fan sands encased in mudrocks. Regional 2D seismic mapping of the Central and Northern North Sea established this relationship placing these base of slope deepwater turbidite sands within/encased by the surrounding deepwater shales which could act as pressure seals. Within these deepwater clays normal faulting with throws of 10 to 50 milliseconds two way time, dips of 5 to 40 degrees, plan view spacing of 100 to 1000 metres and with a polygonal fault pattern were noted.

Post depositional processes have significantly changed the original small and large scale geometry and reservoir characteristics of these deepwater sediments. Kilometre scale areal extent sandstone intrusions, pockmarks, syndepositional polygonal faulting and mud mounding all indicate significant remobilisation of sediment syn and post deposition.

Evidence for large scale intrusion from 3D seismic datasets are detailed from deepwater sands within the Lower Eocene of UK North Sea Blocks 21/4 and 5 and Norwegian North Sea Block 24/9 and include: (i.) cross cutting seismic amplitudes (calibrated to massive sands) of between 10 to 50 milliseconds two way time (10 to 50 metres thick) dipping between 5 to 40 degrees originating from within the Balder Formation below the Lower Eocene with an areal extent of 5 kilometres radius(Lower Eocene Block 24/9); (ii) similarity of 100 to 2000 plan view conical low angle cross cutting amplitudes (calibrated to massive sands – 10 to 50 milliseconds two way time/ 10-50 meters thick) to conical low angle (5 to 25 degrees) polygonal faulting (Lower Eocene 21/4 and 5); and (iii) cross cutting relationship of massive sands within core data in Eocene sediments of Norwegian North Sea well 24/9-5 and 6.

Intrusion of these massive sands is interpreted to have followed pre existing weaknesses in the Lower Eocene clays. In the case of the Lower Eocene of Blocks 21/4 and 5 polygonal faults, and higher angle faults of unknown origin in the Lower Eocene of Block 24/9. Both these intrusive intervals are located over regional highs, the Renee Ridge/Forties Montrose High (21/4 and 5) and regional saddle/structural high of the South Viking Graben (24/9).

Mechanisms for overpressure build up include burial dewatering of clays and the introduction of hydrocarbons including gas. Hydrocarbons have generated about these structural highs from the Upper Jurassic marine source rocks from the Palaeocene to Recent. It is postulated that migration of these hydrocarbons may have preferentially accumulated about these regional highs and be trapped in the Lower Eocene sediments coeval with migration. Petrographic analysis of poikilotopic ferroan carbonate cements from the massive sands within the interpreted kilometer scale intrusion complex in Norwegian North Sea Block 24/9 indicate delta 13C ranges of between +20 and –35 O/oo. The negative values indicate a partly hydrocarbon origin of this ferroan carbonate cement. As this cement is also of an early origin (high minus cement porosities of 30 to 40 percent), an early cement phase related to hydrocarbon migration /accumulation constrains the Early Eocene intrusion complex of Norwegian North Sea Block 24/9 to shallow depths of burial (less than 1000 metres). The trigger mechanism for overpressure release is postulated earthquake activity during the Eocene.

The involvement of migrating hydrocarbons, possibly gas may explain the process for such large scale sandstone intrusion and sediment remobilisation. The scale of pressures involved are significantly larger than ones needed to form typical outcrop exposures of intrusions a few metres wide. Within this thesis the Upper Miocene sandstone intrusion of Yellow Bank Creek of Santa Cruz, California is a documented wrench fault related large scale sandstone intrusion of a kilometre length and with a sill dyke thickness of 40 metres thick. This intrusive complex contains hydrocarbon stained dolomitic cements with delta C13 values of +20 to –35O/oo indicating a hydrocarbon intrusive phase to the cement similar to the Norwegian North Sea 24/9 intrusion.

Upper Eocene Belton Member deepwater sediments of Norwegian North Sea Block 24/9 were resolved on 3D seismic and calibrated with well data. These Upper Eocene sediments contain high amplitude (10 to 50 milliseconds two way travel time) half graben fault bounded lows surrounded by low amplitude higher margin areas. These lows are 100 to 3000 metres in plan view extent with the fault bounded side formed of low or partly high amplitude and the dipping strata into the fault plane formed of the high amplitude. Well calibration indicates this high amplitude limb to be a massive sand of 10 to 50 metres thick. These high amplitude lows are interpreted as fault bounded lows possibly related to polygonal faulting at the palaeoseabed which preferentially captured deepwater sands at this base of slope position. The faulted margin to these lows contain interpreted smeared/intruded sands leading to the discontinuous high amplitude response.

This thesis not only documents that large scale sandstone intrusion occurs but that seafloor topography can also significantly constrain deepwater sedimentation. This seafloor topography can not only be in the form of seafloor polygonal faulting but also seafloor mounding. Middle Miocene age Utsira Mounds of UK North Sea Blocks 16/27, 29 and 30 were studied using 3D seismic and well data. These mounds are 1 to 10 kilometres circular to elongate mounds in plan view, are formed of upto 150 metres of massive sand, have differential compaction relief of 50 to 100 metres and are an onlap fill sequence onto previous mud mounds. From 2D seismic interpretation these mounds occur 200 to 300 kilometres southerly of a shallow marine region in the Middle Miocene of the North Sea. Deepwater sediments are interpreted to have deposited from this northerly source area into a kilometre scale mud mounded area of this study area. The mechanism of kilometre scale palaeo seafloor mud mounding is poorly understood but could include gas hydrates, diapirism of mud or gas mounding of the seafloor by escaping hydrocarbons.

The scale of this sediment remobilisation indicates that very large pressures were involved, but this thesis did not attempt to quantify this but rather document the scale of remobilisation. The role of hydrocarbon migration is put forward as a role in large overpressures, especially gas, either to within intrusions or acting to

create seafloor mounding. The sequential generation of intrusions by fluid flow along faults is also highlighted (seismic pumping)

All these examples highlight to the geoscientist they should be aware of the small to very large scale nature of sediment remobilisation which can significantly change primary depositional geometries and physical properties of deepwater sediments. For instance sand remobilisation may connect otherwise unconnected sand bodies, produce cleaner sands as part of the intrusion process, or create seafloor mounding/polygonal faulted lows which acts as a constraint on deepwater sedimentation. Hydrocarbon fields are contained within these Lower Tertiary deepwater sands of the North Sea such as Gryphon, Balder, Alba, Harding/Forth and Grane field, all of which are either controlled in there original deposition by sediment mounding (Gryphon) or have been post depositionally remobilised as metre to 10's of metre thick sand intrusions. These 10's of metre metre thick to kilometre plan view extent scale intrusions are producible parts of these field and in some cases are the field. The scale of sand remobilisation demonstrated in this thesis indicates that incorrect interpretation of these remobilisation features will lead to incorrect reservoir modelling and subsequent exploration and development "surprises".

ACKNOWLEDGEMENTS

Primarily, I would like to thank my supervisors at Imperial College, Dr. Joe Cartwright and Dr. Lidia Lonergan for their invaluable advice, guidance and enthusiasm throughout this research. A special thanks goes to my fellow postgraduate colleagues who made my research time all the more colourfull : Nick Lee, Edwin Tervoort, Dustin Lister, Dr. Sharon Squire, Dr. Gary Hampson, Dr. Richard Jolly, Dr. "Big" Dave Dewhurst, Dr. Richard Evans and Dr. Renaud Bouroullec.

Outside college I thank all the members of the Birkbeck College Cricket and Hockey team who I spent many hours playing with on the pitch and in the bar. Your humour, friendship and drinks in the clubhouses of Southern England kept me amused. Simon Foister is especially thanked for explaining the finer points of leg spin and the ability to continue bowling even with three deep midwickets under intense provocation by the opposition. The Pyle family, Steve, Lynda, and their children Robert and Catherine are thanked for looking after me towards the end of my research. My friends Phil, Tim, Geoff and Chris are thanked for their ability to talk about anything but my thesis and rather the more important points of a golf match we had played or the next cricket match we were to be involved in.

I would like to thank PanCanadian Petroleum UK for allowing me to work for them and subsequently employing me in Calgary. Without their support financial and moral support this thesis would never have been finished. A special thanks goes to Ian McIlreath, Alan Booth, Graham Dore and Chris Payton of PanCanadian. While completing the thesis in Calgary I also thank all the members of my soccer team who helped me acclimatise to Canadian life : Dr. Andrew Willis, Toni Mutismo, Jessica de la Fuente, Sean, Marlon, Ian, Ronaldo, Geoff, Jim, The Neville Brothers, Kent, Scott and the "trolley dollys", Anita, Imka, Nicole and honourary "dolly" Kelly.

I thank my primary PhD sponsors Fina UK, and secondary sponsors AAPG, PESGB, Geological Society of London and the Stern Trust of the University of London for financing the thesis.

A final thanks to the England Cricket Team who in 2000 managed to beat the West Indian Cricket Team for the first time in living memory. If they could achieve this impossible task it gave me hope that I could finish a PhD.

CONTENTS

pages

Abstract

Acknowledgements

Content

List of Figures

List of Tables

CONTENTS

1 Introduction **1-9**

1.1 Aims of study 1
1.2 Database 1
1.3 Sediment remobilisation : a definition 2
1.4 Previous work on sediment remobilisation within Eocene sediments of the North Sea 2
1.5 Organisation of Thesis 5

2 Geological setting of the pre-Tertiary and Tertiary of the North Sea - factors affecting sediment remobilisation **10-26**

2.1 Introduction 10
2.2 Pre Tertiary 10
2.2.1 Palaeozoic 10
2.2.2 Late Permian/Early Triassic 11
2.2.3 Middle Jurassic and Early Jurassic to Early Cretaceous 11
2.2.4 Late Cretaceous/Tertiary 11
2.3 Tertiary 12
2.3.1 Palaeocene – sequence 1 12
2.3.2 Eocene – sequence 2 13
2.3.3 Oligocene - sequence 3 13
2.3.4 Miocene – sequence 4 14
2.3.5 Summary – 2D seismic interpretation of Eocene to Miocene 14
2.4 Burial History and hydrocarbon/fluid migration 16
2.5 Polygonal faulting 17
2.6 Conclusions 17

3 Kilometre scale Lower Eocene sandstone intrusions, offshore Norway, block 24/9, North Viking Graben **27-106**

3.1 Introduction 27
3.2 Geological Setting 27
3.2.1 Late Palaeocene to Lower Eocene depositional setting 28

3.3 Late Palaeocene to early Eocene stratigraphy 29
3.4 Data 29
3.4.1 Seismic data 29
3.4.2 Well data 29
3.5 Description 29
3.5.1 Seismic interpretation 30
3.5.2 Well data 32
3.5.2.1 Wireline data 32
3.5.2.2 Core data 33
3.5.2.2.1 Gravity flow and deepwater mass transport mechanisms 33
3.5.2.2.2 Lithofacies of core in Balder sediments of wells 24/9-5 and 6 37
3.5.2.2.3 Lithofacies Associations 38
3.5.2.2.4 Lithofacies summary 39
3.5.2.3 Core Samples 40
3.5.2.3.1 Thin section petrography 41
3.5.2.3.2 Fluid inclusion screening 42
3.5.2.3.3 Cathodoluminescence 43
3.5.2.3.4 Scanning Electron Microscopy (SEM) 44
(a) Backscattered electron image mode (BSEI) 44
(b) Cathodoluminescence (SEM CL) 45
(c) Energy dispersive X-ray analysis (microprobe analysis) 45
3.5.2.3.5 Isotopes – C13 PDB and O18 SMOW 47
3.5.2.3.6 Biostratigraphy of clay clasts 51
3.6 Discussion 53
3.7 Outcrop Intrusion Analogue : Giant scale (kilometre) Upper Miocene sandstone intrusions of Yellow Bank Creek, Santa Cruz County, California, USA 55
3.7.1 Aims 55
3.7.2 Location and geological setting 55
3.7.3 Description of Yellow Bank Creek intrusion 56
3.7.4 Interpretation 60
3.8 Conclusion 61

4 Lower Eocene giant scale sandstone intrusions in UK Central North Sea offshore Blocks 21/3, 4, 5 107-188
4.1 Lower Eocene giant scale sandstone intrusions in UK Central North Sea Blocks 21/4 and 5 107
4.1.1 Aims 107
4.1.2 Geological Setting 107
4.1.3 Database 109
4.1.3.1 Seismic data 109
4.1.3.2 Well data 109

4.1.4 Seismic interpretation 109
4.1.4.1 Horizon interpretation 109
4.1.4.2 Description of Lower Eocene amplitude structures 110
4.1.4.2.1 Well calibration 110
4.1.4.2.2 Seismic interpretation 111
4.1.5 Interpretation 114
4.1.5.1 Sea bed pockmarks 115
4.1.5.2 Sandstone intrusions 116
4.1.5.3 Deep versus shallow origin 119
4.1.6 Summary 119
4.2 Outcrop analogues 120
4.2.1 Tourelle Formation sandstone intrusions, Ordovician deepwater sediments of Quebec, Canada 120
4.2.1.1 Location and geological setting 120
4.2.1.2 Description of small scale sandstone intrusions 121
4.2.1.2.1 Facies description 121
4.2.1.3 Interpretation 123
4.2.2 Baldwin Creek Upper Miocene sandstone intrusions, Santa Cruz County, California, USA 124
4.2.2.1 Location and geological setting 124
4.2.2.2 Description of small scale sandstone intrusions 125
4.2.3 Horton Bluff formation storm related sandstone dykes and collapse structures in lake sediments of Devonian - Carboniferous age, Nova Scotia, Canada 125
4.2.3.1 Location and geological setting 125
4.2.3.2 Facies description 125
4.2.3.3 Description of circular "collapse" features 127
4.2.3.4 Interpretation 127
4.3 Summary 128

5 Syn to post depositional polygonal faulting of the Upper Eocene Belton Member deepwater sands of Norwegian offshore Block 24/9 189-234
5.1 Introduction 189
5.2 Geological Setting 190
5.3 Stratigraphy 190
5.4 Database 190
5.4.1 Seismic data 190
5.4.2 Well data 191
5.5 Seismic interpretation 192
5.5.1 Lower part Norwegian North Sea Block 24/9 192
5.5.2 Upper part Norwegian North Sea Block 24/9 193
5.6 Interpretation 194

5.7 Conclusion 196

6 Lower to Middle Miocene Utsira Formation deepwater mounds of the Central North Sea, UK 16/27, 28, 29 and Norwegian offshore Blocks 15/9 (Zweigler *et al.*, 1999) 235-282

6.1 Introduction 235
6.2 Geological Setting 235
6.3 Stratigraphy 236
6.4 Database 237
6.4.1 Seismic data 237
6.4.2 Well data 237
6.5 3D seismic interpretation 238
6.5.1 Block 16/27 (UK North Sea offshore) 238
6.5.1.1 Description 238
6.5.1.2 Interpretation 239
6.5.2 Block 16/28 to 16/29 (UK North Sea offshore) 239
6.5.2.1 Description 239
6.5.2.2 Interpretation 241
6.5.3 Block 15/9 (Norwegian North Sea offshore) 242
6.6 2D Regional Seismic Interpretation 243
6.7 Conclusion and petroleum potential 245

7 Implications of large scale post depositional sandstone remobilisation 283-315

7.1 Introduction 283
7.2 End members of large scale remobilisation 283
7.2.1 Large scale clastic intrusion and pockmarks 284
7.2.1.1 Large scale clastic intrusions 284
7.2.1.2 Why are some intrusions small scale and some large scale? 285
7.2.1.3 Summary 289
7.2.1.4 Pockmarks 290
7.2.2 Seafloor mounding 291
7.2.2.1 Gas hydrate mounds 292
7.2.2.2 Mud volcanoes/diapirs 294
7.2.2.3 Sand gas mounds 295
7.2.2.4 Summary 295
7.2.3 Origins of syn- to early post-depositional faulting and structures in Block 24/9 296
7.2.3.1 Examples 296
7.2.3.2 Summary 297
7.2.4 Large scale remobilisation model for the Eocene to Miocene of the North Sea 297
7.3 The impact of reservoir remobilisation to reservoir geology of deepwater sediments 299
7.3.1 Reservoir remobilisation : impact on reservoir geometries/properties 299

8 **Conclusions and future research** **316-319**
8.1 Conclusions 316
8.2 Future Work 317

References **320-347**

Quote **348**

LIST OF FIGURES

Chapter 1

1.1	Location map of North Sea study areas and seismic datasets	6
1.2	Model for deepwater Tertiary sand remobilisation and intrusion (from Dixon *et al.*, 1995)	7
1.3	Model for deposition and post-depositional remobilisation of the Tertiary Gryphon Field (from Newman *et al.*, 1993)	8
1.4	Model for depositional and post-depositional remobilisation of the Tertiary Balder field (Jenssen *et al.*, 1993)	9

Chapter 2

2.1	Geological cross section across the North Viking Graben through Norwegian North Sea block 24/9 (CNST82-09 regional seismic line)	19
2.2	Geological cross section across the Central North Sea passing through UK Blocks 21/3, 4 and 5(CNST82-04 regional seismic line)	20
2.3	Summary chart of Cenozoic depositional episodes, lithostratigraphy, tectonic events and oceanographic events	21
2.4	Lower Eocene palaeogeographic map of the North Sea	22
2.5	Middle to Upper Eocene palaeogeographic map of the North Sea	23
2.6	Oligocene palaeogeographic map of the North Sea	24
2.7	Middle Miocene Utsira Formation palaeogeography over the North Sea	25
2.8	Migration routes of Jurassic sourced hydrocarbons into Tertiary sediments of the North Sea	26

Chapter 3

3.1	Location map of Norwegian offshore North Sea Block 24/9 (partly from PESGB, 1997)	62
3.2	Geological cross section across the North Viking Graben through Norwegian North Sea Block 24/9 (from CNST82-09 regional seismic line)	63
3.3	Elongate Tertiary sandstone bodies/Balder Formation equivalent (from Timbrell *et al.*, 1993)	64
3.4	Balder palaeogeography map about the North Viking Graben (Michelson *et al.*, 1995)	65
3.5	Stratigraphy of the late Palaeocene to early Eocene of Norwegian North Sea Block 24/9 (redrawn from Knox and Holloway, 1992)	66
3.6	Intra-Jurassic two way time map and Balder anomaly two time map over Norwegian North Sea Block 24/9	67
3.7	Near Top Jurassic two way time map of Norwegian offshore North Sea Block 24/9	68

3.8	Top Chalk structure contour map of Norwegian offshore North Sea Block 24/9	69
3.9	Top Balder two way time map and Top Balder to Sele amplitude map of Norwegian offshore North Sea Block 24/9	70
3.10	Near top Jurassic to top Chalk isochron of Norwegian offshore North Sea Block 24/9	71
3.11	Top Balder to Chalk isochron of Norwegian North Sea Block 24/9	72
3.12	Interpreted Jurassic to Chalk seismic horizon line through Norwegian North Sea Block 24/9	73
3.13	Top Balder reservoir two way time map of Balder Formation amplitude anomaly Norwegian offshore North Sea Block 24/9	74
3.14	Norwegian North Sea Block – Lower Eocene sandstone intrusion – crossline 3800	75
3.15	Norwegian North Sea Block – Lower Eocene sandstone intrusion – crossline 3884	76
3.16	Norwegian North Sea Block – Lower Eocene sandstone intrusion – crossline 3900	77
3.17	Norwegian North Sea Block – Lower Eocene sandstone intrusion – crossline 4000	78
3.18	Norwegian North Sea Block – Lower Eocene sandstone intrusion – inline 6475	79
3.19	Norwegian North Sea Block – Lower Eocene sandstone intrusion – inline 6600	80
3.20	Norwegian North Sea Block – Lower Eocene sandstone intrusion – inline 6649	81
3.21	Norwegian North Sea Block – Lower Eocene sandstone intrusion – inline 6700	82
3.22	High amplitude east west oriented trend within the Balder interval - possible turbidite feeder channels, in Norwegian offshore Block 24/9	83
3.23	Correlation of the Upper Palaeocene and Eocene for wells 24/9-5, 24/9-6 and 25/7-5, offshore Norwegian North Sea (Fina Norway Report, 1998)	84
3.24	Geological cross section through Upper Palaeocene and Eocene for wells 24/9-5, 24/9-6 and 25/7-5, offshore Norwegian North Sea (Fina Norway Report, 1998)	85
3.25	Core description sheet for Norwegian North Sea well 24/9-5	86
3.26	Core description sheet for Norwegian North Sea well 24/9-6	87
3.27	Core description key for Lower Eocene sediments in Norwegian North Sea wells 24/9-5 and 6	88
3.28	Gravity flow processes and sediment flow types temporally and spatially (after Hampton, 1972 and Lowe 1979, 1982)	89
3.29	Deepwater transport and depositional processes (partly from Collinson and Reading, 1997)	90
3.30	Core photographs of a massive sand from Norwegian North Sea well 24/9-6	91
3.31	Core photograph of a high angle sand/shale contact from	92

Norwegian North Sea well 24/9-6
3.32 Core photograph of a high angle intrusive sandstone dyke from Norwegian North Sea well 24/9-5 93
3.33 Core photograph of a high angle quartz cemented planes within massive sands from Norwegian North Sea wells 24/9-6 94
3.34 Plane polarised light image of a massive injected sand from Norwegian well 24/9-5 (Sample 0188-2031 metres measured depth) 95
3.35 Cathodoluminescensce image of a massive injected sand from Norwegian North Sea well 24/9-5 (Sample 0188 – 2031 metres measured depth). 95
3.36 Model of fluid migration for Norwegian North Sea Block 24/9 96
3.37 Model of Lower Eocene clastic injection model in Norwegian North Sea Block 24/9 97
3.38 Location map of Yellow Bank Creek, Santa Cruz, California, USA (after Thompson *et al.*, 1999) 98
3.39 Stratigraphy of Miocene of Santa Cruz region, Califronia, USA (after Thompson *et al.*, 1999) 99
3.40 Sandstone intrusion map of Yellow Bank Creek, Santa Cruz, California, USA (after Thompson *et al.*, 1999) 100
3.41 Cliff cross section of the Yellow Bank Creek sandstone intrusions, Santa Cruz, California, USA (after Thompson *et al.*, 1999) 101
3.42 Ten metre thick sandstone sill passing into a fifteen metre wide sandstone dyke, five hundred metres southeast of the Yellow Bank Creek sandstone intrusion, Santa Cruz, California, USA 102
3.43 Dolomite cemented sandstone with the appearance of "bubbles" and "pipes" at centimetre to metre scale, representing flow texture within the Yellow Bank Creek sandstone intrusion, Santa Cruz, California 103
3.44 Flow texture/limonite recent weathering within poorly cemented sandstone in the Yellow Bank Creek intrusion, Santa Cruz, California, USA 104
3.45 Petrographic thin section of a ferroan dolomite cemented sand in plane polarised light of the Yellow Bank Creek intrusion, Santa Cruz, California, USA 105
3.46 Cathoduluminescence photomicrograph of a ferroan dolomite cemented sand of the Yellow Bank Creek intrusion, Santa Cruz, California, USA 105
3.47 Model of sequential formation of the Yellow Bank Creek intrusion, Santa Cruz, California, USA (after Thompson *et al.*, 1999) 106

Chapter 4

4.1 Location map of UK Central North Sea Blocks 21/3, 4, 5 and 15/18 130
4.2 North Sea Palaeocene palaeogeography (redrawn from 131

Sutter, 1980)
4.3 Forties palaeogeography map (deepwater sediment) about UK North Sea Blocks 21/4 and 5 132
4.4 Geological cross section across the Central North Sea, passing through UK Blocks 21/3, 4 and 5 (from CNST82-04 regional geological seismic line) 133
4.5 Lower Eocene palaeogeographic map of the North Sea 134
4.6 Seismic cross section of a polygonally faulted Lower Eocene section that contains a high amplitude, circular, low angle, cone shaped anomalies within UK Central North Sea Blocks 21/3, 4 and 5 135
4.7 Near Top Jurassic two way time structure contour map over UK Central North Sea Blocks 21/3, 4 and 5 136
4.8 Top Cretaceous two way time structure contour map over UK Central North Sea Blocks 21/3, 4 and 5 137
4.9 Top Palaeocene (Balder Tuff) two way time structure contour map over UK Central North Sea Blocks 21/3, 4 and 5 138
4.10 Two way time isopach between near base Jurassic and near top Cretaceous over UK Central North Sea Blocks 21/3, 4 and 5 139
4.11 Two way time isopach between Top Cretaceous and Top Palaeocene over UK Central North Sea Blocks 21/3, 4 and 5 140
4.12 Structural elements map of the area about UK Central North Sea Blocks 21/3, 4 and 5 141
4.13 Composite log of UK North Sea well 21/5-1 over the Lower Eocene section 142
4.14 Seismic cross section of a polygonally faulted Lower Eocene section that contains a high amplitude, circular, low angle, cone shaped anomaly calibrated by UK North Sea well 21/5-1 143
4.15 Composite log of UK North Sea well 21/5-3 over the Lower Eocene section 144
4.16 Seismic and well calibration of UK North Sea well 21/5-3 145
4.17 UK Central North Sea wells 21/5-1 and 21/5-3 which penetrate the Lower Eocene cone shaped amplitude anomalies 146
4.18 Maximum amplitude extraction between 30 to 70 milliseconds two way time above the top Palaeocene structure map over UK Central North Sea Block 21/3, 4 and 5 147
4.19 Seismic cross section of a high amplitude, low angle cone shaped anomaly, with basal apices located above a fault at Top Balder level, through the UK Central North Sea Blocks 21/3, 4 and 5 148
4.20 Structure contour map of Lower Eocene conical amplitude anomaly – example A – UK North Sea Block 21/5 149
4.21 A Lower Eocene conical amplitude anomaly within UK North Sea Block 21/5 – example A 150
4.22 Structure contour map of Lower Eocene conical amplitude anomaly – example B – UK North Sea Block 21/5 151
4.23 A Lower Eocene conical amplitude anomaly in UK North Sea Block 21/5 152

4.24	Three dimensional representation of selected Lower Eocene amplitude anomalies over UK Central North Sea Blocks 21/3, 4 and 5	153
4.25	Structure contour map of Lower Eocene conical amplitude anomaly – example C – UK North Sea Block 21/5	154
4.26	Charisma Geocube flattened on part ofTop Balder UK North Sea Block 21/5. Timeslice is 30 metres (30 msecs TWT) above Top Balder showing polygonal fault pattern	155
4.27	Charisma Geocube flattened on part of Top Balder UK North Sea Block 21/5. Timeslice is 70 metres (70 msecs TWT) above Top Balder showing polygonal fault pattern	156
4.28	Seismic cross section through (a)compound and (b)individual Lower Eocene conical amplitude anomalies over UK Central North Sea Blocks 21/3, 4 and 5	157
4.29	Comparison of Lower Eocene polygonal fault patterns to the scale and plan view geometry of Lower Eocene amplitude anomalies over the southern part of UK North Sea Block 21/4 and 21/5	158
4.30	UK North Sea Block 21/5 – seismic example (inline 4644) of Lower Eocene polygonal faults and conical amplitude anomalies	159
4.31	UK North Sea Block 21/5 – seismic example (inline 4754) of Lower Eocene polygonal faults and conical amplitude anomalies	160
4.32	UK North Sea Block 21/5 – seismic example (inline 4866) of Lower Eocene polygonal faults and conical amplitude anomalies	161
4.33	UK North Sea Block 21/4 and 5 Lower Eocene high amplitude conical structures, polygonal and Balder fault map superimposed upon eachother	162
4.34	Top Balder structure contour map of UK Block 15/18 3D seismic survey of Balder age pockmarks (Cole, 1998)	163
4.35	Seismic cross section of Balder aged pockmarks over UK Block 15/18 with well calibration (Cole, 1998)	164
4.36	Model for the formation of Balder aged pockmarks over UK Block 15/18 (Cole, 1998)	165
4.37	Model for Lower Eocene conical amplitude anomlies as pockmarks in UK Central North Sea Blocks 21/3, 4 and 5	166
4.38	Model for the formation of Lower Eocene conical amplitude anomalies as sandstone intrusions in UK Central North Sea Blocks 21/3, 4 and 5	167
4.39	Timing of hydrocarbon generation from Jurassic organic rich source rocks about UK Central North Sea blocks 21/3, 4 and 5 (Mason *et al.*, 1995)	168
4.40	Location map of Tourelle formation at Cap Ste-Anne, Quebec, Canada	169
4.41	Line drawing of wave cut platform of the base Tourelle formation, exposing a 70 metre thick section, by 100 metres wide of clastic intrusions, in deepwater shales, silts and fine sands, Cap Ste-Anne, Quebec, Canada	170
4.42	Three sedimentary logs from the base to top of the exposure	171

of the basally injected deepwater sediments of the Tourelle Formation, Cap Ste Anne, Quebec, Canada
4.43 Terminations of intruded of intruded sandstone sills with bulbous and fingerlike geomtries in the basal deepwater sediments of the Tourelle Formation, Cap Ste Anne, Quebec, Canada 172
4.44 Terminations of intruded sandstone sills with bulbous and fingerlike geometries in the basal deepwater sediments of the Tourelle Formation, Cap Ste Anne, Quebec, Canada 173
4.45 Jacking apart of country rock by intruded sandstone sill in the basal deepwater sediments of the Tourelle Formation, Cap Ste Anne, Quebec, Canada 174
4.46 "V" shaped, low angle intrusion within the basal deepwater sediments of the Tourelle Formation, Cap Ste Anne, Quebec, Canada 175
4.47 Model for injection of clastic dykes and sills from an out of plane deepwater channel sand within the basal deepwater sediments of the Tourelle Formation, Cap Ste Anne, Quebec, Canada (Hiscott, 1979) 176
4.48 Dominant intrusive mechanisms of sills from the Ordovician Tourelle Formation, Quebec, Canada and the Ordovician Rosroe Formation, Co.Mayo, Ireland (Lonergan *et al.*, 1999) 177
4.49 Remobilisation features within the Ordovician Rosroe Formation, Co.Mayo, Ireland (Lonergan *et al.*, 1999) and Ordovician Tourelle Formation, Quebec, Canada 178
4.50 Line drawing of wavecut platform exposing low angle, conical shaped dyke sandstone intrusions in the Upper Miocene Santa Cruz diamotaceous Mudstone, Baldwin Creek, Santa Cruz, California, USA 179
4.51 "V" shaped sandstone intrusions in the Upper Miocene Santa Cruz diatomaceous Mudstone, Baldwin Creek, Santa Cruz, California, USA 180
4.52 "V" shaped intrusions in the Upper Miocene Santa Cruz Diatomaceous Mudstone, Baldwin Creek, Santa Cruz, California, USA 181
4.53 Location map of Tournaisian Horton Bluff Formation, Horton Bluff, Nova Scotia, Canada (from Martel *et al.*, 1993) 182
4.54 Idealised sedimentary facies sequence at Horton Bluff, of the Tournaisian Horton Bluff Formation, Nova Scotia, Canada (partly from Martel *et al.*, 1993) 183
4.55 Sections measured at Horton Bluff, of the Tournaisian Horton Bluff, Nova Scotia 184
4.56 Hummocky sand facies (B) lense with intrusive sandstone dykes at the base into facies (A) offshore clays at Horton Bluff, of the Tournaisian Horton Bluff Formation, Nova Scotia, Canada 185
4.57 Circular "collapse" structures within the hummocky sand facies (B) lenses at Horton Bluff of the Tournaisian Horton Bluff Formation, Nova Scotia, Canada 186
4.58 Cross section through a circular "collapse" structure within the hummocky sand facies (B) lenses at Horton Bluff of the 187

Tournaisian Horton Bluff Formation, Nova Scotia, Canada
4.59 Model of circular collapse structures and basal dykes within the hummocky sand facies (B) lenses at Horton Bluff of the Tournaisian Horton Bluff Formation, Nova Scotia, Canada 188

Chapter 5

5.1 Location map of Norwegian offshore North Sea Block 24/9 (partly from PESGB, 1997), with portions of block interpreted through the Upper Eocene Belton Member 198
5.2 Geological cross section across the North Viking Graben through Norwegian North Sea Block 24/9 (from CNST82-09 regional seismic line) 199
5.3 Palaeogeographic map of the Middle to Upper Eocene strata in the North Sea 200
5.4 Well calibration/stratigraphy of the Upper Eocene Belton Member in the Norwegian North Sea Block 24/9 (from well 24/9-2 and 24/9-5 201
5.5 Norwegian North Sea well 24/9-2 over the Upper Eocene Belton Member and Grid Member 202
5.6 Norwegian North Sea well 24/9-5 over the Upper Eocene Belton Member 203
5.7 Norwegian North Sea well 24/9-6 over the Upper Eocene Belton Member and Grid Member 204
5.8 Norwegian North Sea well 24/9-2 penetration through the Upper Eocene Belton Member – crossline 1966 205
5.9 Norwegian North Sea well 24/9-2 penetration through the Upper Eocene Belton Member – inline 6484 205
5.10 Norwegian North Sea Block Upper Eocene Belton Member Top structure map 206
5.11 Top Belton Member Upper Eocene two way time structure contour map and amplitude map over Norwegian North Sea Block 24/9 207
5.12 Examples of three dimensional images of Upper Eocene Belton Member polygonally faulted deepwater sediments of Norwegian North Sea Block 24/9 (see figure 5.11 and 5.18 for location) 208
5.13 Seismic cross section of Upper Eocene Belton Member polygonally faulted deepwater sediments of Norwegian North North Sea Block 24/9 209
5.14 Norwegian North Sea Block 24/9 seismic inline 6205 through the Upper Eocene Belton Member example A 210
5.15 Norwegian North Sea Block 24/9 seismic crossline 1600 through the Upper Eocene Belton Member example A 211
5.16 Norwegian North Sea Block 24/9 seismic crossline 2452 through the Upper Eocene Belton Member example B faulted low 212
5.17 Seismic line through the Belton Member of Norwegian North Sea wells 24/9-5 and 6 213
5.18 Structure contour map of the Upper Eocene Belton Member Member about wells 24/9-5 and 24/9-6 214

5.19	Amplitude map of Upper Eocene Belton Member about Norwegian North Sea wells 24/9-5 and 6	215
5.20	Isopach map between intra Oligocene and Belton Member structure contour map over Norwegian North Sea wells 24/9-5 and 6	216
5.21	Structure contour map of a fault bounded low within the Upper Eocene Belton Member in Norwegian North Sea Block 24/9 – C	217
5.22	Norwegian North Sea Block 24/9 seismic crossline 3788 through the Upper Eocene Belton Member example C faulted low	218
5.23	Norwegian North Sea Block 24/9 seismic crossline through the Upper Eocene Belton Member example C faulted low	219
5.24	Norwegian North Sea Block 24/9 seismic crossline 3808 through the Upper Eocene Belton Member example C faulted low	220
5.25	Norwegian North Sea Block 24/9 seismic crossline 3818 through the Upper Eocene Belton Member example C	221
5.26	Norwegian North Sea Block 24/9 seismic crossline 3828 through the Upper Eocene Belton Member example C faulted low	222
5.27	Norwegian North Sea Block 24/9 seismic crossline 3838 through the Upper Eocene Belton Member example C faulted low	223
5.28	Norwegian North Sea Block 24/9 seismic crossline 3848 through the Upper Eocene Belton Member example C faulted low	224
5.29	Norwegian North Sea Block 24/9 seismic crossline 3858 through the Upper Eocene Belton Member example C faulted low	225
5.30	Norwegian North Sea Block 24/9 seismic crossline 3868 through the Upper Eocene Belton Member example C faulted low	226
5.31	Top Belton Member structure contour map about Norwegian North Sea wells 24/9-5 and 6 – example D faulted lows	227
5.32	Intra Oligocene structure contour map over Norwegian North Sea wells 24/9-5 and 6. Note polygonal fault pattern (partly from Tervoort, 2000)	228
5.33	Seismic example (inline 3918) through Upper Eocene Belton Member about Norwegian North Sea wells 24/9-5 and 24/9-6	229
5.34	Seismic example (inline 3910) through Upper Eocene Belton Member about Norwegian North Sea wells 24/9-5 and 6	230
5.35	Seismic example (inline 3888) through Upper Eocene Member about Norwegian North Sea wells 24/9-5 and 6	231
5.36	Seismic example (inline 3872) through Upper Eocene Belton Member about Norwegian North Sea wells 24/9-5 and 6	232
5.37	Depositional and post depositional model of the Upper Eocene Belton Member and Grid Member	234
5.38	Schematic reconstruction of fault development in UK North Sea Blocks 16/23 and 24 (Whitbread and Anderton, 1997)	235

Chapter 6

6.1	Location map of studied 2D and 3D surveys in UK Central North Sea Blocks 16/27, 28 and 29	247
6.2	Regional east west geological cross section of the Mid Miocene Utsira formation over the Central North Sea through UK blocks	248

16/27, 28, 29 and Norwegian North Sea Blocks 15/9 (CNST 82-04 regional seismic line)
6.3 Stratigraphy of the Middle Miocene Utsira Formation, North Sea, from Norwegian North Sea block 15/9 (Zweigler *et al.*, 1999) 249
6.4 Intra-Jurassic structure contour map over UK North Sea Blocks 15/30, 16/26 and 16/27 250
6.5 Top Chalk structure contour map over UK North Sea Blocks 15/30, 16/26 and 16/27 251
6.6 Top Balder structure contour map over UK North Sea Blocks 15/30, 16/26 and 16/27 252
6.7 North/South seismic line through the Tertiary to Top Jurassic strata of UK North Sea Block 16/27 253
6.8 Seismic cross section through Lower to Middle Miocene Utsira Mounds of Central North Sea Blocks 16/27 254
6.9 Structure contour two way time map of the Top Utsira mounds over UK Central North Sea Blocks 16/27 255
6.10 UK Block 16/27 – Utsira mounds – crossline 1902 256
6.11 UK Block 16/27 – Utsira mounds – crossline 2000 257
6.12 UK Block 16/27 – Utsira mounds – crossline 2200 258
6.13 UK Block 16/27 – Utsira mounds – crossline 2300 259
6.14 UK Block 16/27 – Utsira mounds – crossline 2400 260
6.15 UK Block 16/27 – Utsira mounds – crossline 2500 261
6.16 UK Block 16/27 – Utsira mounds – crossline 2600 262
6.17 UK Block 16/27 – Utsira mounds – inline 4800 263
6.18 Structure contour map of Top Utsira mound surface with pinchout to the west of this surface against the Fladen Ground Spur over UK North Sea Block 16/27 264
6.19 Model of Middle Miocene Utsira mound formation over UK Central North Sea Blocks 16/27 265
6.20 Base Cretaceous, Top Sele and Top Oligocene structure contour map over UK North Sea Blocks 16/28 and 16/29 266
6.21 Seismic cross section, northeast/southwest oriented through Utsira mounds and location of Jurassic fault blocks below these mounds in UK North Sea Blocks 16/28 and 16/29 267
6.22 Time structure contour map of Top Utsira mounds over UK North Sea Blocks 16/28 and 16/29 268
6.23 Seismic/well calibration through UK North Sea well 16/29-4 over the Lower to Middle Miocene Utsira Formation 269
6.24 Composite log of UK North Sea well 16/29-4 over the Miocene Utsira formation 270
6.25 Seismic/calibration through UK North Sea well 16/29-3, 5, 1 and over the Lower to Middle Miocene Utsira Formation 271
6.26 Composite log of UK North Sea well 16/29-1 over the Miocene Utsira Formation 272
6.27 Composite log of UK North Sea well 16/29-5 over the Miocene Utsira Formation 273
6.28 Composite log of UK North Sea well 16/29-3 over the Miocene Utsira Formation 274

6.29	Seismic/well calibration over UK North Sea well 16/29-2 through Lower to Middle Miocene Utsira Formation	275
6.30	Composite log of UK North Sea well 16/29-2 over the Miocene Utsira Formation	276
6.31	Seismic/well calibration over UK North Sea well 16/28-12 through Lower to Middle Miocene Utsira Formation	277
6.32	Composite log of UK North Sea well 16/28-12 over the Utsira Formation interval	278
6.33	Seismic cross section with generalised well calibration of Utsira mounds over UK Central North Blocks 16/28 and 16/29	279
6.34	Model of Middle Miocene Utsira mound formation over UK Central North Sea blocks 16/28 and 16/29	280
6.35	Model of giant scale differential compaction/density inversion pillows in fine grained sediments in the Oligo-Miocene in the Faeroe-Shetland Trough (Davies *et al.*, 1999)	281
6.36	Middle Miocene Utsira Mounds palaeogeography over the UK North Sea Blocks 16/28 and 16/16/29	282

Chapter 7

7.1	Three part classification scheme for large scale remobilisation in Eocene to Mio-Pliocene sediments of the North Sea	302
7.2	Model of seismic pumping (from Muir Wood, 1994)	303
7.3	Gas expansion versus depth graph	304
7.4	Three main processes contributing to clastic intrusion (from Lonergan *et al.*, 1999)	305
7.5	Clastic intrusion development with: (a) no pre-existing weaknesses and (b) pre existing weaknesses (from Lonergan *et al.*, 1999)	306
7.6	Generalised formation of pockmarks (from Hovland and Judd, 1988)	307
7.7	Giant gas mound from the Gulf Coast of Mexico (Brooks *et al.*, 1984)	308
7.8	Giant gas mound model from the Gulf Coast of Mexico (Brooks *et al.*, 1984)	309
7.9	Seismic cross section through Mio-Pliocene gas mounds (Brooke *et al.*, 1995)	310
7.10	Time slice through Mio-Pliocene gas mounds (Brooke *et al.*, 1995)	311
7.11	Seismic cross section of potential gas chimneys from the Jurassic to sea bed via Mio-Pliocene gas mounds (Brooke *et al.*, 1995)	311
7.12	Model for formation of Mio-Pliocene gas mounds (Brooke *et al.*, 1995)	312
7.13	Model of large scale remobilisation features in the Eocene to Miocene of the North Sea	313
7.14	Impact of polygonal faulting on reservoir geometry (Cartwright *et al.*, 1999)	314
7.15	Examples of remobilisation affects on deepwater reservoirs	315

Chapter 8

8.1 Contrasting interpretations of reservoir geometry from the same well calibration 319

TABLES

Table 1	Balder aged core samples for Norwegian North Sea wells 24/9-5 and 6	40
Table 2	Weight percentage of total oxides measured from core samples of structureless massive Balder aged sandstone samples of Norwegian North Sea well 24/9-5 and 6	46
Table 3	C13 PDB and O18 SMOW O/oo values from core samples of structureless maasive Balder aged sandstone samples of Norwegian North Sea well 24/9-5 and 6	48
Table 4	Weight percentage of total oxides measured from dolomite cemented sands from the Yellow Bank Creek intrusion, Santa Cruz County, California	57
Table 5	C13 PDB O/oo values from dolomite cemented sands from the Yellow Bank Creek intrusion, Santa Cruz County, California	58

CHAPTER 1. INTRODUCTION

1.1 Aims of study

The Eocene to Mio-Pliocene sediments of the Central and Northern North Sea contain deepwater hydrocarbon reservoirs, comprised predominantly of mudrocks with occasional submarine fan sands. Post depositional processes have significantly changed the original small and large scale geometry and reservoir characteristics of these sediments (Dixon *et al.*,1995, Jenssen *et al.*, 1993; Newman *et al.*, 1993, Lonergan and Cartwright, 1999). This thesis attempts to document in detail several 3D seismic examples (figure 1.1 and chapters 2 to 6) of large scale post depositional remobilisation from these Eocene to Mio-Pliocene sediments, calibrated to well and core data. Comparisons to field analogues are made, with specific reference in detail to significant locations in California and East Coast Canada. The origins and impact of large scale post depositional remobilisation are reviewed (chapter 7) in the light of the current work and within the literature, in order to develop a model for the remobilisation of certain North Sea deepwater sandstones. Finally, the pitfalls of interpreting deepwater sediments (chapter 7) as wholly primary depositional in character, though they may have been affected by large scale remobilisation, highlight how reservoir characteristics can be improved and downgraded by the remobilisation process and that remobilised reservoirs act as significant hydrocarbon reservoirs. Chapter 8 outlines the conclusions regards sediment remobilisation and future work.

1.2. Database

This study involved the use of over 6000 line kilometres of 1982 and 1986 vintage reflection seismic over the UK and Norwegian part of the North Sea. The northern limit of data lies within UK Block 9, the southern limit lies in UK Block 30, the eastern limit passes variably east across the Norwegian/UK

median line and as far west as the Outer Moray Firth (figure 1.1). 3D seismic data sets used in this study include:

Chapter 3 and 6 : Norwegian North Sea Block 24/9

Chapter 4 : UK North Sea Block 21/3, 4 and 5 and 15/18

Chapter 5 : UK North Sea Block 16/27, 29 and 30

Well and core data were used to calibrate these 3D seismic surveys and observed seismic features are described within individual chapters. Fieldwork upon large and small scale remobilisation relevant to seismic and well/core scale features observed on the subsurface data was undertaken upon:

Chapter 3 : Upper Miocene, Yellow Bank Creek, Santa Cruz, California.

Chapter 4 : Ordovician Tourelle Formation, Quebec, Canada.

:Upper Miocene diatomaceous shales, Baldwin Creek, Santa Cruz, California.

: Carboniferous Horton Bluff Formation, New Brunswick, Canada.

1.3. Sediment remobilisation : a definition

Reservoir remobilisation within this thesis is defined as : "Any comprehensive redistribution of reservoir units from their original depositional configuration caused by post depositional processes of liquefaction and fluidisation related to pore pressure build up". Originally deposited deepwater sediments of the Eocene to Miocene of the North Sea contain several examples attributed to post depositional remobilisation documented in the literature as outlined below.

1.4. Previous work on sediment remobilisation within Eocene sediments of the North Sea

Since the advent of 3D seismic technology since the early 1980's the establishment of significant oil exploration within the deepwater sands in the Eocene of the North Sea has provided a wealth of new data on these sediments. Observations from 3D seismic, well and core data has indicated that the original

deepwater sediment reservoir geometry and sediment porosity and permeability, has in many cases been significantly changed after initial deposition. Within the North Viking Graben the Lower Eocene contains several hydrocarbon fields interpreted to be within deepwater sediments. Several of these oilfields have been documented as having been affected by sediment remobilisation. Below is a description of these fields with specific reference to sediment remobilisation.

(i) Forth Field

In the Forth Field (to the west of Norwegian North Sea Block 24/9 and located on the Eocene palaeo-slope) some underlying section is missing and this suggests a more erosive origin for the base of the sandbody (Alexander *et al.*, 1992; Dixon *et al.*, 1995). The massive sands which make up the greater part of the sandbody are overlain by thinner interbedded sandstones and mudstones. The massive sands thin rapidly on the flanks of the accumulation. Slide scars are interpreted to have extended down a slope from a shelf edge source area and themselves become the sites for sand accumulation near the base of slope. High density flows, which could possibly have been true turbidity currents, possibly sandy debris flows, are interpreted to have been largely confined to the depression, thereby explaining the absence of clear overbank sands (Dixon *et al.*, 1995). Burial of the massive sands, probably to the depths of many tens of metres and the resultant differential compaction and dewatering of the muds led to overpressuring and to the deformation of the sand mass through diapiric movement and injection of sands upwards as complexes of anastomosing sandstone sills and dykes (Dixon *et al.*, 1995, figure 1.2). Diapirism and injection may have been triggered by contemporaneous seismicity or it may have developed more gradually. In some cases pressures have been interpreted to have been relieved through the movement of faults and the expulsion of sand and water along fault surfaces (Dixon *et al.*, 1995). Diapirism may have led to the development of steep margins (15 degrees) to the sand.

(ii) Gryphon field

The Gryphon Field (to the west of Norwegian North Sea Block 24/9 and located on the Eocene palaeo-slope) conforms to a similar general model

whereby sand distribution was strongly controlled by pre-existing topography with rapid wedging out of sands on the sloping pre-existing flanks (Newman *et al.*, 1993). Later sands, deposited after the main Balder tuffs, reflect not only offset stacking due to differential compaction but also adjustment through soft sediment failure and faulting. Sand was extensively injected along the fault surfaces (figure 1.3).

(iii) Balder field

The Balder field is located to the east of Norwegian North Sea Block 24/9 and on the northwestern margin of the Utsira High. Hydrocarbons are trapped in thick massive submarine fan sandstones which were deposited from high-density turbidity currents derived from the East Shetland Platform (Jenssen *et al.*, 1993). They have formed close to the Paleocene sandstone pinch-out and form thick mounded reservoirs in the field. High relief mounded geometries are believed to have been caused by a complex interaction between deposition and syn- and post depositional soft-sediment deformation processes. Slumping, sliding and sand remobilization were the dominant deformational processes. Associated sand injections into overlying shales occurred during the soft-sediment deformation processes. During the Early Eocene associated sand injections into overlying shales occurred during the soft-sediment deformation processes which dominantly. The sandstones which have excellent reservoir properties, appear to be in pressure communication and have common oil-water contacts which is probably related to the soft-sediment deformation processes with associated sand injections (Esso Norge pers.comm. 1999) (figure 1.4).

(iv) Grane field

The Lower Eocene Grane hydrocarbon field is similar in character to the Balder Field (Norsk Hydro pers. comm., 1999) and is interpreted to have been deposited from shelf sands on the East Shetland platform as mounded deepwater sediments against the Utsira High to the east. Wells and core data within the Lower Eocene sediments have observed small scale sandstone intrusions and pressure communication between apparently isolated sand mounds.

(v) Alba field

The Alba field within UK North Sea Block 16/26 is interpreted to have been deposited as a northwest/southeast oriented Middle Eocene deepwater sand body, 9km long and 1.5km wide and formed of up to a 100 metres of massive sand, separated internally by mm to metre scale shale breaks. Lonergan and Cartwright (1999) observed that over 70% of the field perimeter was fault contact and MacLeod *et.al.* (1999) noted that much of the field had low angle high amplitude seismic "wings" coming off from the main sand body. Recent well/core calibration of these "wings" by MacLeod *et al.* (1999) has shown these to be discordant to bedding and intrusive in nature with massive sand bed thicknesses up to 20 metres thick.

1.5. Organisation of Thesis

As established from the previous section 1.4, discrete documented examples within Eocene deepwater sediments of the North Sea contain unusual large scale seismic and well /core calibrated geometries attributed to postdepositional remobilisation of deepwater sediments. This thesis describes previously undocumented interpreted large and small scale remobilisation features from the Eocene to Miocene of the North Sea from 2D seismic and 3D seismic, calibrated to core data (chapters 3, 4, 5 and 6). The stratigraphical and geological history of these sediments is established first (chapter 2), highlighting the specific factors which have influenced sediment deposition and subsequent remobilisation of these strata. Description of these North Sea Tertiary examples is compared where relevant within each chapter to studied field outcrop examples that are geometrical and/or scale analogues. Finally chapter 7 summarises the literature beyond the Tertiary of the North Sea pertinent to types of remobilisation, processes involved and establishes a model for deepwater sediment remobilisation in the Eocene to Miocene of the North Sea, concluding with the possible affect this may have on reservoir continuity and reservoir characteristics.

Figure 1.1 Location of 2D and 3D seismic datasets used in this North Sea study. (partly from PESGB (1997); Jones *et al.*, (1999); Pegrum and Spencer, (1990))

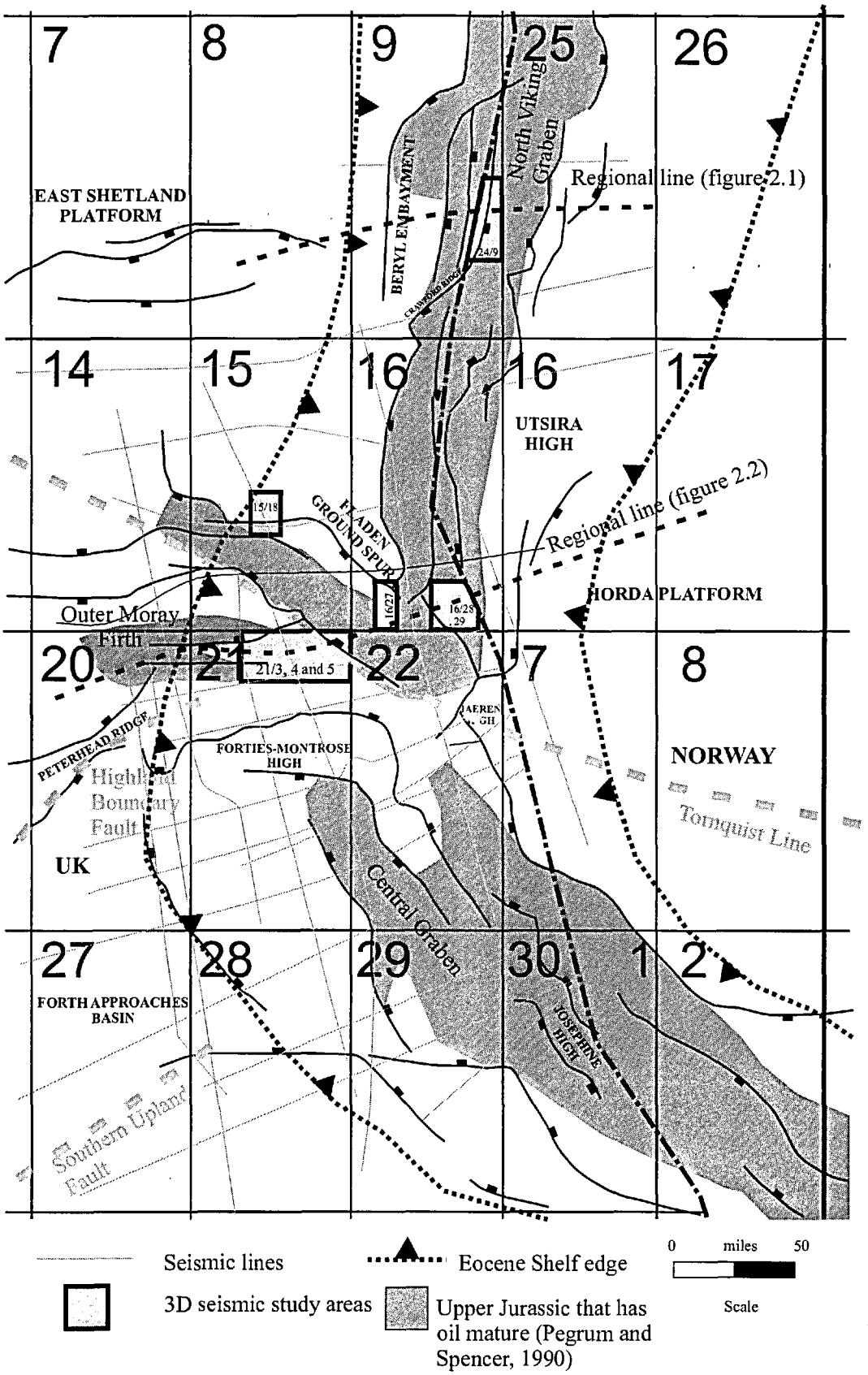


Figure 1.2. Model for deepwater Tertiary sand remobilisation and intrusion (from Dixon *et al.*, 1995)

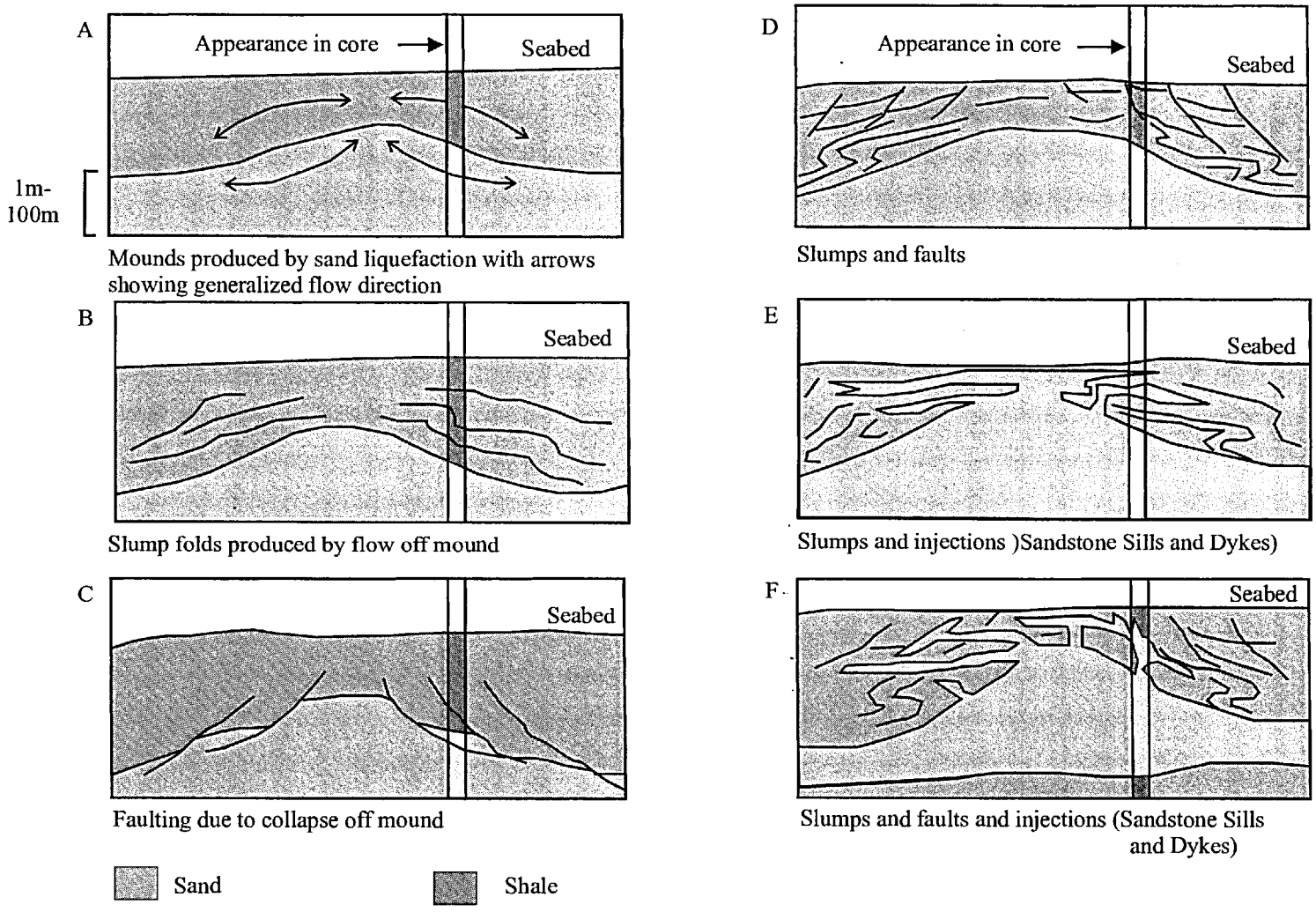


Figure 1.3. Model for deposition and post depositional remobilisation of the Tertiary Gryphon Field (from Newman *et al.*, 1993)

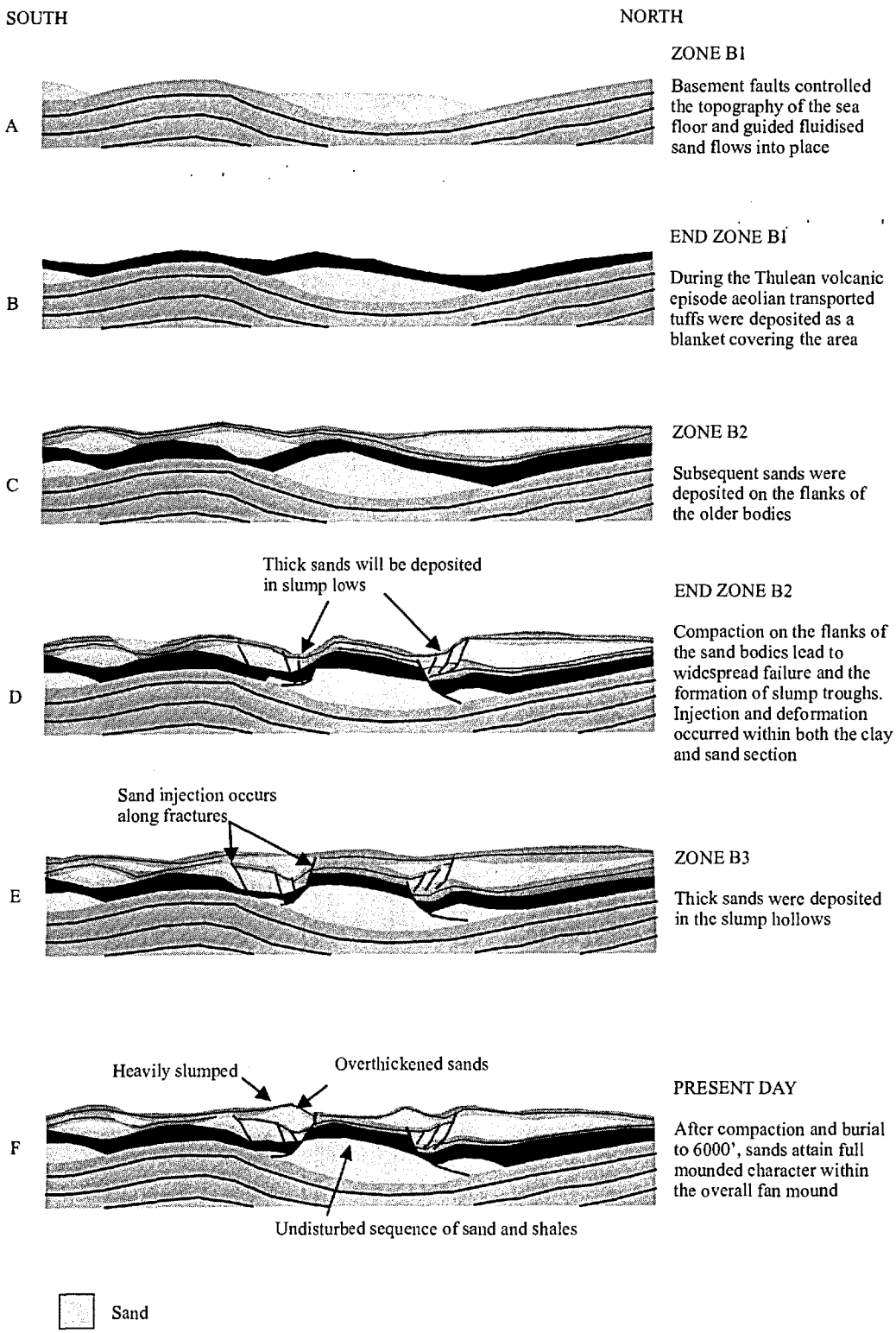
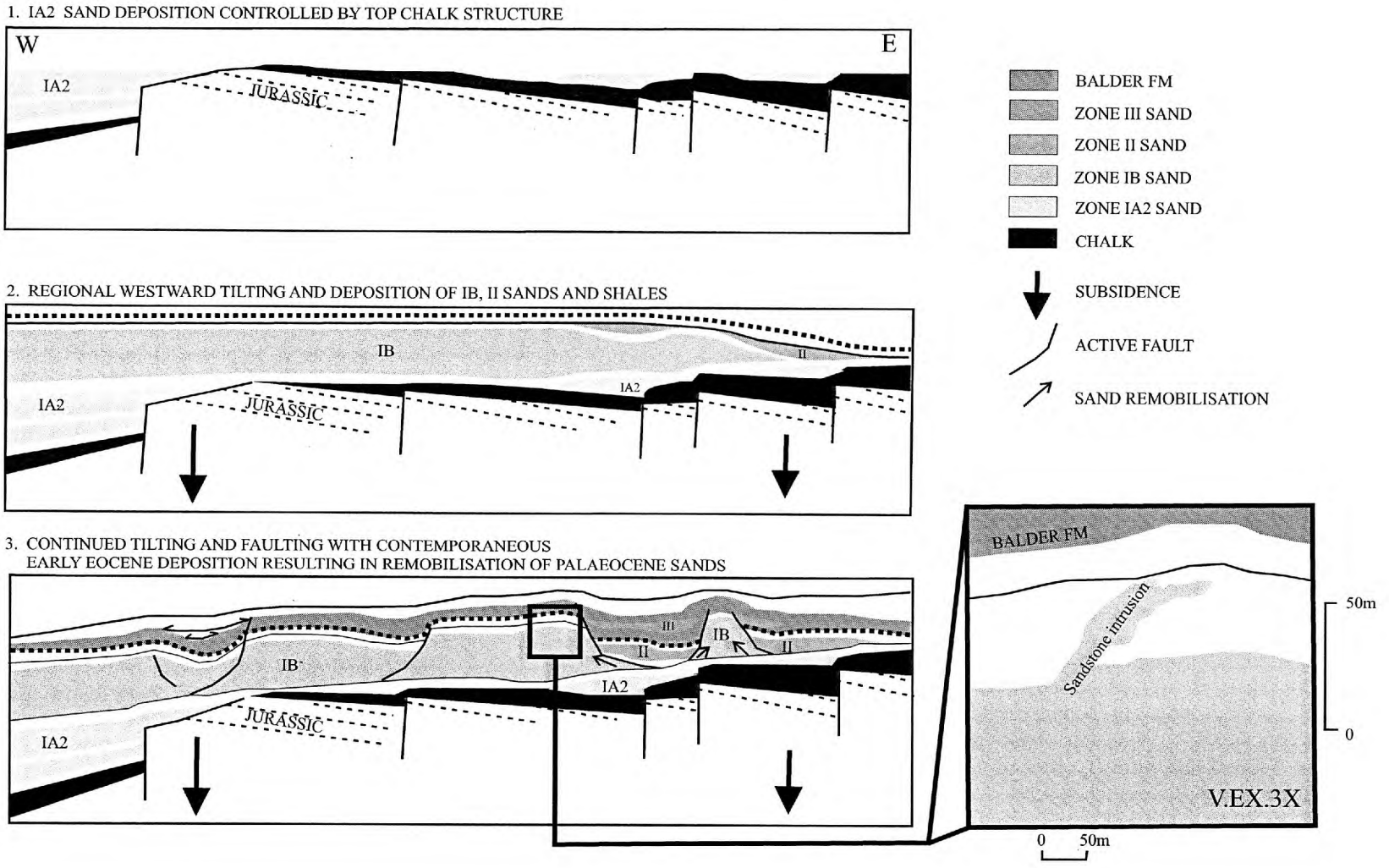


Figure 1.4. Model for depositional and post depositional remobilisation of the Tertiary Balder field (Jenssen *et al.*, 1993)



CHAPTER 2. GEOLOGICAL SETTING OF THE PRE-TERTIARY AND TERTIARY OF THE NORTH SEA-FACTORS AFFECTING SEDIMENT REMOBILISATION

2.1 Introduction

This chapter highlights the factors and geological framework which have controlled remobilisation features within the deepwater sediments of the Eocene to Mio-Pliocene of the North Sea. Pre Tertiary sedimentation and structuration established the location of basinal and intra-basinal areas which may have generated (expelled water and/or hydrocarbon) and focused fluid, respectively. Tertiary sediments are reviewed, outlining stratigraphy and palaeogeography which constrains lithology and distribution. Timing of events that could cause possible inversion and or fault activity within the Tertiary and periods of hydrocarbon generation are highlighted as being particularly significant in the context of the post depositional remobilisation processes to be described later in the thesis.

2.2 Pre Tertiary

Four major deformational events superimposed onto a Palaeozoic structural framework delineates post Carboniferous to pre Tertiary sedimentation within the North Sea: Late Permian/Early Triassic, Middle Jurassic, latest Jurassic/earliest Cretaceous and Late Cretaceous (Jones *et al.*, 1999). These structural events and trends have importantly controlled the location of the Upper Jurassic marine source rock.

2.2.1 Palaeozoic

Caledonian aged structures formed during progressive collision of Baltica with Laurentia during the Late Silurian-Early Devonian. The dominant structural trends in the North Sea and surrounding onshore areas are trends of major NE-SW Caledonian fault zones (Great Glen Fault, Highland Boundary Fault and

Southern Uplands fault) and WNW-ESE (Tornquist line) (Jones *et al.*, 1999 and see figure 1.1). Subsequently late Carboniferous to Early Permian Variscan deformation emplaced a W-E oriented grain on the North Sea (Coward, 1993; Platt, 1995).

2.2.2 Late Permian/Early Triassic

North Sea basin evolution during this time was dominated by the development of a widespread rift system that resulted from the separation of Scandinavia from Greenland (Ziegler, 1990a, b). The Central North Sea is suggested by Cartwright (1990) to have originated as a pull apart basin between two reactivated Tornquist trend basement shears. Continental sedimentation predominated through Permian and Triassic times (Glennie, 1998a, b; Fisher and Mudge, 1998), with salt deposition during the Lower Permian over the central and southern parts of the Northern North Sea becoming mobile and affecting basin geometry through time (Fisher and Mudge, 1998).

2.2.3 Middle Jurassic and Early Jurassic to Early Cretaceous

During the Late Triassic to Middle Jurassic, the degree of rifting decreased, passing into a thermal subsidence phase centred on the Central North Sea (Ziegler, 1982). In the Toarcian-Aalenian, a thermally induced dome centred close to UK blocks 21/3, 4 and 5 was established (Ziegler 1982; Underhill and Partington, 1993; Davies *et al.*, 1999a) and associated with Bathonian-Callovian volcanism (Smith and Richie, 1993; White and Latin, 1993). Collapse and rifting of this region centred about UK North Sea blocks 21/3, 4 and 5 through the Mid-Late Jurassic to Early Cretaceous, caused continental sediment (Pentland formation) equivalents of these and the Middle Jurassic volcanics to pass upwards into a succession of deepwater/shallow marine sequences that progressively onlapped and expanded out from the centre of this rift.

2.2.4 Late Cretaceous/Tertiary

Rifting terminated in the Late Jurassic to early Cretaceous and the Early to Late Cretaceous was a period dominated by thermal subsidence. The Late Cretaceous sea level rise established carbonate chalk sedimentation, which progressively overstepped the basin margins (Oakman and Partington, 1998).

2.3 Tertiary

Interpretation of approximately 6000 line kilometres of CNST 82 and CNST 86 2D regional seismic (figure 1.1) was undertaken to compare regionally correlatable seismic stratigraphic units with these interpreted by Galloway *et al.*(1993) and Martinsen *et al.* (1999) for the Eocene to Miocene of the North Sea. Over 100 wells were used to constrain lithology for defined intervals. Biostratigraphic constraints are poor for this dataset, as composite logs of variable vintage were used. Where seismic lines crossed interpreted 3 D seismic datasets with recent composite well logs, interpreted horizons could be better constrained for age and lithostratigraphy.

The following descriptions of the main four Palaeocene to Miocene sequences are taken from Galloway *et al.* (1993), Jordt *et al.* (1995) and Martinsen *et al.* (1999), and they have been identified here as exemplified by interpreted seismic lines figure 2.1 and 2.2. For a summary chart of the North Sea Cenozoic depositional episodes, nomenclature, tectonic events and oceanographic events (taken from Galloway *et al.*, 1993) see figure 2.3. Figure 2.3 incorporates these events with the Palaeogene lithostratigraphy of Knox and Holloway (1992), Jones and Milton (1994) and Miocene lithostratigraphy from Zweigler *et al.* (1999).

2.3.1 Palaeocene - approx. 65-51 Ma (Martinsen *et al.*, 1999) – sequence 1

Early Palaeocene times began with regional uplift of the Shetland and Scottish Massif (Nadin and Kusznir, 1995) by up to 1 to 3 kilometers (Green, 1986, 1989; Thomson *et al.*, 1999). This has been attributed to thermal doming, volcanism and movement of the Iceland hotspot (Nadin and Kusznir, 1995). In addition, a complex interaction of Atlantic margin compression and compression

related to Alpine collision (Ziegler, 1982; Cartwright, 1989 and Eggink *et al.*,1996), occurred south of the Tornquist line in the Central North Sea (Zoback, 1992). Initial relative sea level fall and reworking of Chalk from the uplifted basin margins occurred as deepwater mixed carbonate siliciclastic unit called the Lower Palaeocene Maureen Formation succession (Johnson, 1987). Repeated uplift of the Scottish/Shetland Massif through the Palaeocene resulted in the shedding of a series of eastward stepping shallow to deepmarine successions (Andrew and Forties submarine fans) across the Moray Firth, the East Shetland Platform and the Forth Approches basin (Galloway *et al.*, 1993). No sediment thickening is seen from the East: Scandinavia not acting as a significant source region at this time.

2.3.2 Eocene - 51 to 31 Ma (Joy, 1996; Martinsen *et al.*, 1999) – sequence 2

Late Paleocene Beauly and Balder Formation sediments mark renewed uplift of Scotland (Galloway *et al.*,1993), with progradation of these intervals eastwards. Collapse of the platform in response to opening of the Norwegian and Greenland Sea and concomittant eruption of volcanic rocks along the Hebridean margin, led to transgression of the basin margin, subsequent sediment starvation and the deposition of the Balder Tuff horizons from these volcanics (Knox and Morton, 1988). Subsequent Eocene sequences prograded eastwards into the North Sea Basin forming the Tay, Frigg and Alba submarine fans. From the early Eocene onwards sea level continued to rise to the present day, punctuated by N-S compressional events related to Alpine convergence as in the early Eocene and late Eocene (Kooi *et al.* 1989). These events may have been periods of localized fault seismicity as can be seen over the Renee Ridge where Lower Eocene sediments markedly thin (figure 2.2).

2.3.3 Oligocene - 31 to 24 Ma (Martinsen *et al.*, 1999) – sequence 3

A further basinward shift in deposition occurs in the Oligocene, with sediment derived from both the Scottish/Shetland region and from Scandinavia (Galloway *et al.*, 1993) for the first time in the Cenozoic. The separation of

Greenland and Norway is recognised by a change to a more Arctic microfauna in Oligocene lithologies (Berggren and Gradstein, 1981).

2.3.4 Miocene - 25 to 8 Ma – sequence 4

A significant unconformity of variably between 25 Ma to 8Ma is developed across the North Sea. The Utsira Formation is variably dated between Middle to Upper Miocene and is believed to be related to a fall in sea level and uplift of the Norwegian margin at this time (Galloway *et al.* 1993). Martinsen *et al.* (1999), summised that the Atlantic Ocean was connected to the Polish Platform via the North Sea at this time, with Utsira sands being supplied laterally from the Scandinavian and East Shetland basin margin in the North Viking Graben and reworked by basinal currents southwards into the Central North Sea (Galloway *et al.*, 1993) from a shallow shelf as interpreted by Rundberg (1989). A candidate fluvial tributary system running southwards has been identified by Rundberg (1989) in Norwegian block 35/8, with incision into the underlying Oligocene. Galloway *et al.* (1993) has noted large scale mounds within the Utsira formation of UK blocks 16 and suggests that during the lowstand in the Lower to Middle Miocene, erosion and bypass of the shelf resulted in the deposition of contourite mounds. The origin of these mounds will be discussed in chapter 6.

2.3.5 Summary – 2D seismic interpretation of Eocene to Miocene

The author undertook a 2D seismic interpretation using a seismic dataset previously outlined in section 1.2 (figure 1.1) covering the Lower Eocene, Upper Eocene, Oligocene and Miocene intervals of the North Viking Graben and Central North Sea. The study was completed to establish the position of shelf, slope and basinal position of strata within these four intervals, so the above intervals within which the 3D seismic datasets of chapters 3, 4, 5 and 6 could be put into a broad palaeogeographic context. Each interpreted surface (Top Lower Eocene – figure 2.4, Top Upper Eocene – figure 2.5, Top Oligocene – figure 2.6 and Top Miocene – figure 2.7) was identified as being seismically correlatable across the seismic dataset. No attempt was made to establish the sequence

stratigraphic character of wireline character as the purpose of this interpretation was to locate the 3D seismic datasets within gross lithological packages and determine the likelihood of primary deepwater sand compartmentalisation. Between these horizons well data established whether each well contained sand (sand prone) or no sand (clay prone) to establish gross lithology in a palaeogeographic context. The depositional slope break was established where there is a clear break in clinoform geometry (Emery and Myers, 1996) and coincided with a change from a maximum thick to thinning strata. The slope/basin break was more difficult to establish but was taken as basinward of the shelf/slope break and as a significant basinward thinning of the strata. Downlap onto the sequence below occurred within the slope and basinal setting.

Based on interpretation of this 2D seismic dataset, the following important observations can be made:

(i.) Lower Eocene to Middle/Upper Eocene maps (figures 2.4 and 2.5) indicate the geometry of progradation of shelf/slope clinoforms towards the basin centre from the western margin. The interpreted western margin shelf is variably sandy and shaley, whilst the slope and basin sediments are mud-dominated.

(ii.) The Oligocene map (figure 2.6) indicates progradation of shelf/slope clinoforms from the western and eastern basin margins into the basin centre. The eastern basin margin was not observed on seismic, though the slope clinoforms were. The western shelf is variably sandy and shaley, while the slope and basin sediments are mud dominated.

(iii.) The Miocene map (figure 2.7) indicates no stratal progradation from the west and east margins, but onlap onto the previous Oligocene sequence. Located in the environs of UK Quad 16 are mounds with kilometre scale wavelengths and vertical relief of up to 100 metres. Well calibration (see chapter 6) shows that these mounds are formed variably of sandstone and mudstone. East and west of UK Quad 16, the mounds pinchout before the onlap margin of the Miocene sediments and to the south pinchout and thin progressively southwards as parallel strata of clay-prone sediments.

(iv.) Throughout the Eocene to Miocene slope and basinal clay-prone successions, systems of minor ,normal faults are observed, with throws

between 10 to 50 msecs and fault spacings between 100 and 1000 metres. These are the polygonal fault systems of Cartwright (1994a, b)

(v.) Approximate calculation of minimum palaeowater depths of more than 300 msecs TWT (approximately 300 metres compacted) for base of slope sediments can be calculated from the vertical height difference of the shelf/slope break to the slope/basin break. Uncompacted palaeowater depths would place this figure much deeper.

The literature review and 2D seismic analysis of the Eocene to Miocene sediments of the North Viking and Central North Sea highlight a broad west to east prograding variably sandy shelf to mud rich slope and basin sediments during the Eocene. The Oligocene continued to prograde basinwards but from both the west and east with a variably sandy shelf and mud prone slope and basin sediments. The Miocene strata are mounded about UK Quad 16 and strata onlaps the previous Oligocene slope sediments.

3D seismic datasets described in this thesis are located within the mud prone, densely faulted intervals of slope/basin strata. This establishes that any deepwater sand prone sediment deposited within this Eocene to Miocene mud prone slope/basin interval could be compartmentalised/isolated from other sand prone sediments, such as those sandy sediments on the shelf or other deepwater sandy sediments. These sediments could also be affected during and after their deposition by the normal faulting described (see section 2.5) and dewatering/hydrocarbon generation below, especially from the Jurassic (section 2.4).

2.4. Burial History and hydrocarbon/fluid migration

Timing of hydrocarbon generation from the Upper Jurassic marine source rocks varies considerably across the basin and is significantly affected by Cenozoic sedimentation rates and heat flow (Cornford 1998). It is important to note that Upper Jurassic marine shales within this succession, subsequently act as a hydrocarbon generating source rock over large areas of the North Sea (Barnard and Barstow 1996)(figure 1.1). Work by Fisher and Miles (1983) over the Outer

Moray Firth-South Viking Graben, Goff (1983) over the East Shetland Platform and Barnard and Barstow (1996) over the Witch Ground Graben indicate progressive expansion of oil and gas mature Upper Jurassic regions through the Late Cretaceous to Neogene. Migration of petroleum fluids and gas expelled porewater due to burial will all require a migration path through the overburden of Cretaceous and Tertiary. Cornford (1998) suggests three mechanisms for fluid migration: (1) migration through halokinetically controlled fractures; (2) lateral movement through Tertiary connected deepwater sand bodies; (3) along basement faults (figure 2.8.). Although all these migration routes may ultimately lead to release of fluid pressure updip to seabed, if trapped, this fluid may create overpressure and subsequently be released as injected phenomena. Examples of this process are discussed in chapters 3 and 4.

2.5. Polygonal faulting

Polygonal faulting is widely observed within the fine grained units of the Eocene to Miocene of the North Sea. First noted by Cartwright (1994a, b) these normal faults (as seen on the 2D seismic lines described in section 2.3) occur as seismically resolvable offsets of between 10 to 100 metres, have fault trace spacings 100 to 500 metres, with fault traces randomly oriented and exhibiting radial strain (Cartwright and Lonergan, 1996). These faults have been ascribed to three dimensional dewatering of fine grained sediments and can be seen to pervasively deform the deepwater sediments of the Eocene Miocene sediments of the North Sea (Cartwright and Lonergan, 1996). They may affect the deposition of deepwater sediments as seen in the Upper Eocene Belton Member sands of chapter 5 and post depositionally affect Tertiary reservoirs such as the Middle Eocene Alba field of the Central North Sea (Lonergan *et al.*,1999). They may also act as routes for fluid migration.

2.6. Conclusions

A north (North Viking Graben)/south (Central North Sea) rift system with a westerly rift arm (Moray Firth) was active from Middle Jurassic times through

to the Early Cretaceous. An Upper Jurassic marine source rock was located regionally throughout the rift section which generated hydrocarbons about the respective 3D seismic study areas in this thesis from Eocene to Recent. Post rift thermal sag of the North Sea basin from Late Cretaceous onwards to present day was affected by Atlantic opening and Alpine compression during the early Palaeocene, early Eocene, late Eocene and middle Miocene. These periods marked the boundary between periods of submarine deposition initially from the Scottish/Shetland margin eastwards into the North Sea. It is within these deepwater Tertiary sediments that the Lower Eocene Balder Formation turbidite sands of Norwegian block 24/9 located in the centre of the North Viking Graben (chapter 3), the Lower Eocene deepwater clays of UK North Sea blocks 21/3, 4 and 5 located over the Renee Ridge (chapter 4), the Upper Eocene Belton Member polygonally faulted deepwater sands located in Norwegian block 24/9 (chapter 5) and the Middle to Late Miocene Utsira mounds of UK blocks 16/27, 28 and 29 (chapter 6) are to be found. Subsequent chapters describe these case studies as proposed large scale sediment remobilisation phenomena from the North Sea, compare relevant field analogues where available and finally outline processes and the affects remobilisation in general may have on reservoirs. The impact of hydrocarbon migration to this process is outlined.

Figure 2.1. Geological cross section across the North Viking Graben through Norwegian North Sea block 24/9 (from CNST82-09 regional seismic line)

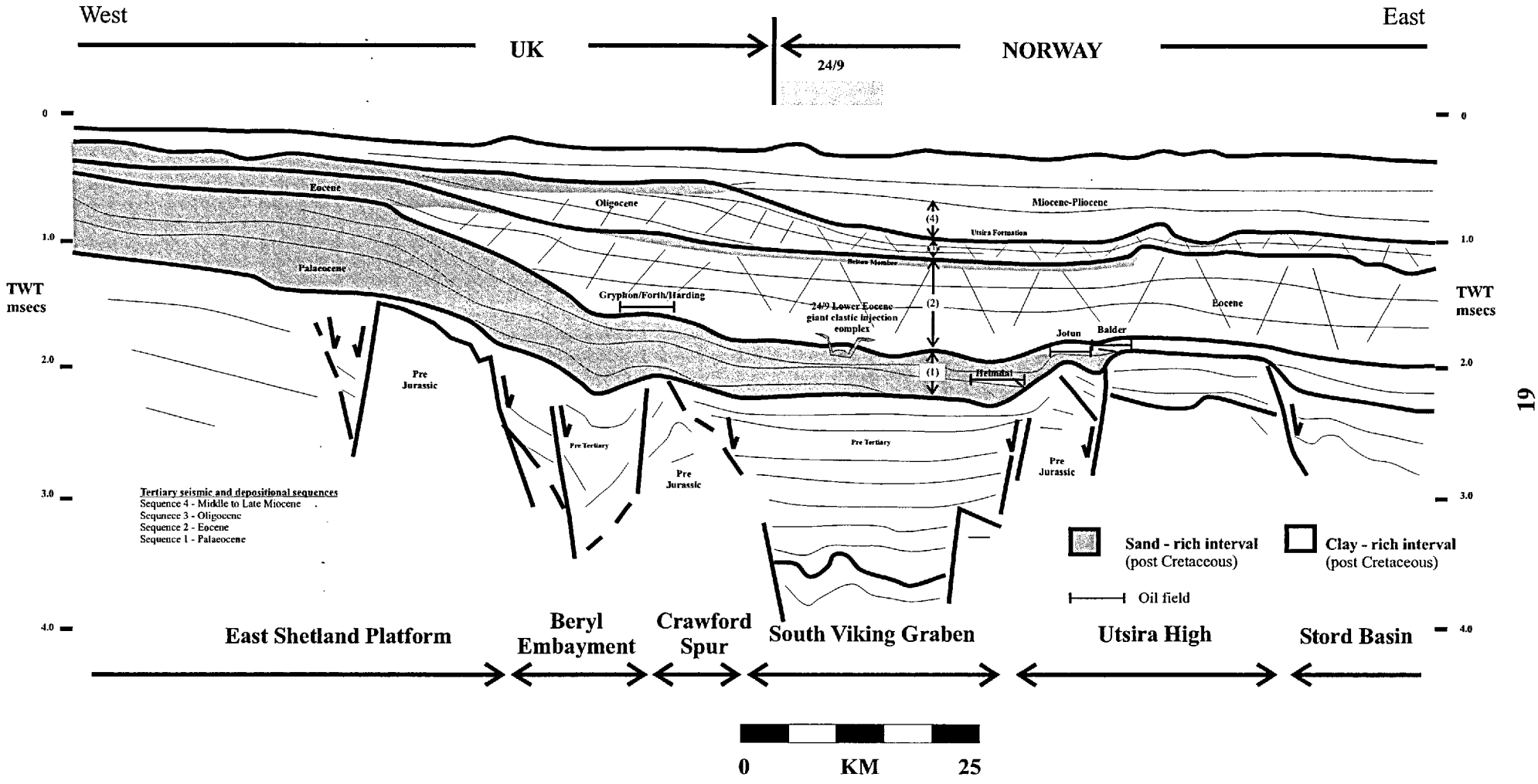


Figure 2.2. Geological cross section across the Central North Sea passing through UK blocks 21/3, 4 and 5 (from CNST82-04 regional seismic line)

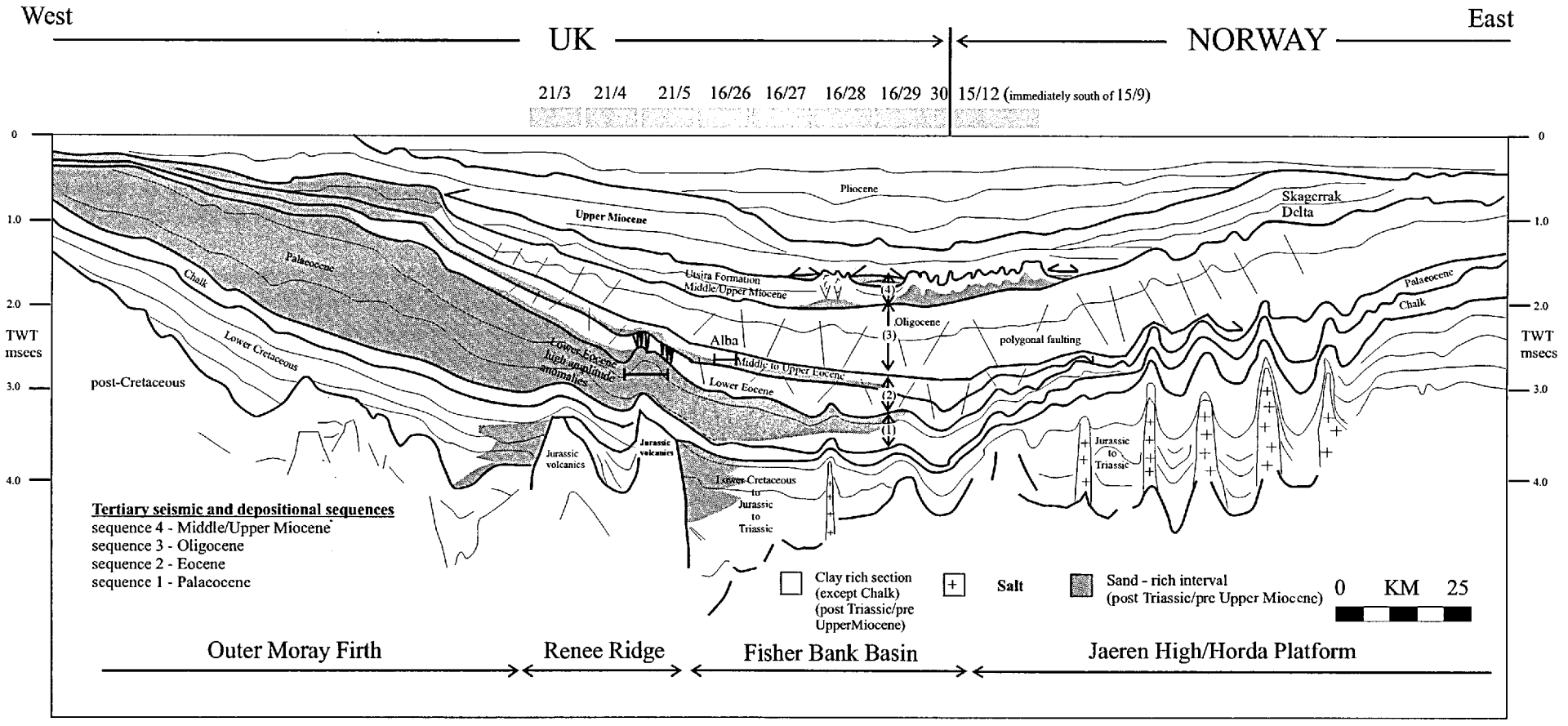
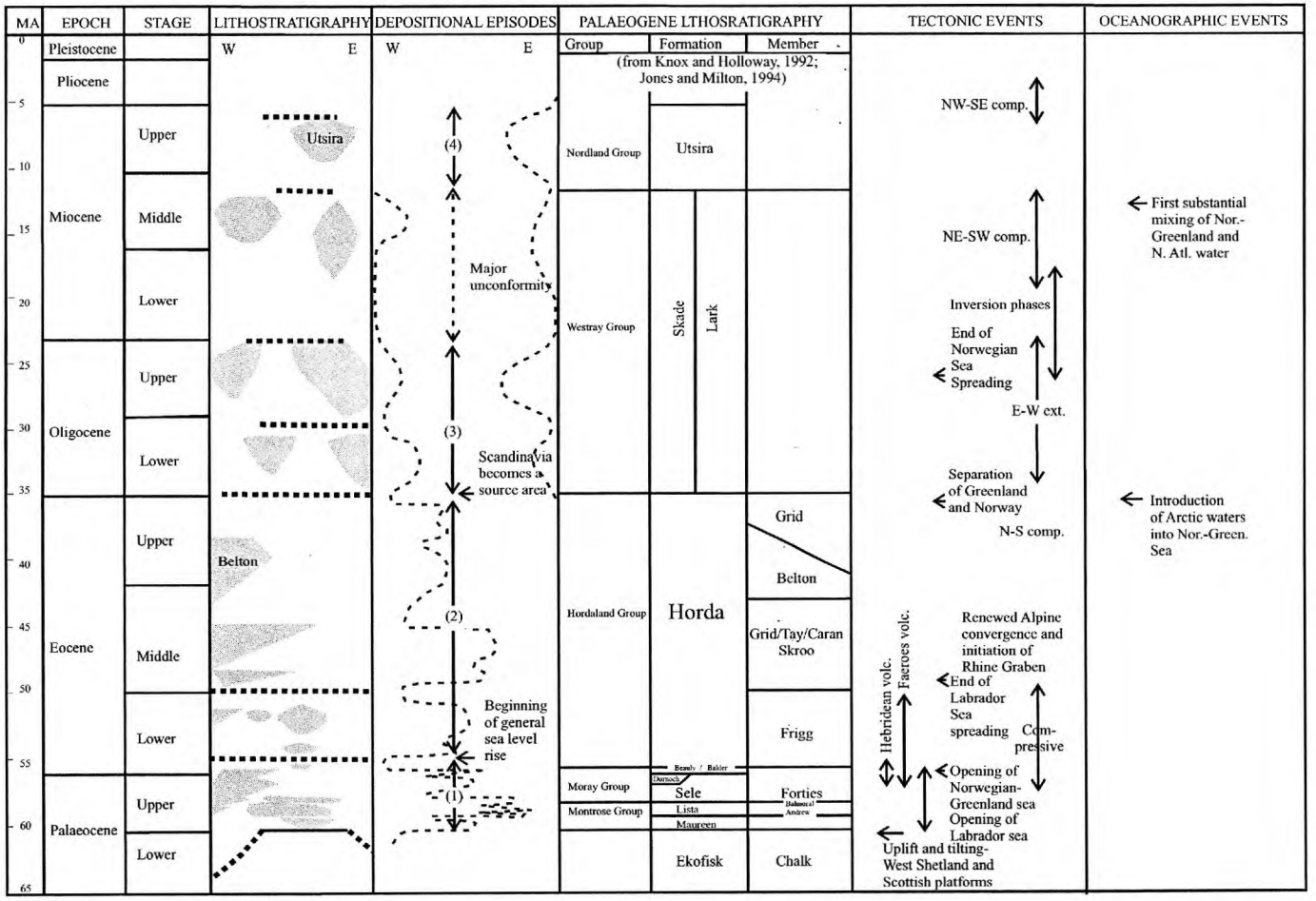


Figure 2.3. Summary chart showing the North Sea Cenozoic depositional episodes, lithostratigraphy, tectonic events and oceanographic events (partly from Galloway *et al.*, 1993; Knox and Holloway, 1992; Jones and Milton, 1994)



Note 1 : Numbered depositional episodes equate to those on interpreted regional seismic lines figures 2.1 and 2.2.
Note 2 : Utsira Formation lithostratigraphy from Zweigler *et al.* (1999).

Figure 2.4. Lower Eocene palaeogeographic map of the North Sea (faults from PESGB, 1997)

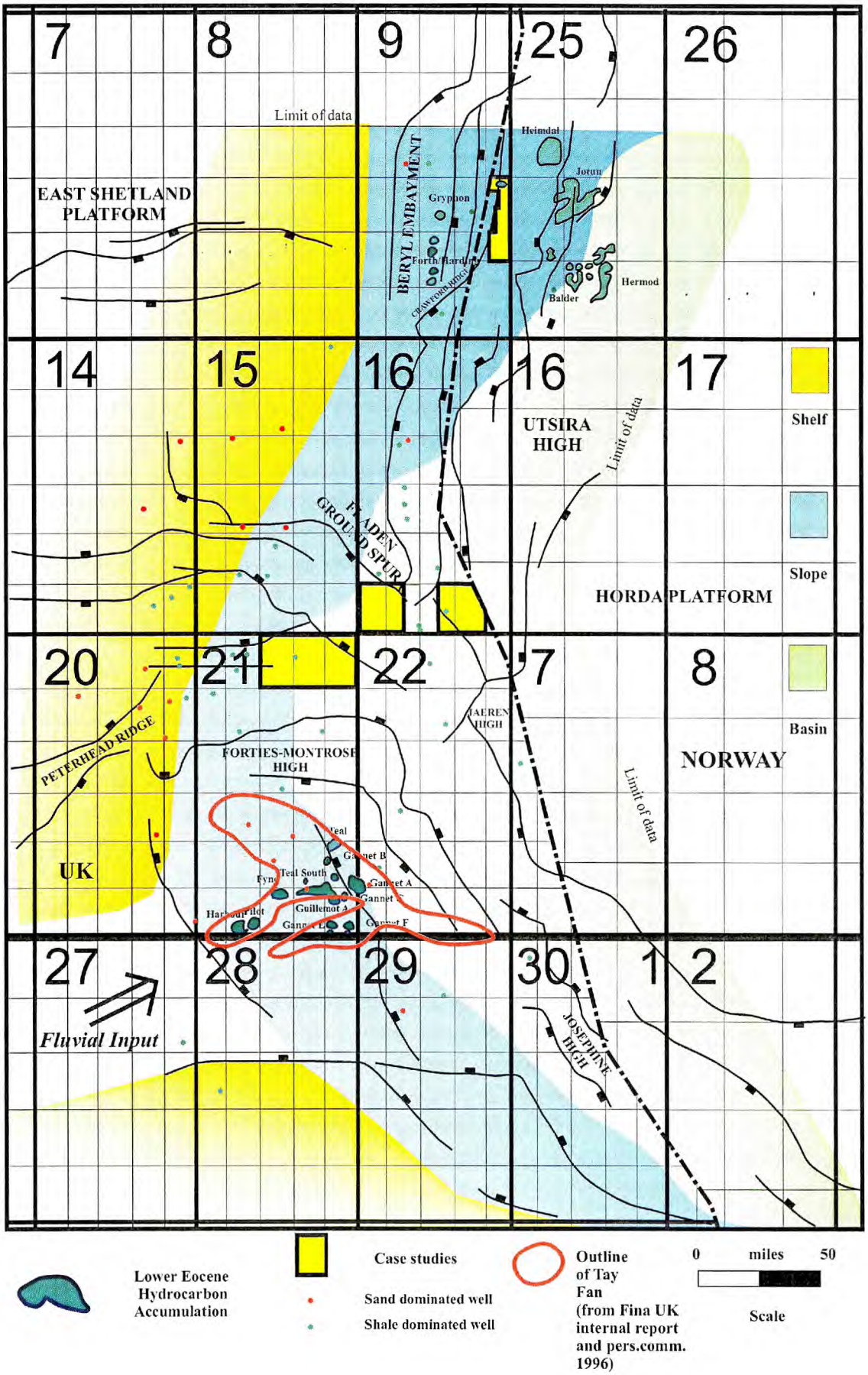


Figure 2.5. Middle to Upper Eocene palaeogeographic map of the North Sea (faults from PESGB, 1997)

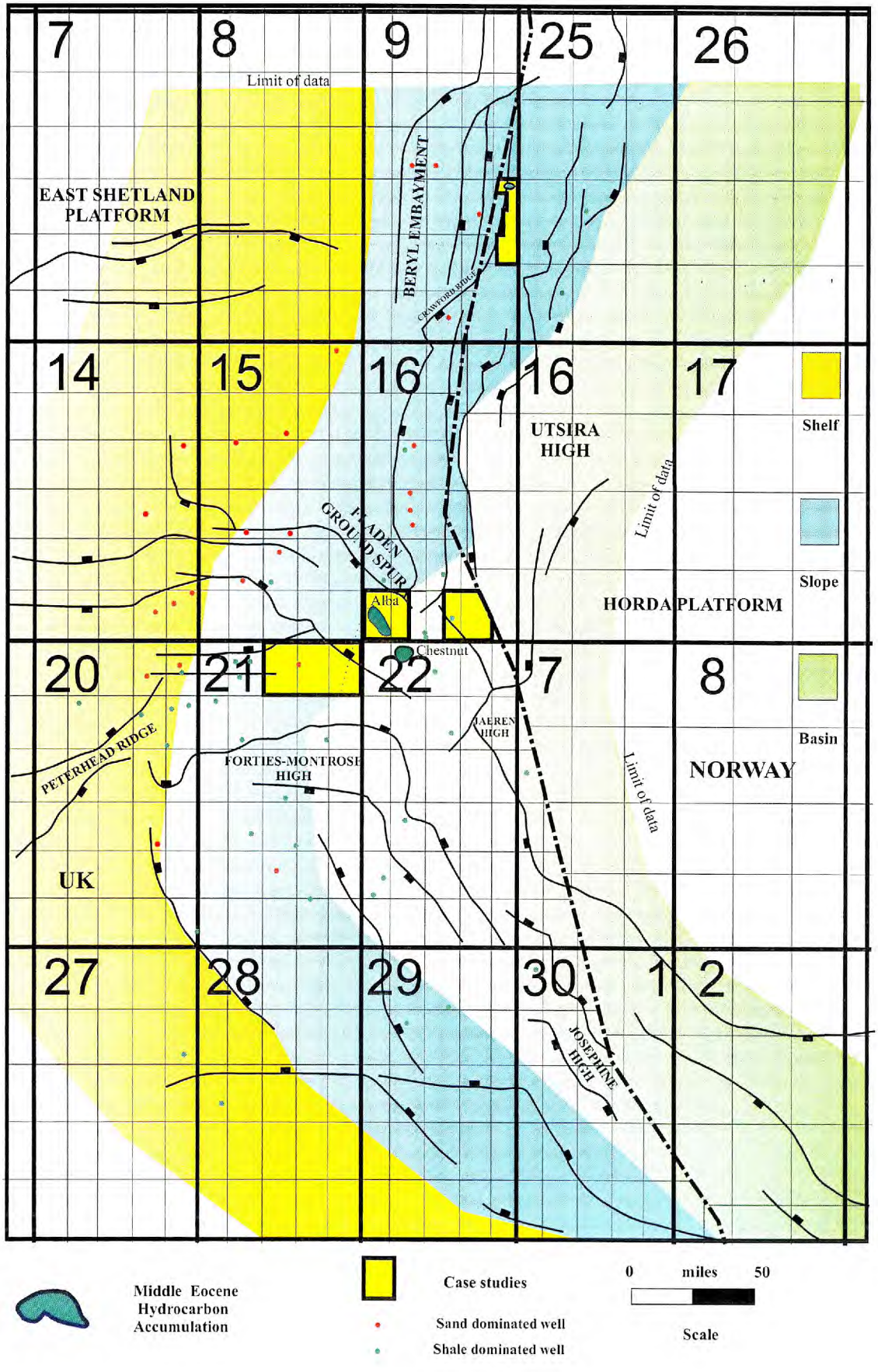


Figure 2.6. Oligocene palaeogeographic map of the North Sea (faults from PESGB, 1997)

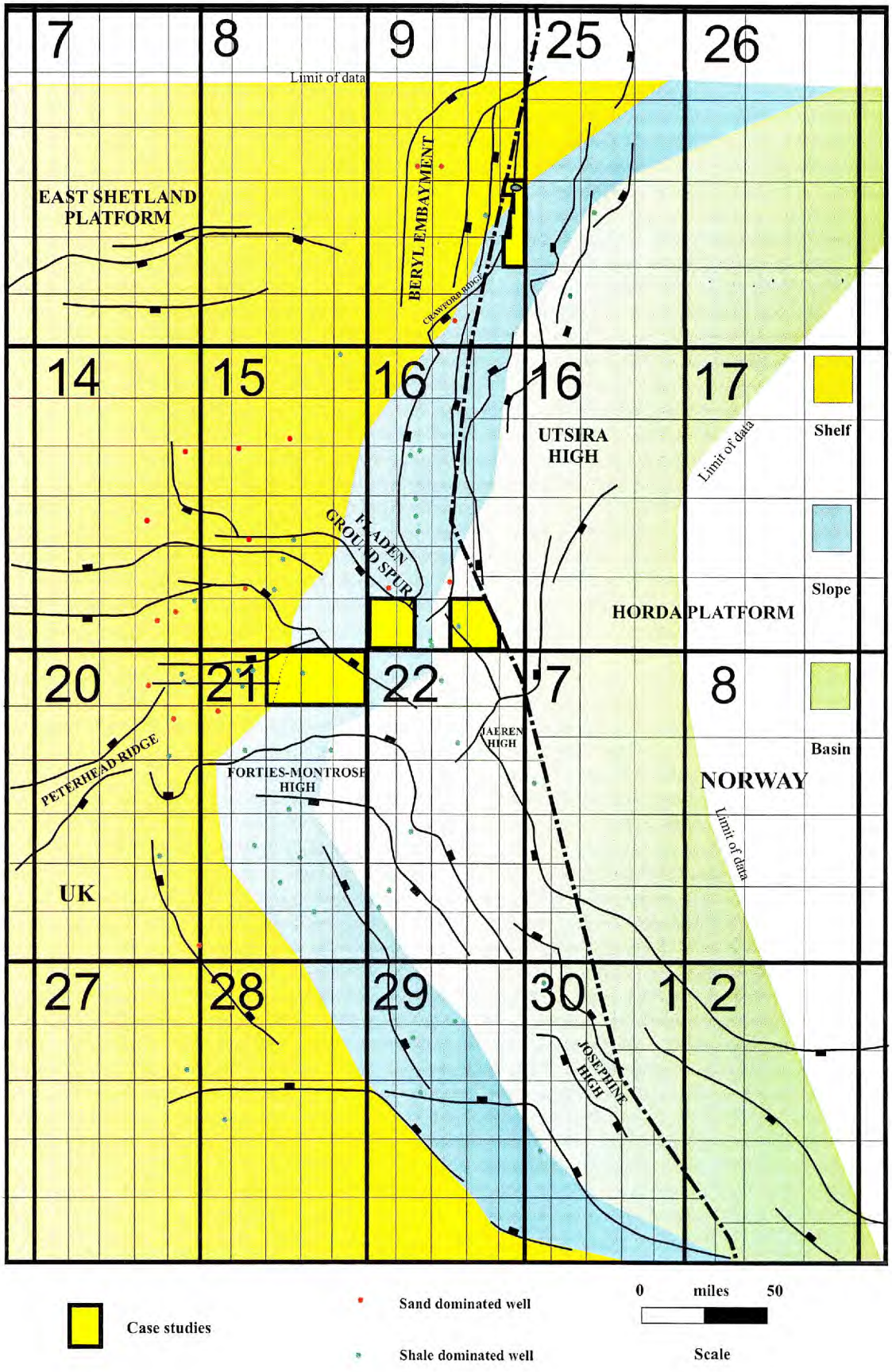


Figure 2.7. Middle Miocene Utsira formation palaeogeography over the North Sea

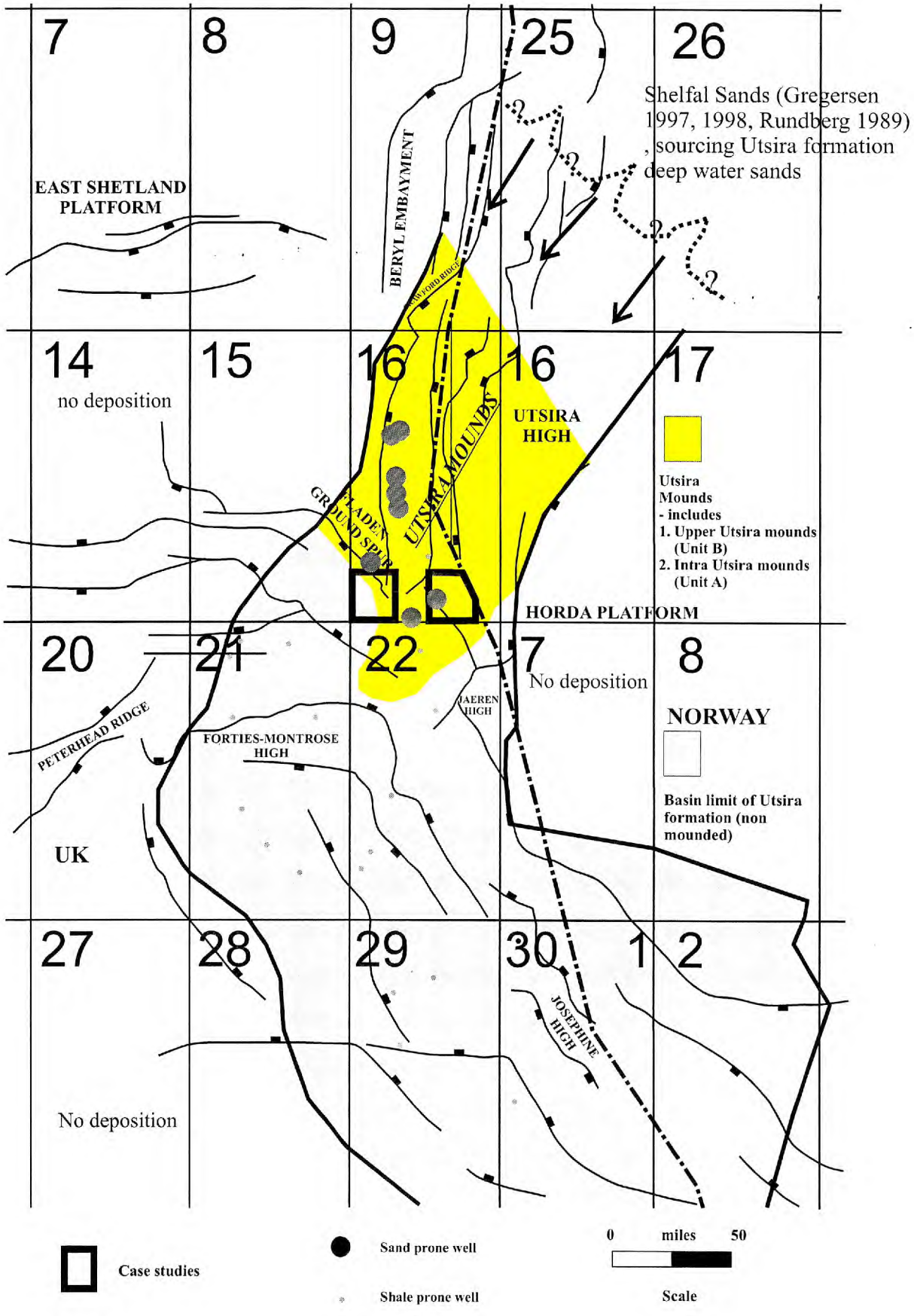
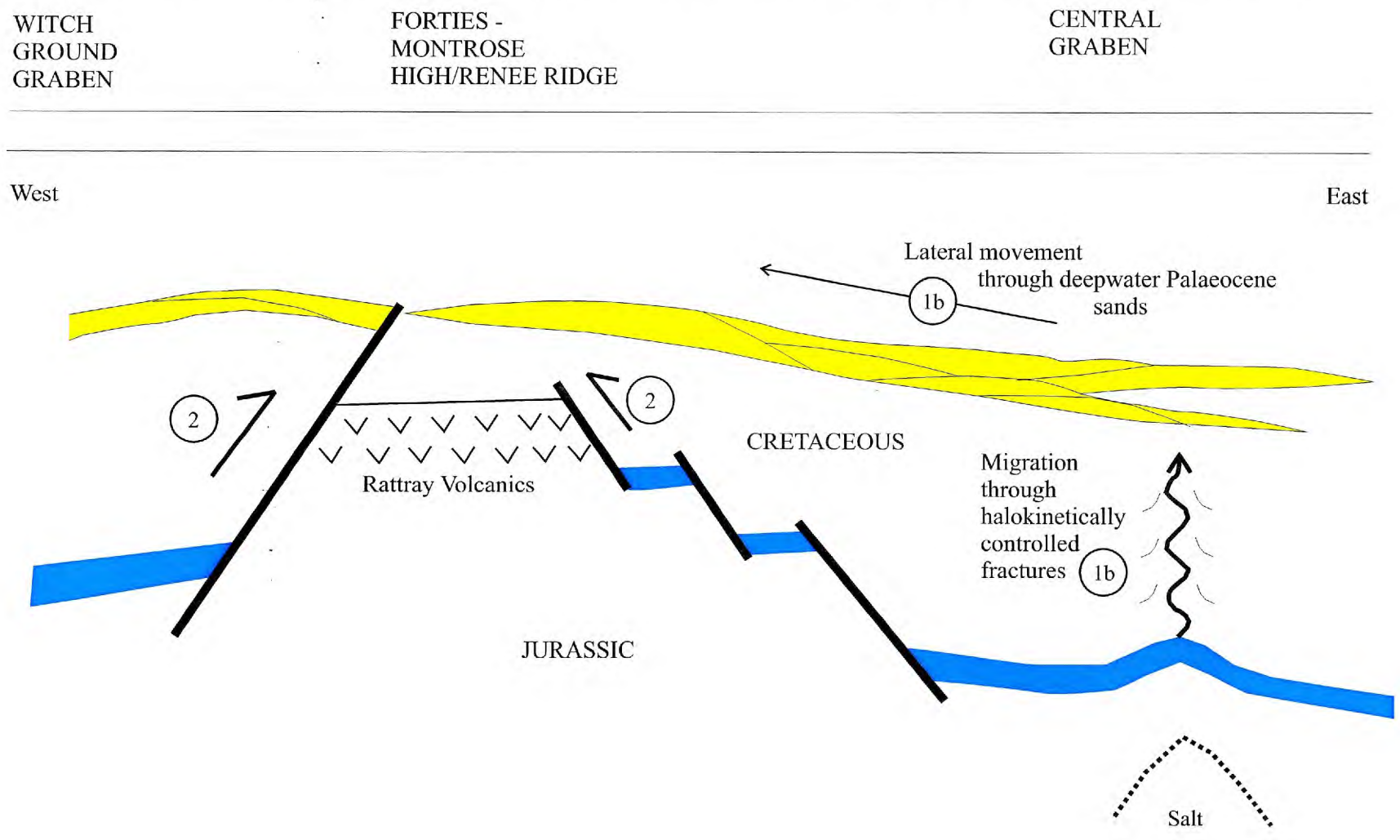


Figure 2.8. Migration routes of Jurassic sourced hydrocarbons into Tertiary sediments of the North Sea:
Migration into Tertiary deepwater sands draped over structural highs (e.g. Forties - Montrose High) is probably from the main graben, vertically via salt or fault-related fractures (1a) and then laterally up-fan from distal to proximal facies (1b). An alternative pathway via faults bounding the basement high (2) has been proposed (after and redrawn from: Wills and Peattie, 1990; Wills, 1991)



CHAPTER 3. KILOMETRE SCALE LOWER EOCENE SANDSTONE INTRUSION, OFFSHORE NORWAY, BLOCK 24/9, NORTH VIKING GRABEN

3.1 Introduction

The study area is located in the axis of the South Viking Graben within Norwegian Block 24/9 (figure 3.1). A 3D seismic survey, calibrated by two wells (24/9-5 and 6) with core within the Lower Eocene Balder Formation were used to investigate this interval. This data was primarily used to interpret seismic amplitude anomalies which originate from the Balder Formation and cross-cut stratal reflections upwards at an angle of between 10 to 40 degrees up to 300 metres of Lower Eocene stratigraphy in the northern part of the block.

3.2 Geological setting

Norwegian offshore Block 24/9 is situated in the axis of the South Viking Graben. This graben is bounded to the west by the north/south trending fault bounded East Shetland Platform and to the east by the north/south trending fault bounded Utsira Platform (figure 3.1). The study area is situated in the deepest part of the North Viking Graben with Jurassic marine source rocks of the syn rift section buried to over 9000 feet (Fina Norge, 1998). As described in Chapter 2 the Cretaceous section extends over most of the North Sea including Norwegian Block 24/9 and oversteps the platform margins as a marine clastic/carbonate succession(Lower and Middle Cretaceous) and then as the carbonate Chalk (Upper Cretaceous) post-rift fill as sea level rose and tectonic activity was at a minimum. The Late Cretaceous to Middle Miocene was a period of renewed tectonic activity related to the opening of the Atlantic (see chapter 2 for more detailed discussion), and produced a series of prograding clastic sequences from Scotland eastwards and then within the Oligocene an additional source from the east. Regional geoseismic cross-section figure 3.2 illustrates this overall stratal succession.

3.2.1 Late Paleocene to Lower Eocene depositional setting

During the latest Palaeocene, Block 24/9 was part of the development of an extensive sand system into the Viking Graben (Timbrell, 1993), with Block 24/9 situated in the distal, deepwater portion. Oilfield reservoirs of this age include the Gryphon and Forth field in the UK sector and the Balder Field in the Norwegian sector. These sands have been interpreted as part of a low-stand systems tract which coincided with the progradation of the basin slope from the East Shetland Platform to the east (Timbrell, 1993).

Timbrell (1993) has shown the main sandbodies to occur as elongate bodies or as strings of sand-rich pods aligned down slope (figure 3.3). These bodies are made up predominantly of thick massive sands apparently deposited by high density turbidity currents. The sandbodies appear to trend downslope from several different points on the shelf edge (Michelsen *et al.*, 1995, see figure 3.4) and the overall system does not appear to conform to a fan but more a ramp or slope apron (Michelson *et al.*, 1995). The sand bodies themselves have quite sharp lateral limits though there is evidence of levees on the flanks of some examples. Some of the elongate bodies appear quite strongly sinuous in plan view. Detailed biostratigraphic studies have shown that superficially sheet-like sands are in fact, products of imbricate off-set stacking caused by lateral emplacement being controlled by differential compaction of earlier units. Detailed stratigraphic evidence from interbedded shales suggest that very little erosion was involved in the initiation of many sandbodies and this led Timbrell (1993) to suggest that the sandbodies are akin to accretionary channel complexes rather than being cut-and-fill channels.

As noted earlier, throughout these Palaeocene to Lower Eocene deepwater fine grained sediments polygonal faulting exists which disrupts the geometry of sediments. These polygonal faults have been described by Cartwright (1994a, b) Cartwright and Lonergan (1996, 1997) and Lonergan and Cartwright (1996 and 1999) and Lonergan, Cartwright and Jolly (1998). They have been attributed to volumetric contraction during early compactional dewatering on the basis of detailed strain measurements carried out using high resolution three dimensional

seismic data. They have typical fault displacements of 10 to 50 metres and fault spacings of 100 to 1000 metres (Tervoort, 2000 and Lister, 2000).

3.3 Late Palaeocene to early Eocene stratigraphy

Stratigraphic nomenclature for the late Palaeocene to early Eocene for Norwegian North Sea Block 24/9 is taken from Knox and Holloway (1992)(figure 3.5). Late Palaeocene Lista Formation deepwater shales are time equivalent to the Heimdal Sandstone Member deepwater sands. Stratigraphically above these units is the late Paleocene/early Eocene Sele Formation deepwater shales within which is the older Teal Sandstone Member deepwater sands and the younger Hermod Sandstone Member. Stratigraphically above these units is the early Eocene Balder Formation formed of deep marine shales and volcanic tuff, above which are the deepwater shales of the Horda Formation.

3.4 Data

3.4.1 Seismic data

Seismic interpretation was undertaken on a 3D seismic data set 10km wide (E/W) and 34 km long (N/S) with line spacing at 12.5 metres. Data quality is generally good allowing the mapping of several horizons and fault patterns. The data was interpreted on the GeoQuest Charisma workstation system.

3.4.2 Well data

Three wells within block 24/9 (24/9-5 to 6) and well 25/7-5 have been studied. Two wells 24/9-5 and 24/9-6 have core taken through the Lower Eocene Balder interval, within sand/shale units.

3.5 Description

Interpretation of 2D seismic and the 3D seismic dataset in conjunction with analysis of the well data (wireline correlation, core description, facies analysis, thin section petrography, isotope analysis) has formed the bulk of the description of the Lower Eocene strata within Norwegian North Sea Blocks 24/9.

3.5.1 Seismic interpretation

Structure maps were produced from an interpretation of an intra-Jurassic event (figure 3.6) and a near to Jurassic event (figure 3.7), Top Chalk/Top Cretaceous (figure 3.8), Top Balder (figure 3.9) and Top Balder Reservoir. Well calibration (figure 3.23) of wells 24/9-5 and 6 to sesimic (figures 3.14 to 3.21) for the Tertiary sediments indicates the following seismic amplitude responses:

(i) Top Balder Formation – a slower shale (Horda Formation above) down into a faster sonic wireline response into the Balder Formation producing a strong positive amplitude response.

(ii) Top Balder Sandstone Member – a slower Balder Formation shale down into a faster Balder Sandstone Member sonic wireline response producing a strong positive amplitude response.

Calibration of the Top Chalk indicated slower Palaeocene shales/sands passing into a faster sonic wireline response carbonate of the Chalk (figure 3.12). The intra Jurassic and near Top Jurassic event was mapped as a strong positive seismic amplitude event and was taken as arbitary events several hundred milliseconds two way time below the Top Chalk event (figure 3.12). These events were primarily selected as they appeared regionally most able to be correlated across the seismic dataset.

Isopach maps have also been completed between the near top Jurassic event and Top Chalk (figure 3.10), Top Chalk and Top Balder (figure 3.11).

The intra Jurassic map (figure 3.6) outlines the basement structural elements across the block. Block 24/9 is situated in the middle of the North Viking Graben, with the top of the Jurassic reaching depths of greater than 8000 feet. The deepest parts of the Jurassic are within a N-S orientated trough of the North Viking Graben in the central/southerly part of the block. In addition to this

N-S tectonic trend, several faults have been mapped that are east/west oriented. To the north of block 24/9, several of these east/west faults are prominent and cross cut the north/south oriented trough of the North Viking Graben. In addition, the trough shallows to this northern location and forms a structural saddle, which further passes to the North into a deepening N-S oriented trough. Burial history work (Fina, 1990) indicates that the Jurassic has been buried to within the oil and then gas window from the Eocene to Recent.

The Top Chalk (figure 3.8) and Top Balder (figure 3.9) mirror the near Top Jurassic with each horizon deepening into a north/south oriented trough. Isopach maps between the near Top Jurassic and Chalk show thickening of strata into this north/south oriented trough. This indicates the effect tectonic/thermal subsidence or infill of previous topography has had from the Jurassic to the end Cretaceous.

The Tertiary section as previously described in this chapter and chapter 2, from the Palaeocene to Eocene, is a clastic deep marine sequence, derived from the west. The isopach map between the Top Chalk and Top Balder/Palaeocene (figure 3.11) corroborates this fact by showing thinning of this sediment package from west to east.

A high amplitude interval occurs 50 to 100 milliseconds two way time below the top Balder horizon and within the Balder Formation (figure 3.13). The amplitude anomaly has been mapped following the upper positive amplitude (figure 3.14 to 3.21). This amplitude event is 3 kilometres wide (N/S) by 5 kilometres long (E/W), with an approximate orientation east/west. The high amplitude event below the top Balder is upto 50 milliseconds thick two way time. It is observed to be directly above a a Top Balder structural high of the same vertical relief (figure 3.9). Along the periphery of the amplitude feature, the amplitude anomaly steepens considerably between 10 to 40 degrees. The amplitude steps upsection with a thickness of 10 to 50 milliseconds through the Top Balder horizon and up to 200 milliseconds above this horizon. At an approximately common height the amplitude anomaly changes from being subvertical and cross cutting strata to paralleling seismic strata (figures 3.14 and 3.21). The amplitude anomaly then extends for up to 5 kilometres laterally with a thickness of 10 to 50 milliseconds two way time. Subregional mapping by Fina

Norge (1998), has outlined the high amplitude anomaly to be on trend with a series of elongate, east/west oriented, amplitude anomalies immediately to the west, which they interpreted to be deepwater, turbidite feeder channels (figure 3.22).

Amplitude maps by Fina Norge (1998) immediately below the above amplitude anomaly, within Upper Palaeocene deep water sediments, show amplitudes which equate to a sand prone section from well correlations. These amplitudes have been postulated to be offset by Fina Norge (1998) by a series of east/west and north/south wrench faults, though mapping of these faults is difficult on individual seismic lines, as little or no offset can be noted in the vertical plane. The author was unable to reproduce these amplitude maps within the Palaeocene and correlating these inferred faults in the Upper Palaeocene to the faults on the near Top Jurassic was not possible as the faults could not be followed between the intervening stratigraphic sections.

3.5.2. Well data

Calibration of the amplitude anomaly immediately below the Balder horizon is via two wells, 24/9-5 and 24/9-6. Both wells have cored intervals which tie to the intra-Balder Formation amplitude anomaly. Core description by the author has been completed for both wells with samples of cemented portions of sand being taken for thin section petrography, cathodoluminescence, scanning electron microscopy, isotope (carbon and oxygen) and fluid inclusion screening.

3.5.2.1. Wireline data

Wells which penetrate the Balder amplitude anomaly (24/9-5 and 24/9-6) calibrate the anomaly as a partly hydrocarbon filled fine to medium grained massive sand. Figure 3.23 shows the correlation (Fina Norge, 1998) of the 24/9-5 and 24/9-6 wells within the Upper Palaeocene with well 25/7-5, 4.5 kilometres to the east. This correlation outlines the restricted nature of the Balder sandstones and the continuity of the turbidite sand units immediately below in the Hermod, Teal and Heimdal about these wells. Removing the sand from the section (Fina

Norge, 1998), indicates how isopachous are the intervening shales. Correlations have been based on a combination of biostratigraphy (Robertson Research 1998) and wireline log picks. A geological cross section, calibrated to these wells and to the seismic shows the interpreted stratal relationships (figure 3.24), hydrocarbon accumulations and position of cored intervals.

3.5.2.2. Core data

Well 24/9-5 and 24/9-6 both have core taken in the Balder sand over the following measured depth intervals:
24/9-5: 2000m - 2033.1 metres and 2048.3m - 2052.8metres
24/9-6: 2022.1m - 2045.1 metres

The above core has been described by the author (figure 3.25 and 3.26), then divided into deepwater lithofacies and lithofacies associations. The interpretation of deepwater sediments is briefly reviewed prior to the description of the lithofacies schemes applied to these core descriptions.

3.5.2.2.1. Gravity flow and deepwater mass transport mechanisms

Clastic deposition in submarine fans takes place by a variety of gravity flow processes. Following early experimental work (e.g. Kuenen, 1937; Bagnold, 1956; Middleton 1966a, b; Middleton and Hampton 1973, 1976) four end members were proposed on the basis of grain support mechanism within a continuum of sediment gravity flow processes; debris flow; grain flow; fluidised flow and turbidity flow (figure 3.28). Hampton (1972) recognised the role of debris flow in generating turbidity currents downslope and the concept was developed to produce a diagram relating sediment flow types temporally and spatially (figure 3.28). This scheme was modified by Lowe (1979, 1982) to include flow rheology (fluid or plastic) in addition to particle support mechanism. Lowe (1982) also stressed the continuous nature of sediment gravity flow processes when proposing end member flow types. Included within this continuum of deepwater transport and deposition are rockfall, slides and slumps (figure 3.29), though these are not defined as flow.

i) Rockfall

These are short lived events in which blocks of lithified material fall down a steep subaqueous slope with minimal interference between falling clasts. Large clasts are usually involved and, on arriving at the foot of the slope they collide with and bounce over similar clasts which had fallen earlier. Together they make up the subaqueous equivalent to a scree slope or talus apron. Subaqueous slopes steep enough to allow this type of movement are confined to active fault scarps, the margins of carbonate platforms and the heads of incised canyons. In many cases, rock falls will be triggered by some external event such as an earthquake or major storm. The deposits will be wedges of chaotic breccia with clasts sometimes up to 100's of metres. The breccias commonly have high porosities which tend to be filled by pelagic and hemipelagic fall-out (Collinson and Reading, 1997).

ii) Slides

Slides also involve large blocks of lithified or partially lithified sediment which move in isolation or as associated clusters in continuous contact with underlying slope sediments. The blocks move without any associated internal deformation as all the shear is concentrated on basal slip surfaces where the blocks slide over the slope sediment. In the head area of a slip the decollement surface may have a listric character, minor faults may also be present. Many slides involve relatively rapid movements in discrete events, but the possiblity also exists for material to slide more slowly over protracted time intervals by a process of creep. Slide deposits are characterised by large, often isolated blocks of lithified material, often limestones, in otherwise fine grained background sediments. Some olistoliths may be up to hundreds of metres or even kilometres in dimension. Creeping layers may show some internal fragmentation along small extensional faults giving them a similarity with certain subaerial landslides (Collinson and Reading, 1997)

iii) Slumps

Slumps share some of the features of slides and in some ways are gradational with them. They may occur over a wide range of scales with the largest slump layers covering many hundreds of square kilometres.

The bulk of displacement is concentrated on a basal slip surface, in some cases located at a lithological boundary or at some particularly weak horizon. Because slumping involves plastic deformation, a slump will freeze once the shear forces fall below some critical value. Within slumps it is common to find a wide variety of styles of deformation, ranging from brittle to plastic as the nature of the slump varies along its length. It is probable that one of the main consequences of slumping is to act as a starting process for a whole range of other sediment gravity flows which develop through the down slope acceleration, dilution and transformation of slumps as below (Collinson and Reading, 1997)

iii) Debris flow

Hampton (1972) described the transition from landslide to debris flow, agitation and the incorporation of water combining to reduce shear strength and causing internal shear throughout the sliding mass. Clasts are buoyed within the flow, supported by internal strength of the mud matrix, and deposition is by "freezing" of the flow when the driving stress is reduced below shear strength (Middleton and Hampton, 1976).

iv) Grain flow

The transport mechanism for grain flow is dispersive pressure due to grain to grain collisions preventing grain settling (Middleton and Hampton, 1976). Lowe (1979) considered grain flow to represent the transition between plastic and fluid behaviour, the density of the flow (>30% grains to fluid) giving frictional strength and therefore plastic rheology. Although not thought to be volumetrically significant as a single transport mechanism, dispersive pressure probably contributes significantly to other forms of gravity flow, notably high density turbidity flow (Lowe, 1982).

v) Liquefied and fluidised flow

Both liquefied and fluidised flow involve the relative movement of grains and interstitial fluid. However, liquefaction involves particles settling downwards through the fluid, displacing it upwards, whereas grains are temporarily suspended by upward fluid movement during fluidisation, in which there is no net downward movement (Lowe, 1976). Liquefied and fluidised flows, in a similar fashion to grain flows, may only be a transient process between flow initiation and eventual deposition or may provide part of the transport mechanism

in combination with other flow types. Loosely packed fine sand with a depositional porosity of 40 to 50 % is particularly susceptible to liquefaction due to excess pore pressures. Deposition of liquefied and fluidised flows is in response to loss of expelled pore fluid (Middleton and Hampton, 1976) often resulting in various fluid escape structures (Lowe and LoPiccolo, 1974; Lowe, 1975).

vi) Turbidity current flow

Turbidity current flow is supported by the upward component of fluid turbulence. Experimental surge type turbidity current flows were initially described by various authors (eg Kuenen and Migliorini, 1950; Middleton, 1966a and 1966b). Often derived from grain flows (Hampton, 1972), turbidity currents can move over low gradient slopes for long distances due to the hypothetical (ie as yet unobserved) state of auto-suspension (Middleton and Hampton, 1976) where sediment is eroded at the head of the flow and deposited in the body and tail (Allen, 1982).

Turbidity flow can be divided into two types - low density and high density - dependant largely on the grain size population involved in the flow and grain concentration. Low density turbidites usually consist of clay to fine sand grade material with a grain density of 20 to 30% contrasting with high density flow consisting of medium sand to cobble sized particles at concentrations of greater than 30% (Middleton, 1967; Lowe, 1982).

Low density turbidite flows, as described by Bouma (1962), show internal structure produced by decelerating flow and change from suspended (Ta) to bedload transport and subsequent deposition by traction sedimentation forming the Bouma Tb and Tc divisions. The overlying part of the unit (Td and Tc) results from direct suspension sedimentation.

High density turbidity currents (>30% grain density) were proposed by Kuenen and Migliorini (1950) and are well described by Lowe (1982). Lowe (1982) subdivided high density turbidites into sandy and gravelly flows. In sandy flows dispersive pressure is negligible, except possibly at the base of a flow where shear rates between bed and flow are highest (Middleton, 1967). Lowe (1982) proposed three stages of sedimentation from such a flow; a traction sedimentation stage during which various bedforms may be produced (S1); a

traction carpet stage when sediment "freezing" can result in the deposition of inversely graded layers (S2); and a suspension stage (S3) where high fallout rates suppress traction sedimentation creating a dense cohesionless layer which is prone to secondary water escape structure formation, in particular dish and pillar structures (Lowe and LoPiccolo, 1974; Lowe, 1975). The latter division - S3 - is equivalent to Bouma's (1962) Ta division.

Within the context of these gravity flow deposits, the core from the Balder formation and Heimdal formation was described and interpreted.

3.5.2.2.2. Lithofacies of core in Balder sediments of wells 24/9-5 and 6

1) Sands

Sm - Massive (figure 3.30)

Buff to pale yellow, massive, fine to medium grained sand units cm to metre bedded, generally loose or poorly cemented with occasional moderately to well cemented carbonate. Rare dish structures occur. Rare low angle cross bedding. Millimetre to centimetre scale carbonaceous material occur occasionally. Millimeter to centimetre scale dark grey clay clasts occur rarely. Base and top of unit are sharp and parallel to bedding.

Environment of deposition

High density turbidite or grain flow deposit.

Sg - Normally graded

Buff to pale yellow, upward fining units of fine to medium grained sand units, cm to dm bedded, generally loose or poorly cemented with occasional moderately to well cemented carbonate. Occasionally laminated. Base of sequences sharp or low angle erosive base with sharp, bedding parallel top. Occasionally loaded base.

Environment of deposition

High density turbidite with progressive waning flow.

Si - Injected sands

Pale grey, massive, fine to medium grained, sand, cm to metre bedded, with no internal fabric. Sharp tops and bases. Intrusive sands may be sills or dykes. Dykes may be intruded up to 65 degrees (figure 3.31 and 3.32). Sands may have quartz cemented subvertical to vertical planes (figure 3.28). Sands are generally uncemented and rarely moderately to well carbonate cemented.

Environment of deposition

Sandstone intrusions.

2) Mudstones (clay/silt)

Mh - horizontally laminated

Dark grey to dark olive green, mm laminated, rarely bioturbated mudstones.

Environment of deposition

Deep water, basinal shales

Mg - normally graded

Dark grey to dark olive green, mm laminated, rarely bioturbated mudstones. Upward fining units cm to dm scale.

Environment of deposition

Low density waning turbidite deposit.

3) Tuffs/Tuffaceous mudstones/Tuffaceous sandstones

Tg - normally graded

Olive green to dark brown, mm to cm laminated claystone with mm fragments of siliceous tuff shards. Fining upwards mm to metre scale units.

Environment of deposition

Low or high density turbidite deposit part of a waning flow with associated erosion of or concurrent fallout of volcanic tuff.

3.5.2.2.3 Lithofacies Associations of core in Balder sediments of wells 24/9-5 and 6

1) Sand dominated

S1 - Massive sands

Formed of Sm massive sand and thin less than 1 metre layers of Mh horizontally laminated mudstone lithofacies interpreted as either proximal high density turbidites or grain flows interbedded by periods of non turbidite sand deposition represented by laminated clays. Alternatively these sands may have been deposited as above and subsequently remobilised into these massive sands.

S2 - Interbedded Massive Sands and Mudstones

Lithofacies as above with Sg normally graded massive sands and Mg normally graded mudstones. This lithofacies association is interpreted as the S1 lithofacies but more distal/lower density to the main flow either from the source or peripheral to the flow.

2) Mud dominated

M1 - Mudstones

Composed of only Mh horizontally laminated mudstones, this lithofacies association is interpreted as being a basinal mudstone, with no affect of turbidite sand deposition.

M2 - Mudstones with graded silts/tuffs/tuffaceous sands

Composed of a mixture of horizontally laminated clays, normally graded clays, normally graded tuffaceous sediments and normally graded sands. This lithofacies association is formed of low density distal turbidite sediments with tuffaceous fall-out and hemipelagic muds.

3.5.2.2.4 Lithofacies summary

Cores of Lower Eocene sediments in 24/9-5 and 24/9-6 are interpreted to represent sediments deposited within a deepwater clastic system. Massive sands (S1) can be equated to the Ta division of Bouma (1962). Interbedded Massive sand and Mudstones (S2) represent either grain flows, high density turbidites of the Ta to c division of Bouma (1962) or remobilisation of these sediments. Rare clay interbeds represent cessation of flow and a return to low density turbidites or hemipelagic deposition. Increased content of clay beds represents a more distal

location to the flow. Horizontally laminated mudstones (M1) indicate areas of hemipelagic deposition with graded tuffaceous mudstones/siltstones and sandstones representing decelerating turbidite flow within a background of volcanic tuff fall out equivalent to the Tc-d divisions by Bouma (1962).

Throughout these above lithofacies all contain some observable sedimentary structure(s) and when combined can be interpreted to turbulent or grain flow such as graded bedding, erosive bases, cross bedding, massively bedded and lamination. Intruded sands described were wholly different to these primary turbidity sediments. The intrusive sediments (Si) were massive with no internal fabric and appeared to be a lighter pale grey colour than the "dirtier" looking turbidite sediments. Importantly, these sediments had cross-cutting relationships with the surrounding strata, either low or high angle. Only strata with demonstrable cross-cutting relationships were intrepreted as intrusive. Many more intrusive beds may exist in these core as it may be that several of the other massive beds described and attributed to turbidity or grain flow processes which have no observable discordant bedding relationships are in fact intrusive sills (see chapter section 4.2.1.).

3.5.2.3. Core samples

In an effort to further understand the potential fluid flow through these sediments, sandstone samples that appeared cemented were taken for laboratory analysis. Twenty sandstone samples were taken from both cores of 24/9-5 and 24/9-6. Of these, 9 samples were cemented enough to warrant being analysed and are listed below (Table 1)(and on the core description sheets figures 3.25 and 3.26):

Table 1

24/9-5

Sample	Depth (MD metres)
0179	2010.3m
0185	2010.8m
0181	2013.4m
0182	2019.6m

0183 2032.2m

0186 2033.2m

24/9-6

Sample Depth (MD metres)

0188 2031.1m

0195 2034.4m (no isotopes run on this sample)

0191 2034.9m

These samples were thin-sectioned and the following techniques/apparatus used to analyse them: petrography, scanning electron microscopy, cathodoluminescence, carbon and oxygen isotopes and screening for fluid inclusions.

3.5.2.3.1 Thin Section Petrography

i.) Methodology

Petrographic descriptions of the thin sections were undertaken of the cemented sandstones. Thin sections were stained with Alizarine Red S to differentiate calcite from dolomite and Potassium Ferrocyanide to differentiate ferroan and non-ferroan minerals (Friedman, 1959; Dickinson, 1966). Observations were made and recorded photographically on a Leitz Ortholux microscope fitted with an Olympus 2 camera. Grain shape and sorting were estimated by comparison with the charts of Powers (1953) and Pettijohn *et al.* (1972) respectively. Sands described were either Massive (Sm) or Massive injected (Si) and were nearly all similar to the description below:

ii.) Petrographic description

Fine to medium grained sandstone (quartz arenite; Pettijohn, 1975) formed of monocrystalline and very minor polycrystalline quartz) which is moderately sorted and is generally composed of subangular to subrounded detrital quartz grains. The samples observed display point contacts indicating very weak compaction.

The detrital mineralogy is dominated by monocrystalline quartz. Polycrystalline and microcrystalline (chert) quartz grains are sparsely distributed. Minor feldspar grains include K-feldspar (orthoclase with minor microcline) and plagioclase feldspar. Rare rock fragments are predominantly composed of dissolute, fine grained and possibly argillised volcanic grains. Rare mica muscovite and biotite mica flakes are commonly altered to clay minerals and locally buckled and splayed at the end.

The authigenic mineralogy comprises rare, very incipient, quartz overgrowths and with 95% of the cement a partially or wholly pore occluding poikilotopic ferroan calcite cement (as confirmed by the red staining from the Alizarine Red S and Potassium Ferrocyanide preparation). Very rare, poorly crystalline booklets of kaolinite are recognized, formed in porosity before the ferroan calcite cement. Figure 3.34. is a plane polarized photomicrograph of such a sandstone. Quartz grains also show variable levels of etching by the ferroan calcite cement.

(iii) Petrographic interpretation

These quartz arenite sandstones are mineralogically mature and texturally moderately mature, indicating some reworking/winnowing of grains, before deposition into deepwater. Diagenetic history began with minor quartz overgrowths, followed by minor kaolinite and finally a ferroan calcite cement, which may totally occlude porosity originally up to 30 to 35% by volume, now preserved by this cement. This high minus cement porosity coupled with common "floating" grains and a lack of compaction effects, indicates a relatively early formation of the ferroan cement due to the high minus cement porosity observed. This minus porosity could also be interpreted to indicate preservation of overpresure within these sediments as overpressure would create high porosity. The poikilotopic nature of the ferroan calcite cement has been ascribed by Tucker (1981) to infer an early formation of the cement. These are important points to note as if these sands were remobilised or injected then this constrains this process to occurring early and/or shallow in the burial of these sediments.

3.5.2.3.2 Fluid inclusion screening

Using a times 50 light microscope no fluid inclusions could be observed in any of the carbonate cements of these samples. Wilkinson pers.comm. (1999) indicated this may mean a low temperature of cement formation, probably below 60 degrees celsius, not allowing fluid inclusion formation. Alternatively fluid inclusions may have formed at higher formation temperatures, but due to the pervasive cleavage network within calcite cements, fluid inclusions may be destroyed by this network and leak the inclusion contents.

3.5.2.3.3 Cathodoluminescence

i.) Methodology (partly from Coneybeare, 1996)

Cathodoluminescence microscopy (CL) was used to observe luminescence effects in carbonates to determine qualitatively compositional differences between and within the poikilotopic ferroan calcite phase. These sections were made in a similar fashion to ordinary thin sections but were lapped and then polished to 30 microns thickness. Observations were made using a Technosyn luminescence chamber attached to a vacuum pump and mounted on a Nikon petrographic microscope. The electron beam was generated using a variable current and a 15kV potential difference between a tungsten steel cathode disk and an annular anode within an evacuated glass tube, and fired obliquely down onto the speciman surface.

CL within a mineral can be attributed to intrinsic or extrinsic centres of luminescence (Walker, 1985). Intrinsic centres are due to crystal imperfections such as lattice defects and mechanical damage. Extrinsic centres are acquired from the conditions in which a mineral precipitated and relate to the mineral chemistry. These centres vary in their response to excitation by an electron beam and can be divided into two main types:

1.) activator centres - where the emission of light is highly likely on decay from the excited state, eg Mn 2+ in calcite

2.) quencher centres - where the centre is close to a radiationless groundstate even when excited and produces little or no radiation, eg Fe 2+ in calcite.

It is the concentration of these luminescent centres that governs the intensity and colour emission. The causes of CL in quartz are not yet fully understood although it is apparently related to thermal history (Walker, 1985). Different CL colours in feldspars are due to various ionic substitutions (eg F 2+ for Al 3+ and Mn 2+ for Ca 2+).

ii.) Description/Interpretation

CL images of the Balder Formation massive sands in Norwegian North Sea wells 24/9-5 and 6 show very dull orange brown to non-fluorescence of the poikilotopic ferroan calcite cement, with the quartz grains non-fluorescent(figure 3.35). No CL zoning is observed within the poikilotopic ferroan calcite cement. As explained quartz grains generally have no fluorescence with the Fe component of the calcite cement suppressing fluorescence in the ferroan calcite cement. The lack of zoning indicates a single fluid flow phase of ferroan calcite cementation which occluded the porosity in one event.

3.5.2.3.4. Scanning Electron Microscopy (SEM)

i.) Methodology (partly from Coneybeare, 1996)

In this study a Hitachi 2500 SEM was primarily used, with a JEOL 733 SEM being utilised for element mapping and a Hitachi S-800 Field Emission SEM (FESEM) for detailed observations. Images were acquired from a number of types of radiation resulting from the incidence of an electron beam on a specimen surface.

a.) Backscattered electron image mode (BSEI)

i) Methodology (partly from Coneybeare, 1996)

The number of backscattered electrons emitted from a point on a sample surface is a function of the atomic number of the mineral at that point. The contrast and brightness of a mineral viewed in the backscatttered mode varies with the mean atomic number of the mineral composition. On polished flat surfaces, differences in contrast can separate differences in atomic number with a resolution of 0.12 (Hall and Lloyd, 1981).

BSEI requires a negative potential to be applied to the collector, repelling the lower energy secondary electrons but allowing the higher energy (>50eV) backscattered electrons to reach the scintillator.

Samples required for backscattered electron imaging require a flat, polished upper surface. A carbon coat is applied prior to observation.

ii.) Description/Interpretation

Backscattered images highlighted the poikilotopic nature of the ferroan calcite cement with each cemented region encompassing upto several sand grains at a time.

b.) Cathodoluminescence (SEM CL)

i.) Methodology (partly from Coneybeare, 1996)

CL effects produced on the SEM by electron beam excitation are focused via a lens into a light guide and then onto a photo-multiplier. CL features in silicate minerals, notably quartz and feldpar, were examined using carbon coated polished thin sections. Carbonate cements are not easily studied on the SEM due to the smearing effect produced by the long persistence of the luminescence generated in carbonate minerals.

ii.) Description/Interpretation

SEM CL outlined the quartz grains as darker, non fluorescing areas and the ferroan calcite cement as dull fluorescing ferroan calcite cement. As in the convential CL technique described earlier these images indicate no zoning of the ferroan calcite cement.

c.) Energy dispersive X-ray analysis (microprobe analysis)

i.) Methodology (partly from Coneybeare, 1996)

X-rays are emitted as a result of electron beam excitation and the displacement within an atom of an electron from an inner to an outer shell, followed by a return to the original energy state. This energy transition involves the release of fluorescence and X-rays, the wavelength of which are related to the atomic number of the excited atom.

An energy discriminating system (EDS) was used for the microprobe analysis. The fluorescent X-ray beam is passed to a solid state lithium drifted silicon detector, kept cool by liquid nitrogen, and the resulting signal divided by a

multichannel pulse height analyser. Using a beryllium detector window, the lowest atomic mass detectable is sodium with an atomic number of eleven.

Quantitative and qualitative analyses was performed on the carbonate cements within sandstones using a Link System 869 analyser with a 15 kV potential difference, a current of about 2mA and a 40mm working distance. Quantitative analyses were calculated using ZAF4 software, correcting atomic number, absorbtion and fluorescence effects. The beam diameter limits analysis to grains approximately greater than 4 microns.

ii.) Description and results

This technique allowed whole screen mapping of the poikilotopic ferroan calcite cement for MnO, MgO and FeO. This technique involves the analysing machine probing a sample area for the above constituents in this case over a 10 micron grid pattern. The resulting maps showed little variation for the above components and as such are not presented here. Below are the ranges which were determined for the above mapped oxides as a weight percentage of total oxides measured and are presented in table 2 below.

Table 2

Well 24/9-5 (poikilotopic ferroan calcite)

Sample	Depth(metres)	MnO min	MnO max	FeO min	Feo max	MgO min	MgO max
0179	2010.3m	1.155	1.648	0.995	1.738	0.411	0.577
0185	2010.8m	1.55	2.604	1.853	0.823	0.351	0.88
0181	2013.4m	0.841	1.091	2.191	2.268	0.874	1.105
0183	2032.2m	8.584	9.554	2.689	3.101	1.09	1.198

Well 24/9-6 (poikilotopic ferroan calcite)

Sample	Depth(metres)	MnO min	MnO max	FeO min	Feo max	MgO min	MgO max
0188	2031.1m	0.171	0.261	1.682	2.65	0.004	0.211
0191	2034.9m	0.641	1.082	0.123	1.052	0.213	0.421

iii.) Interpretation

Whole screen mapping of the ferroan calcite cement indicates FeO levels to be the same or double MnO and up to eight times the level of MgO. The

predominance of fluorescence suppressing FeO over the potentially fluorescing MnO and MgO and the generally higher than 1% weight percent of FeO explain the dull fluorescence of this cement. Again, a lack of observable zonating or variation in the above components indicates no sign of episodic cement growth in this cement.

3.5.2.3.5. Isotopes - C13 PDB and O18 SMOW and O18 PDB

i.) Methodology (from Coneybeare, 1996)

Isotopes of carbon (C12 and C13) and oxygen (O16 and O18) were measured from ferroan carbonate cements. The carbon isotope compositions of authigenic carbonate were used to determine the source of carbon involved in cement precipitation (Curtis, 1977; Irwin *et.al.*, 1977; Curtis and Coleman, 1986; Coleman and Raiswell, 1981) and the oxygen isotopic signatures to give the possible source of the formation fluid (eg seawater, meteoric water) and also to provide evidence of the physical and chemical processes that may have influenced the original fluid composition (eg mixing) (Longstaffe, 1986).

During a chemical reaction, molecules bearing the lighter isotope of an element react more readily than those with a heavier isotope resulting in isotopic fractionation (Hoefs, 1987).

A number of factors govern the ratio of oxygen isotopes during the formation of an authigenic phase, but the most notable are the initial isotopic composition of the precipitating fluid and temperature (Longstaffe, 1986). Experimental work has established fractionation factors for calcite (Friedman and O'Neil, 1977). If temperatures can be constrained, the type of fluid present during the precipitation of a mineral can therefore be determined as both seawater and meteoric water have diagnostic isotopic signatures, although these have been modified by chemical and physical processes (e.g. evaporation and mixing). Conversely, if the composition of the original fluid is known, the temperature of precipitation can also be estimated.

The carbon isotopic composition of carbonates reflects the source of bicarbonate involved in precipitation. The initial carbon isotope composition of pore fluid at the sediment water interface for marine water will be similar to that

of seawater. During burial, the influence of CO2 generation from the decomposition of organic matter surviving occurs generating characteristic isotopic compositions (Tissot *et al.*, 1974; Curtis, 1978; Irwin *et al.*, 1977).

The accuracy to which absolute isotopic abundances can be measured is much poorer than the precision with which relative differences in abundance can be determined. It is for this reason that isotopic analyses are quoted as del with reference to standards (Hoefs, 1987)

$$\text{del O/oo} = \frac{\text{Rsample - Rstandard}}{\text{Rstandard}}$$

Ferroan calcite cements were selected for carbon and oxygen isotope analysis with a small piece (about 0.5 gram sample) of each sample broken and crushed using an agate pestle and mortar. Samples were sent to the Scottish Universities Research and Reactor Centre, Glasgow, Scotland where analysis was completed by staff at the facility. About 2mg of powdered sample was weighed in a nickel boat and loaded, with standards and duplicates, onto a carousel for automatic analysis. Standard samples were dispersed amongst the samples to check accuracy and to identify any "memory effect" from the incomplete dissolution of previous samples. The carousel was loaded onto a sample changer which allowed one sample to drop into phosphoric acid at 90 degrees celsius every 20 minutes. Following dissolution, a series of valves allowed the evolved CO2 gas to pass, via a nitrogen cooled water trap, into the evacuated mass spectrometer system where the isotopes of carbon and oxygen were measured.

ii) Results

Of the 20 samples taken from the 24/9-5 and 6 well cores in the Lower Eocene, 8 samples were analysed for C13 PDB and O18 SMOW isotopes, as only these samples had sufficient amounts of carbonate cement for analysis. The areas of cementation in the core did not appear to relate to lithology boundaries and occurred as either more cemented areas or as small fractures.

The results of the analysis are plotted on the core description sheets, as a series of graphical plots (figure 3.25 and 3.26) and are tabulated below (table 3):

Table 3

Well 24/9-5

Sample	Depth (metres)	C13 PDB(O/oo)	O18 SMOW(O/oo)
0179	2010.3m	-2.04	+20.2
0185	2010.8m	-5.96	+21.29
0181	2013.4m	-32.97	+21.96
0182	2019.6m	+3.39	+19.17
0183	2032.2m	-17.22	+21.45
0186	2033.2m	-1.32	+20.84

Well 24/9-6

Sample	Depth (metres)	C13 PDB(O/oo)	O18 SMOW(O/oo)
0188	2031.1m	+14.34	+20.82
0191	2034.9m	-17.87	+21.08

(iii) Interpretation - Carbon 13 PDB

The wide range of Carbon 13 PDB (+15 to -33 O/oo) are characteristic of ferroan calcite cements (Mozley and Burns, 1993). Differentiated mixing between bicarbonate, derived from oxidation/sulphate reduction and methanogenic fermentation, is the most likely cause of wide ranging carbon isotope ratios within studied ferroan calcite cements (Watson *et al.*, 1995). High positive C13 PDB values in ferroan calcites suggest that methanogenic fermentation processes probably acted to cause C13 PDB of bicarbonate within pore waters to increase with increasing burial depth, as the sediment column passes through the zones of dominant bacterial oxidation/sulphate reduction and burial fermentation (Irwin *et al.*, 1977). In contrast, the more negative values of the ferroan calcite cement may have formed due to the microbial oxidation of hydrocarbons (Watson *et al.* 1995). Carbonates derived from the chemical oxidation or bacterial conversion of hydrocarbons/organic matter typically have C13 PDB values more negative than –25 0/oo PDB (Russell *et al.* 1967; Donovan 1974; Donovan et.al. 1974; Gould and Smith 1978; Roberts *et al.* 1989). C13 PDB values for Viking Graben oils range from -27.5 to -31 O/oo PDB (Cornford 1990) and secondary biogenic carbonate material having low C13 could be expected to result from microbial oxidation of Viking Graben crude oil (Gould and Smith 1978).

Irwin *et al.* (1977) suggest that bicarbonate activities sufficient to reach carbonate supersaturation are unlikely in the zone of near surface bacterial

oxidation because of upward diffusion of bicarbonate into the depositional waters. However bacterial reactions and carbonate supersaturation can occur at depth in the meteoric aquifers especially when oil is present (Connan, 1984). The association of pyrite can suggest that sulphate reduction was also contributing bicarbonate to these cements (Watson *et al.*, 1995). Sulphate reducing bacteria cannot utilise petroleum products directly, but other organisms associated with oxidation of hydrocarbons can convert oil into suitable materials from metabolism by sulphate reducers (Krouse 1977). Oxidation of methane, derived from deeper in the sediment column, yields extremely isotopically light bicarbonate with C13 PDB values of -30 to -60 0/oo (Hathaway and Dyers 1969; Raiswell 1987) may also be from an isotopically negative bicarbonate source. Less negative values than C13 PDB of <-25 0/oo may indicate contributions of isotopically heavier carbon released during methanogenic fermentation. Abiotic thermal decarboxylation can produce carbonates with C13 PDB values of approximately -15 0/oo (Watson *et al.*, 1995), though the process generally occurs at extreme depths related to low grade metamorphism. Petrographic evidence (high "minus" cement porosity, point contact between grains and poikilotopic nature of cement) indicates a shallow depth of cementation, indicating this deep source to be unlikely.

The high levels of Fe indicate an excess of Fe available, which often occurs after sulphate reduction, implying cement formation after all marine water sulphur had been used up by initial microbial oxidation of this sulphur source (Coleman 1985). In addition a high ferroan cement indicates reducing conditions within the pore waters . This can be attributed to the progressive reduction in pore water oxygen levels by bacterial oxidation immediately upon deposition of the sediment and during progressive burial. A burial depth of between 100 to 1000 metres is suggested for similar cements by Watson *et al.* (1995) of Balder aged sands for the Forth Field in the North Viking Graben of the North Sea.

Watson *et al.* (1995) suggest a more complicated isotope history for calcite cements from the Forth Field. Meteoric flushing resulted in the precipitation of non ferroan carbonate cements with progressively more negative C13 PDB values. When meteoric flushing ceased, sulphate reducing bacteria continued to produce C13 PDB depleted bicarbonate and H2S which reacted with

available Fe to form authigenic pyrite when sufficient sulphate was available. After oxygen and sulphate where exhausted, methanogenic fermentation is interpreted to have continued forming poikilotopic ferroan calcite.

From the C13 isotope data range exhibited in the data presented in Table 2, it is concluded that a potential hydrocarbon source could have been the source of the poikilotopic ferroan calcite cement, from the petrographic evidence, cementation most probably occurred at a shallow depth of burial.

(iv.) Interpretation – O18 SMOW

Values of O18 SMOW vary between + 19.17 and + 21.96 O/oo within poikilotopic ferroan calcite cement and have a similar range to similar poikilotopic ferroan calcite cements within coeval Lower Eocene deepwater sands of the Forth field of UK North Sea Block 9/23 (Watson *et al.*, 1995). These values of O18 SMOW have been ascribed to an original marine pore fluid of – 1.2O/oo SMOW (Shackleton and Kennett, 1975) which has been subsequently buried and isotopically enriched in heavier O 18 during burial and reach a carbonate cementation temperature of 14 to 35 degrees celsius. Watson *et al.* (1995) assumed a a geothermal gradient of 2 degrees celsius per 100 metres and an Eocene palaeo seafloor temperature of 14 degrees. This places the depth of carbonate cementation to be less than 1000 metres burial. The carbonate cement values within the Balder age sands of 24/9 are 30 kilometres downdip to the east of the age equivalent Forth field deepwater sands. There seems no reason to suggest that these Balder sediments did not follow the same O18 SMOW isotope history, the pore fluid being derived from an Eocene marine pore fluid that was buried less than thousand metres before carbonate cementation.

3.5.2.3.6. Biostratigraphy of clay clasts

Within several of the massive sands (Sm) millimeter to centimetre scale dark grey clay clasts occur. It was considered possible that these could have originated from a stratigraphically deeper level, and were then transported upwards during remobilisation. In order to test this hypothesis, samples of these clay clasts, as listed below, were removed from the core in Norwegian North Sea

wells 24/9-5 and 6 and sent to the Robertson Group, Llandudno, Wales (Robertson 1998), for an analysis of the biostratigraphic origin of these samples, as listed below:

24/9-5

Two samples have been examined at 2015.4m (massive sand/Sm) and 2018.4m (massive sand/Sm). The samples have been processed both as bulk samples and selectively for mudstones. In the latter, mudstone lithologies have been picked from the bulk sample and processed separately. Both selectively picked mudstone samples were found to be barren. Bulk sampling of the ditch cutting at 2015.4m proved barren also, although the sample at 2018.4m yielded an impoverished assemblage with a pyritised diatom *Coscinodiscus sp.1* indicative of Zone MP(P)6 of 'lowermost' Eocene - 'uppermost' Paleocene age recorded. The poor recovery was probably the result of predominantly sandy lithologies.

24/9-6

Two samples have been examined at 2025.6m (intrusive sand/Si) and 2034.4m (massive sand/Sm). The samples have been processed selectively for mudstones. Processing of the mudstones at the base of the core 2025.6m produced poor microfaunas of an indeterminate age. The mudstone cored at 2034.4m yielded an abundant and diverse assemblage of pyritised diatoms. This assemblage is indicative of subzone MP(P)6A of late Paleocene age.

Samples indicate difficulty in defining exact ages due to the small amount and poor quality of microfossils. Age dates that have been given by the Robertson Group suggest a late Palaeocene age of the mud clasts, indicating them to be coeval with the sediment they are contained within.

If the massive sands were intrusive in nature, then the clay clast biostratigraphy indicates these sands were derived from coeval sediments. Intrusive sediments could have been laterally injected a small to large distance, but not vertically from older or younger than late Palaeocene sediments.

3.6 Discussion

A 3km by 5km high amplitude bedding parallel body within the Balder formation of Norwegian North Sea Block 24/9 has observed discordant high amplitude strata that originate from the side of this body. These high amplitudes cross cut the Balder Formation and continue discordantly upsection upto 300 msecs TWT into the Lower Eocene. Wireline and core calibration (well 24/9-5 and 24/9-6) indicates the amplitude body to be encased within the Balder Formation clays and to be formed of a mixture of a sequence of turbidite sands and shales with occasional small scale sandstone intrusions. These sands were constrained linearly E-W on deposition and were sourced from a shelf to the West.

Petrographically the cemented sands from the core are similar to those described by Watson *et al.* (1995) of the Lower Eocene deepwater sands of the Forth Field in UK North Sea block 9/23b - a poikilotopic ferroan calcite cemented sand with a high "minus cement" porosity exhibiting +20 0/oo O18 SMOW interpreted to relate to an original meteoric fluid. Dixon and Pearce (1995) suggest that the equivalent shelf edge sands to the west on the East Shetland Platform contain biodegraded oils and that within the Balder aged Forth field sands had hydrocarbons emplaced in the Paleocene to Early Eocene, the time of hydrocarbon maturation of the Upper Jurassic marine source rock over 24/9. The formation of high positive and negative C13 PDB values in the ferroan calcite cements can be ascribed partly in the negative value case to the breakdown of hydrocarbons at the time of cementation by microbial activity, whereas positive values can be attributed to methanogenic fermentation during burial. Petrographic information from high "minus cement" porosities constrains the depth of cementation to shallow, as partly corroborated by lack of fluid inclusions and the low levels of compaction in thin section of these sands. Watson *et al.* (1995) further note that the average +20 O18 O/oo SMOW be attributed to an originally meteoric pore fluid with original postulated –1.2 O18 O/oo SMOW. The temperature of formation of the final +20 O18 O/oo SMOW would have required a temperature of formation close to 14 to 35 degrees celsius equating to a depth of burial of no greater than 1000 metres. The relative depth of

formation of the ferroan calcite cement constrains the cement formation and puts a maximum relative depth of intrusion of the small scale intruded sands that these samples were taken from. The process of ferroan calcite cementation may have been coeval with intrusion, but also may have been later.

The potential migration of hydrocarbons at shallow burial into these Balder aged sands highlights the need for a migration route into these sands. Potential cross fault trends at the Upper Jurassic level in 24/9 may have been reactivated in Eocene times, thus acting as a migration route for generating hydrocarbons at this time to the northerly saddle area in 24/9. Watson *et al.* (1995), from their studies on the Lower Eocene Forth field and from Alexander *et al.* (1992) on the Forth field and *Dixon et al.* (1995) of the Gryphon and Forth field area suggest this migration process along faults to be related to seismic activity in the Eocene. This tectonic activity is ascribed to sea-floor spreading in the Norwegian Greenland Sea during Eocene times, causing periodic remobilisation of near surface/sea bed sediments. Post-Eocene migration may have been initiated by Alpine tectonic movement (Le Pichon *et al.*, 1988) or continual opening of the Atlantic. Remobilisation and slumping of Balder aged reservoirs soon after burial is ascribed to this seismic activity by Dixon *et al.* (1995) and Alexander *et al.*, (1992).

Migration of fluid/gas during the Eocene into the isolated turbidite sands of 24/9-5 and 6 is likely in this area as these sediments are located above a regional saddle in the Jurassic. Migrating fluids would have preferentially flowed into this structurally higher location (figure 3.36). Eocene fault activity may have diverted fluid flow up into the early Eocene Balder age deepwater sands. Since these deepwater sands were isolated within surrounding shales, any fluid increase within this body would subsequently have created a buildup of overpressure. This overpressure would then have been released during seismic activity as faults opened, injecting sand and overpressured fluid as small to large scale sand intrusions producing the intrusion complex (figure 3.37). Processes of clastic intrusion are discussed further in chapter 7.

3.7. Outcrop Intrusion Analogue : Giant scale (kilometre) Upper Miocene sandstone intrusions of Yellow Bank Creek, Santa Cruz County, California, USA. (Molyneux, 1999; Thompson 1995, 1996 and 1999)

3.7.1 Aims

This outcrop location is one of only two (the other Harms, 1965) documented field examples of kilometre-scale sandstone intrusions in the world. Field descriptions are partly taken from Thompson 1995, 1996 and Thompson *et al.* (1999) with original work by the author analysing the delta C13 PDB isotopic composition of the cements within the outcrop to understand the fluid source of the cement and possibly that of the intruding fluid. A comparison of the intrusive geometries and cement analysis of the Californian intrusion, to that of the Lower Eocene age Balder age intrusion complex in Norwegian North Sea Block 24/9 was intended to outline any common features and/or processes between the two large scale intrusions.

3.7.2. Location and geological setting

This large scale sandstone intrusion is located 5 miles southwest along the coast from Santa Cruz, California, which is itself located 70 miles south of San Francisco (figure 3.38). The locality, known as Yellow Bank Creek or Panther Beach, is along the northwestern edge of the exhumed Majors oil field (figure 3.38). The Majors oil field lies on the crest of a basement high that is the core of a gentle plunging anticline. Here oil probably has been sourced in rocks underlying the Upper Miocene Santa Margarita Sandstone (figure 3.39) and has migrated updip into the coarser-grained, cross-bedded facies of this formation (Philips, 1990). Sandstone intrusions derived from the Santa Margarita Sandstone, including hydrocarbon saturated bodies have intruded the overlying Upper Miocene Santa Cruz Mudstone (Erickson *et al.*, 1994; Thompson, 1995).

Sandstone intrusions in the Santa Cruz Mudstone include sills and dikes, with the latter typically being steeply dipping and oriented northwest (Phillips, 1990; Erikson et.al., 1994; Thompson, 1995). The intrusion at Yellow Bank

Creek is the largest of the local intrusions, being at least 300m in width, extending at least twice that distance inland, and no more than 550m offshore (Thompson, 1995). Thompson (1995) showed that the intrusion consists of at least two parts that merge into a single body in an offshore direction (figure 3.40). This intrusion is arguably the largest subaerially exposed sandstone intrusion in the world and may be an analogue for large bodies of remobilised sand in the Tertiary of the North Sea.

3.7.3 Description of Yellow Bank Creek intrusion

The intrusive nature of the Yellow Bank Creek intrusion has long been recognized (Newson, 1903). A cross section of the intrusion (figure 3.41) indicates the discordant bedding relationships of the intrusion and the internal features that exist. Another significant intrusion exists 500m along the coast SE of the Yellow Bank intrusion and is important to note as it is formed of a 8m thick sandstone sill which passes into a 20 metre wide sandstone dyke (figure 3.42). Off the main intrusion at Yellow Bank Creek, three lithologic features exist within the internal structure of the intrusion:

(1) Hydrocarbon-bearing masses: Darker, commonly gray masses cut across and locally parallel the limonite stained banding (see below). The darker sandstones have the appearance of bubbles and pipes (figures 3.43) which often contain what appear to be flow texture (figure 3.44). The dark sandstones have tar residues and are cemented by dolomite (Thompson, 1995).

The hydrocarbon bearing masses appear to be analogous to the buoyant rise of light material in response to density instability. At the "bubbles" locality (figure 3.43) the hydrocarbon-bearing masses clearly cross cut the limonite stained banding, indicating the oil migrated and replaced pre-existing fluids, after the limonite stained banding began to develop. At the southeast flank of the intrusion the hydrocarbon-bearing pipes or sand masses may directly intrude previously emplaced water saturated sands (Thompson, 1995). Below is a review of petrographic work completed by the author on 6 samples of the dolomitically cemented sand from Yellow Bank Creek intruded sands. For methodology of petrographic and isotope data, refer to 3.5.2.3

(i) Petrography

Samples in thin section (figures 3.45) are not stained (colourless) when Alizarin Red S and Potassium ferrocyanide was applied, indicating the cement present to be a ferroan dolomite. This ferroan dolomite cement is formed of 0.1mm equant, interlocking, pore occluding crystals forming 30 to 40 percent of the field of view. The sample is formed of a fine to medium grained quartz (80 to 90% predominantly monocrystalline, occasionally polycrystalline) with 5-10% moderately altered lithic fragments and 5-10% moderately altered microcline and orthoclase feldspar (subarkosic/sublith arenite; Pettijohn, 1975). Grains are moderately sorted, subangular to subrounded, with moderate sphericity.

Mineralogically these sands are moderately mature, with a source area from an igneous/metamorphic terrain and/or reworked sedimentary source. Texturally these sands are moderately mature. No fluid inclusions were observed in the dolomite cement.

(ii) Cathodoluminescence

Samples in CL show multiple zoned ferroan dolomite cemented crystals (figure 3.46). Zones vary from dull to bright yellow fluorescence, repeated several times throughout any one crystal. Commonly the dolomite cement is dull in the centre and lighter to the edge of each crystal. Explanations of these observations will follow in subsequent sections.

(iii) SEM - Energy dispersive X ray analysis (micro probe analysis)

Whole screen mapping of the dolomite cement measured MnO, MgO and FeO. Below in Table 4 are the range of these values in weight percent of oxide.

Table 4

Sample	MgO%	MnO%	FeO%
YB2 1	10.372	.048	.017
YB2 2	10.138	.012	.012
YB2 3	9.900	.071	.566
YB2 4	9.900	.008	.390
YB2 5	9.971	.019	.351
YB3 1	10.212	.014	.031
YB3 2	10.394	.055	.021

YB3 3	9.856	.025	.658
YB3 4	7.543	.093	1.834

This mapping indicates yellow fluorescing areas of dolomite cement to have FeO levels below the reliable detectable limit of the machine (Giddins pers. comm. 1999) with the dark/dull fluorescing parts of the dolomite cement having FeO weight percent of between 0.35 and 1.834 weight percent. MnO and MgO levels do not vary which indicates that the increased FeO levels are the suppressor of fluorescence in the sample (Walker, 1985). Additionally original observations from carbonate staining indicating a wholly ferroan dolomite cement are incorrect and that the cement has an evolution from a non ferroan dolomite at the edge of each crystal to a progressively more ferroan dolomite towards the centre of the crystal, though each cement crystal may have numerous alternating fluorescing zones.

(iv) Isotopes - C13 PDB

Below in table 5 are the isotope data for 6 samples taken from dolomitically cemented sands of the Yellow Bank Creek intrusion. Analysis of the ferroan versus the non ferroan dolomite cement was not undertaken due to time and cost.

Table 5

	C13 PDB O/oo
YB1	3.14
YB2	0.63
YB3	7.20
YB4	7.99
YB5	-12.48
YB6	6.95

Values of C13 PDB have a range similar to that of ferroan calcite cements in Norwegian offshore block 24/9 in the Lower Eocene Balder injected/remobilised sand of this chapter and of the Forth field (Watson *et al.*, 1995). As in the block 24/9 case the wide negative to positive range of C13 is

ascribed in the negative case to breakdown of hydrocarbon/organic matter by microbial activity. Positive C13 PDB values are related to methanogenic fermentation/bacterial oxidation/sulphate reduction of pore waters during shallow burial.

(v.) Interpretation

Analysis of the cement indicates it to be a zoned, alternately of non ferroan and ferroan calcite. This indicates a variably reducing (ferroan) and non reducing conditions (non ferroan). High "minus" cement porosity could be attributed to early cementation of the intruded sands, soon after intrusion. Whether the dolomite cement is formed at the time of intrusion is difficult to confirm, though as noted the cement formed relatively soon after intrusion. Cementation was episodic as noted by the well defined cement zoning and alternated between reducing and non reducing conditions. The reducing component could be interpreted to be organic rich/hydrocarbon bearing pore fluids. Delta C13 PDB isotope composition of the ferroan and non ferroan dolomite together show a positive and negative range similar to that of the ferroan calcite cement in the Early Eocene Balder age sands of Norwegian North Sea Block 24/9. As in 24/9 (see section 3.5.2.3.5) this isotope range is interpreted to have been generated from a hydrocarbon/organic rich pore fluid.

(2) Limonite-stained banding: Iron-stained layering may be fluid flow banding or diagenetic weathering of the outcrop as Liesegang rings (Carl & Amstutz, 1958; Gibbons, 1978) (figure 3.44).

(3) Vertical granulation seams (figure 3.44): these less than 10 cm, near vertical, quartz seams exist within the outcrop, especially near the south east end of the intrusion where a faulted contact exist with the country rock. These seams are commonly related to fault activity, in the deepwater Tertiary sands of the North Sea case, and form due to postdepositional faulting of mounded sand sides (Dixon *et al.*, 1995) and are similar to features seen in the Norwegian 24/9-5 and 6 core (figure 3.33).

(4) Dish structures

These are millimetre to centimetre scale dewatering structures. Dish structures are formed during the process of water escape within a sand prone bed and appear as concave up shallow dish like features (Lowe and LoPiccolo, 1974; Lowe, 1975; and Allen, 1982), formed of clay (Hurst and Buller, 1984).

3.7.4. Interpretation

Thompson (1999) outlined a model for the formation of the intricate banding and intrusion as follows (figure 3.47):
Initially, water saturated sands intruded and developed flow banding. Shortly thereafter, hydrocarbons migrated in, cross cutting some of the early-formed banding in the water-saturated sands. Thus, the hydrocarbon front arrived in the later stages of emplacement of the entire intrusion. Hydrocarbon migration occurred both as a fluid replacement phenomena and as intrusions of hydrocarbon-bearing sand. Later oxidising aqueous fluids, perhaps even modern groundwater, superimposed the limonitic staining.

The timing and depth of the intrusion are only broadly constrained. The intrusion must have occurred after deposition and burial of the Santa Cruz Mudstone (i.e. post 7 Ma), but before the deposition of the terrace deposits which cap the cliffs (approx. 125 Ka; Anderson and Menking, 1994). Apatite fission track analysis carried out by Geotrack (Thompson 1995) on the intrusive sand and vitrinite reflectance of a sample from the intruded Santa Cruz Mudstone indicate that the temperatures of the intrusion and the intruded rocks never exceeded 50-60 degrees celsius. This would indicate the maximum depth of burial of these sediments and thus a maximum depth intrusion formation to be less than 1500 metres assumming a palaeo seafloor temperature of approximately 15 degrees and a geothermal gradient of 30 degrees celsius per 1000 metres.

Thompson (pers.comm. 1999) suggests that the intrusion began as a vertical dike along its southeastern faulted margin and expanded into sills to the northeast and northwest. Cause of injection is postulated to be related to fault activity along regional wrench faults (Thompson 1995) and related fluid expulsion along these faults at the time of hydrocarbon migration creating the

necessary fluid pressure to remobilise the sand volumes (Thompson pers. com. 1999 and see chapter 7 for a fuller explanation of the process). The influence of gas as a contributory factor to remobilise the volumes of sand involved is suggested (Thompson et.al., 1999). The relationship of maturation of the source rock for the hydrocarbons in the intrusion has not been documented and requires further work to constrain the relative timing and comparison geochemically to oils in the Yellow Bank Creek intrusion

3.8 Conclusion

Both the early Eocene Balder age intrusion complex in Norwegian North Sea Block 24/9 and the Upper Miocene intrusion of Santa Cruz, California are of large scale and extend areally over a kilometre. They are both related in some way to a migrating hydrocaron bearing fluid as noted from isotopic analyses of the cements within the intruded sands, but whether these cements were part of the intrusion process cannot definitively be established. Both intrusions formed at a maximum depth of 1000 meters or less of sediment overburden. Both intrusions are interpreted to be related to fault activity which emplaced large volumes of fluid into sand bodies to drive the intrepreted high pressure clastic intrusion process.

These two examples prove that large scale clastic intrusion can occur beyond the millimetre to centimeter scale documented most commonly in the literature. Chapter 4 describes another interpreted large scale sandstone intrusion complex from the Lower Eocene of UK North Sea Blocks 21/3, 4 and 5.

Figure 3.1. Location map of Norwegian offshore North Sea Block 24/9 (fault elements from PEGSB, 1997)

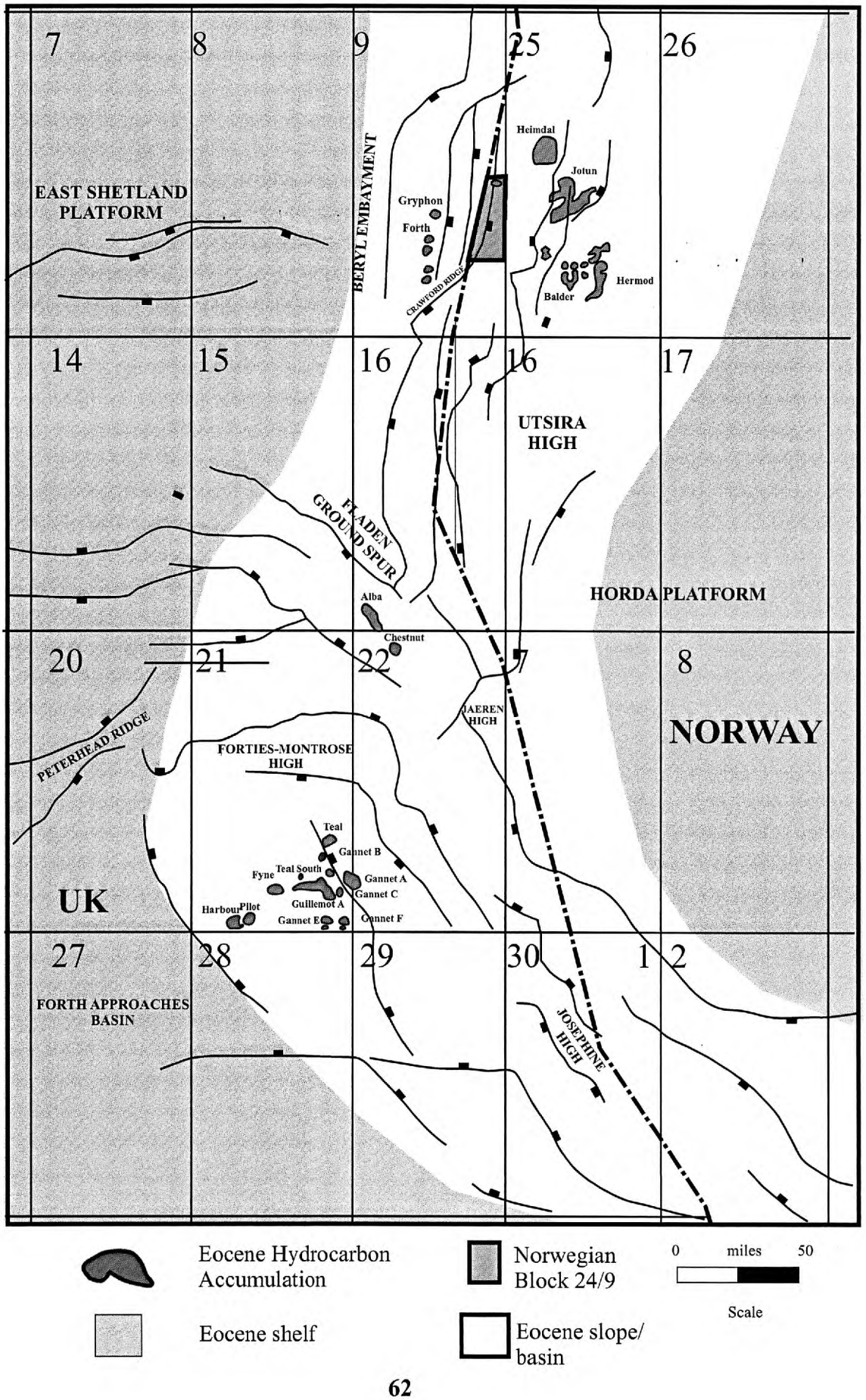


Figure 3.2. Geological cross section across the North Viking Graben through Norwegian North Sea Block 24/9 (from CNST82-09 regional seismic line)

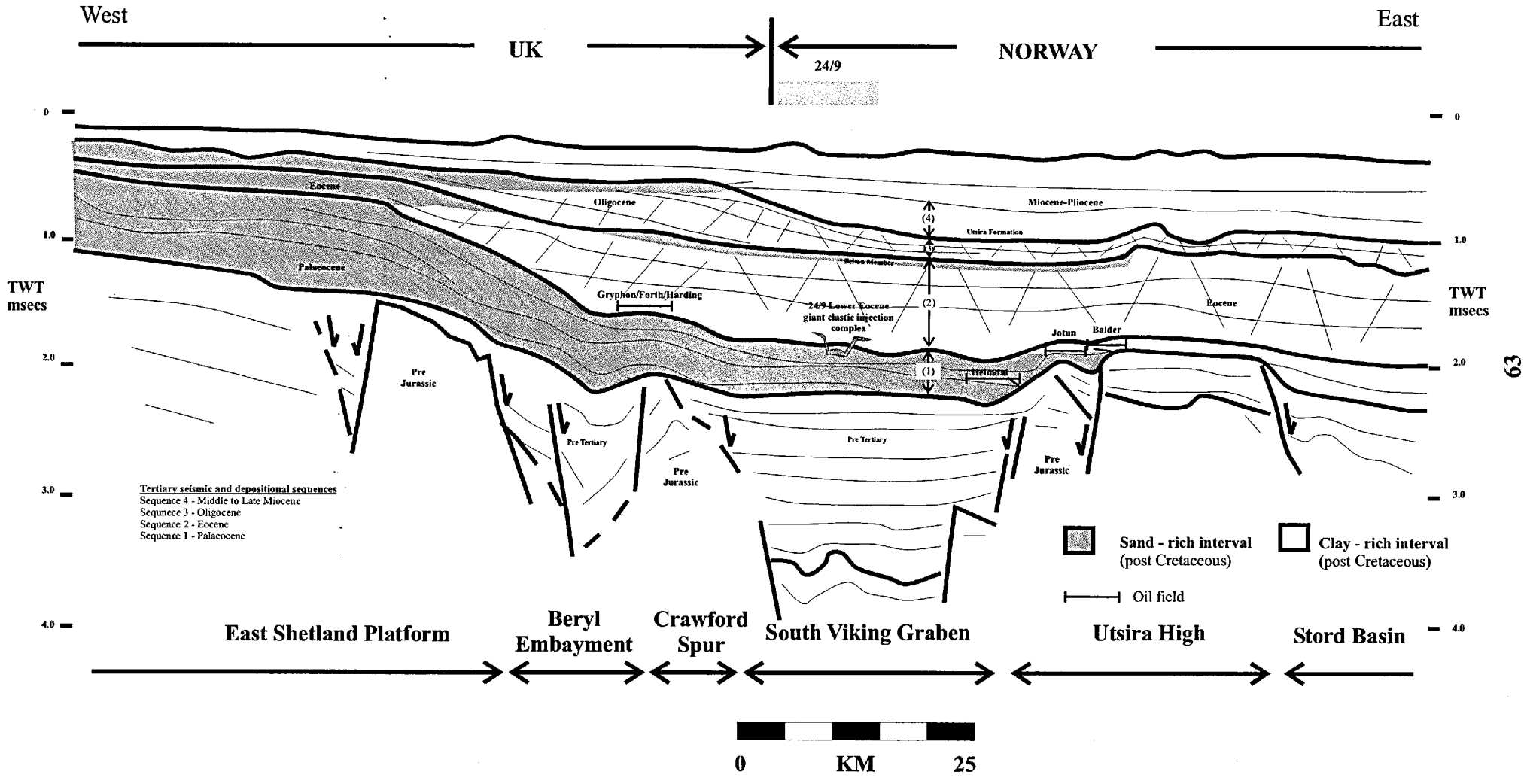


Figure 3.3. Elongate Tertiary sandstone bodies (Balder Formation equivalent (from Timbrell *et al.*, 1993)

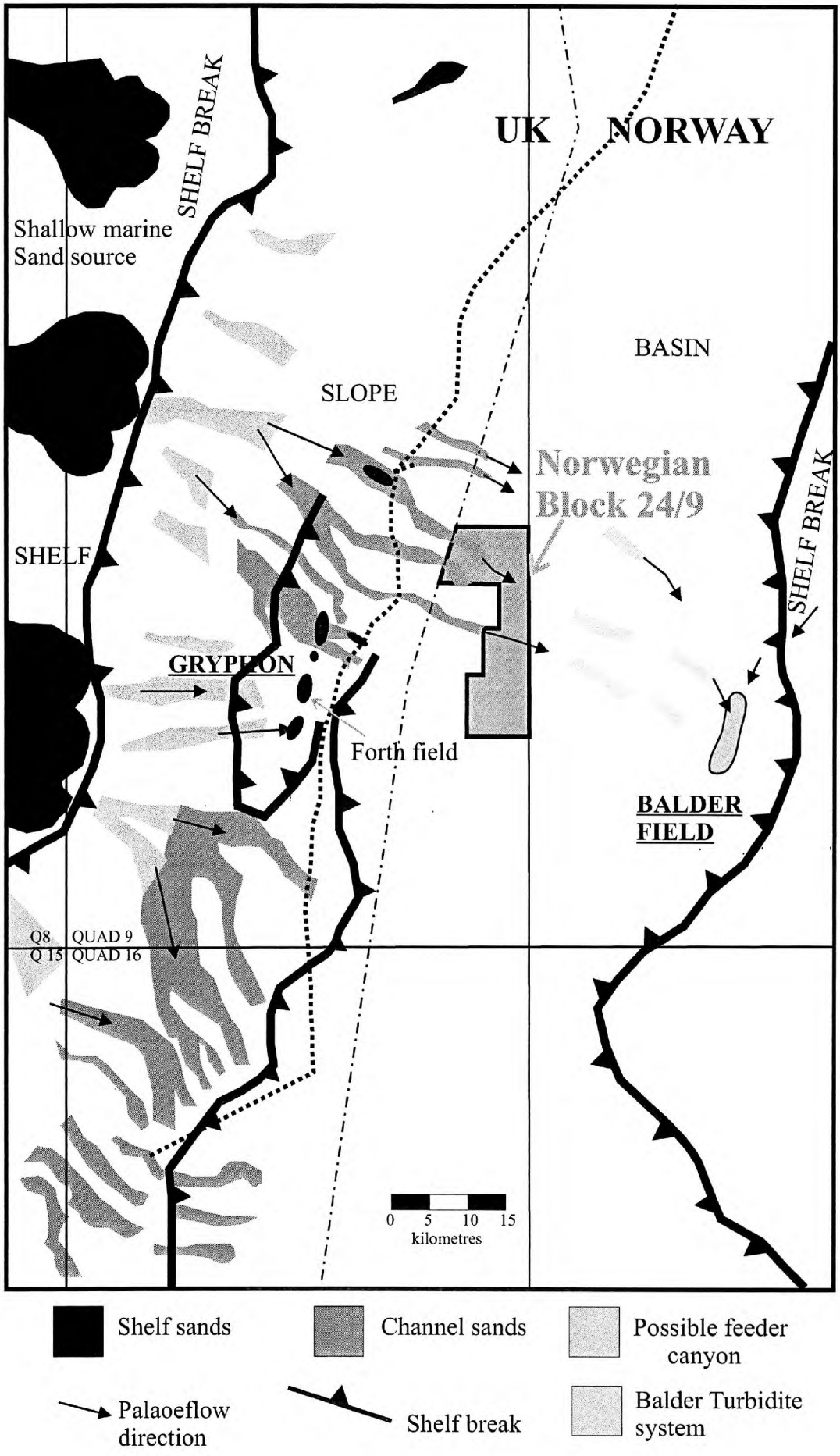


Figure 3.4. Balder palaeogeography map about the North Viking Graben (Michelson *et al.*, 1995)

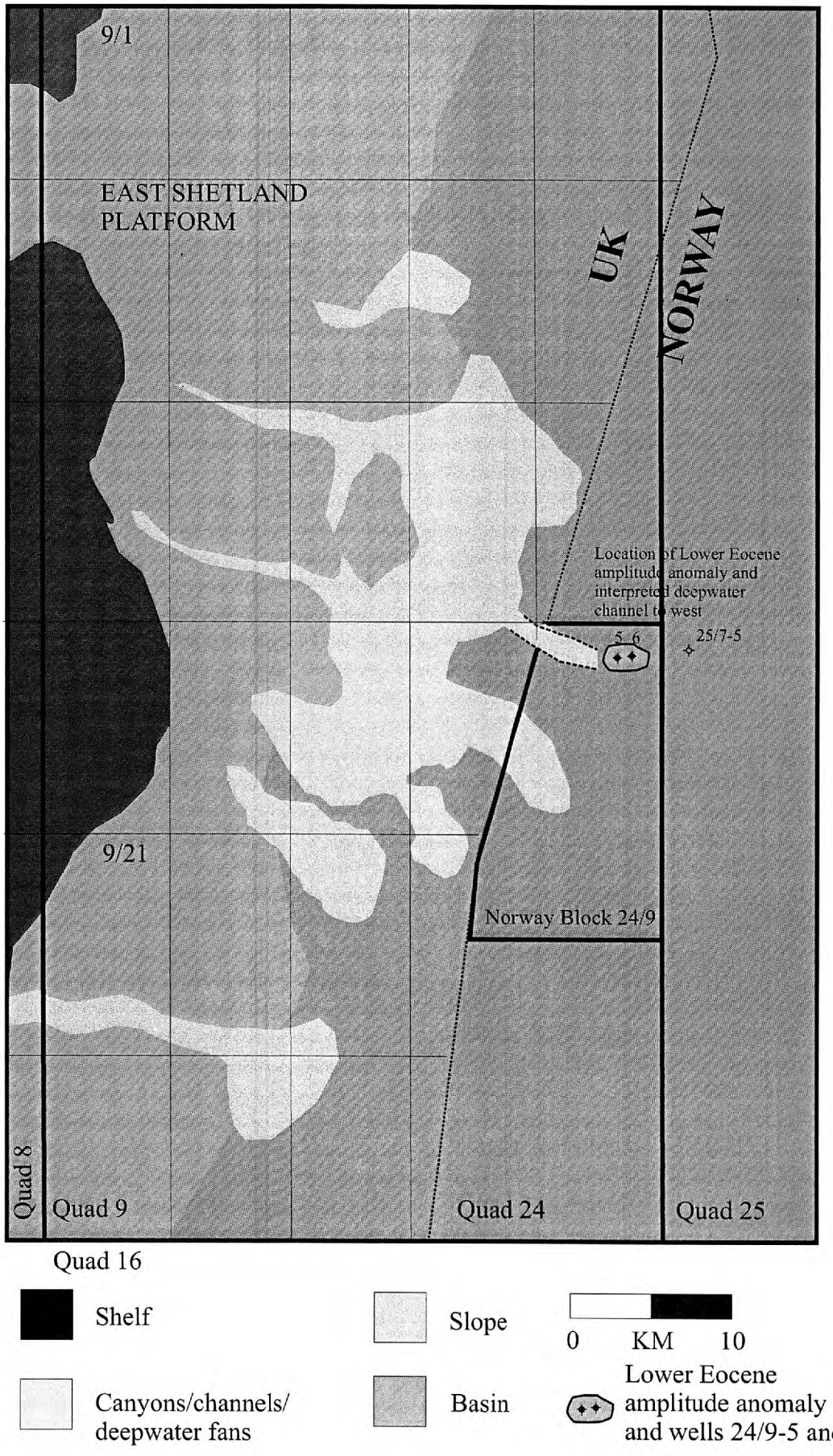


Figure 3.5. Straigraphy of the late Palaeocene to early Eocene of Norwegian North Sea Block 24/9 (redrawn from Knox and Holloway, 1992)

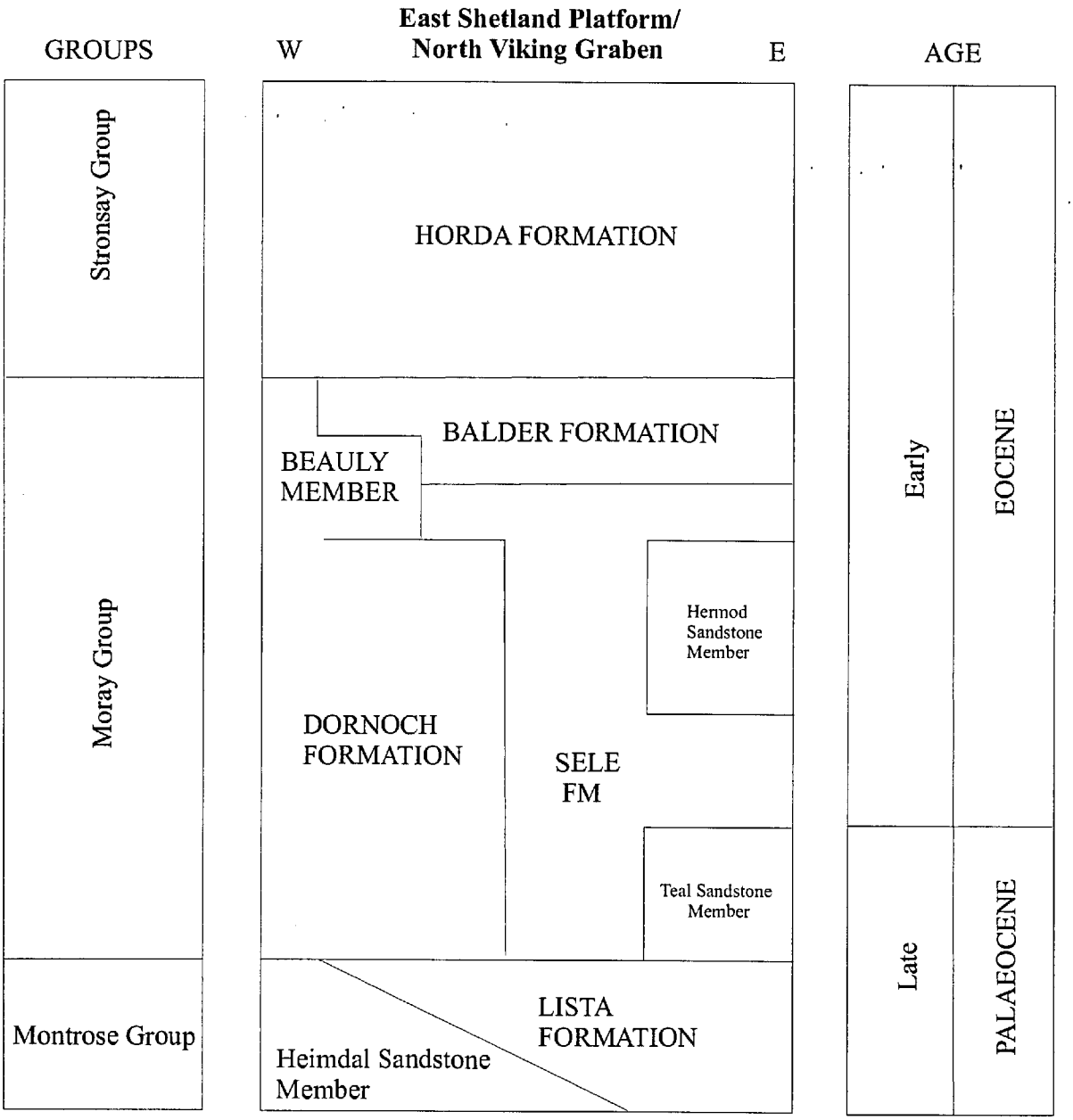


Figure 3.6. Intra-Jurassic two way time map (yellow)(Fina Norge, 1998) and Balder anomaly two way time map (red) over Norwegian offshore North Sea Block 24/9 (see figure 3.1 for scale). Intra Top Jurassic fault trends north/south and east/west, with the Balder anomaly above such a set of cross faults. The Balder anomaly is situated where the intra-Jurassic rises to the north, positioned above an intrabasinal high.

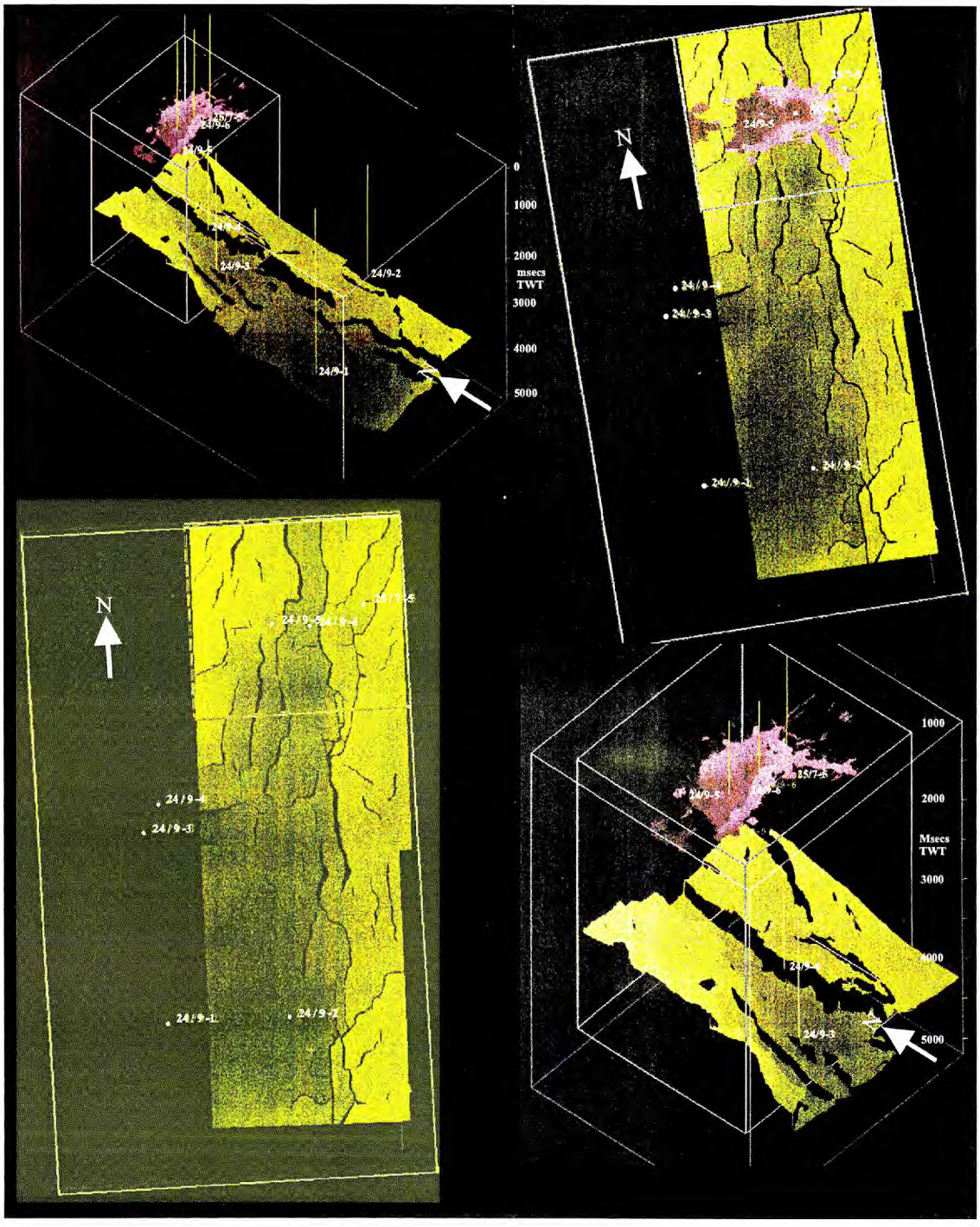


Figure 3.7. Norwegian North Sea Block 24/9 - Near Top Jurassic structure contour map

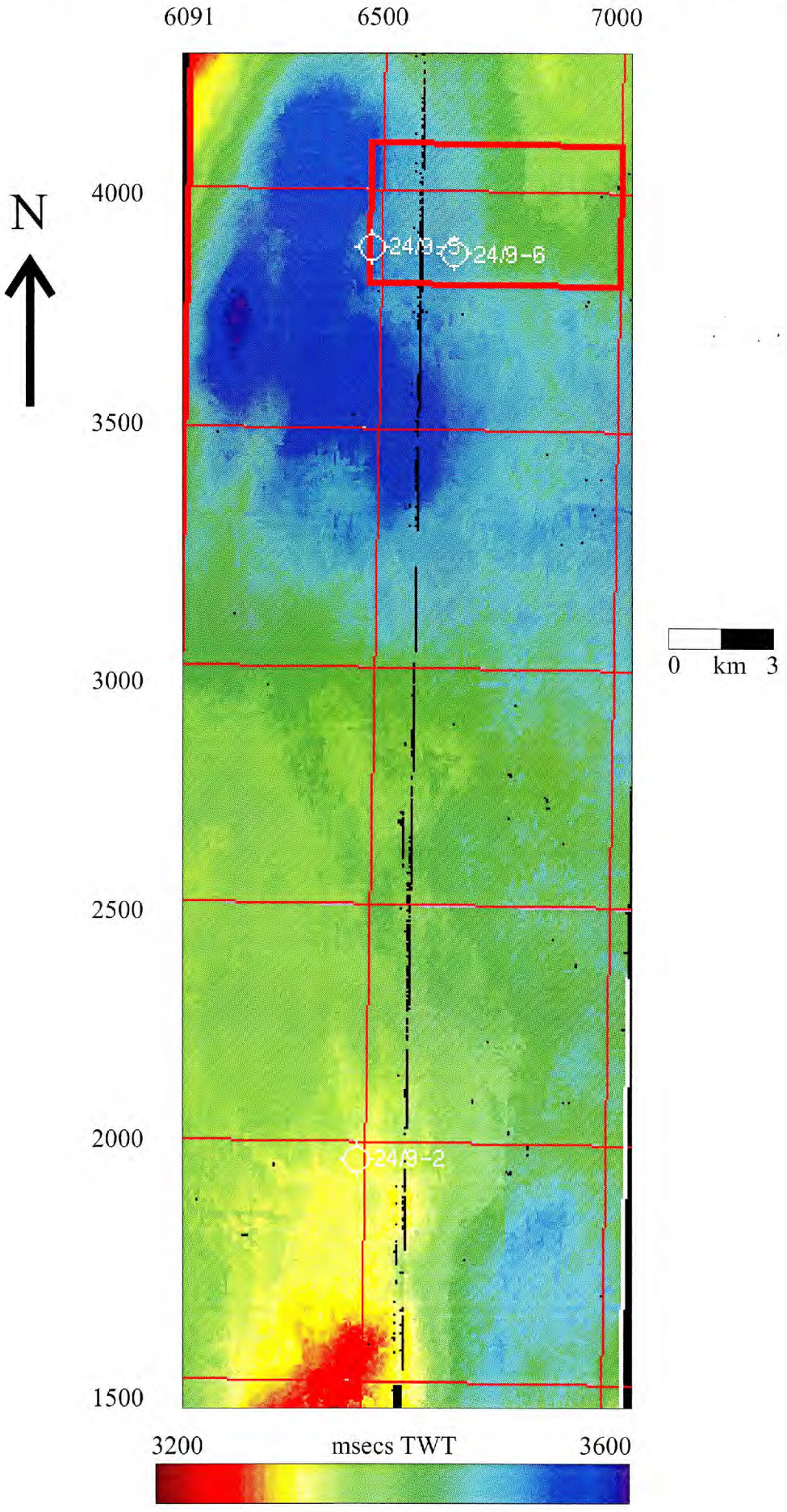


Figure 3.8. Norwegian North Sea Block 24/9 - Top Chalk structure contour map.

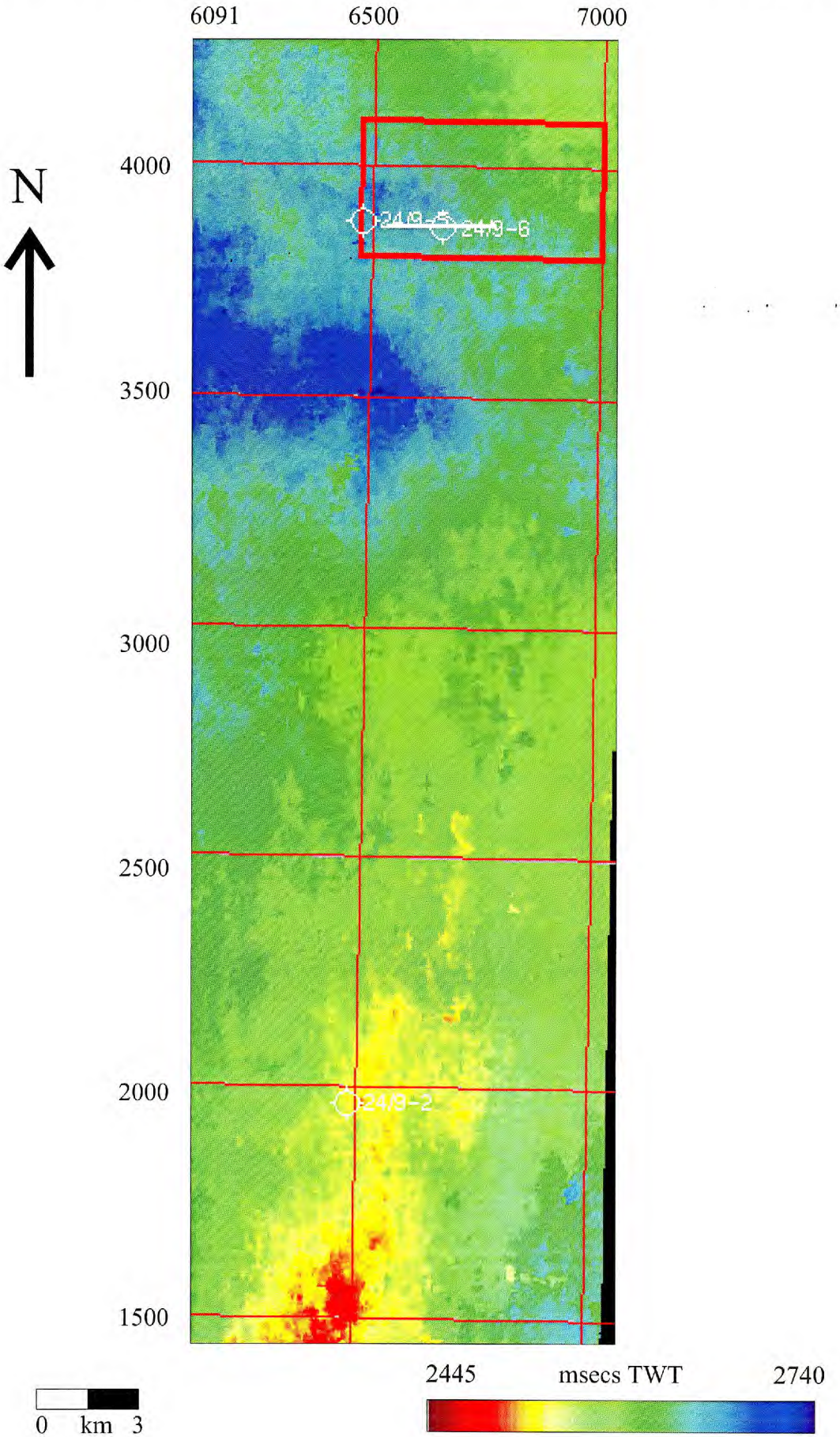


Figure 3.9. Top Balder two way time map and maximum amplitude map between Top Balder and Top Sele. Note location of high amplitude intra Balder anomaly about wells 24/9-5 and 6.

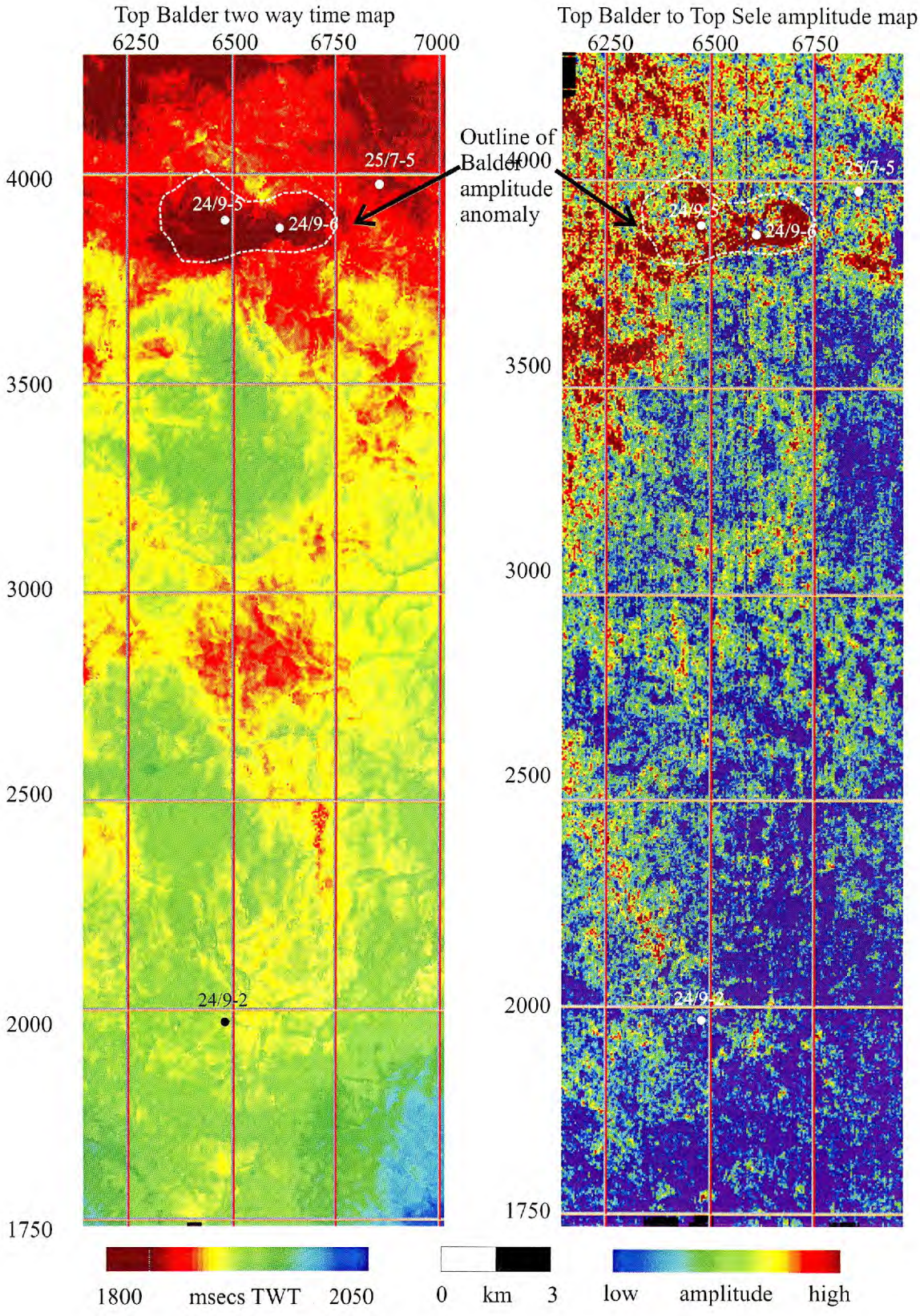


Figure 3.10. Norwegian North Sea Block 24/9 - Near top Jurassic to top Chalk time isochron

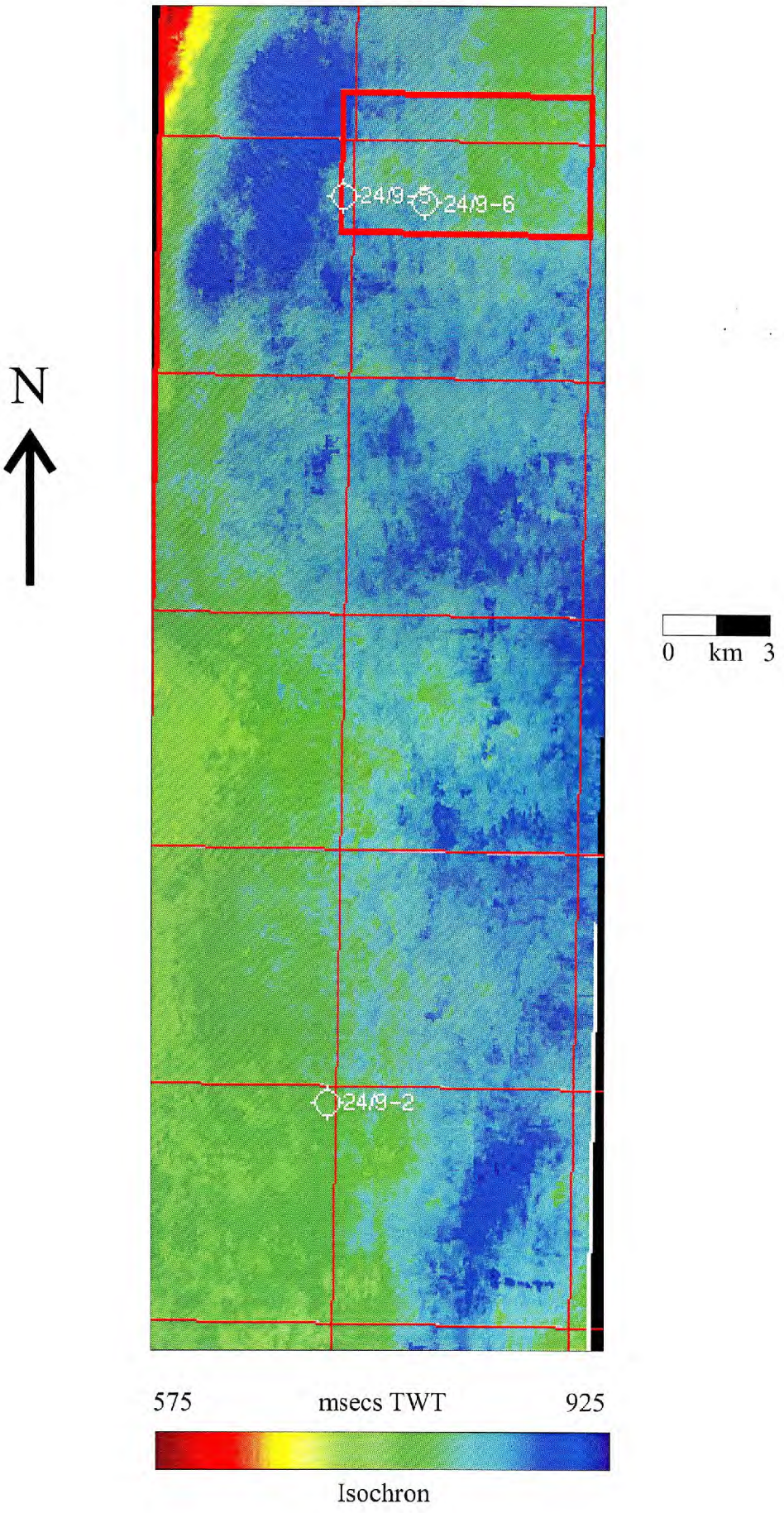


Figure 3.11. Norwegian North Sea Block 24/9 - Top Balder to Chalk isochron

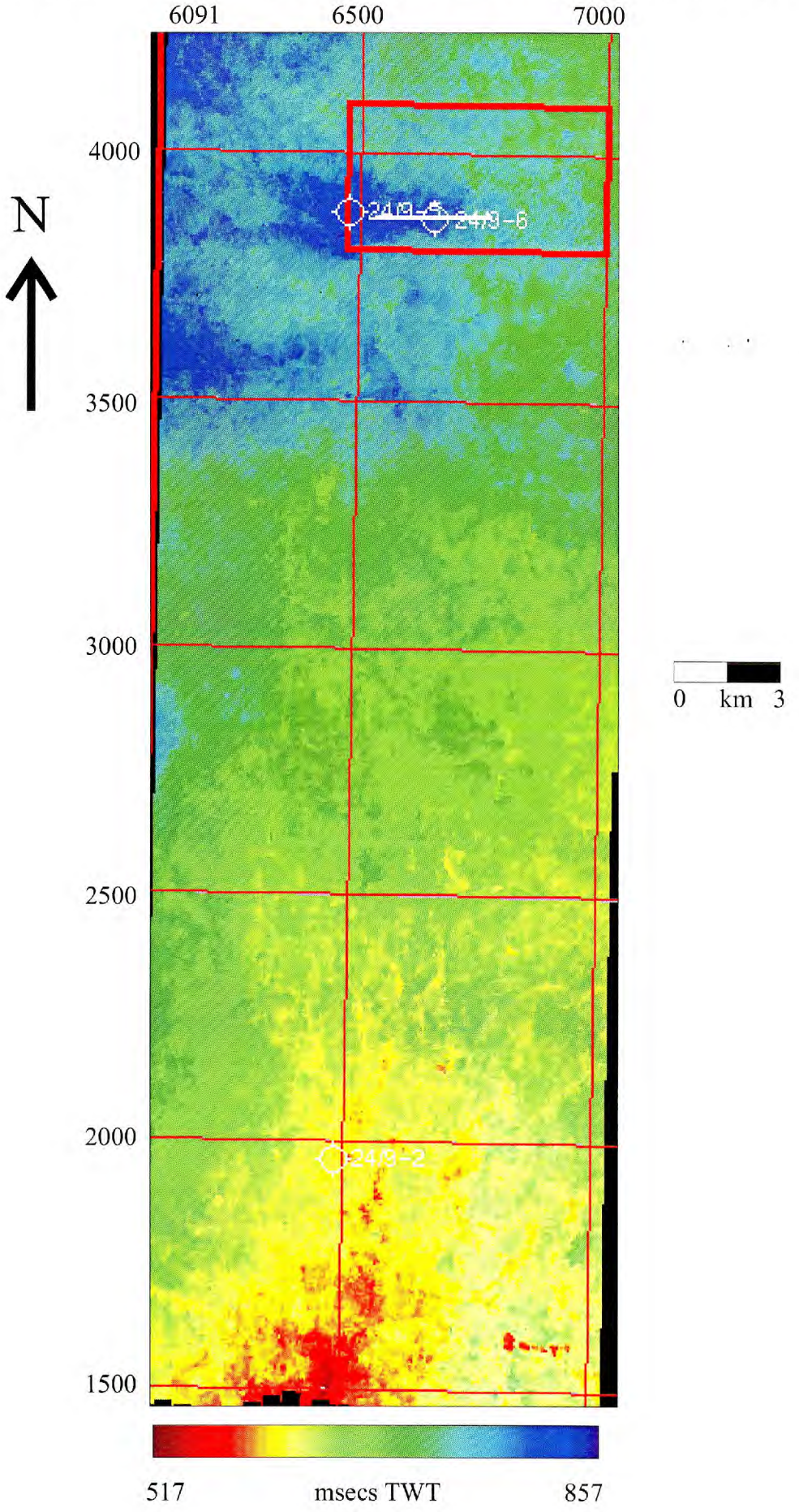


Figure 3.12. Regional seismic line through the Tertiary to Jurassic strata of Norwegian North Sea Block 24/9. Location of line see figure 3.36.

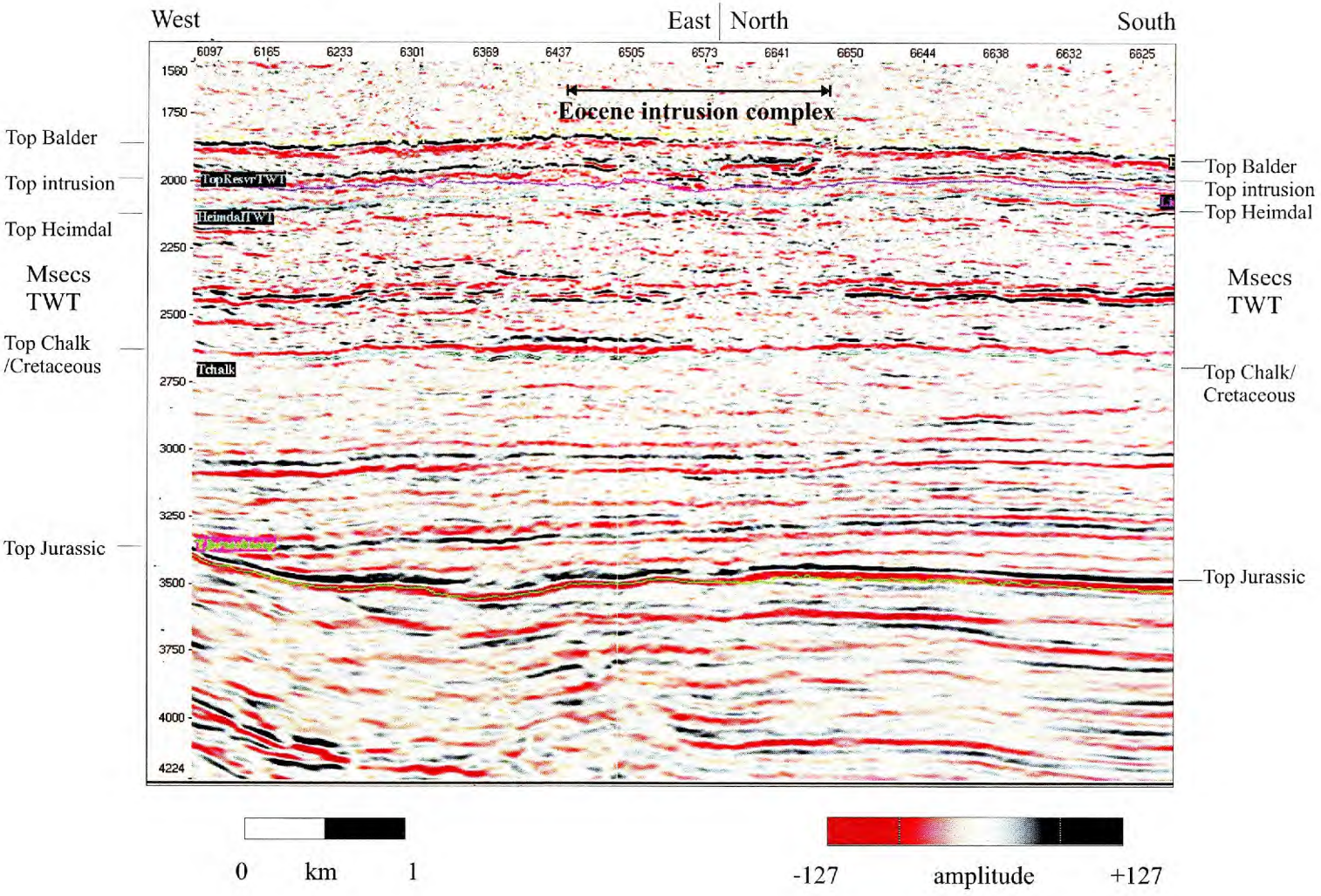


Figure 3.13. Top Balder reservoir two way time map of Balder Formation amplitude anomaly Norwegian offshore North Sea Block 24/9

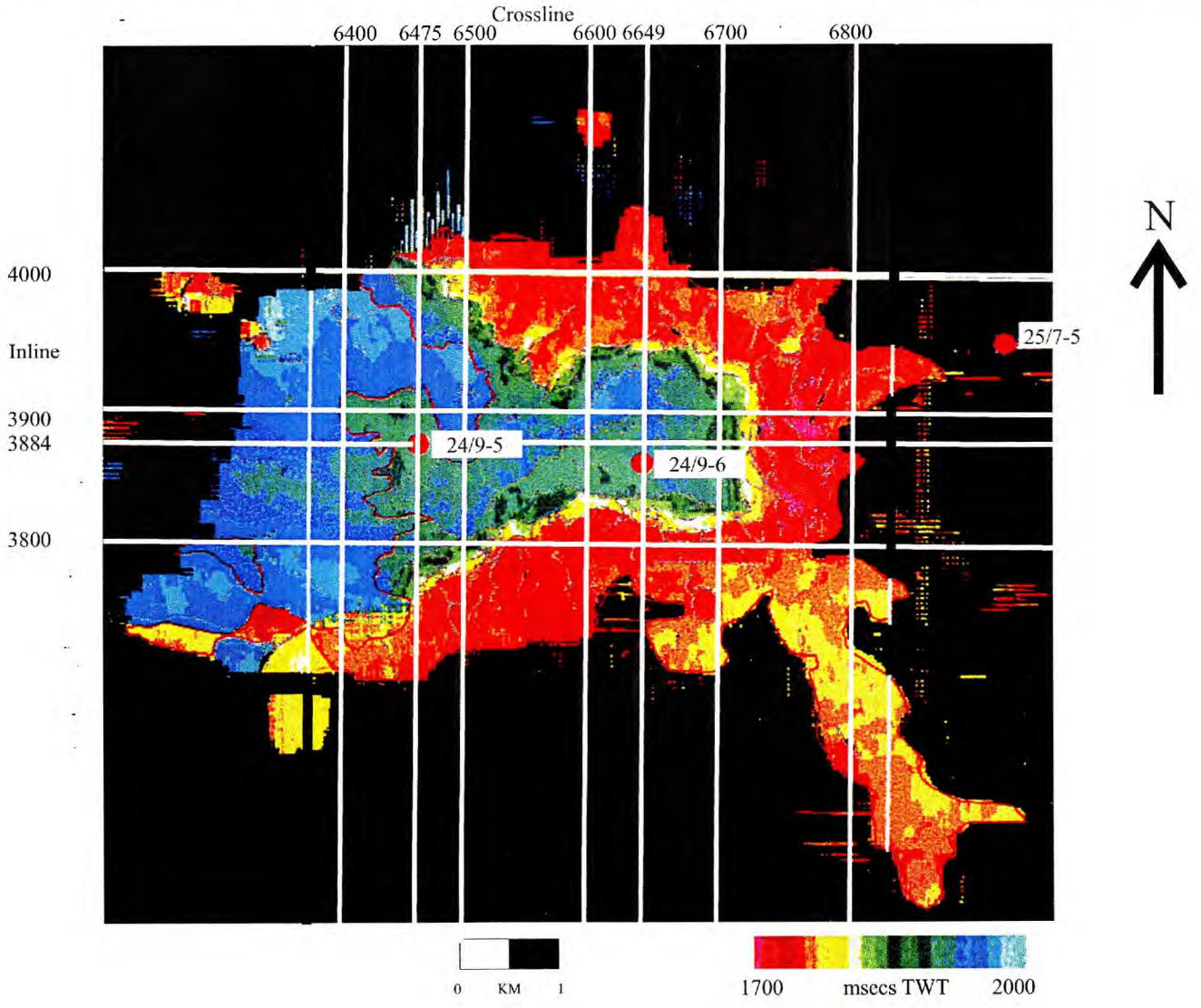


Figure 3.14. Norwegian North Sea Block 24/9 - Lower Eocene intrusion - crossline 3800

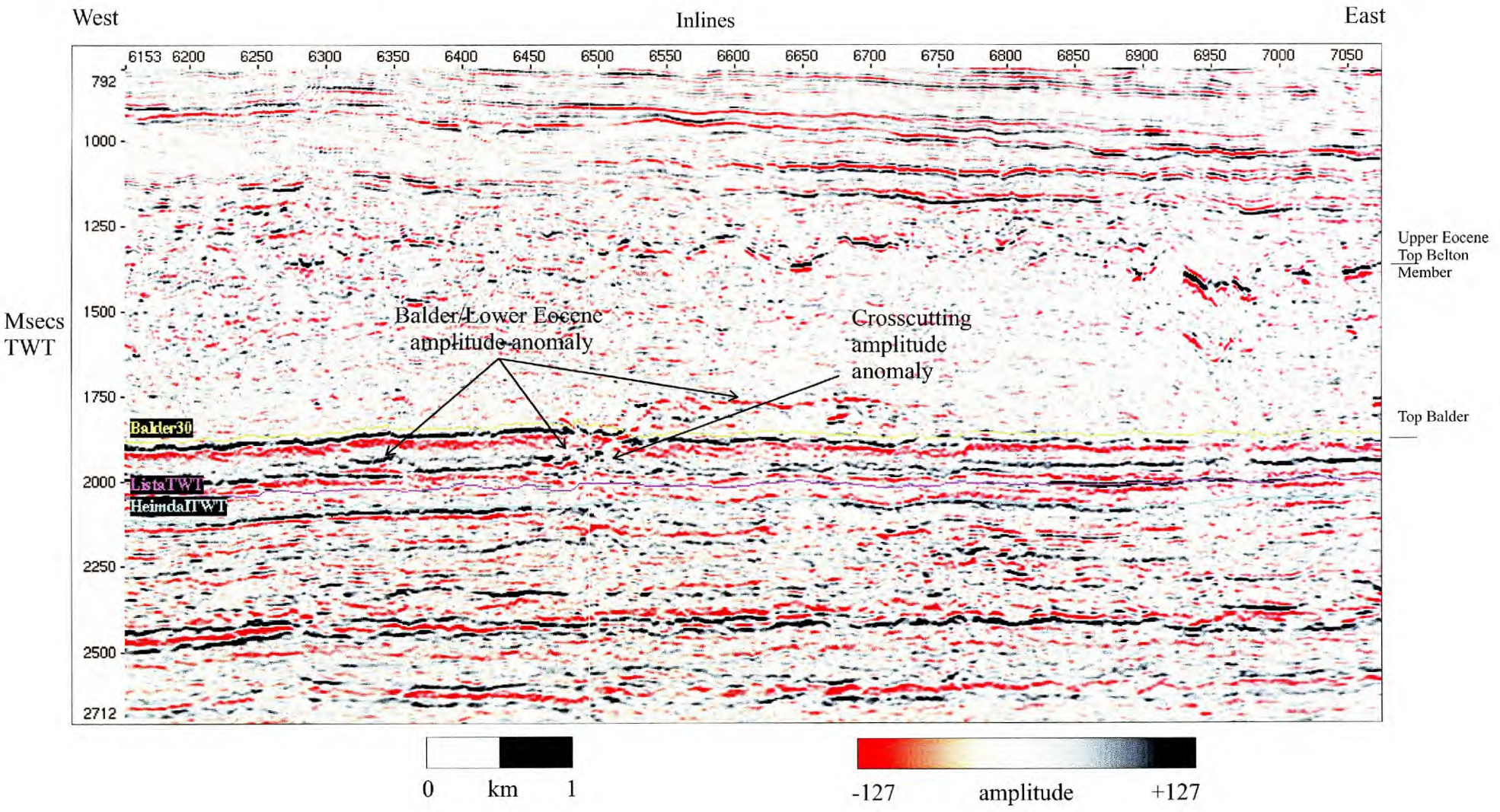


Figure 3.15. Norwegian North Sea Block 24/9 - Lower Eocene sandstone intrusion - crossline 3884

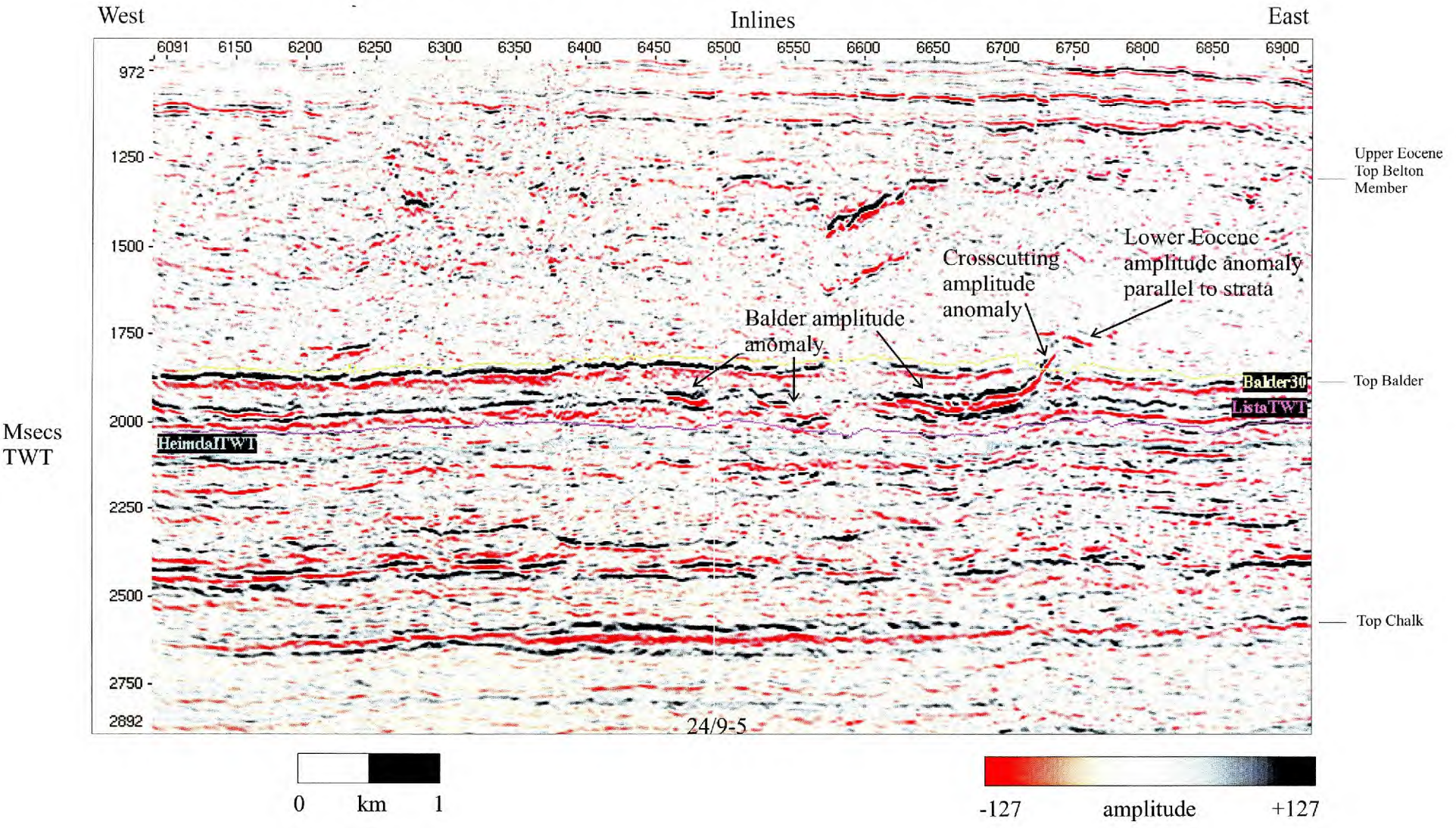


Figure 3.16. Norwegian North Sea Block 24/9 - Lower Eocene sandstone intrusion - crossline 3900

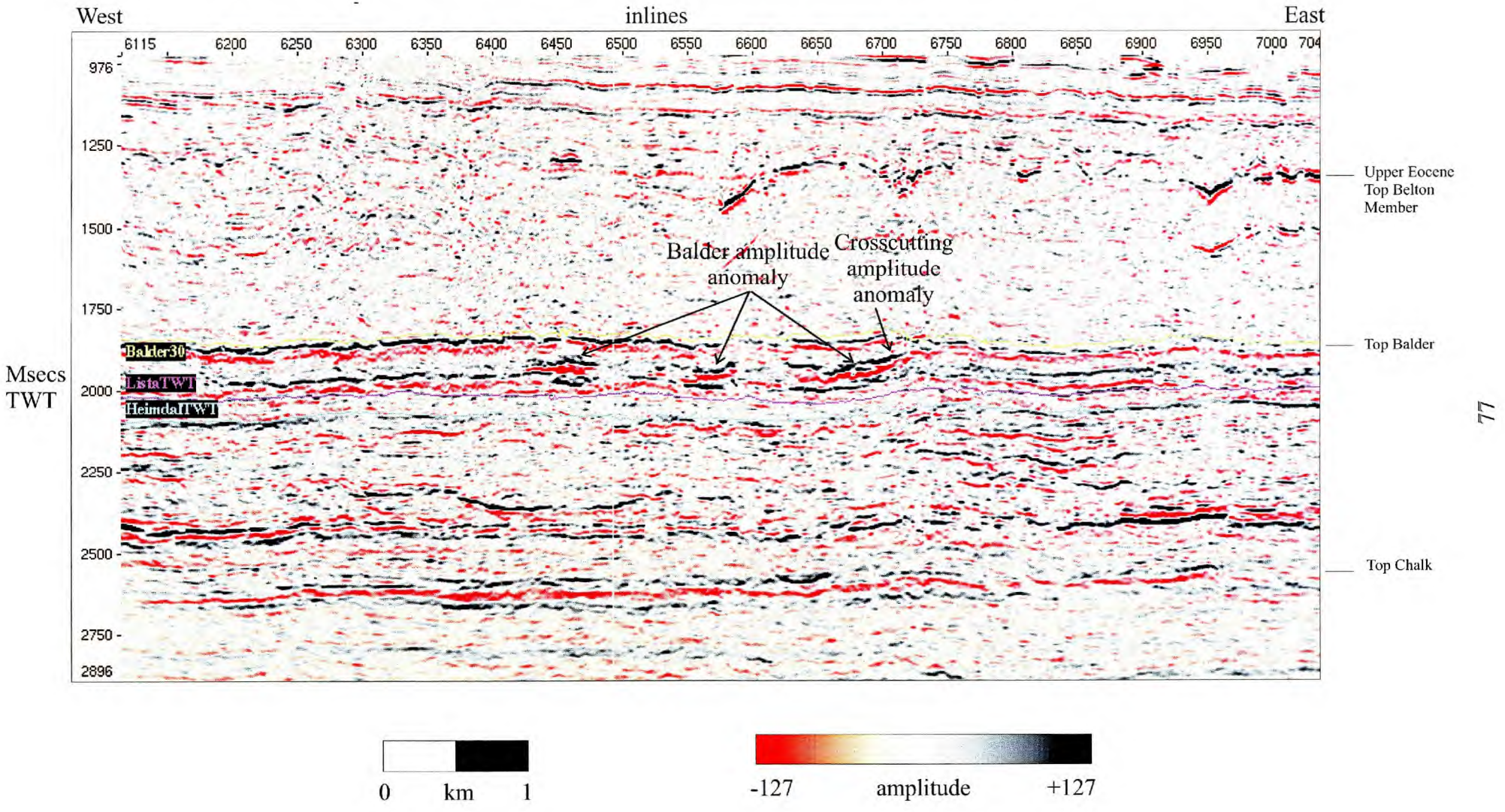


Figure 3.17. Norwegian North Sea Block 24/9 - Lower Eocene sandstone intrusion - crossline 4000

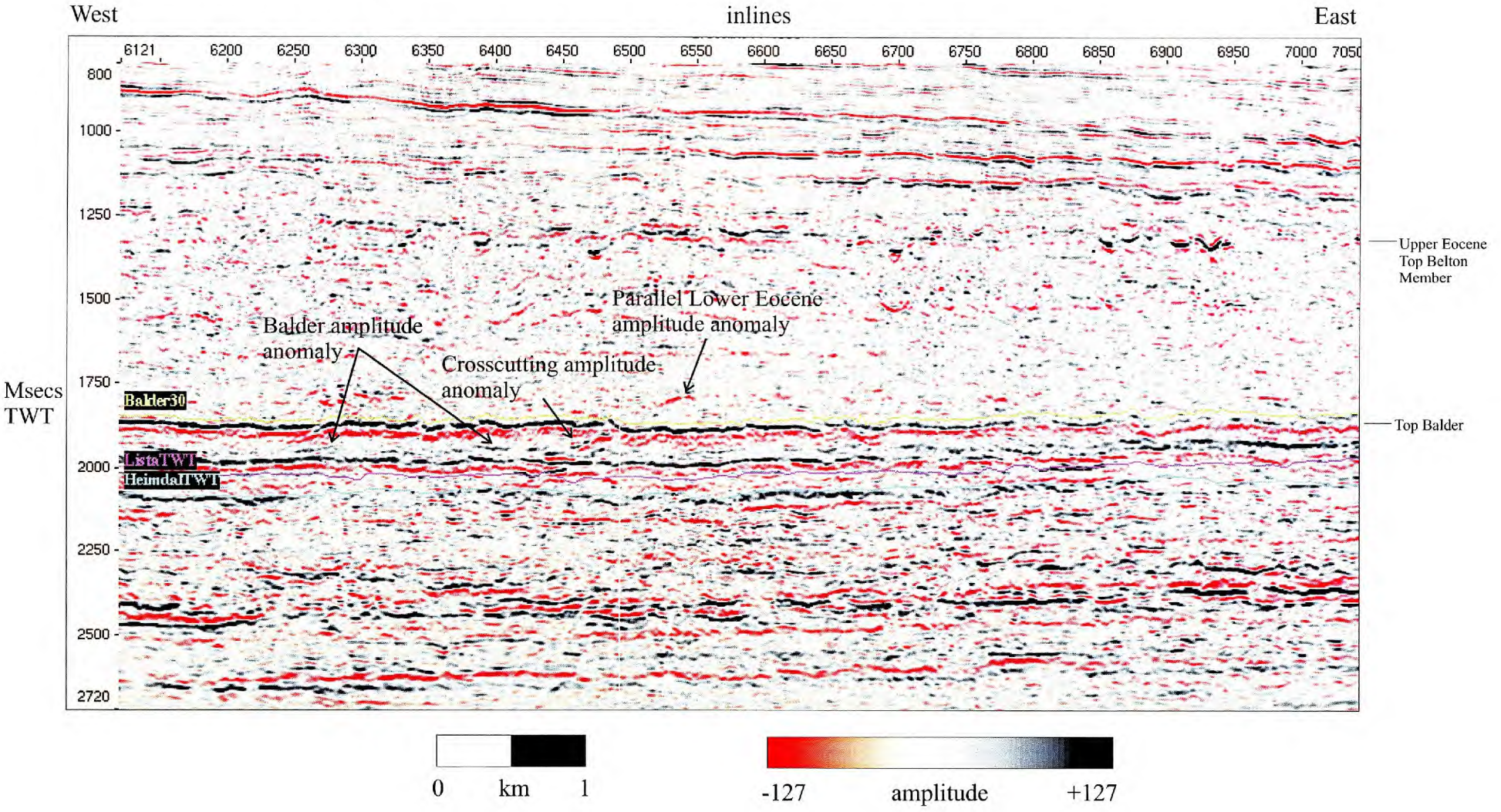


Figure 3.18. Norwegian North Sea Block 24/9 - Lower Eocene sandstone intrusion - inline 6475

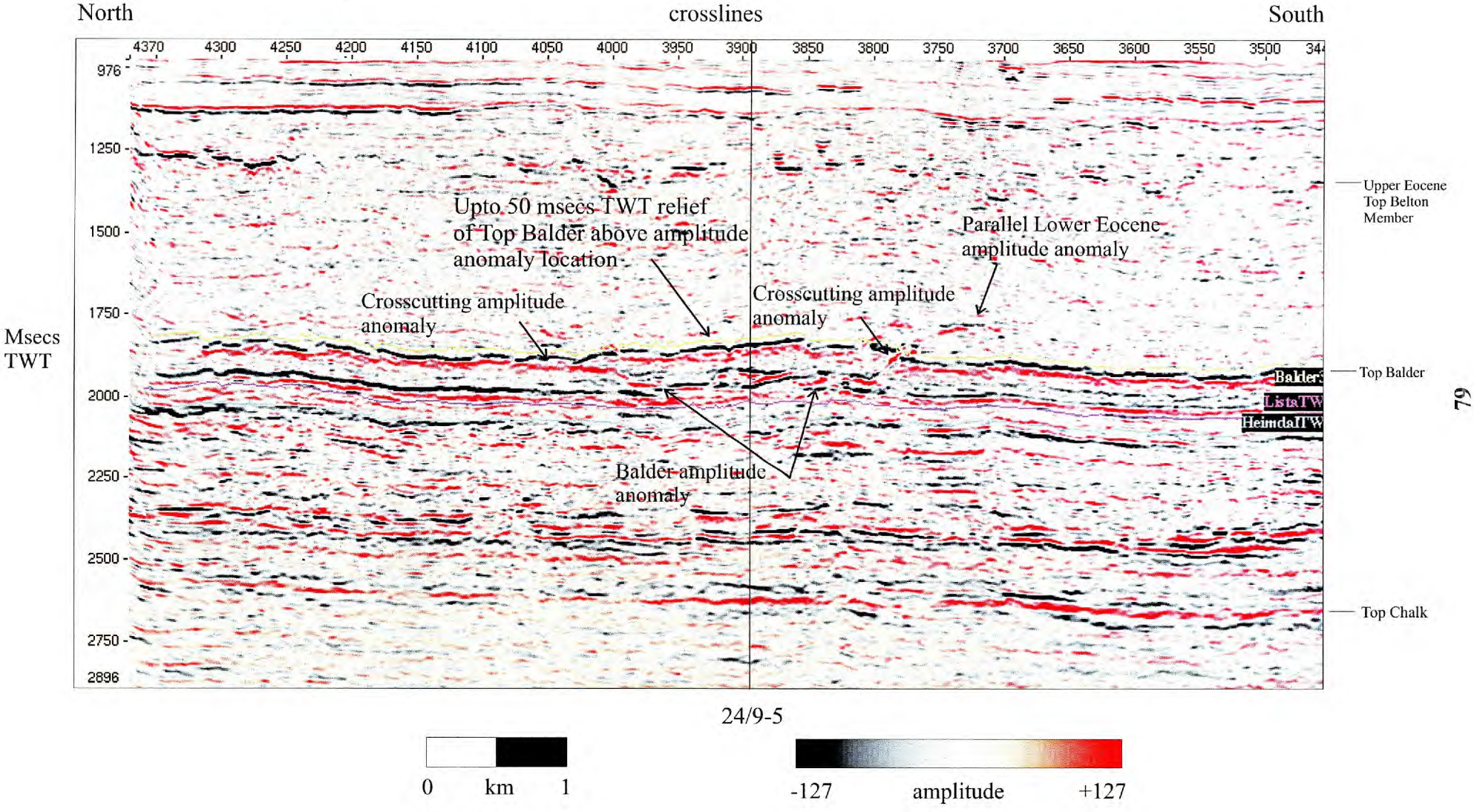


Figure 3.19. Norwegian North Sea Block 24/9 - Lower Eocene sandstone intrusion - inline 6600

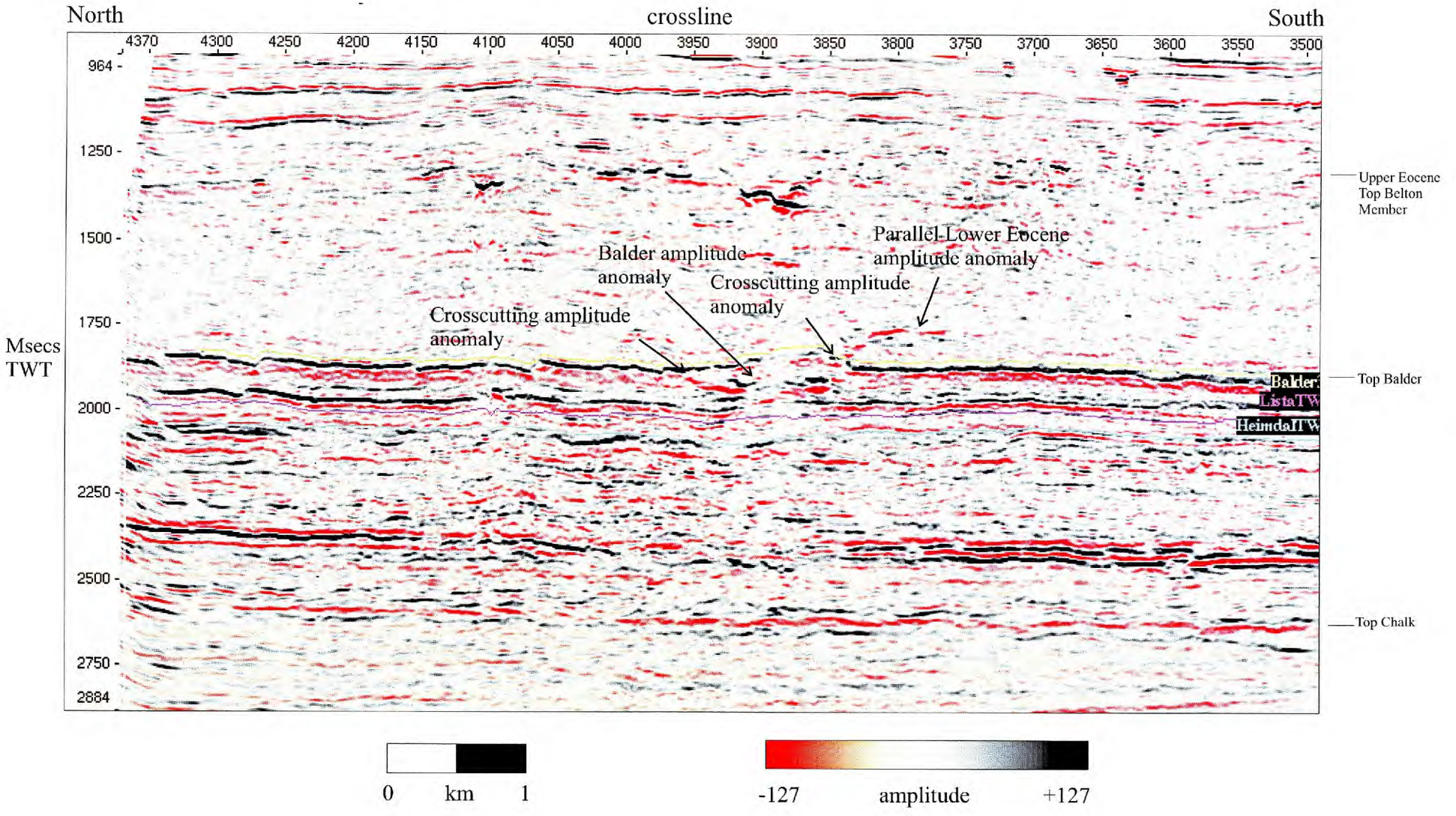


Figure 3.20. Norwegian North Sea Block 24/9 - Lower Eocene sandstone intrusion - inline 6649

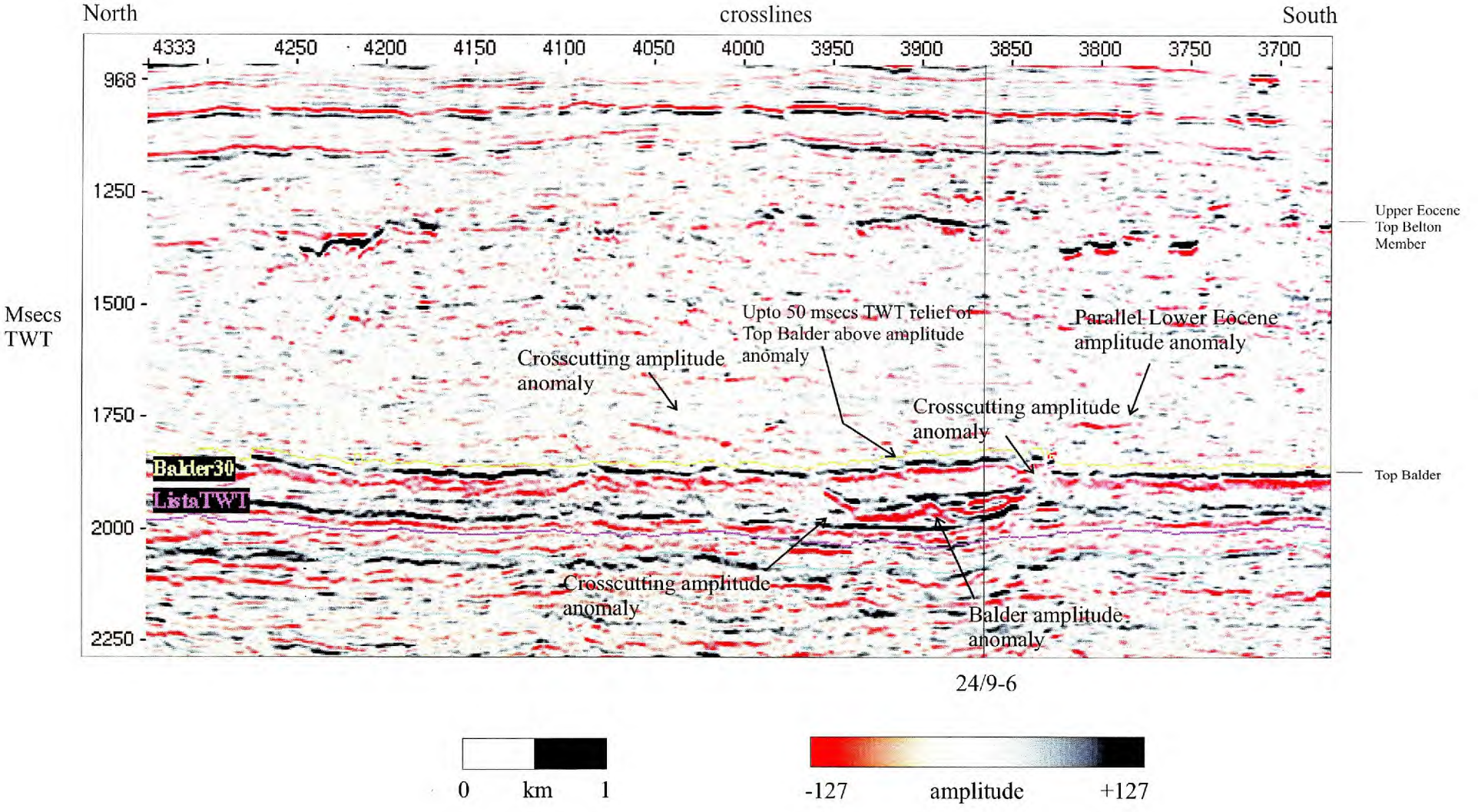


Figure 3.21. Norwegian North Sea Block 24/9 - Lower Eocene sandstone intrusion - inline 6700

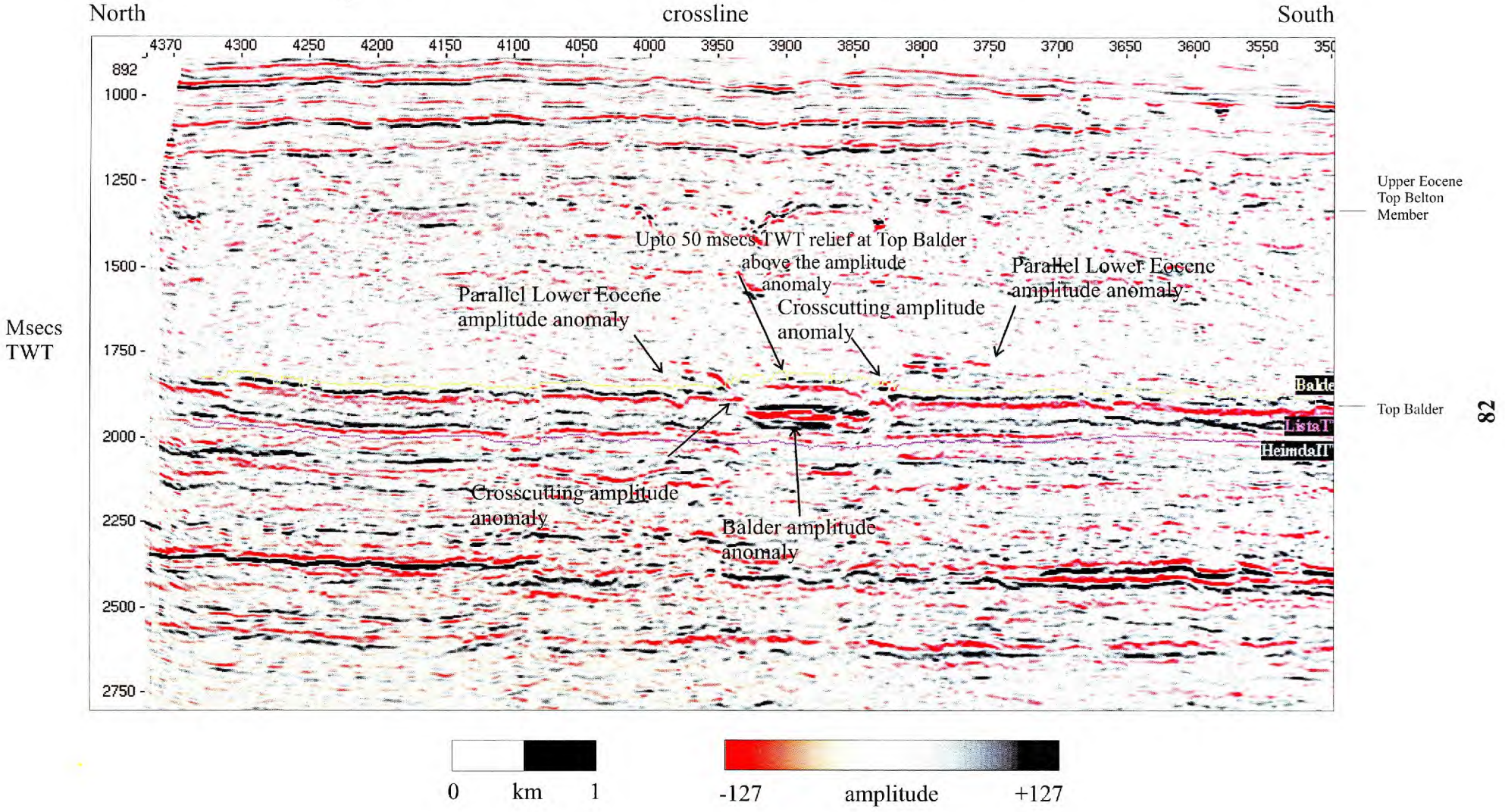


Figure 3.22. High amplitude east west oriented trend within the Balder interval - possible turbidite feeder channels, in Norwegian offshore North Sea Block 24/9 (partly after Fina, 1998)

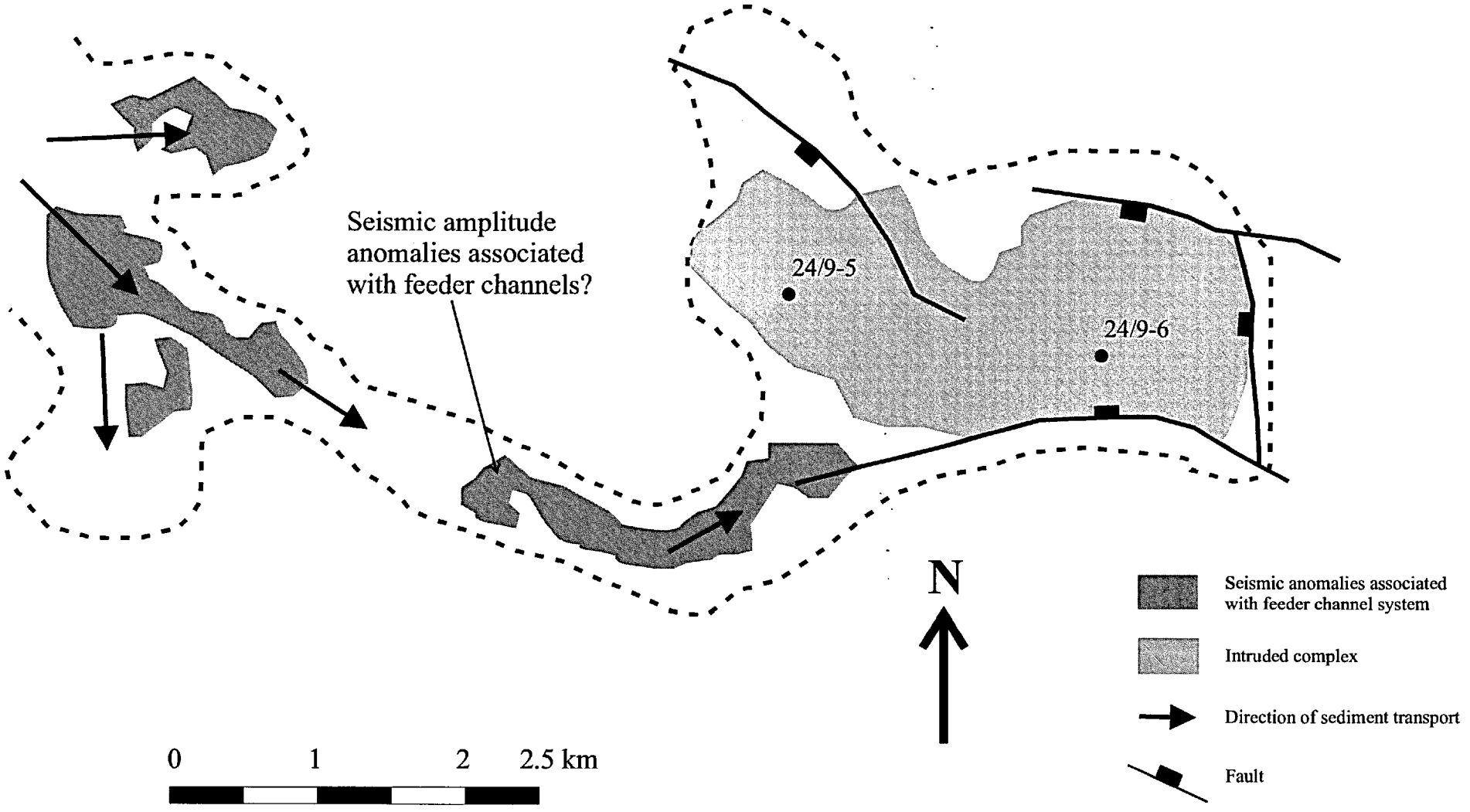


Figure 3.23. Correlation of the Upper Palaeocene and Eocene for wells 24/9-5, 24/9-6 and 25/7-5, offshore Norwegian North Sea (partly from Fina Norway Report, 1998)

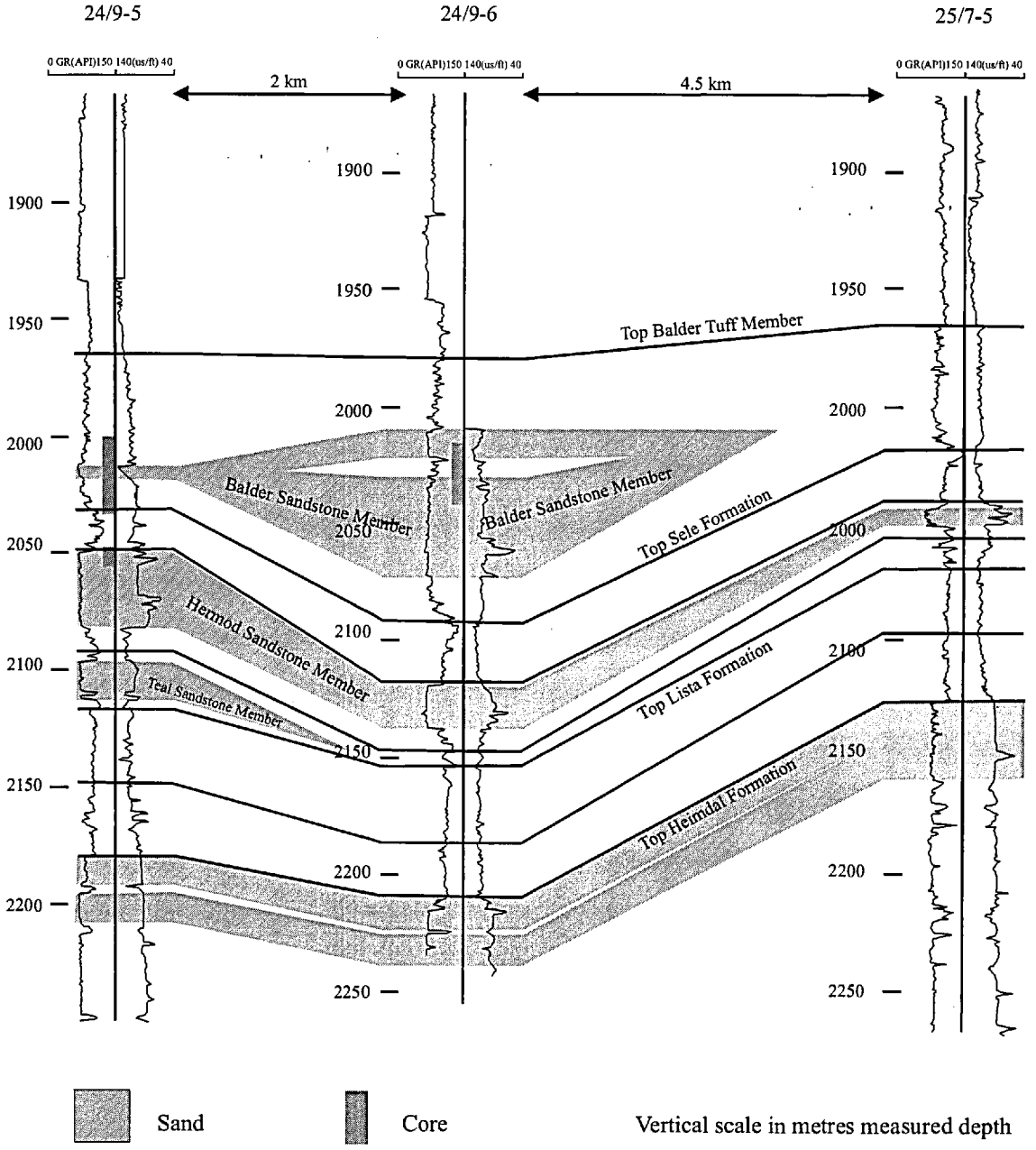


Figure 3.24. Geological cross section through Upper Palaeocene and Eocene for wells 24/9-5, 24/9-6 and 25/7-5, offshore Norwegian North Sea (partly from Fina Norway Report, 1998)

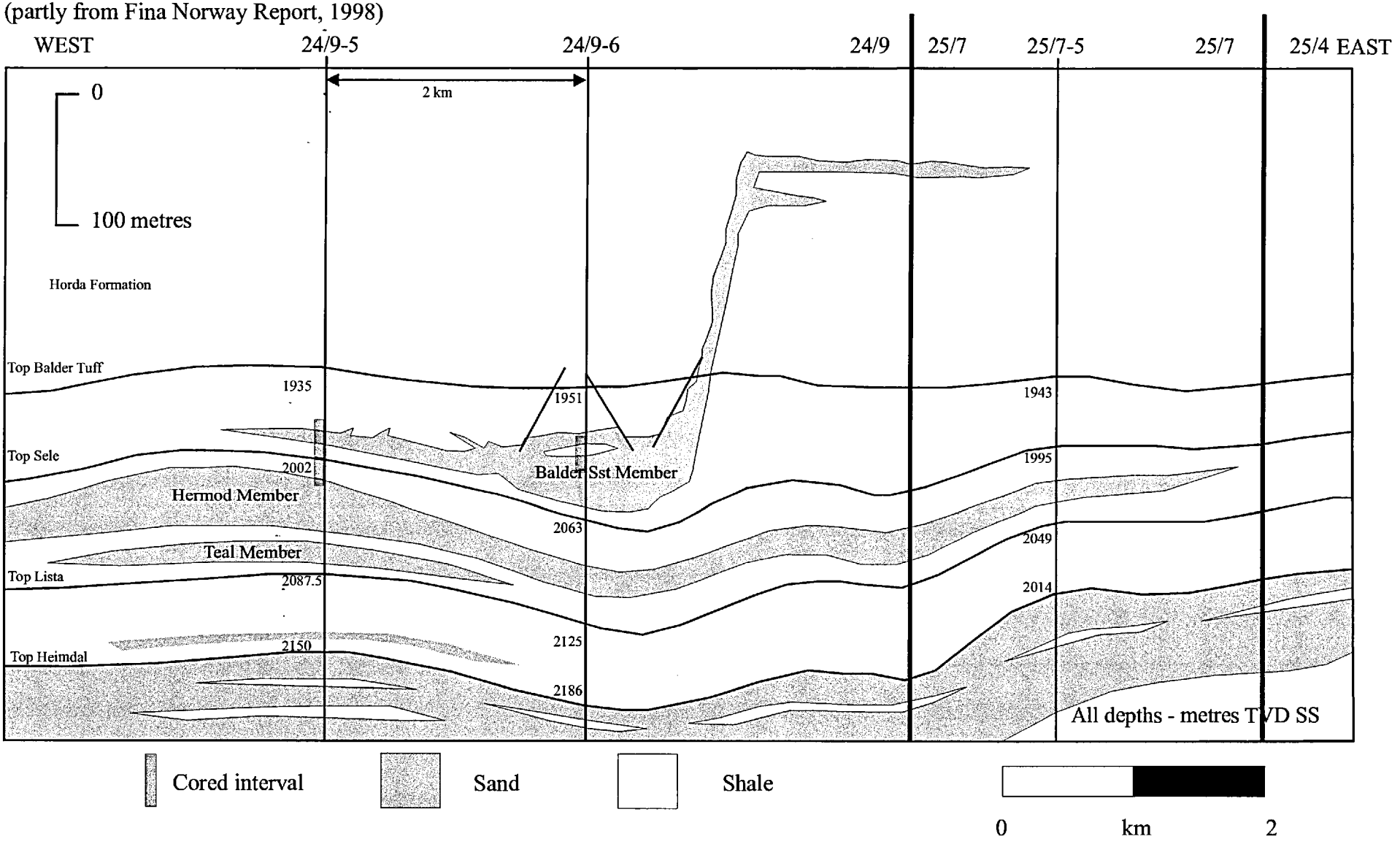
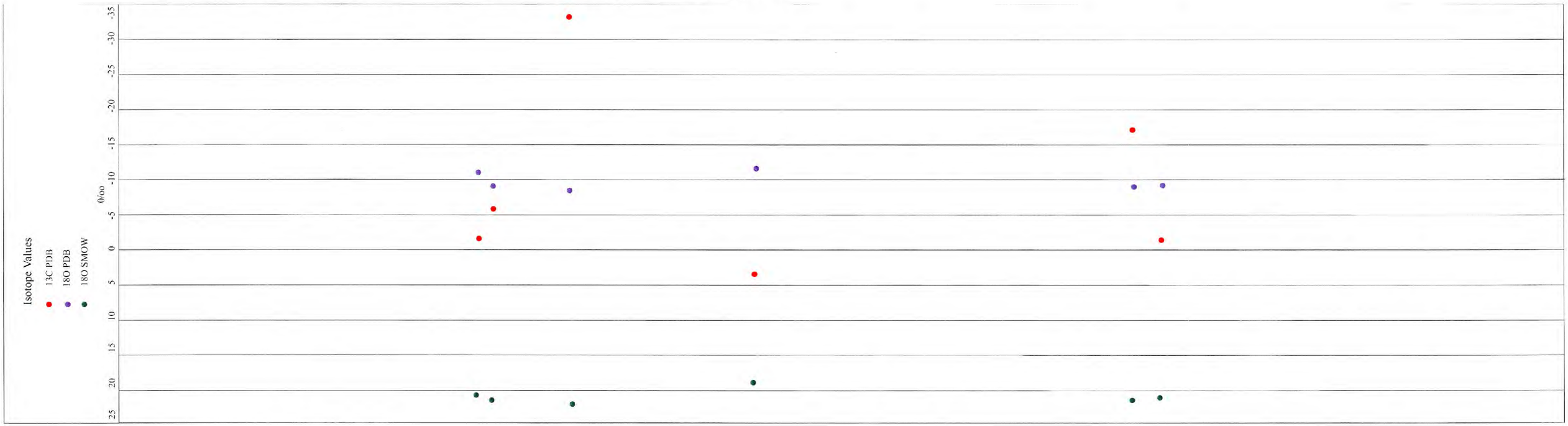


Figure 3.25. Core description sheet for Lower Tetiary interval of Norwegian North Sea well 24/9-5



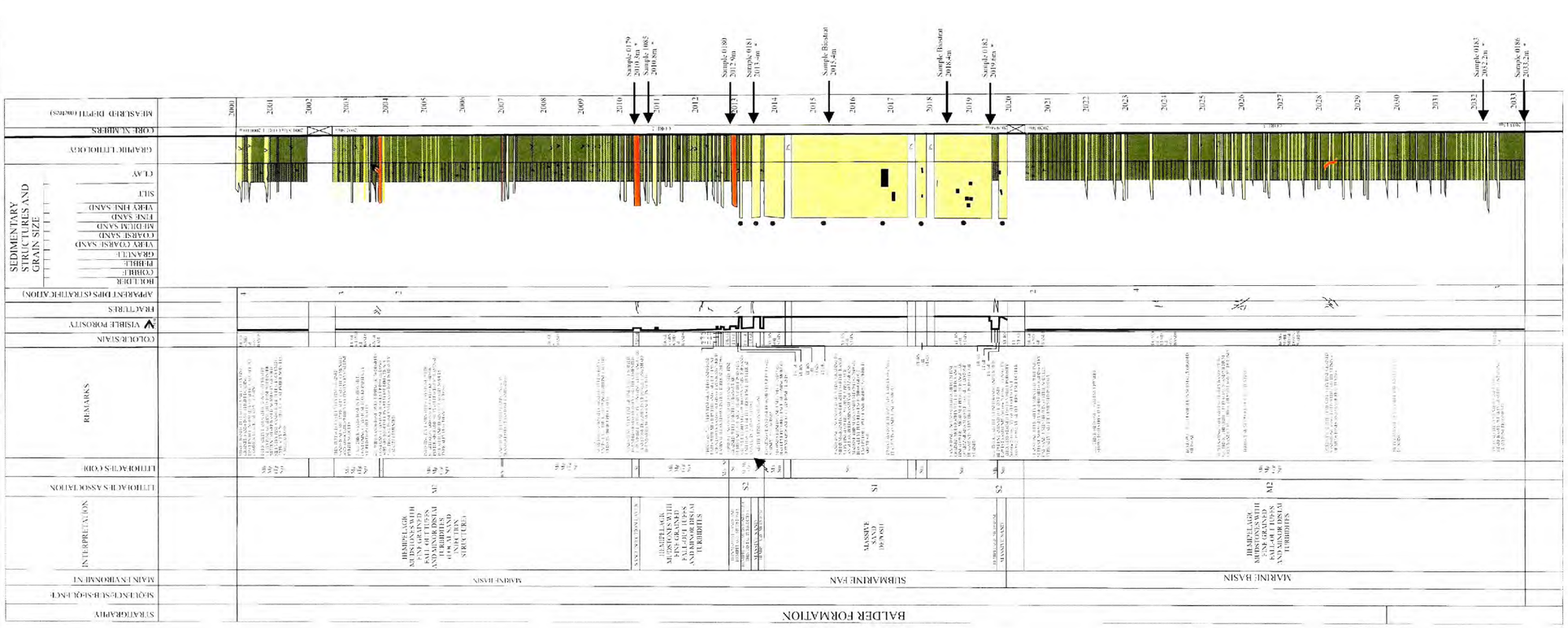


Figure 3.26. Core description sheet of the Lower Tertiary for Norwegian North Sea well 24/9-6

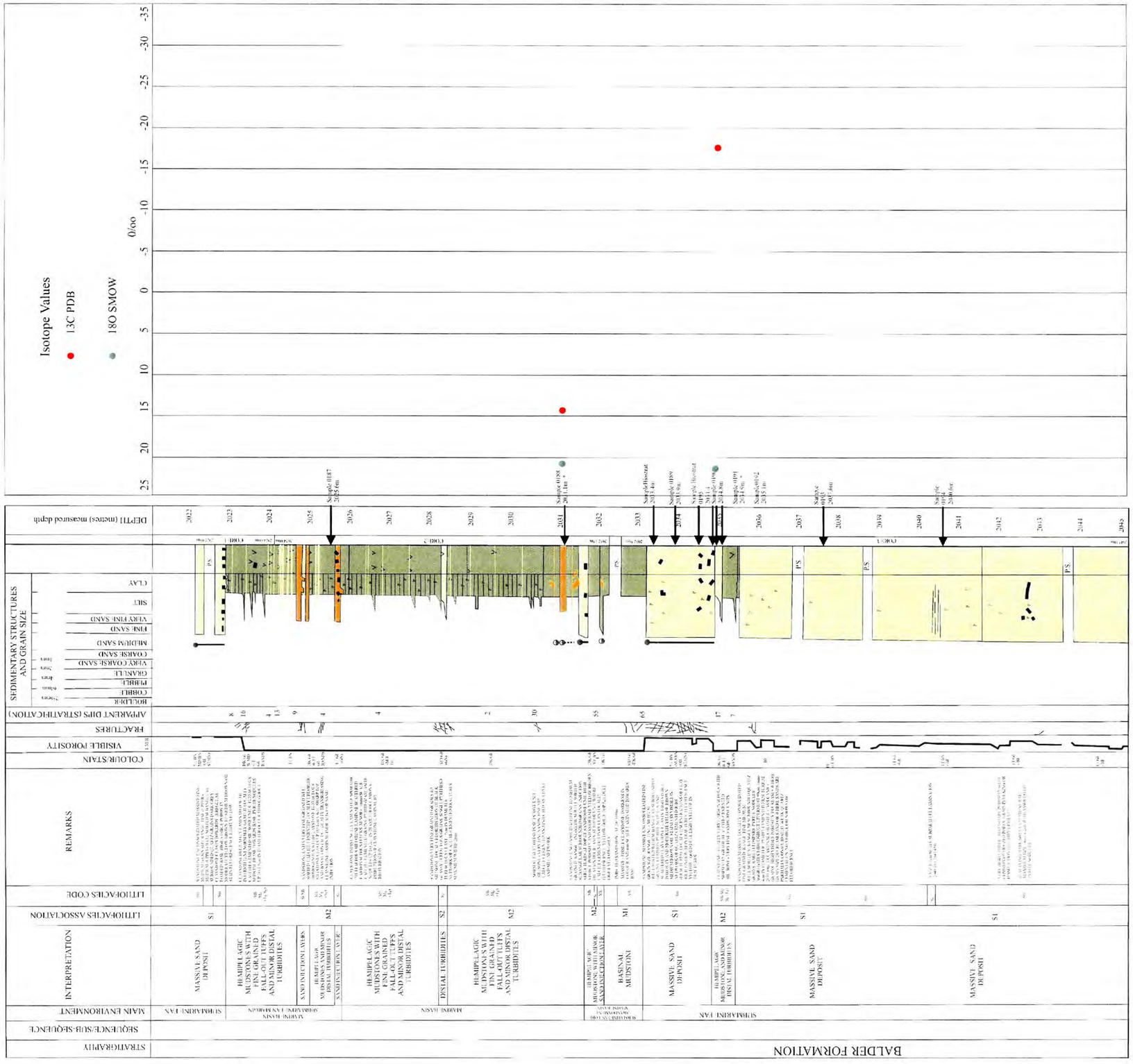


Figure 3.27. Core description key for Lower Eocene sediments in Norwegian North Sea wells 24/9-5 and 6

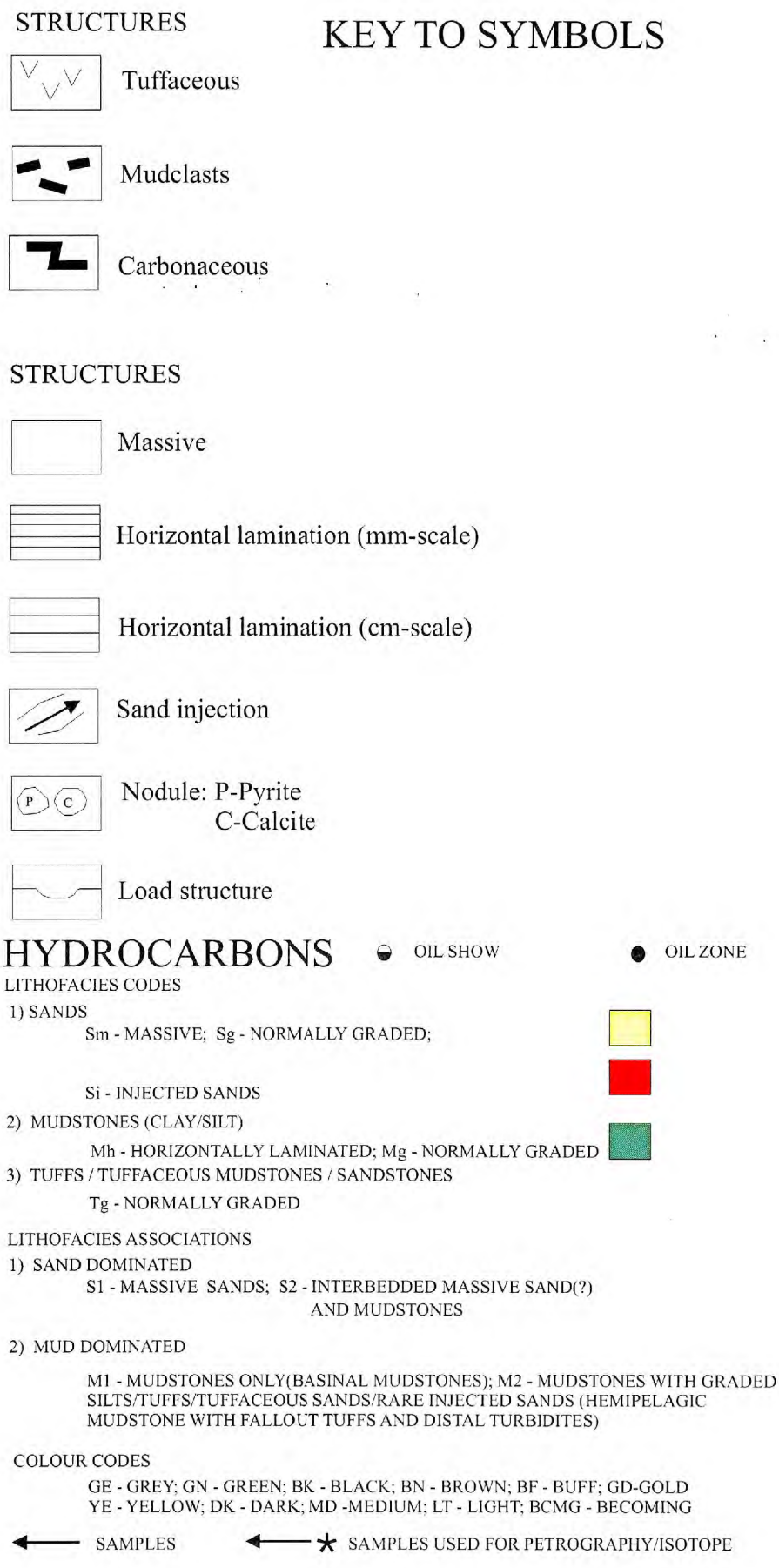
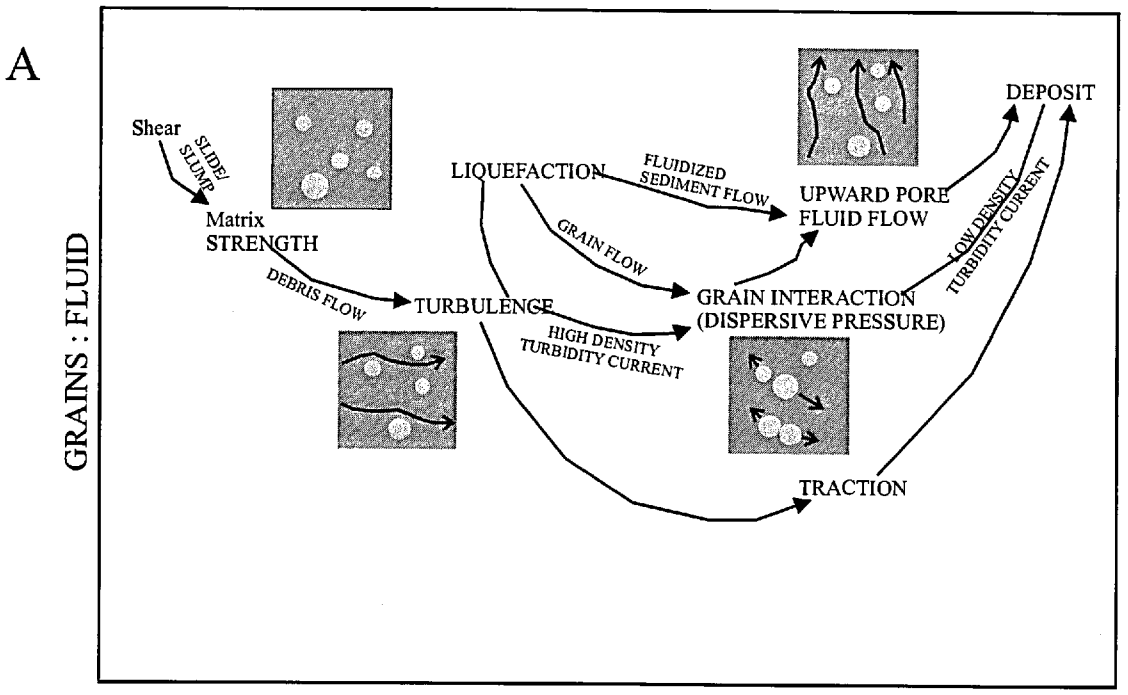


Figure 3.28. (a) Gravity flow processes and (b) Sediment flow types temporally and spatially (from Coneybeare, 1996 (after Hampton, 1972 and Lowe 1979, 1982))



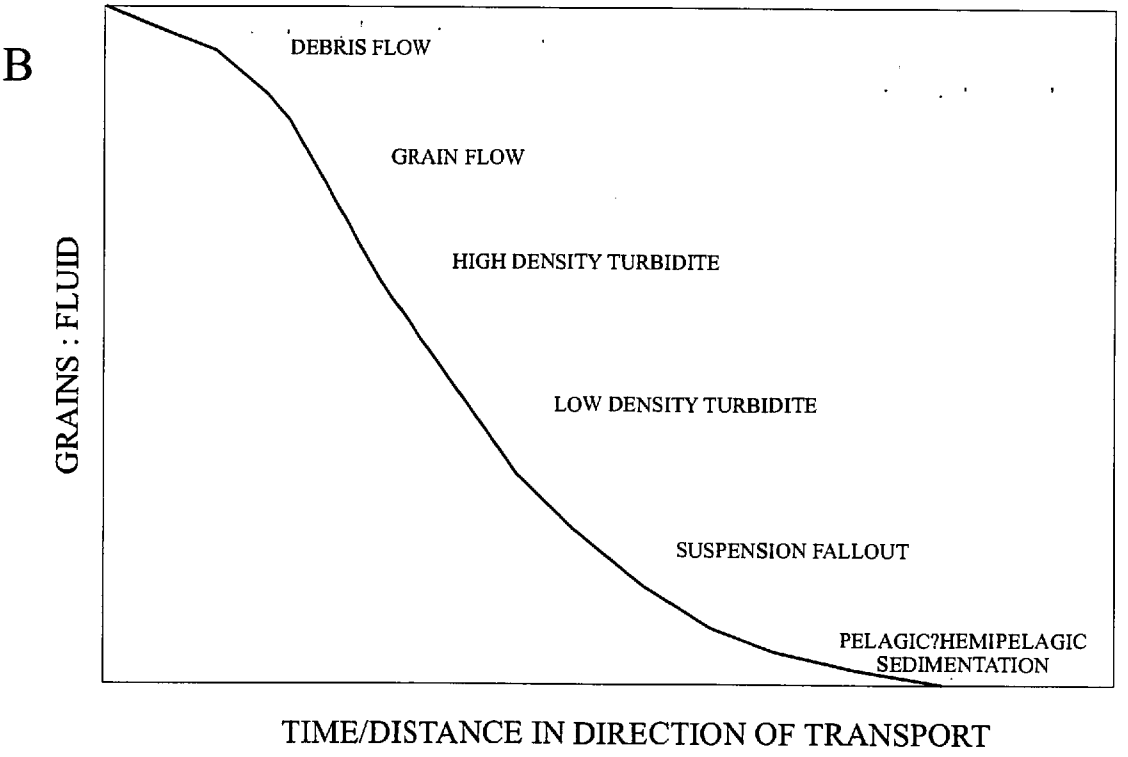


Figure 3.29. Deepwater transport and depositional processes (partly from Collinson and Reading, 1997)

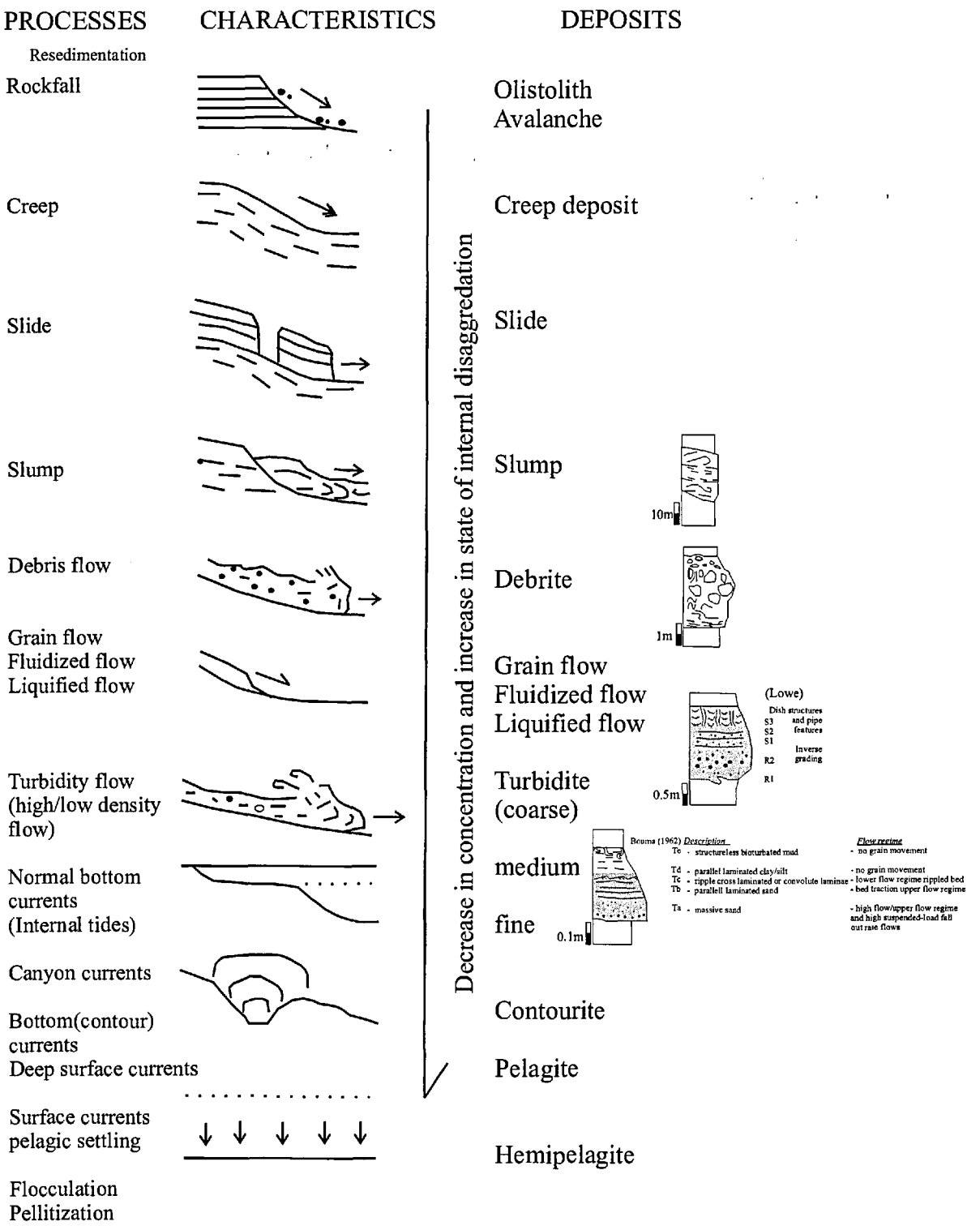


Figure 3.30. Core photographs of a Balder age massive sand from Norwegian North Sea well 24/9-6



Figure 3.31. Core photograph of a Balder age high angle sand/shale contact from Norwegian North Sea well 24//9-6

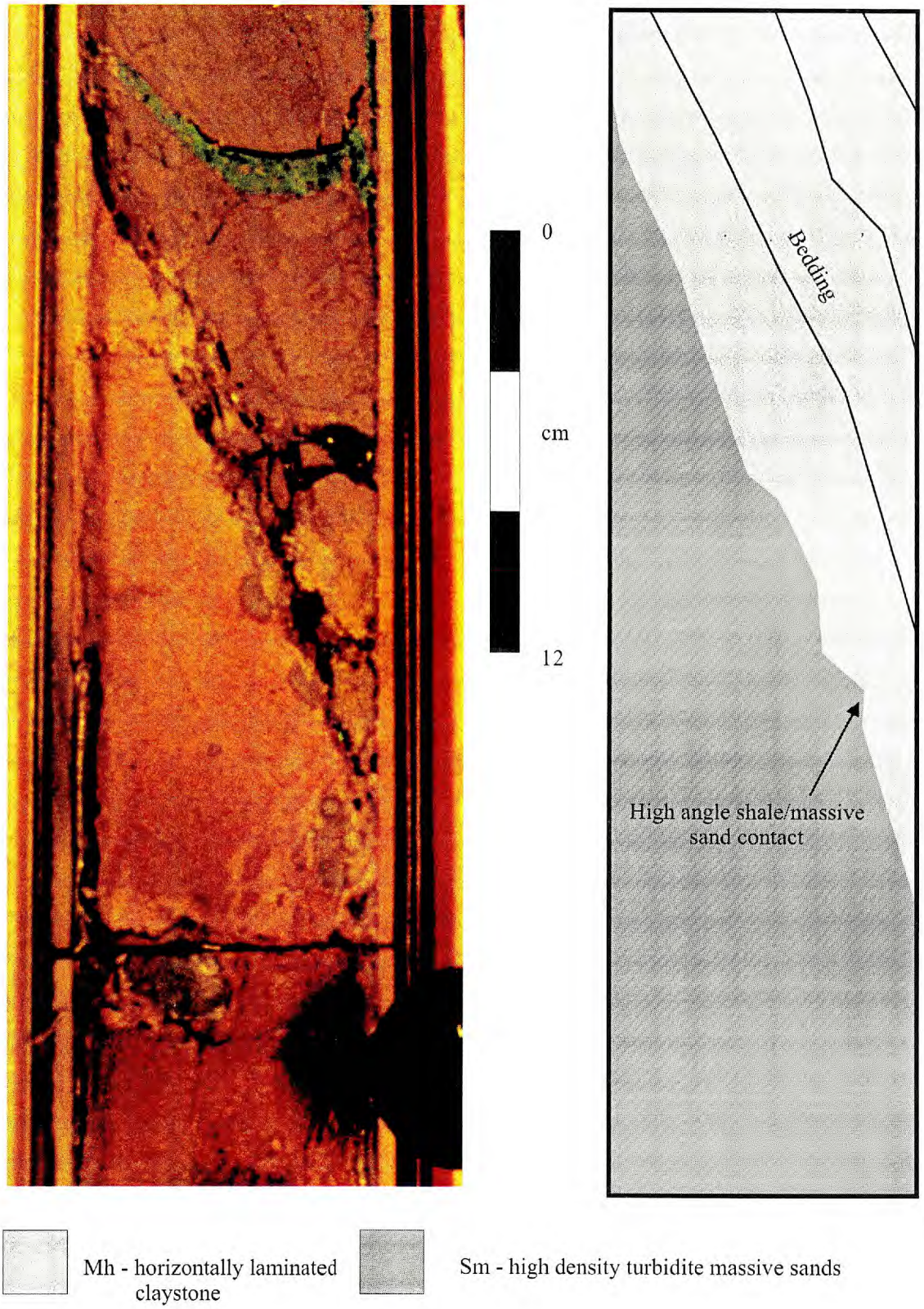


Figure 3.32. Core photograph of a Balder age high angle intrusive sandstone dyke from Norwegian North Sea well 24/9-5

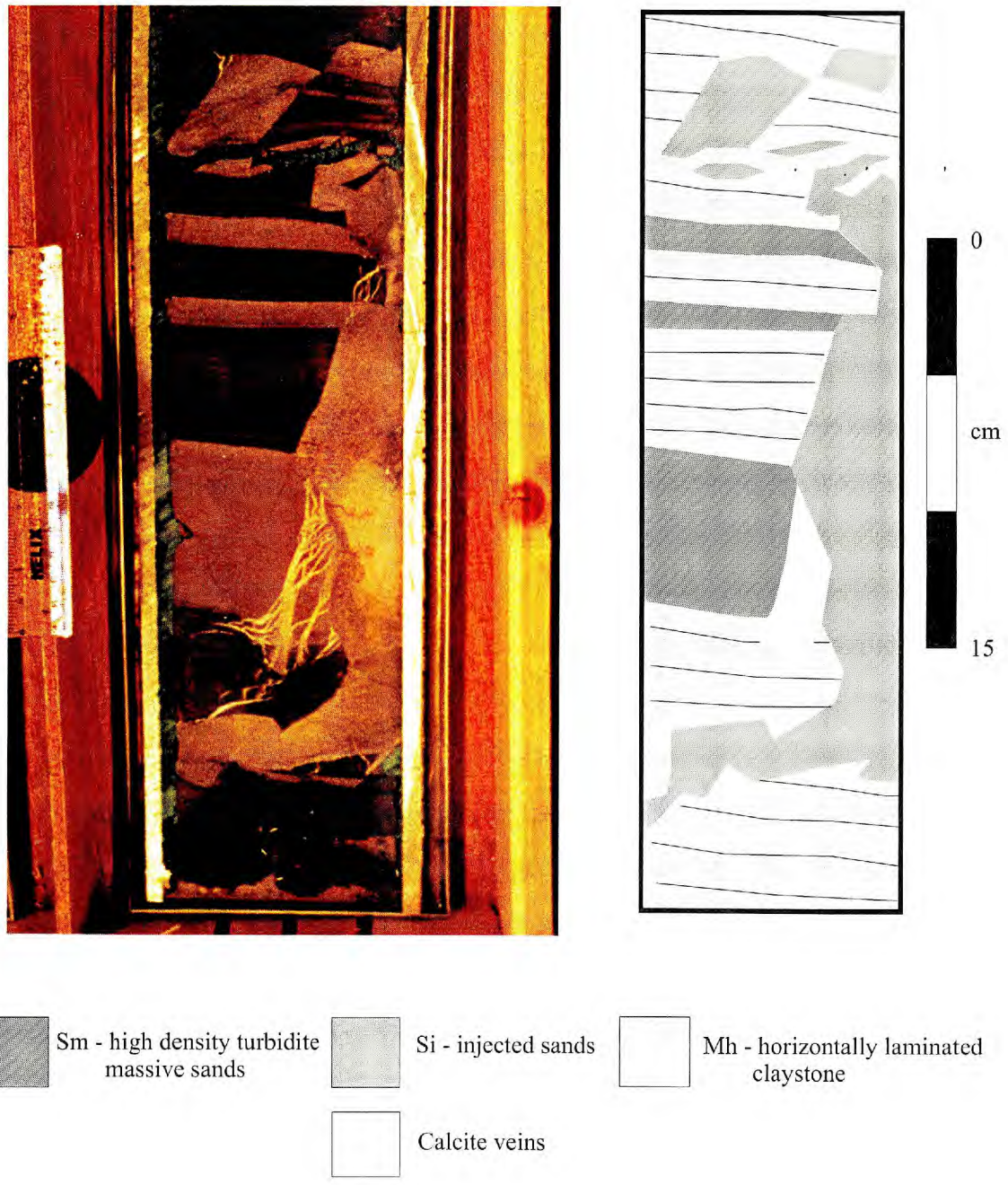


Figure 3.33. Core photograph of high angle quartz cemented planes within massive sands from Norwegian North Sea well 24/9-6

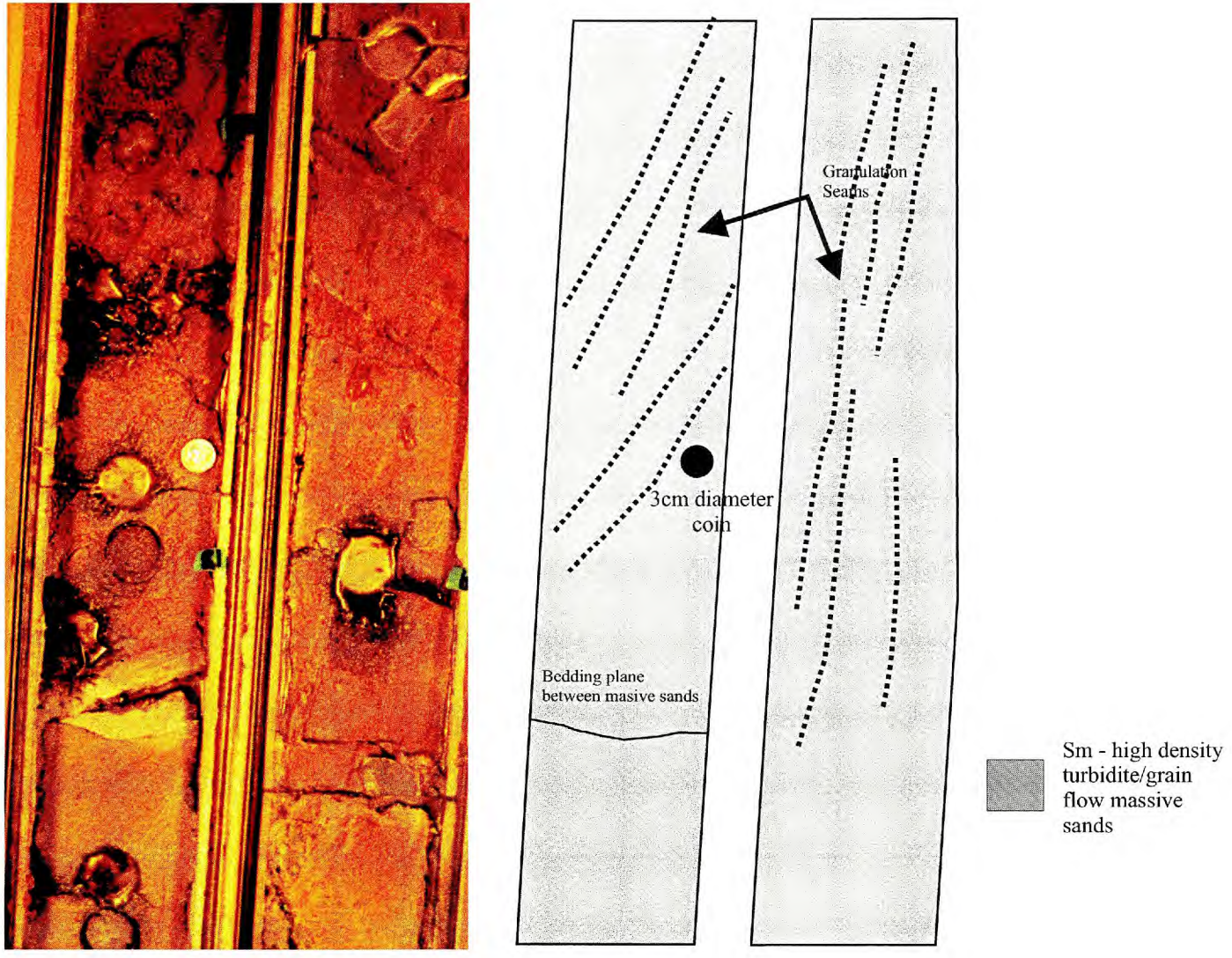


Figure 3.34. Plane polarised light image of a massive injected sand from Norwegian well 24/9-5 (Sample 0188 - 2031 metres measured depth)

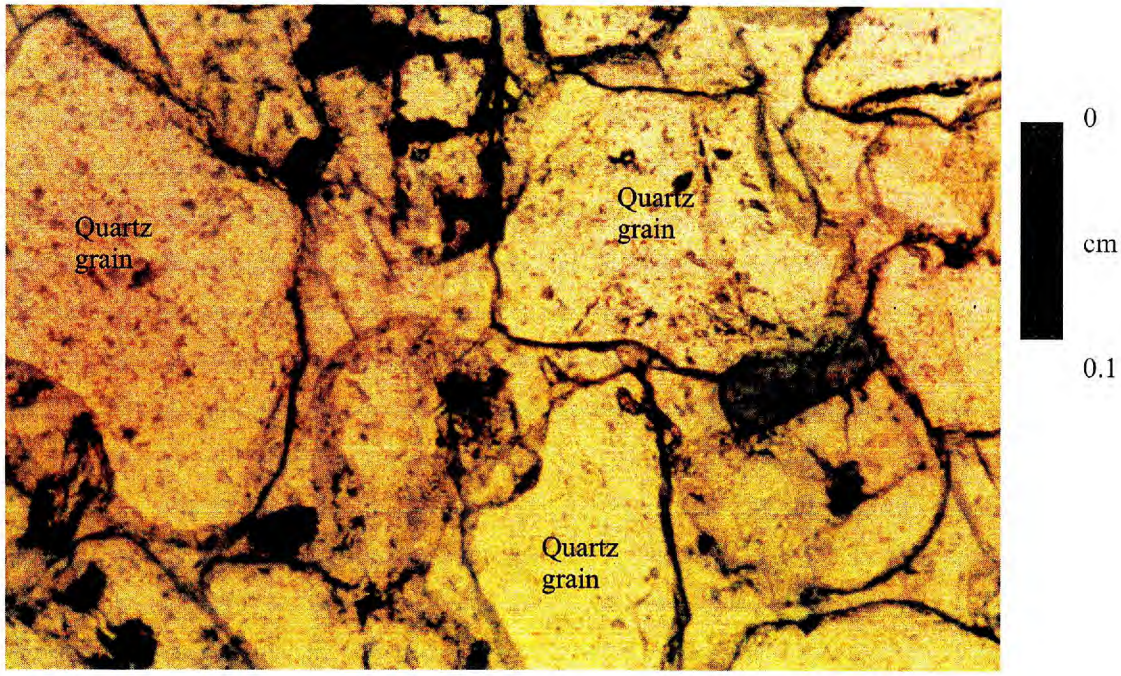
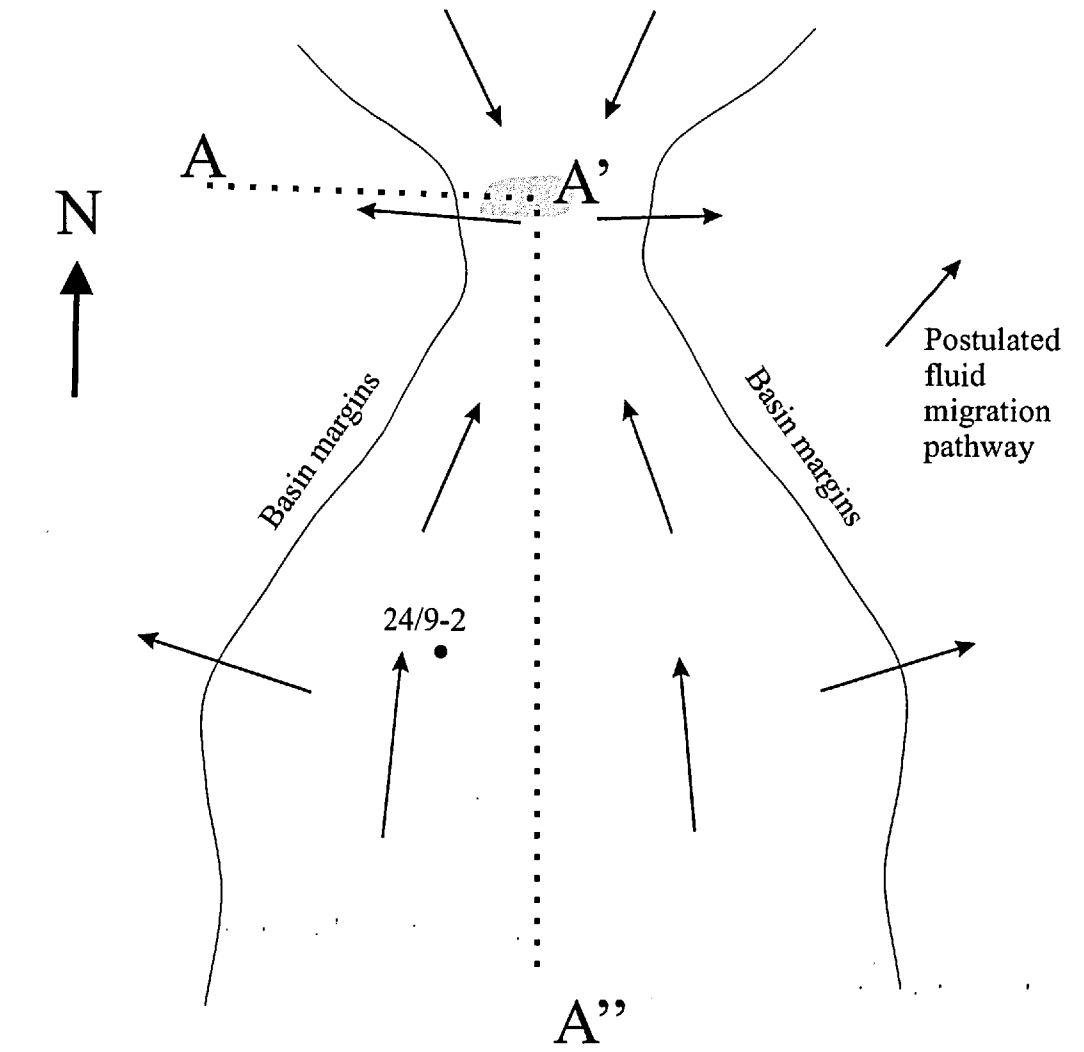


Figure 3.35. Cathodoluminescence image of a massive injected sand from Norwegian North Sea well 24/9-5 (Sample 0188 - 2031 metres measured depth). Note quartz grains are dark and the surrounding ferroan calcite cement is dull/poorly luminescing exhibiting no zoning. Ferroan calcite cement is poikilotopic (a single ferroan calcite crystal encompasses, large areas around the quartz grains).



Figure 3.36. Model of Fluid migration about Norwegian North Sea Block 24/9



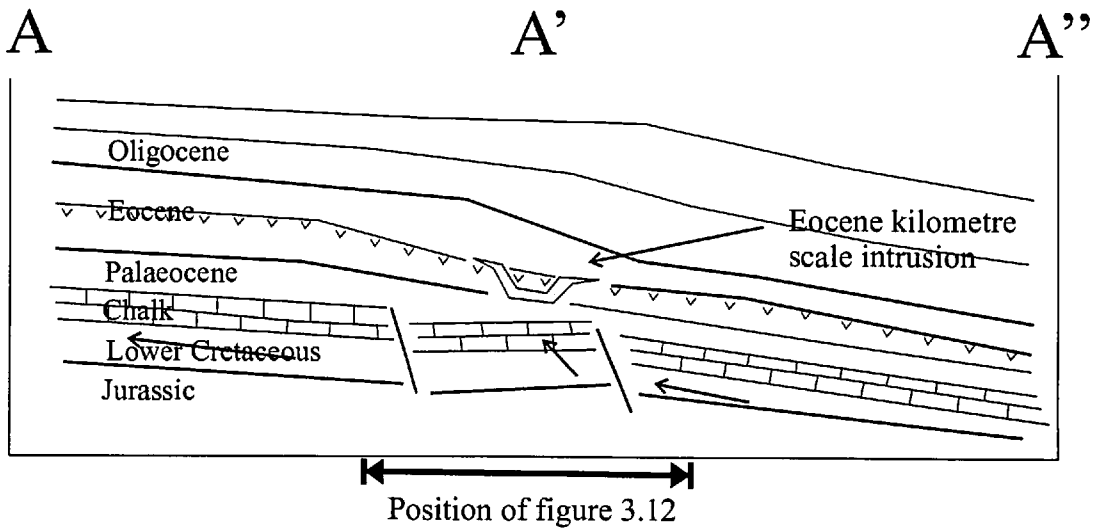
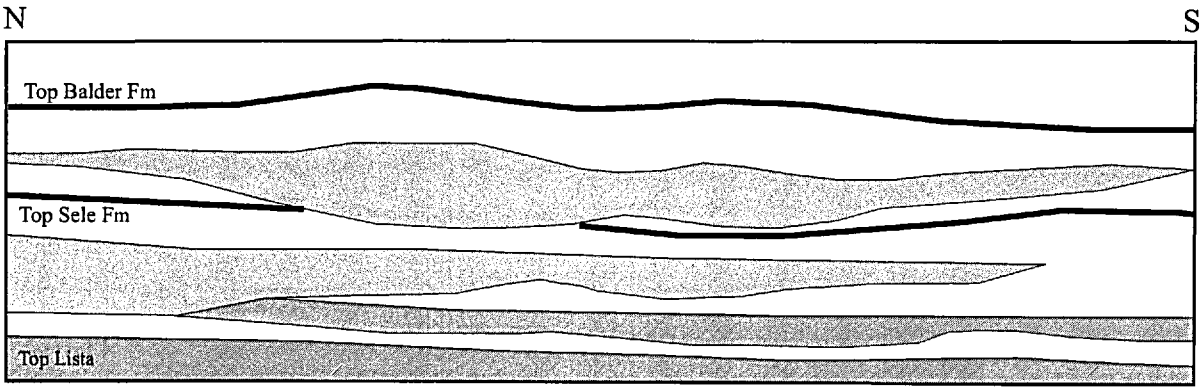


Figure 3.37. Model of Lower Eocene clastic injection model in Norwegian North Sea Block 24/9

(1) Balder Deposition (Upper Palaeocene)
- deposition of deepwater sands



(2) Post-Balder Remobilisation
- intrusion of Balder sands along possible wrench faults

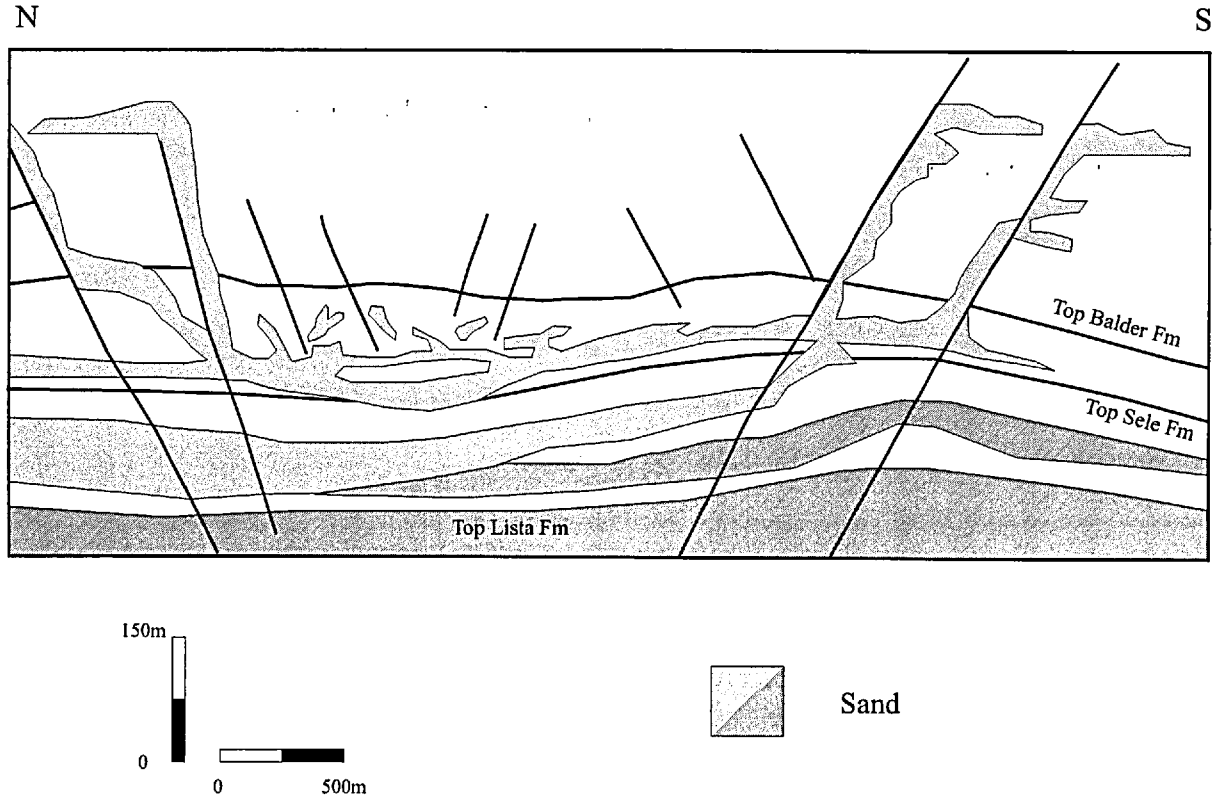


Figure 3.38. Location map of Yellow Bank Creek, Santa Cruz, California, USA (after Thompson *et al.*, 1999)

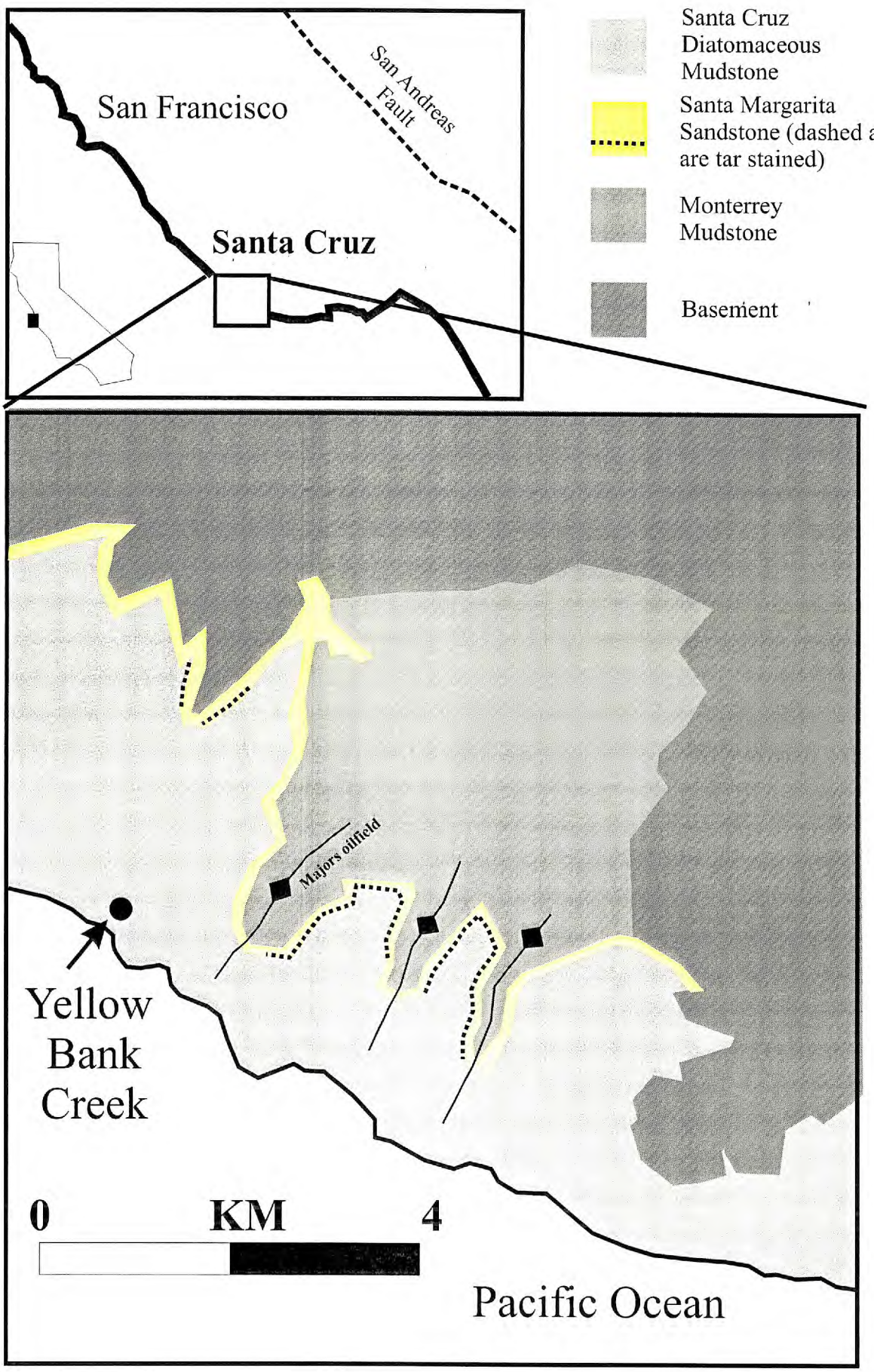
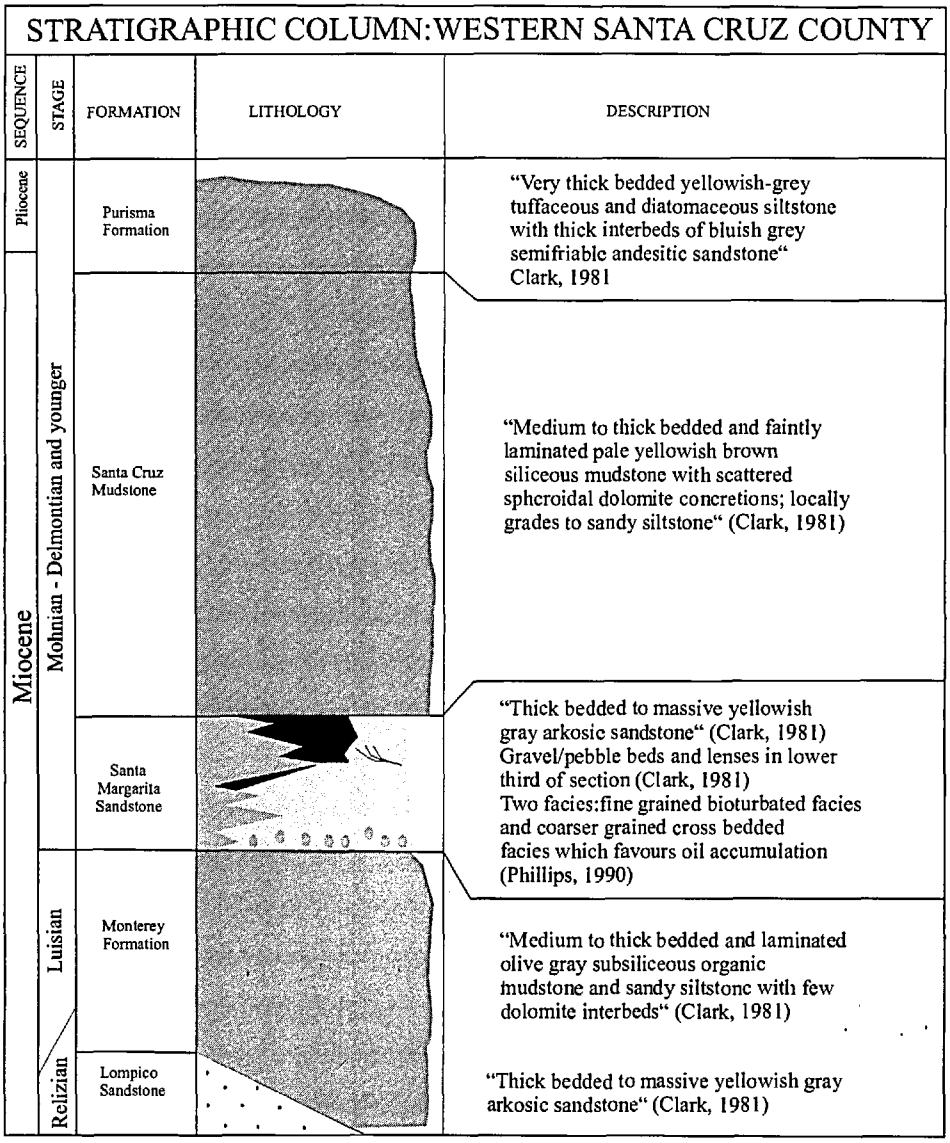


Figure 3.39. Stratigraphy of Miocene of Santa Cruz region, California, USA (after Thompson *et al.*, 1999; modified from Clark, 1981)



STRATIGRAPHIC THICKNESSES

Purisma Formation: Exposures mostly eroded, thickness measured at 150m (+), with as much as 180m exposed in Felton Quadrangle and 820m exposed in Laurel Quadrangle Quadrangle (Clark, 1981).
Santa Cruz Mudstone: Thickness is 140m at the western extent of Santa Cruz, 385m in the Shell Davenport Borehole no.1 (Clark and Babb, 1981).
Santa Margarita Sandstone: Thickness varies from 80m to 130m (Phillips, 1990), and is a maximum of 95m on the southwest slope of Ben Lomond Mountain (Clark, 1981)
Monterey Formation: Thickness of 810m on the north limb of the Scotts Valley syncline, and > 600m in Shell Davenport Borehole no.1 (Clark, 1981)
Lompico Sandstone: Thickness varies from 60 to 240m (Clark, 1981)

fine grained bioturbated sand
coarse grained cross bedded sand
hydrocarbon accumulation
massive sandstone
siliceous mudstone/ siltsone

Figure 3.40. Cliff cross sections of the Yellow Bank Creek sandstone intrusions, Santa Cruz, California, USA (after Thompson *et al.*, 1999)

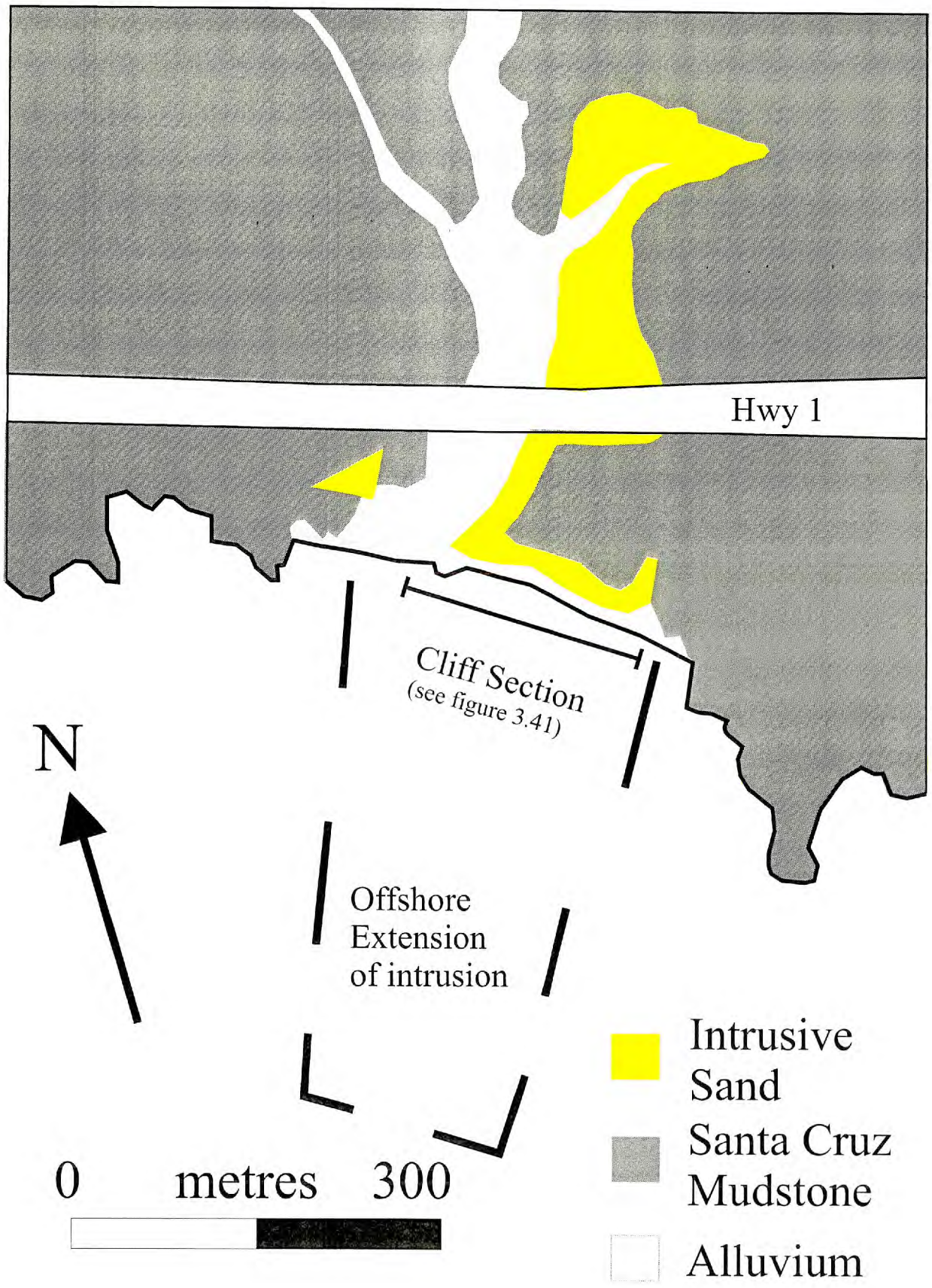


Figure 3.41. Cliff cross section of the Yellow Bank Creek, Santa Cruz, California, USA (partly after Thompson *et al.*, 1999)

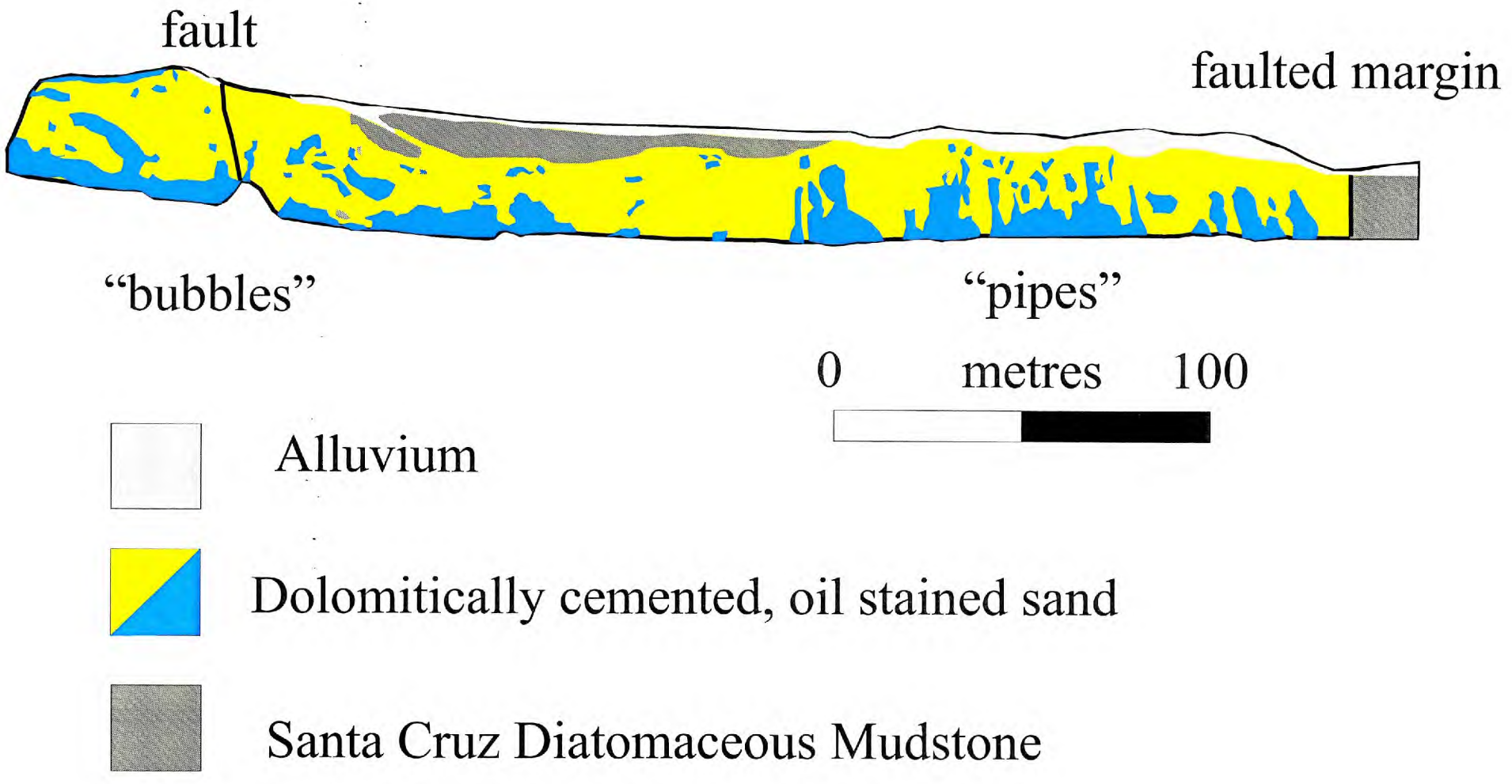


Figure 3.42. Ten metre thick sandstone sill passing into a fifteen metre wide sandstone dyke, five hundred metres southeast of the Yellow Bank Creek sandstone intrusion, Santa Cruz, California, USA

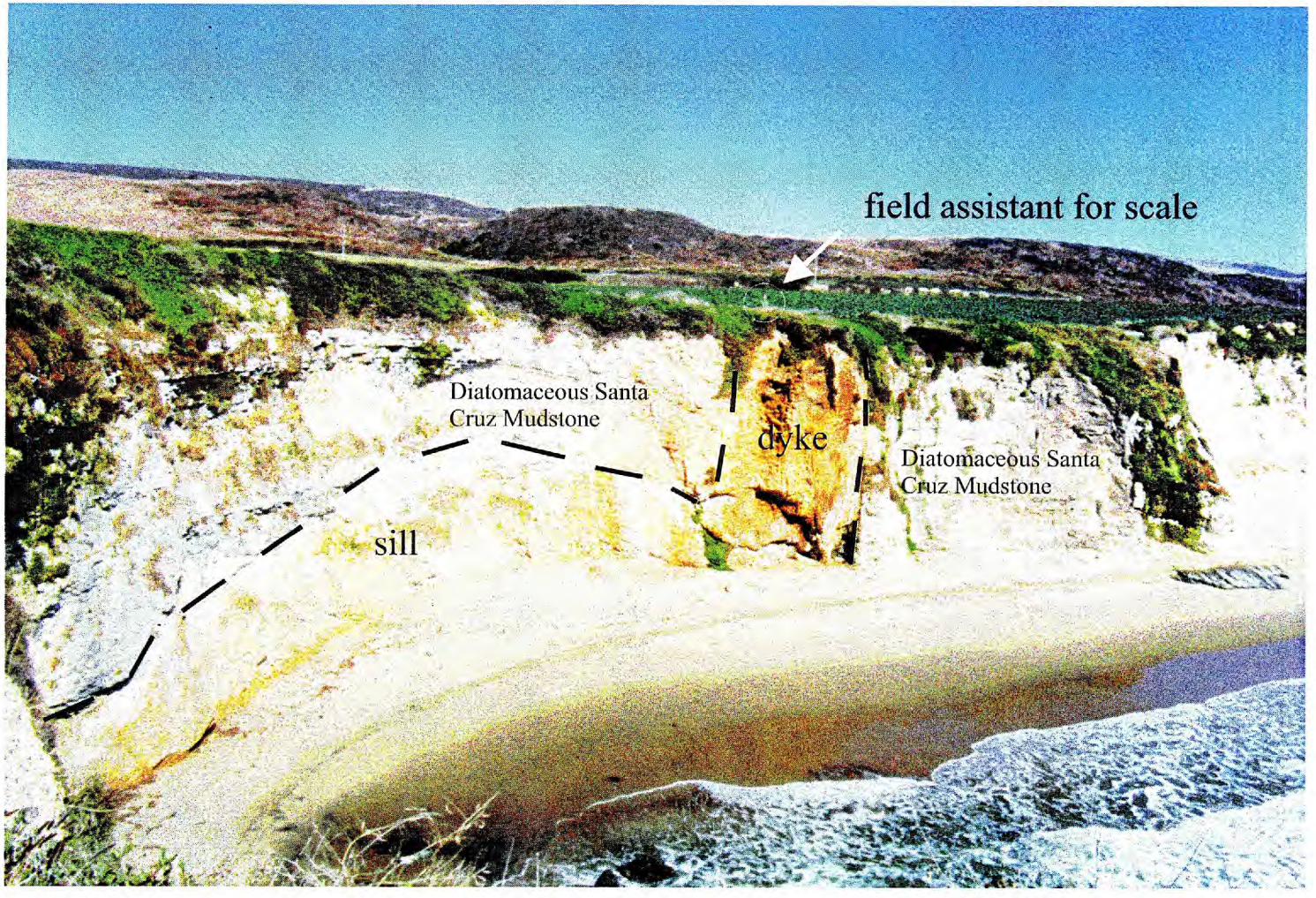


Figure 3.43. Dolomite cemented sandstone with the appearance of "bubbles" and "pipes" at centimetre to metre scale, representing fluid flow texture within the Yellow Bank Creek sandstone intrusion, Santa Cruz, California, USA.

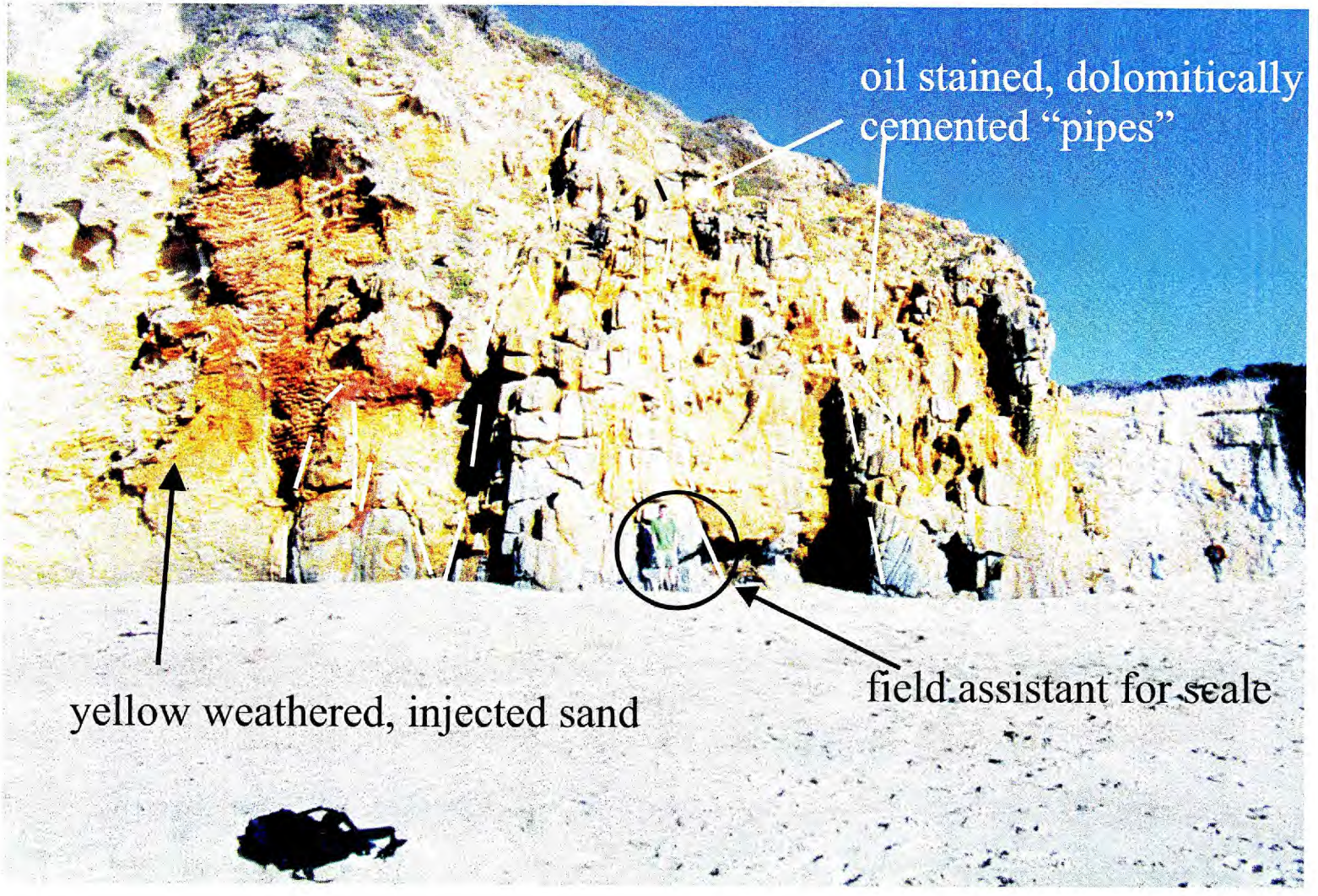


Figure 3.44. Flow texture or limonite staining and granulation seams within poorly cemented sandstone in the Yellow Bank Creek intrusion, Santa Cruz, California, USA

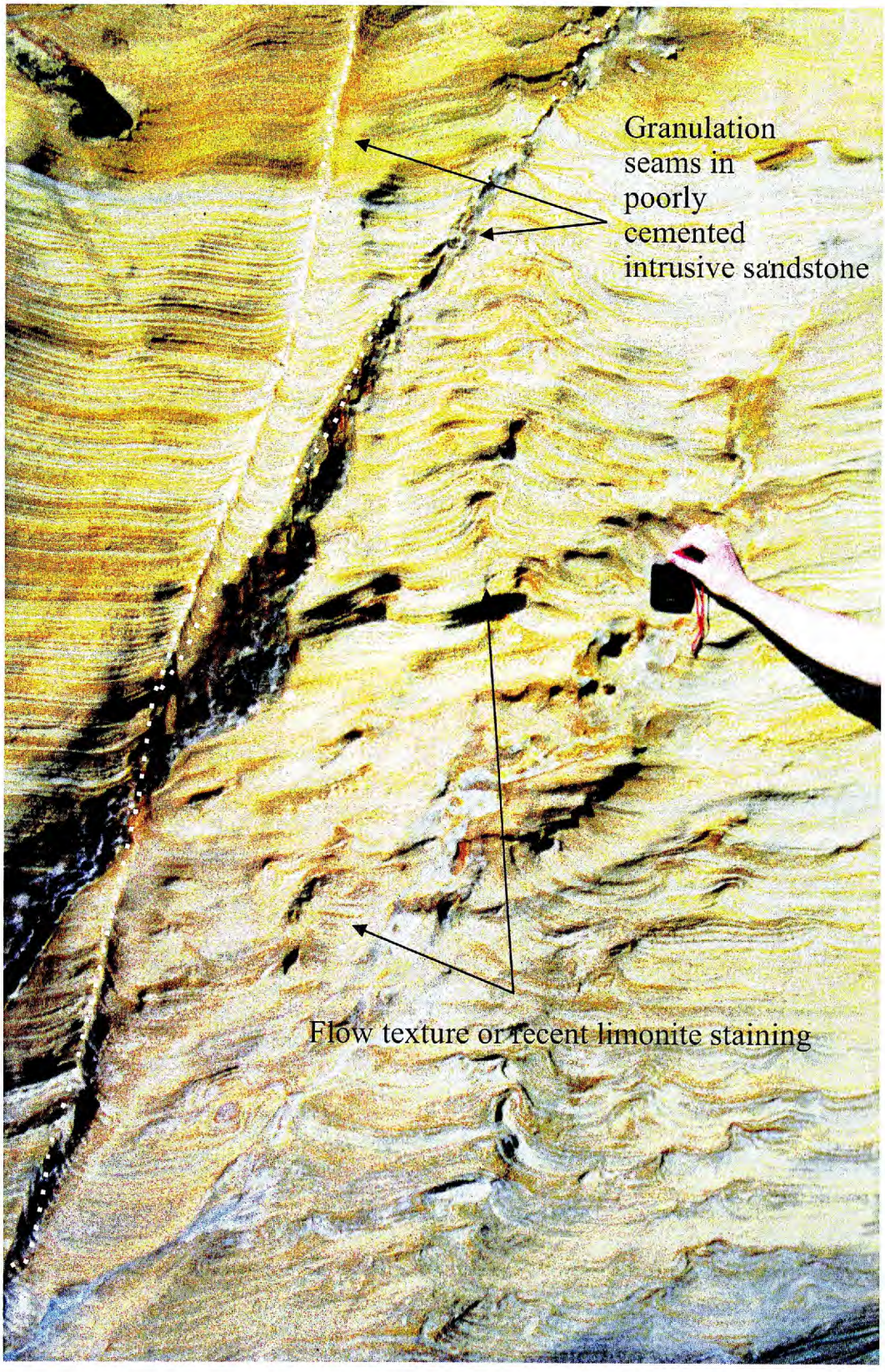


Figure 3.45. Plane polarised light image of an intruded massive sand (Sqtz) cemented with dolomite (d). Lithic fragments occur (Lith). Yellow Bank Creek, Santa Cruz, California.

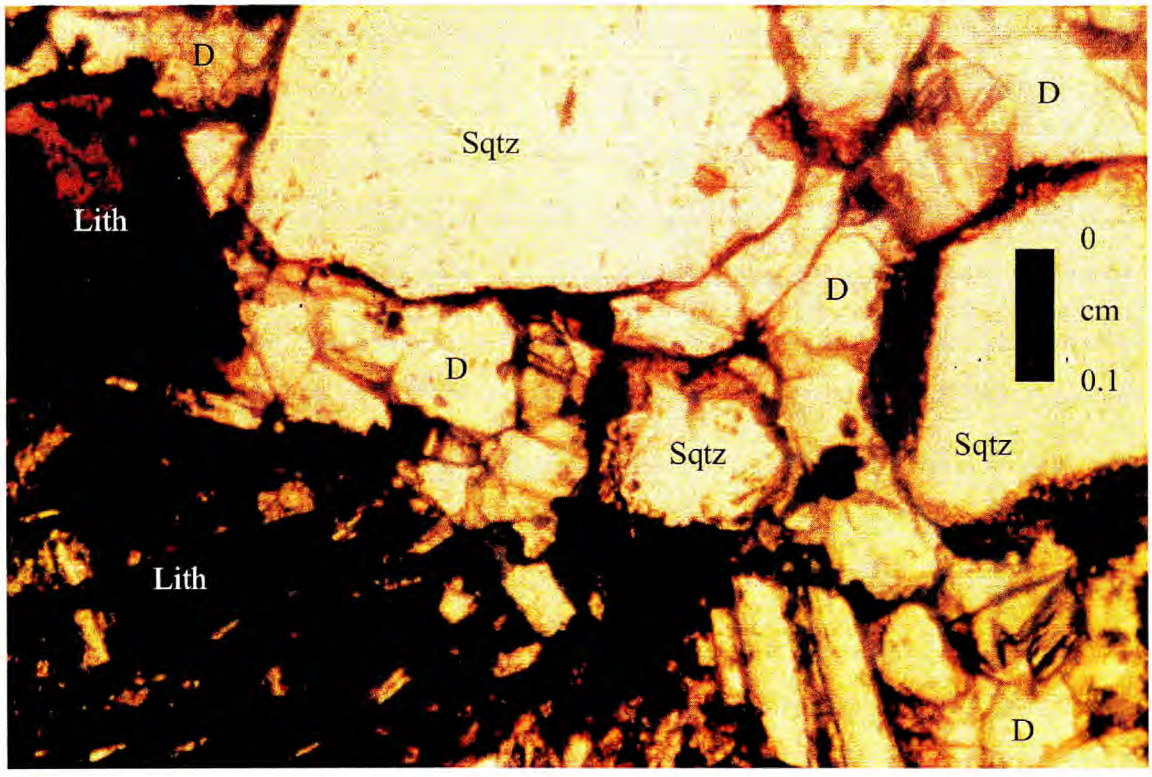


Figure 3.46. Cathodoluminescence image of an intruded massive sand and lithic fragments (opaque)cemented with multiple zoned, highly yellow luminescing non ferroan dolomite (nfd) and non fluorescing ferroan dolomite(fd).

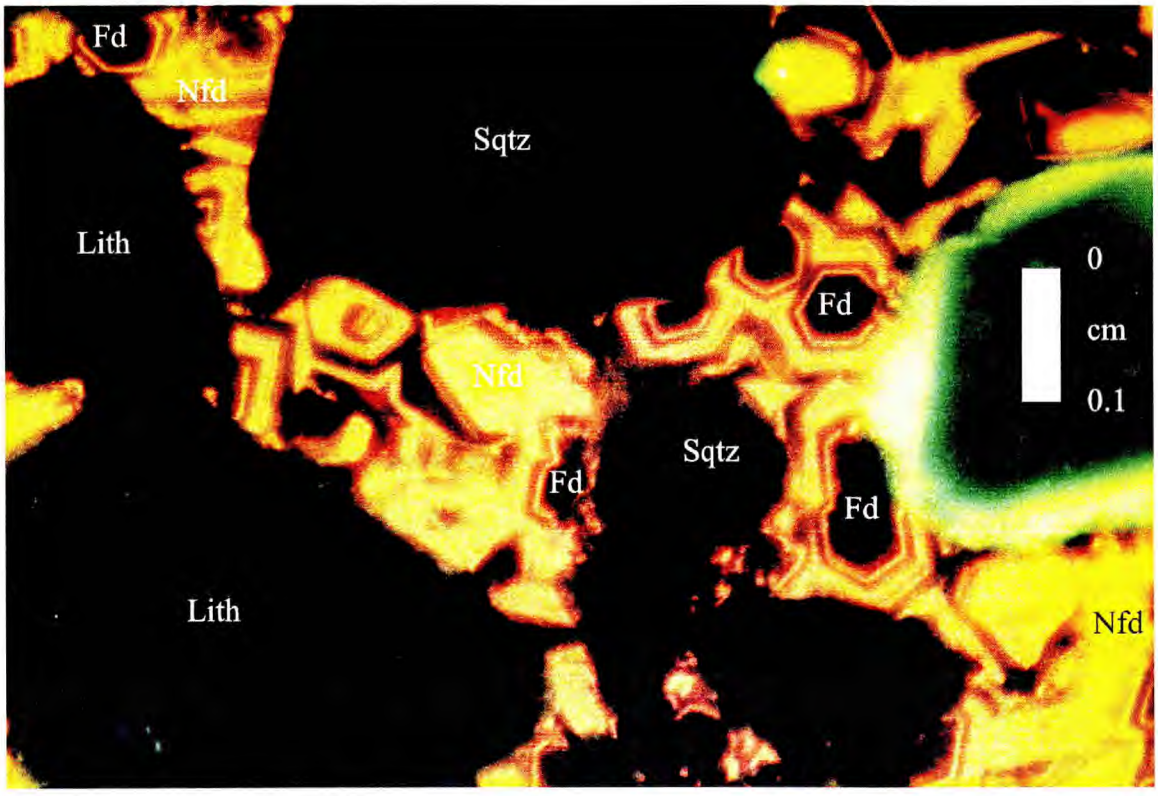
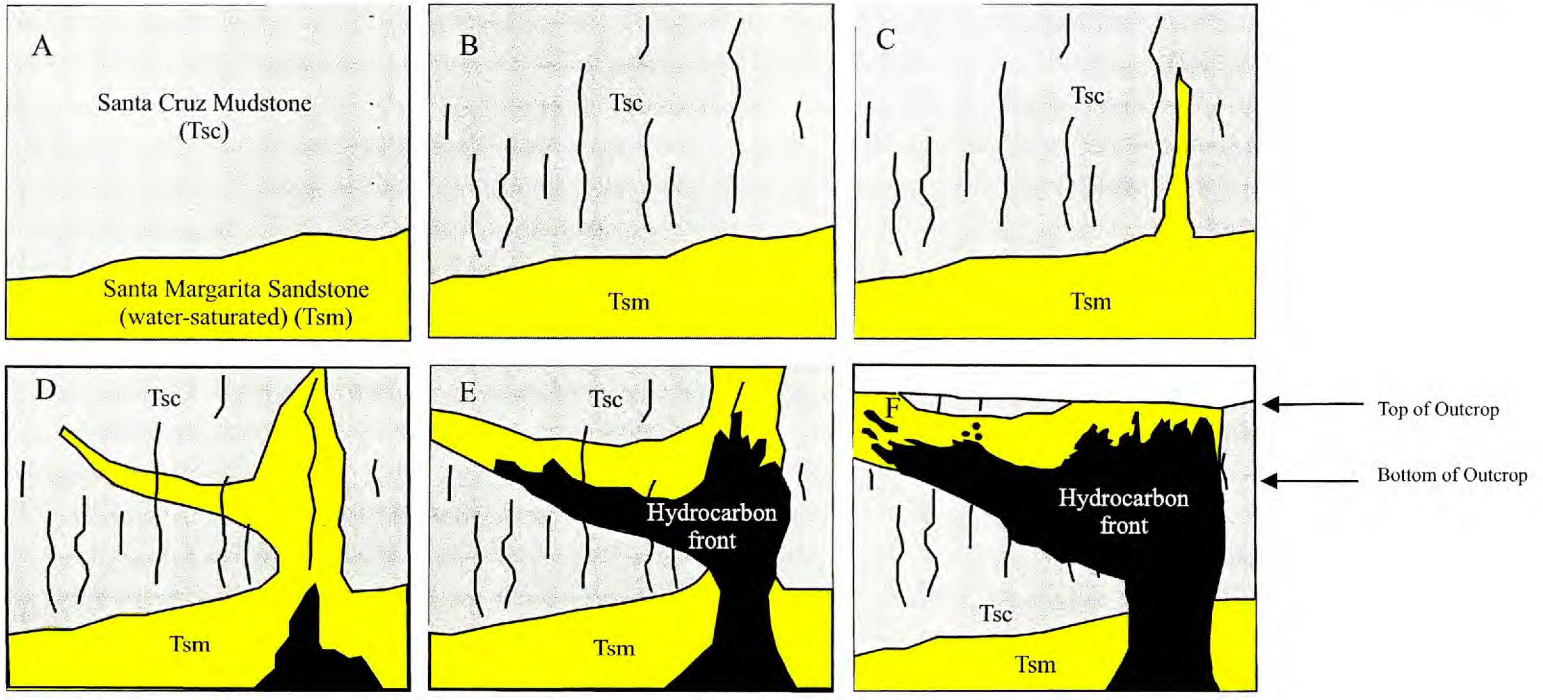


Figure 3.47. Model of sequential formation of the Yellow Bank Creek intrusion, Santa Cruz, California (Thompson *et al.*, 1999)



A. Middle to late Miocene sedimentation of the Santa Margarita Sandstone and the overlying Santa Cruz Mudstone
B. Late Cenozoic fracturing or faulting is most intense in relatively brittle siliceous mudrocks of the Santa Cruz Mudstone and less pronounced in unlithified, water-saturated parts of the Santa Margarita Sandstone
C. Vertical injection of water-saturated sands from the bioturbated facies of the Santa Margarita Sandstone along a fracture or fault creates a dike
D. Horizontal breakout of the water-saturated sands along bedding planes in the Santa Cruz Mudstone creates a sill extending from the dike. Flow banding develops in the sill at this stage. A hydrocarbon front begins to migrate into the intrusion, being sourced from layers (cross-bedded facies?) in deeper levels of the Santa Margarita Sandstone
E. Continued fluidized sediment flow from the Santa Margarita Sandstone and emergence of the hydrocarbon front which is injected into the water-saturated intrusion as immiscible bodies of petroleum and hydrocarbon front which is injected into the water-saturated intrusion as immiscible bodies of petroleum and hydrocarbon bearing sands. These form vertically elongated "pipes" in the area of the dike and spheroidal "bubbles" which cut across the flow banding in the area of the sill. Dolomitic cementation occurs within the hydrocarbon front.
F. Uplift and erosion expose the intrusion to groundwater flow which produces complex patterns of limonite staining. Arrow show an outcrop geometry that is similar to the seacliff of Body I of the intrusion at Yellow Bank Creek

CHAPTER 4. LOWER EOCENE GIANT SCALE SANDSTONE INTRUSIONS IN UK CENTRAL NORTH SEA OFFSHORE BLOCKS 21/3, 4 and 5

4.1. Lower Eocene giant scale sandstone intrusions in UK Central North Sea Blocks 21/4 and 5

4.1.1. Aims

This chapter addresses the possibility that large and small scale sandstone intrusions can be formed with a low-angle conical geometry. Within UK Central North Sea Blocks 21/3, 4, 5 located 150km east of Scotland (figure 4.1), Lower Eocene kilometre-scale, low-angle conical seismic amplitude anomalies are observed on 3D seismic data within polygonally faulted Lower Eocene base-of-slope deepwater clays. The blocks are located above a structural high, the Renee ridge with the Fisher Bank Basin to the east, the Witch Ground Graben to the north, Outer Moray Firth to the west and the Forties Montrose High to the South. Several hydrocarbon accumulations occur in the area, namely the Lower Cretaceous Britannia field located over Blocks 15/29, 30 and 16/26 and 27 and the Middle Eocene age Alba field of Block 16/26. Factors such as hydrocarbon generation from the Jurassic in the Eocene about this subregional structural high and other palaeo-cone shaped features such as Lower Eocene age kilometre-scale pockmarks of the Outer Moray Firth, plus other field outcrop cone shaped clastic intrusive geometries are considered as possible explanations for the Lower Eocene amplitude anomalies in UK North Sea Blocks 21/4 and 5.

4.1.2. Geological Setting

Blocks 21/3, 4 and 5 are located about the mid-Cimmerian, Middle Jurassic North Sea triple junction (Underhill and Partington, 1994) and the related present day subcrop of Rattray Volcanics (figure 4.1). Rifting of the basement from Middle Jurassic to the Early Cretaceous produced a significant

rift sequence in which a succession of marine shales and deep and shallow marine sands were deposited (Glennie, 1998a). Upper Cretaceous Chalks extend across the whole of the study area and record the onset of post rift thermal subsidence and sea level rise (Glennie, 1998a). Palaeocene sediments were deposited as a series of turbidite fans and across the study area are located about a base of slope position (figure 4.2 and 4.3). They contain variable amounts of deepwater sand and are related to the previous description in chapter 2 of uplift of the Scottish mainland at this time due to Atlantic rifting and the formation of a clastic system flowing along the Inner and Outer Moray Firth and into the Central North Sea. This episode of clastic progradation formed during a period of progressive relative sea level fall (den Hartog Jager *et al.*, 1993) and deposited the Maureen, Andrew and Forties fan systems. Early Eocene sedimentation began with the deposition of the Sele deep-marine shale and subsequently Balder deep marine clays and volcanic tuffs. They mark the start of a progressive sea level rise (den Hartog Jager *et al.*, 1993) with the Balder marking a period of volcanism as evidenced by tuffaceous material within the formation. Lower Eocene to Middle Miocene deepmarine sediments are predominantly mud prone, except on the shelf which is variably sandy, and progressively backstep landward as sea level rises, with individual sequences within the study area prograding into the basin centre.

Figure 4.4 is a geoseismic section and line drawing through the study area and shows the sequence of Jurassic rifting, Upper Cretaceous chalk deposition, Palaeocene clastic progradation and Eocene to Middle Miocene sea level rise punctuated by progradation of sediment into the basin centre. The Tertiary within the Palaeocene section is a sandy shelf, passing into a variably sandy slope section of deepwater sands, and muddy basin plain sediments. The Eocene to Middle Miocene section is a sandy shelf, with a mud prone slope, rare deepwater sands and muddy basin plain sediments (figure 4.5). Blocks 21/3, 4 and 5 are located in a deepwater base of slope position. Throughout this Eocene to Middle Miocene slope/basinal mud prone section, there are numerous normal faults (figure 4.6). As previously noted in chapter 2 they are polygonal faults and are ascribed to three dimensional dewatering of clays (Cartwright and Lonergan, 1996). They are typically radial in plan view, are 100

to 500m apart, dip at 5-30 degrees, have normal displacements of between 10-50m but may be up to 300m in extreme cases (Lister, 2000). It is within the polygonally faulted Lower Eocene section that high amplitude, circular, low angle, cone shaped anomalies occur (figure 4.6). They are 0.5 to 2km across, 100-300m high and dip at 5-25 degrees (compacted) and contain 20-30 metres of sand calibrated from wireline logs. This chapter describes, then outlines the possible origin of these features.

4.1.3. Database

4.1.3.1. Seismic data

The seismic data used over blocks 21/3, 4, 5 (figure 4.1) is a 3D seismic data set shot by PGS Exploration AS in 1995, imaging down to four seconds two way time with a line spacing of 12.5 metres and subsequently processed by CGG. The data was interpreted on a workstation using Geoquest Charisma.

4.1.3.2. Well data

Well data over the 3D seismic study area, contains the wells below: 21/3-1, 21/3-2, 21/3-3, 21/3-4, 21/4-1, 21/4-2, 21/4-3, 21/4-4, 21/5-1, 21/5-2, 21/5-3 and 21/5-4. All wells were loaded on the workstation. In addition paper composite logs were used. It should be noted no core has been taken in the sand prone section of the Lower Eocene for these wells, so calibrations of the seismic are made to the wireline log data only. Age dates for calibration of seismic events are made from composite log formation names from the wells above where these wells penetrate relevant strata. These horizons were subsequently confirmed by Fina UK (Fina UK pers comm. 1998)

4.1.4. Seismic Interpretation

4.1.4.1. Horizon interpretation

The Near Top Jurassic map (figure 4.7) shows an eastwest oriented regional structural high over blocks 21/4 and 5 which persists through the Top Cretaceous (figure 4.8) and Top Palaeocene (figure 4.9) structure maps. This high is called the Renee Ridge and is a prominent positive feature from at least the Jurassic to the Tertiary. Isopach maps between the base Jurassic and Top Jurassic (figure 4.10) and the Top Cretaceous and Top Paleocene (figure 4.11) show thinning over the Renee ridge and sediment thickening away from it indicating its presence and topographic effect on sedimentation through these times. The Renee Ridge is significantly downthrown to the North and East and internally faulted (Fina UK pers.comm. 1997; figure 4.12) and links to the south with the faulted North South oriented Forties Montrose horst block. Either side of these two linked faulted highs exist graben lows – the Witch Ground Graben to the North, the Fisher Bank Basin to the East and the South Buchan Basin to the West. The outline of the Lower Eocene low angle, high amplitude anomalies in figure 4.12 locates these features above the Renee Ridge. These Lower Eocene amplitude anomalies are described below.

4.1.4.2. Description of Lower Eocene amplitude structures

4.1.4.2.1. Well calibration

Of the 12 wells in Blocks 21/3, 4 and 5 only one well (21/5-1 : figures 4.13 and 4.14) fully penetrates the "V" structures, a second well, (21/5-3 : figure 4.15 and 4.16) clips the very edge of one of these cone shaped anomalies. Of the remaining wells, the Lower Eocene section has a high gamma ray, shaley, wireline character. The two wells that penetrate these cone shaped anomalies have a blocky wireline character equating to sand.

Well 21/5-1 has three sand layers :

upper sand - 20 metres thick

middle sand - 25 metres thick

lower sand - 15 metres thick

Well 21/5-3 has an interbedded section of thin sands which has a combined thickness of:

sand layers - 10 metres

Geoseismic summary figure 4.17 is a west/east transect through UK Blocks 21/3, 4 and 5 showing the relationship between Lower Eocene wells which penetrate only shale and wells 21/5-1 and 3 which penetrate the Lower Eocene low angle high amplitude anomalies. All the above thicknesses are measured depth along hole, with the 21/5-1 well deviated 30 degrees within the Lower Eocene from the vertical into a structure dipping at 20 degrees in the same direction. In this well true sand thickness is half the above value (10m, 12.5m and 7.5 metres respectively). Well 21/5-3 is a near vertically drilled well into the edge of a structure dipping at 10 to 20 degrees. Measured depth sand thickness approximates to actual thickness of the sand bed.

Sonic values of the Lower Eocene sands are acoustically faster than the surrounding clays. In addition the upper massive sand in well 21/5-1 exhibits fast, sonic spikes at the sand/shale boundary. It should be noted that neither well was cored in these intervals. Calibrated to seismic these well petrophysical characteristics produce a strong positive event at the upper shale/sand boundary and a strong negative event at the lower sand/shale boundary in the sandy horizons in wells 21/5-1 and 21/5-3. It should be noted that well 21/4-4 contains a basal twenty metre thick (20 msec TWT) sand (figure 4.17) calibrated to Lower Eocene strong amplitudes.

4.1.4.2.2. Seismic interpretation

A maximum amplitude extraction, taken between 30 to 70 milliseconds two way time above the top Palaeocene structure contour map (figure 4.18), exhibits a Northwest oriented set of amplitudes in blocks 21/4 and 21/5. These amplitudes represent the cone shaped amplitude anomalies of the Lower Eocene. They are characterised on vertical seismic profiles by their distinctive "V" shaped profiles, and their high seismic amplitudes in comparison to the low amplitude of the background sedimentary units in the Lower Eocene interval containing them (figure 4.19). They

are confined to the interval between two regionally correlatable marker horizons, the Top Balder and the Top intra-Lower Eocene. The basal apices of the amplitude anomalies are usually angular, occur close to the Top Balder surface, and significantly, often coincide closely with fault offsets of that surface (figure 4.19).

The amplitude anomalies consist of a strong peak and trough ranging from about 10-30 milliseconds in time 'thickness'. The acoustic character of this doublet reflection is found to be fairly uniform within the context of a single conical anomaly as noted from the strong amplitude extraction map (figure 4.18), seismic cross sections (figure 4.21 and 4.23) and timeslices (figure 4.27). The conical shape of these anomalies has been established by mapping the zero crossing within the reflection doublets using sequential lines at a 12.5m spacing. Figures 4.20, 4.22 and 4.25 are three structure contour map examples of these Lower Eocene conical amplitude anomalies. The individual conical amplitude anomalies have been displayed in three-dimensions to outline their geometry (figure 4.24). The circular to sub-circular planform geometry is one of the characteristic features of these anomalies.

Figure 4.26 and 4.27 are images of the Lower Eocene sequence of part of UK Blocks 21/4 and 5 using the Charisma function called Geocube. Geocube allows a cube volume view of the seismic data. These inline, crossline and timeslice views of the Lower Eocene interval shows the conical nature of the high amplitude anomalies and how they appear to tip out basally near the Top Balder surface (figure 4.27). Figure 4.26 is a timeslice 30 milliseconds below the previous Geocube figure. Note the apparent similarity in plan view dimensions of polygonal faults to the Lower Eocene conical amplitude anomalies. Typical dimensions of the anomalies are 0.5 to 2km in diameter, and 100-300m in vertical extent. The flanks dip inwards at between 5° and 25° (uncorrected for compaction).

The Lower Eocene amplitude map (figure 4.18) reveals a NW-SE trending zone of high amplitude, consisting of two regions of almost continuously high amplitude response (region I and II), separated by an intervening region with a blobby, discontinuous patchwork of high amplitude features with generally circular or elliptical planform geometry (region III). Highlighted on this image are the three sub-areas containing the examples (A, B and C) of individual conical amplitude anomalies (figures 4.20, 4.22 and 4.25). These are both located in the central region

(III) of discontinuous amplitude response. The more continuous regions (I and II) also consist of conical amplitude anomalies, but they are closely spaced or even compound in form (figure 4.28a) rather than isolated as in figure 4.28b. These cross sections show a suite of "V" shaped amplitude anomalies set in a background of generally low amplitude reflections. Importantly, it has been noted that the Lower Eocene strata containing the amplitude anomalies is pervasively deformed by small normal faults with modest throws (<50 milliseconds two way time – Tervoort, 2000; Lister, 2000). These form part of the polygonal fault network recognised on a regional scale at this stratigraphic level (Tervoort, 2000; Lister, 2000).

The precise observation and quantification of polygonal fault geometry and displacement over UK North Sea Blocks 21/4 and 5 has been made by Tervoort (2000) on prominent reflectors within the Oligocene. Polygonal fault geometry and fault plane dip within this interval are respectively similar to the plan view geometry and dip of the Lower Eocene high amplitude cone shaped anomalies. Within the Lower Eocene as demonstrated above, structure contour mapping of the cone shaped amplitude anomalies is possible. The surrounding Lower Eocene shale prone section however has few mappable horizons to display the exact nature of the relationship of the polygonal faulting to the cone shaped amplitude anomalies. Fortunately a small area immediately west of the Lower Eocene amplitude anomalies about well 21/5-1 allowed mapping of the plan view geometry of the polygonal faults over a 6km by 6km area (figure 4.29). Plan view geometry indicated a polygonal fault pattern, with fault displacements between 10 to 50 msecs. Polygonal fault dips appear similar to the dip of the conical amplitude anomalies (5 to 25 degrees) as can be seen on east west seismic lines figure 4.30, 4.31 and 4.32 through these features.

The relationship of the polygonal faults to Lower Eocene amplitude anomalies is encapsulated with figure 4.33. This figure summarises a detailed series of 4 msec TWT interval time slice interpretations from near Top Balder to near Top Lower Eocene over the region of isolated cone shaped amplitude anomalies. This figure highlights the following:

(i) Top Balder faults appear to follow the basal termination of many of the amplitude anomalies.

(ii) Planform polygonal fault geometry at 60 and 80 msecs TWT above the Top Balder surface, where observable, appear to be the same scale as the conical amplitude anomalies.

The external and internal stratal relationships to the amplitude anomalies are not sufficiently precisely constrained to allow the conclusion that the high amplitude doublet reflections are discordant with the stratal reflections in the post-Balder interval. The relationship between stratal reflections on either side and internally of the inclined high amplitude reflections is not clear, and has not been possible to correlate any marker horizons from one side to the other. However, if the dip of the Top Balder and Top Lower Eocene is assumed to be concordant with that within the Lower Eocene interval, then the Lower Eocene amplitude anomalies would cross cut Lower Eocene strata.

The above relationships are interpreted as showing that the amplitude anomalies are preferentially developed along fault planes. Polygonal fault systems commonly exhibit complex linkage geometries between variably striking fault planes, and it is common for linked faults to form polyhedral forms including cones, pyramids and prisms (Cartwright, 1994a, b). It is probable, therefore, that the sand bodies responsible for the conical amplitude anomalies have adopted a geometrical form based on the geometry of the pervasively developed polygonal fault system affecting the Lower Eocene.

4.1.5. Interpretation

No reports exist in the literature of directly comparable structures imaged by seismic data to those described here. We considered the possibility that the amplitude anomalies could be wholly primary sedimentary features, such as channelised turbidite deposits. The cross-sectional geometry of the amplitude anomalies does resemble the seismic expression of channel bodies developed within some highly channelised turbidite deposits (Pickering *et al.*, 1995). In addition, the location of the study area is in a base-of-slope position, so it is ideally located for this type of deposit. However the continuous nature of the amplitude anomalies from the base to the top of these fetaures is difficult to explain in a primary depositional channel. The

amplitude equates to a near constant sand thickness, which in a deepwater channel is nearly impossible as sand deposited within such a channel would be deposited either at the base and/or on the side. In the case of the sand at the side of the channel, this would be gravitationally unstable and probably collapse to the lowest part of the channel. As a result it would be expected that the resultant amplitude for this primary depositional scenario to have a basal amplitude related to the sandy "channel" fill and the sides of the "channel" to have a variable amplitude responses (discontinuous deposited sand/gravitationally collapsed). It is far more probable that these conical amplitude anomalies are some type of post-depositional feature formed from a possible Lower Eocene deepwater sand. From a review of the literature, only two possible genetic mechanisms match most of the basic observations described above. These are discussed in turn below:-

4.1.5.1 Sea bed pockmarks

Pockmarks form by the explosive venting of gas and water through a muddy substrate (Hovland and Judd, 1988). They do not occur in sandy substrates. They are circular or elliptical in plan view and commonly have steep margins that are often modified by collapse after initial excavation. Pockmarks have been documented to be up to 500m in diameter (Prior *et al.*1989), though they are more commonly less than 100m wide. They are often lined at their bases with muddy or sandy rubble related to the ejection of primary sedimented material. A recent study of a 3D seismic survey from UK Quad 15 (Cole, 1998) has found evidence of palaeo-pockmarks at a similar stratigraphic level to the amplitude anomalies described within the Upper Palaeocene/Lower Eocene Balder horizon. These circular to elliptical structures have diameters of 1-2km, and are up to 100m deep (figure 4.34), and are filled with sand (figure 4.35 for well calibration) transported from the nearby shelf margin. These Quad 15 pocks have some similarities with the amplitude anomalies in our study area, but they differ in having flat bases, and only limited development of any flanking high amplitude reflections. These features are interpreted to have formed by escape of fluids from basinal sediments through the Balder aged shelf sands of UK Quad 15 (figure 4.36).

The similarity in scale with the amplitude anomalies of UK North Sea Block 21/3, 4 and 5 and the naturally conical geometry of pockmark craters of UK Blocks 15/18 are strong arguments in favour of a pockmark origin for the amplitude anomalies in the study area. However, it is difficult to explain the consistency of the amplitude response over the flanks of the cones over vertical distances of over 100m unless there was a crater of this depth which was filled entirely with sand (figure 4.37). This would imply that a pockmarked region was subsequently the locus for a major sand depositional episode (figure 4.37), and this filled all the craters developed on the seabed. Whilst not impossible from a paleogeographic perspective, this model does call for a uniform thickness of sand to have deposited at the base of the pockmarks and also along the sides. This would be required to have stayed gravitationally stable, without collapsing to the centre of the pock. It is likely depositional thickness in a pockmark would be variable and that post deposition, sand would likely collapse/slump to the centre of the pocks. This would give variable seismic response from thicker sands at the centre of the pock with amplitude thinning upwards along the sides of the structures. This is not seen on seismic, where the seismic response of the "anomaly" remains constant from base to top. We also need to ask why there was a region of intense pockmark development in this specific area in the first place. This could be explained as the study area is located over a regional high that may have acted as a focus for expelling basinal fluids, leaking to palaeoseabed to create the pocks. In summary, pockmarks offer a possible analogue for the structures described from the study area but the constant amplitude seen on seismic from the top to the bottom of these conical features does not favour a pockmark interpretation at present.

4.1.5.2. Sandstone intrusions

An alternative model to pockmarks is that of post-depositional remobilisation and intrusion of fluidised sandstones. Processes of liquefaction and fluidisation of previously deposited deepwater sands have been invoked in several recent studies of Eocene reservoirs in the North Sea to explain sandstone dykes and sills observed in cores and on 3D seismic (Alexander *et al.*, 1992, Newman *et al.*, 1993; Dixon, 1995; Lonergan and Cartwright, 1999). Common to these studies is the concept that

depositionally isolated sandbodies could have become overpressured during early burial, and then liquefied through an external triggering mechanism such as earthquake shaking or hydrocarbon migration. Sandstone intrusions are widely described in the literature (Allen, 1982). Most published descriptions of sedimentary intrusions involve sandstone dikes or sills injected into finer-grained strata (e.g. shales). However, the vast majority of the described examples involve relatively small-scale intrusions with thicknesses generally less than a few metres. Descriptions of reservoir-scale intrusions are rare, namely the tectonically influenced intrusions from the Miocene of the coastal region of central California (Newsom, 1903; Thompson 1995, 1996; Molyneux, 1999) and the Precambrian of the Southern Front Range, Colorado (Harms, 1965). These rare examples do show, however, that larger-scale intrusions are physically possible.

A model for the formation of the Lower Eocene amplitude anomalies of UK Blocks 21/3, 4 and 5 as sandstone intrusions is envisaged as follows (figure 4.38):

• Lower Eocene claystones with a very fine grain size were deposited with a thickness from 200-400m, and soon after deposition, polygonal faults began to deform this interval (figure 4.37a)(Cartwright, 1994a, b). These claystones formed a very effective top seal to underlying deepwater sandstones of late Palaeocene and early Eocene age. Note, that nearby wells updip from the study area indicate the presence of a deepwater turbidite sand fairway of early Eocene age (Fina UK pers.comm., 1997), hence the possibility that the sands in the cone shaped anomalies may have originally been deepwater turbidite sands. Pore fluids within the deepwater sands were probably trapped by the claystone seals above, and by isolation from updip migration routes.

• The location of the study area above a regional structural high (4.37b) meant that this area was an obvious focus for any aqueous and hydrocarbon fluids that were being expelled from the Jurassic kitchen areas and overlying Cretaceous mudstone and chalk successions. The onset of hydrocarbon generation in the local kitchens surrounding the study area has been constrained as late Palaeocene by thermal and maturity modelling (Mason *et al.*, 1995, figure 4.39). Fluids (particularly gas) migrating vertically at crestal leak-off points from the Jurassic into the Cretaceous

and reaching Palaeocene or Eocene sands that were already possibly overpressured could further inflate their fluid pressure because of the highly impermeable overburden of Lower Eocene shales.

• Pressure inflation within the shallow sand reservoirs would not by itself initiate liquefaction (Nichols, 1994, 1995), and some form of triggering mechanism is required. Two possible triggers are considered (figure 4.37c): (1) propagation of polygonal faults into the top of the sandbodies, or (2) earthquake events. Polygonal faults are known to have been forming at this time and were locally influencing deposition and remobilisation in the nearby Alba Field (Lonergan *et al.*, 1998; Lonergan and Cartwright, 1999). Propagation of normal faults into pressure-inflated and possibly gas-charged sandstones may have been sufficient by itself to initiate upwards injection along the fault planes. The elevated pore-fluid pressures in the sandstones and immediately overlying topseal units could have reduced local values of effective stress sufficiently to allow dilation of the fault planes and facilitate upwards injection.

Equally plausible is the role of earthquakes, during which large volumes of water/gas could have been seismically pumped upsection (Sibson 1975, 1994; Jaffri, 1993; Muir Wood, 1994) from nearby basement faults flanking major structures such as the Renee Ridge. Although these basement faults were not reactivated in any major phase of movement in the Eocene, minor inversion events with a strike-slip component are known from this area (R. Laver, personal communication, 1997). The fluid flux during and after earthquakes and the shaking during the earthquake are both contributory factors that could have initiated liquefaction in shallow sands (c.f. Reimnitz and Marshall, 1965). Upwards injection of these sands would follow the same routes for easy exploitation of injection-related failure of the top seal as above i.e. along existing polygonal fault surfaces wherever possible.

• Upwards injection would have been limited by the bleed-off of pressure in the sands as they were transported upwards. Upwards transport was probably by fluidised flow i.e. where the sand grains are moved by the velocity of the pore fluids (Nichols *et.al.*, 1994; Nichols, 1995). To achieve sufficient fluid velocity, the pressure differential between the site of liquefaction (the sandbody) and the upward limit of

the intrusion must be sufficient that frictional effects do not dominate and prohibit sand transport. Given the shallow depth at which this process may have been occurring (<500m), it is possible that the sandstone injections propagated to the seabed, and formed sand volcanoes (4.37d). The area about well 21/4-4 appears to be located about the high point of the regional structural high called the Renee Ridge and as such may have been the locus of any fluid migration. About this area (region I) it should be noted that several amplitudes (figure 4.17) exist calibrated to sands throughout not just the Lower Eocene, but the whole Eocene. The lateral extent of these amplitudes is not more than a few kilometres laterally and may document a series of sandy intrusions and/or palaeoseabed pockmarks/seabed sand extrusions. Pressure communication between the source sands and the seabed would have provided a large pressure differential to sustain a fluidised flow, and gas expansion during ascent could have played a major role in maintaining upward velocity (Jenkins, 1930). This might explain the observation that the upper limits of the amplitude anomalies are at a consistent stratigraphic horizon, presently about 300m above the Top Balder (approximately 500 m before compaction). Sandstones are occasionally found at this level, and it is also possible, therefore, that they may have been extruded and reworked locally.

4.1.5.3 Deep versus shallow origin

Currently the amplitude anomalies are at 2000 metres below sea level which is the maximum burial depth (M.Cope pers.comm., 1999). The possibility exists that the intrusions may have formed at these depths. It is considered unlikely that intrusion occurred at these deeper depths as all the cone shaped intrusions have upper terminations against an intra Lower Eocene marker, which appears to be a shale/shale boundary. As explained, extrusion of sand at the palaeo-seabed would explain a shallow origin of the cone shaped anomalies, but once buried this boundary has the same lithological characteristics above and below i.e. clay. It is difficult to understand how this boundary would act as a subregional cap to these injected features if they formed at great depth.

4.1.6. Summary

In conclusion, the preferred model for the amplitude anomalies in the study area is that they represent conical sandstone injection structures into a pre-existing low angle polygonally faulted very fine grained clay during or very soon after deposition of this clay. The source for the sand may either be stratigraphically autothonous i.e. from within the Balder or Early Eocene or, more speculatively, could be allochthonous i.e. from source units within the Palaeocene (or deeper?). The injection mechanism may have been triggered by overpressure release due to local fault propagation, or driven by external triggers such as seismic pumping during earthquake events. The presence of a Jurassic hydrocarbon kitchen below (which in this area was close to the oil window in the Eocene), would have supplied gas and oil charged gas during the Eocene with gas expansion potentially playing an important role in the injection mechanics.

4.2. Outcrop analogues

Several geometrically similar, low angle, cone shaped sandstone intrusions have been identified in the literature and subsequently studied in the field. Though of variable origins and of small scale, they all show that this low angle, cone shaped geometry is possible.

4.2.1. Tourelle Formation sandstone intrusions, Ordovician deepwater sediments of Quebec, Canada.

4.2.1.1. Location and geological setting

The Ordovician Arenigian aged Tourelle Formation crops out in the Quebec Appalachians (St-Julien and Hubert, 1975) and is characterised by thick-bedded, coarse, massive sandstones. Small scale clastic intrusions, mostly low angle dykes and sills have been documented by Hiscott (1979) within this Tourelle formation at Cap Ste-Anne, along the southern shore of the St. Lawrence River (figure 4.40). Steeply dipping strata along a 100m wide wave cut platform allowed detailed re-examination of these intrusions.

The Tourelle Formation conformably overlies the Lower Ordovician Cap des Rosiers Group (Hiscott, 1979), which he interprets as a slope and base of slope assemblage dominated by interbedded red or green shale and abundant thin rippled, dolomitic siltsones. It is within this basal zone that the clastic injections of fine, medium and coarse grained sandstones are located (figure 4.40).

4.2.1.2. Description of small scale sandstone intrusions

This basal zone of intrusion measuring 70m from base to top of section and extending 100m parallel to bedding along the wave cut platform, was studied by undertaking the following:

(i) Photographing the exposure from a nearby cliff section and undertaking a detailed line drawing of the exposure in the field (figure 4.41)

(ii) Undertaking 3 sedimentary logs from the base to the top of the exposure to document lateral changes in sill and dyke location (figure 4.42).

(iii) Photographing and detailed line drawings in the field of individual dyke and sill geometries and relationships (figures 4.43, 4.44, 4.45 and 4.46).

4.2.1.2.1 Facies description

(A) Claystone purple/grey

Description

Purple to dark grey, mm bedded, clay grade, claystone. Rare *Zoophycus* trace fossils.

Environment of deposition

Deepwater hemipelagic claystone (low energy deposit with deepwater trace fossil *Zoophycus*) in association with other deepwater facies.

(B) Interbedded fine sandstone and claystone commonly current rippled (mm to cm bedded)

Description

Interbedded very well non calcareous cemented fine sand, laminated sandstone with minor interbeds of mm laminated claystone. Sandstone current rippled throughout. Beds millimetre to centimetre thick

Environment of deposition

Low energy turbidite waning flow division Tc (Bouma 1962) of current rippled sands with claystone interbeds recording suspension drop out from a very dilute, low energy flow.

(C) Interbedded fine sandstone and claystone (cm to dm bedded)

Description

Interbedded very well cemented non calcareous cemented fine sand grained, laminated sandstone with minor interbeds of mm laminated claystone. Beds centimetre to decimetre bedded.

Environment of deposition

Sand packages representing high energy turbidite flows with claystone interbeds recording suspension drop out from a dilute, low energy flow.

(D) Massive sandstone

Description

Very well non calcareous cemented fine to medium grained pale buff to light brown sand, occasionally micaceous. Individual beds may vary between 50 to 1000 centimetres, be stacked/amalgamated, massive and contain rare low angle centimetre to metre scale cross beds and very rare planar laminations. Bases of individual units are occasionally erosive with rare granule grade lags. Individual units are flat topped with erosive bases and thin and thicken across the scale of the wavecut platform.

Environment of deposition

Channelised (?) and/or sheet (?) turbidite sands, occasionally stacked on top of eachother.

(E) Massive intrusive/remobilised sand

Description

The predominant sandstone intrusion is of sandstone bedding parallel sills, 1 to 500 cm thick, formed of fine to medium grained sand very well non calcareous cemented, with a massive appearance. Subordinate to the sills are variably angled discordant to bedding dykes with the same massive appearance. The sand appears very light grey to white in colour which is very different from the other sand facies. Intrusions are sharp topped and based but where they terminate can end in a bulbous termination or split into further, but less thick intrusions (figure 4.43 and 4.44). This leads to rapid changes of bed thickness across the outcrop. Intrusions will often exhibit jacking up of the beds as they have intruded into the country rock (figure 4.45). Over the portion of the wavecut platform immediately above the Cap des Rosiers Group shales and the base of the massive turbidite sand, *all such massive sands are intrusive*. All the massive sands step upsection at some point, either as steeply dipping dykes or < 20 degree dipping dykes (figure 4.42). This stepping up section of intrusions if extrapolated as an angle would approximate to a 5 to 20 degree angle (uncompacted), similar to the "V" structures of UK blocks 21/3, 4, 5, though of a smaller scale. Finally, a low angle intrusive dyke exists in this outcrop (figure 4.46), which mirrors the geometry of the "V" structures, being fed from a high angle basal dykes.

4.2.1.3. Interpretation

Hiscott (1979) interpreted this seventy metre thick section of sandstone intruded turbidite succession to have been caused by liquefaction/fluidisation and injection laterally of an out of plane of section turbidite sand body (figure 4.47). Hiscott (1979) summised the injection process to have been relatively early after sedimentation, approximately 20 to 60 metres below palaeo-seabed as many of the dykes are severely ptygmatically folded. This outcrop confirms that low angle sandstone intrusions occur and significantly affect sandstone distribution. The origin of the intrusive complex, if correct, may be an explanation for the Lower Eocene UK block 21/3, 4 and 5 high amplitude structures, where an isolated deepwater sand body is interpreted to have remobilised along the edges of the body to create intruded "wings" off the side.

In this case, injection occurs along polygonal faults. Intrusion occurs at the edge of a turbidite sand body has most probably occurred due to an increase in pore pressure due to sand volume reduction.

Lonergan *et al.* (1999) outline a similar scale intrusion with near identical features to the Tourelle Formation within deepwater sediments of the Ordovician Rosroe Formation of Western Ireland. These sands have been interpreted by Archer (1984) to represent turbidite deposits formed within the North Mayo Trough, Western Ireland. The dominant intrusive mechanism is via sills and occurs in two ways:

(i) Stoping - where the host sediment is incorporated as rafts within the intrusion (figure 4.48A). this process forms fingerlike, sharp injections into the surrounding strata, similar to figure 4.43 of the Tourelle Formation

(ii) Dilation - the forceful pushing apart of the host sediment to create space, with the cohesistivity of the host sediment controlling the emplacement mechanism (figure 4.48B). This creates bulbous ended sills which show deformation about the injection tip, similar to figure 4.44 of the Tourelle formation.

Within both the Rosroe Formation and to some extent the Tourelle formation, several remobilisation features occur (figure 4.49): (a) fluidised beds, (b) dewatering pipe structures, (c) ball and dyklets, (d) wings, (e) dykes, either stoped or blunt ended and (f) sill and dyke complexes.

4.2.2. Baldwin Creek Upper Miocene sandstone intrusions, Santa Cruz County, California, USA.

4.2.2.1. Location and geological setting

Clastic intrusions of Late Tertiary age crop out over a broad area from eight to fifteen kilometers west of the town of Santa Cruz, California, USA (figure 3.38) in both quarries (Eldridge, 1901) and along the coastal sea cliffs (Newsom, 1903). The intrusions represent the upward, fluidized injection of sands from the Santa Margarita Sandstone into fractures within the overlying Santa Cruz Mudstone (Clark, 1981; Eldridge, 1901; Newsom, 1903; Page and

Holmes, 1945; and Phillips, 1981) (figure 3.39). The timing of intrusion is poorly understood, but has been attributed (Casey Moore pers.comm. 1998) to the Pacific plate reorientating 4 Ma (Atwater, 1998).

4.2.2.2. Description of small scale sandstone intrusions

Sandstone intrusions in Baldwin Creek are small scale, unlike the associated giant scale intrusion at Yellow Bank Creek (described in chapter 3) five kilometres east. A set of intrusions at Baldwin Creek are exposed on a wave cut platform. These intrusions are a series of low angle (<45 degrees), subcircular conical sandstone intrusions between 5 and 50 centimetres thick, fed by near vertical (>45 degrees) sandstone intrusions between 5 and 50 centimetres thick. Figure 4.50 is a line drawing of the wavecut platform that the intrusions are exposed. Figures 4.51 shows a "V" shaped intrusion in the cliff and figure 4.52 the low angle sandstone intrusions on the wavecut platform.

4.2.3. Horton Bluff formation storm related sandstone dykes and collapse structures in lake sediments of Devonian-Carboniferous age, Nova Scotia, Canada.

Horton Bluff on the Bay of Fundy, Nova Scotia contains spectacular examples of small scale sandstone dykes. These downwardly injecting intrusions resulted from the sudden deposition of lens shaped storm deposited sand bodies on a muddy lake floor, and are formed within the Devonian-Carboniferous Horton Bluff formation (Martel *et al.*, 1993). The intrusions were previously described by Hesse and Reading (1978) as upwardly injecting sand dykes. These sand bodies are postulated to have subsequently failed concentrically forming low angle circular collapse features.

4.2.3.1. Location and geological setting

The Horton Bluff Formation and overlying Cheverie Formation, together comprise the Horton Group (Bell, 1929), of Tournaisian age (Bell, 1960; Utting *et al.*, 1989) in the Wolfville-Truro region of Nova Scotia (figure

4.53). The outcrops studied at Horton Bluff were interpreted previously as an ancient lake sequence based upon fossils (Bell, 1960) and reptilian and amphibian populations (Carroll *et al.*, 1972; Sarjeant and Mossman, 1978).

4.2.3.2 Facies description

The sediments at Horton Bluff comprise repeating lacustrine cycles of 1 to 10 metres thickness (Martel *et al.*, 1993) as noted from sedimentary logging (figure 4.54). Each sequence (figure 4.55) fines up from (A) offshore fine grained clays with fish and ostracods; into (B) storm generated hummocky cross stratified siltstone to fine sandstone; (C) shore face wave-rippled sandstone; (D) shore face planar-bedded siltstone containing mudcracks and tree casts; (E) lake fringing marsh green mudstones with roots, tree casts and mudcracks and (F) subaerial dolomitic soil horizons with roots. The dykes and circular "collapse" features occur within the hummocky cross-stratified siltstone to fine sandstone unit of facies type B.

The hummocky facies occur as lenses of silt and sand upto 40 cm thick, encased within the fine grained clays of facies A (figure 4.56). These lenses occur laterally at consistent stratigraphic horizons, are regularly spaced at between 30 to 150cm and are typically ovoid in plan view, 0.3-3 m wide and up to 6 m long. The top of each lens is convex up with shale layers onlapping this surface indicating surface topography generated by these sands. The base of the lenses are concave up and often show an erosive contact with the underlying shale. In other cases the basal sand contact has sunk into the underlying clay as balls and pillows. These lenses of sand contain low angle truncation surfaces and antiformal surfaces that are attributed to hummocky cross-stratification as described by Dott and Bourgeois (1982) and represent subaqueous sand deposition during a storm. The sand lenses may also contain planar laminated sand, massive to faintly laminated sand and are often capped by wave-rippled sands and silts. The dykes inject from the base of each of the lenses. The dykes range from 1 cm to 40 cm wide and 5 cm to 5 metres long. The dykes are ptygmatically folded, as a result of the greater compaction of the surrounding shale relative to the originally vertical sand filled dyke, a factor of 2.3 times in

this case (Martel *et al.*, 1993). Ptygmatic folding is a common feature of dykes that have been injected into surrounding sediment during early burial. Shale compacts at a greater rate than the vertical sandy dyke and as a consequence, the vertical dyke compresses to give this "snake like", ptygmatic appearance. Consequently, the dykes original length is much longer than seen in outcrop today. It is also important to note that the dykes as well as the sandy lenses appear to have a consistent orientation. The dykes and sandy lenses are parallel to wave ripple crests which are parallel to the palaeo-shoreline (Martel *et al.*, 1993), implying that wave action was a possible control on dyke formation.

4.2.3.3. Description of circular "collapse" features

The circular "collapse" structures as described by Hesse and Reading (1981), occur within the centre of the hummocky sand lenses. They measure between 3 to 15 m across (figure 4.57) and are circular in plan view. In cross section (figure 4.58), within the flat lying hummocky cross-stratified lenses, the central portion displays steep (up to 70 degrees) dipping beds on the outside of the circular structures with dip decreasing to horizontal towards the centre. The centre of these circular features contain fractured and brecciated siltstone of the hummocky sand/silt facies. These circular collpase features are onlapped by Facies A offshore clays.

4.2.3.4. Interpretation

The hummocky sand lenses are interpreted by Martel (1993) as storm deposited, lens-shaped sandbodies on the low energy muddy lake bottom of the Horton Bluff Group (figure 4.59). These sand bodies formed oriented lenses, deposited parallel to the lake shoreline. The initial storm scoured into the muddy lake bottom. Subsequent sand deposition during and immediately after the storm, deposited hummocky cross-stratified sands, massive and faintly laminated sands, planar sands and finally wave rippled sands into scours. These represent a waning of the storm and deposition of sequentially lower energy bedforms. The deposition of rapidly deposited storm sands loaded the soft clay

of the lake floor, causing the clay within the first few centimetres of the lake bottom to act plastically, due to the surface sediments high initial pore fluid content, and formed load features. They are seen in the outcrop as sandy layers detaching into the soft clay layer below as balls and pillows of sand. Below the load structures, (5 to 25 cm below lake bottom) these clays underwent brittle failure represented by downwardly injected sand dykes. These dykes formed parallel with the impinging storm front (Martel *et al.*, 1993). Brittle, as opposed to plastic failure occured at this depth below the lake bottom as mud cohesion increased dramatically at shallow (possibly a few centimetres) depth below the sediment water interface as water was lost due to rapid compaction of overlying sediment (Martel *et al.*, 1993). Consequently the competency of the clay strata deeper below the lake bottom increases markedly and instead of plastically deforming as sandy load balls, the clay fails in a brittle sense, due to the deposited storm sand which inject downwards as sand dykes.

The sandy lenses continued to build up as a gentle mounded topography above the lake floor. In some cases these sandy lenses subsequently collapsed as circular faulted structures in the centre, due to possible gravity collapse or a further storm/earthquake event shocking the unconsolidated sandy lens and causing the sediment to fail.

The remaining geometry of mounded sandy lenses with circular collapsed central portions was subsequently mantled by clay, signifying a return to low energy conditions in the lake. Compaction over geological time, was greater in the surrounding clays than the vertical sandstone dyke. To accommodate the extra shortening of the clay, the dyke folded, forming "ptygmatic" folds. Figure 4.43 summarises the formation of these sandstone dykes. The assertion by Hesse and Reading (1981) that these dykes are injected upwards is incorrect, as in no case is the sandstone "source" bed for these dykes found at the base of the lower portion of any dyke, but always at the top of a dyke as the hummocky sand lenses. These hummocky sand lenses represent another low angle, conical sand filled geometry.

4.3. Summary

Low angle, cone shaped sandstone intrusions and cone shaped post depositional geometries occur at small scale, as seen by the field examples, and possibly at large scale in the subsurface seismic case study from the Lower Eocene of UK Blocks 21/3, 4, 5. From the injection examples outlined, their origin is common in that a sand body is required to be isolated within an impermeable unit such as shale. The triggering mechanism for injection requires a build up in overpressure (local sediment dewatering or tectonic focussing of basinally expelling fluids into the sands) and a sudden release of this overpressure by sudden shocking such as by a storm or earthquake. The depth of these processes is poorly constrained, except where ptgymatic folding of the sandstone intrusions can be measured or analysis of cement fabrics (relative compaction of sediment from minus cement porosity) can be undertaken. In the case of the Lower Eocene over UK Blocks 21/3, 4 and 5 no core material exists for such an analysis.

Figure 4.1. Location map of UK Central North Sea blocks 21/3, 4, 5 and 15/18 (partly from PESGB, 1997)

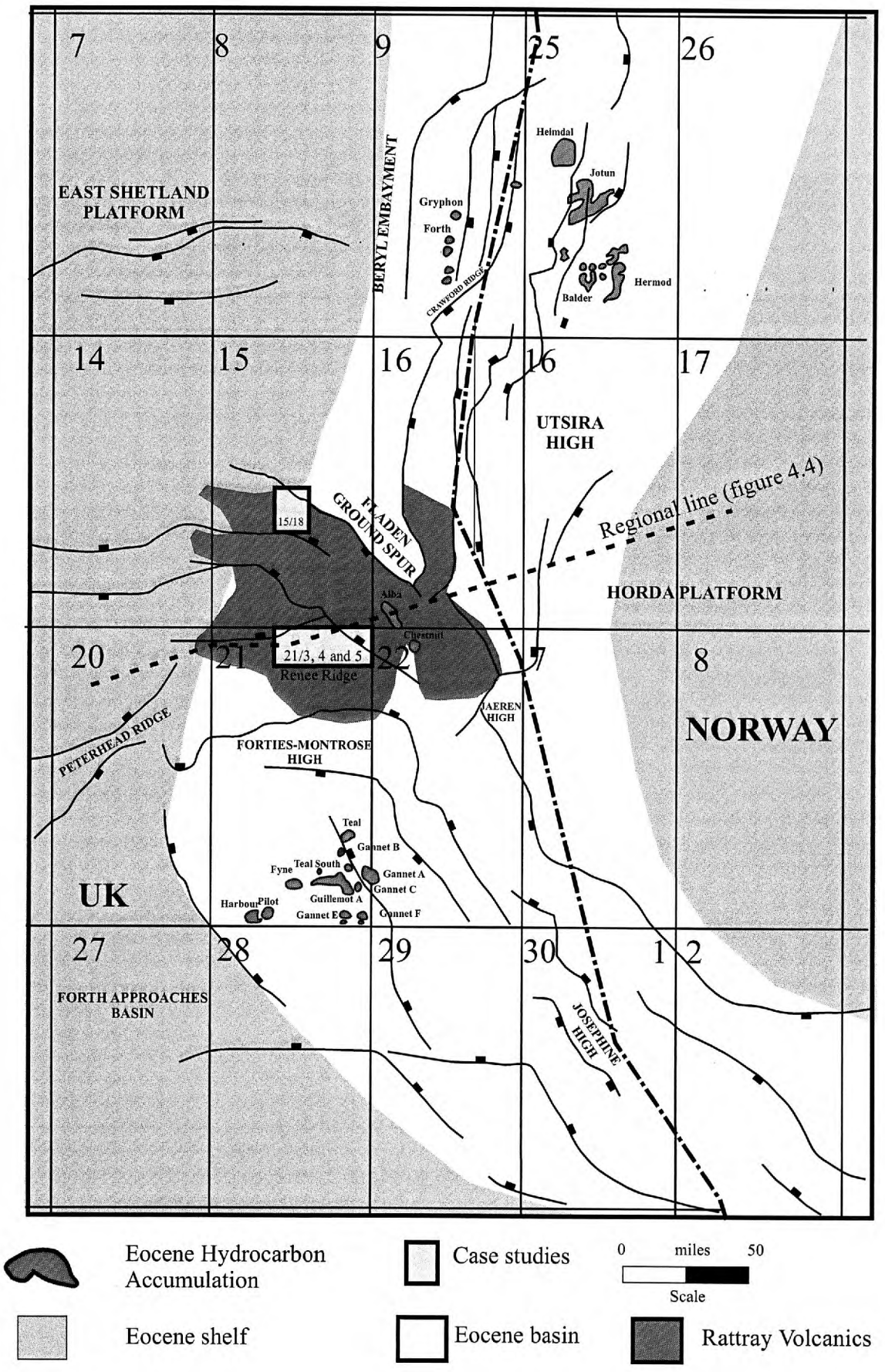


Figure 4.2. North Sea Palaeocene palaeogeography (redrawn from Sutter, 1980)

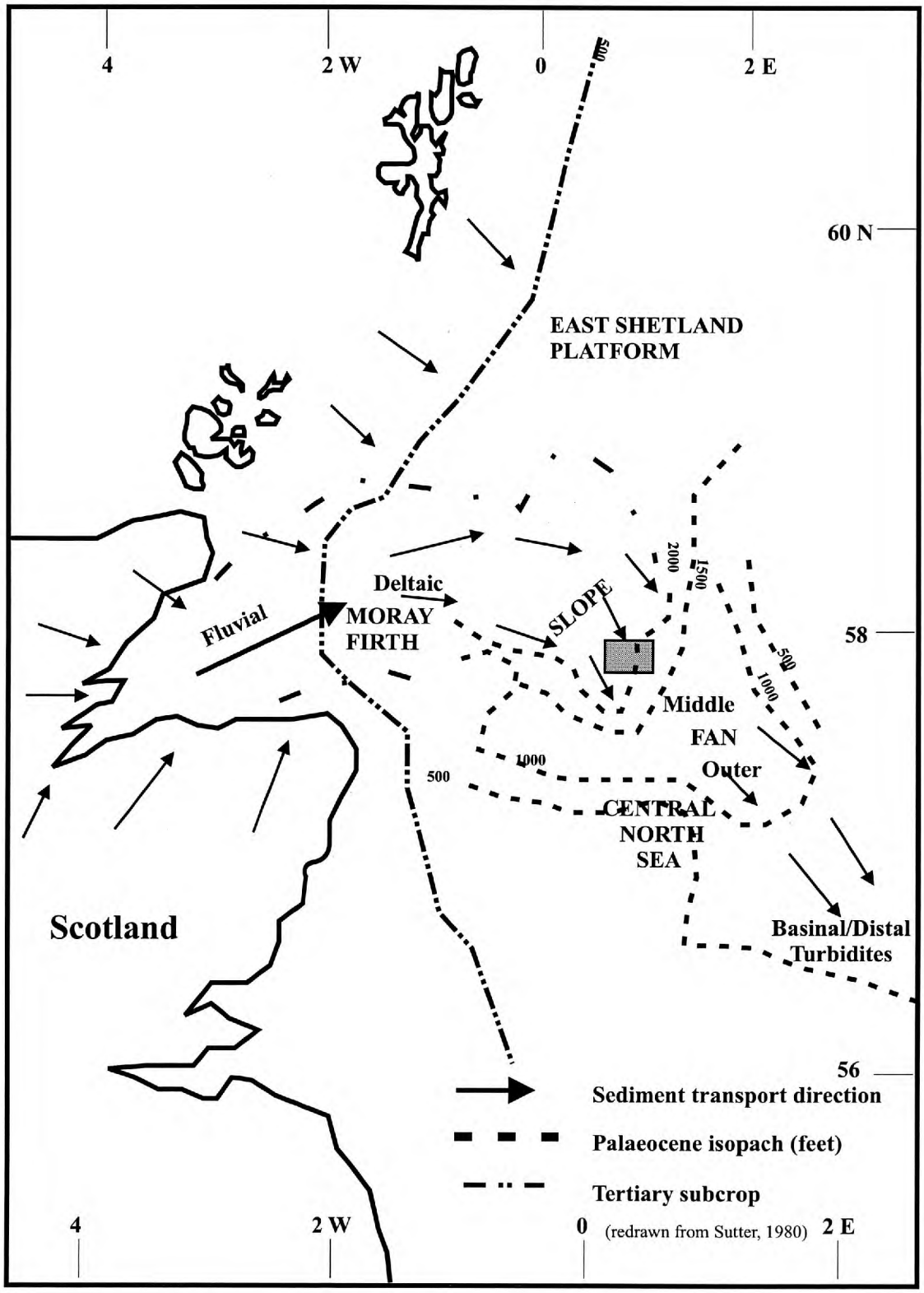


Figure 4.3. Forties palaeogeography map (deepwater sediments) about UK North Sea Blocks 21/4 and 5 (partially redrawn from Fina UK pers. comm. 1996)

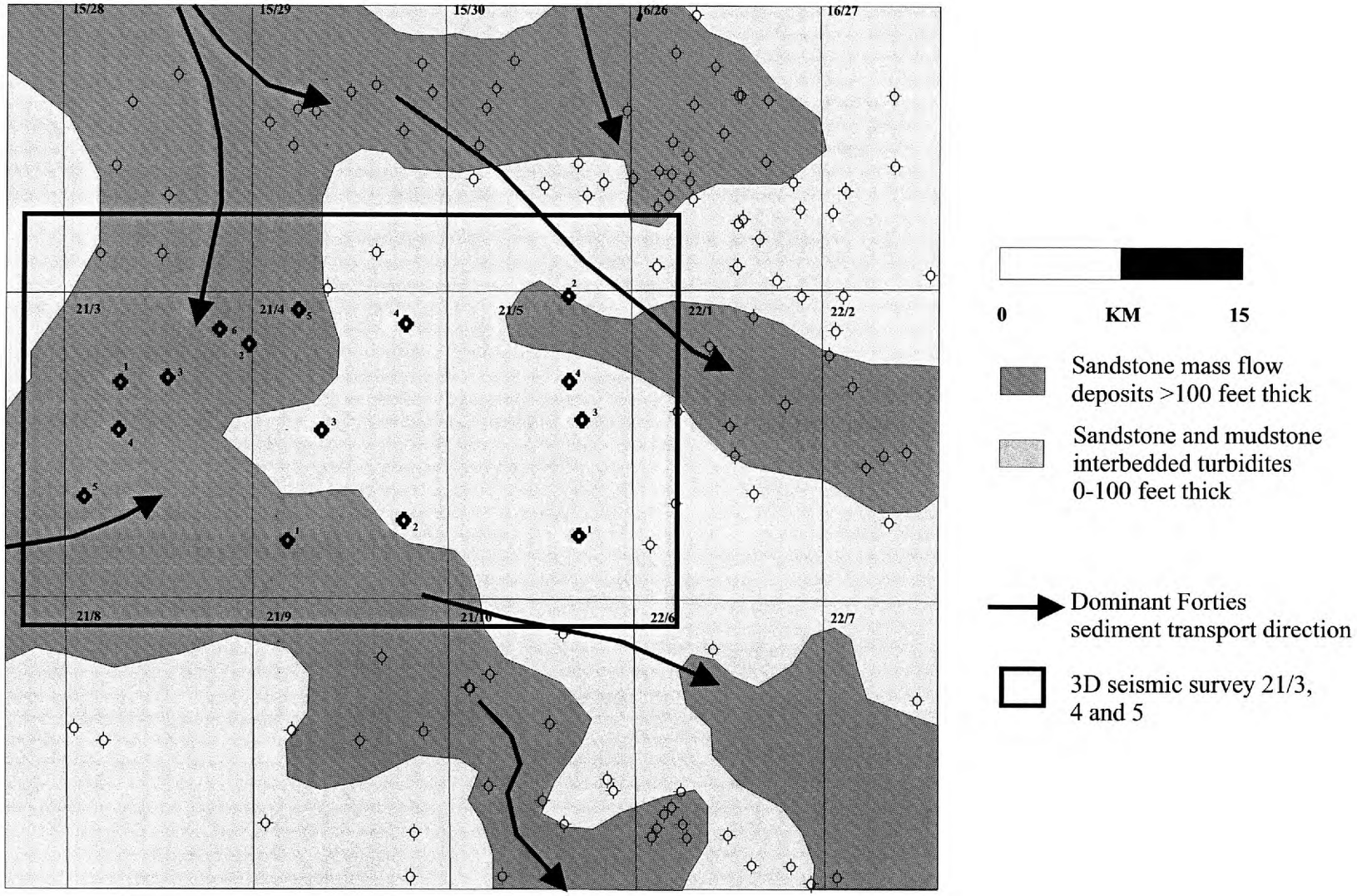


Figure 4.4. Geological cross section across the Central North Sea passing through UK Blocks 21/3, 4 and 5 (from CNST82-04 regional seismic line)

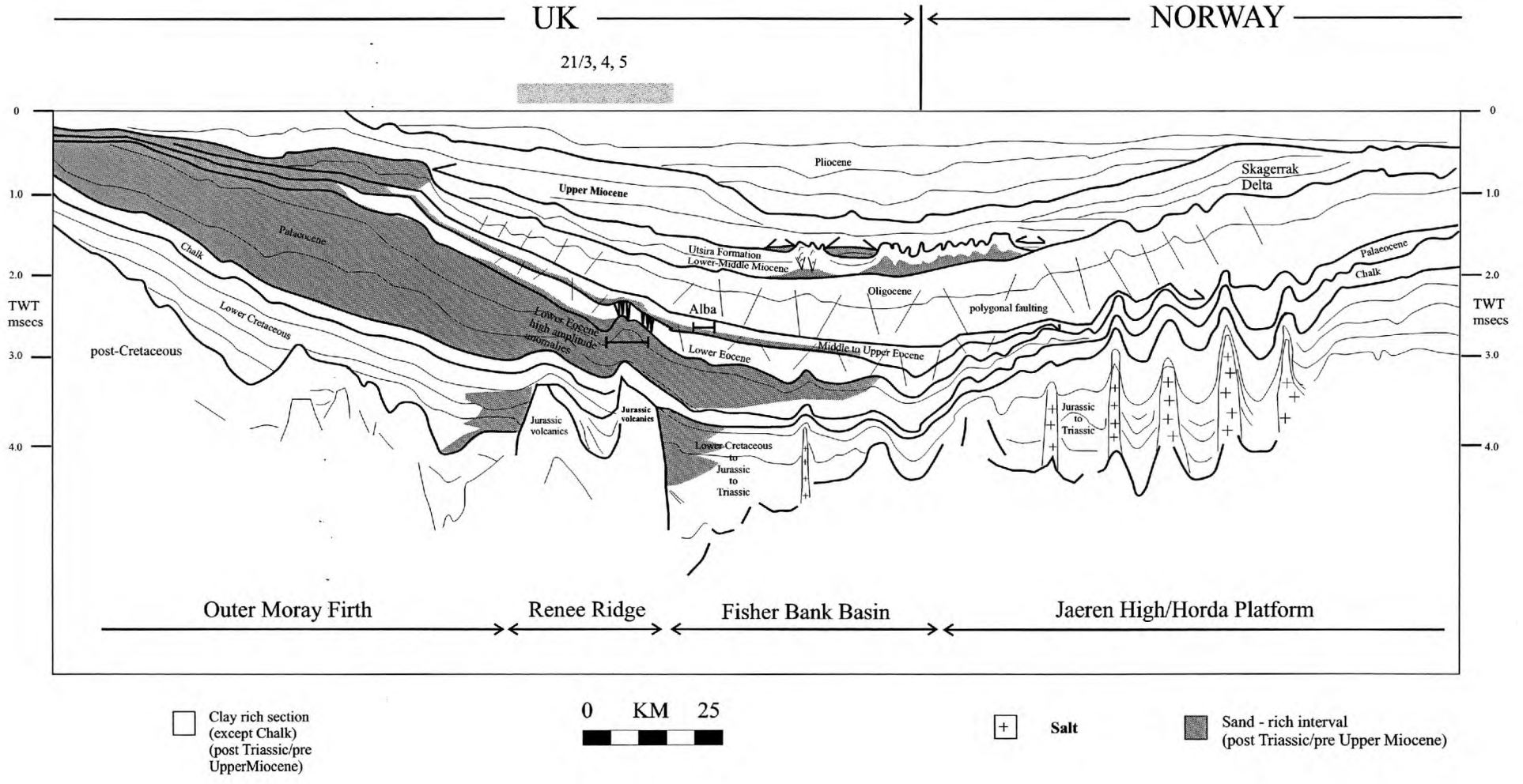


Figure 4.5. Lower Eocene palaeogeographic map of the North Sea (faults from PESGB, 1997)

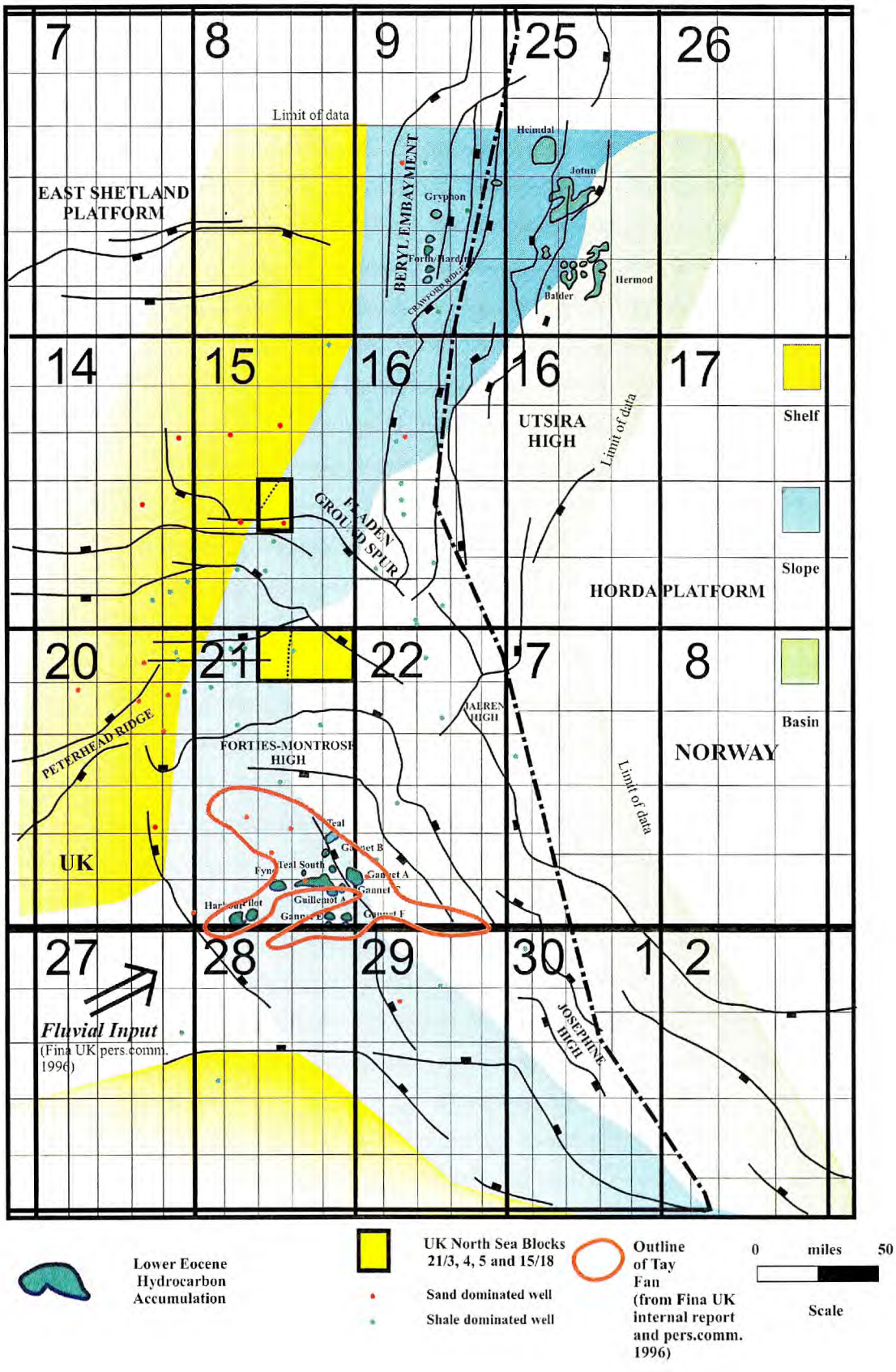


Figure 4.6. West/east seismic inline 3500 through UK North Sea Blocks 21/3, 4 and 5.

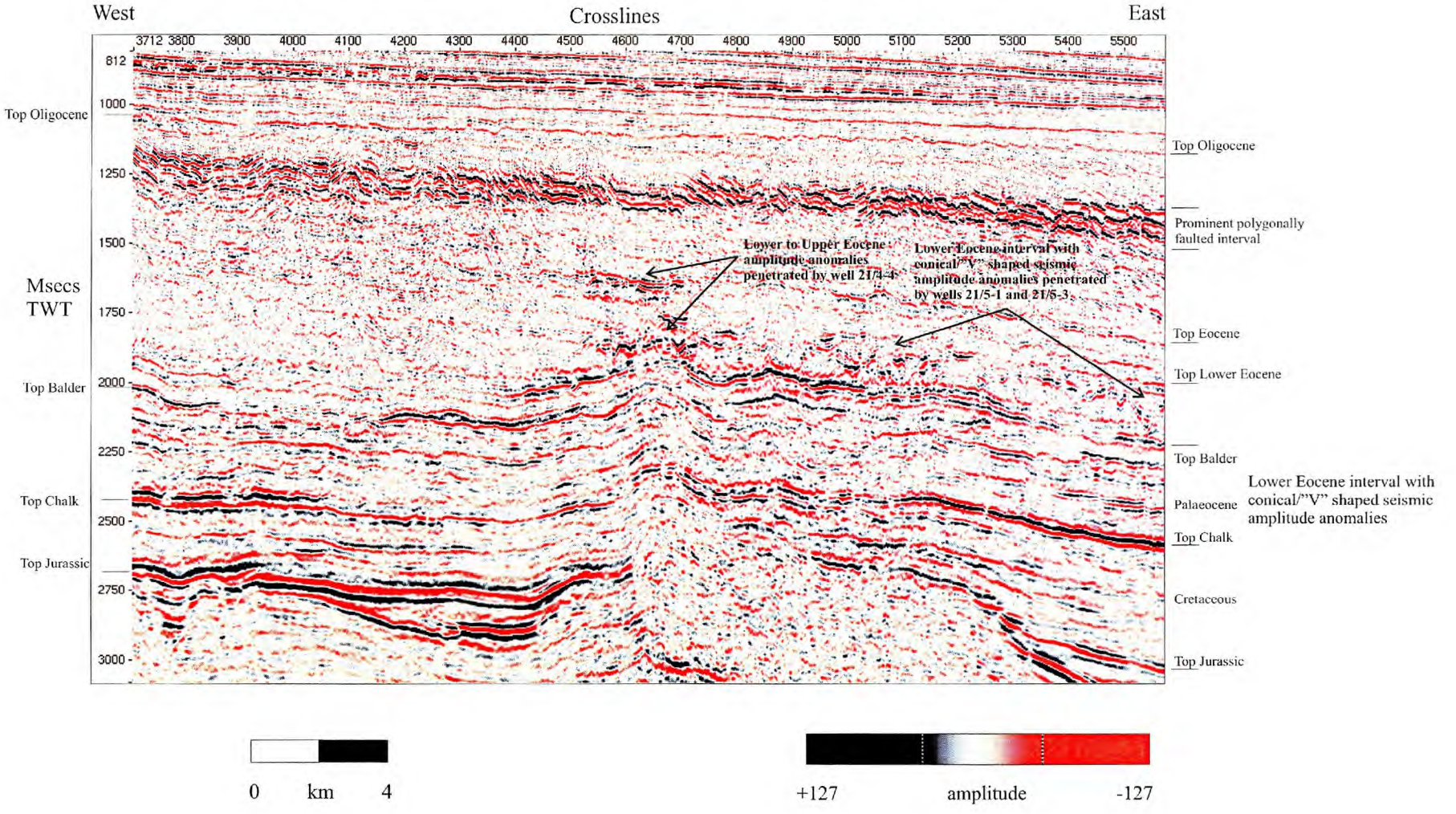


Figure 4.7 Near Top Jurassic two way time structure contour map over UK Central North Sea Blocks 21/3, 4 and 5

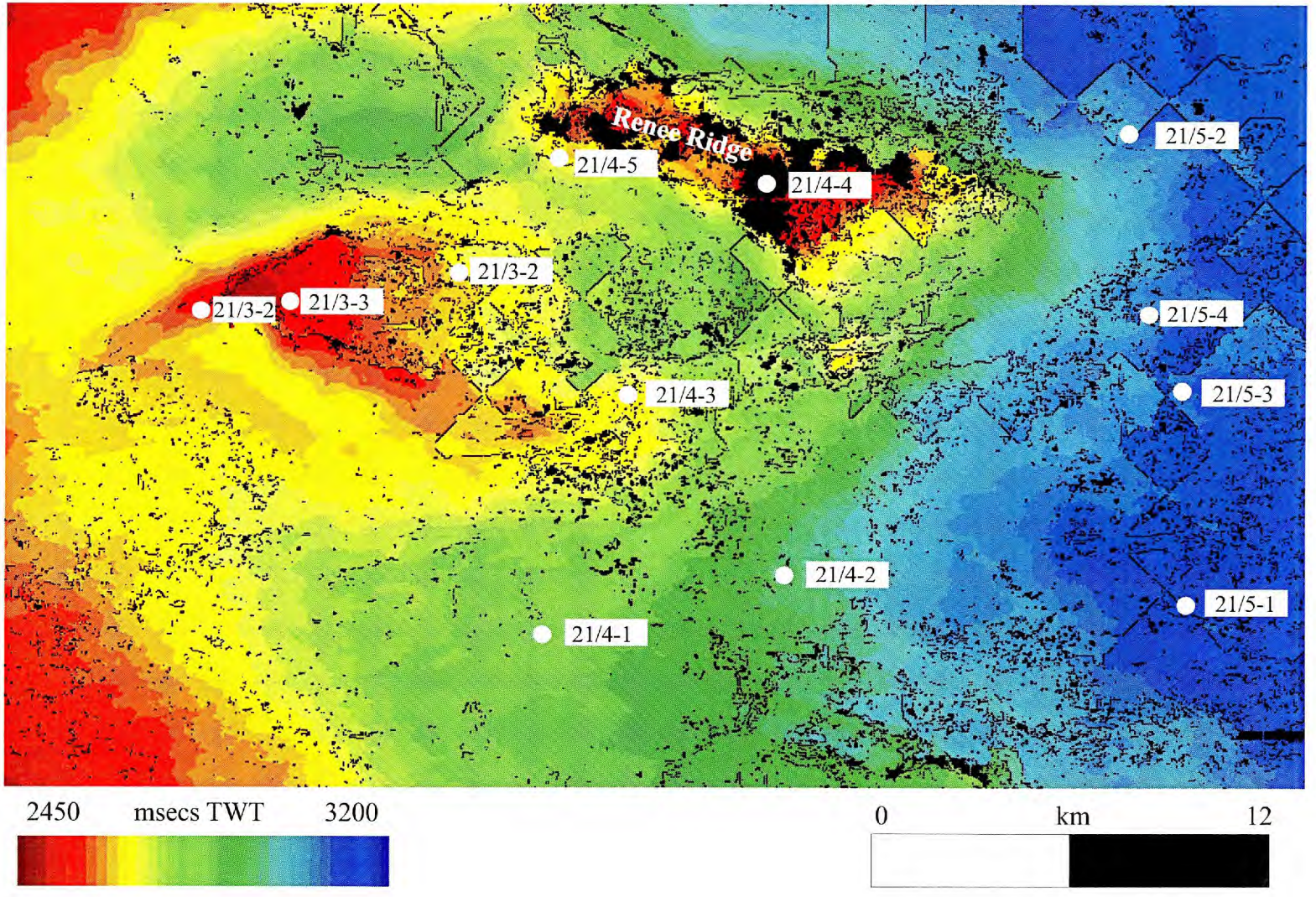


Figure 4.8. Top Cretaceous two way time structure contour map over UK Central North Sea Blocks 21/3, 4 and 5

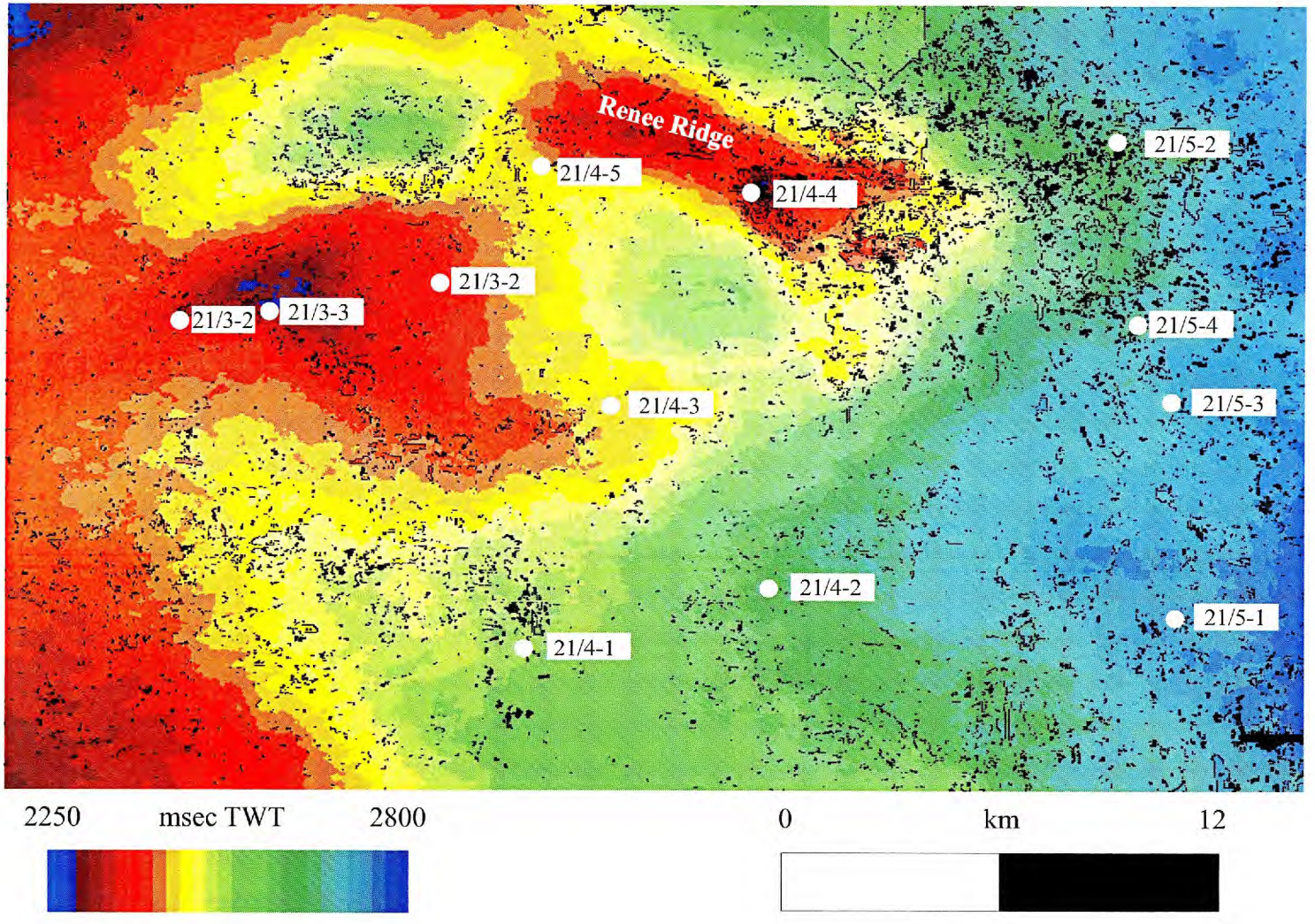


Figure 4.9. Top Palaeocene (Balder Tuff) two way time structure contour map over UK Central North Sea Blocks 21/3, 4 and 5

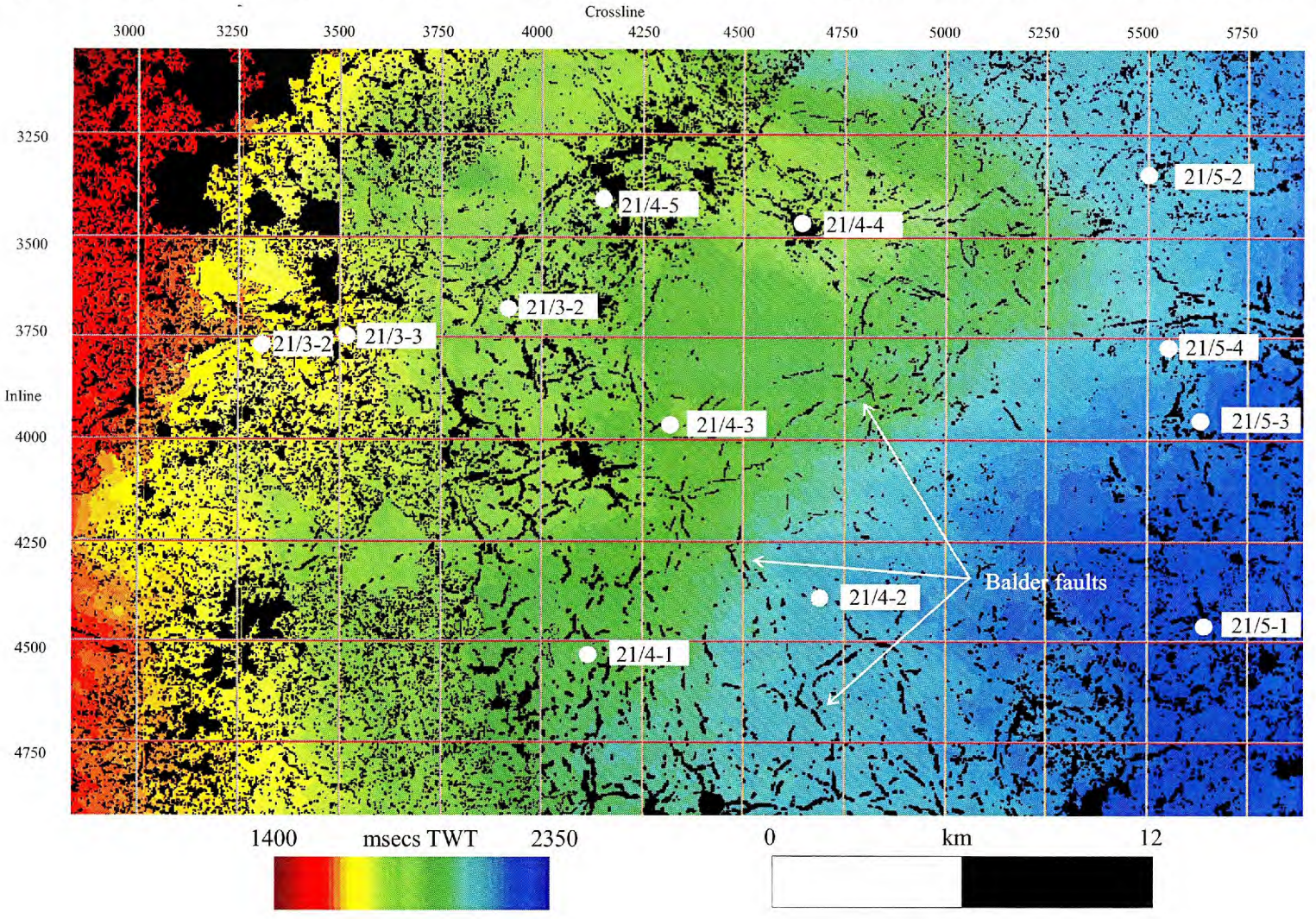


Figure 4.10. Two way time isopach between near base Jurassic and near top Jurassic over UK Central North Sea Blocks 21/3, 4 and 5

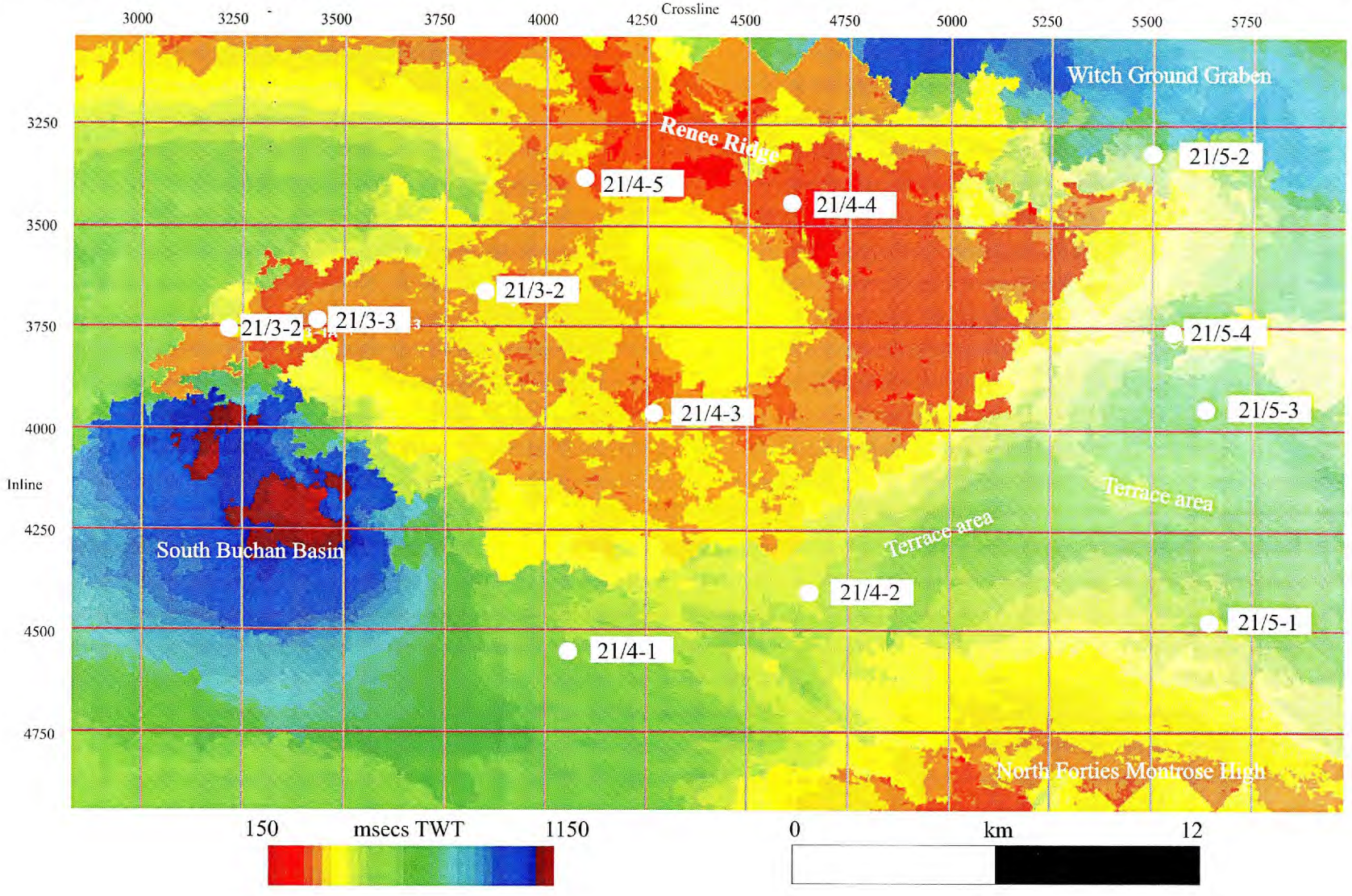


Figure 4.11. Two way time isopach between Top Cretaceous and Top Palaeocene over UK Central North Sea Blocks 21/3, 4 and 5

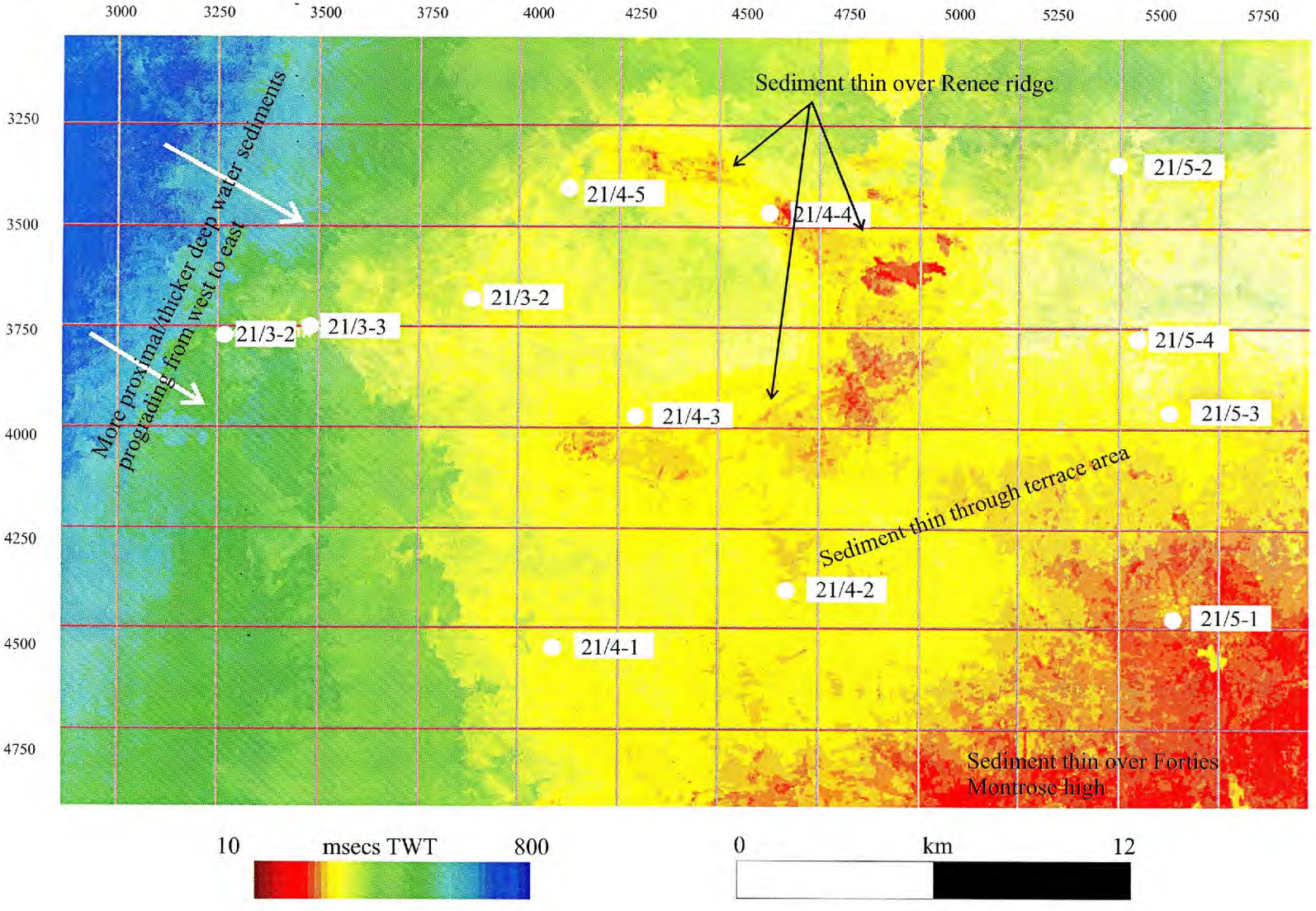


Figure 4.12. Structural elements map of the area about UK Central North Sea Blocks 21/3, 4 and 5 (partly from Fina UK pers. comm. 1996)

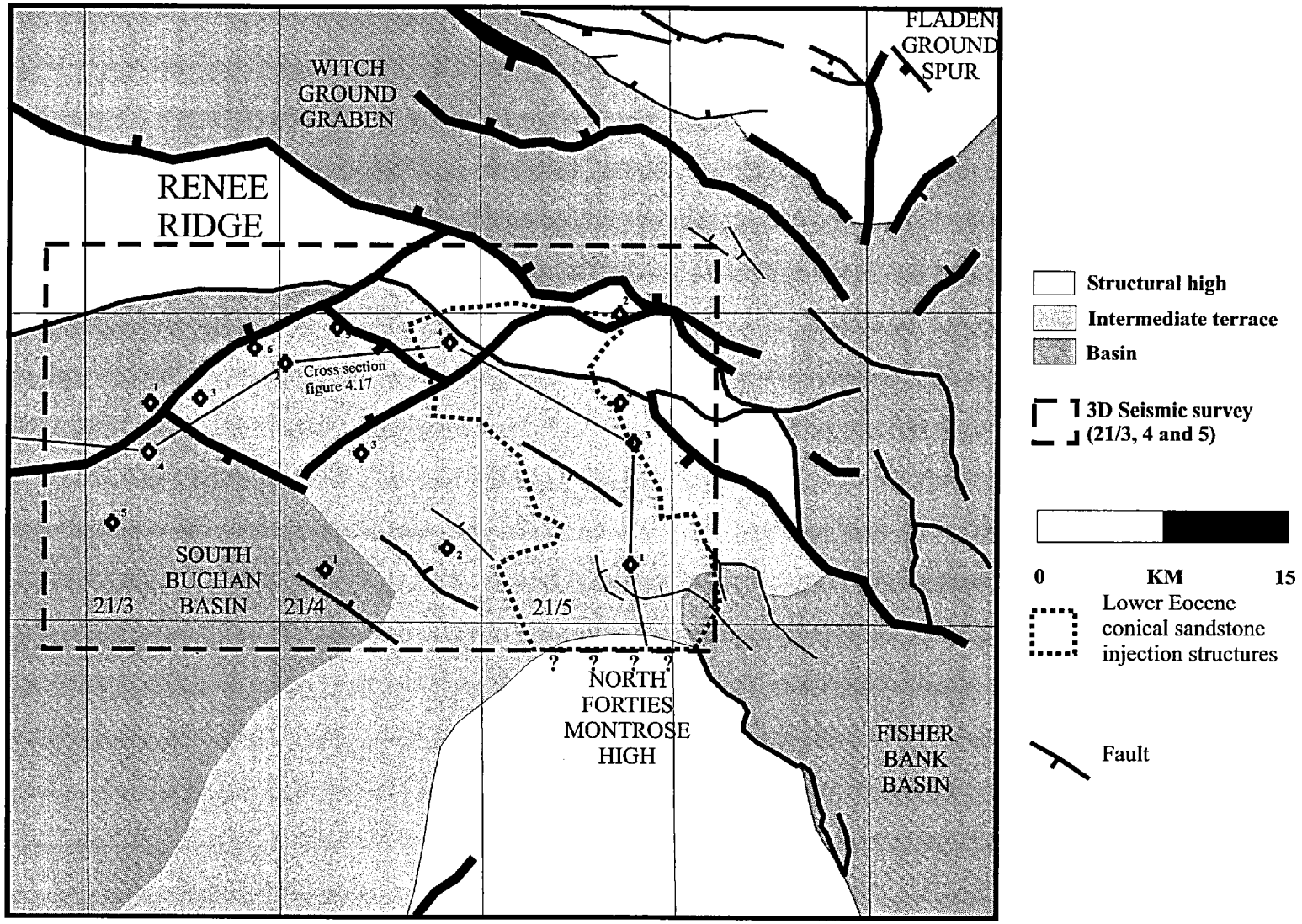


Figure 4.13. Composite log of UK North Sea well 21/5-1 over the Lower Eocene section

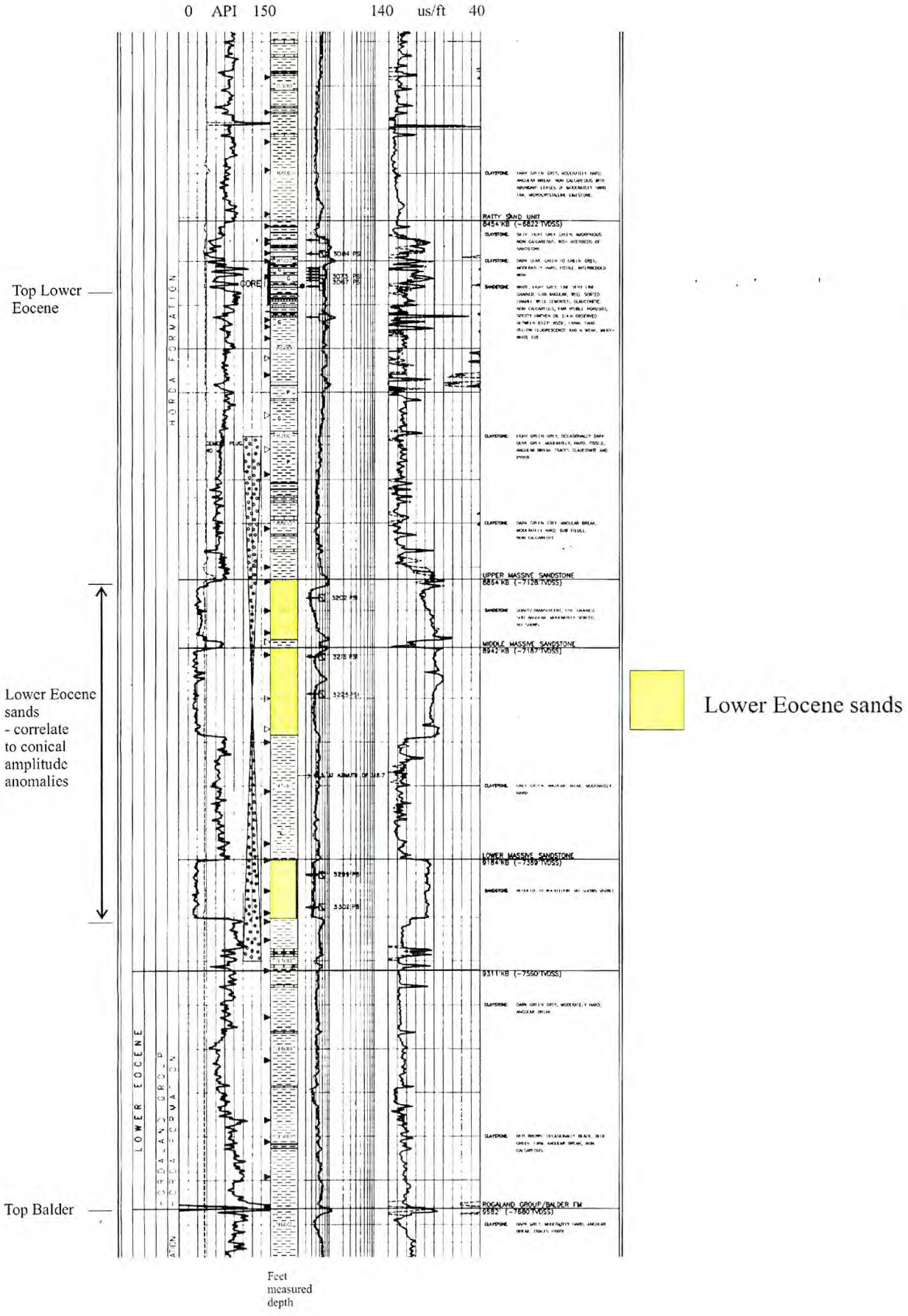


Figure 4.14. Seismic cross section of a polygonally faulted Lower Eocene section that contains a high amplitude, circular, low angle, cone shaped anomaly calibrated by UK North Sea well 21/5-1

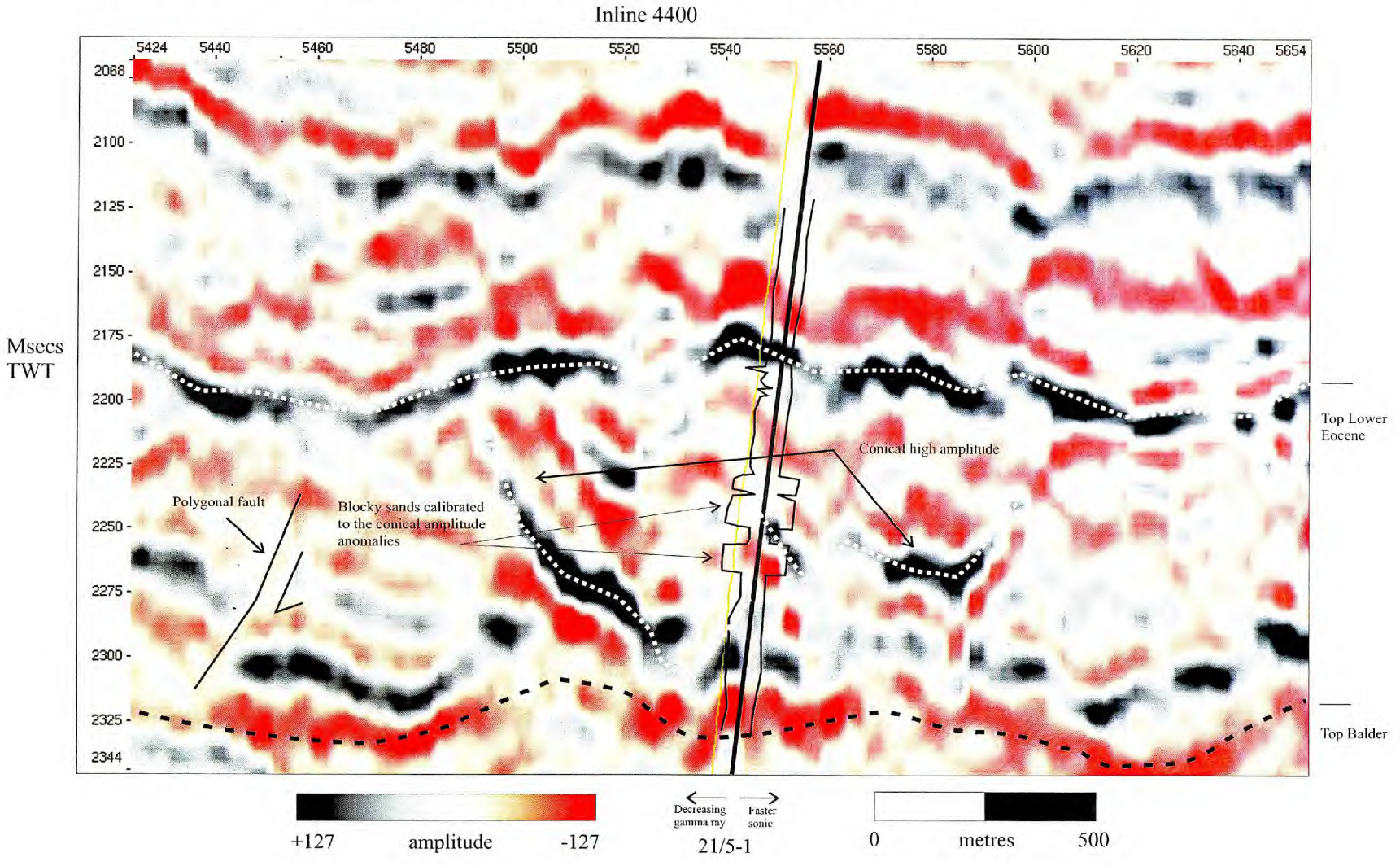


Figure 4.15. Composite log of UK North Sea well 21/5-3 over the Lower Eocene section

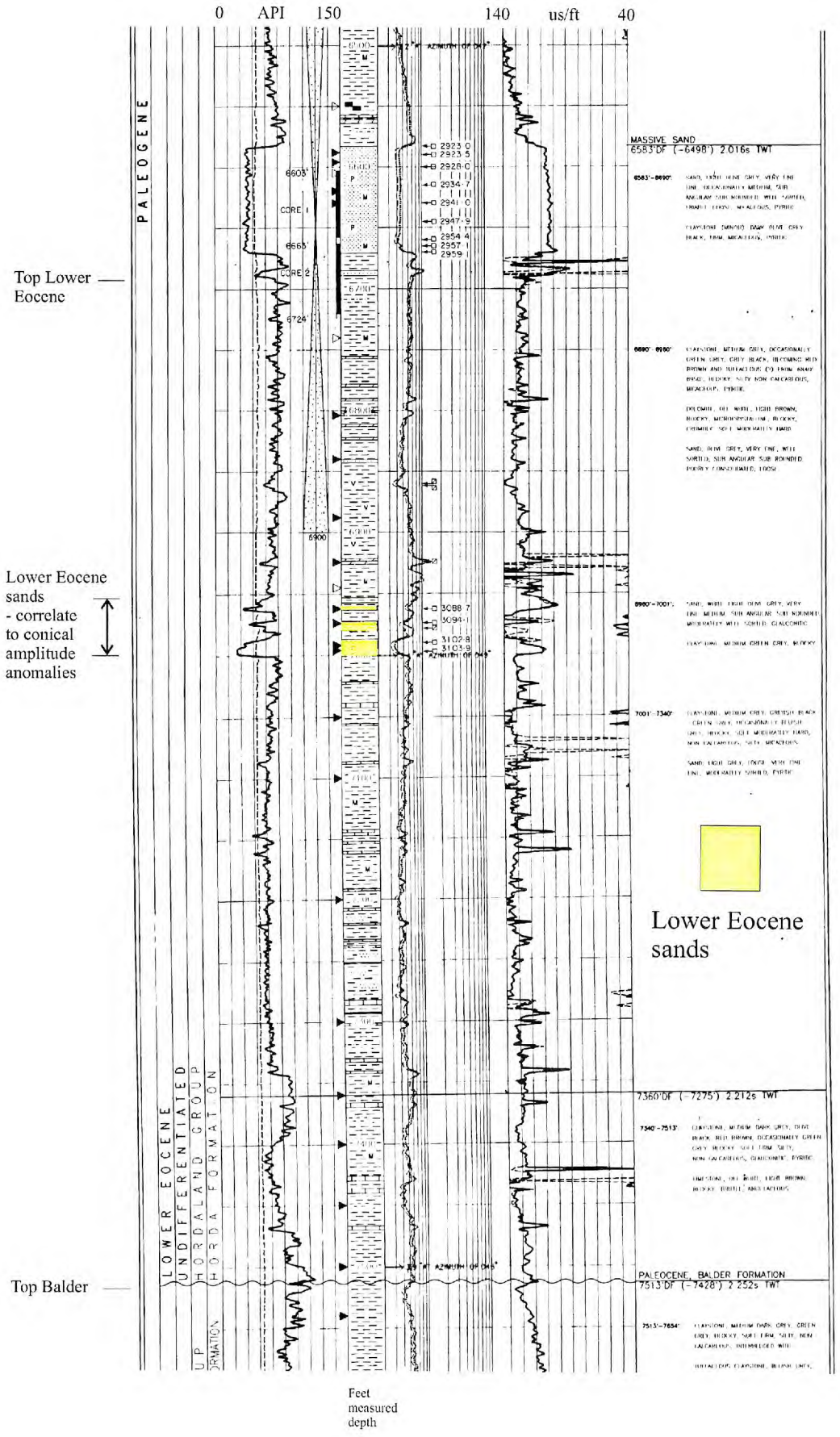


Figure 4.16. Seismic and well calibration of UK North Sea well 21/5-3 (inline 3968)

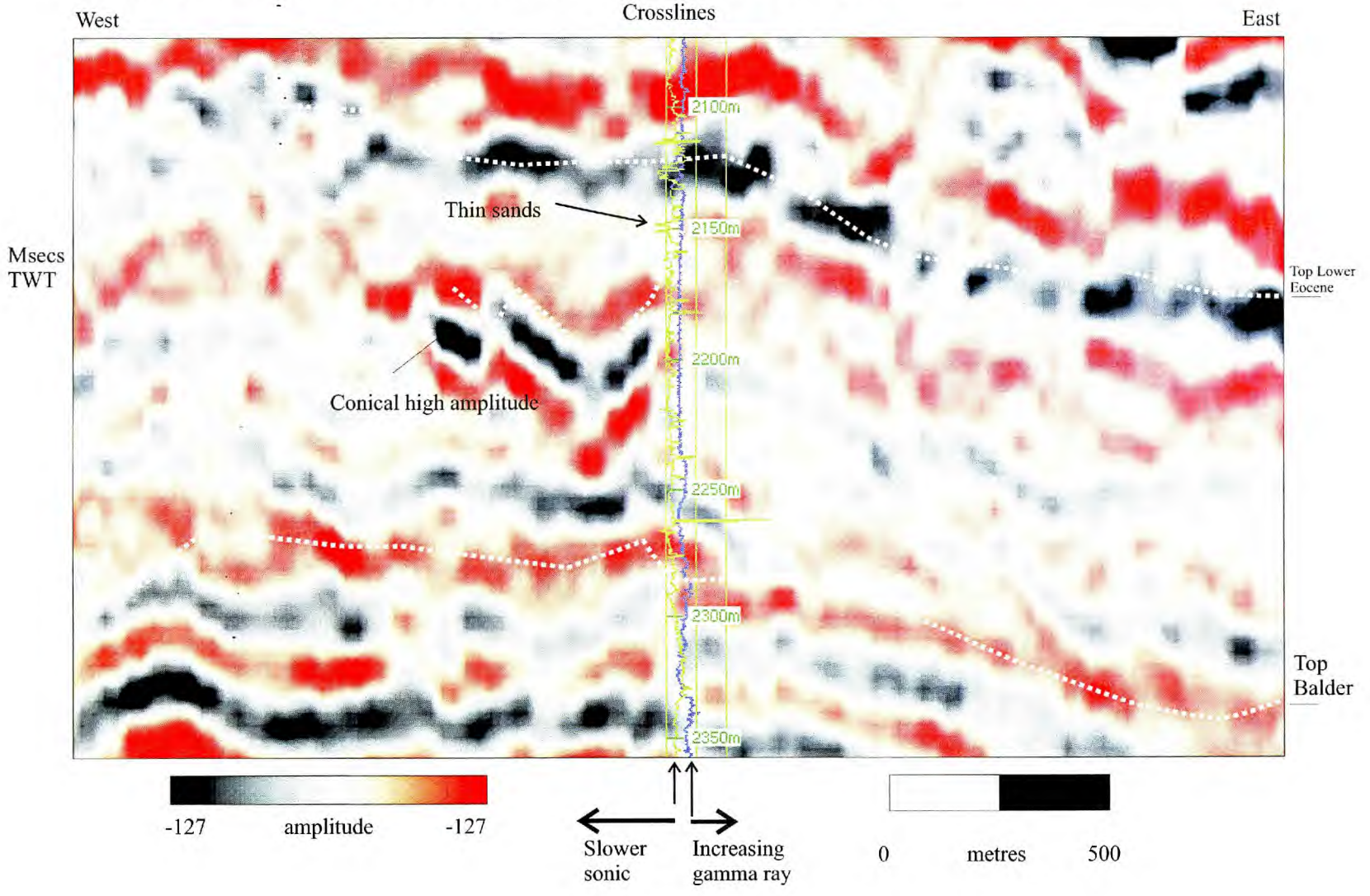


Figure 4.17. UK Central North Sea wells 21/5-1 and 21/5-3 which penetrate the Lower Eocene cone shaped amplitude anomalies

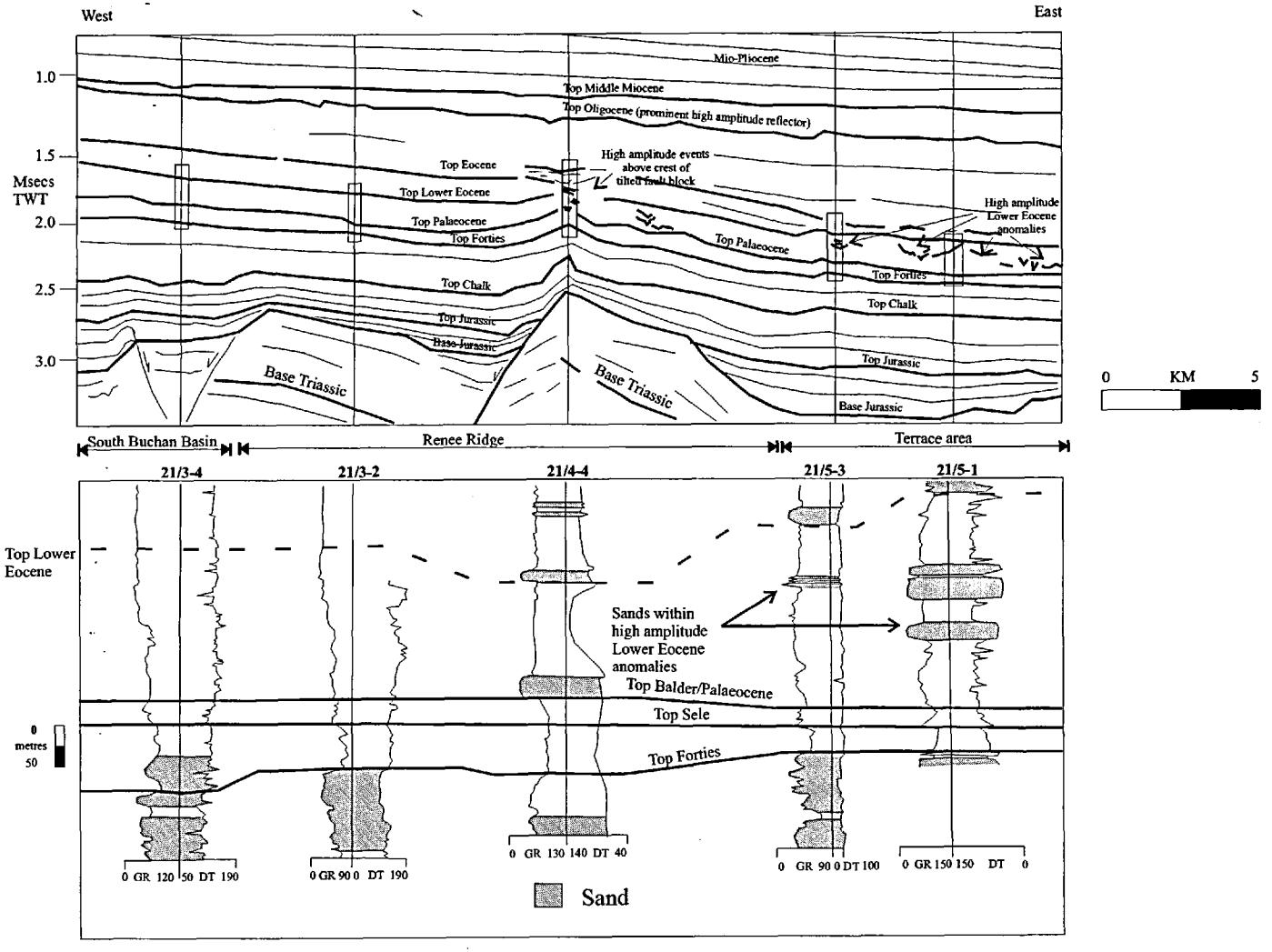


Figure 4.18. Maximum amplitude extraction between 30 to 70 milliseconds two way time above the top Palaeocene structure map over part of UK Central North Sea Blocks 21/4 and 5

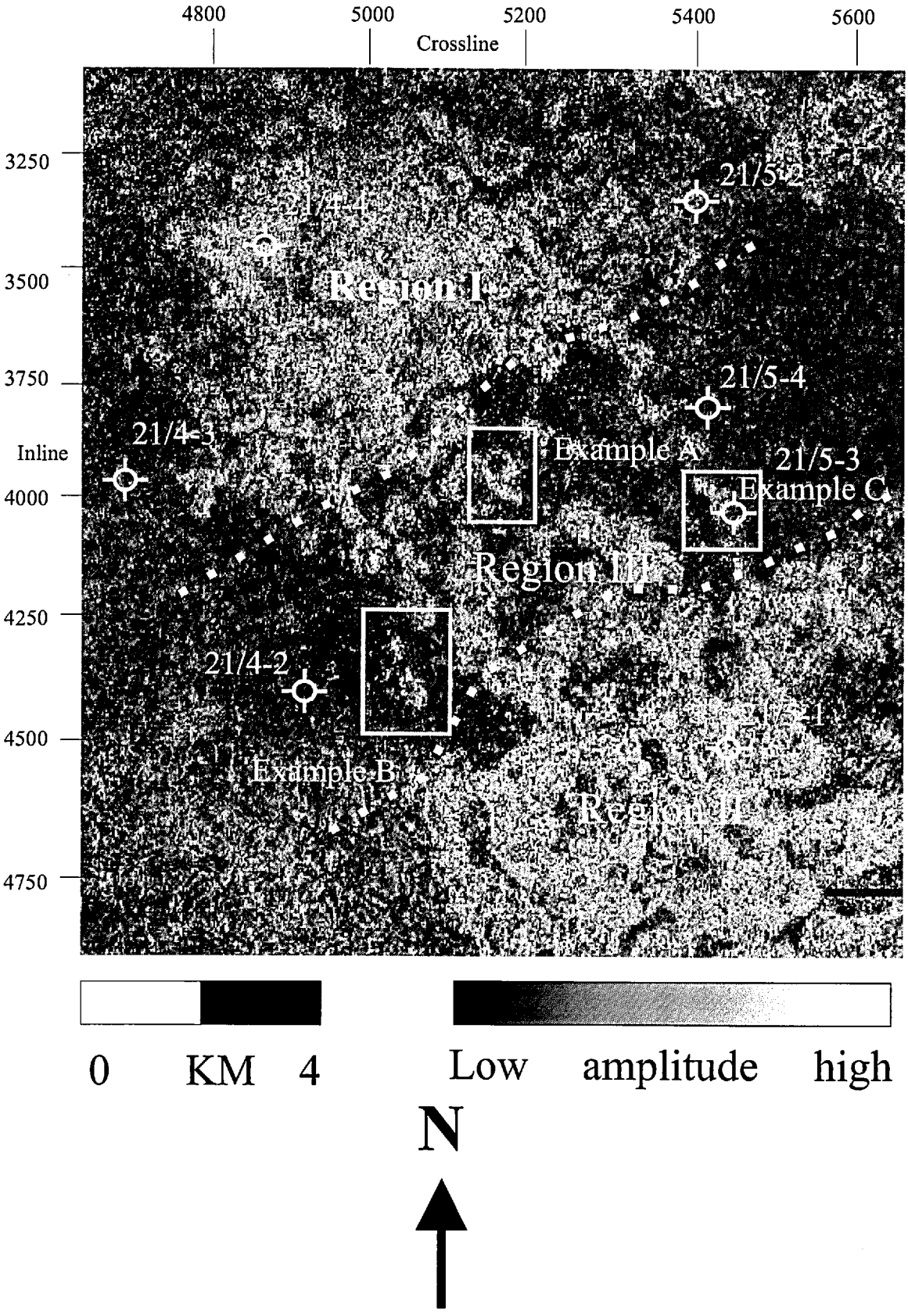


Figure 4.19. Seismic cross section of a high amplitude, low angle cone shaped anomaly, with basal apices located above a fault at top Balder level, through the Central North Sea Blocks 21/3, 4 and 5

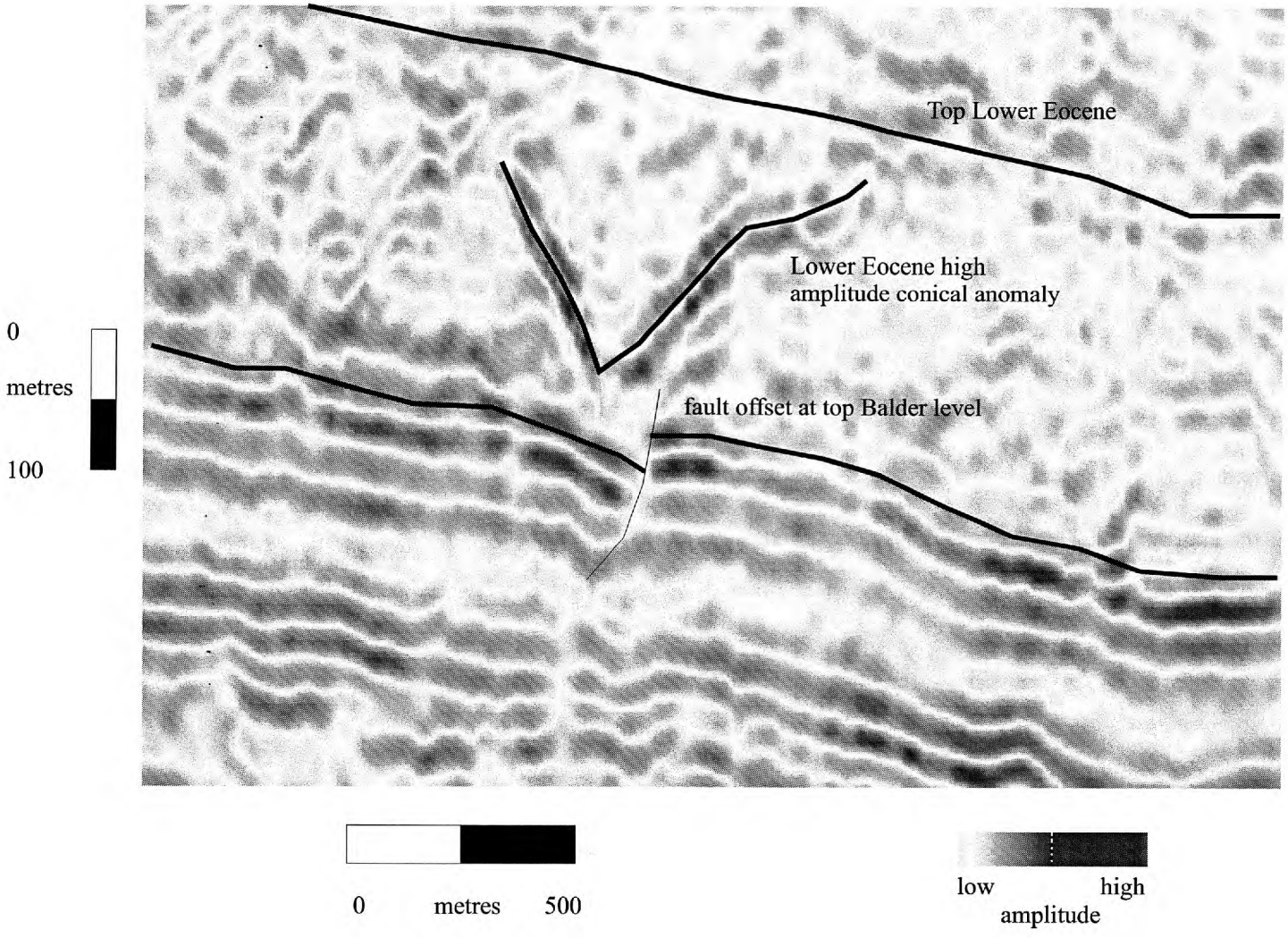


Figure 4.20. Structure contour map of Lower Eocene conical amplitude anomaly - example A - UK North Sea Block 21/5

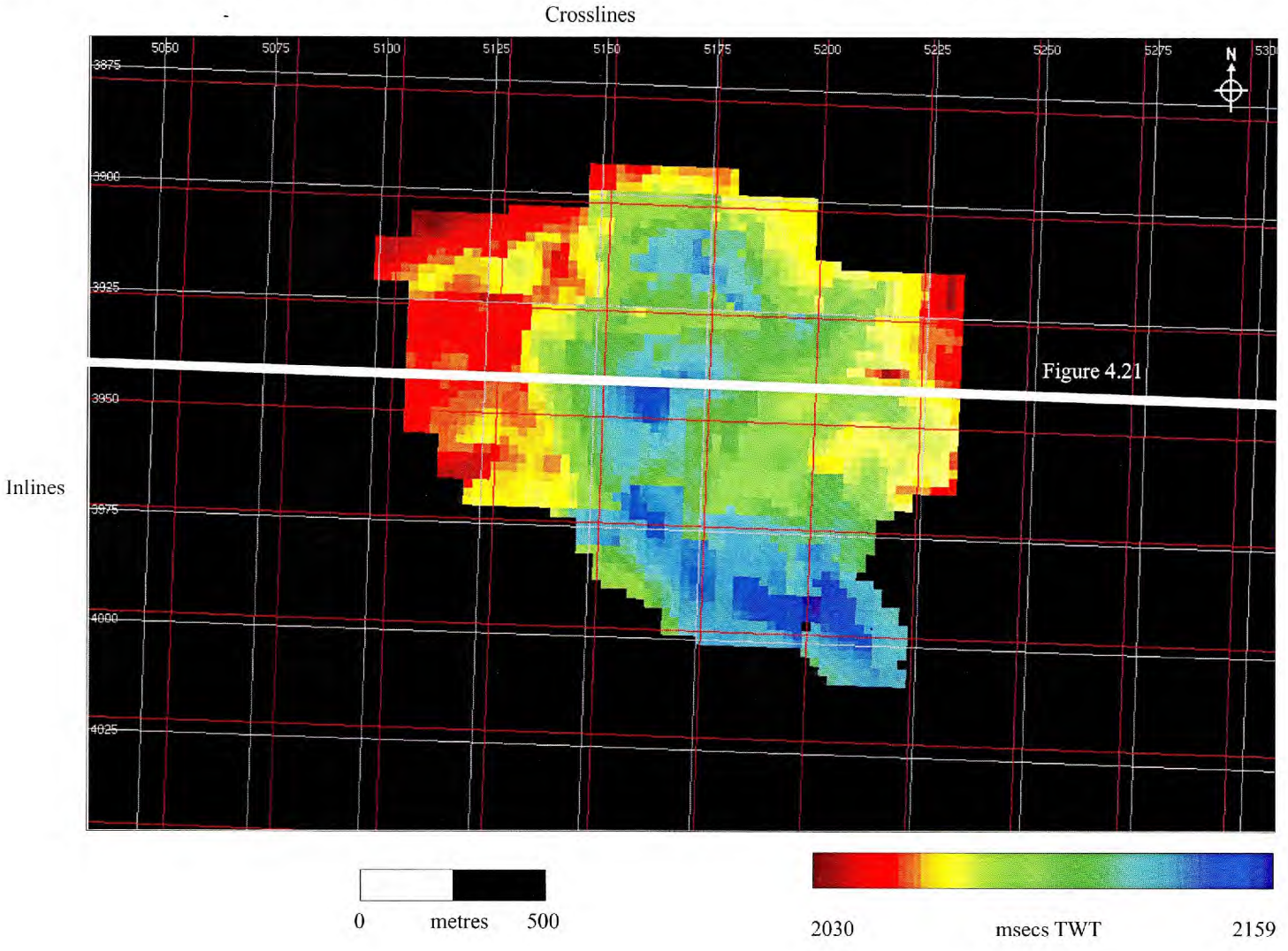


Figure 4.21. A Lower Eocene conical amplitude anomaly within UK North Sea Block 21/5 - example A

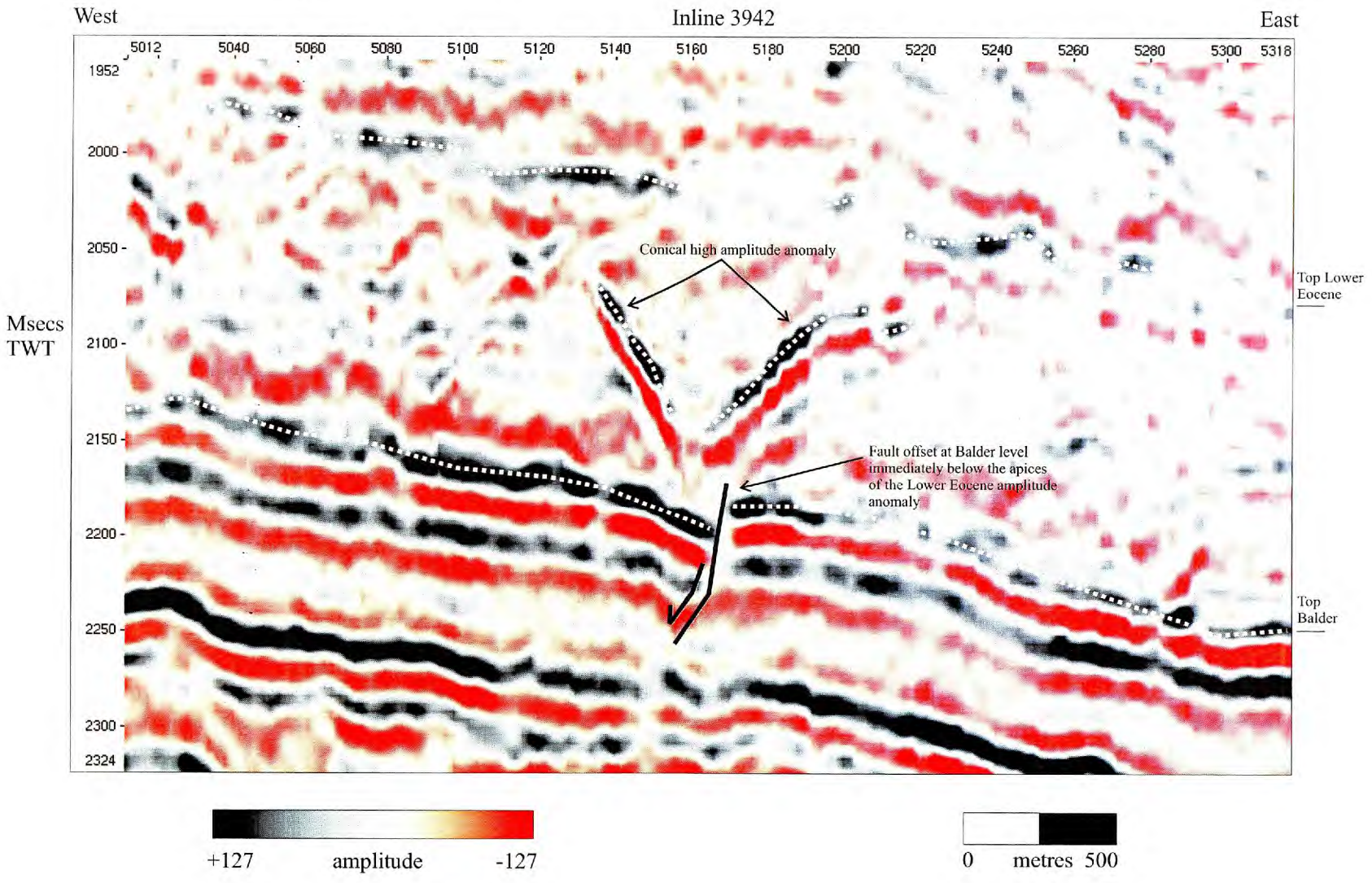


Figure 4.22. Structure contour map of Lower Eocene conical amplitude anomaly - example B - UK North Sea Block 21/5

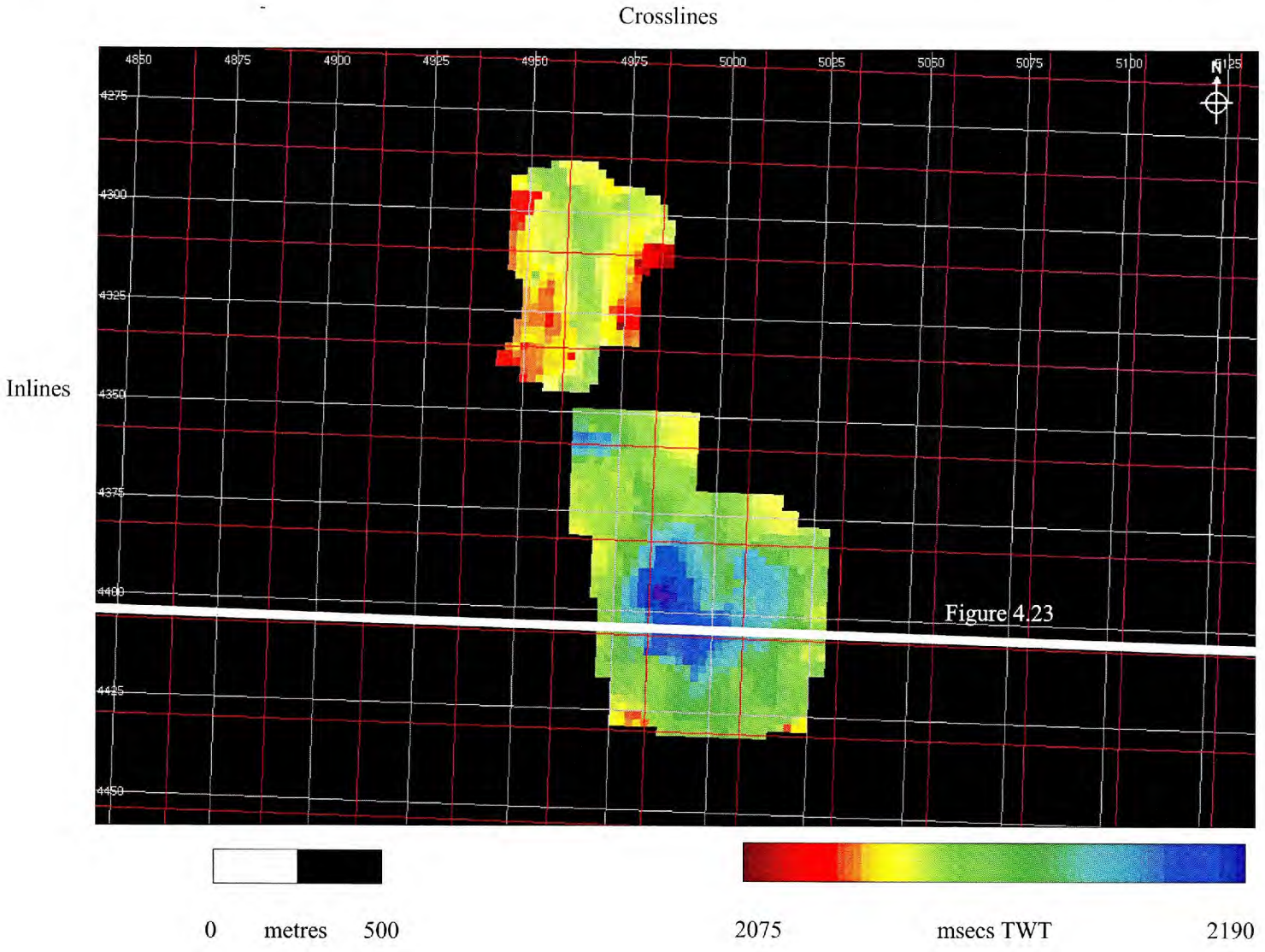


Figure 4.23. A Lower Eocene conical amplitude anomaly in UK North Sea Block 21/5

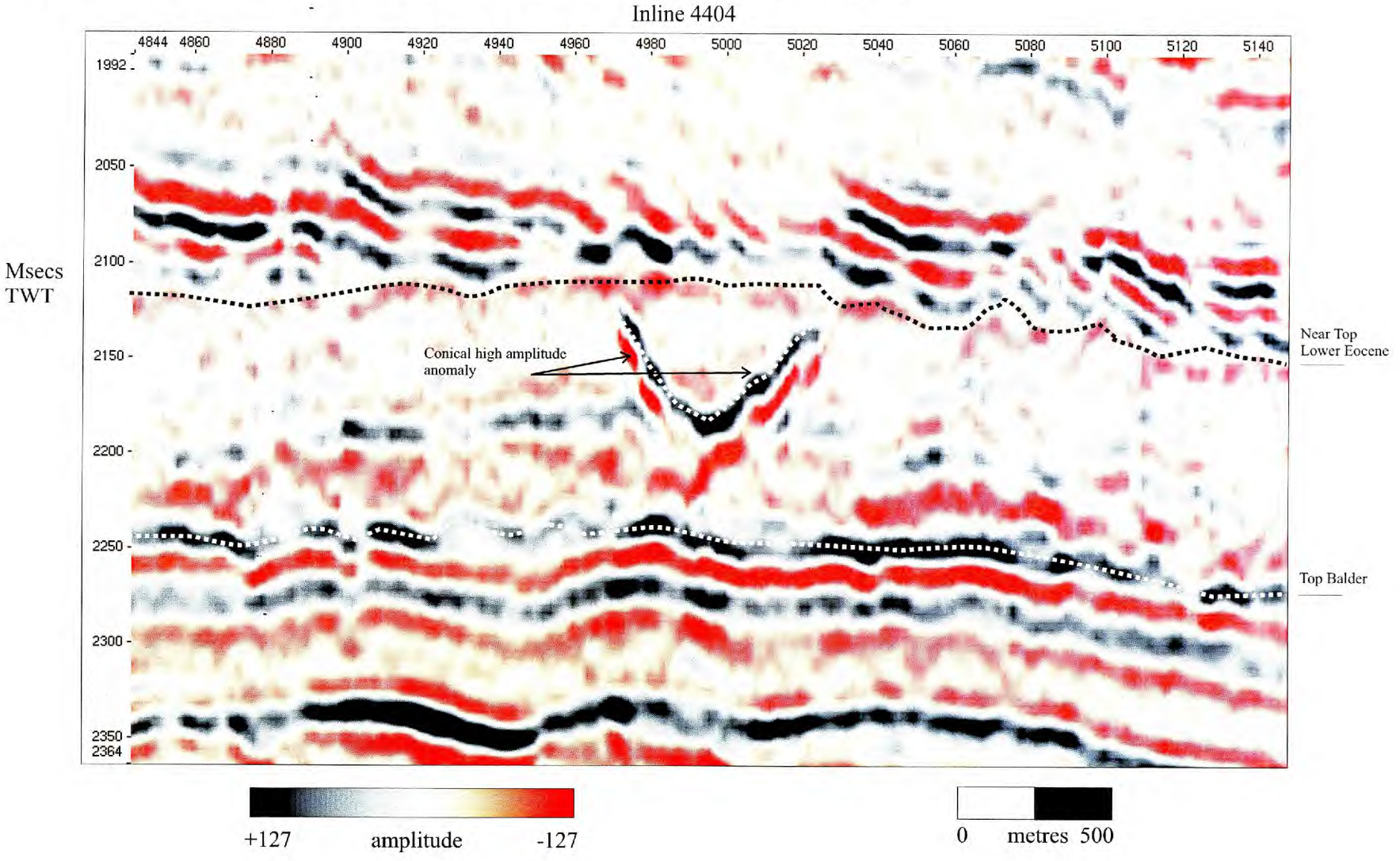


Figure 4.24. Three dimensional representation of selected Lower Eocene amplitude anomalies over UK Central North Sea 21/4 and 5

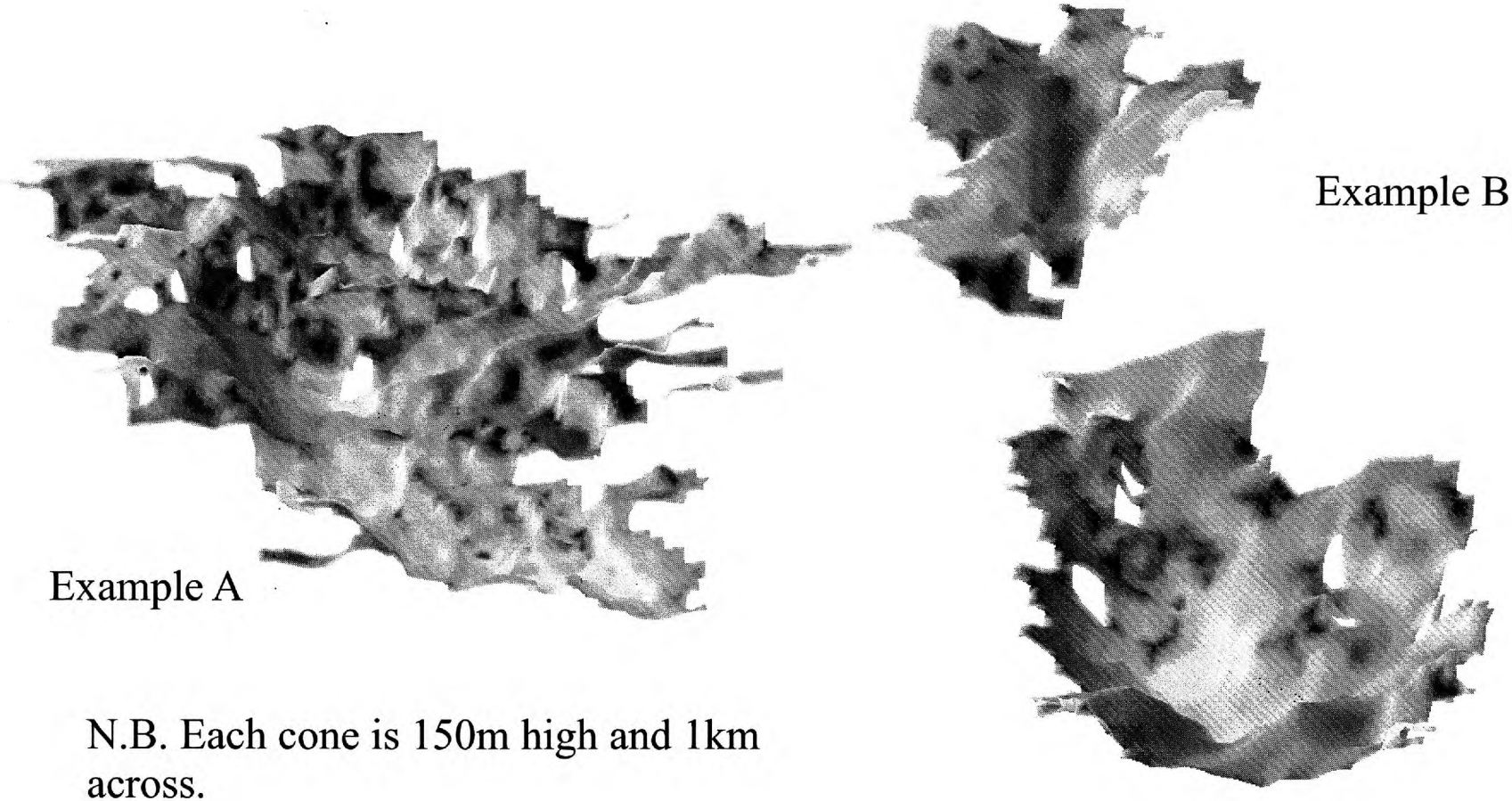


Figure 4.25. Structure contour map of Lower Eocene conical amplitude anomaly - example C - UK North Sea Block 21/5

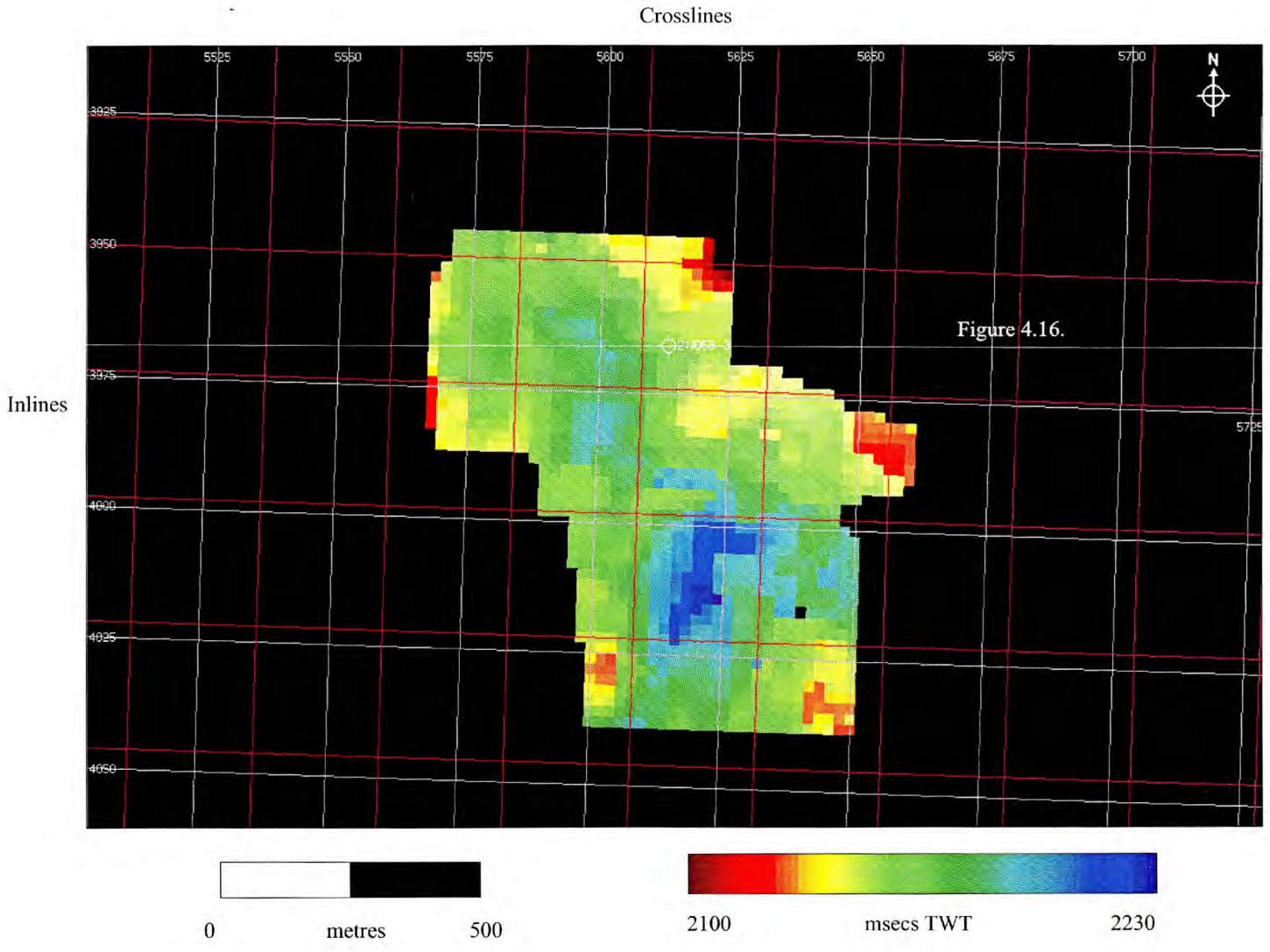


Figure 4.26. Charisma Geocube flattened on Top Balder UK North Sea Block 21/5 . Timeslice is 30 metres (30 msecs TWT) above top Balder. Note polygonal fault pattern on timeslice - the same plan view geometry as Lower Eocene conical high amplitude features in figure 4.27.

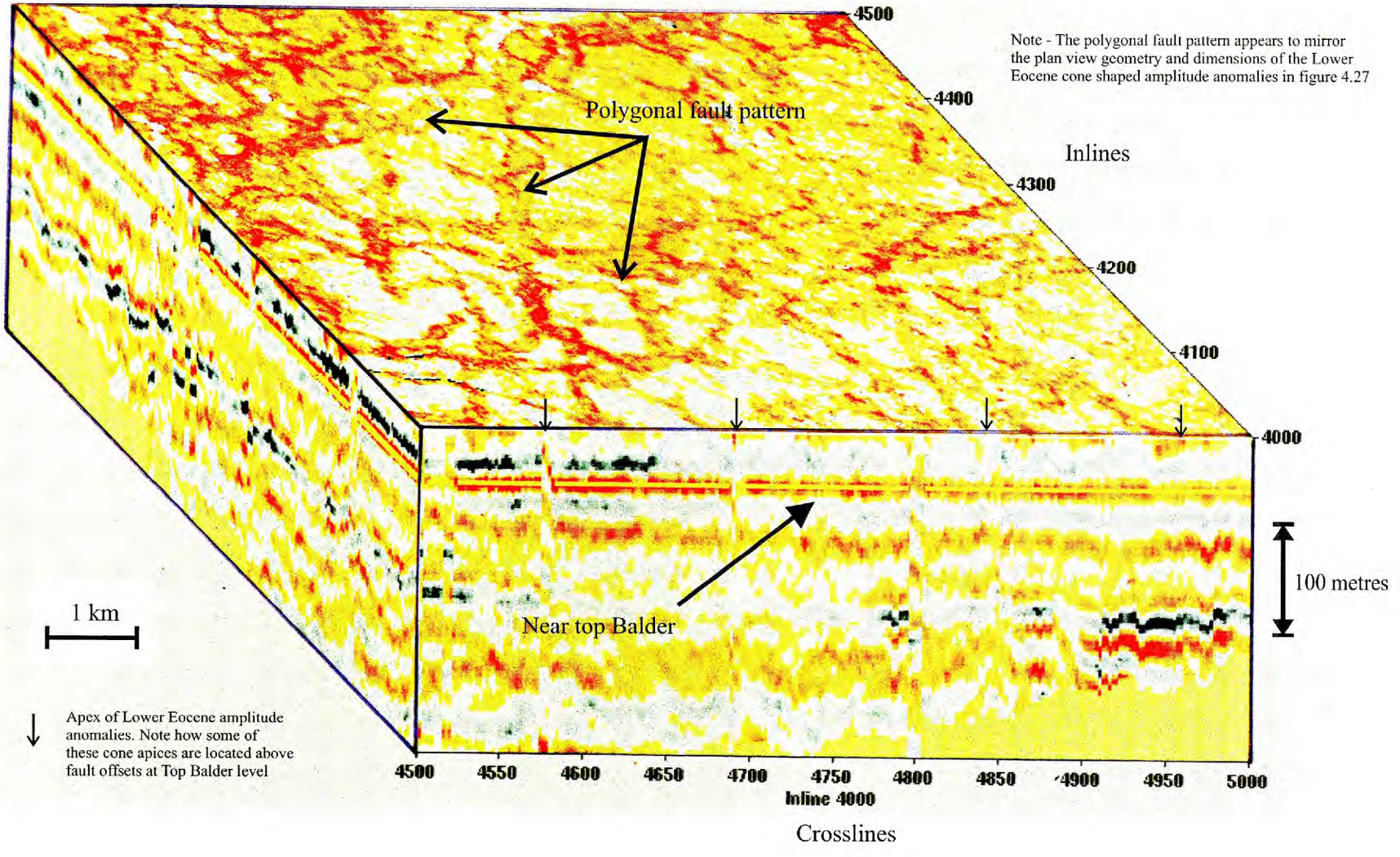


Figure 4.27. Part of UK North Sea Block 21/5 Charisma Geocube image, flattened on the Top Balder Horizon. Note conical high amplitude features, terminating basally against the Top Balder horizon on timeslice 70 milliseconds above Top Balder.

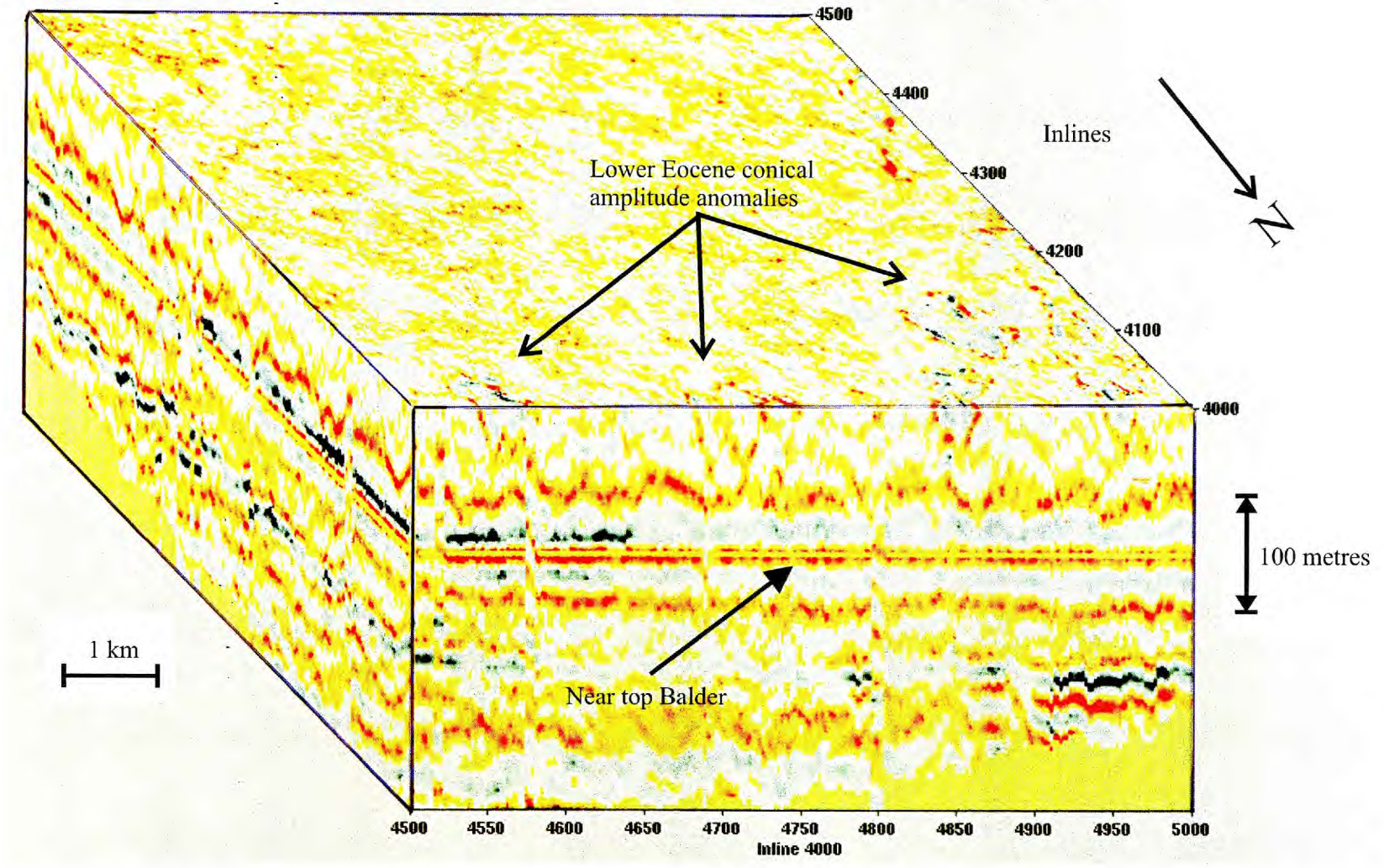


Figure 4.28. Seismic cross sections through (a) compound and (b) individual Lower Eocene conical amplitude anomalies over UK Central North Sea Blocks 21/3, 4 and 5

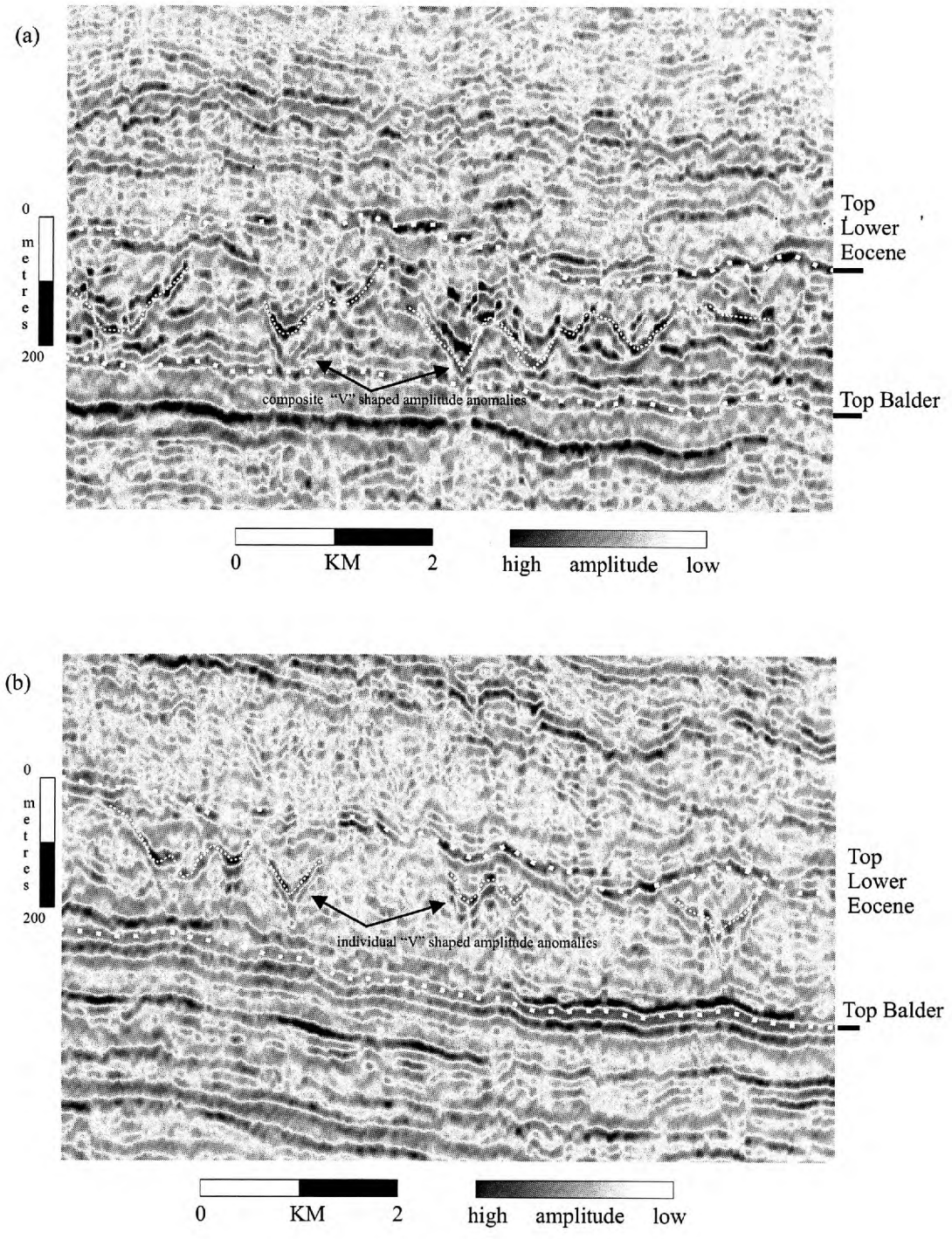


Figure 4.29. Comparison of Lower Eocene polygonal fault patterns to the scale and plan view geometry of Lower Eocene amplitude anomalies over the southern part of UK North Sea Block 21/4 and 21/5.

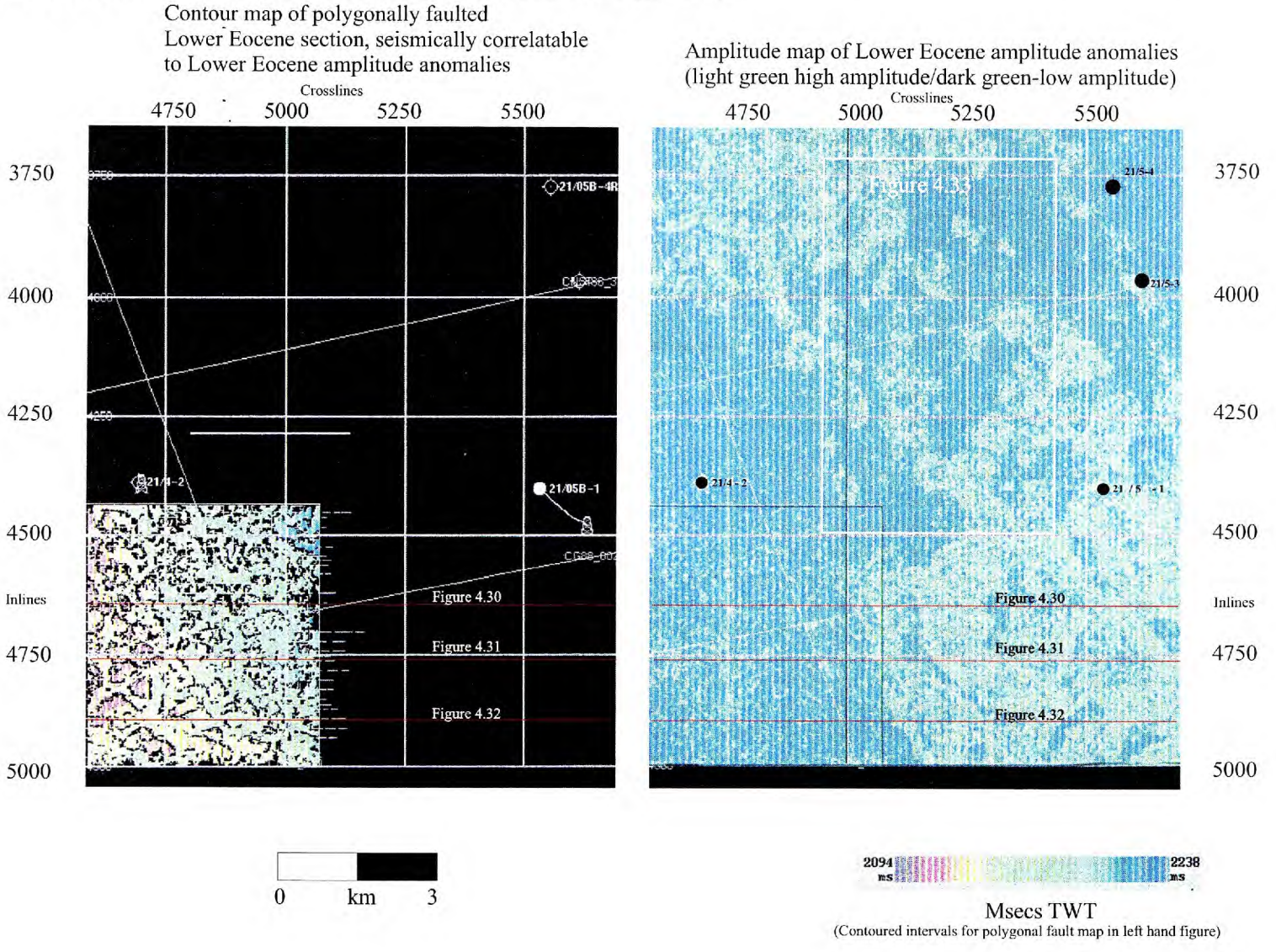


Figure 4.30. UK North Sea Block 21/5 - seismic example (inline 4644) of Lower Eocene polygonal faults and conical amplitude anomalies. Note similar scale, geometry and dip of polygonal faulting to the conical amplitude anomalies.

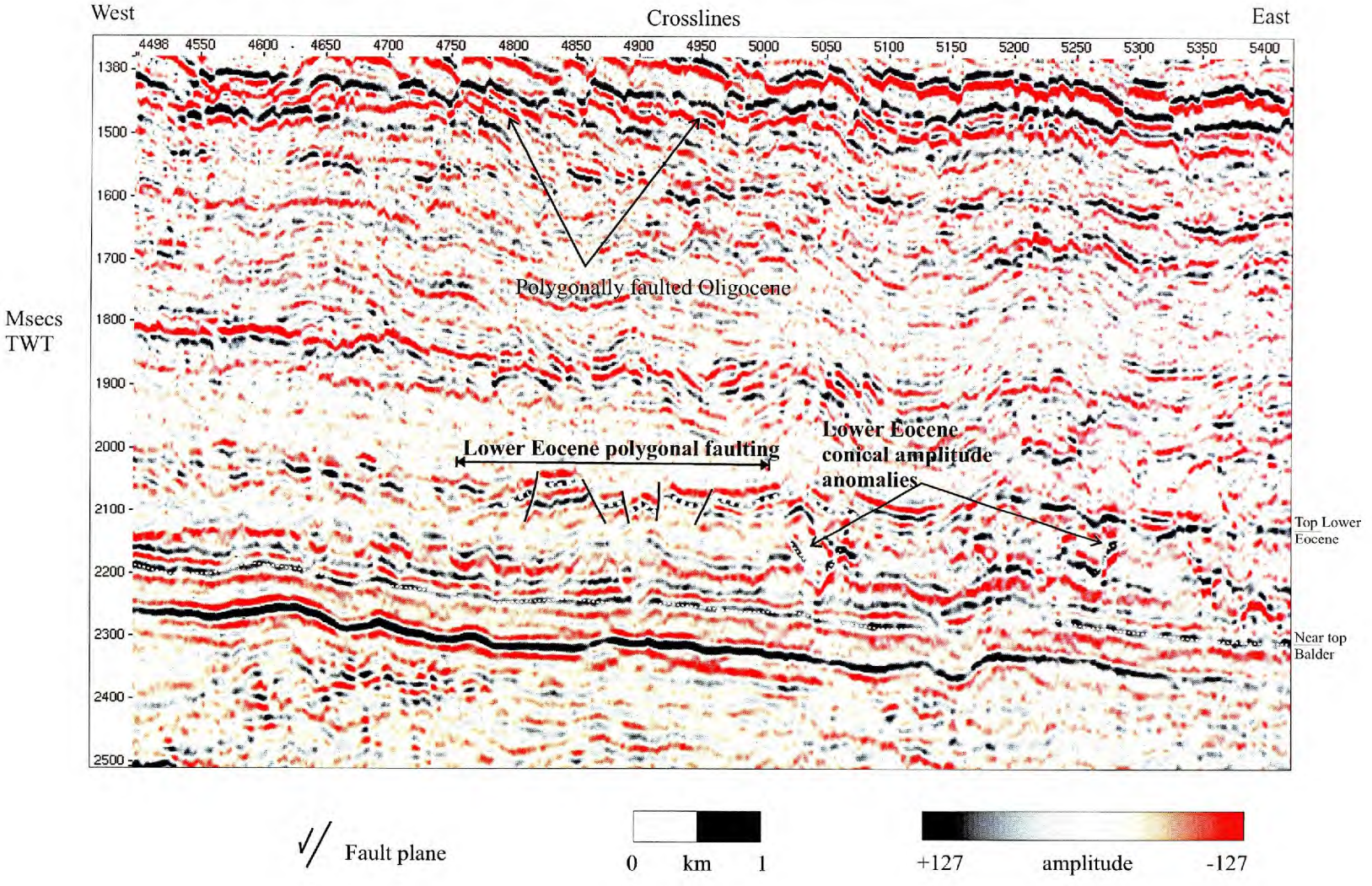


Figure 4.31. UK North Sea Block 21/5 - seismic example (inline 4754) of Lower Eocene polygonal faults and conical amplitude anomalies. Note similar scale, geometry and dip of polygonal faulting to the conical amplitude anomalies.

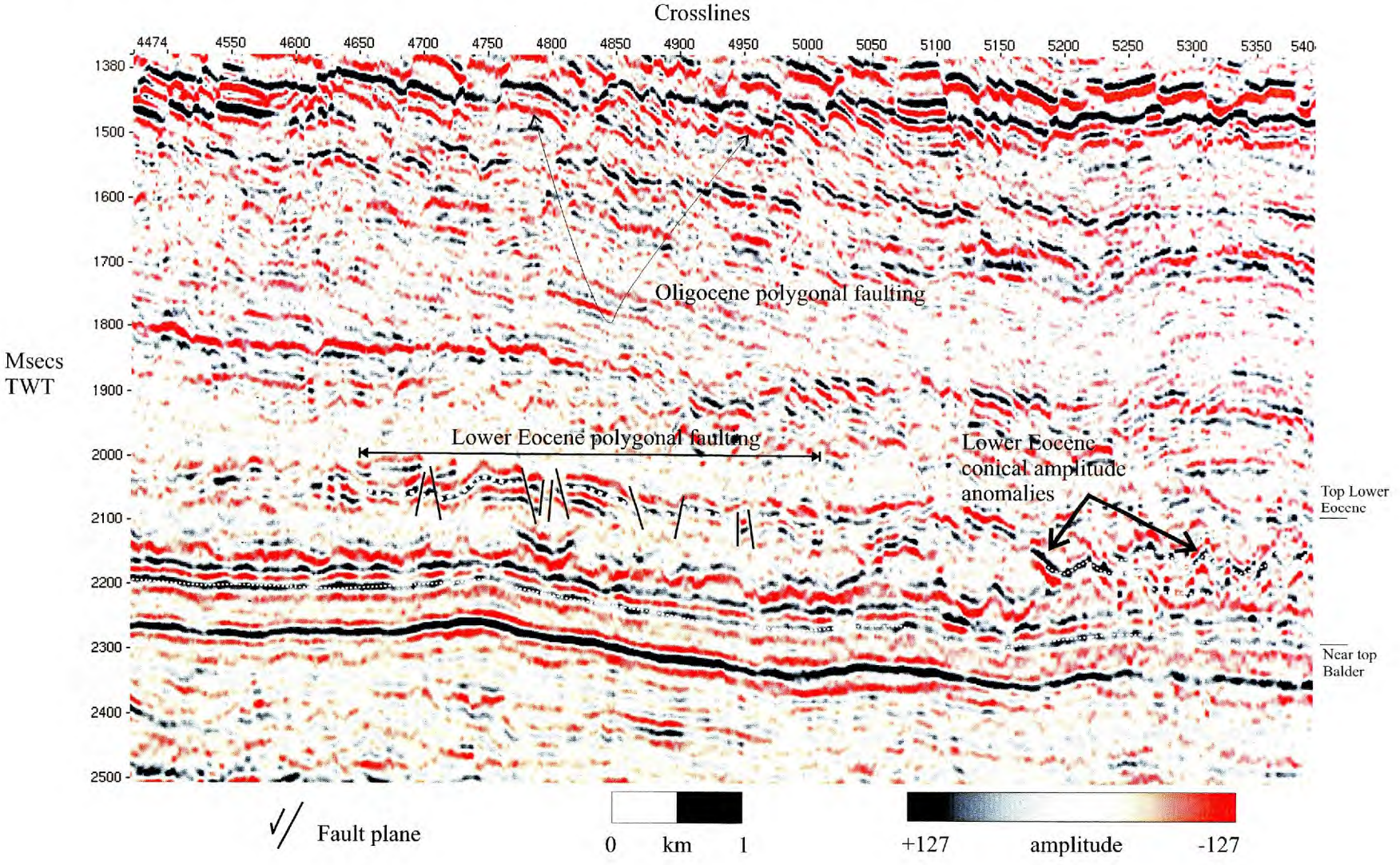


Figure 4.32. UK North Sea Block 21/5 - seismic example (inline 4866) of Lower Eocene polygonal faults and conical amplitude anomalies. Note similar scale, geometry and dip of polygonal faulting to the conical amplitude anomalies.

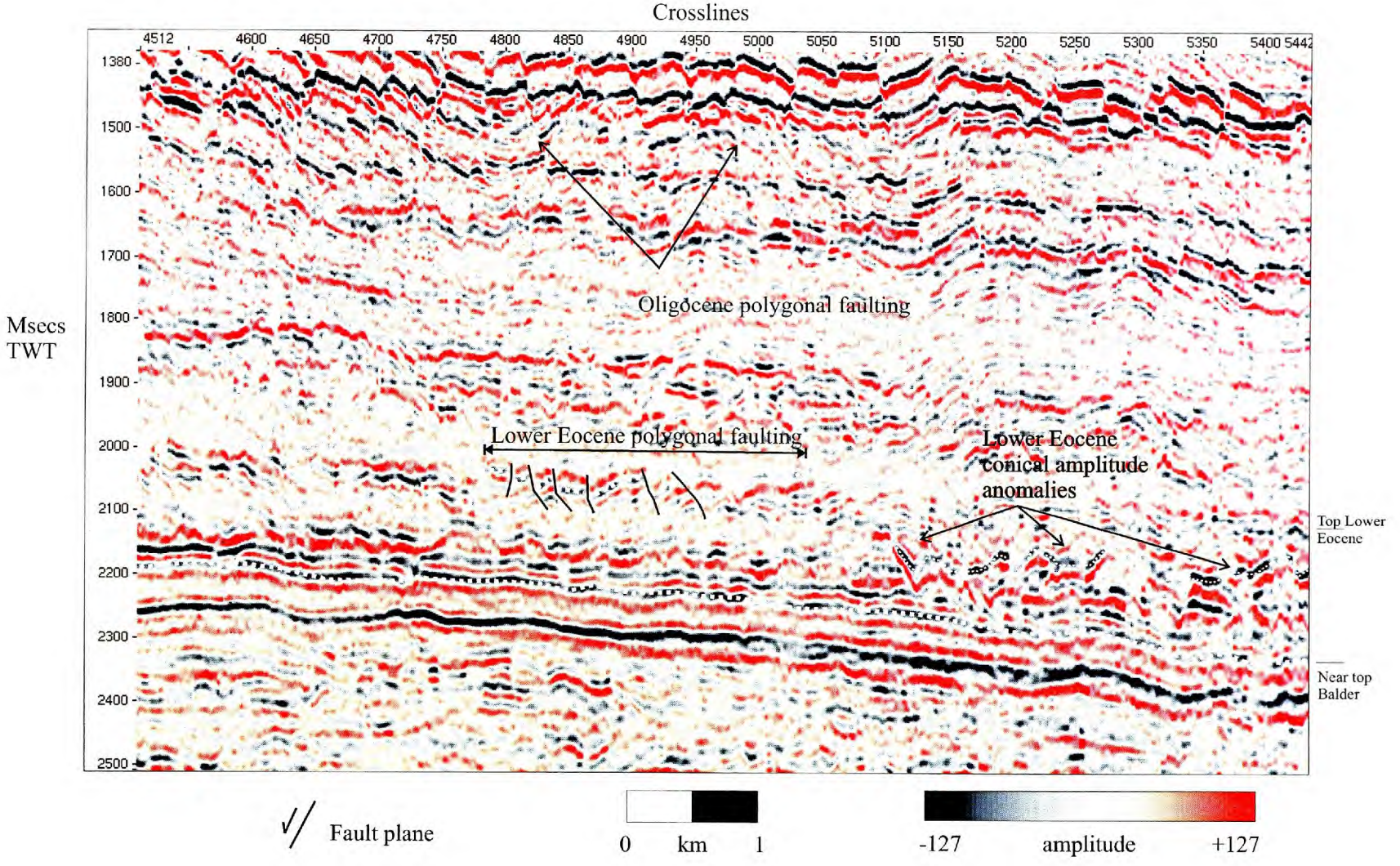


Figure 4.33. Within UK North Sea Block 21/4 and 5 Lower Eocene high amplitude conical structures, polygonal and Balder fault map superimposed upon eachother

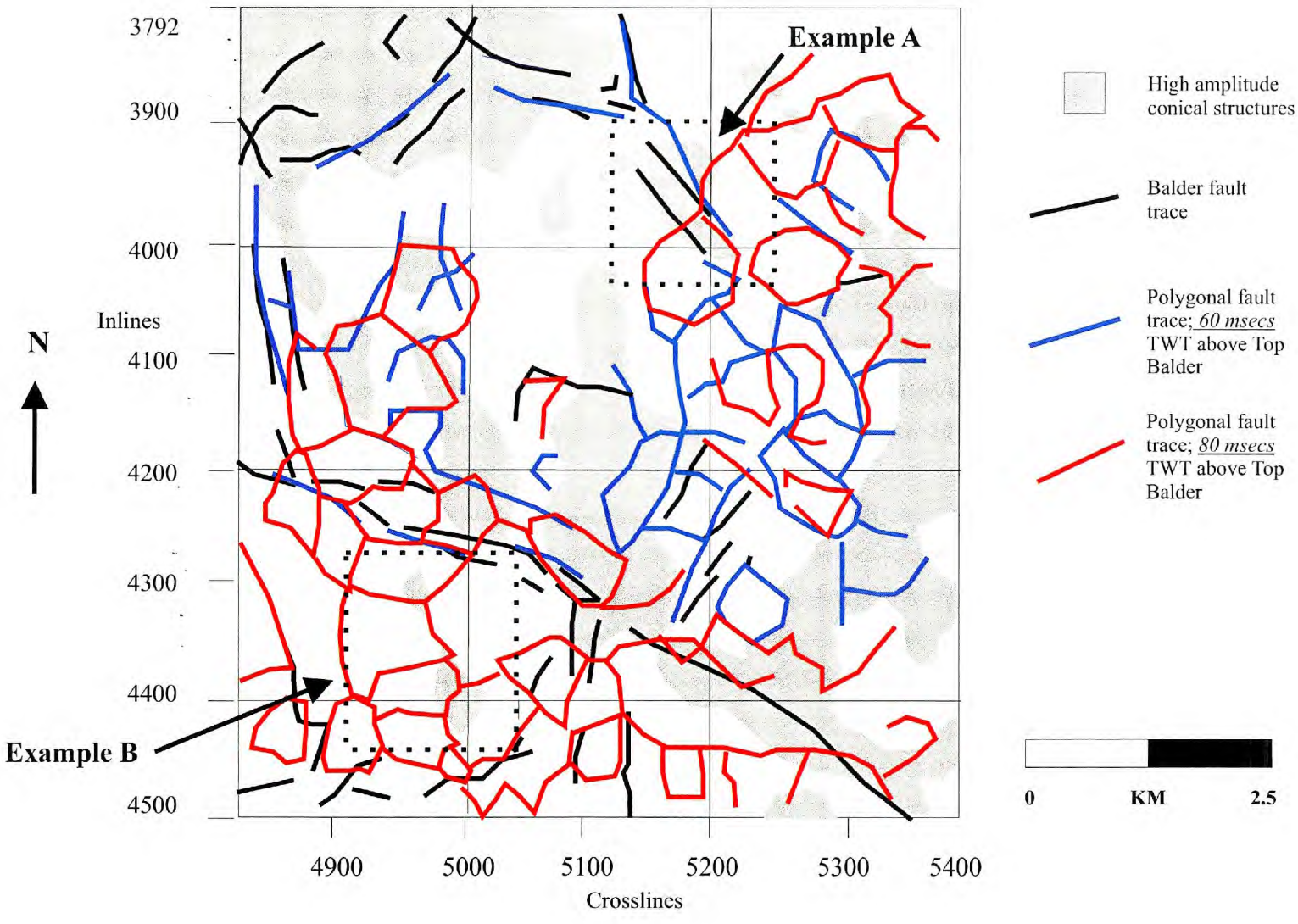
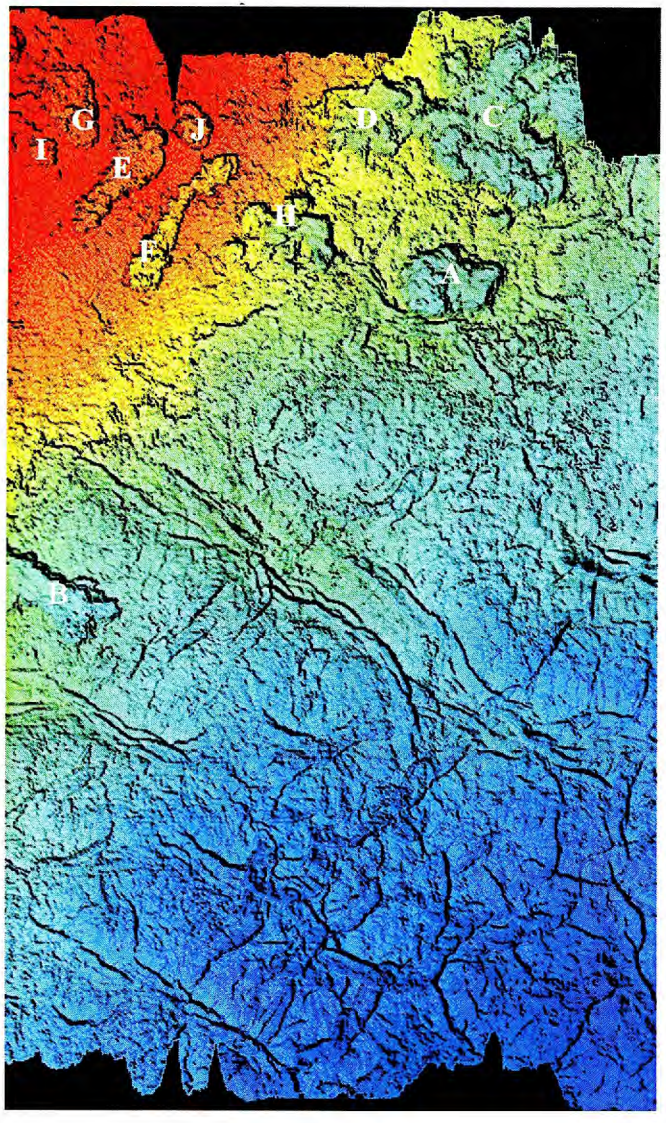
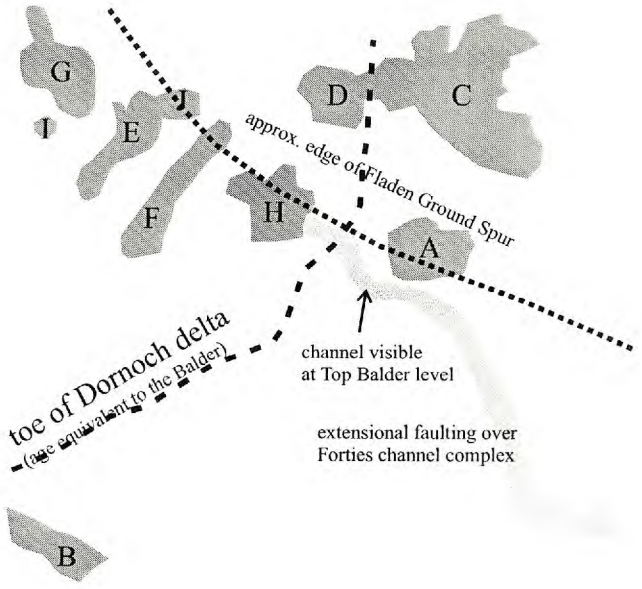


Figure 4.34. Top Balder structure contour map of UK Block 15/18 3D seismic survey with pockmarks marked (redrawn from Cole, 1998)



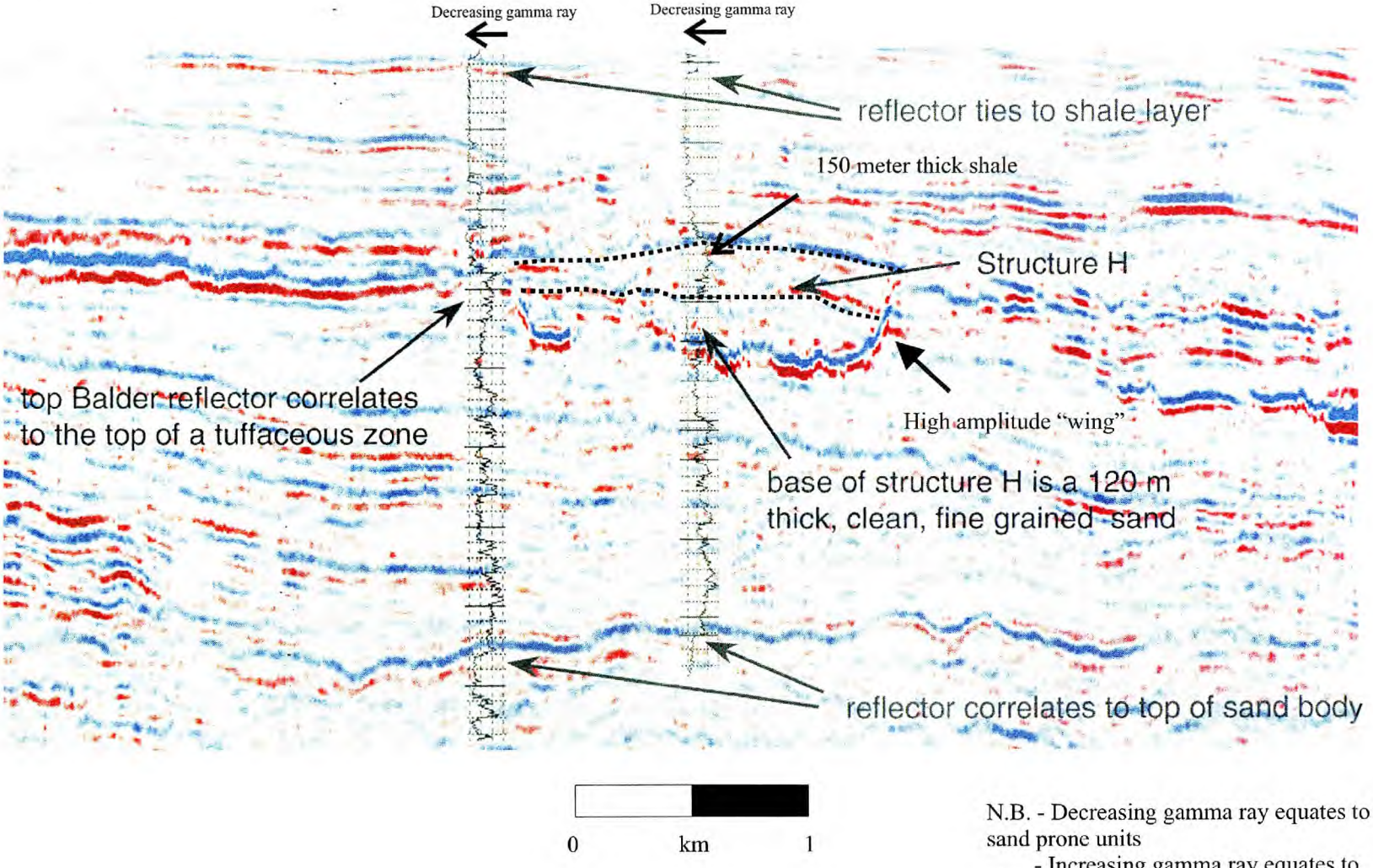


H - crater name

O KM 2

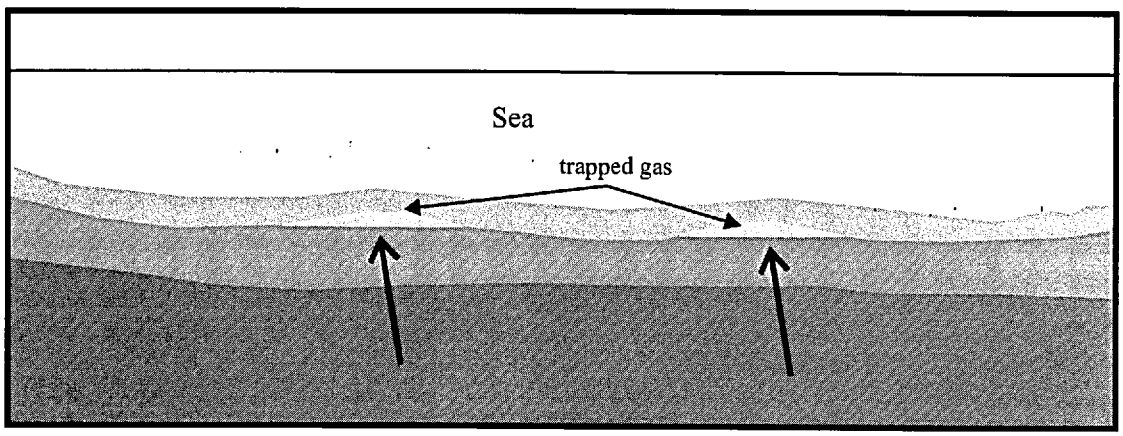
N.B. Red to blue colour contours equate to 200 msecs TWT

Figure 4.35. Seismic cross section of Balder aged pockmarks over UK Block 15/18 (redrawn from Cole, 1998)

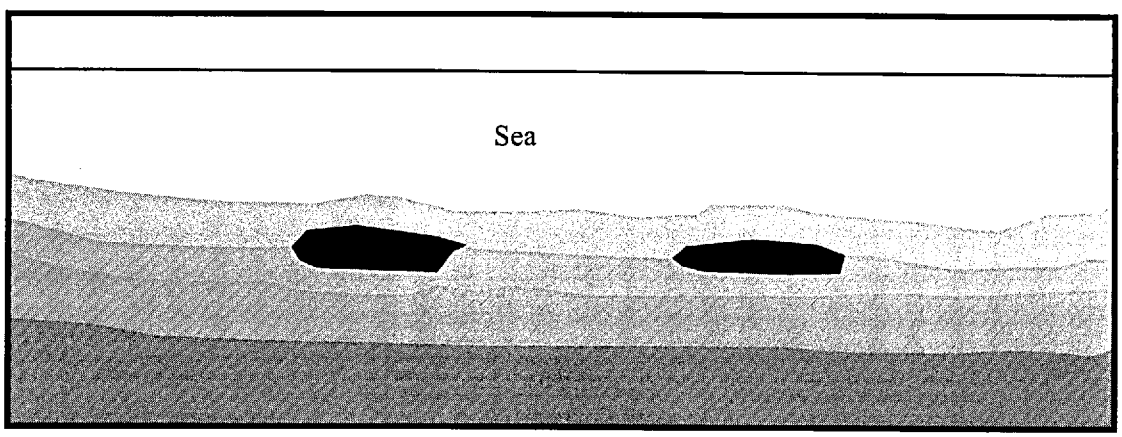


N.B. - Decreasing gamma ray equates to sand prone units
- Increasing gamma ray equates to clay prone units

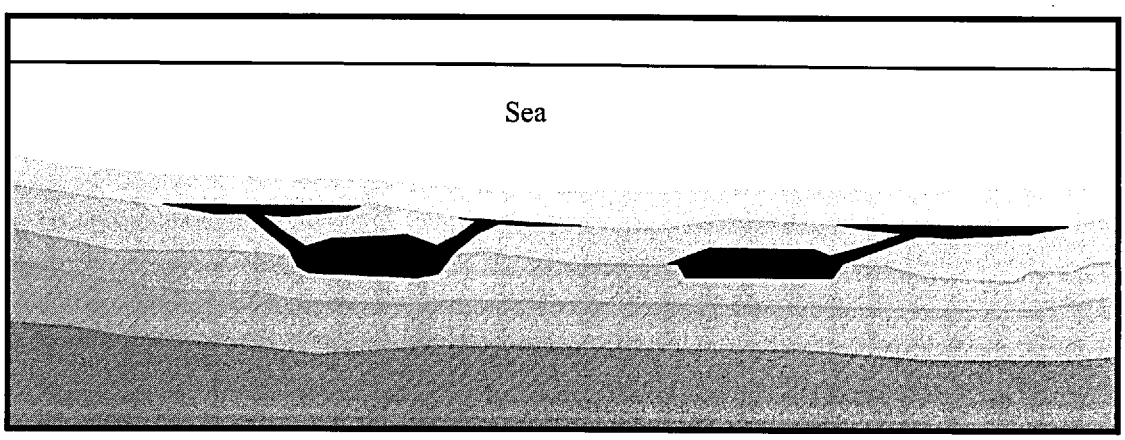
Figure 4.36. Model for the formation of Balder aged pockmarks over UK Block 15/18 (redrawn from Cole, 1998)



1 Gas, migrating up the Mesozoic fault systems, is stored in a "reservoir" unit beneath the tuffaceous Balder formation. The sea floor domes up before catastrophic failure produces the large craters



2 The composite craters are infilled with sand and overlain by a 100m thick mudstone unit. Differential compaction produces the mounded topography seen on the seismic data



3 Sandstone dykes are intruded into the overlying sediment and may also break the surface to be deposited as remobilized sand "pods". A kilometre of sandy sediment has since been deposited over the structures

Figure 4.37. Model for Lower Eocene conical amplitude anomalies as pockmarks in UK Central North Sea Blocks 21/3, 4, 5

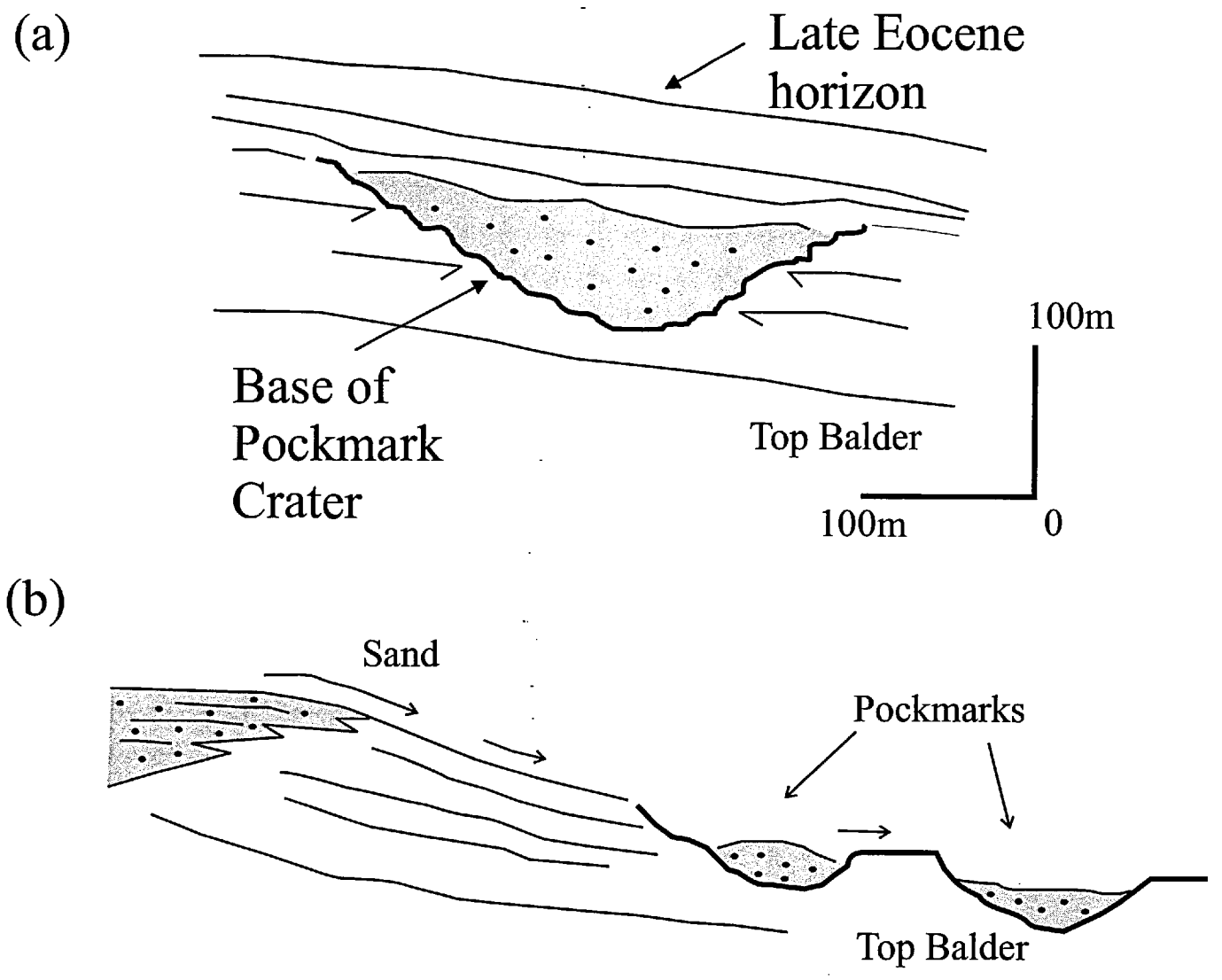


Figure 4.38. Model for the formation of Lower Eocene conical amplitude as sandstone intrusions in the UK Central North Sea Blocks 21/3, 4, 5

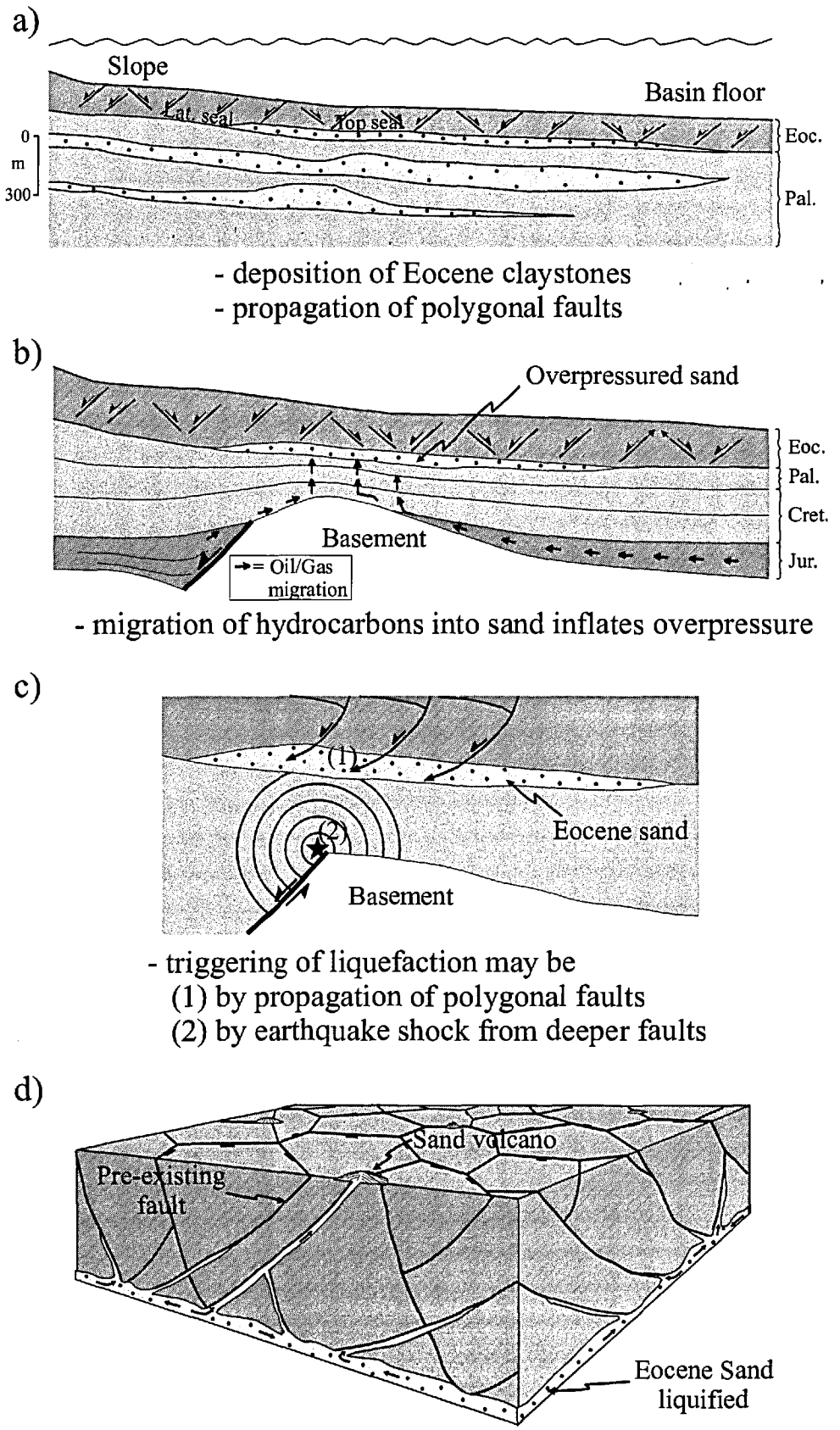


Figure 4.39. Timing of hydrocarbon generation from Jurassic organic rich source rocks about UK Central North Sea Blocks 21/3, 4, 5 (redrawn from Mason *et al.*, 1995)

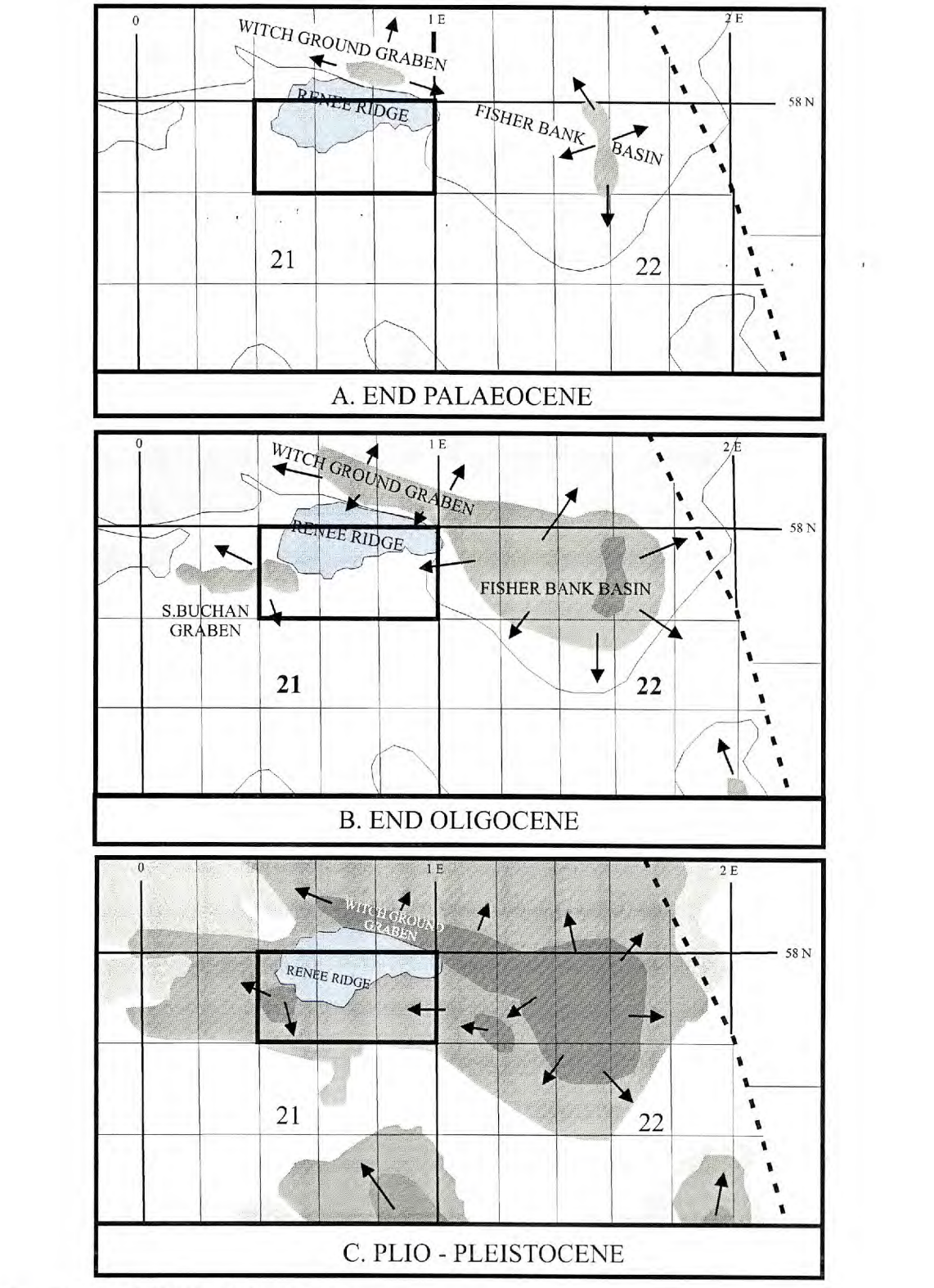
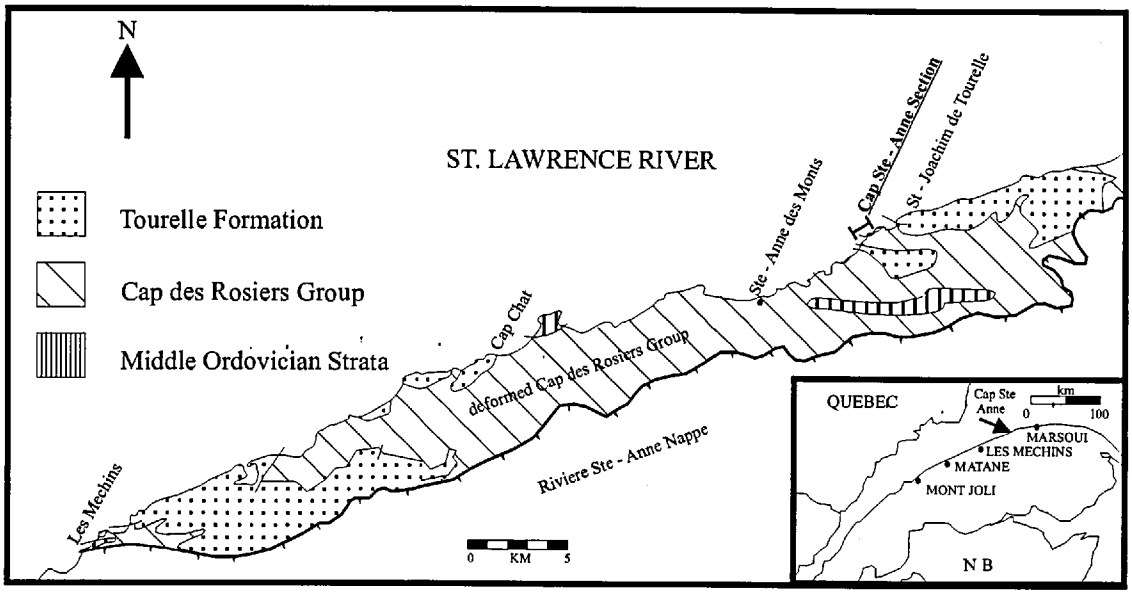


Figure 4.40. Location map of Tourelle formation at Cap Ste-Anne, Quebec, Canada



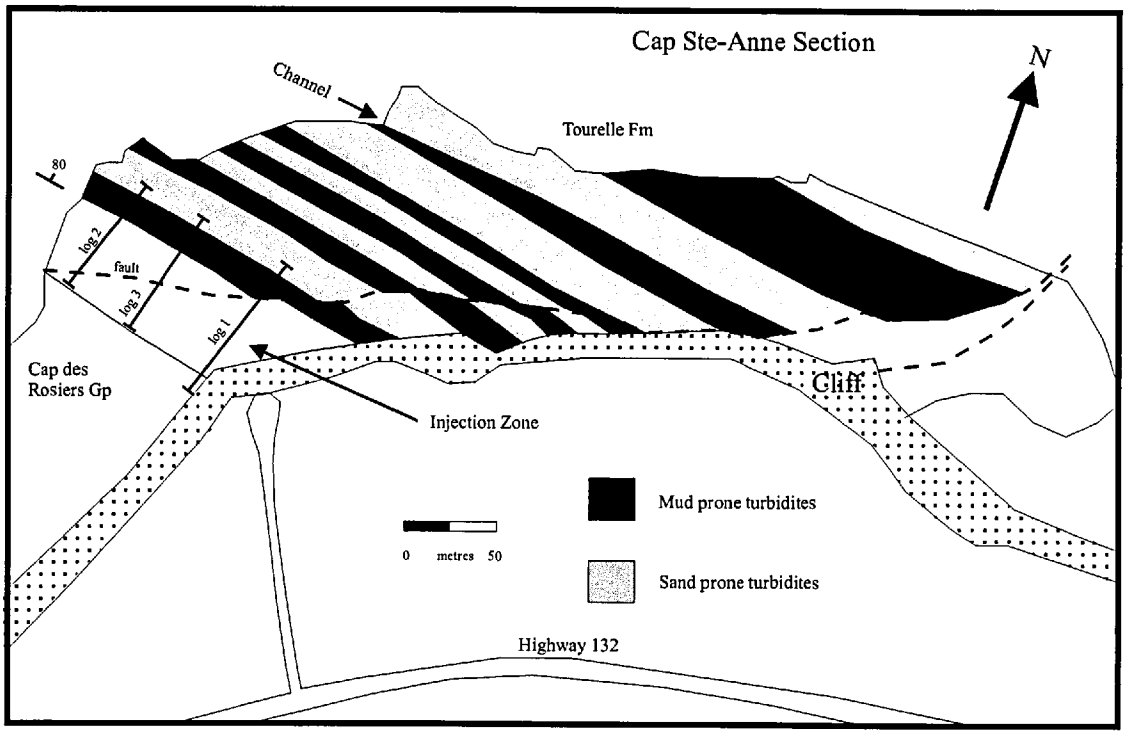


Figure 4.41. Line drawing of wave cut platform of the base Tourelle formation, exposing a 70 metre thick section, by 100 metres wide of clastic intrusions, in deepwater shales, silts and fine sands, Cap Ste-Anne, Quebec, Canada

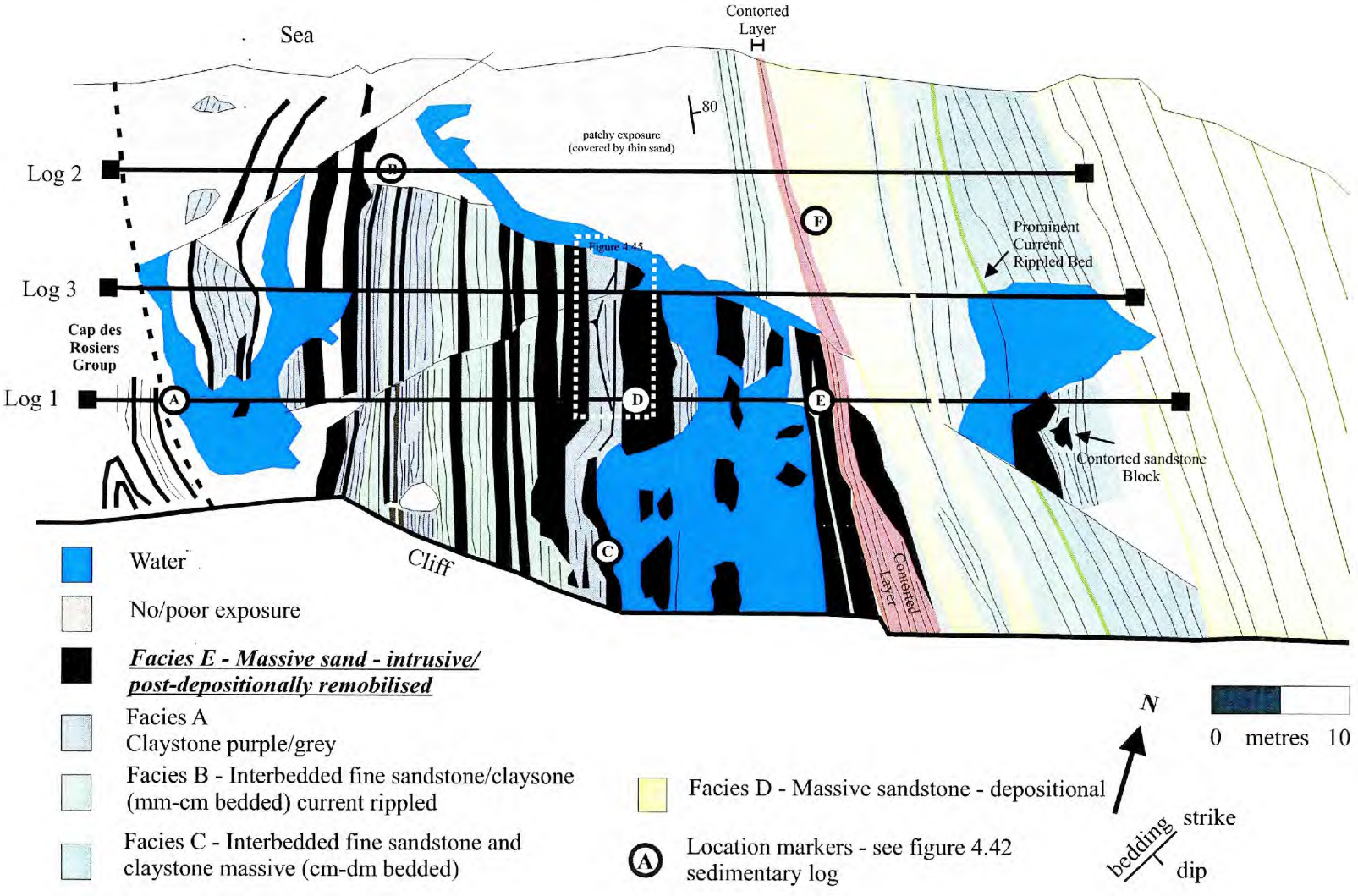


Figure 4.42. Three sedimentary logs from the base to top of the exposure of injected sandstone intrusions in deepwater sediments of the Tourelle Formation, Cap Ste Anne, Quebec, Canada

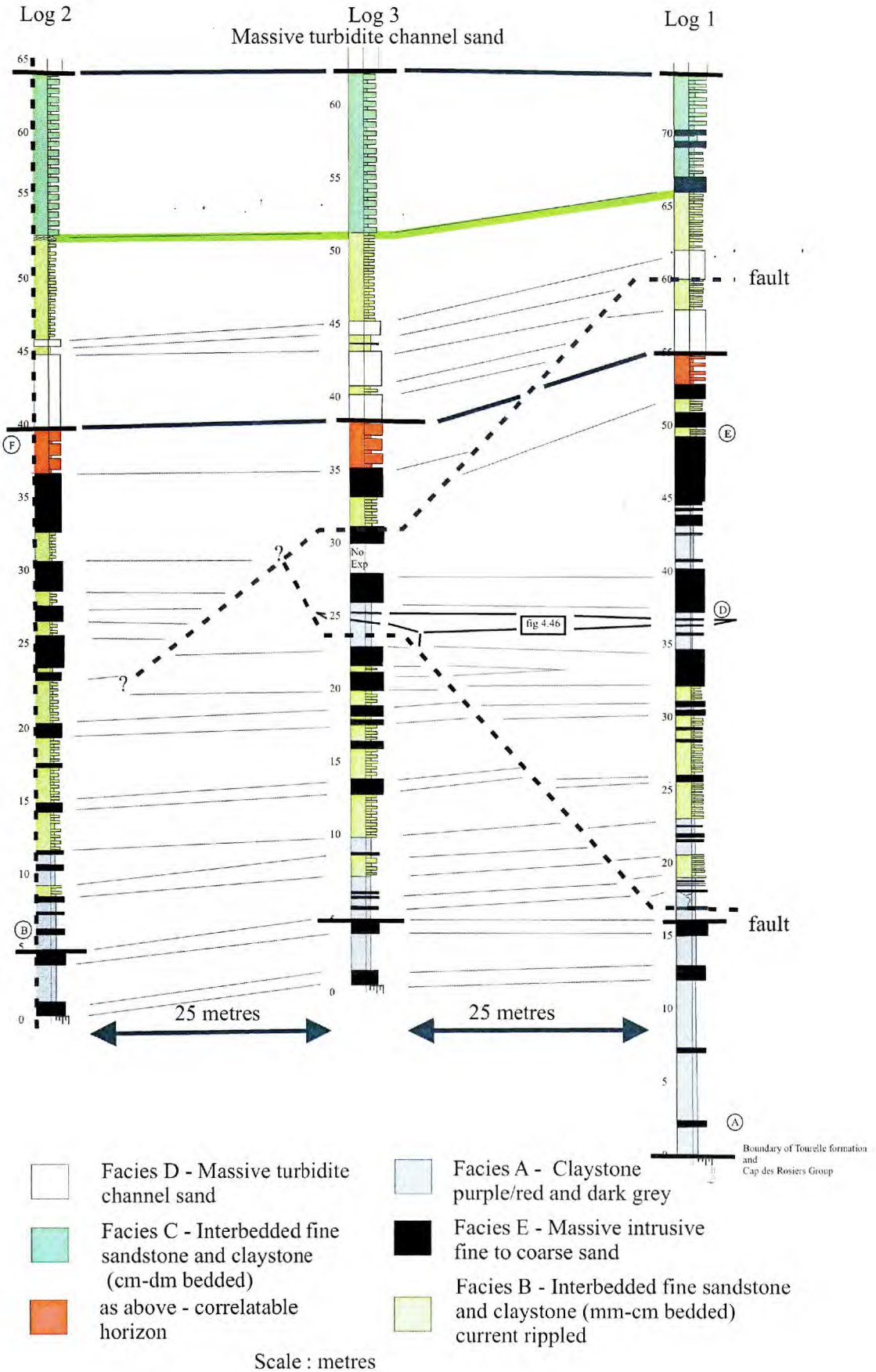


Figure 4.43. Termination of intruded sandstone sills with bulbous and fingerlike geometries in the basal deepwater sediments of the Tourelle Formation, Cap Ste Anne, Quebec, Canada

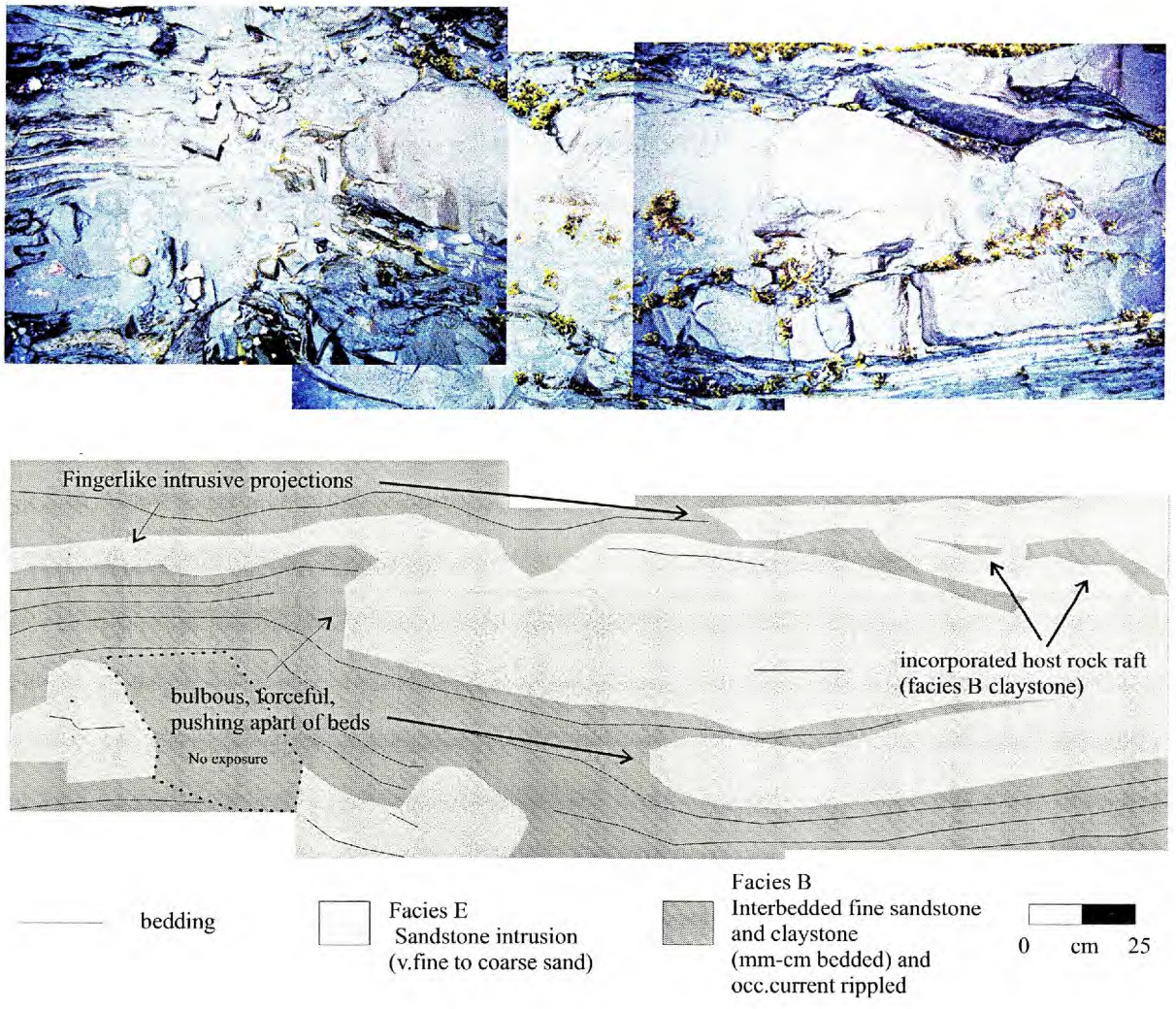


Figure 4.44. Terminations of intruded sandstone sills with bulbous and fingerlike geometries in the basal deepwater sediments of the Tourelle Formation, Cap Ste Anne, Quebec, Canada

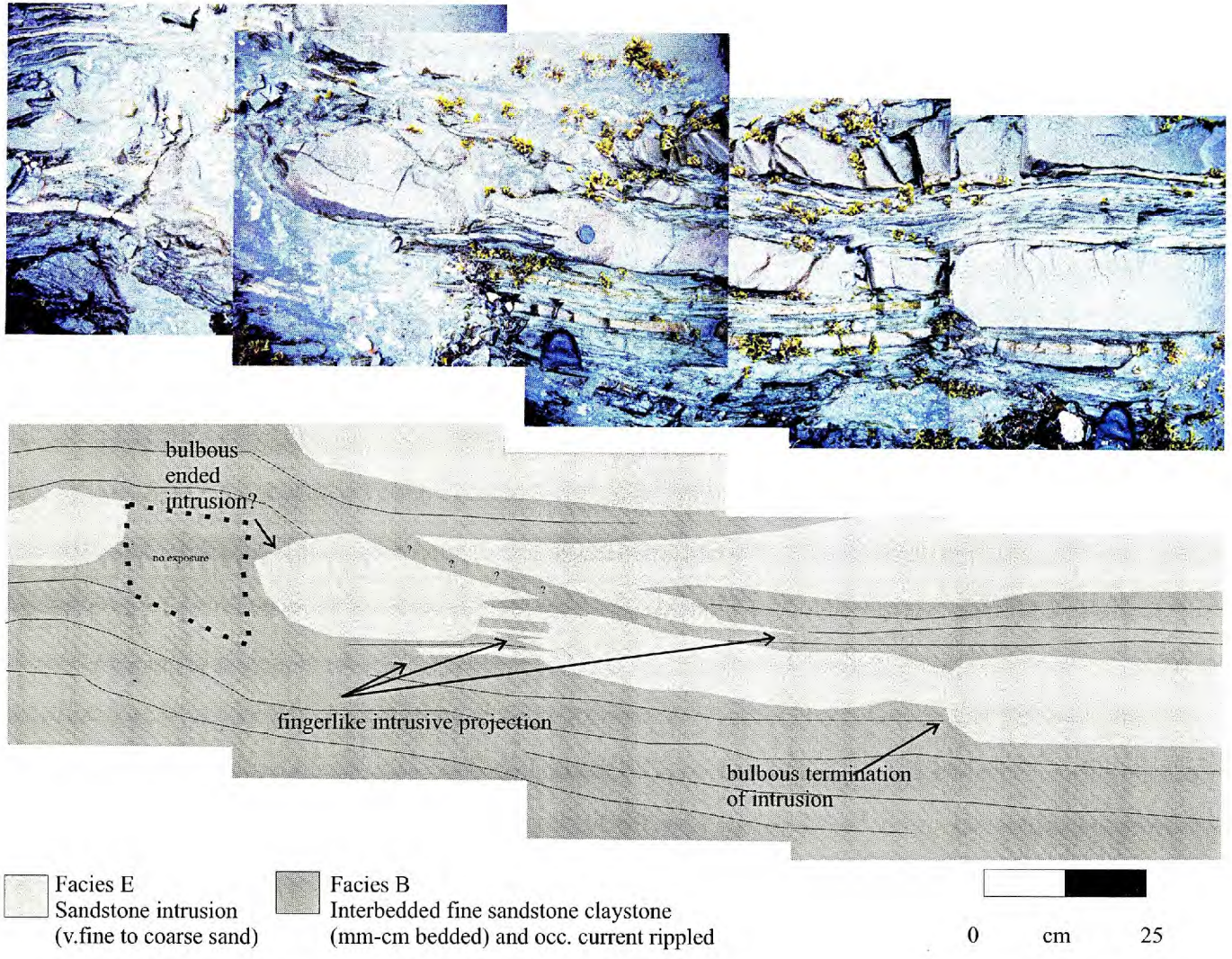
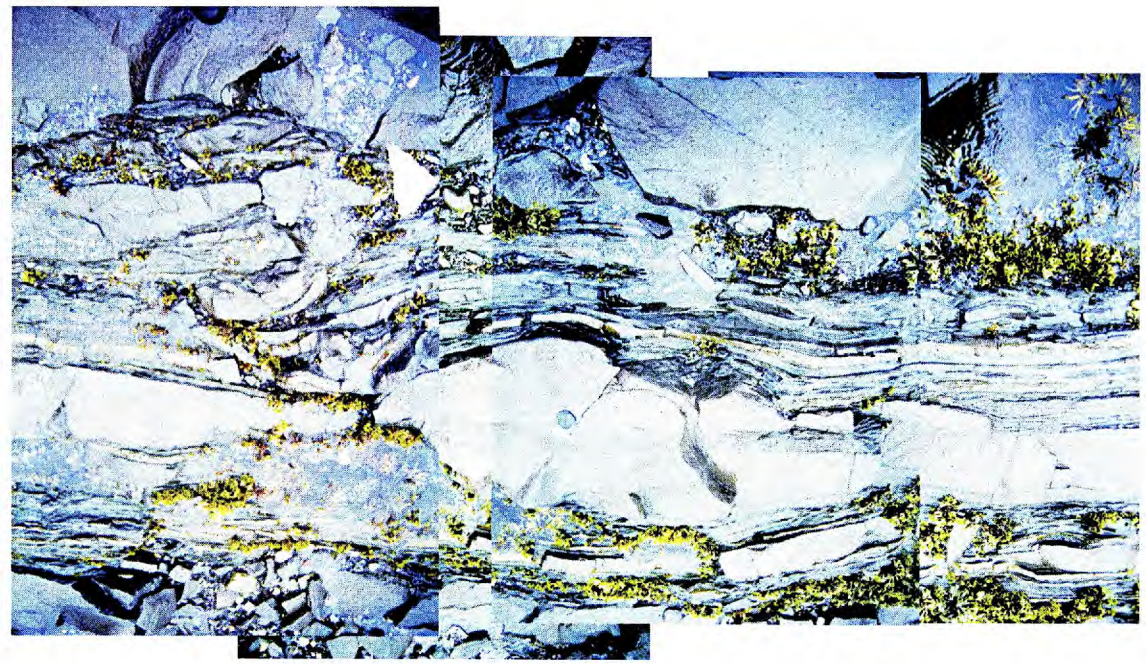


Figure 4.45. Jacking apart of country rock by intruded sandstone sill/dykes in the basal deepwater sediments of the Tourelle Formation, Cap Ste Anne, Quebec, Canada



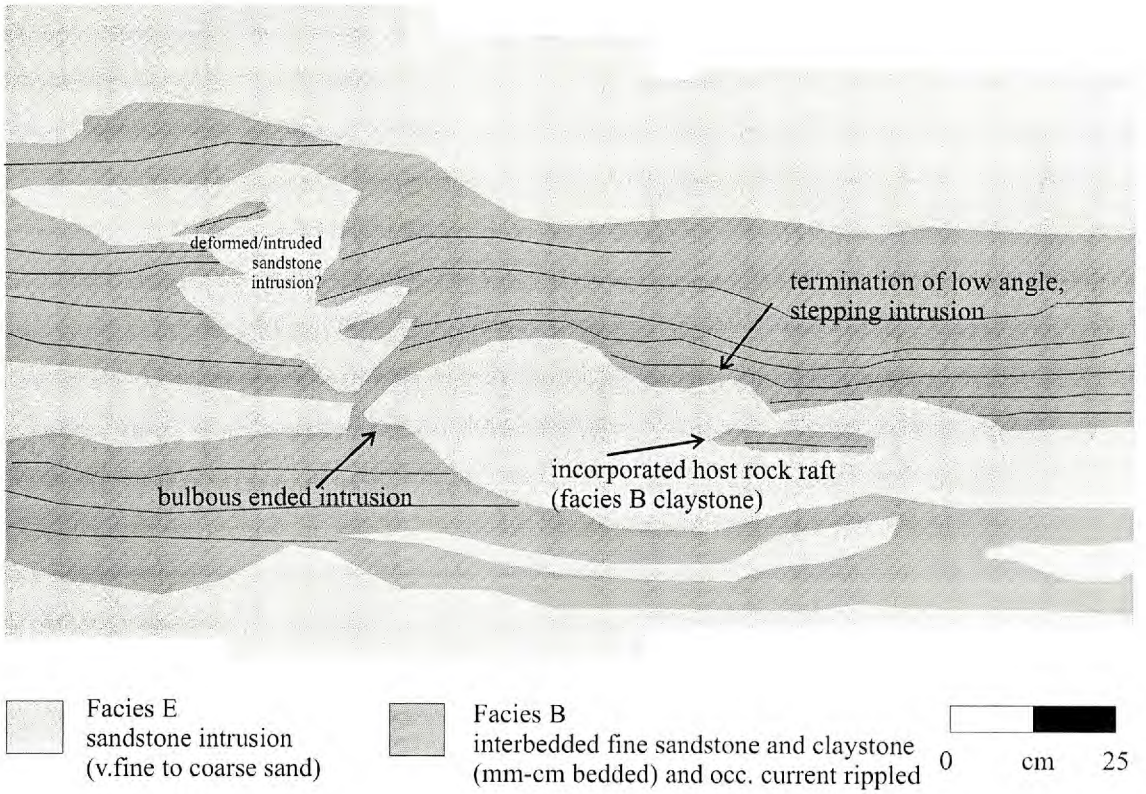


Figure 4.46. "V" shaped, low angle intrusion within the basal deepwater sediments of the Tourelle Formation, Cap Ste Anne, Quebec, Canada

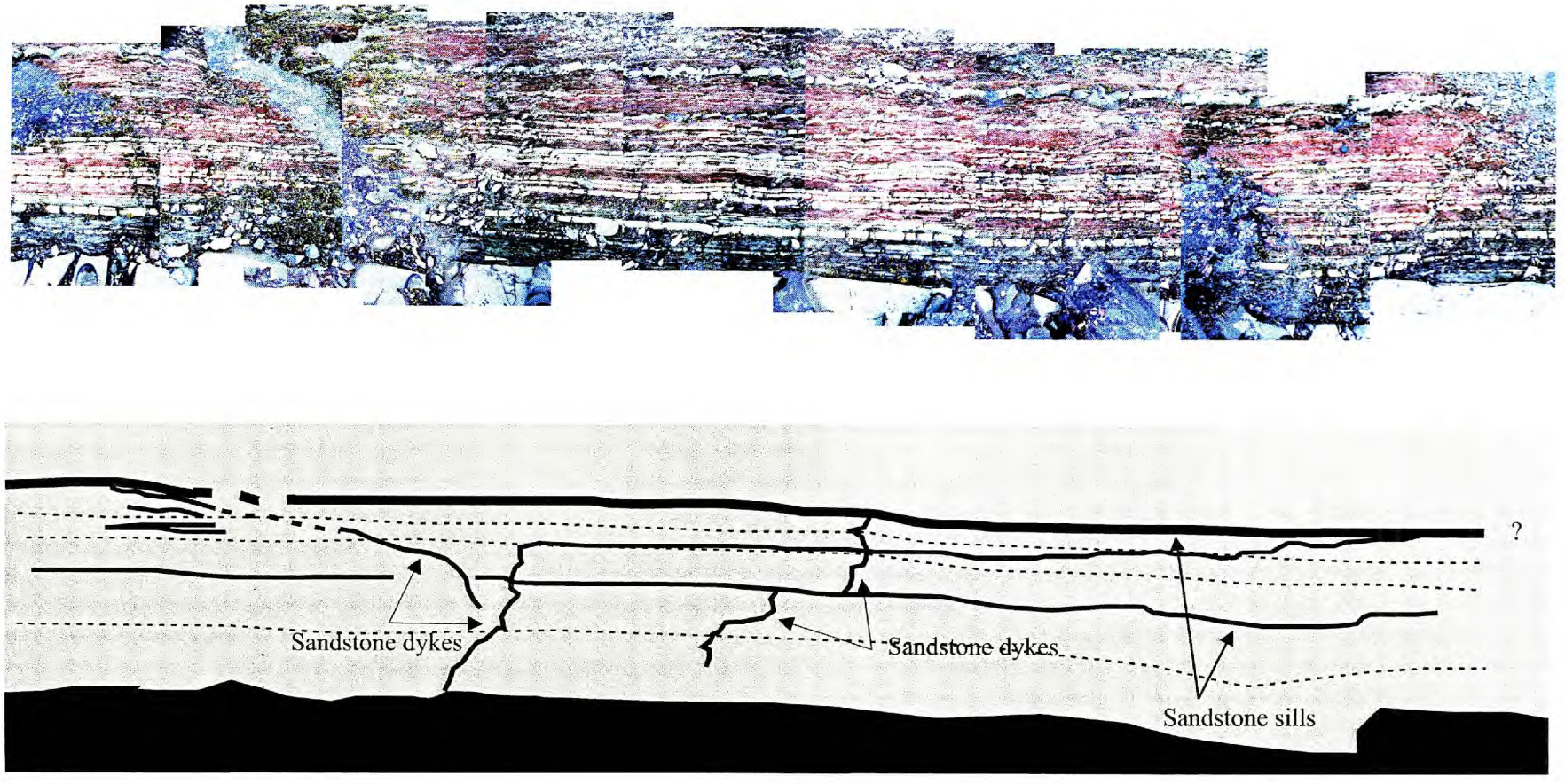
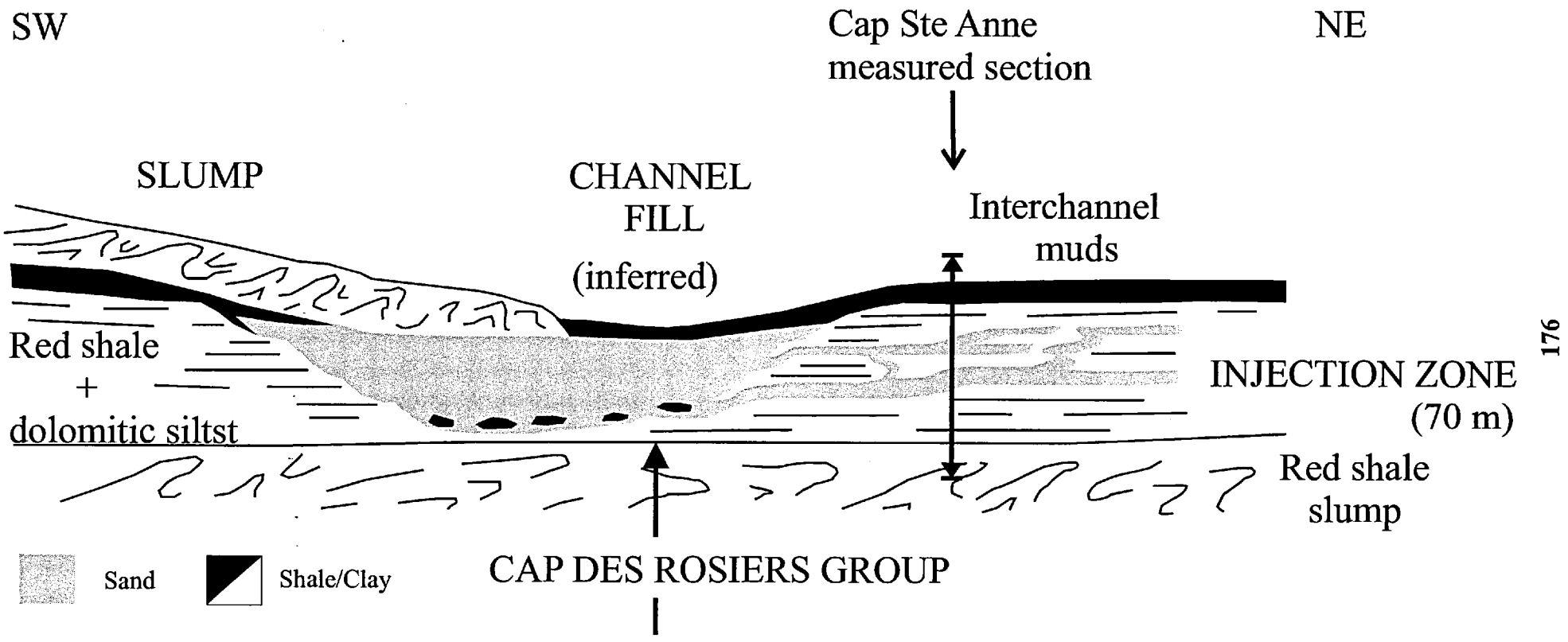


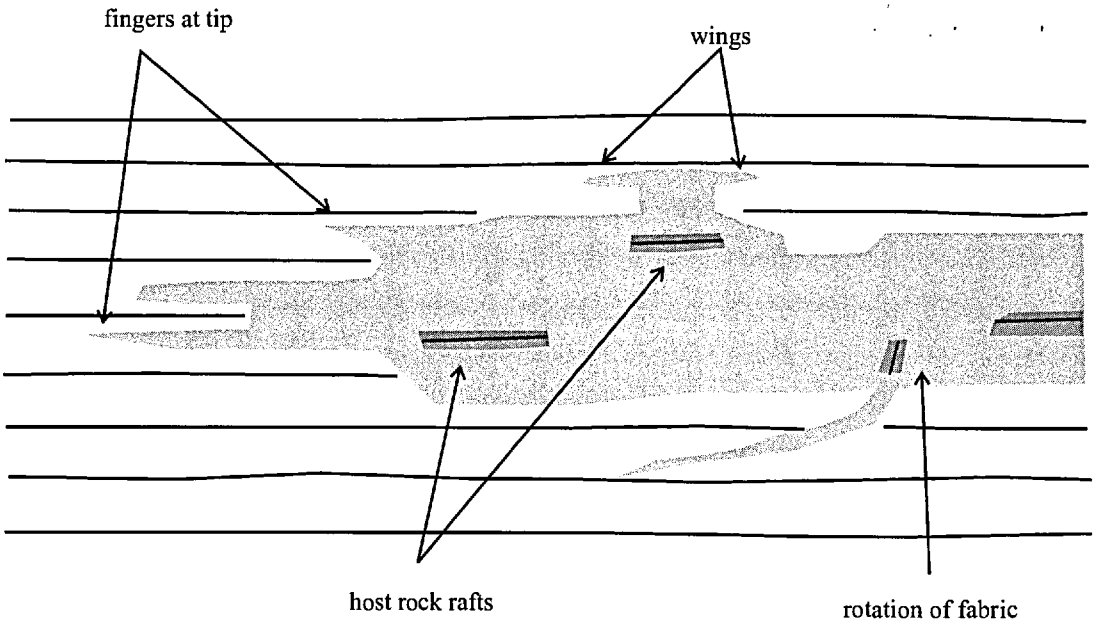
Figure 4.47. Model for injection of clastic dykes and sills from an out of plane deepwater channel sand within the basal deepwater sediments of the Ordovician Tourelle Formation, Cap Ste Anne, Quebec, Canada (Hiscott, 1979)



Note. In this model, liquefied sand is interpreted as injected laterally and upward from a sand-filled channel subjected to loading under a subaqueous slump. Impermeable red clay shales at the base of the formation prevent dissipation of excess pore fluid pressures from the liquefied sands as they flow outward from the channel margin (Hiscott 1979)

Figure 4.48. Dominant intrusive mechanisms of sills from the Ordovician Tourelle Formation, Quebec, Canada and the Ordovician Rosroe Formation, Co. Mayo, Ireland (redrawn from Lonergan *et al.*, 1999)

A. STOPING - host sediment is incorporated as rafts within the intrusion



B. DILATION - the forceful pushing apart of the host sediment

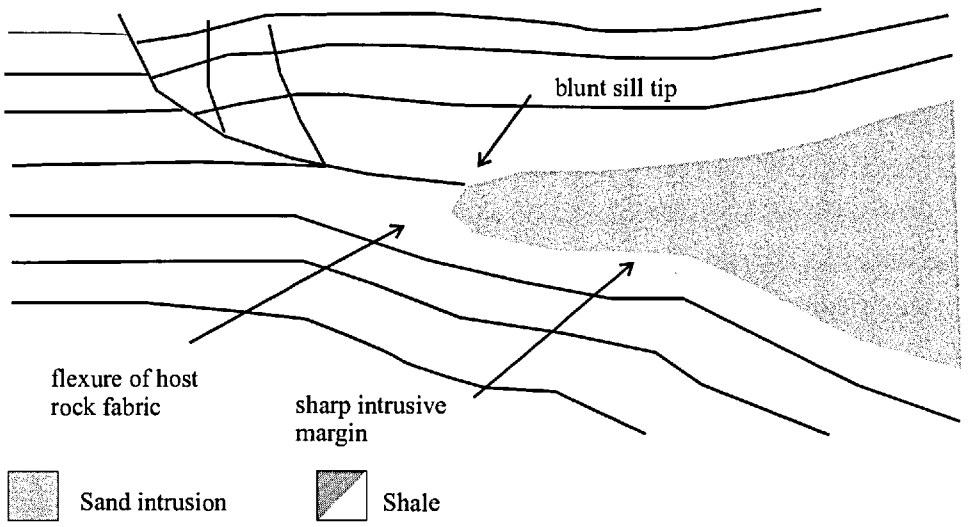


Figure 4.49. Remobilisation features within the Ordovician Rosroe Formation, Co.Mayo,Ireland and Ordovician Tourelle Formation, Quebec, Canada (partly redrawn from Lonergan *et al.*, 1999)

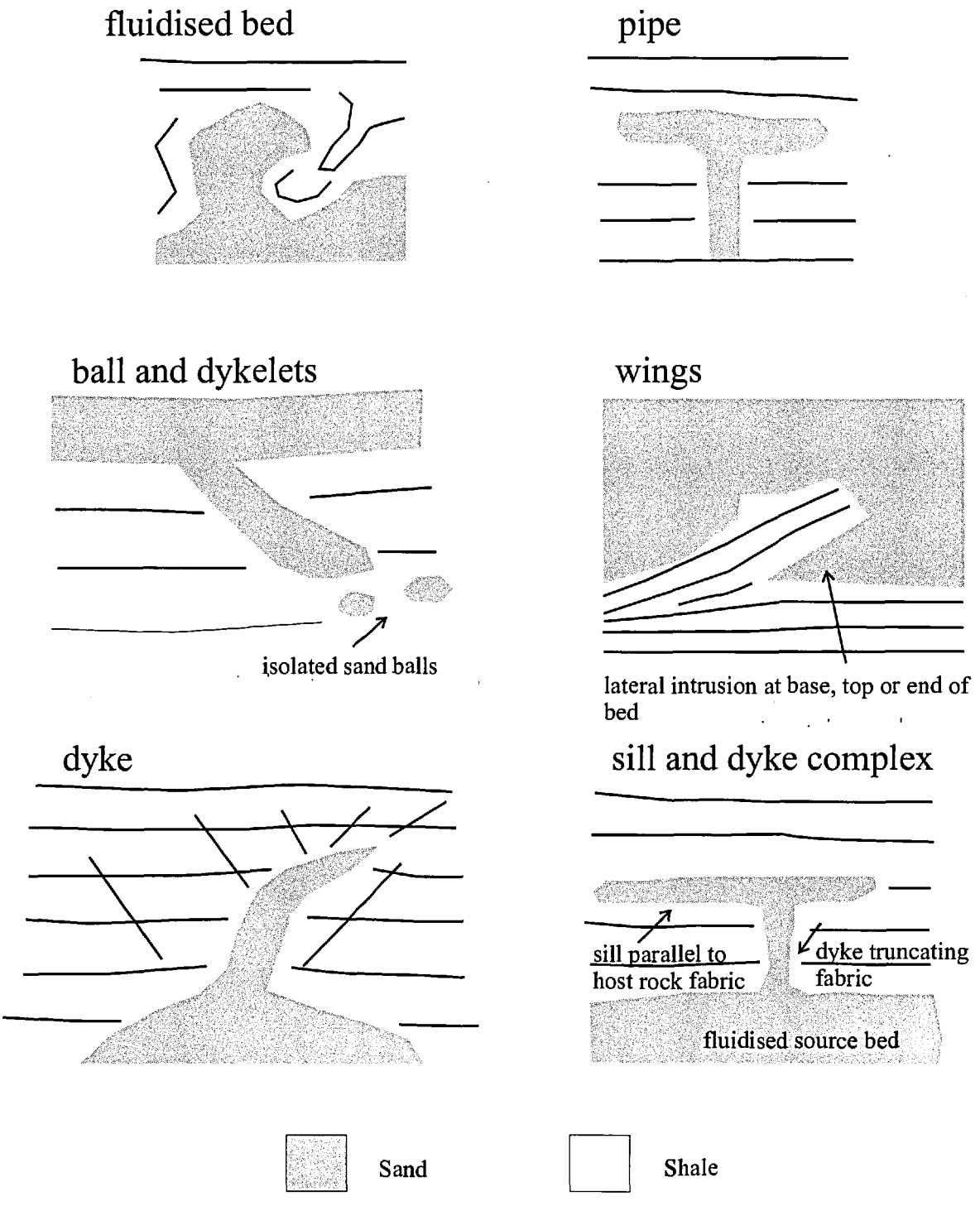
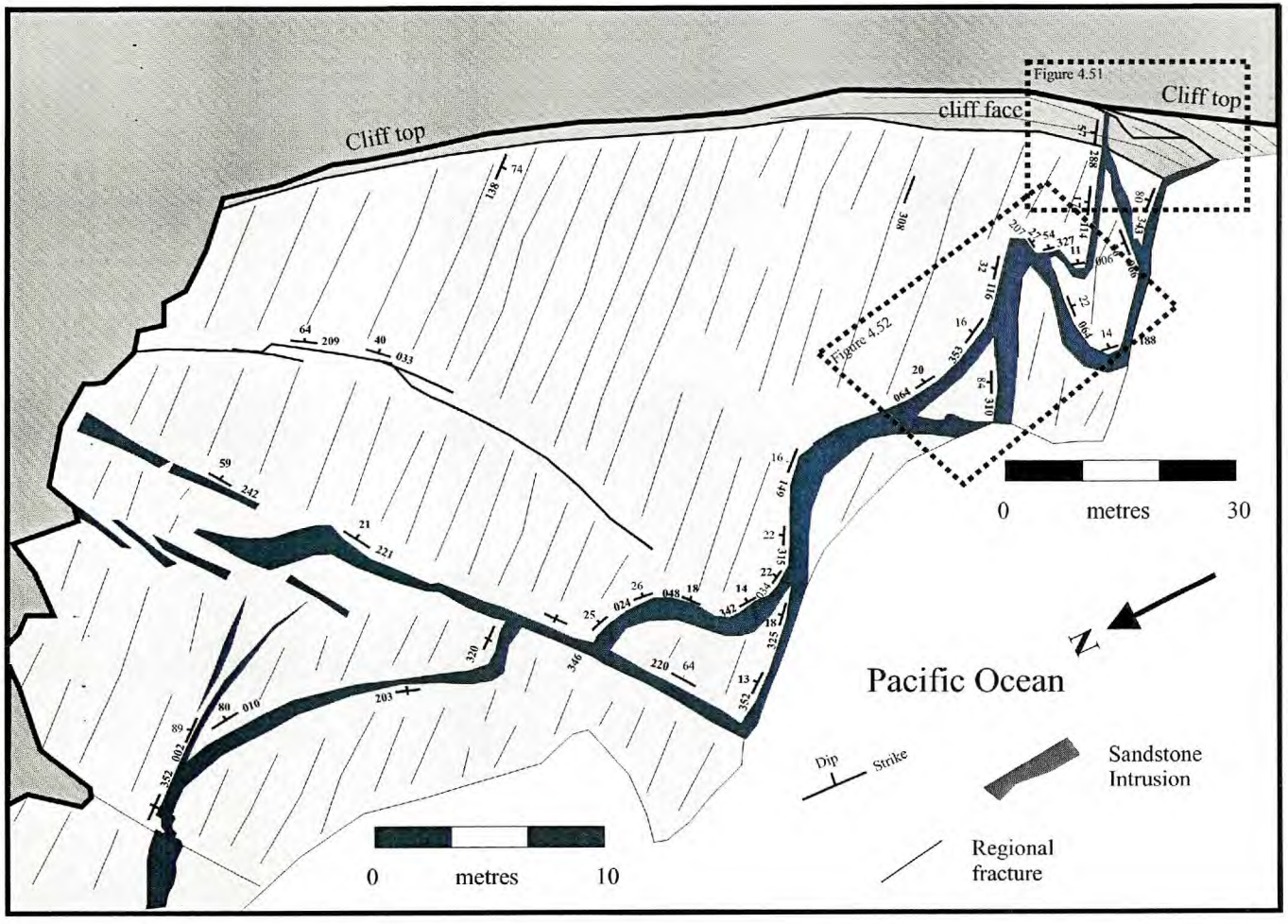


Figure 4.50. Line drawing of wavecut platform exposing low angle, conical shaped dyke sandstone intrusions in the Upper Miocene Santa Cruz diamotaceous Mudstone, Baldwin Creek, Santa Cruz, California



N.B. Sketch section taken from North to South hence perspective problem with scale.

Figure 4.51. A "V" shaped sandstone intrusion in the Upper Miocene Santa Cruz Diamotaceous Mudstone, Baldwin Creek, Santa Cruz, California, USA

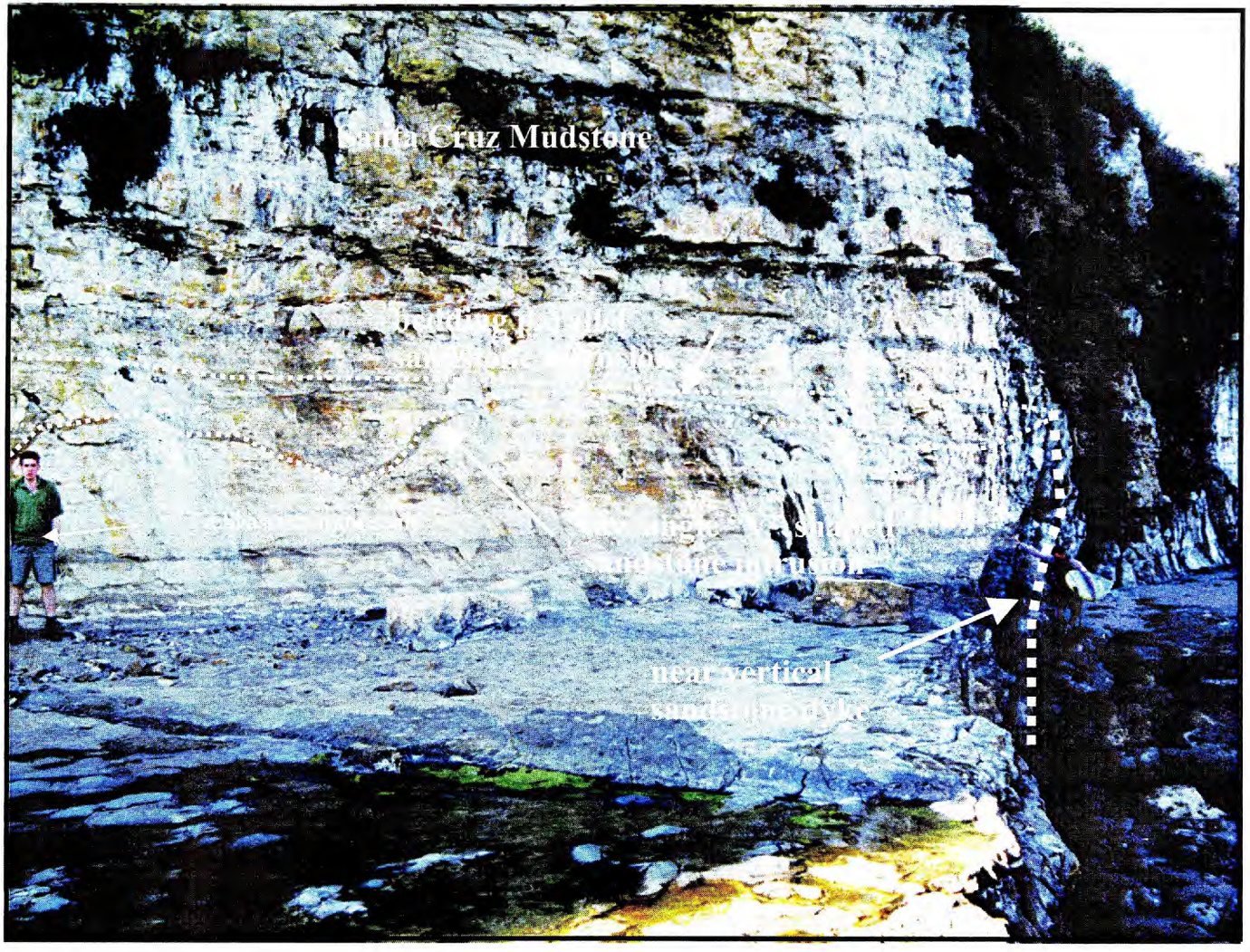


Figure 4.52. "V" shaped sandstone intrusions in the Upper Miocene Santa Cruz Diamotaceous Mudstone, Baldwin Creek, Santa Cruz California, USA



Figure 4.53. Location map of Tournaisian Horton Bluff Formation, Horton Bluff, Nova Scotia, Canada (from Martel *et al.*, 1993)

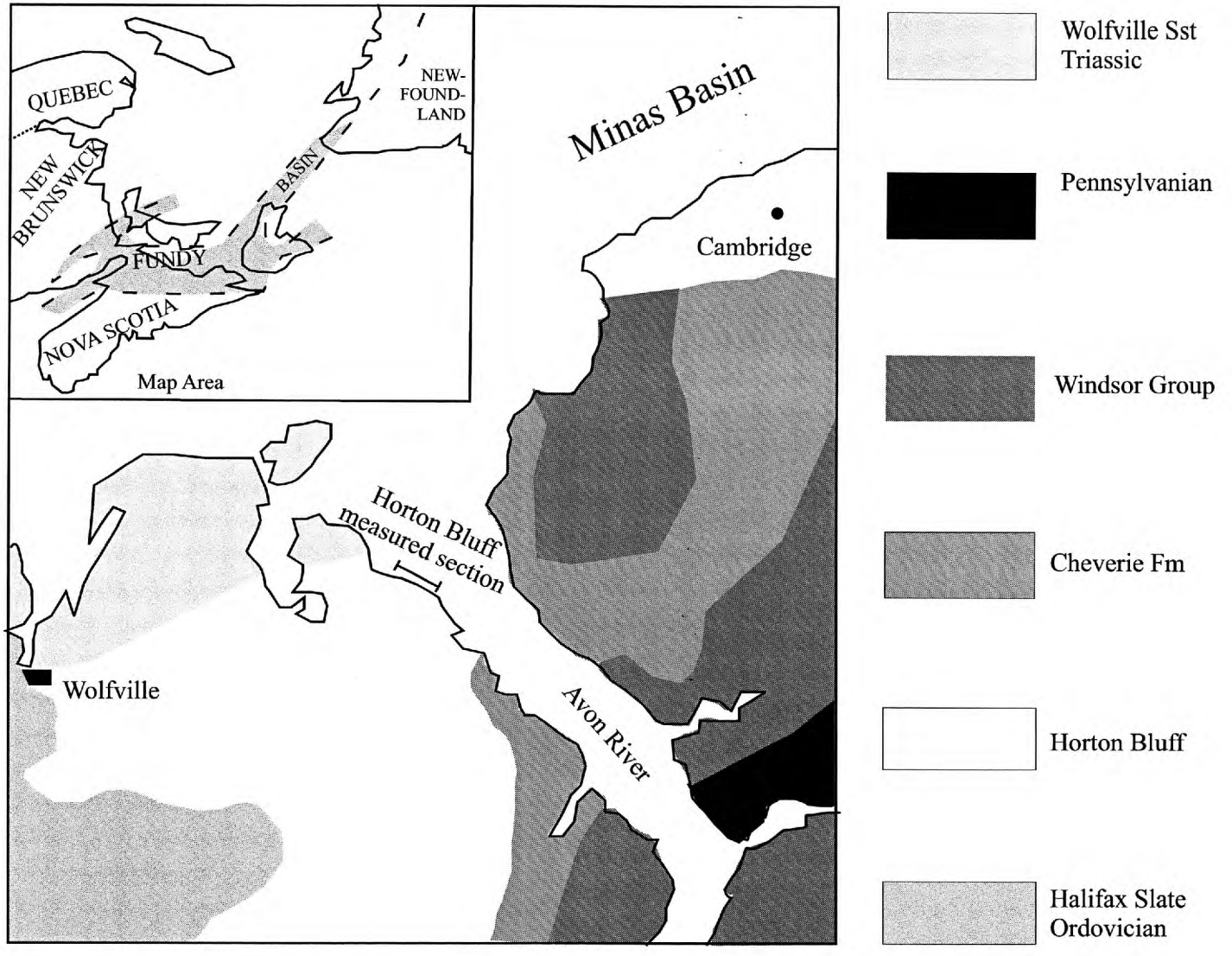


Figure 4.54. Idealised sedimentary facies sequence at Horton Bluff, of the Tournaisian Horton Bluff Formation, Nova Scotia, Canada (partly from Martel *et al.*, 1993)

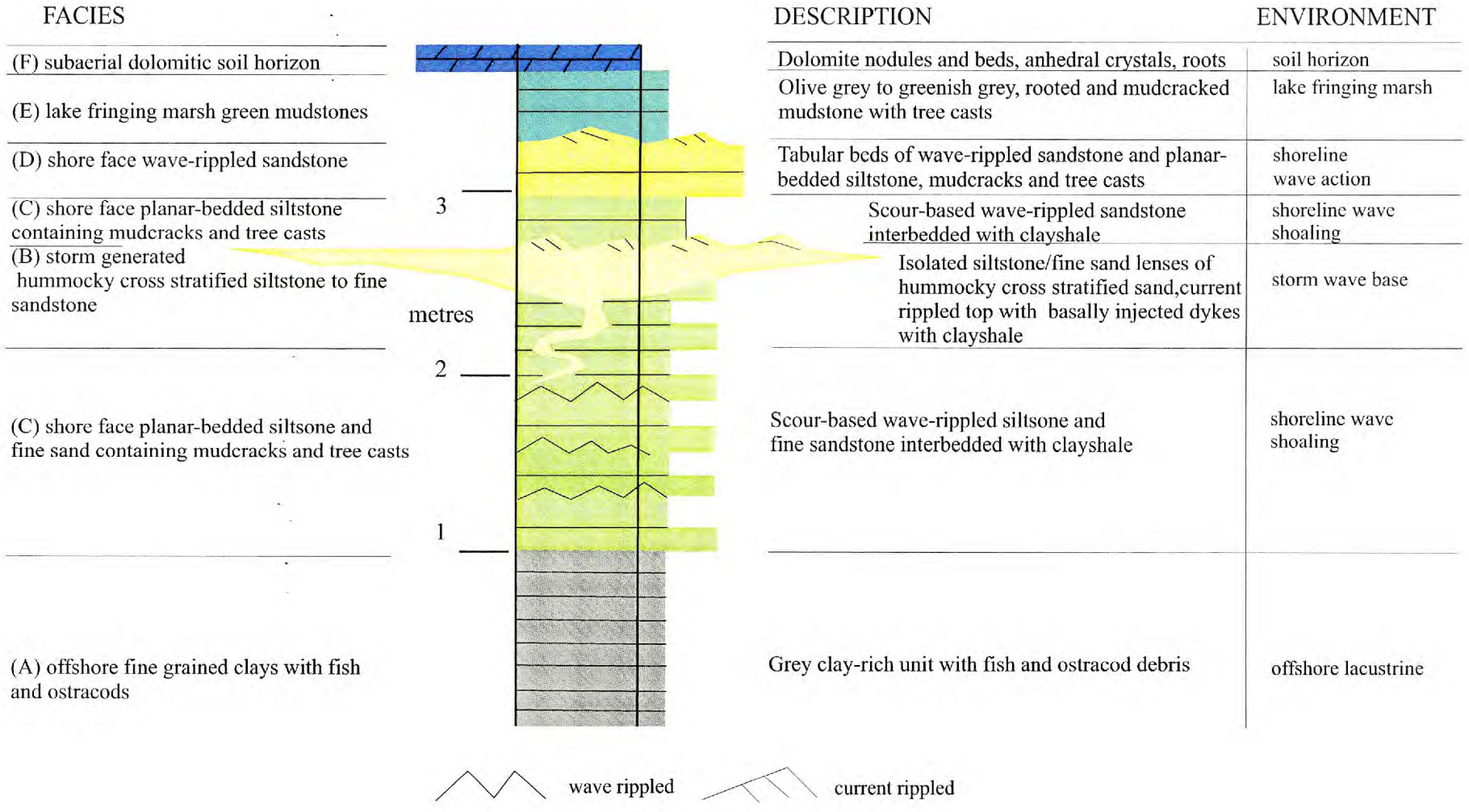


Figure 4.55. Section measured at Horton Bluff, of the Tournaisian Horton Bluff Formation, Nova Scotia, Canada

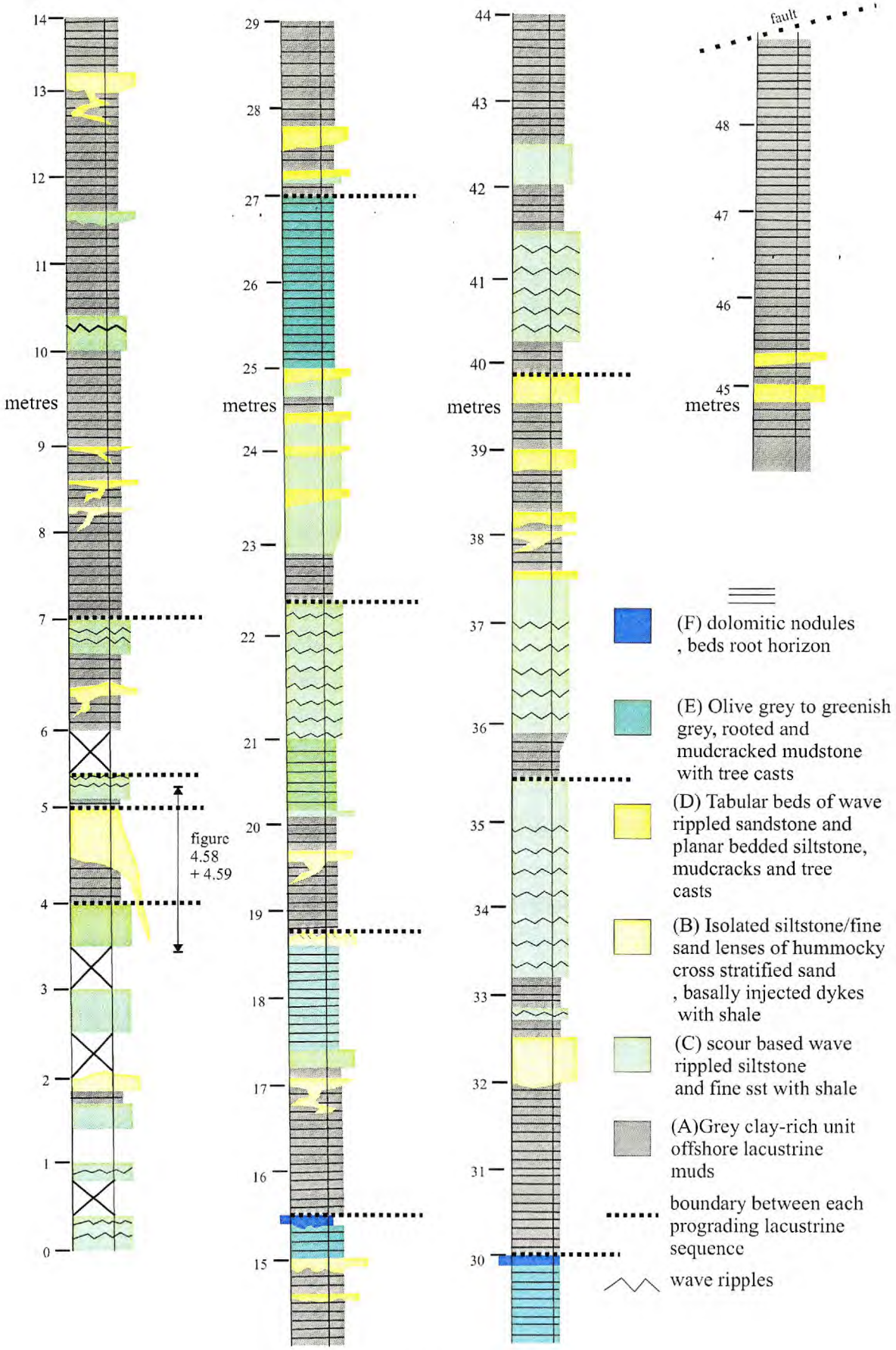


Figure 4.56. Hummocky sand facies (B) lense with intrusive sandstone dykes at the base into facies (A) offshore clays at Horton Bluff, of the Horton Bluff Formation, Nova Scotia, Canada



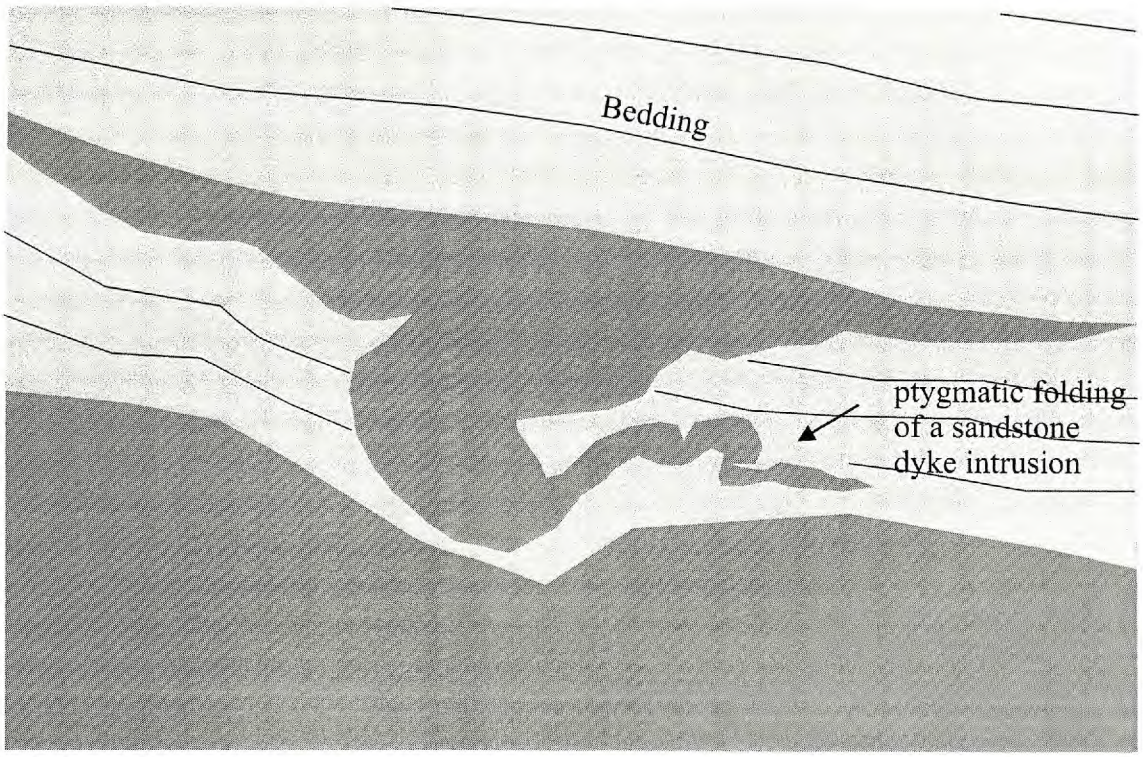


Figure 4.57. Circular "collapse" structures within the hummocky sand facies (B) lenses at Horton Bluff of the Tournaisian Horton Bluff Formation, Nova Scotia, Canada



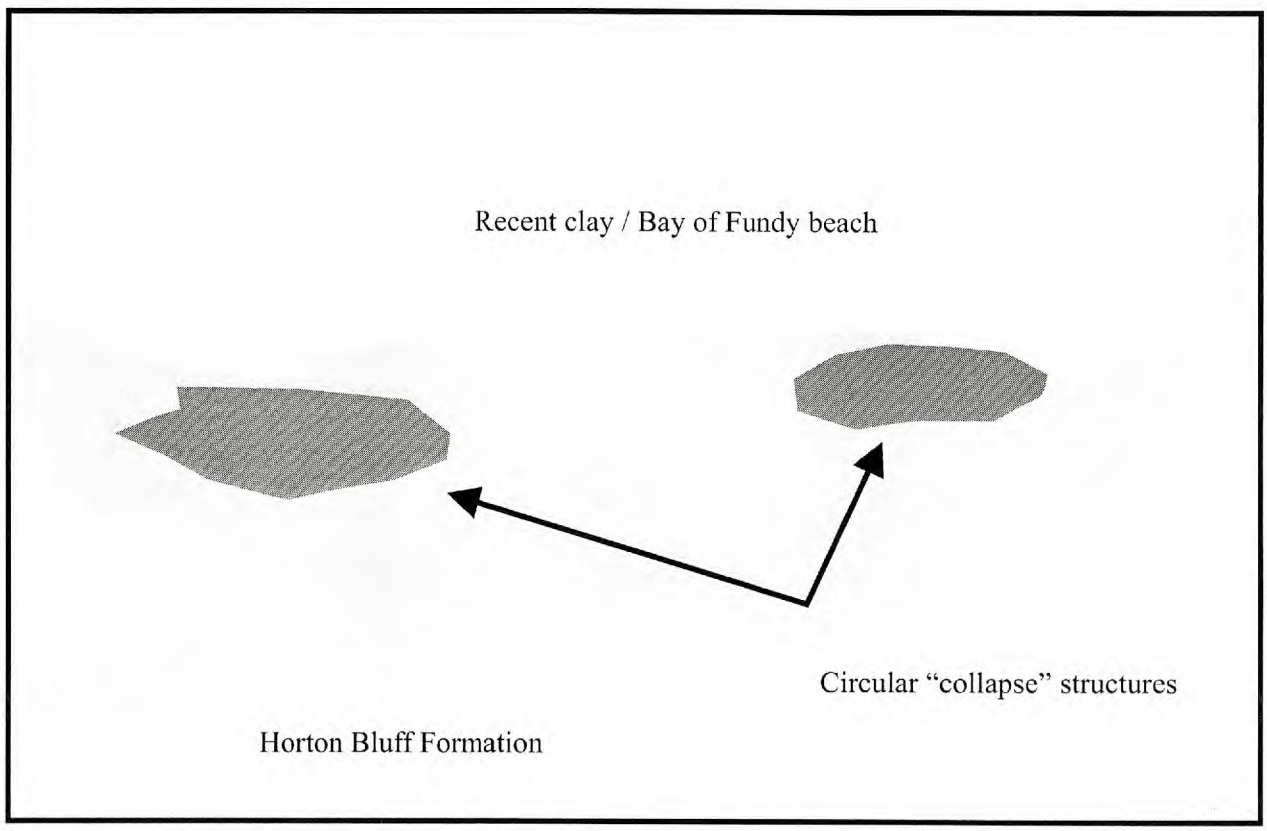




Figure 4.58. Cross section through a circular "collapse" structures within the hummocky sand facies (B) lenses at Horton Bluff of the Tournaisian Horton Bluff Formation, Nova Scotia, Canada



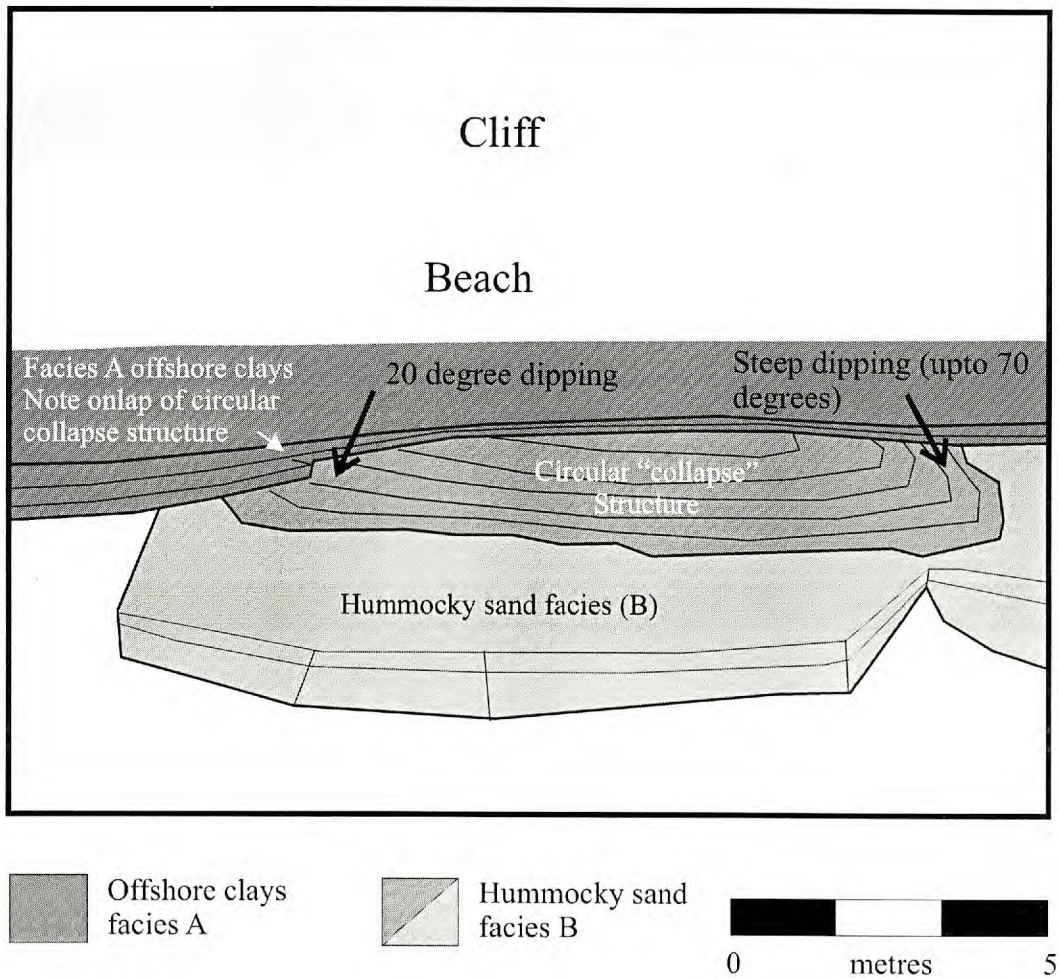
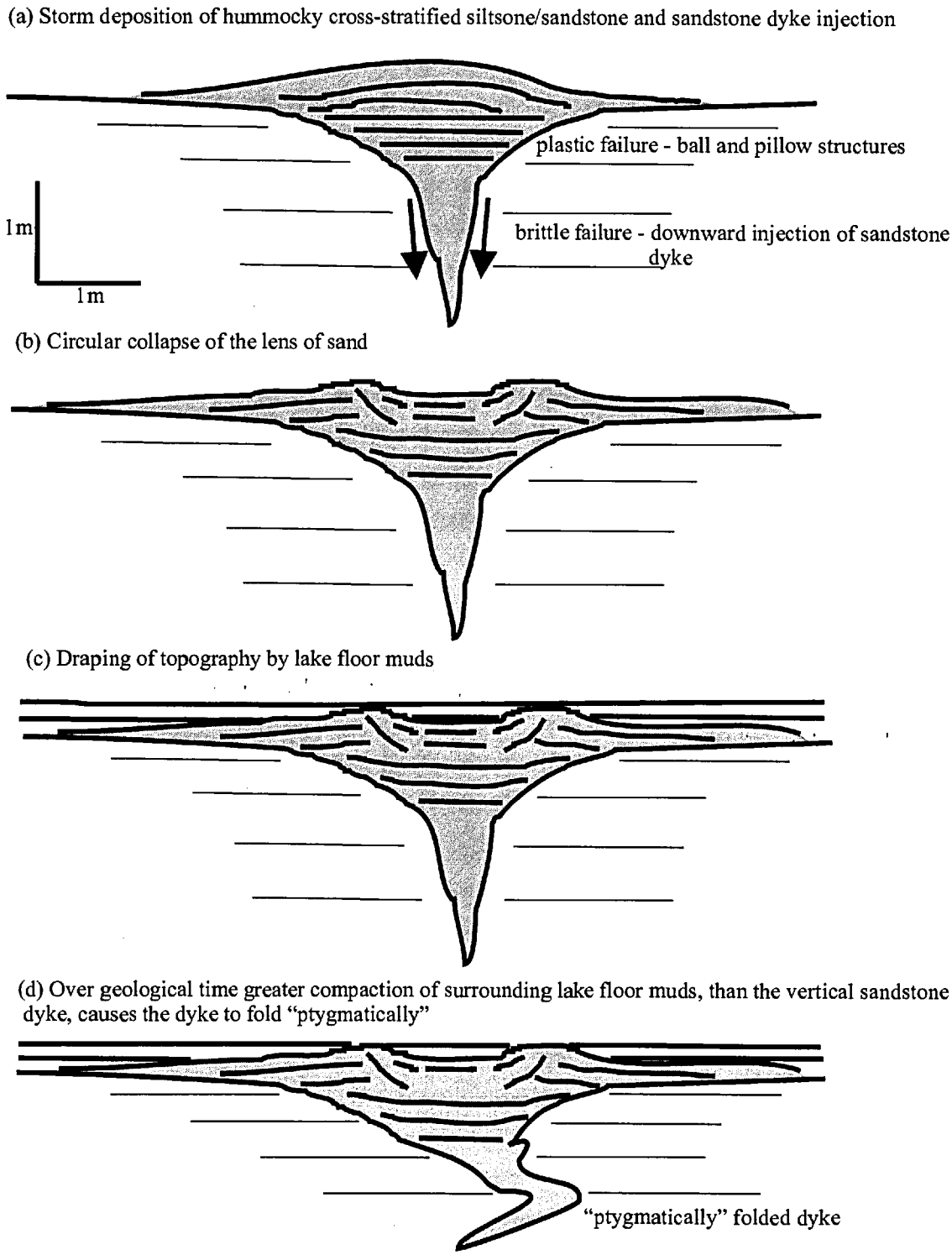


Figure 4.59. Model of circular collapse structures and basal dykes within the hummocky sand facies (B) lenses at Horton Bluff of the Tournaisian Horton Bluff Formation, Nova Scotia, Canada



CHAPTER 5. SYN TO POST DEPOSITIONAL POLYGONAL FAULTING OF THE UPPER EOCENE BELTON MEMBER DEEPWATER SANDS OF NORWEGIAN OFFSHORE BLOCK 24/9

5.1 Introduction

Upper Eocene Belton Member and Grid Formation sediments within Norwegian North Sea Block 24/9 have been analysed using a regional 2D seismic grid, a 3D block specific seismic survey and well data calibrated to the seismic (figure 5.1). Analysis of these high amplitude sandy sediments was undertaken to observe the effect seismic-scale and polygonal faulting may have had on these strata.

5.2 Geological Setting

The Tertiary of the North Viking Graben began with Danian/Thanetian major hinterland rejuvenation related to doming around a mantle hot spot centred under East Greenland (Bowman, 1998). The Early Palaeocene had volcanic activity was possibly related to east-west extension associated with Atlantic rifting and is now grouped as the British and Faeroe-Greenland igneous province. The main impact of this volcanic episode in the North Sea is exemplified by the Andrew Tuff of the Witch Ground Graben. Late Palaeocene volcanic activity associated with the onset of sea-floor spreading in the Norway-Greenland Sea, led to eruption and deposition of widespread tuff marker beds (the Balder Tuff)(Knox, 1988). Restriction of the Northern North Sea, due to the thermal doming, lead to the development of an anoxic basin in the North Sea during the late Palaeocene and early Eocene. Minor inversion in the early Eocene was possibly linked to the final rupture of the North Atlantic (Bowman, 1998; Muir Wood, 1994). This was followed by passive subsidence, leading to a clear marine connection of the North Sea with the North Atlantic (Joy, 1993). Large volumes of material were fed into the North Sea and Faeroe-Shetland Basins as major submarine-fan depocentres (Lovell, 1990). Following successful rifting of the North Atlantic, the Eocene and Oligocene are characterised by reduced rates of

clastic input along the newly developed passive margin. Sedimentation rates were reduced, the hinterland gradually denuded, and a more uniform pattern of deposition established across the North Sea and Faeroe-Shetland Basins.

From the regional 2D seismic analysis (figure 5.2 and 5.3) the Belton Member and Grid Formation are part of the Eocene-Oligocene system which progressively prograded eastward within the North Sea. This Eocene – Oligocene system (Bowman, 1998) contributed less coarse clastic sediment to basinal areas as the effects of the opening of the Atlantic immediately to the west became reduced. The Belton Member represents a rare pulse of deepwater sand into the basinal area of the North Viking Graben, from the East Shetland Platform. The subsequent Grid Formation is part of this coarse clastic pulse and corresponds to the end of the Late Eocene.

The 2D seismic interpretation (figure 5.3) places the Upper Eocene strata of Norwegian North Sea Block 24/9 within a palaeo lower slope / basin plain position, with strata thinning to the east and the sediments directly east of probable shelf clinoforms. Height from the shelf topsets updip to the Belton Member of 24/9 is at least 300 metres, and given the 2D seismic stratal relationships above, the Belton Member throughout 24/9 is interpreted to be probable deepwater sediments.

5.3 Stratigraphy

The Upper Eocene Belton Member is placed immediately below the Grid Formation (Isaksen and Tonstad, 1989). Knox and Holloway (1992) equate the Grid Formation of Isaksen and Tonstad (1989) to their Grid Sandstone Member. Both Grid equivalents and Belton Member (Isaksen and Tonstad, 1989) are placed within the Upper Eocene Horda Formation and the Stronsay Group (Knox and Holloway, 1992; figure 5.4).

5.4 Data base

5.4.1 Seismic data

Evaluation of the Belton Member was undertaken using a 3D seismic dataset spanning offshore Norwegian North Sea Block 24/9. The survey has a 12.5 meter seismic line spacing. Data quality is excellent for the Belton in the lower and upper part of the block. The middle part of the block has a poor data quality and so no maps over this region are presented herein.

5.4.2 Well data

Three wells penetrate the Belton member and Grid Formation in Norwegian Block 24/9: well 24/9-2 (figure 5.4 and 5.5), 24/9-5 (figure 5.4 and 5.6) and 24/9-6 (figure 5.7). None of these wells have been cored in this interval. Age dates and lithostratigraphic member equivalence is taken from the nomenclature on the respective well composite logs and then tied to the 2D and 3D seismic datasets. No independent biostratigraphy to corroborate the composite log tops was undertaken.

(a) Belton Member

The Belton Member from these well calibrations is noted as sand prone intervals (24/9-2 : 45 feet sand; 24/9-5 : 50 feet sand; 24/9-6 : 90 feet sand). Wireline character is blocky with the sandy interval having a faster sonic velocity than the surrounding shales by 10 to 20 us/ft. In the case of 24/9-5 and 24/9-6 there is a prominent fast sonic "spike" at the base of the Belton Member, with a slight sonic "spike" at the upper contact. Cuttings are described as being sandstone, light grey to off white, occasionally iron stained, colourless to milky grains, loose, coarse to medium grained, becoming fine to medium grained with depth, subangular to subrounded, moderately sorted, with an occasional calcite cement.

(b) Grid Formation

The Grid Formation is basally a blocky low gamma ray sand prone section increasing generally in gamma ray and shale content upwards (24/9-2 : 170 feet sand/110 feet shale and silt; 24/9-5 : 100 feet sand/ 70 feet shale and silt; 24/9-6 : 135 feet sand/250 feet shale and silt). Sonic values within the sandy units are faster than the surrounding shales by 10 to 20 us/ft. Cuttings for the sandy sections are described as predominantly loose grains, milky, transparent to

translucent, medium to coarse grained, subrounded, occasionally rounded, with an occasional calcareous cement. Cuttings for the siltstone/clay are described as olive grey to dark green, amorphous to blocky and slightly sticky, with peaty texture, non calcareous, with common black carbonaceous specks, micromicaceous, occasionally pyrite.

5.5 Seismic interpretation

Near top Jurassic (figure 3.7), Top Chalk (figure 3.8), Top Palaeocene (Balder)(figure 3.9) and Top Belton Member (figure 5.10) have been seismically mapped. The maps below the Belton are shown in chapter 3 and indicate Norwegian North Sea Block 24/9 to be situated straddling a North/South oriented Jurassic graben. Tertiary sediments as previously described, thin from east to west as part of the overall eastward prograding Tertiary clastic system. The Belton Member and Grid Formation of Norwegian North Sea Block 24/9 are located within a lower slope position as part of this prograding sequence.

Seismic interpretation of the Belton Member interval has been split up into analysis of the lower part of 24/9 (about well 24/9-2) and the upper part of 24/9 (about wells 24/9-5 and 6) as the central area of the seismic survey is of poor data quality.

5.5.1. Lower part Norwegian North Sea Block 24/9

The Belton Member was mapped line by line in both crossline and inlines by following an upper strong positive amplitude with a lower strong negative amplitude below. This amplitude response has been calibrated by the 24/9-2 well as a 45 foot thick blocky fast sonic sand (figure 5.8 and 5.9). This subsequent Upper Eocene Belton Member structure contour map (figure 5.10) expresses several fault controlled lows (figure 5.12). These lows are expressed as a higher amplitude seismic response than the higher areas as can be observed across the area by an amplitude extraction map about the Belton Member mapped interval (figure 5.11). Example A (figure 5.14 and 5.15) of such a faulted low shows the relationship of the high amplitude Belton Member within the low area, a poor

amplitude response about the fault bounded margin and low amplitude structurally higher areas. Example B of a faulted low is shown in figure 5.16 as a high amplitude fault-bounded low with lower amplitude structurally higher areas. Fault displacements are between 10-50 metres but in rare cases may be 100 to 300 metres. The fault planes are probably a composite, made up of several faults. Observing the strata within the hanging wall of these faulted lows is difficult, so any inference about the relative age of the faulting from stratal relationships is difficult. It can be seen that the faulted hanging wall lows do contain a thicker sediment fill than the footwall which suggests thickening and movement of faults during Belton Member and Grid Formation times. The faulted lows are between 100 to 2000 metres long and 100 to 1000 metres wide.

Mapping the fault pattern below the Belton Member is very difficult, if not impossible as there are only minor amplitude differences within this predominantly shale prone Eocene package and there is an overall low amplitude seismic response. With difficulty, large scale faults can be interpreted to have vertical extents of the thickness of the Eocene package (600 metres) starting from the Belton Member and soling out near the Balder horizon (figure 5.13). Whether all the fault-bounded lows in the Belton interval are part of this deeper network is conjectural due to the quality of the dataset.

5.5.2 Upper part Norwegian North Sea Block 24/9

The Belton Member interval has also been mapped by following the upper strong positive amplitude of this interval. Well calibration (24/9-5 and 24/9-6; figure 5.17) to seismic confirms the seismic response of the Belton Member sands as an upper strong amplitude and a lower negative amplitude related to a sand-prone Belton interval at this location. As in the Lower part of the 24/9 Block, the upper part of block 24/9 structure contour map shows these faulted lows as being areally 100 to 2000 metres long to 100 to 1000 metres wide (figure 5.18). A maximum amplitude extraction about this Belton Member horizon indicates the amplitudes are concentrated within the low fault-bounded areas (figure 5.19). In addition, an isopach between the Belton Member and an

intra-Oligocene horizon indicates the areas of fault bounded lows are isopach thicks and the intervening areas have thinner strata (figure 5.20).

Figures 5.18, 5.19 and 5.20 outline two examples of fault bounded lows (examples C and D) that are described below:

(a) Fault-bounded low C (figures 5.21 to 5.30)

This fault bounded low shows the Belton Member to be of a high amplitude within fault-bounded low. Seismic figures 5.26, 5.27, 5.28 and 5.29 especially show the fault controlled nature of the high amplitude low area. The fault bounded low may itself be faulted as shown in figure 5.23. For this example, it proved difficult to map the fault pattern, however fault-bounded low D proved easier to map and is described below.

(b) Fault bounded low D (figures 5.31 to 5.36)

These fault bounded lows about wells 24/9-5 and 6 indicate the half graben nature of the faulting (figure 5.31), with maximum fault displacements of 50 to 150 msecs (50 to 150 metres). The faulted low about well 24/9-6 is a multiply-faulted half graben, especially shown on seismic figures 5.33 to 5.36. These seismic lines again show the relationship of high amplitude fault bounded lows and the lower amplitude structurally higher areas within the faulted Belton Member interval. In addition 200 msecs TWT above the Belton Member, there are smaller displacement faults. These faults appear to be unconnected to the faulting Belton Member faulting below. This suggests that a boundary exists between the Belton Member fault set and the subsequent Oligocene fault set. Mapping of this Oligocene fault set (Tervoort 2000; figure 5.32) indicates a polygonal fault pattern similar to the polygonal faults described Cartwright (1994a, b). These polygonal faults are organised into composite fault rosettes, with areal dimensions of between 500 to 1000 metres per polygonal fault rosette and composite fault displacements of 10 to 50 msecs with no preferred orientation of fault traces (Tervoort, 2000).

5.6 Interpretation and Analogue horizon

From the regional work the Belton can be designated as a deep water system and the blocky sandy wireline character supports this deepwater affinity (a

massive mass flow /remobilised sand). The main questions arising about the origins of these fault bounded lows are:

(i.) Did the faulting control the Belton deepwater sand deposition or did the faulting compartmentalise the Belton sands post deposition?

(ii.) What caused the faulting?

To address question (i.) it is argued that since the sand is concentrated in the faulted lows (high amplitude response) and not on the higher areas (lower amplitude), that these sediments were concentrated in the faulted lows during deposition. For the faulting to have compartmentalised the Belton sands after deposition, then the Belton Member would be seen as an offset high amplitude event across the whole area, assuming near constant deepwater sand deposition. This is not the case within this interval.

Question (ii.) highlights the origins of the faulting. If the Belton Member faulting had a preferred orientation then it could possibly be ascribed to tectonic faulting or to syn depositional growth faulting gravitationally displacing downslope of the large scale slope clinoforms. As has been noted there appears to be no preferred orientation of the Belton Member faulting, and thus has more the geometrical and dimensional characteristics of the large scale polygonal fault rosettes in the intra Oligocene interval (figure 5.32; i.e. both the Belton Member and Oligocene faulting have no preferred orientation of fault pattern, approximately similar fault displacements and areal fault bounded low dimensions).

From the observations made above, it is suggested here that the Belton deepwater sediments were deposited onto a palaeoseafloor which had a polygonal fault pattern nucleated on it. This polygonal fault pattern may have been similar to the Oligocene fault pattern. Loading of these polygonal fault horsts and lows during deposition by the deepwater Belton sediments may have enhanced the kinematic behaviour of this polygonal faulting and continued to concentrate deepwater deposition into these faulted lows through the Belton to the Grid Formation i.e. they may have behaved as load-driven growth faults. The faulting may also have caused smearing of sand and possible sand injection along these fault planes, which may explain some of the discontinuous high amplitude seismic responses along these fault zones (figure 5.37). The movement of the

fault would variably smear the deepwater deposited sand of the Belton Member along these fault planes syn and post depositionally. Sand intrusion is outlined as a possiblity for this discontinuous fault plane reflector. The mechanism would involve overpressure building up in the areally restricted Belton Member deepwater sands from burial dewatering. Sequential movement along the fault plane could act as a conduit of pressure release for these overpressured Belton sands and potentially inject these deepwater sands up along the fault plane thus giving a series of fault controlled sands (a variable high event).

A possible geometrical analogue to these Upper Eocene Belton Member polygonally faulted lows has been suggested by Whitbread and Anderton (1997) who interpreted a Lower Eocene turbidite sand interval over UK Central North blocks 16/23 and 24. They interpreted similar scales of geometries in cross section and in plan view to the Upper Eocene Belton Member of Norwegian North Sea Block 24/9. They attribute this reservoir geometry to post-depositional remobilisation of an originally deposited turbidite sand (figure 5.38). The original deposition of a deepwater turbidite from the NW, subsequently loaded and pillowed the clay substrate onto which it had been deposited. This process continued and caused low angle fault planes along which sand injected/smeared to create the high amplitude "V" shaped structures as in 24/9 with a down thrown side of high amplitude sand and a fault plane of discontinuous amplitude interpreted to equate to the injected/smeared fault plane. Whitbread and Anderton (pers.comm. 1998) subsequently agreed that these faults may be polygonal in character and instead of the faulting being induced by diapirism and pillowing of the Eocene shaley substrate, deposition into polygonally fault induced lows was a more probable process. In their example the high amplitude response was continuous across the blocks from one fault bounded low to a structurally higher area. This implies that sedimentation was in this case not affected by the polygonal faulting, but was offset post depositionally. This is a significant difference with regard to the timing of the post- to syn-depositional polygonal faulting of the Belton Member sands in Norwegian North Sea Block 24/9.

5.7 Conclusion

The Belton Member is interpreted to be a deepwater mass transport sand, deposited onto a polygonally faulted palaeoseafloor of Eocene clays. Sand deposition was preferentially concentrated into the polygonally faulted lows, while the high areas had thinner amounts of sand deposited. Subsequent Grid Member sands deposited into these polygonally faulted lows which continued to form, accommodating the Grid member sediments. By the end of the period of deposition of the Grid Formation sediments the polygonal fault topography and Eocene polygonal faulting ceased to be active. On resumption of clay deposition in the lower Oligocene, a new set of polygonal faults began to form of similar dimensions to the Belton Member faulting below, with both fault systems apparently unconnected vertically.

Figure 5.1 Location map of Norwegian offshore North Sea Block 24/9 (partly from PESGB, 1997), with portion of block interpreted through the Upper Eocene Belton Member

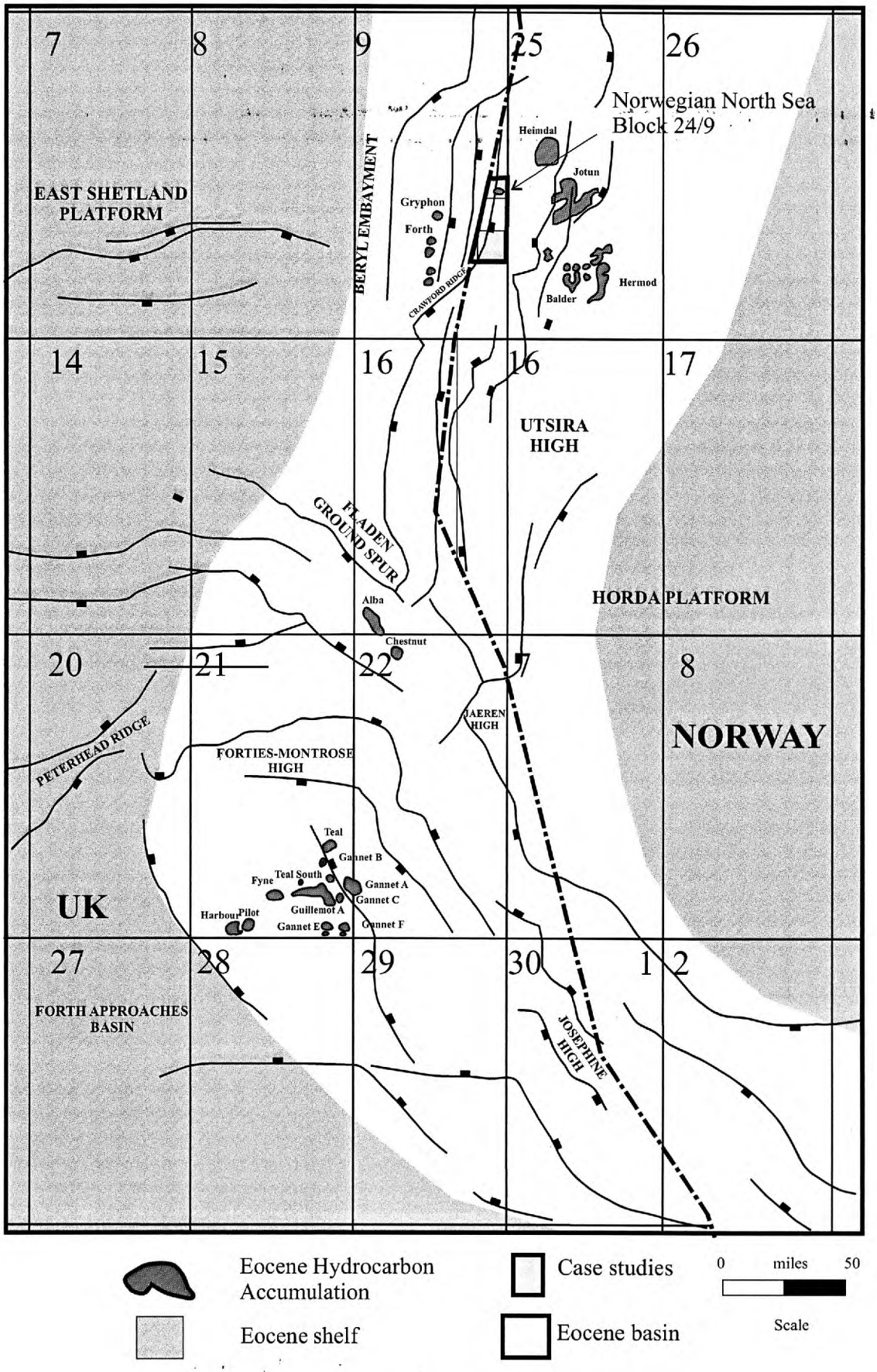


Figure 5.2. Geological cross section across the North Viking Graben through Norwegian North Sea Block 24/9 (from CNST82-09 regional seismic line)

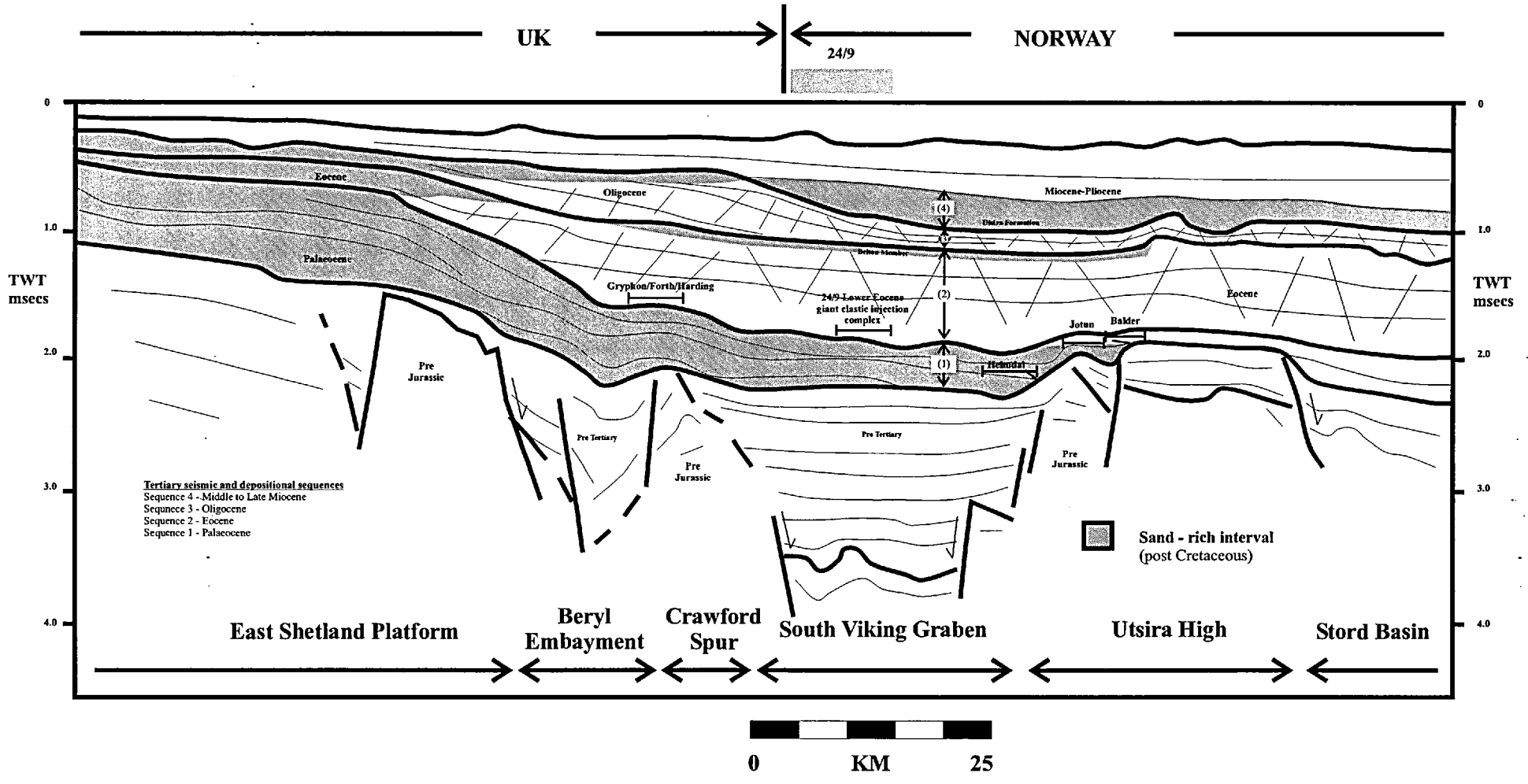


Figure 5.3. Palaeogeographic map of the Middle to Upper Eocene strata in the North Sea

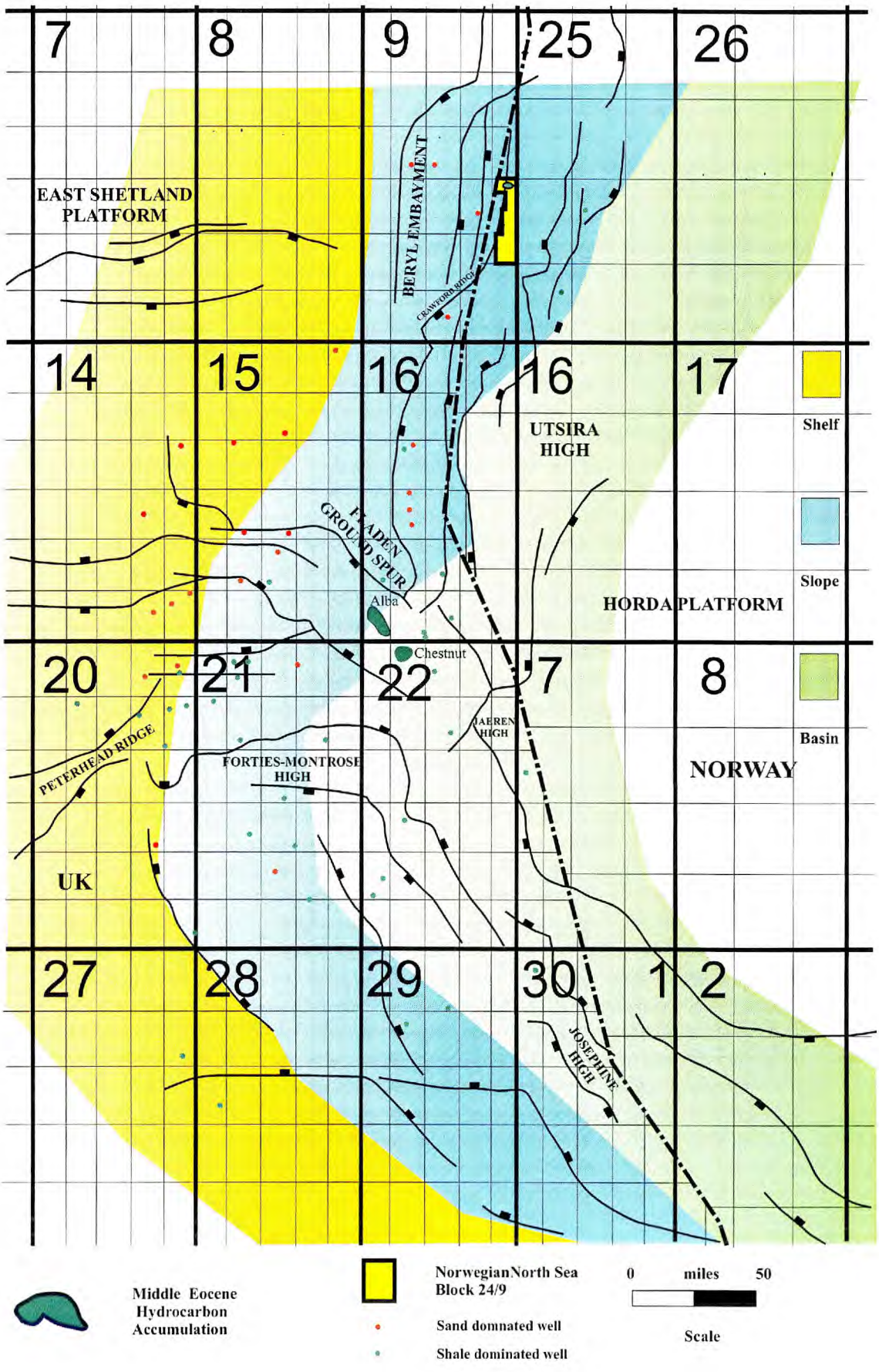


Figure 5.4. Well calibration/stratigraphy of the Upper Eocene Belton Member in Norwegian North Sea block 24/9 (from well 24/9-2 and 24/9-5)

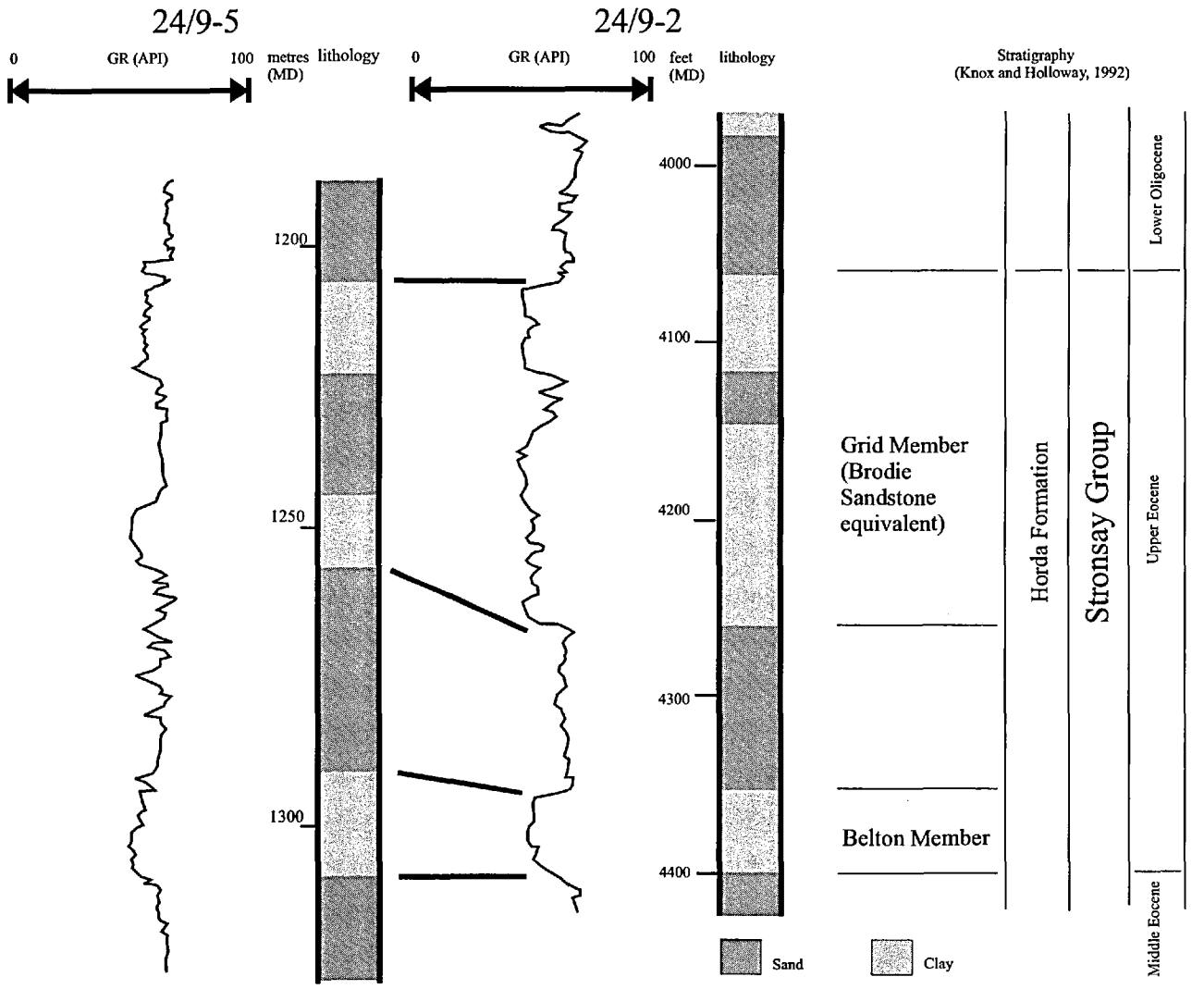


Figure 5.5. Norwegian North Sea well 24/9-2 over the Upper Eocene Belton Member and Grid Member.

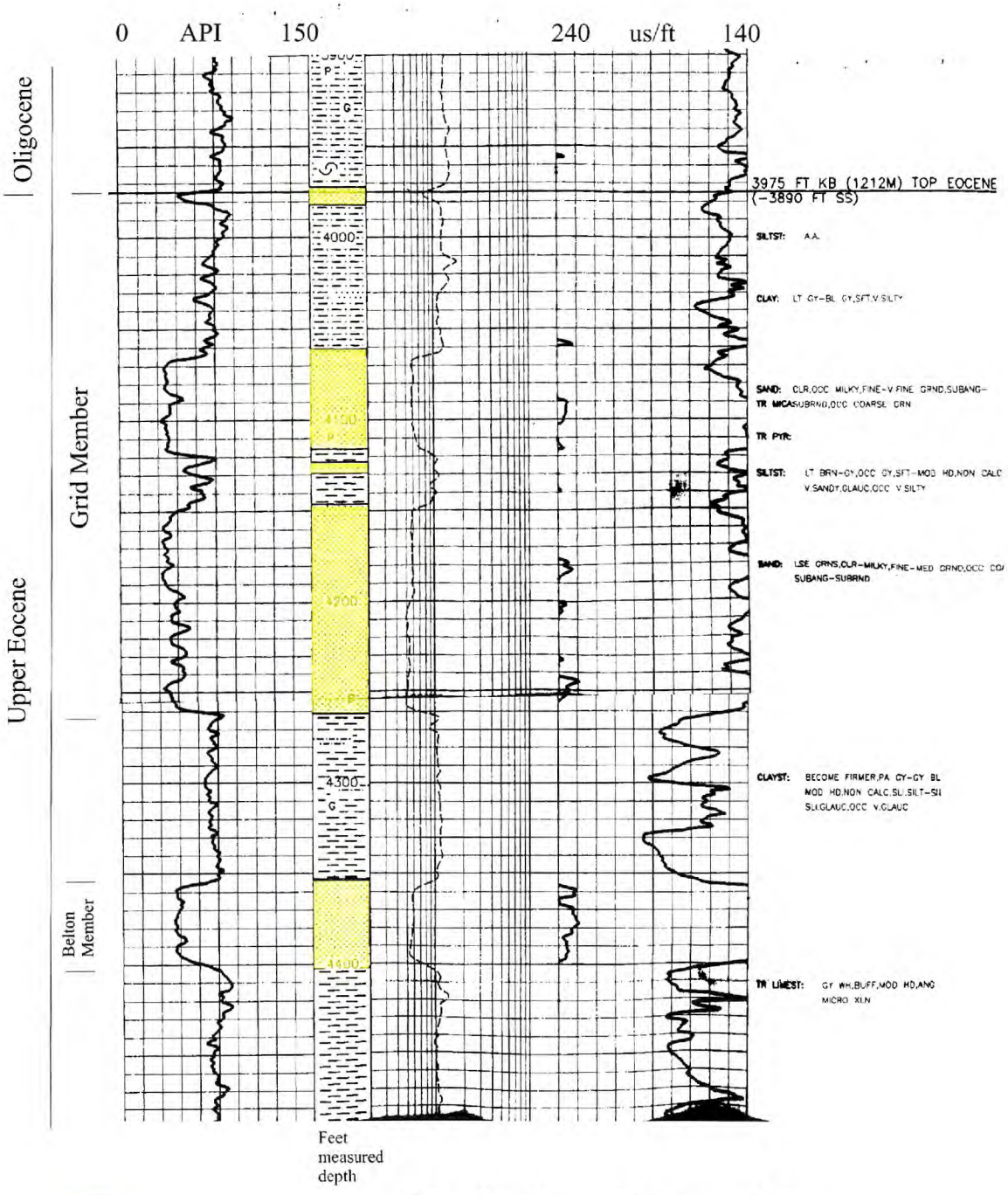


Figure 5.6. Norwegian North Sea well 24/9-5 over the Upper Eocene Belton Member

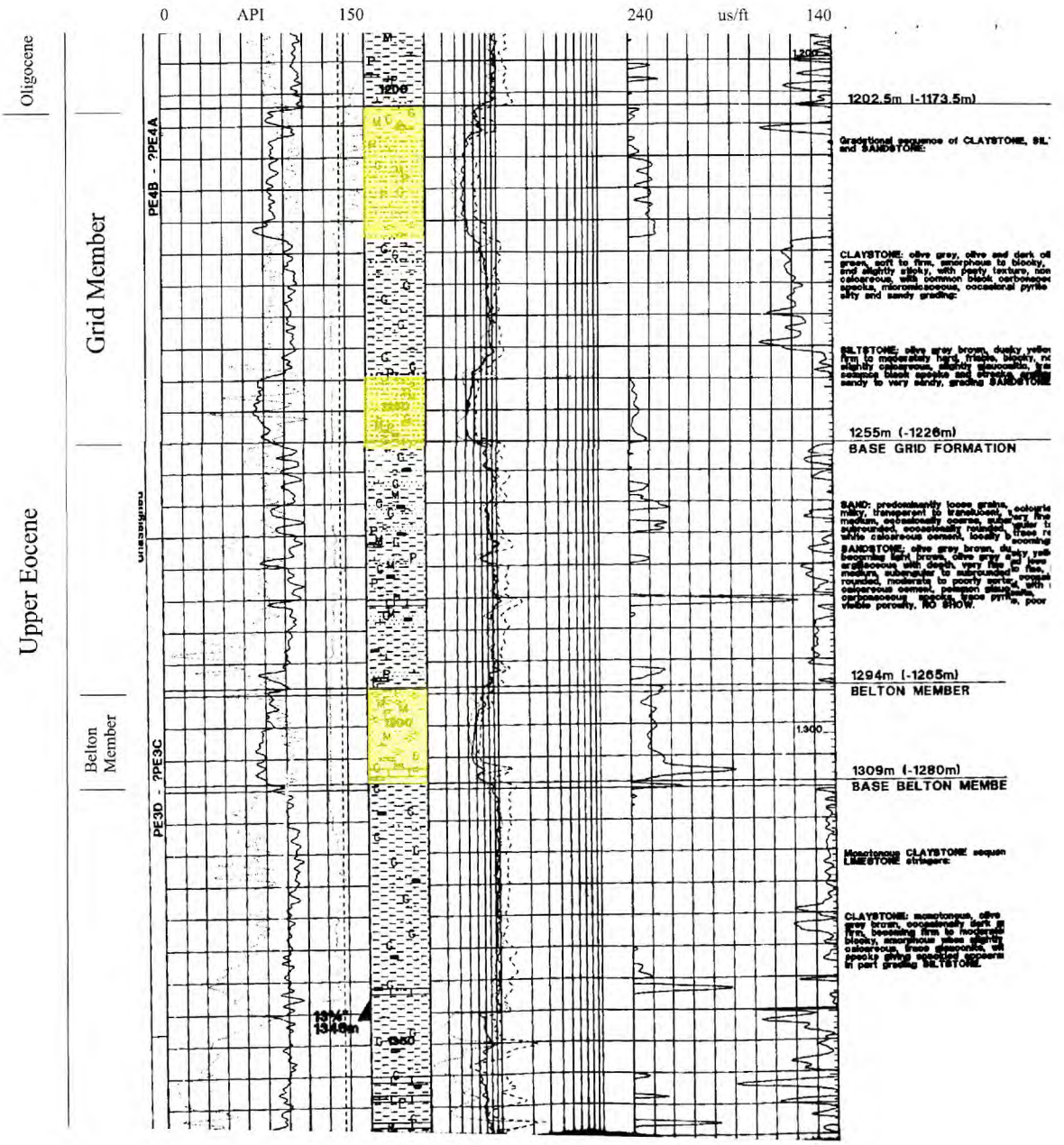
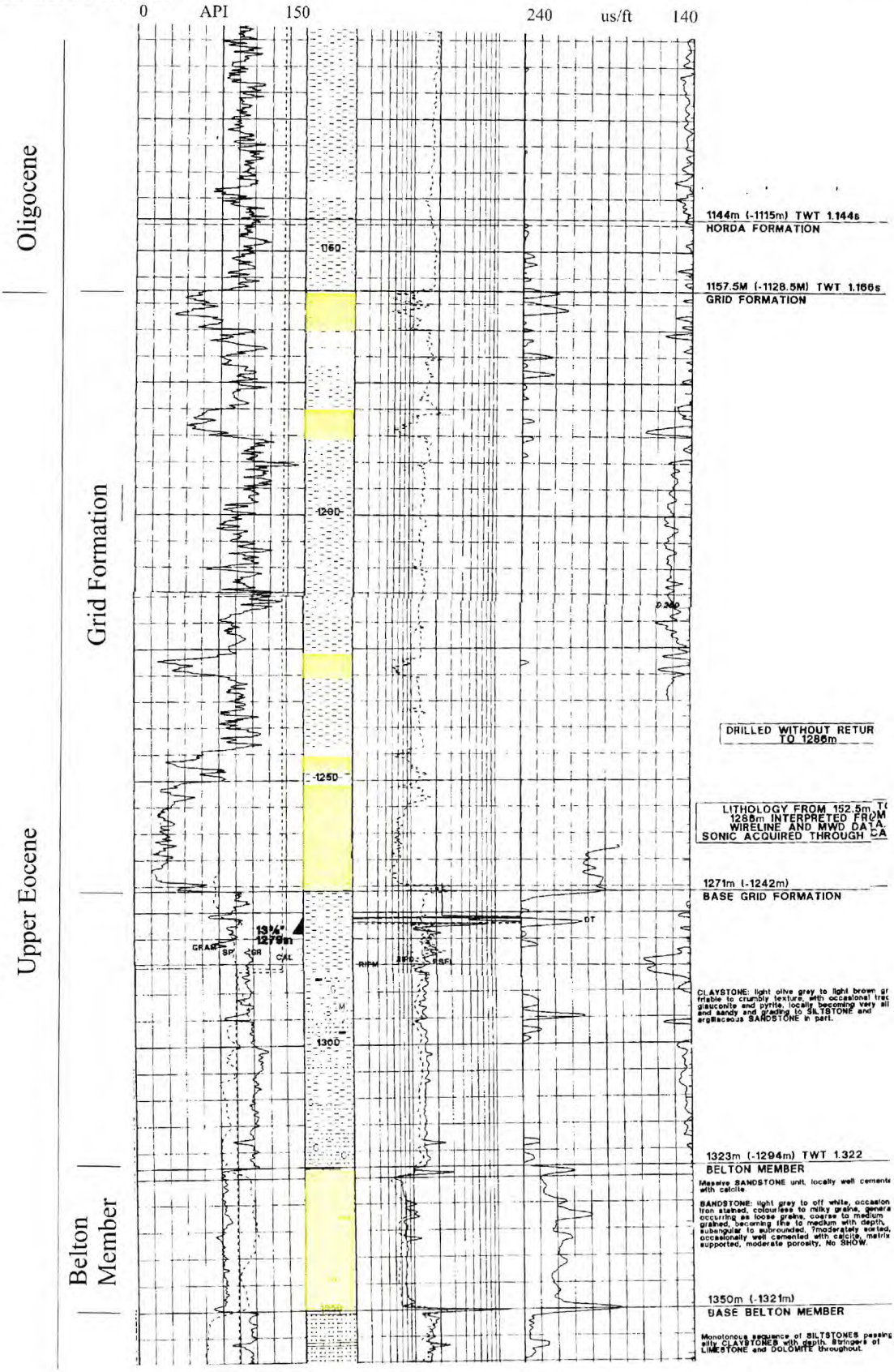


Figure 5.7. Norwegian North Sea well 24/9-6 over the Upper Eocene Belton Member and Grid Member



Belton Member

Belton Member sand thickness : 90 feet

Grid Member sand thickness : 135 feet

Figure 5.8.. Norwegian North Sea well 24/9-2 penetration through the Upper Eocene Belton Member - crossline 1966

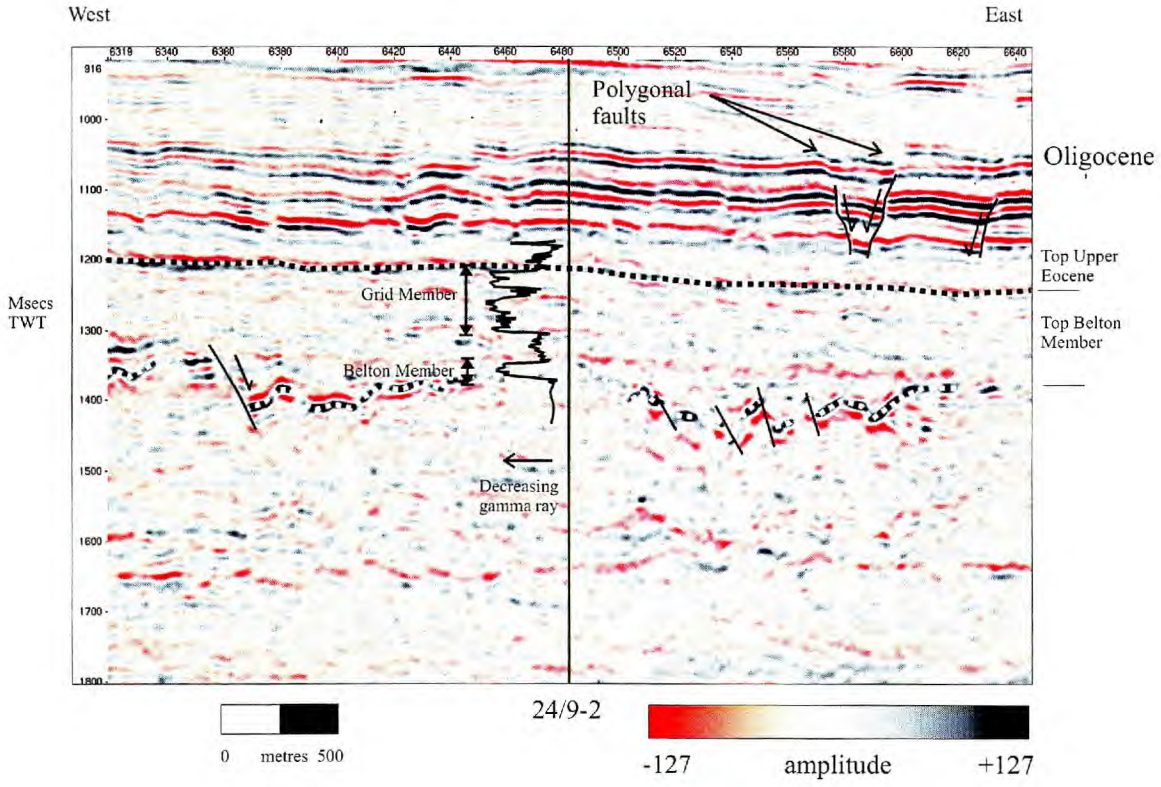


Figure 5.9. Norwegian North Sea well 24/9-2 penetration through the Upper Eocene Belton Member - inline 6484

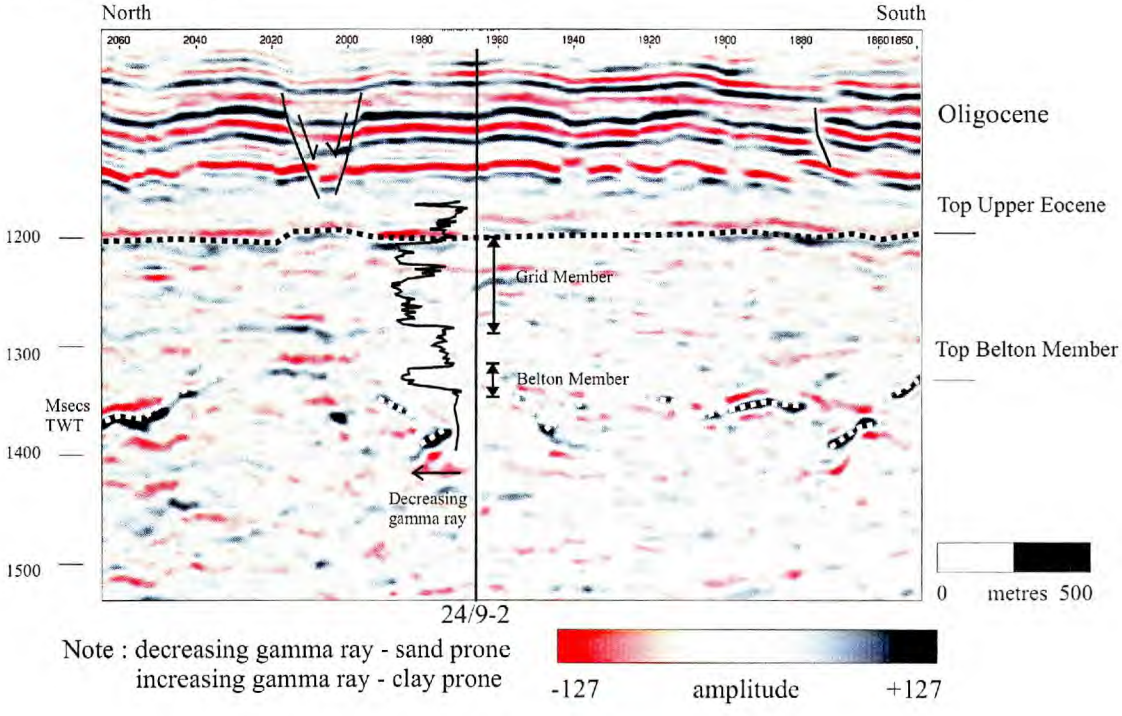


Figure 5.10. Norwegian North Sea Block Upper Eocene Belton Member Top structure map

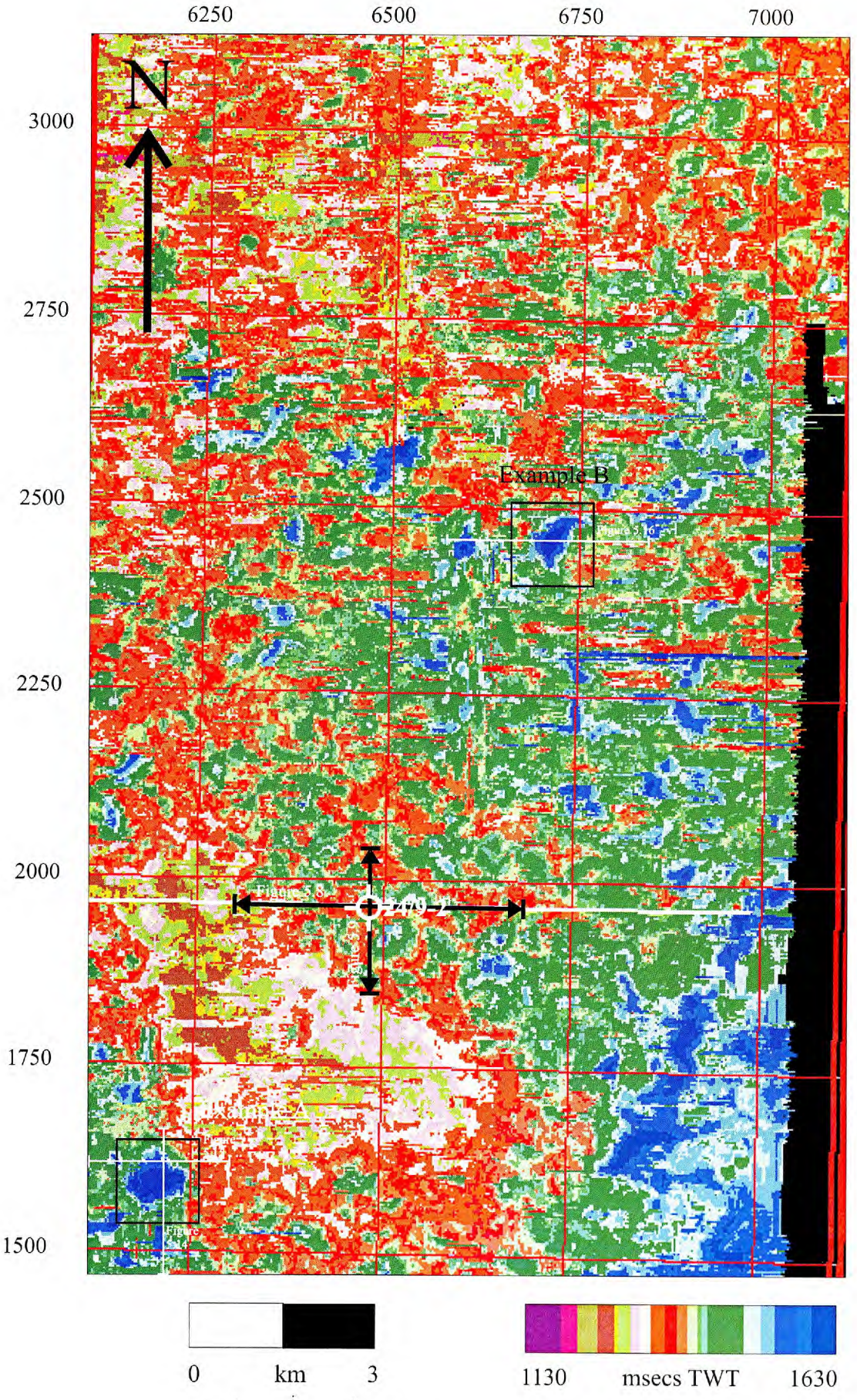


Figure 5.11. Top Belton Member Upper Eocene two way time structure contour map and amplitude map over Norwegian North Sea Block 24/9

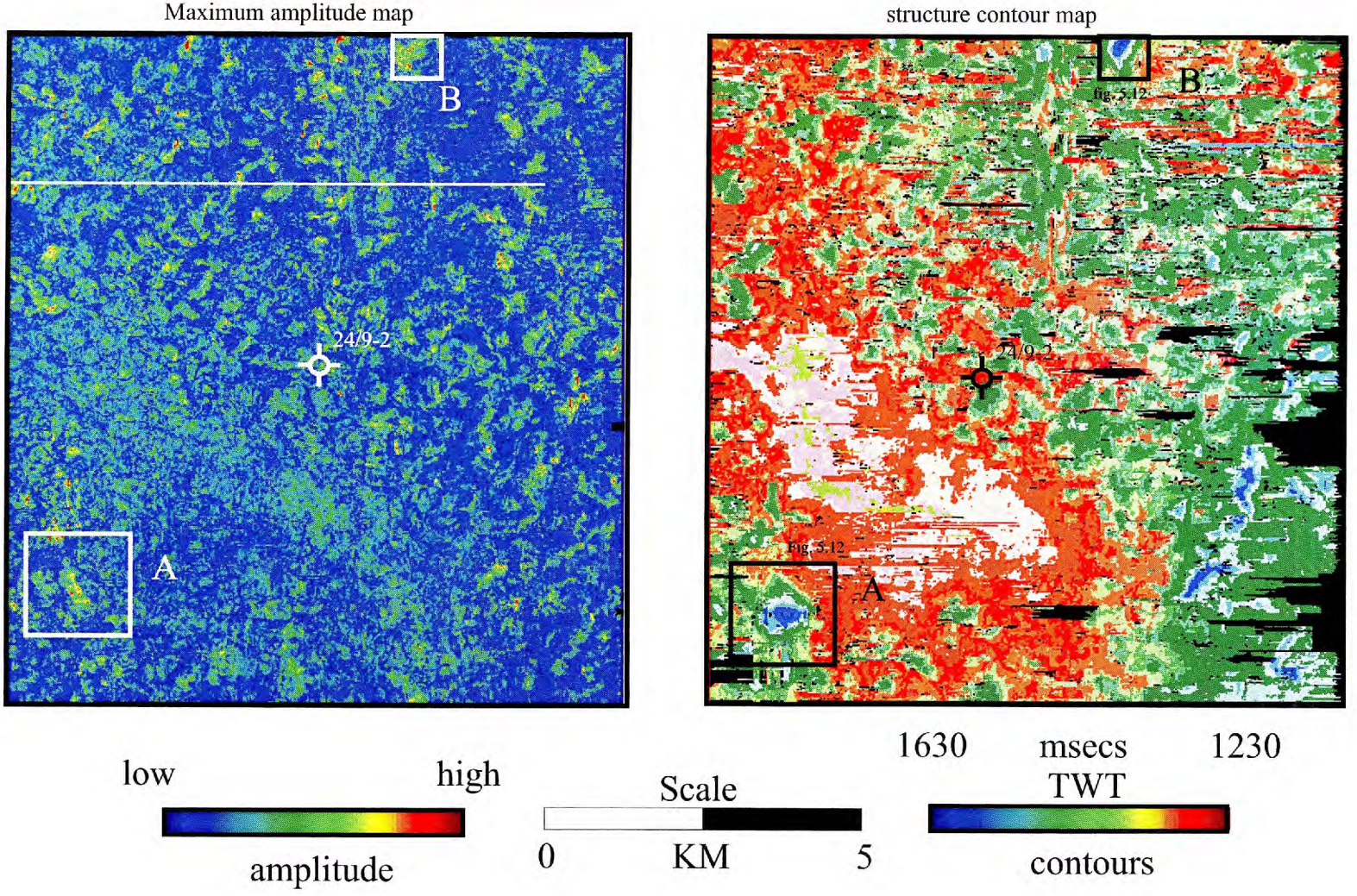


Figure 5.12. Examples of three dimensional images of Upper Eocene Belton Member polygonally faulted deepwater sediments of Norwegian North Sea Block 24/9 (see figure 5.11 and 5.18 for location)

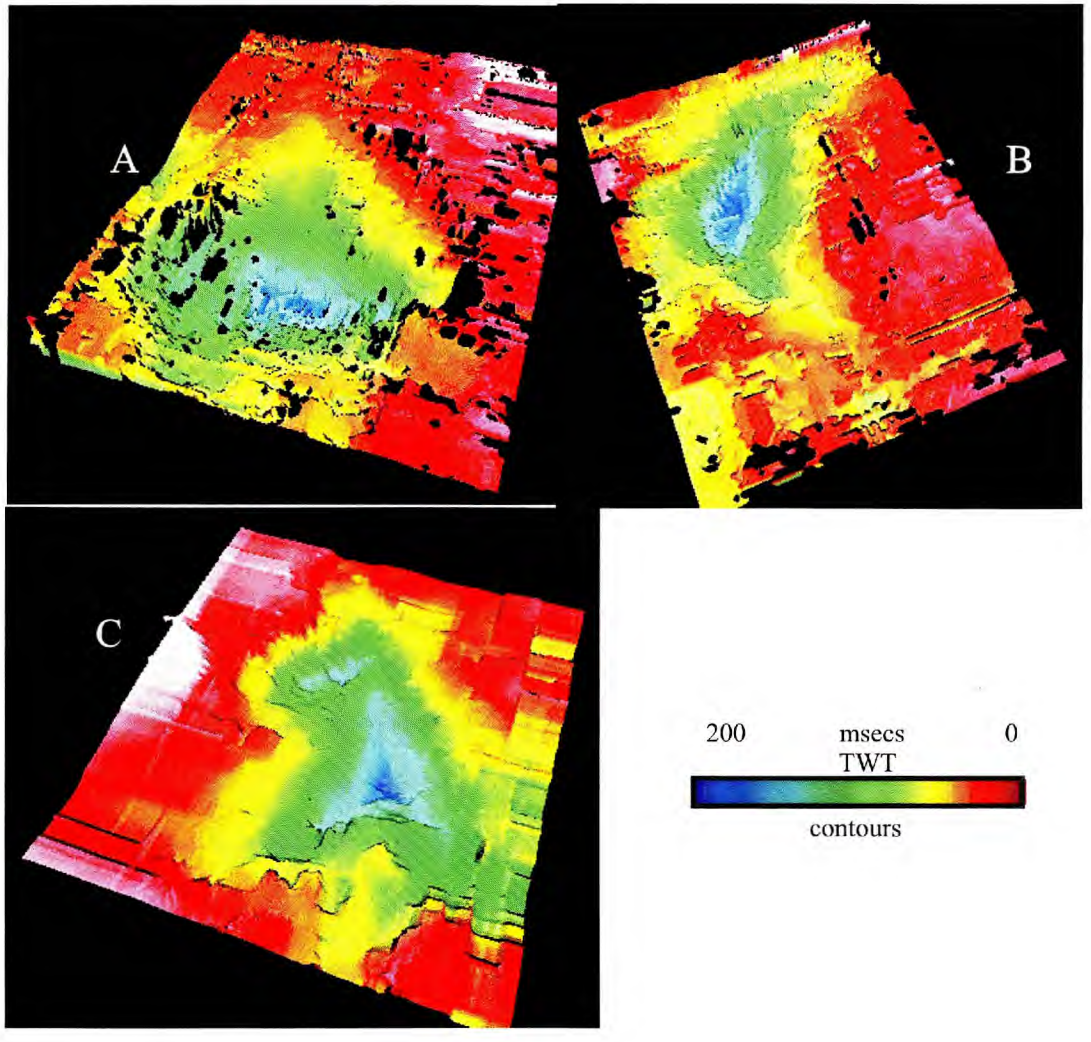


Figure 5.13. Seismic cross section of Upper Eocene Belton Member polygonally faulted deepwater sediments of Norwegian North Sea Block 24/9

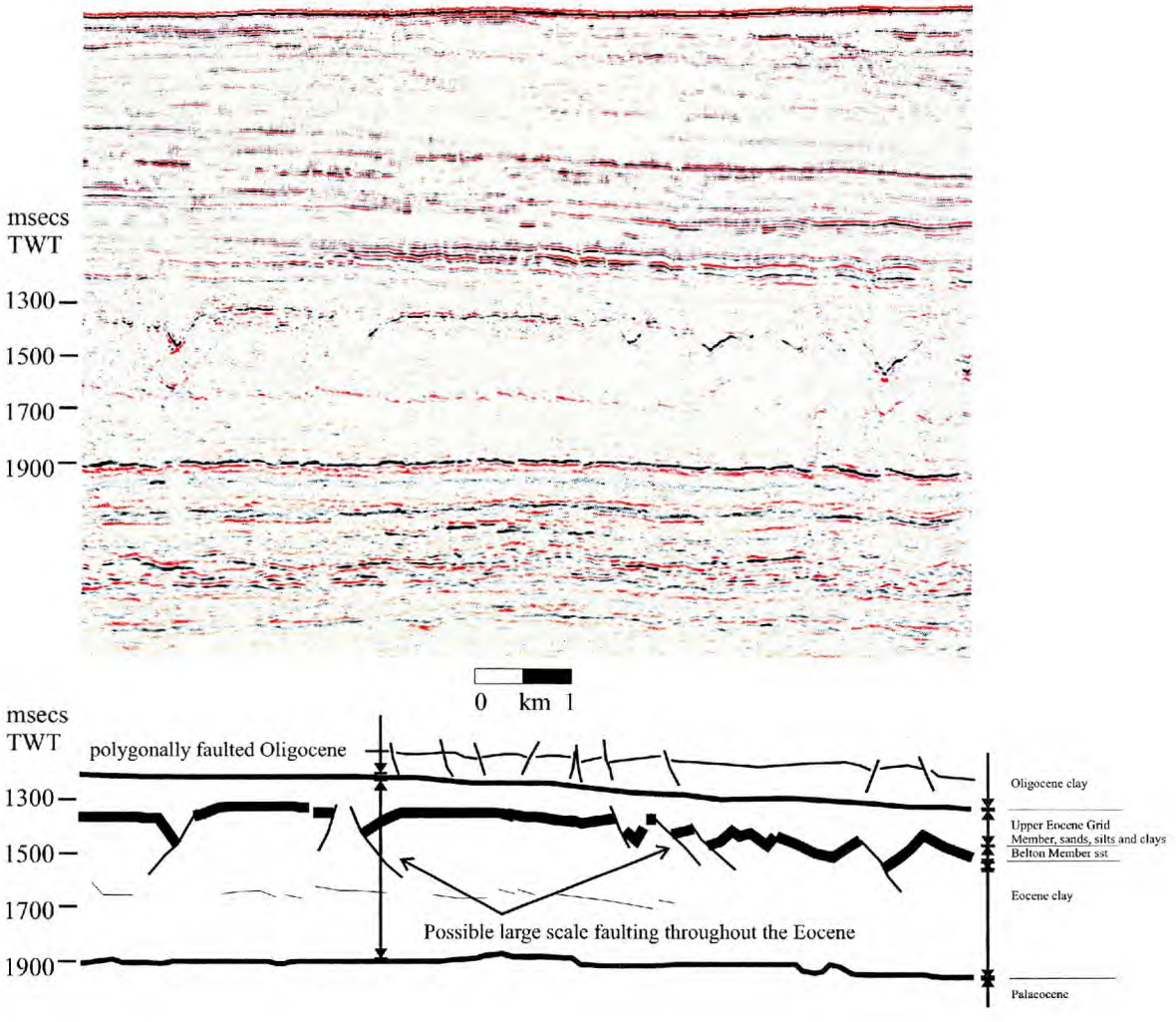


Figure 5.14. Norwegian North Sea Block 24/9 seismic inline 6205 through the Upper Eocene Belton Member example A

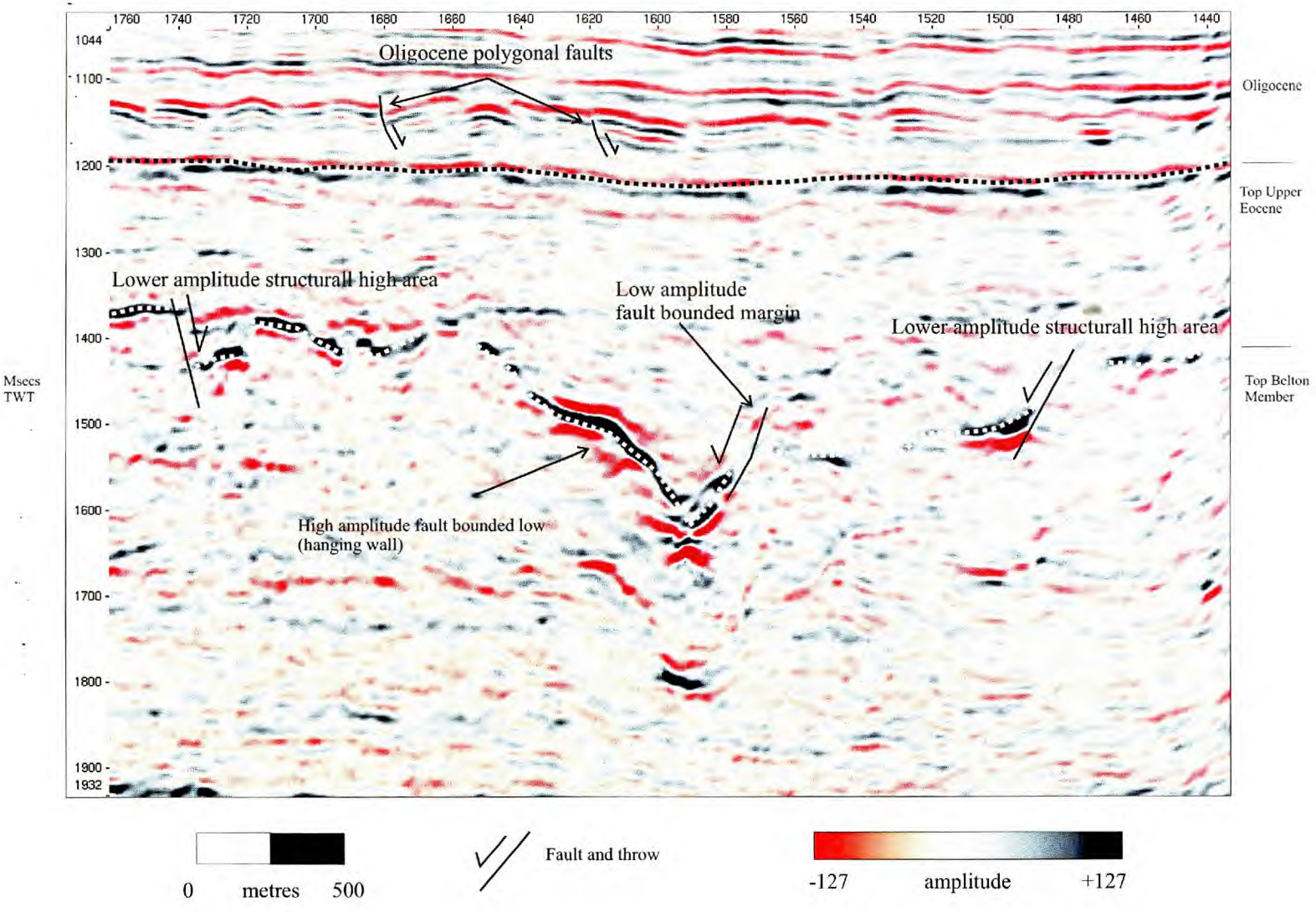


Figure 5.15. Norwegian North Sea Block 24/9 seismic crossline 1600 through the Upper Eocene Belton Member example A

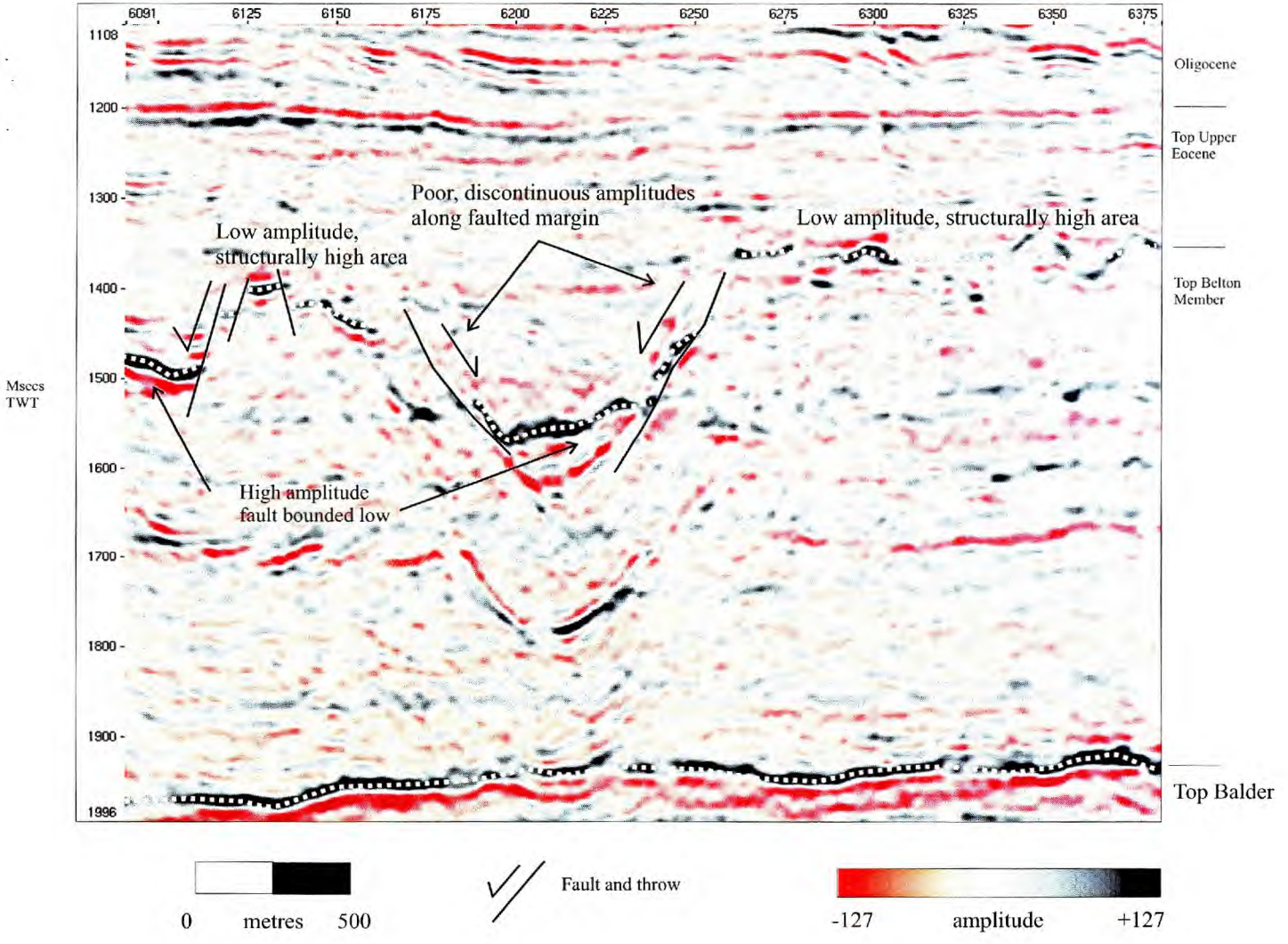


Figure 5.16. Norwegian North Sea Block 24/9 seismic crossline 2452 through the Upper Eocene Belton Member example B faulted low

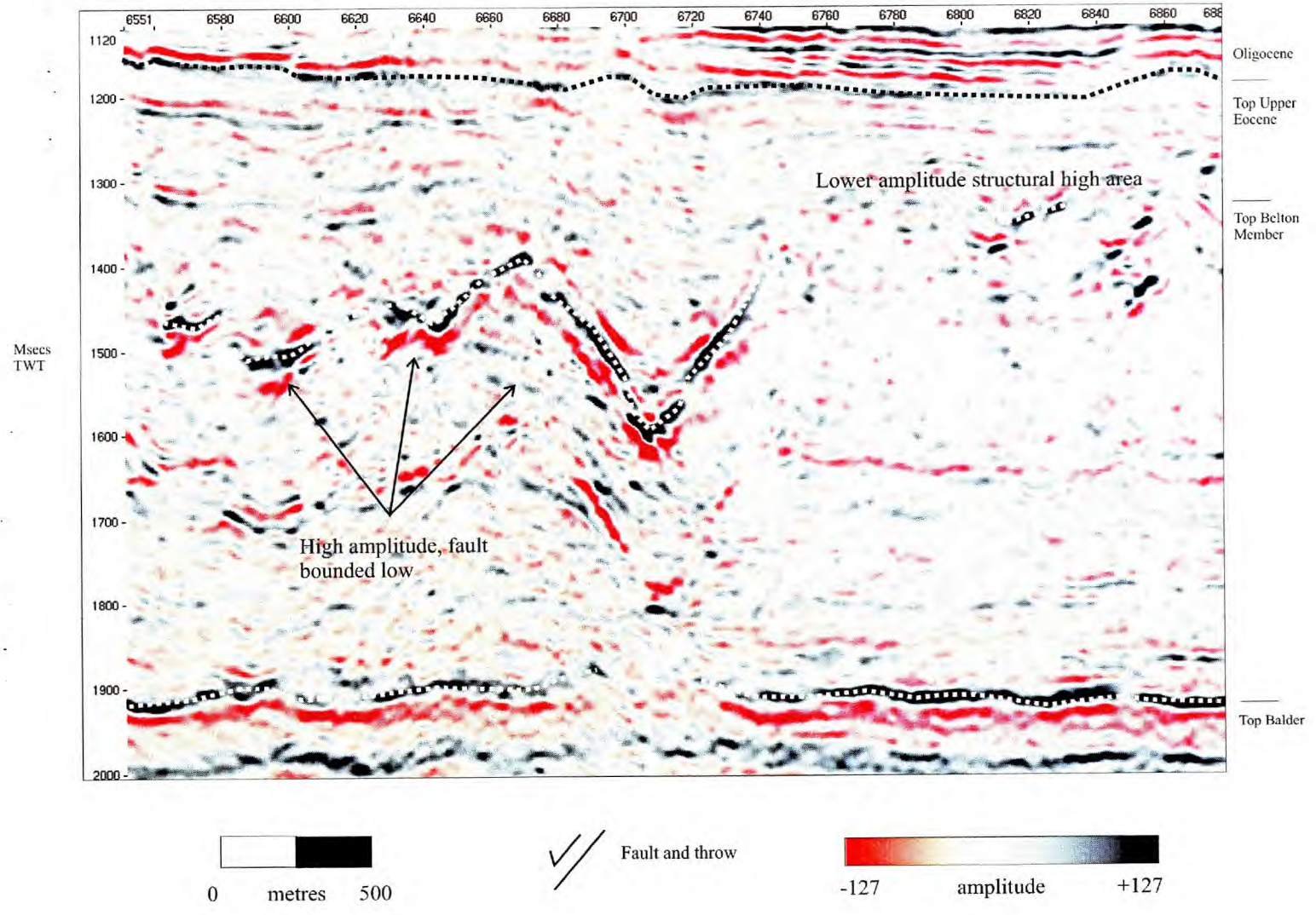


Figure 5.17. Seismic line through the Belton member of Norwegian North Sea wells 24/9-5 and 6 (see figure 5.18 for location)

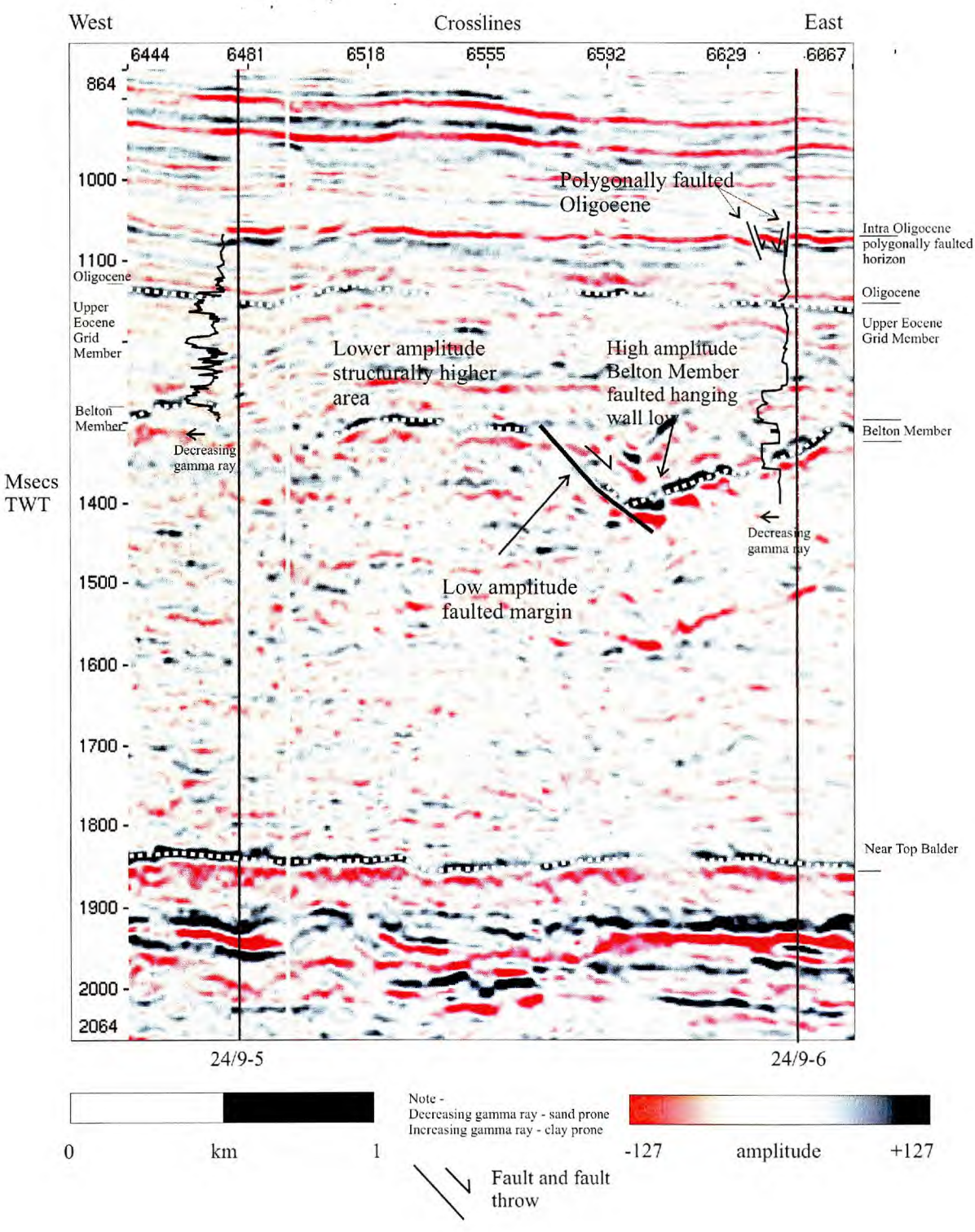


Figure 5.18. Structure contour map of the Upper Eocene Belton Member about wells 24/9-5 and 24/9-6

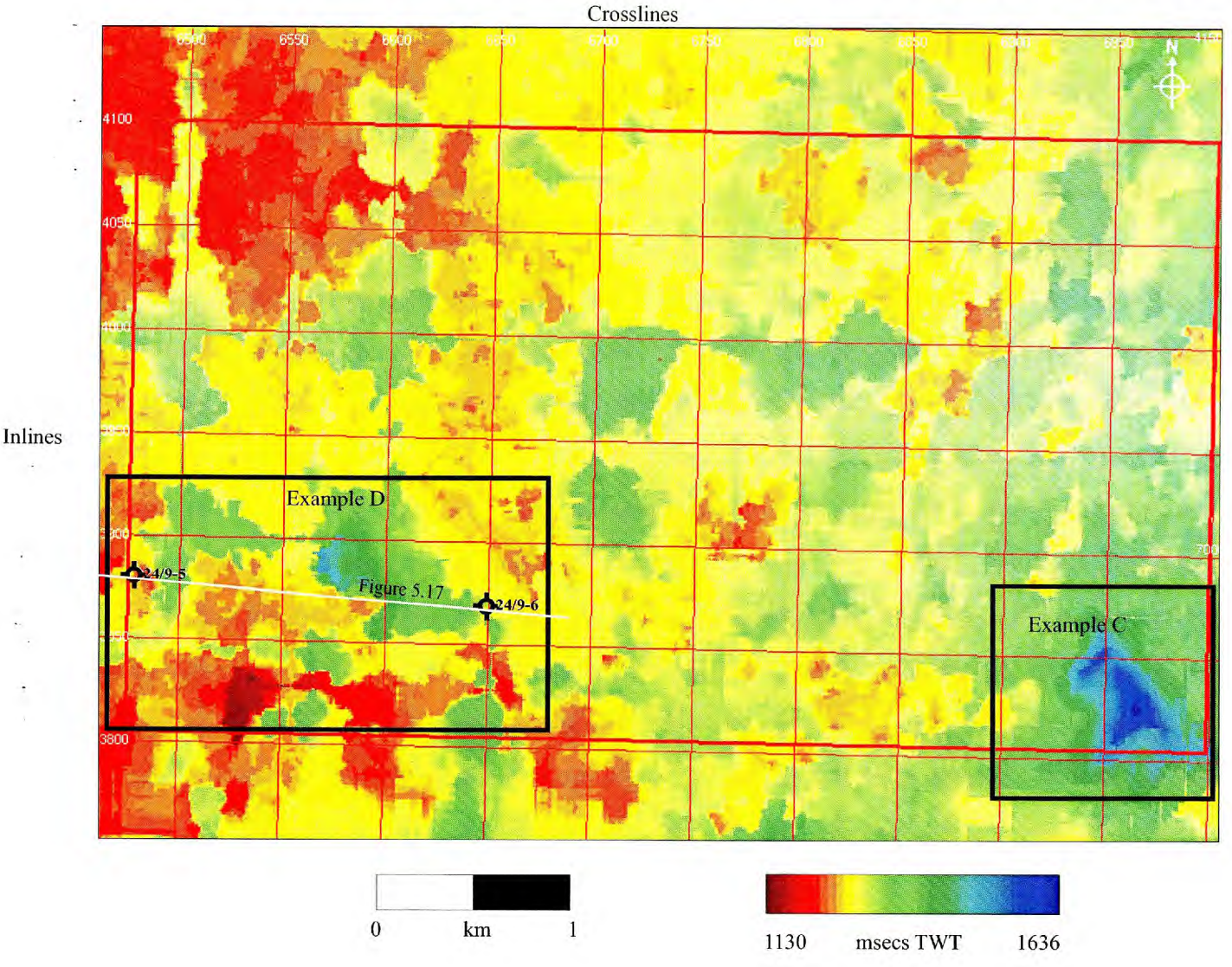


Figure 5.19. Amplitude map of Upper Eocene Belton Member about Norwegian North Sea wells 24/9-5 and 6

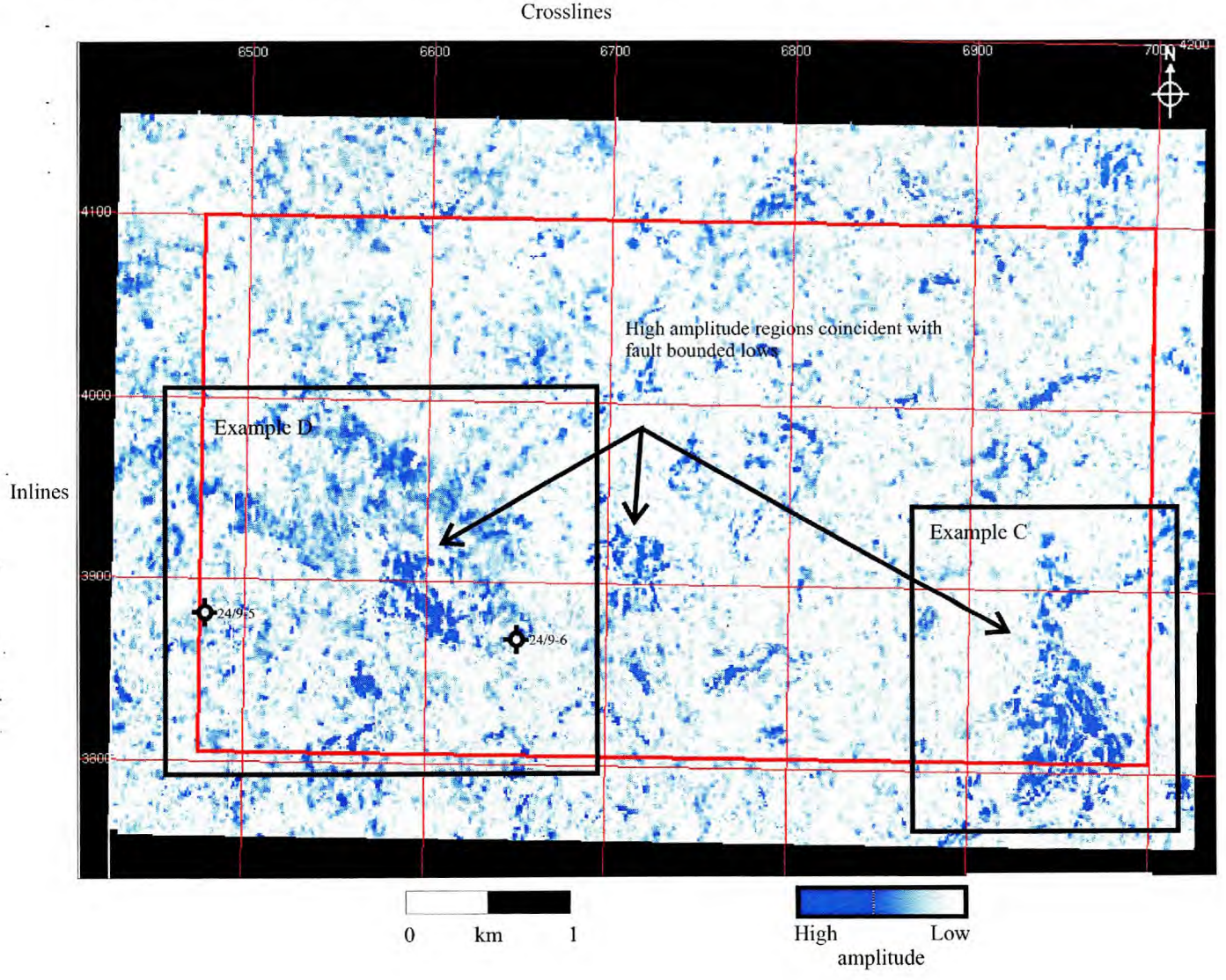


Figure 5.20. Isopach map between intra Oligocene and Belton structure contour map over Norwegian North Sea wells 24/9-5 and 6

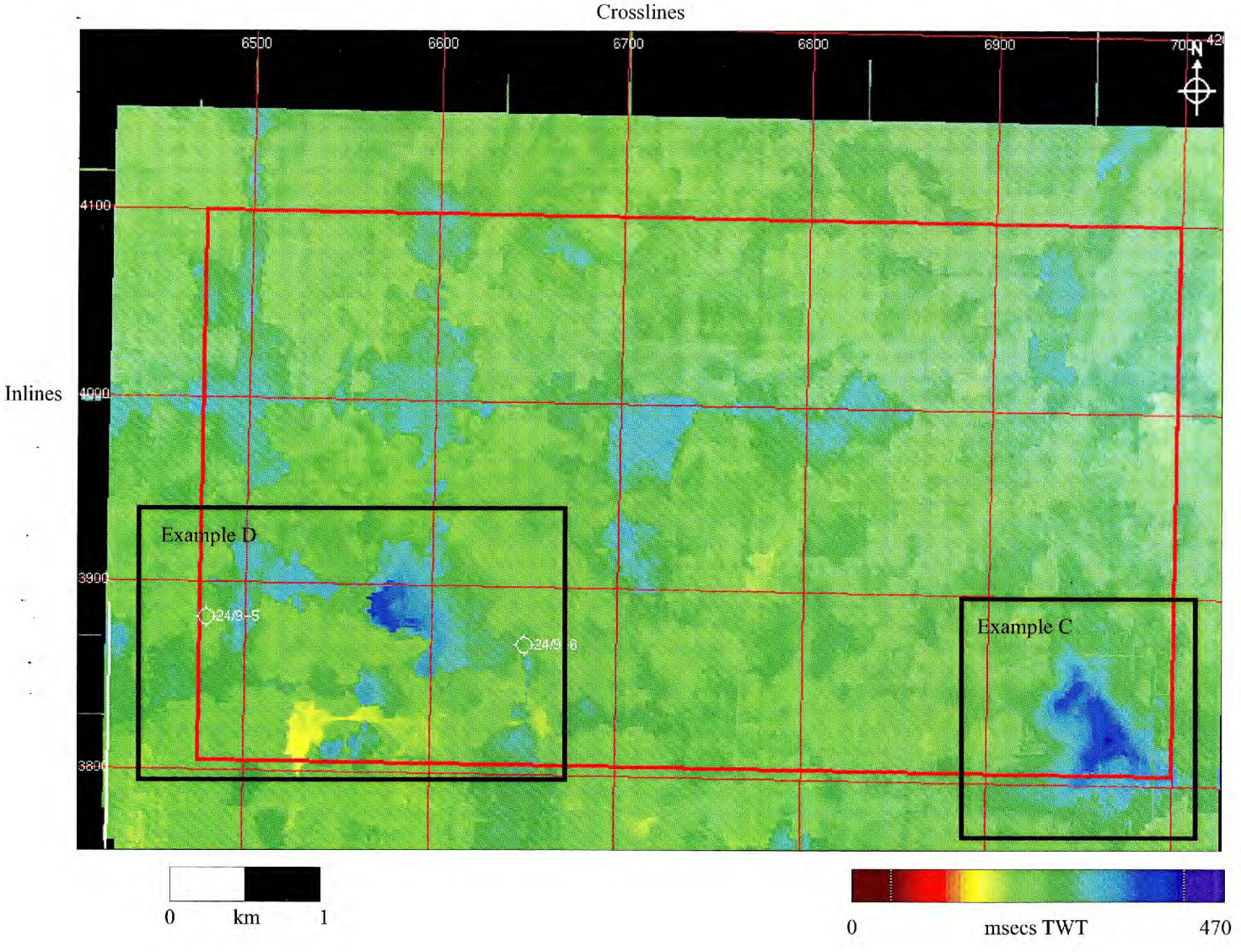


Figure 5.21. Structure contour map of a faulte bounded low within the Upper Eocene Belton Member in Norwegian North Sea Block 24/9 - example C.

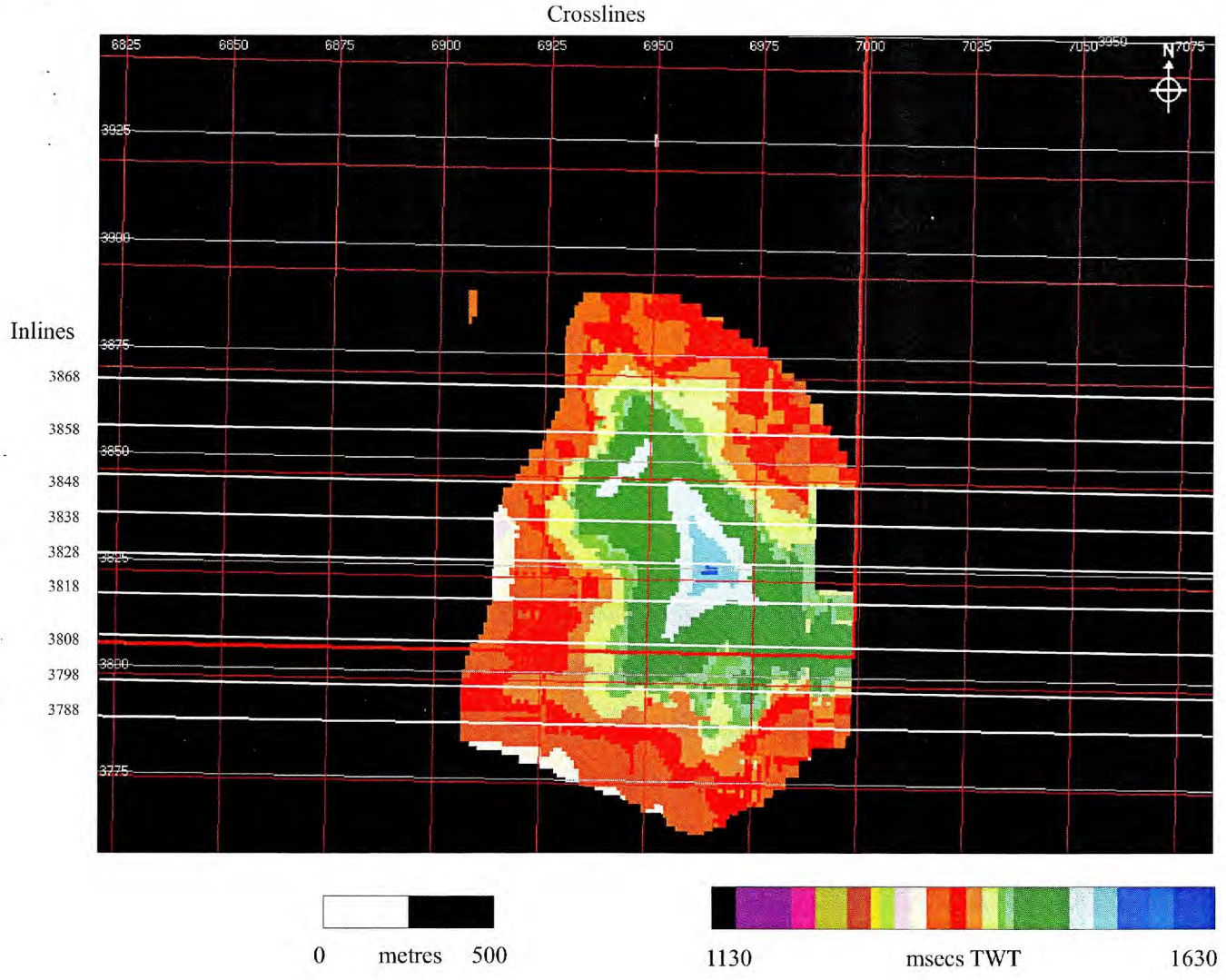


Figure 5.22. Norwegian North Sea Block 24/9 seismic crossline 3788 through the Upper Eocene Belton Member example C faulted low

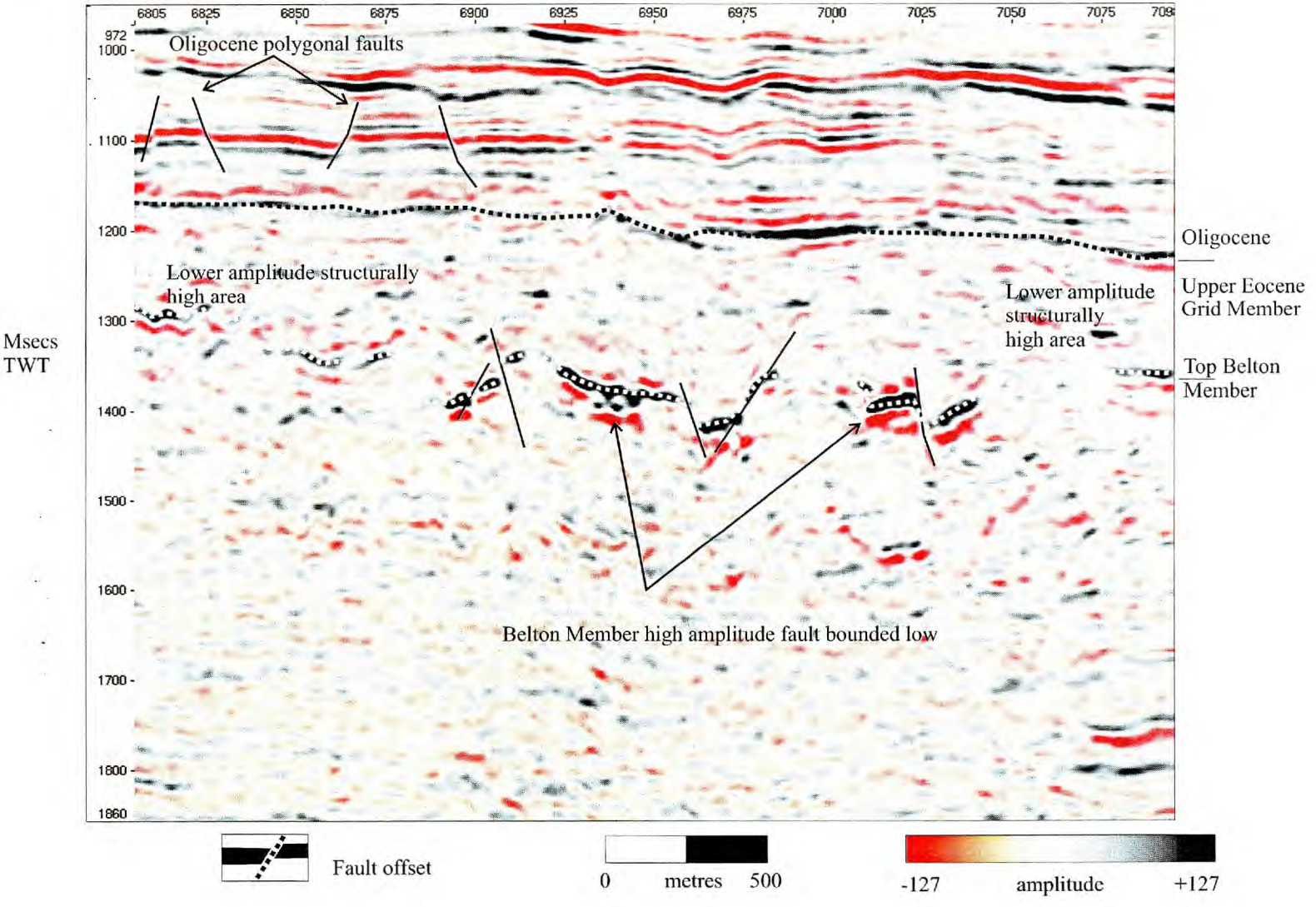


Figure 5.23. Norwegian North Sea Block 24/9 seismic crossline 3798 through the Upper Eocene Belton Member example C faulted low

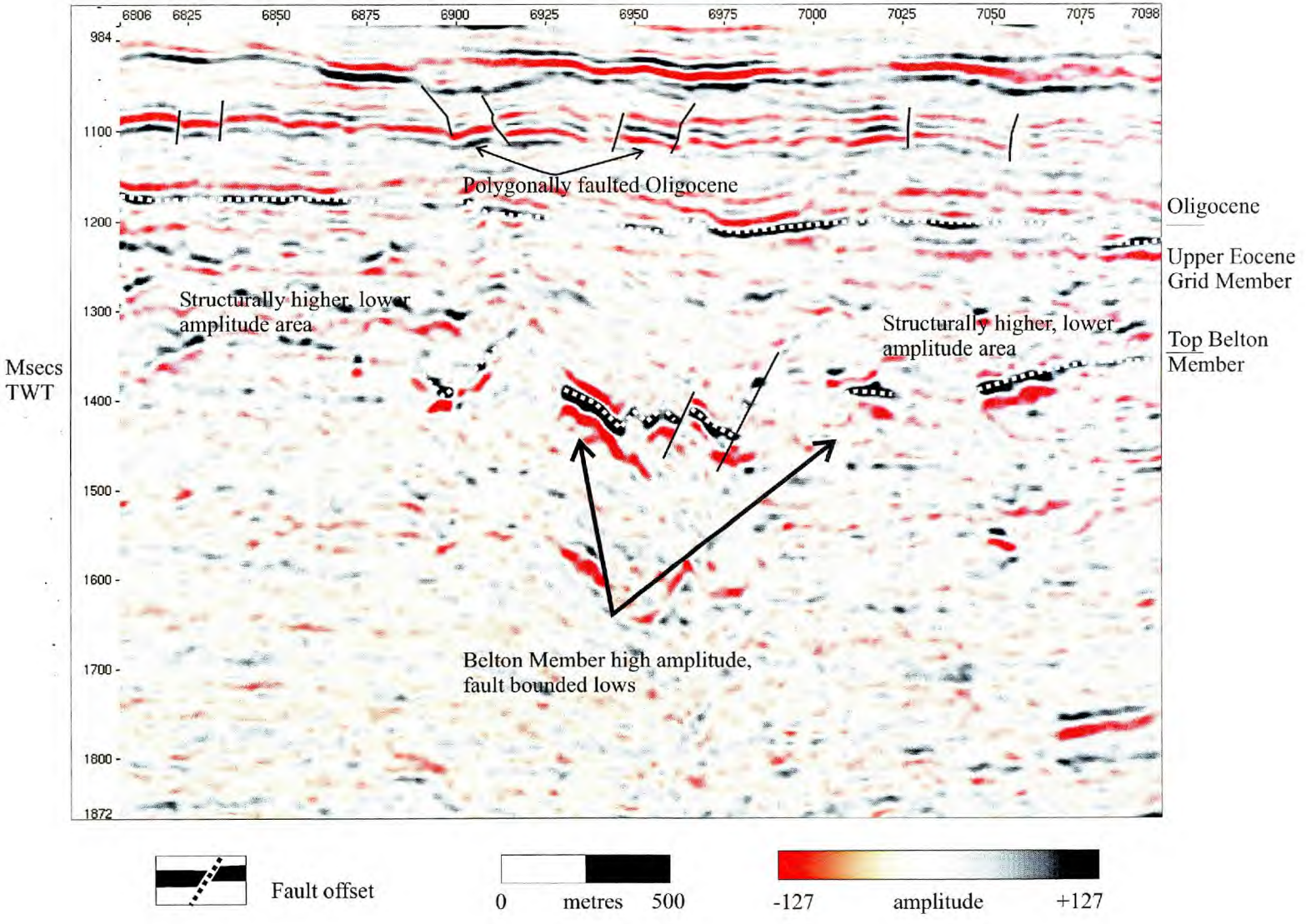


Figure 5.24. Norwegian North Sea Block 24/9 seismic crossline 3808 through the Upper Eocene Belton Member example C faulted low

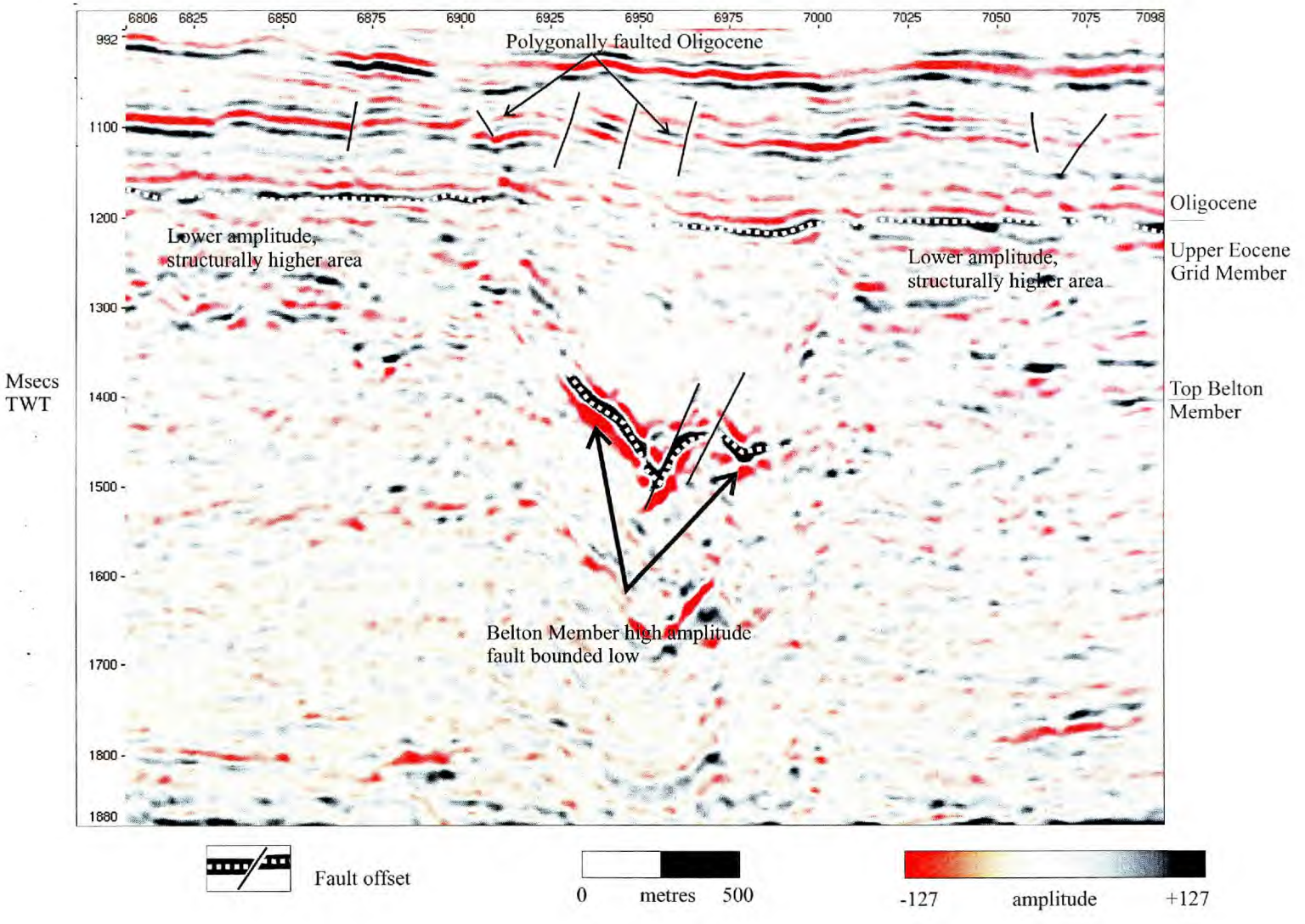


Figure 5.25. Norwegian North Sea Block 24/9 seismic crossline 3818 through the Upper Eocene Belton Member example C faulted low

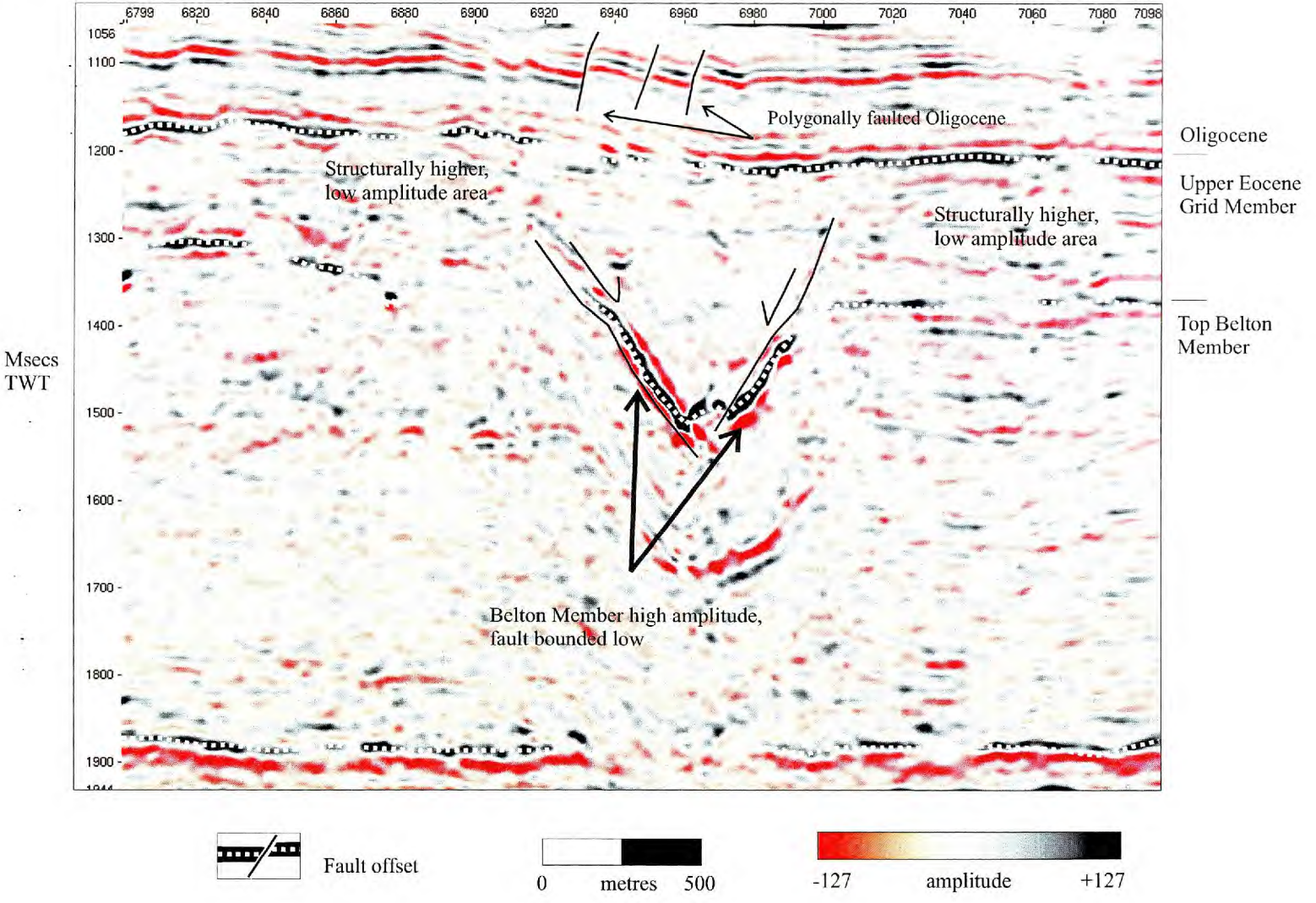


Figure 5.26. Norwegian North Sea Block 24/9 seismic crossline 3828 through the Upper Eocene Belton Member example C faulted low

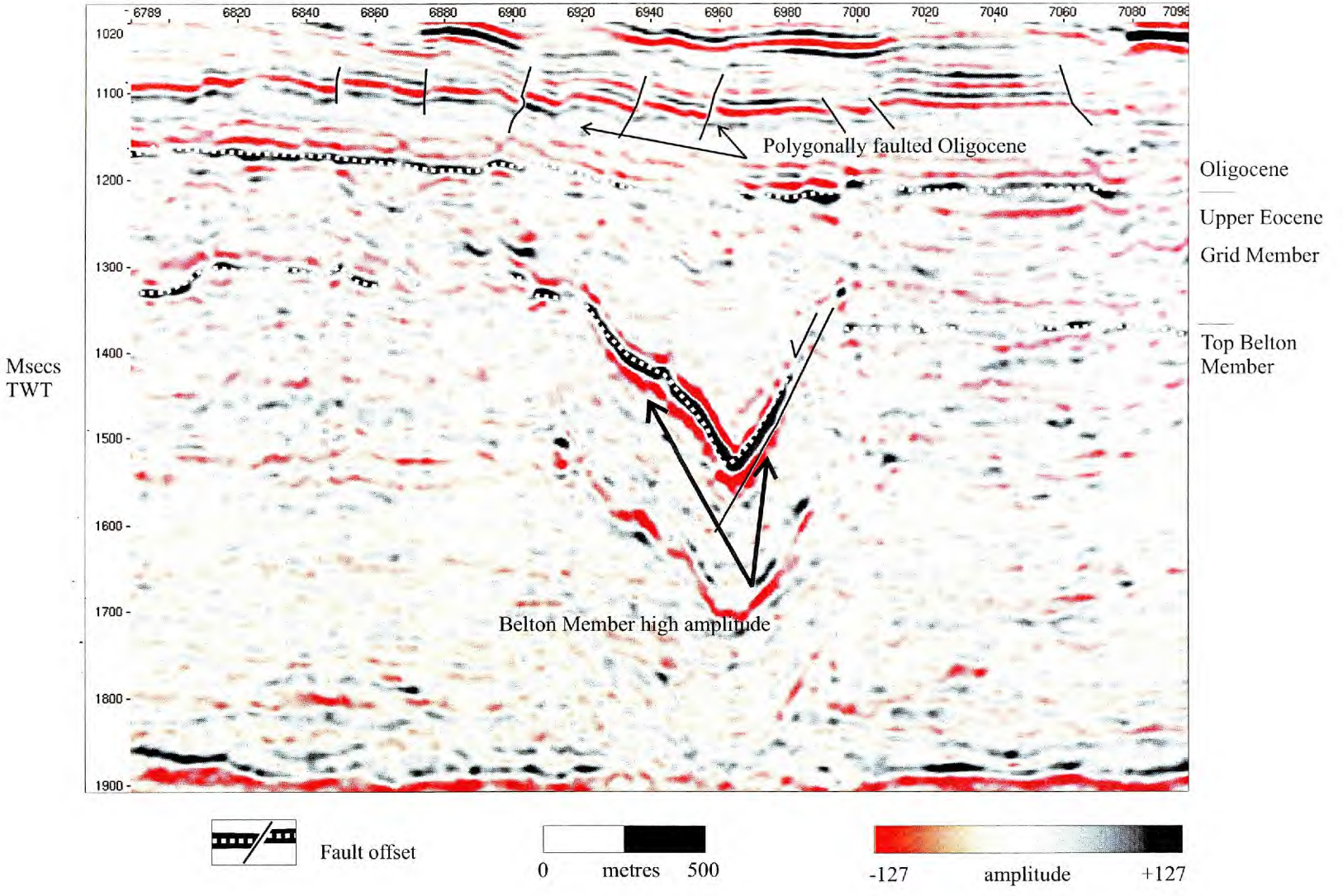


Figure 5.27. Norwegian North Sea Block 24/9 seismic crossline 3838 through the Upper Eocene Belton Member example C faulted low

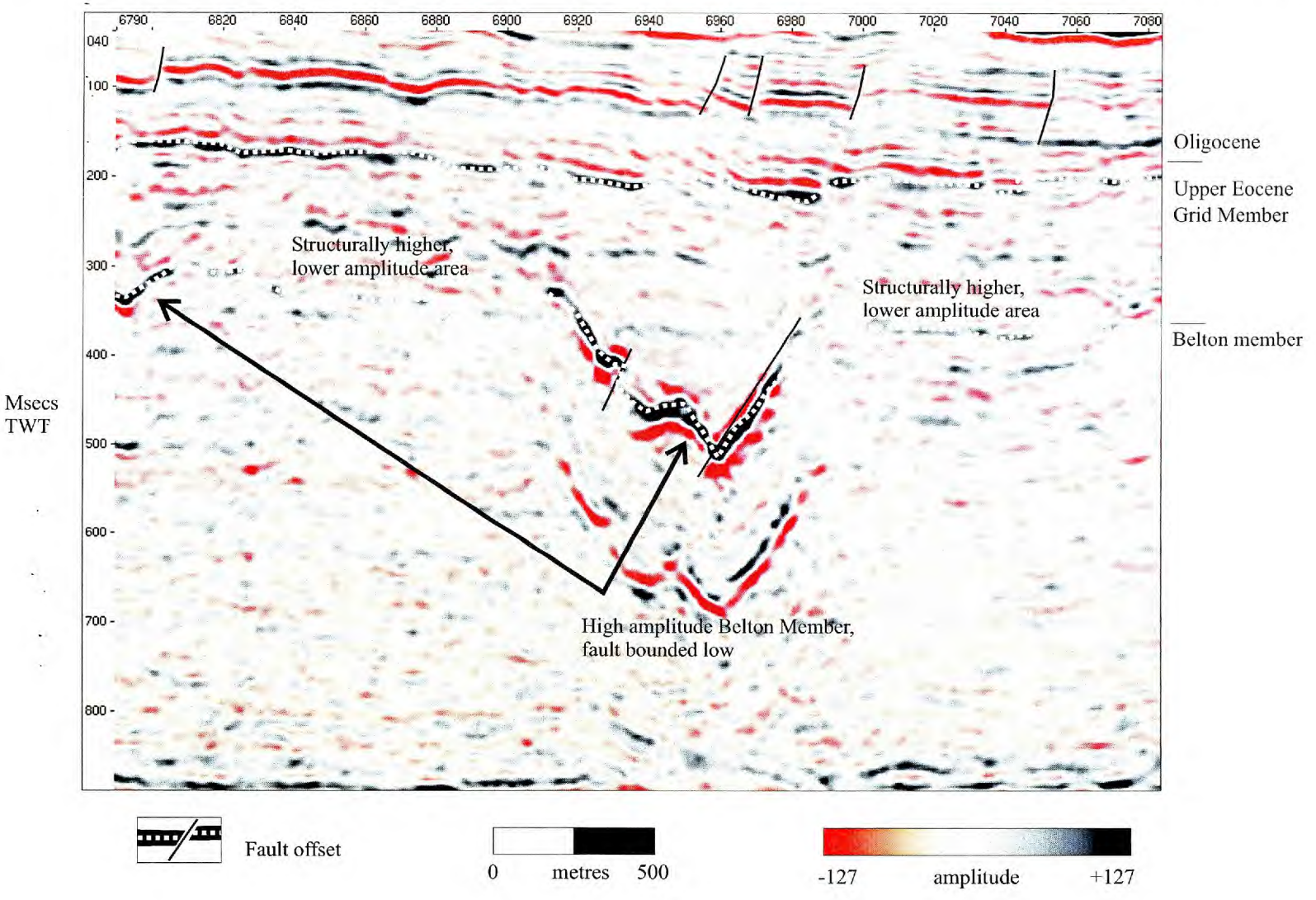


Figure 5.28. Norwegian North Sea Block 24/9 seismic crossline 3848 through the Upper Eocene Belton Member example C faulted low

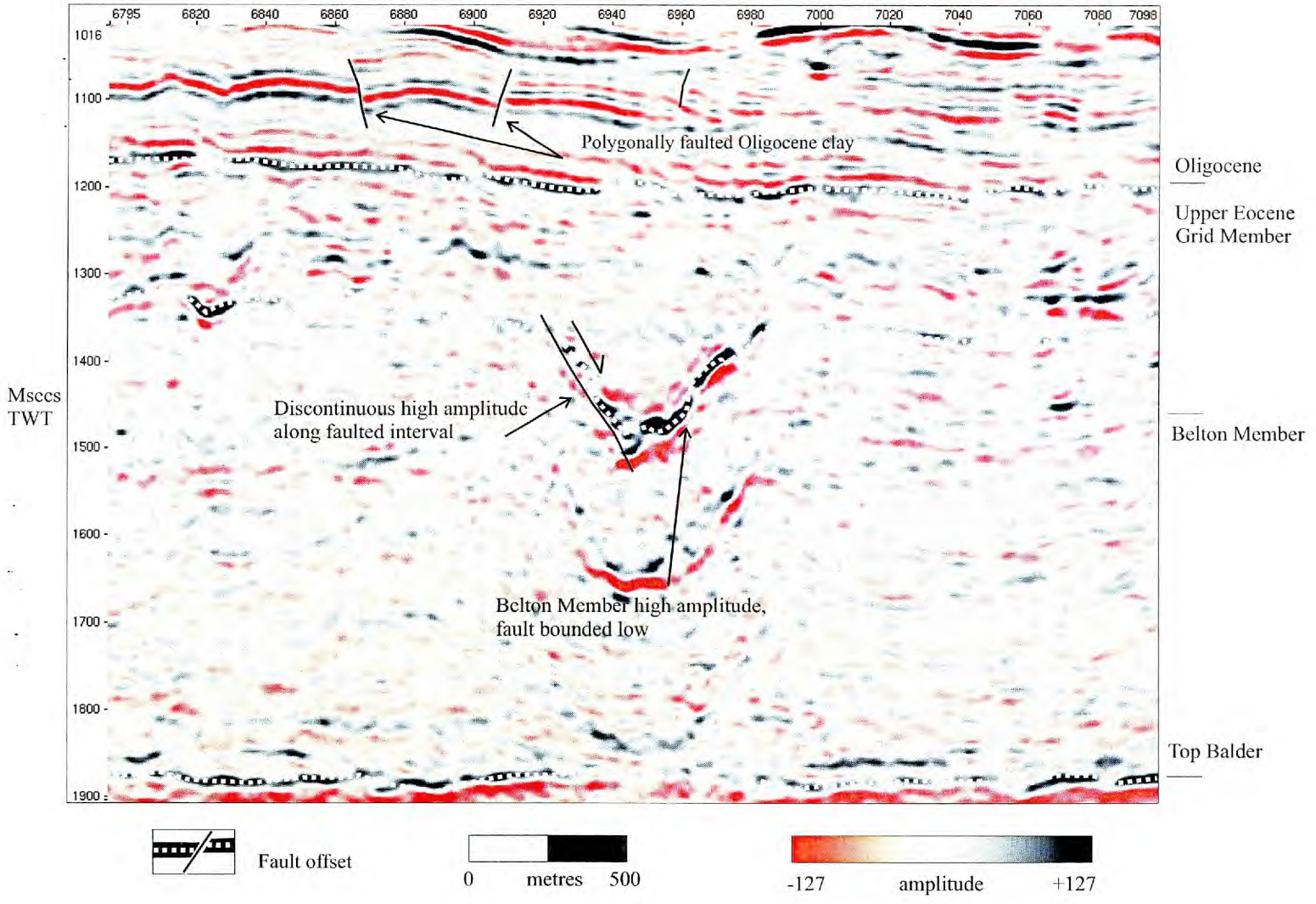


Figure 5.29. Norwegian North Sea Block 24/9 seismic crossline 3858 through the Upper Eocene Belton Member example C faulted low

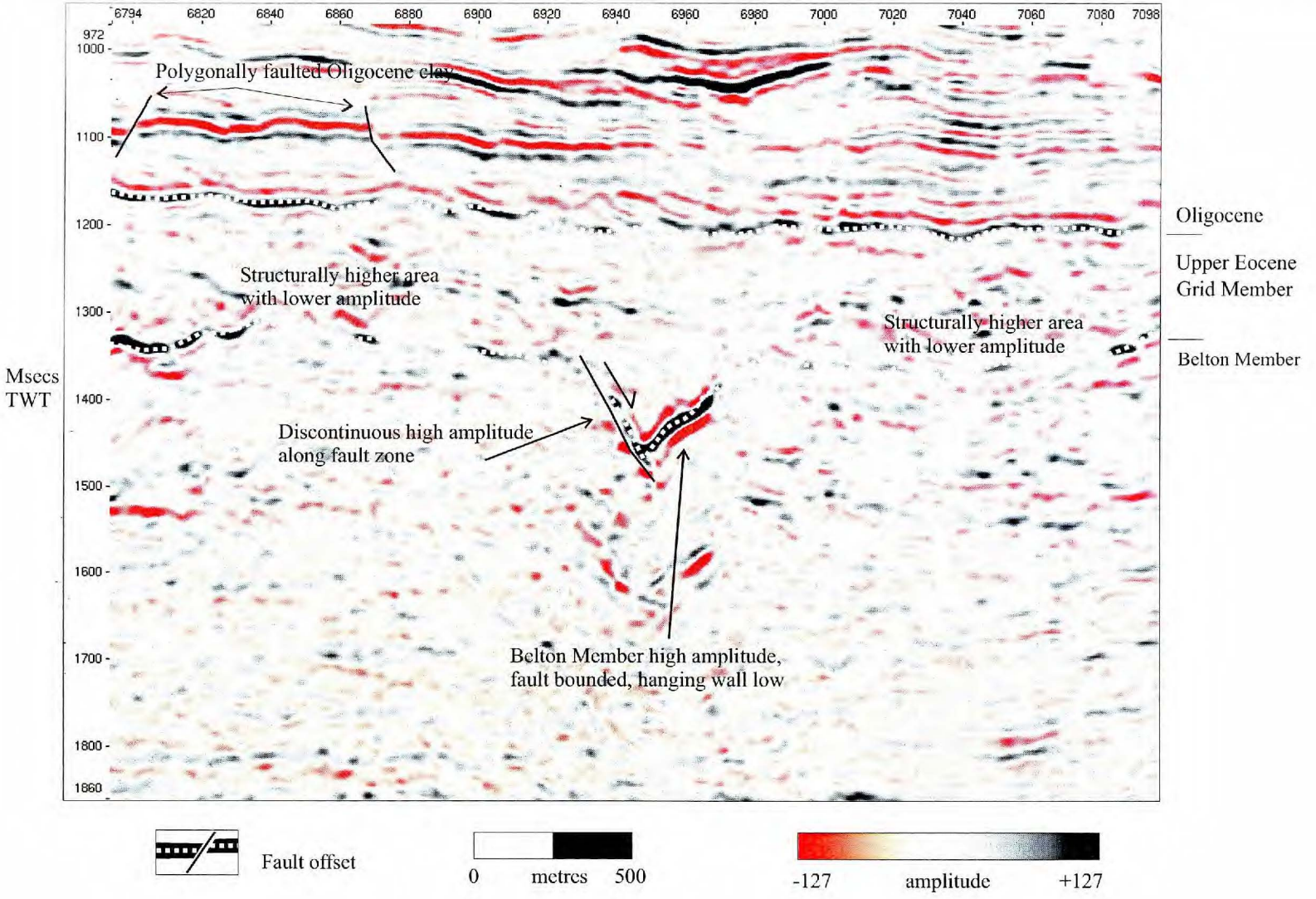


Figure 5.30. Norwegian North Sea Block 24/9 seismic crossline 3868 through the Upper Eocene Belton Member example C faulted low

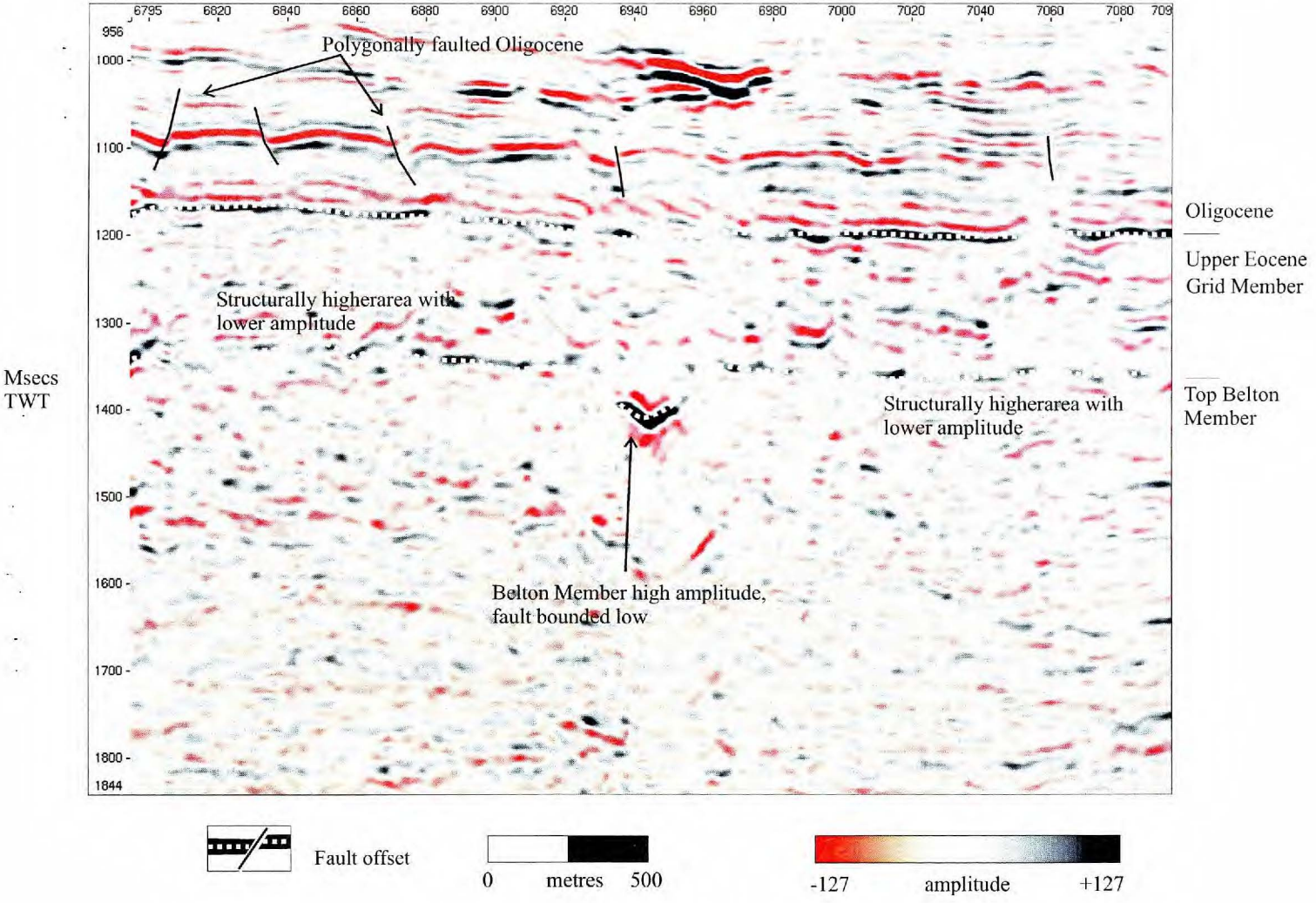


Figure 5.31. Top Belton Member structure contour map about Norwegian North Sea wells 24/9-5 and 6 - example D faulted lows

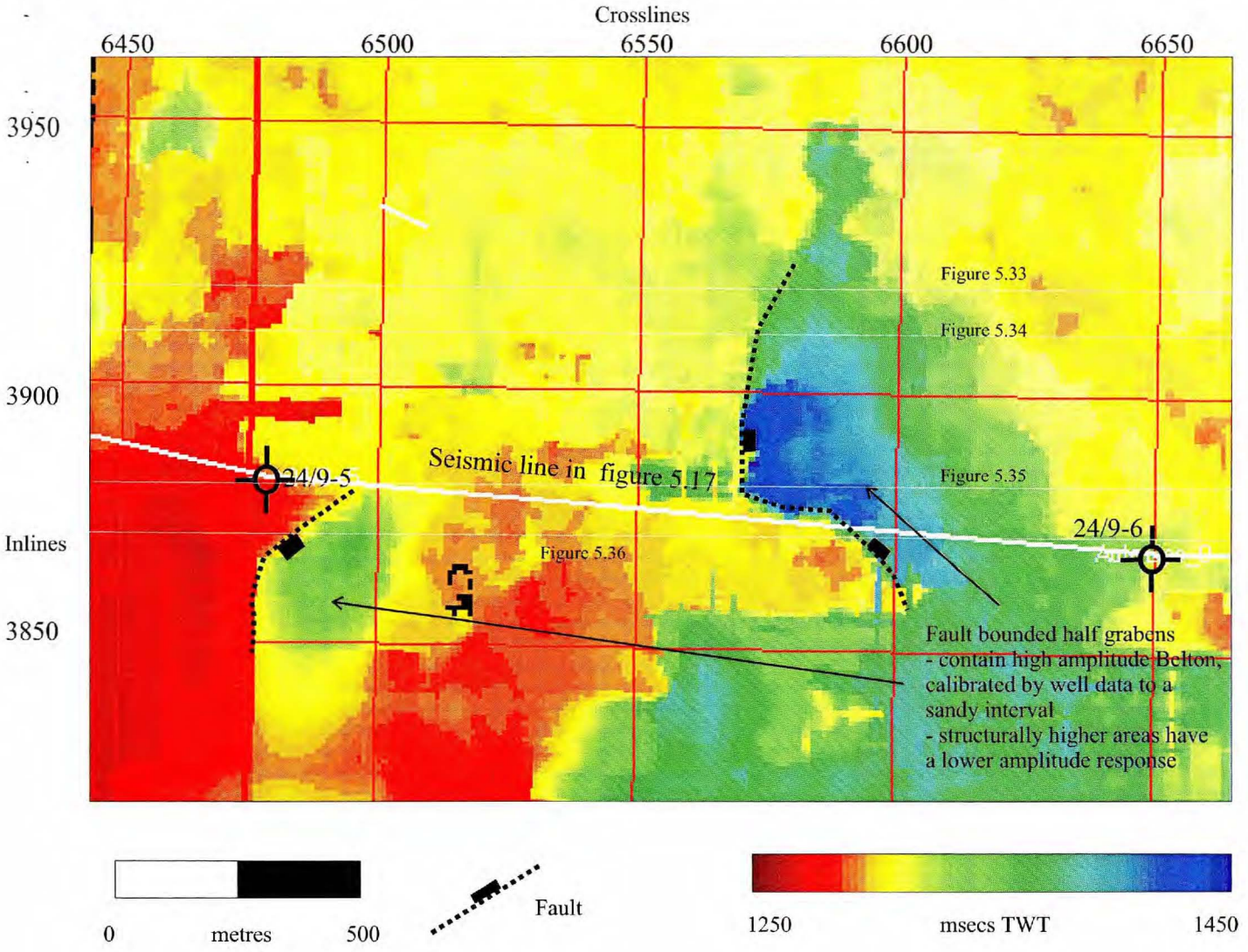


Figure 5.32. Intra Oligocene structure contour map over Norwegian North Sea wells 24/9-5 and 24/9-6. Note polygonal fault pattern (partly from Tervoort, 2000)

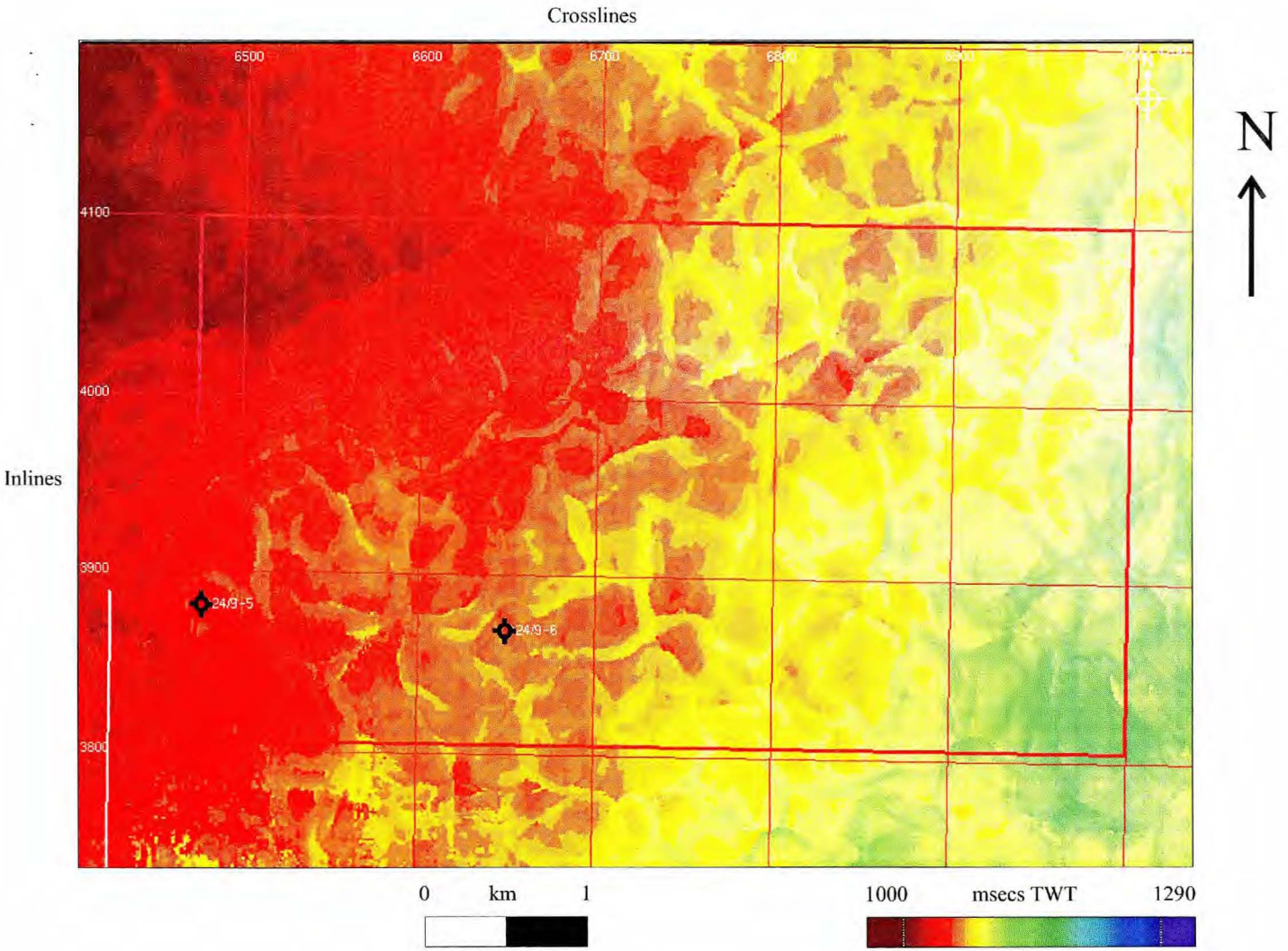


Figure 5.33. Seismic example(inline 3918) through Upper Eocene Belton Member about Norwegian North Sea wells 24/9-5 and 6

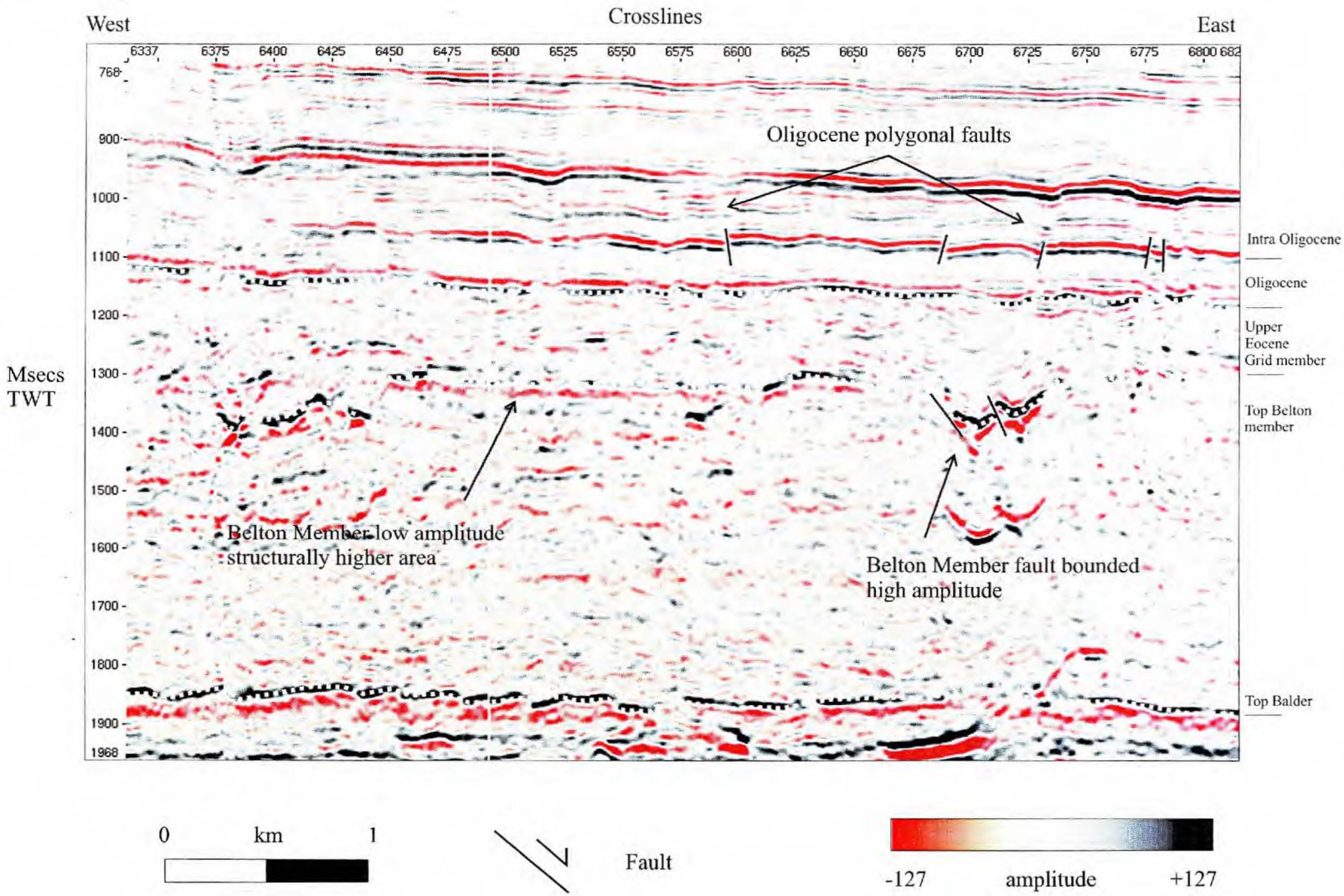


Figure 5.34. Seismic example(inline 3910) through Upper Eocene Belton Member about Norwegian North Sea wells 24/9-5 and 6

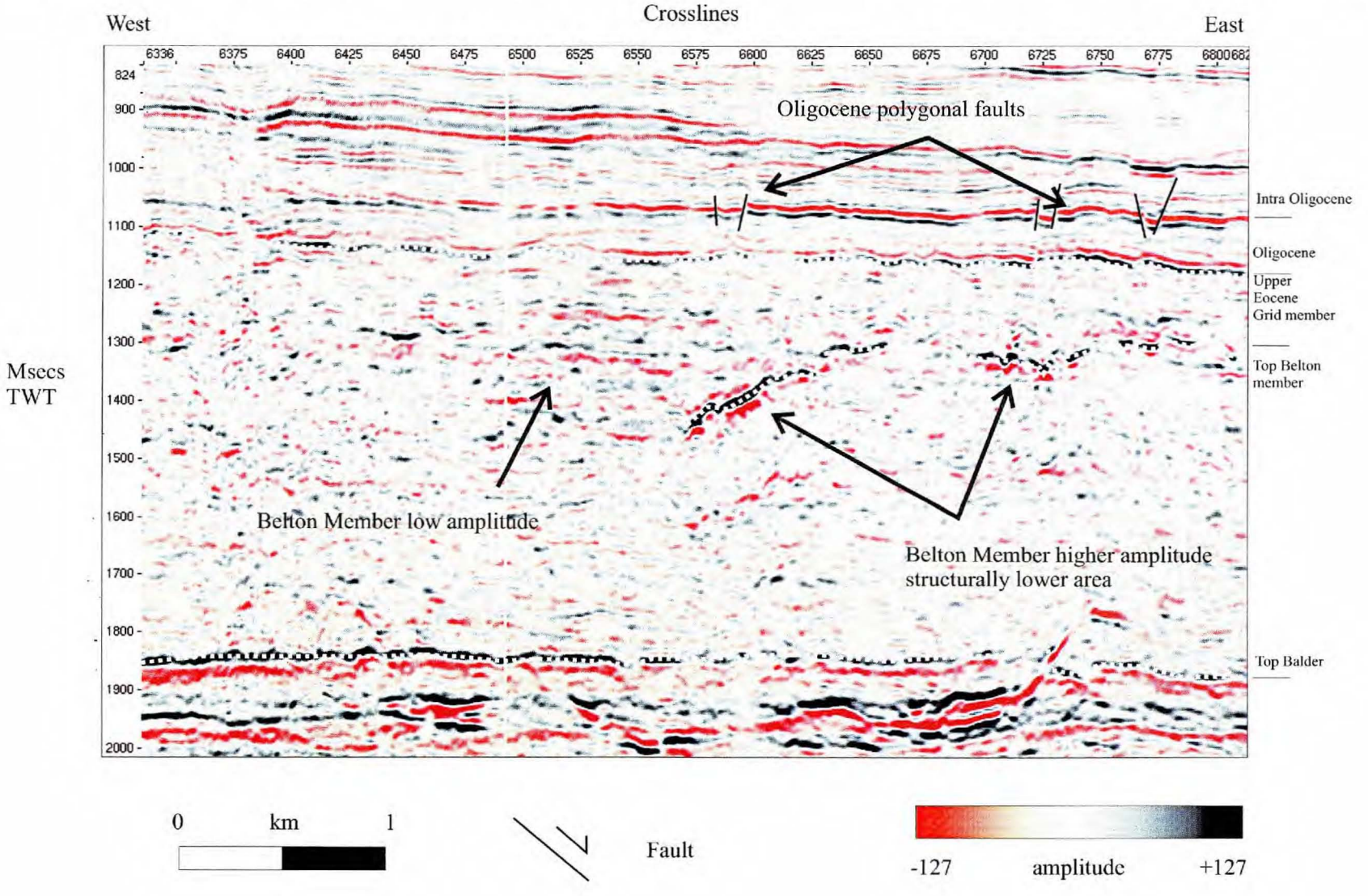


Figure 5.35. Seismic example(inline 3888) through Upper Eocene Belton Member about Norwegian North Sea wells 24/9-5 and 6

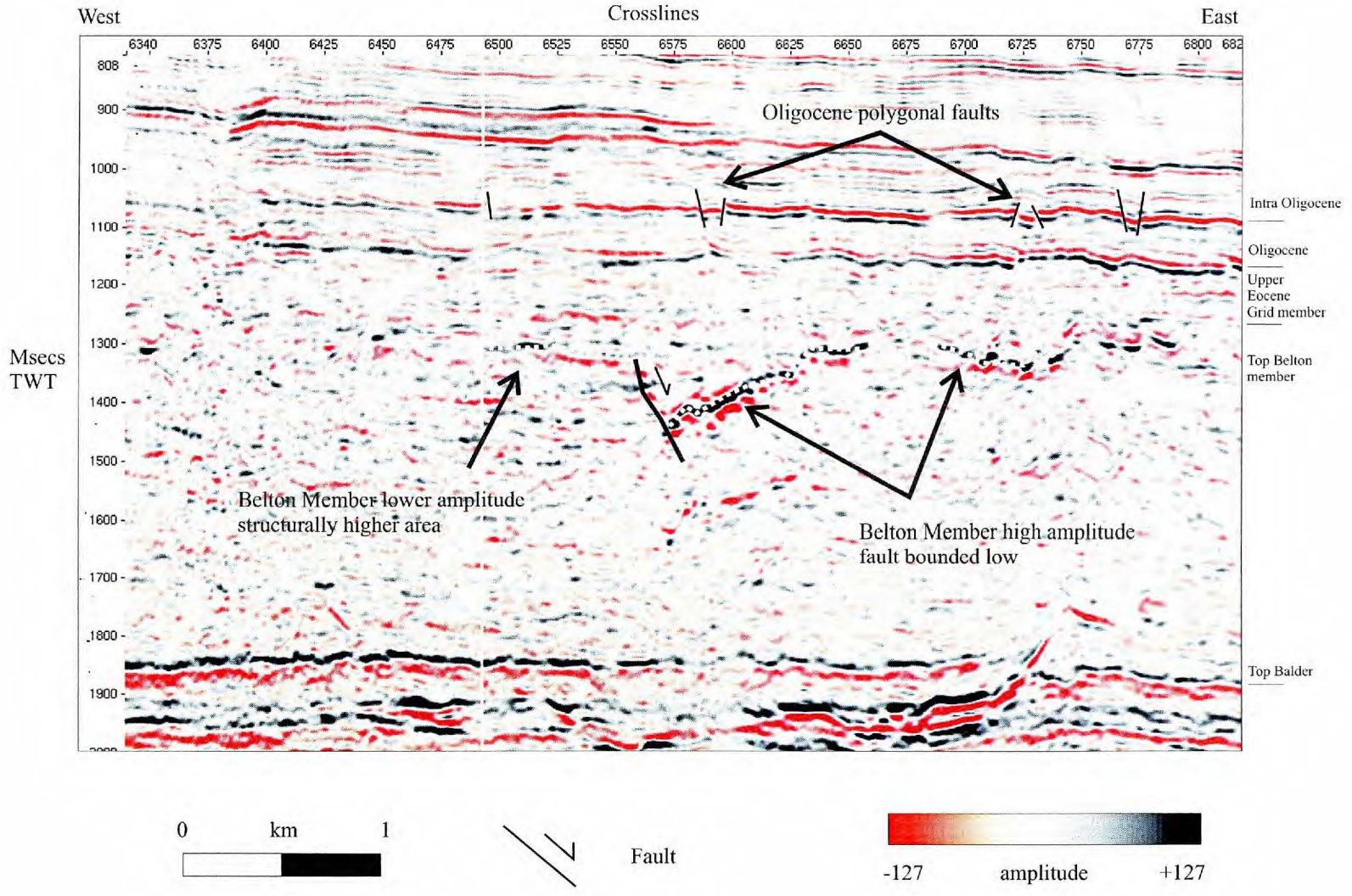


Figure 5.36. Seismic example(inline 3872) through Upper Eocene Belton Member about Norwegian North Sea wells 24/9-5 and 6

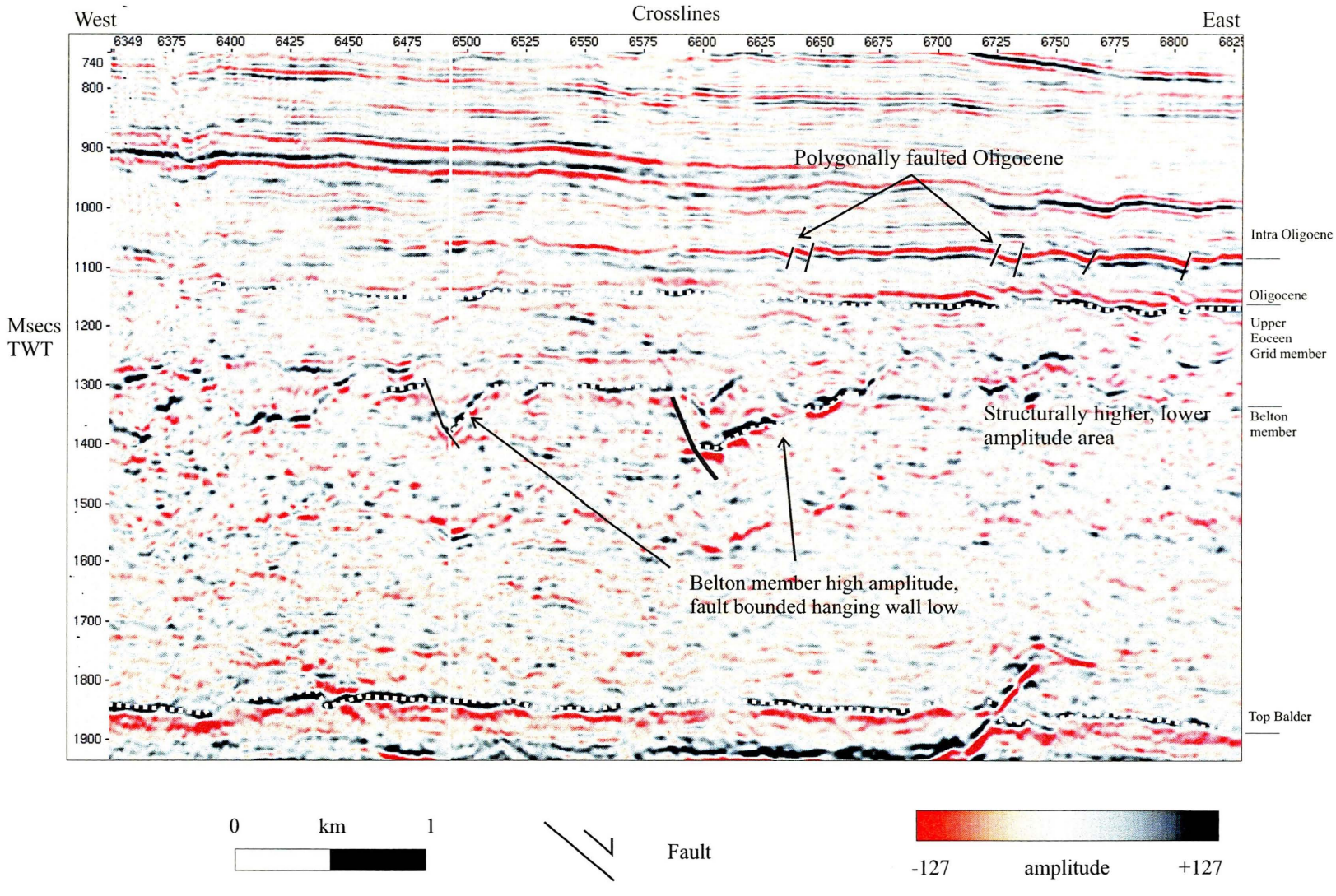


Figure 5.37. Depositional and post depositional model of the Upper Eocene Belton Member and Grid Member

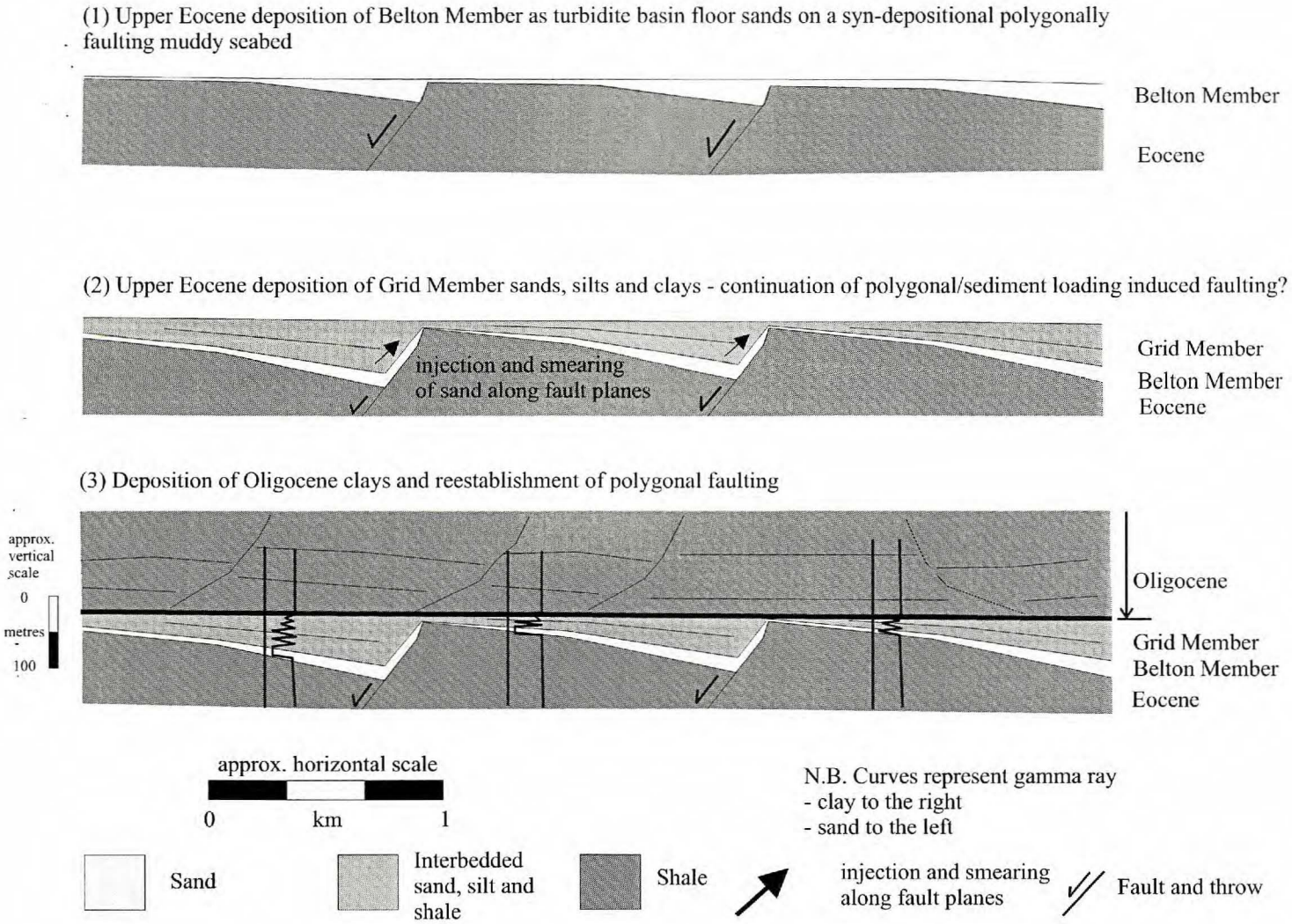
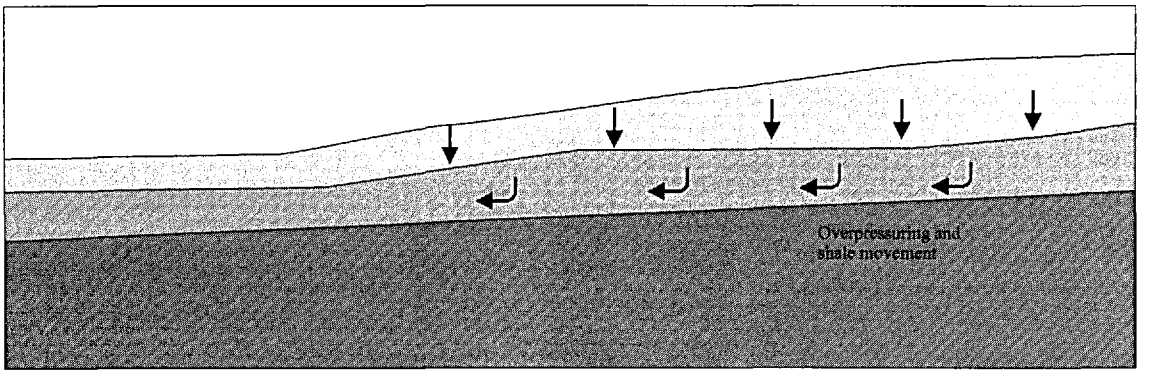
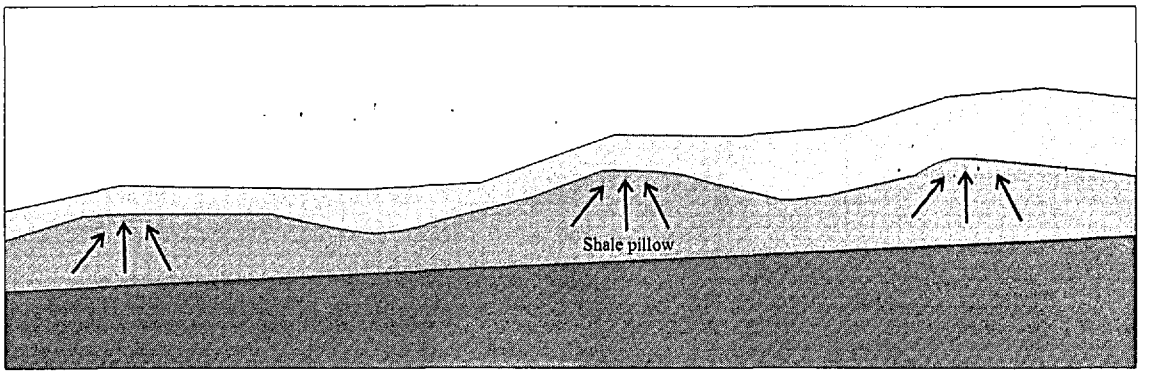


Figure 5.38. Schematic reconstruction of fault development in UK North Sea Blocks 16/23 and 24 (Whitbread and Anderton, 1997)

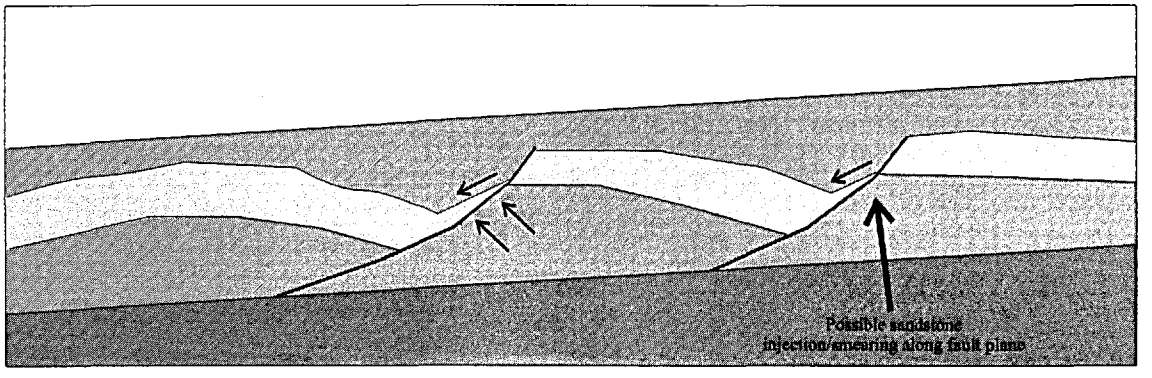
1. Successive anastomosing channels deposit
   Sandstone wedge on water saturated shales



2. Overburden causes shale dewatering
   and overpressures build up



3. Listric faulting caused by overpressures



CHAPTER 6. LOWER TO MIDDLE MIOCENE UTSIRA FORMATION DEEPWATER MOUNDS OF THE CENTRAL NORTH SEA, UK 16/27, 28, 29 AND NORWEGIAN OFFSHORE BLOCKS 15/9

6.1. Introduction

The phenomena of large scale seabed mounding of muddy sediment has been experimentally and theoretically predicted to have similar scales and waveform geometry as by Anketell *et al.* (1970) and as such should be a commonly observed feature of muddy seafloors.

Kilometre-scale seafloor mounding has been previously attributed partly to mud diapirism or gas hydrate mounding (Hovland 1988). Examples of large scale mounds include those described by Vogt (1997) who observed mud-prone sediment hummock fields in the Norway Basin with wavelengths of about a kilometre. Vogt (1997) attributed the mounds to be due to instability and subsequent diapirism of low-density biosiliceous oozes beneath a cover of higher density glaciogenic sandy clays. Davies *et al.* (1999) described giant (km) scale domal features (pillows) from an Oligo-Miocene succession in the Faeroe-Shetland Trough, off the northern coast of the UK. These pillows have a wavelength of 1-2km, an amplitude of about 50m and are characterised by a polygonal geometry and are postulated to have formed by density inversion within deep marine, fine grained sediments.

This chapter describes Lower to Middle Miocene age Utsira Formation kilometre scale mounds formed of sand and mapped with the use of wells on high quality 3D multichannel reflection seismic surveys of UK blocks 16/27 and 16/28, 16/29 (figure 6.1) and calibrated with well data. The mounds have also been observed on 2D seismic data and the stratigraphic interval has been mapped over the North Sea in order to place the mounds into palaeogeographic context.

6.2. Geological Setting of the Utsira Formation

Prior to the Oligocene, sediment transport direction was predominantly from northern Britain and the East Shetland. This sediment provenance was due to uplift related to the opening of the N.E.Atlantic Ocean and the subsequent establishment of an easterly prograding sediment system infilling the North Sea Basin. From the mid-Oligocene to the end of the Oligocene the North Sea Basin was significantly smaller (Rundberg 1989) than at present. Late Oligocene deposition was of basinal silts and clays (Hordaland Group) and sand sedimentation (Skada Formation) was probably related to an eustatic sea-level fall (Isaksen and Tonstad, 1989). Minor progradation occurred along the northern North Sea margin with associated uplift (Ghazi, 1992). This was the first time in the Cenozoic that significant sediment influx was derived from the East.

The Miocene of the northern North Sea was deposited in a shallow marine basin, connecting the deeper Central North Sea Basin to the South and the Norwegian-Greenland Basins to the North. Little tectonism occurred at this time with Early-Middle Miocene sedimentation predominantly consisting of basinal clay.

During the Middle Miocene, a phase of uplift occurred on the Scandinavian margin and led to tilting of the Horda Platform. This created an unconformity along the Scandinavian margin of the North Sea Basin (Ghazi, 1992). Sand deposition of the Utsira Formation was derived from the uplifted Scandinavian margin (Gregersen 1997, 1998). Figure 6.2 is a regional line drawing through the 3D seismic datasets studied and marks the position of the Utsira mounds.

6.3 Stratigraphy

Figure 6.3 indicates the Utsira stratigraphy (from Zweigler *et al.*, 1999). Stratigraphically, the work of Knox and Holloway (1992) on the Palaeogene lithostratigraphic nomenclature of the UK North Sea did not cover the Utsira formation. Deegan and Scull (1977) placed the Nordland Group above the Hordland Group, with the only formation recognized in the Nordland Group, the Utsira Formation. The Utsira formation has been described by Deegan and Scull

(1977) and Isaksen and Tonstad (1989) in the Northern North Sea sections as a fine to coarse grained sandstone, glauconitic with common bioclastic debris. These authors indicate the Utsira sands are similar to the underlying Skade Formation and that it is difficult to separate the two units stratigraphically.

Deegan and Scull (1977) and Isaksen and Tonstad (1989) placed the Utsira formation within the Miocene. Eidvin *et al.* (1999) as part of the Zweigler *et al.* (1999) analysis of the Utsira Formation in the Norwegian North Sea Block 15/9 biostratigraphically dated the Utsira formation within the Middle Miocene to Early Pliocene. The UK North Sea well 16/29-2 contained within section 6.5 (figure 6.30) has been dated by Gradstein *et al.* (1994) to biostratigraphically place the Utsira Formation within the Middle and possibly within the Late Miocene. This report uses the Gradstein *et al.* (1994) and Eidvin *et al.* (1999) Middle Miocene age for the Utsira Formation in this chapter.

6.4 Database

6.4.1. Seismic data

Two 3D seismic surveys have been interpreted over UK Central North Sea Blocks 16/27 and 16/28, 29 (figure 6.1). Seismic lines are spaced at 12.5 metres and so allowed a detailed interpretation of the Utsira mounds. The 2D seismic North Sea regional interpretation of the Utsira formation used over 6000 kilometres of 1982 and 1986 vintage reflection seismic data.

6.4.2. Well data

Of the 3D seismic datasets used to study the Utsira mounds, no wells penetrate the Utsira mounds in block 16/27. However in blocks 16/28 and 16/29 eleven wells penetrate the Utsira mounds of which wells 16/28-12, 16/29-1, 2, 3, 4 and 5 are documented in this study in detail. No core has been taken through the Utsira section in these wells. 30 plus wells have been used in the 2D regional seismic interpretation and are marked on the palaeogeographic map (figure 6.36).

Well data for this study were only used to calibrate whether the Utsira Formation contained sand or no sand (clay dominant).

6.5. 3D Seismic interpretation

6.5.1. Block 16/27 (UK North Sea offshore)

6.5.1.1. Description

Structure contour maps for the Intra Jurassic (figure 6.4), near Top Chalk (figure 6.5) and near Top Balder (figure 6.6) were mapped. Figure 6.7 indicates these horizons mapped on seismic with the top Utsira mound surface onlapping a mounded topography below. The structure contour maps all indicate a broad structural high oriented NW/SE called the Fladen Ground Spur. Over UK North Sea Block 16/27 this structural high is oriented N/S and structural contours appear to deepen to the East and South.

A structure map of the Top Utsira surface (figure 6.9) was constructed over the UK North Sea Block 16/27. Figure 6.8 is a typical example east/west seismic line through this horizon and indicates a mounded Top Utsira surface which onlaps onto an intra Utsira mounded surface. The relationship of the Top Utsira mounds to the onlapped intra-Utsira mounded surface is shown in figure 6.9 in plan view and through a series of mainly east/west oriented seismic lines (figures 6.10 to 6.17). The pinchout limit of the Top Utsira mound surface was also mapped out (figure 6.18) and indicates the Utsira mounds to pinchout close to the East/West limit of the Fladen Ground Spur. It should be noted that the Top Utsira surface is seismically a hard seismic response (strong positive red then strong negative black) with the Top intra Utsira surface a soft seismic response (strong negative black then a strong positive red). A possible explanation of this response could be the Top Utsira sediments are faster velocity sands with the Intra Utsira sediments being slower velocity shales.

These Utsira mounds are 1 to 10 km long, 50 - 150 metres high, circular to elongate, with approximately north-south trends. Internal stratal geometry within the mounds suggests downlap onto the intra Utsira surface with associated thinning of the Top Utsira mounds onto the intra Utsira surface. This thinning

appears to be onto a mounded intra-Utsira surface. Strata above are parallel and concordant with the Top Utsira Mounds, implying that palaeo-seabed topography immediately after Utsira deposition had been infilled. Top Utsira mounds structuration is not related to structuration below the Oligocene with no coincident structures observed on the top intra Jurassic, near Top Chalk and near Top Balder maps. Unfortunately the seismic data was clipped above 1000 msecs TWT, preventing the author from observing the actual stratal relationships above the Top Utsira Mounds. The underlying Intra Utsira mud mounds, which delineate the topography that controls the sediment infill of the subsequent Top Utsira mound sediments, are observed to collapse over several of these structures. This collapse could have occurred after deposition between the mud mounds, although evidence for this is equivical owing to data coverage. A possible subsequent sediment infill exists over the crest of these collapsed mounds.

6.5.1.2 Interpretation

Figure 6.19 outlines the model for Utsira mound formation based on the stratal relationships. Intra Utsira sediments began to mound with subsequent infill by the Top Utsira sediments as evident by stratal onlap. Infilling of this topography produced a flat surface with no topography and onto which subsequent post-Top Utsira sediments deposited parallel to this surface. Subsequent to post Top Utsira sediment deposition, differential compaction of the top Utsira sedimnets occurred, with the Top Utsira thicks becoming mounds and the thins becoming lows. This implies that the Top Utsira mounds are sand thicks and the lows are thinner sediment. Further interpretation of these Utsira mounds is continued in the UK North Sea Block 16/28 and 29 interpretation and description with well calibration.

6.5.2 Block 16/28 to 29 (UK North Sea offshore)

6.5.2.1 Description

Structure contour maps for the base Cretaceous, Top Sele and Top Oligocene were undertaken (figure 6.20). Figure 6.21 indicates the horizons mapped. A broad NE/SW oriented high tracks across the dataset, with the Maureen field highlighted. This region is formed over a series of Jurassic fault blocks as noted from seismic line 6.21 and the expression of these fault blocks as highs on the base Cretaceous map (figure 6.20).

The top Utsira structure contour map (figure 6.22) indicates an approximate N/S, NE/SW and E/W mound crests. The onlap of the Top Utsira surface upon the lower intra-Utsira mound surface is marked on this map. Seismic well calibration of these mounds is best summarised by figure 6.23 of 16/29-4. Here, the well penetrated the crest of the lower intra Utsira mound and indicated this mound to be formed of 300 feet of blocky (wireline) sand (figure 6.24). The seismic line shows the intra Utsira mound is onlapped by the Top Utsira surface. Strata above are concordant and do not appear to onlap this surface. Figure 6.25 is a seismic well calibration across wells 16/29-1 (240 feet Top Utsira sand/ 280 feet intra Utsira sand, figure 6.26), 16/29-5 (260 feet Top Utsira sand/ 250 feet intra Utsira sand, figure 6.27) and 16/29-3 (470 feet Top Utsira sand/ 0 feet intra Utsira sand, figure 6.28). This seismic line shows how both the Top Utsira (unit B) and the Lower Utsira (unit A) can both contain blocky wireline character sand. Strata above the Top Utsira surface are concordant and do not onlap this surface. Seismic (figure 6.29) /well calibration (figure 6.30) of 16/29-2 (540 feet Top Utsira sand/ 30 feet intra Utsira sand) indicates that in this location across the Top Utsira Unit B interval is formed of predominantly sand. A broad Top Utsira mound occurs across this line with onlap of unit B onto the lower unit A. Strata above the Top Utsira surface are parallel and do not onlap this surface. Seismic (figure 6.31)/well (figure 6.32) calibration of 16/28-12 (200 feet Top Utsira sand/ 50 feet intra Utsira sand) indicates broad onlap of the the Top Utsira unit B sands onto the intra Utsira mound surface. Again, strata above the Top Utsira surface are concordant and do not onlap this surface.

Seismic response of the individual surfaces is very variable and leads to difficulty in mapping horizons, especially the top intra Utsira Formation surface. From the well/seismic control presented no horizon appears to match perfectly to

a sand shale boundary and on observing sonic values for such lithologies no obvious velocity difference occurs. Consequently well data calibrates lithologies within these sediments but does not allow lateral estimation of lithology by seismic attribute recognition.

6.5.2.2. Interpretation

Utsira mounds within these 3D seismic datasets have similar dimensions to those within 16/27 and are elongate northeast-southwest trending structures. Seismic cross sections (figure 6.33) indicate a lower and upper unit to the Utsira mounds and well control indicates the mounds are formed of 10 to 150 metres of sand with blocky gamma ray character. Again internal stratigraphy within the Utsira mounds indicates downlap onto the Top Oligocene. The lower intra-Utsira sands (Unit A) appear to have formed as topographic mounds on the seafloor with the following upper Top Utsira sand units onlapping the lower unit. The subsequent sediments are concordant with the Top Utsira indicating that there was no seabed topography after upper Utsira sediment deposition. This implies that immediately post-Utsira sand deposition no sand mounds existed. The Top Utsira mounds appear not to follow structures below the Oligocene surface which indicates if the Top Utsira mounds did not exist during deposition and subsequent tectonics did not form them, then differential compaction of these features may explain their formation. Simply, Unit B, containing thick sands would compact less than the lower unit A clay rich sediment. With time this would cause the Unit B Top Utsira horizon to form highs compared to the more compacted, mud prone lows of Unit A.

Figure 6.34 outlines the progressive formation of these Utsira mounds. Observations of the deeper structures below the Utsira mounds indicates the mounds are located over a series of Jurassic fault blocks as in the case of the Maureen field, located in NE corner of 16/29. In addition gaps on the Top Oligocene surface structure contour map (figure 6.20) have been interpreted as blowout features/potential pockmarks by Cooper (2000) which are located directly below circular gas-induced mounds in Pliocene sediments as described by Brookes *et al.* (1995) and Cooper (2000). The location of the Utsira mounds

above Jurassic fault blocks which may have been fluid/gas migration foci in the Tertiary and the vertical juxtaposition of the location of Lower Oligocene blowout features below and Pliocene gas mounds above suggests that these Utsira mounds may have been influenced by migrating fluids/gas during the Cenozoic. As previously outlined in chapters 3 and 4, the Upper Jurassic marine source rock was mature for oil from Eocene to Recent in the North Sea (Cornford, 1998). Gas anomalies throughout the 16/28 and 16/29 area have been ascribed by Cooper (2000) to be due to previously or actively migrating hydrocarbons(oil and/or gas) from these Upper Jurassic marine source rocks, focused about the upthrown side of Jurassic fault blocks. A relationship between mound formation and fluid migration is possible.

6.5.3 Block 15/9 (Norwegian North Sea offshore)

Zweigler *et.al.* (1999) have made observations of the Utsira mounds from a 3D seismic survey shot and interpreted in 1999 over the Sleipner field in Norwegian offshore North Sea Block 15/9. Well data of 50 plus wells, with average spacings of 250 metres allowed a detailed lateral and vertical calibration of the Utsira Formation mounds over this block by Zweigler *et al.* (1999).

Zweigler *et.al.* (1999) observed the following regionally regards the Utsira Formation:

(i) Utsira formation is confined to the North Sea basin centre, showing east and westward onlap of the basin margin.

(ii) Utsira formation has an irregular base with onlap against local mounds.

(iii) Utsira formation top is irregular with a general dip towards the south.

(iv) Utsira formation is overlain by shaly rocks of the Upper Pliocene Nordland group, which shows downlap onto the Utsira formation.

(v) The lower part of these Upper Pliocene shales are the toes and the thin basinal correlatives to clinoformal wedges prograding from the west to east.

Zweigler *et.al.* (1999), considers evidence from the 3D seismic survey and a dense well database, suggestive of mud volcanism, and is expressed in the form of mud mounds (correlative to the intra Utsira mounds, Unit A) between areas of Utsira sand (correlative to the Top Utsira surface, Unit B). Zweigler *et.*

al. (1999), observed that the sand of the Utsira Formation onlaps the mud mounds/mud volcanoes, and be partly overlain by mud sheets, interpreted as ejected, outflowing mud. Sand deposition of the Utsira sand was at least partly contemporaneous with mud volcanism. Zweigler *et.al.* (1999) noted strong compaction of the mud mounds, which has led to local subsidence anomalies with thickening of sands over the mud volcanoes and downward deflection of the top Utsira Formation. Zweigler *et.al.* (1999) made the observation that the mud mounds are often linked to/triggered by migration of gas. This observation is confirmed by noting the abundance of shallow gas indicators above the mud mounds, such as blurred seismic signals in nearly vertical zones and anomalously strong amplitudes in certain horizons, especially in the upper part of the Pliocene shales.

Zweigler *et.al.* (1999) further noted that the sandy Utsira Formation is easily discernable on well logs, especially by the blocky, low gamma ray signal. Gamma ray and resistivity peaks within the Utsira Formation are most likely due to thin (<1 metre) interbedded shale layers. These shale layers can locally be traced from well to well (<500 metres), but can not be easily traced over larger distances.

Zweigler *et.al.* (1999) described a 9 metre core sample taken from well 15/9-A23. The sample is of sand, grey, homogenous, fine to very fine grained, moderately to well sorted, with no visible sedimentary structures. The grains are angular to sub angular, with some rounded grains. Porosities vary between 27-31% with petrography consisting of primarily quartz, with some feldspar and organic material, and additional minor components such as pyrite, glauconite and chlorite cement.

6.6 2D Regional Seismic Interpretation

Regional 2D seismic interpretation has been undertaken in the Central North Sea and the Northern North Sea for the Utsira formation with figure 6.36 representing the resultant palaeogeographic reconstruction. The Basin is elongated in a north-south direction. Utsira mounds can be noted in northern UK quads 16 about the 3D seismic study areas, and quad 9 (figure 6.1). Well

calibration of these mounds indicates, as in the Block 16/28 and 16/29 interpretation, sand thickness of between 10 to 150 metres, with a blocky wireline character, often with several sands stacked on top of each other. Correlation of individual sand units on the available 2D seismic was very difficult and only the Top Utsira mound pick could be used with any certainty. This horizon when observed southwards passed into progressively thinner and deeper mud prone, parallel strata delineating probable basinal shales. When traced east and west, these shale units onlap the Top Oligocene, indicating the basin margin at this time. 2D seismic was not available beyond UK quad 9 to the north, but according to Gregersen (1997, 1998) equivalent aged strata becomes thinner (50 to 100 milliseconds) with strata being variably parallel, minor mounded to chaotic in appearance, and eventually progradational in character with well calibration indicating a sandy, blocky wireline character. Rundberg (1989) and Gregersen (1997, 1998) interpret the northerly extension of the Utsira Formation to be a shallow marine shelf area. Gregersen (1997, 1998) interpret the Utsira formation to signify a sea level fall in the Middle Miocene which led to the formation of an incised shelf and river systems on the western Scandinavian margin as observed by Gregersen (1997, 1998). This sea level fall is inferred to have caused the deposition of deepwater sands in a southerly direction into the Central North Sea as Utsira formation sands about UK quads 9 and 16. Galloway *et al.* (1993) interprets the Utsira mounds to be some form of originally deposited contourite deposit. Galloway *et al.* (1993) assertian of the deepwater depositional environment of the sands is corroborated by the current author since the depth of the Utsira mounds relative to the palaeoshelf (from regional seismic lines) is at least 500 metres. The interpretation by Galloway *et al.* (1993) of the mounding as due to contourite deposition is regarded here as erroneous. Instead, the descriptions of these mounds from 3D seismic intrepretation in this thesis are consistent with their origin as differential compaction features. Deposition of these sands into deepwater may have involved remoulding of the sediment by sea floor contour currents but there is insufficient core data to refine the general interpretation as a deepwater mass transport depositional process.

The preferred model of mound formation is that deposition of these sands occurred onto either a mounded seafloor (intra Utsira/unit A) created either by

mud diapirism, loading of the seafloor by the Utsira sands, gas hydrate mounding or mounding created by original deepwater sand deposition. Gas hydrate mounding is suggested as a possibility as water depths of 500-1000m at the time of mounding between the Utsira sand mounds puts the Oligocene muds at a seafloor range for gas hydrates to form (Kayen 1991). In addition at this time (middle Miocene) the introduction of colder Norwegian - Greenland waters (Mudge and Bujak 1999) may have allowed gas hydrates to have formed (Kayen 1991). Occasionally intervening mud mounds show collapse over the crest of these features as previously noted. A very similar mode of formation has been documented by Davies *et.al.* (1999) as previously noted (figure 6.35), with onlap fill of a mounded topography followed by collapse of the intervening mud mounds due to some unknown pressure depletion mechanism. In the Utsira mound case the topography has been infilled with sand, rather than mud and thus shows subsequent differential compaction over the sand thicks.

6.7 Conclusion and petroleum potential

Middle Miocene Utsira formation mounds occur over tens of thousands of square kilometres of deepwater basinal shales of the Central North Sea. They show that within deepwater shales, kilometre-scale mud mounding can occur, as predicted by Anketell *et.al.* (1970) and that they significantly affect depositional geometry of deepwater sands. Similar scales of plan view and cross-sectional geometries have been noted by Davies *et. al.* (1999) within the Oligo - Miocene succession of the Faeroe-Shetland Trough and by Vogt (1997) in the Quaternary-Holocene of the Norway Basin. The process of large scale mounding of the sea floor may be an important feature of deepwater basinal settings, hitherto poorly observed. It should be noted that the depositional model of the North Sea Gryphon field (figure 3.5), bears a striking resemblance to the Utsira mound formation model. The turbiditic sands of the Gryphon oilfield appear to be controlled by a mounded sea floor topography of a similar scale to the Utsira mounds. Plan view extents are of kilometres for the Utsira sands which are controlled by intervening seafloor mud mounds and are near identical in

dimensions to the apparent mounding controlling the depositional lows for Balder age deepwater sediment deposition within the Gryphon field.

The ability of the muddy substrate to mound at a kilometre scale is obviously important. Formation of kilometre scale mud mounds could occur via gas hydrate mounding, gas/fluid expansion or mud diapirism (see chapter 7 for discussion). These examples highlight the possibility of deepwater sands which may act as oil reservoirs and have been constrained by seafloor mounds, and may be an important control on deepwater sediment geometry. As the Utsira formation is so shallow in the section, it allows a very detailed observation of this mud mound topography , lithology and internal stratigraphy, otherwise difficult to detail in deeper units due to resolution problems.

Finally, to date the youngest commercial hydrocarbons found in the UK part of the North Sea are within the Lower Eocene Alba field. The Utsira Formation mounds may be a possible target as they contain significant kilometre scale traps with excellent reservoir quality sands. Major risk for this potential play would be hydrocarbon migration through the thick Eocene and Oligocene clay section and the possibility of hydrocarbon biodegradation at these shallow depths (approximately 1000 metres). In addition within Norwegian offshore North Sea Block 15/9, 20 to 50 kilometres east of UK North Sea Blocks 16/27, 28 and 29, the Utsira Formation has been a repository of carbon dioxide disposal from the Sleipner oilfield in this block (Zweigler *et.al.*, 1999). Carbon dioxide has been injected into sands of the Utsira Formation since 1996, the first instance in the North Sea for such carbon dioxide injection into shallower strata. The Utsira may in the future not only be a hydrocarbon reservoir, but a site for widespread carbon dioxide disposal, and hence reduce greenhouse gases released to the atmosphere (Zweigler *et.al.*, 1999) from North Sea hydrocarbon producing fields.

Figure 6.1. Location of 2D and 3D seismic datasets in UK Central North Sea Blocks 16/27, 28 and 29 for study of the Middle Miocene Utsira Formation (partly from PESGB, 1997)

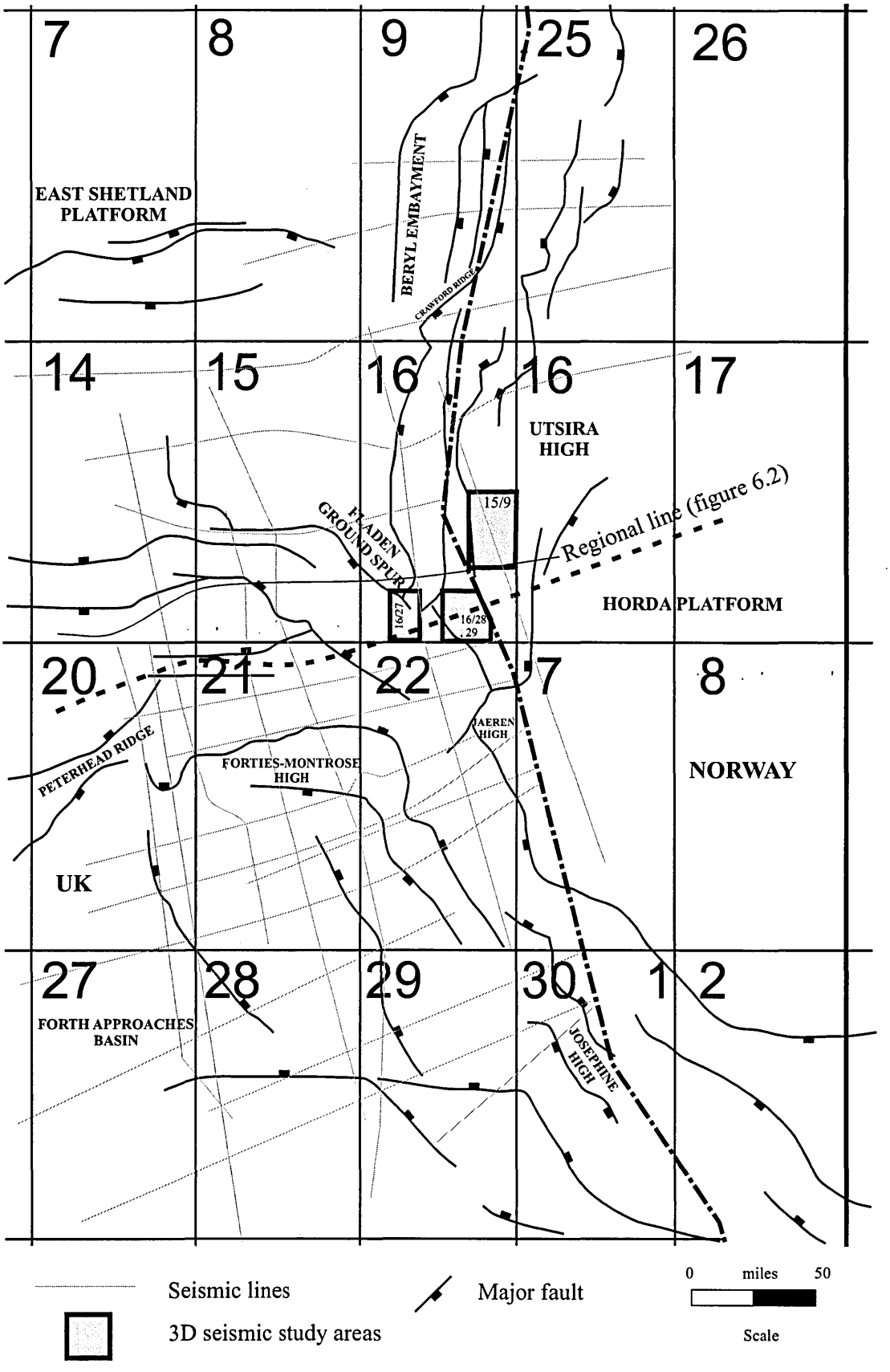


Figure 6.2 Geological cross section across the Central North Sea passing through UK Blocks 16/26, 27, 28, 29 and 30 (interpreted from CNST82-04 regional seismic line)

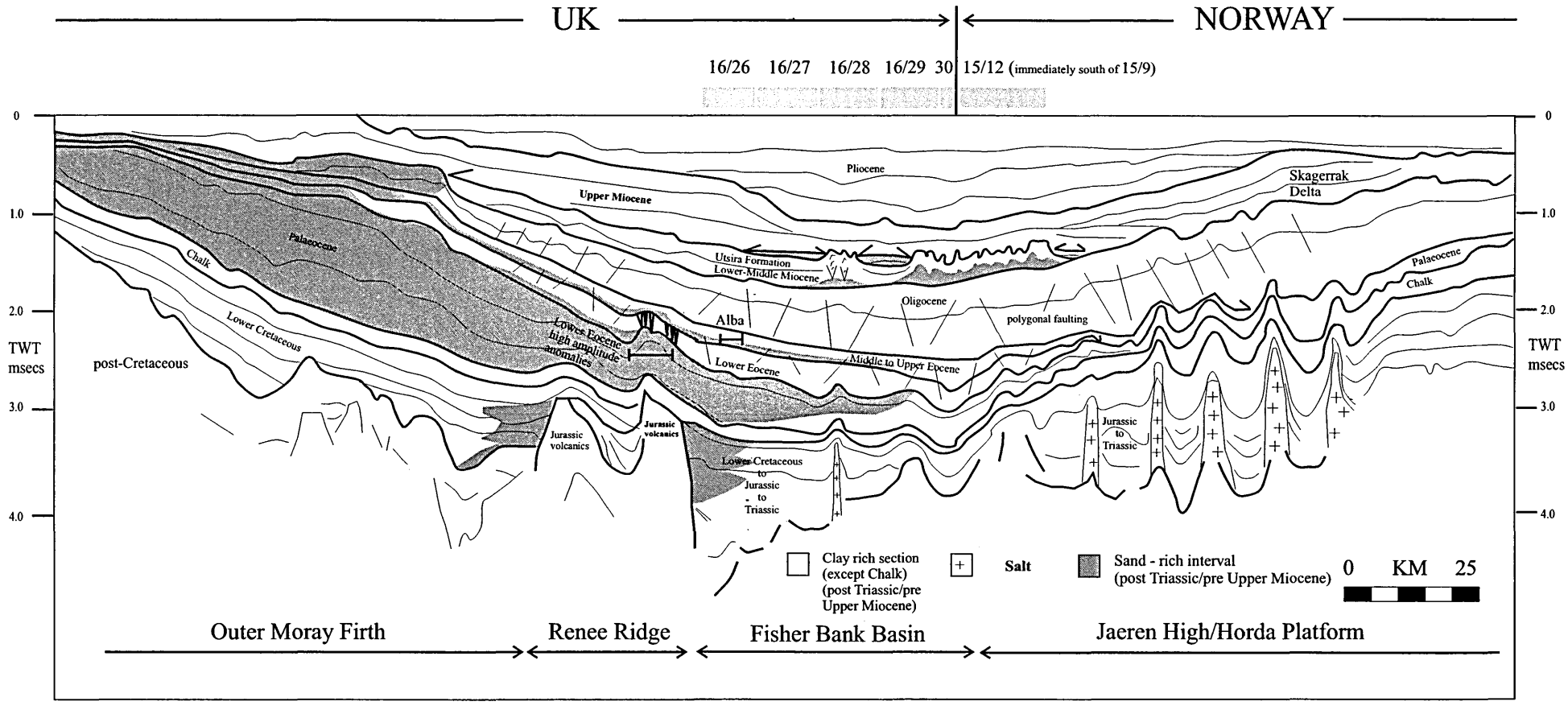


Figure 6.3. Stratigraphy of the Middle Miocene Utsira Formation, from Norwegian North Sea Block 15/9 (from Zweigler *et al.*, 1999)

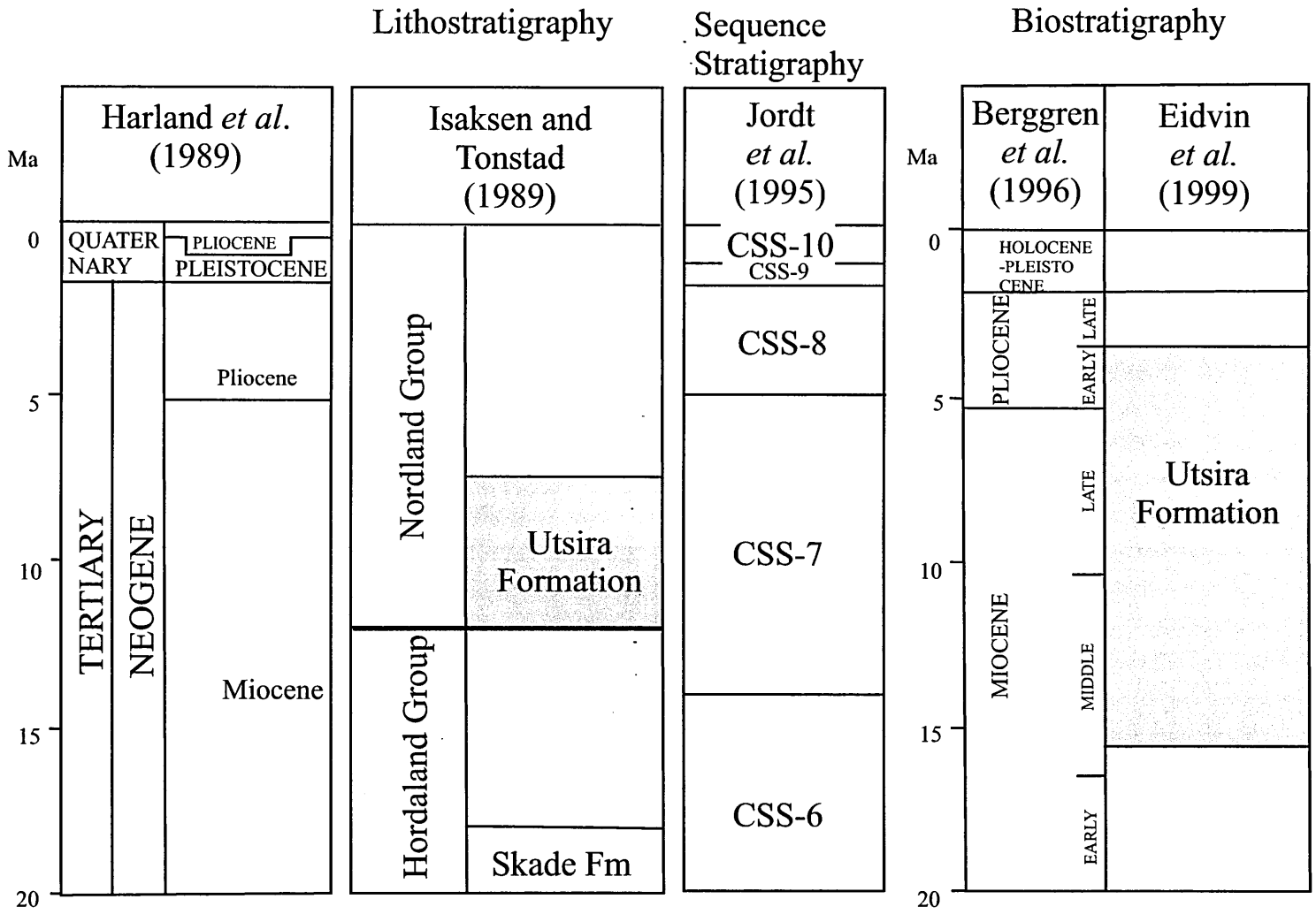


Figure 6.4 Intra Jurassic structure contour map over UK North Sea Blocks 15/30, 16/26 and 16/27

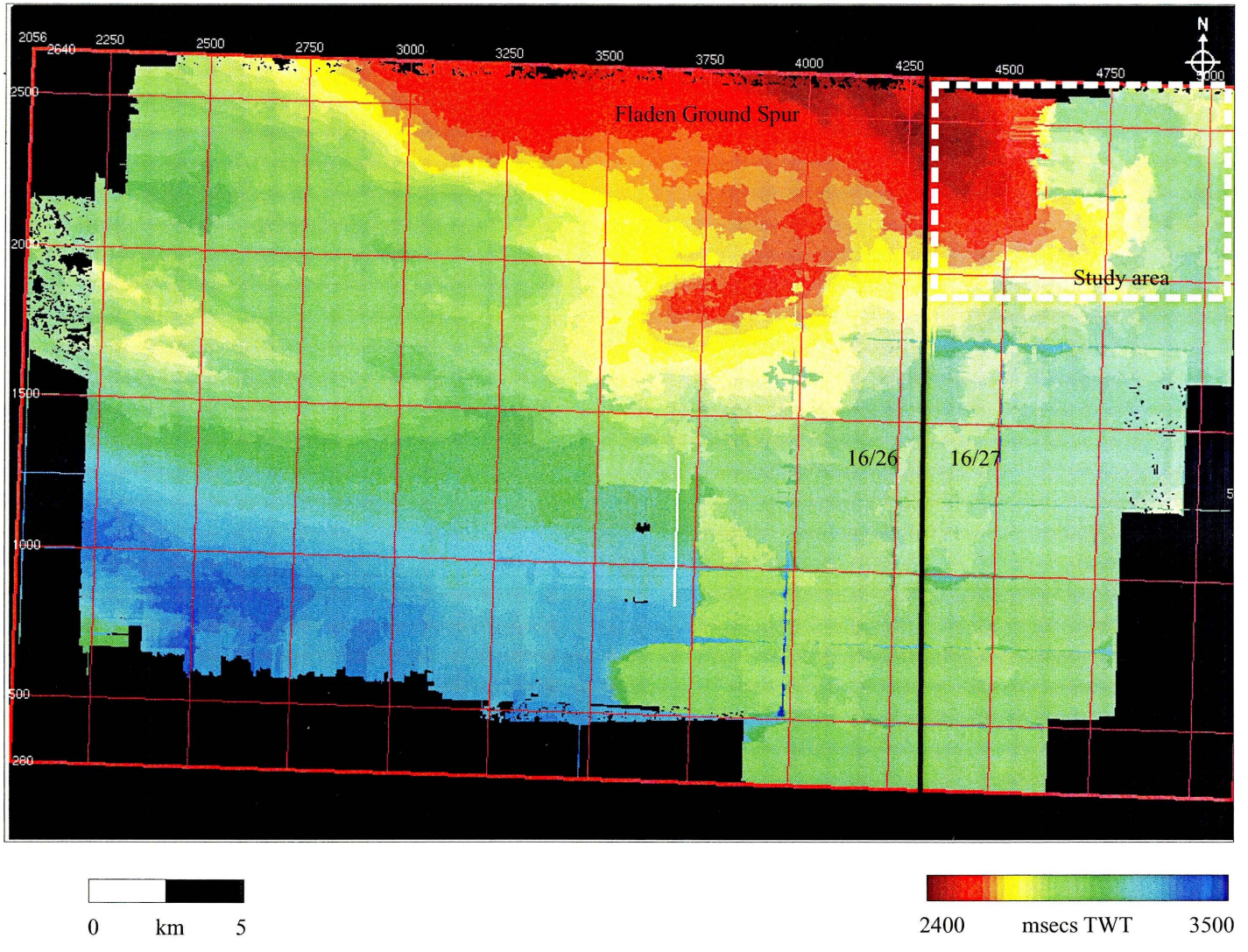


Figure 6.5. Top Chalk structure contour map over UK North Sea Blocks 15/30, 16/26 and 16/27

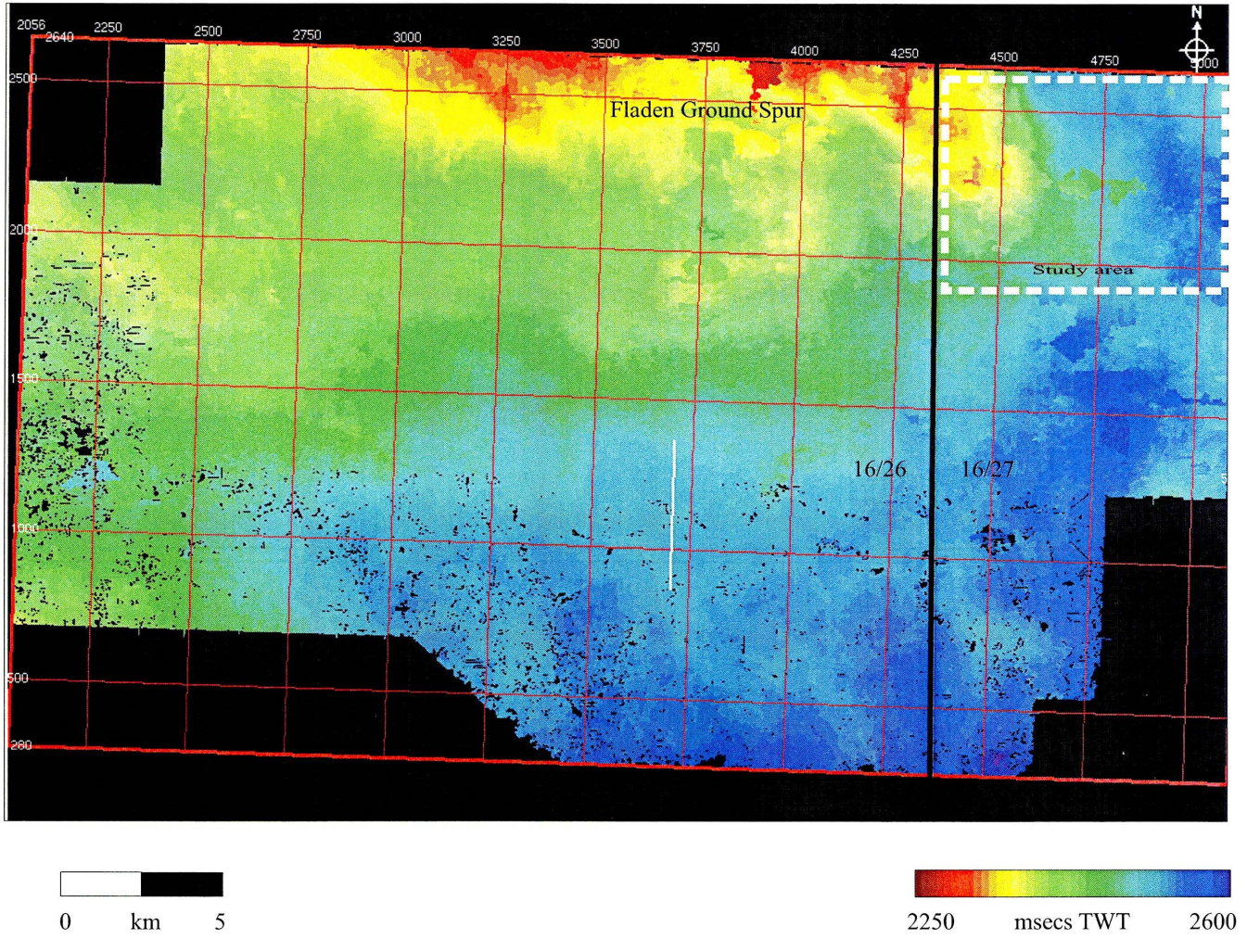


Figure 6.6 Top Balder structure contour map over UK North Sea Blocks 15/30, 16/26 and 16/27

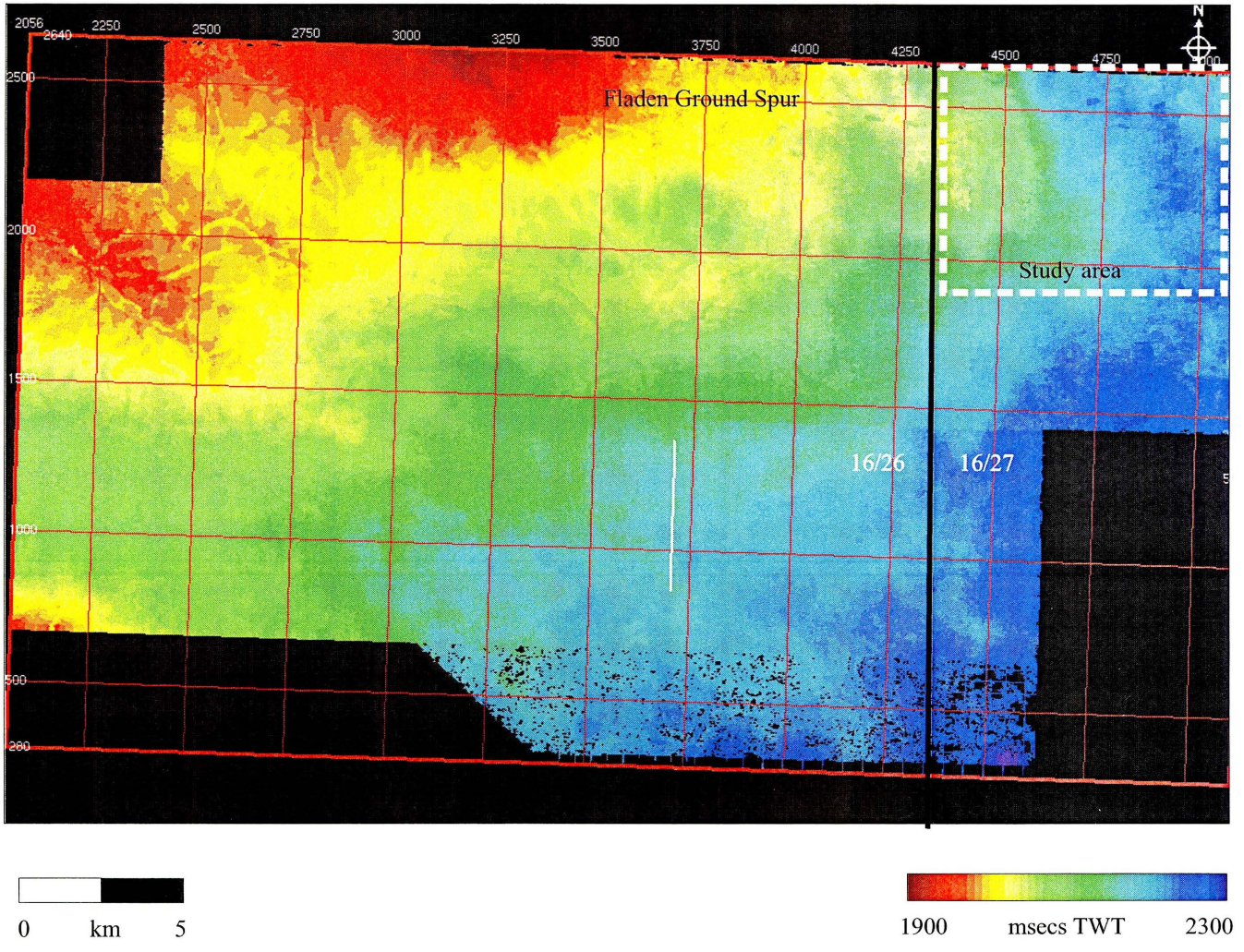


Figure 6.7. North/South seismic line through the Tertiary to Top Jurassic strata of UK North Sea Block 16/27

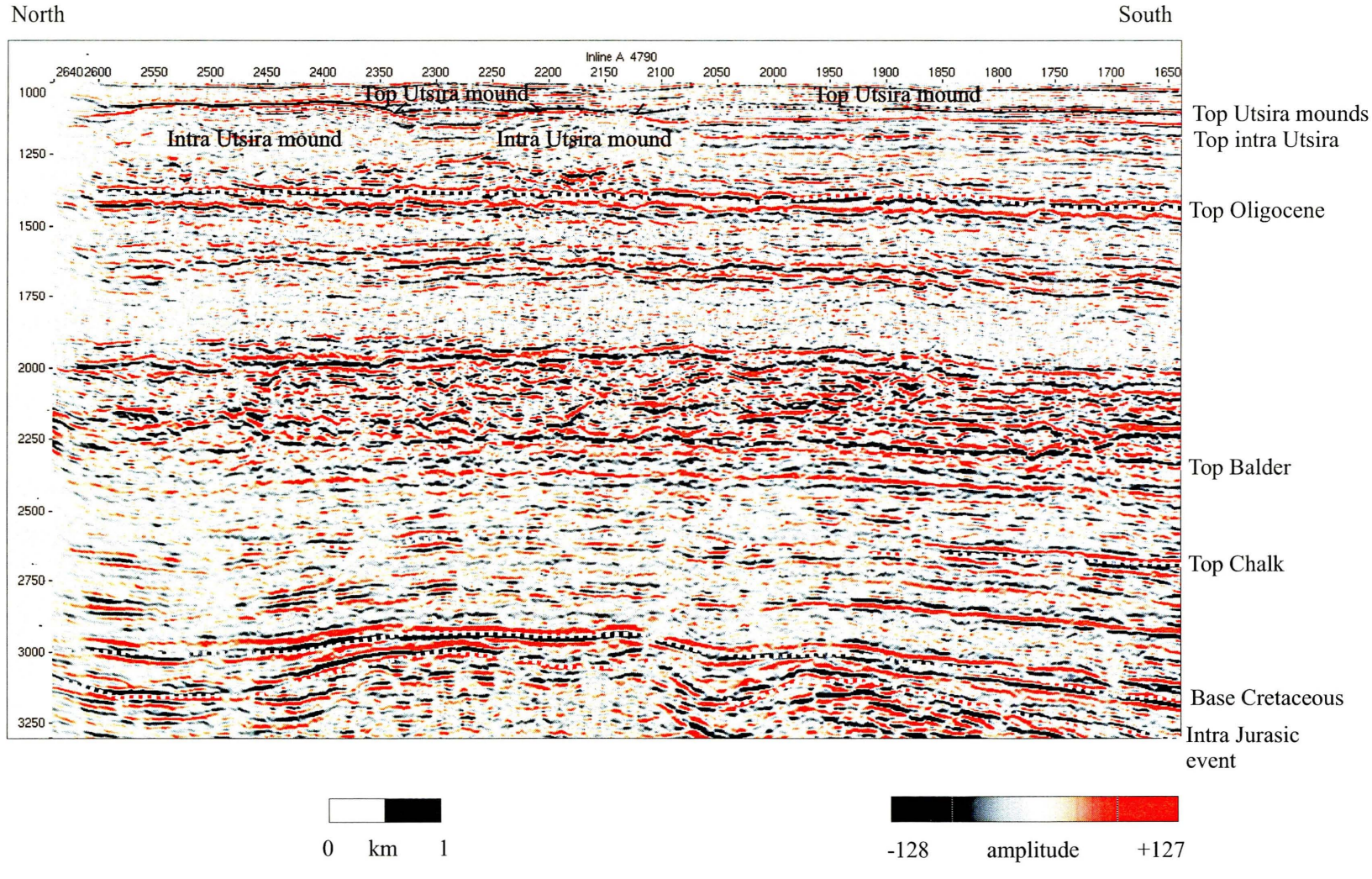


Figure 6.8. Seismic cross section through Lower to Middle Miocene Utsira Mounds of Central North Sea Blocks 16/27

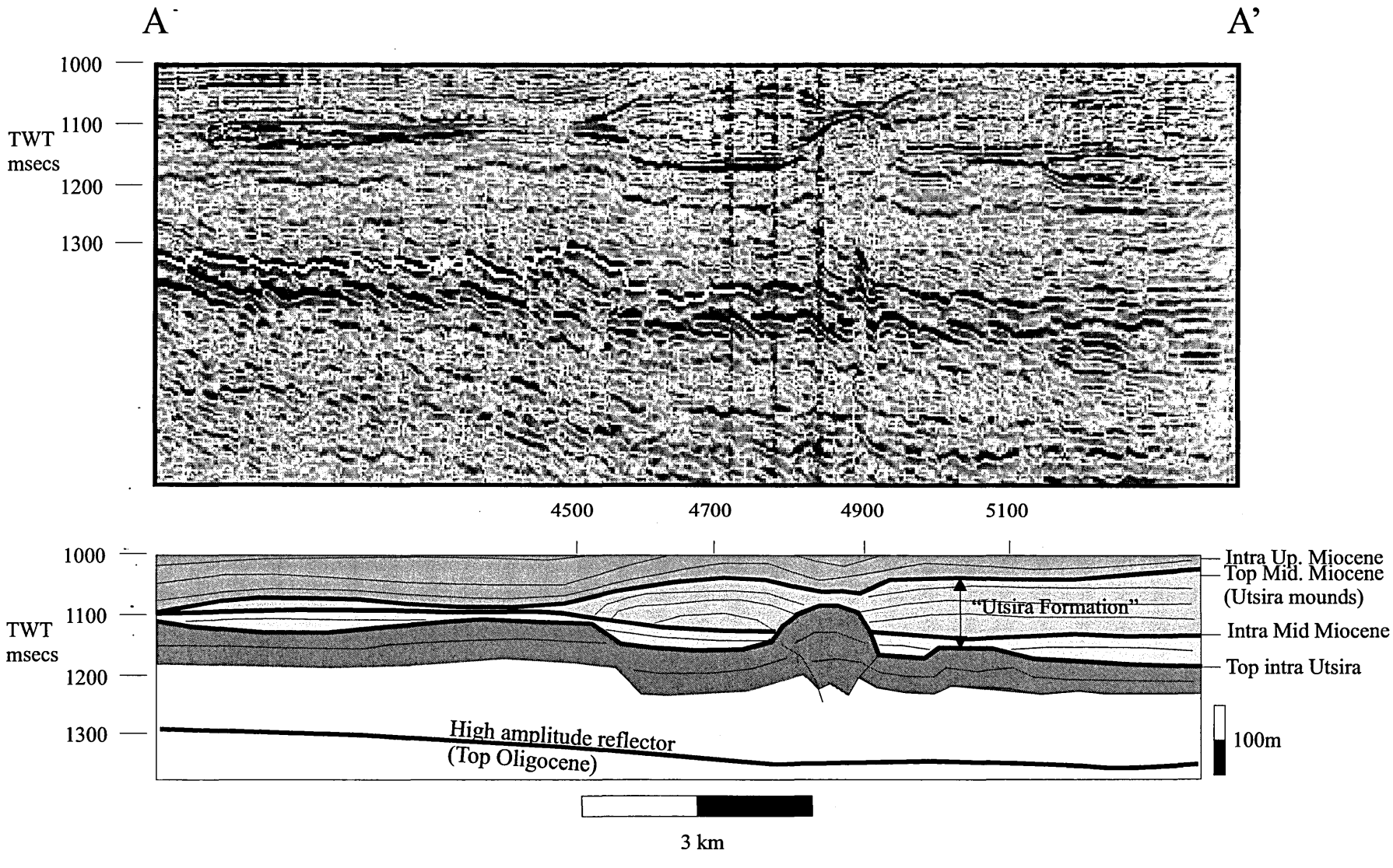


Figure 6.9. Structure contour two way time map of the Top Utsira mounds over UK Central North Sea Block 16/27

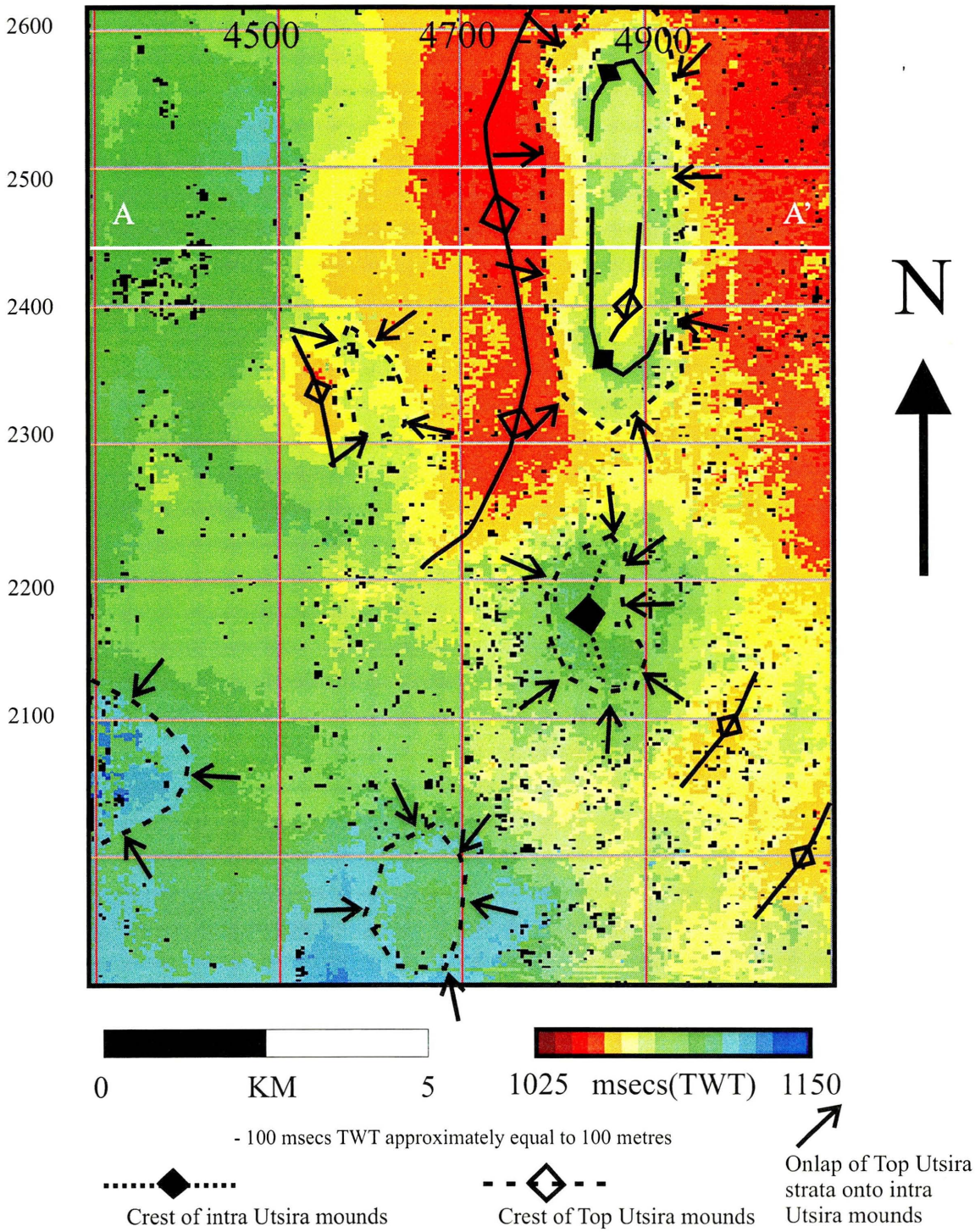


Figure 6.10. UK Block 16/27 - Utsira mounds - crossline 1902

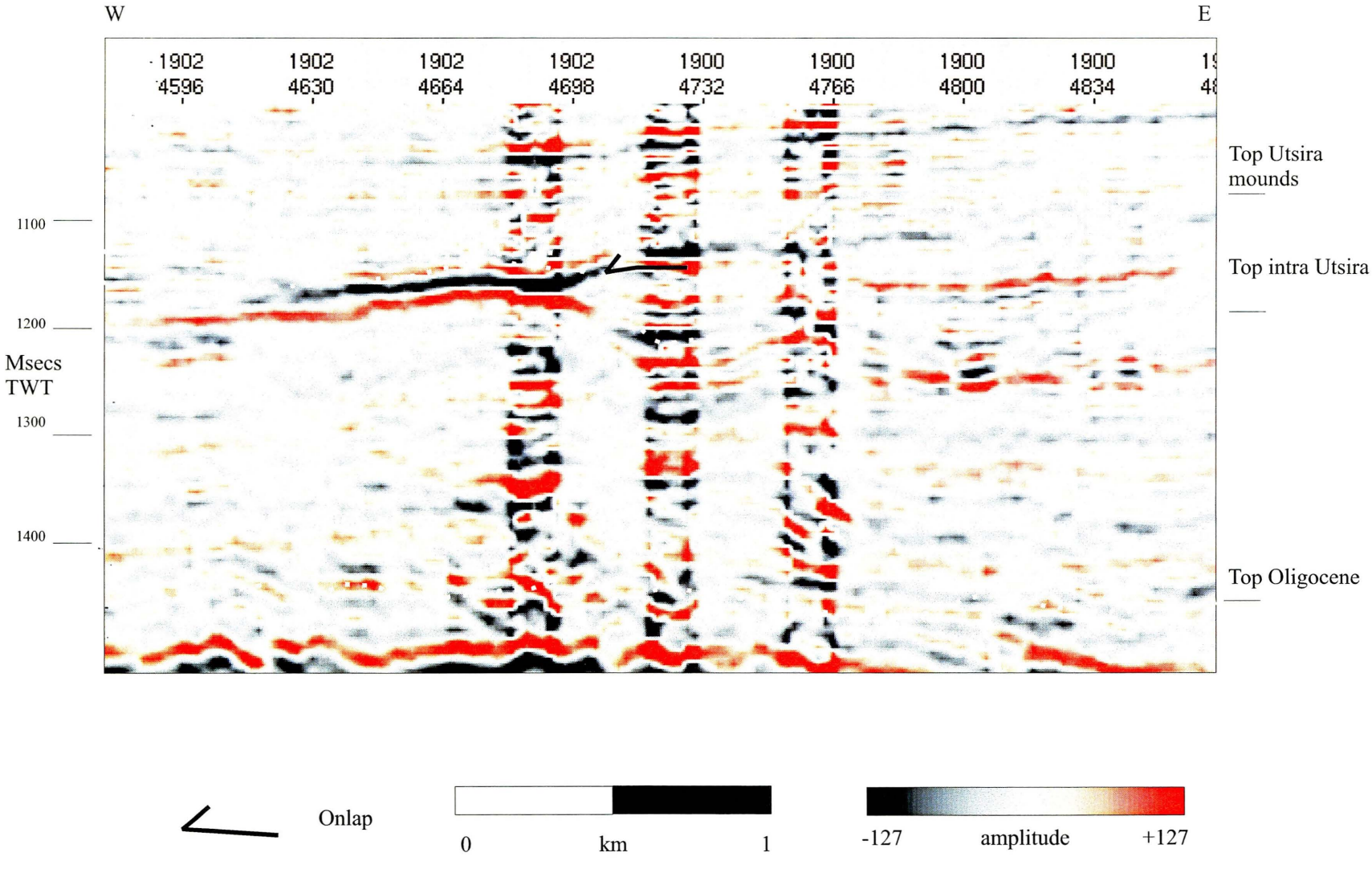


Figure 6.11. UK Block 16/27 - Utsira mounds - crossline 2000

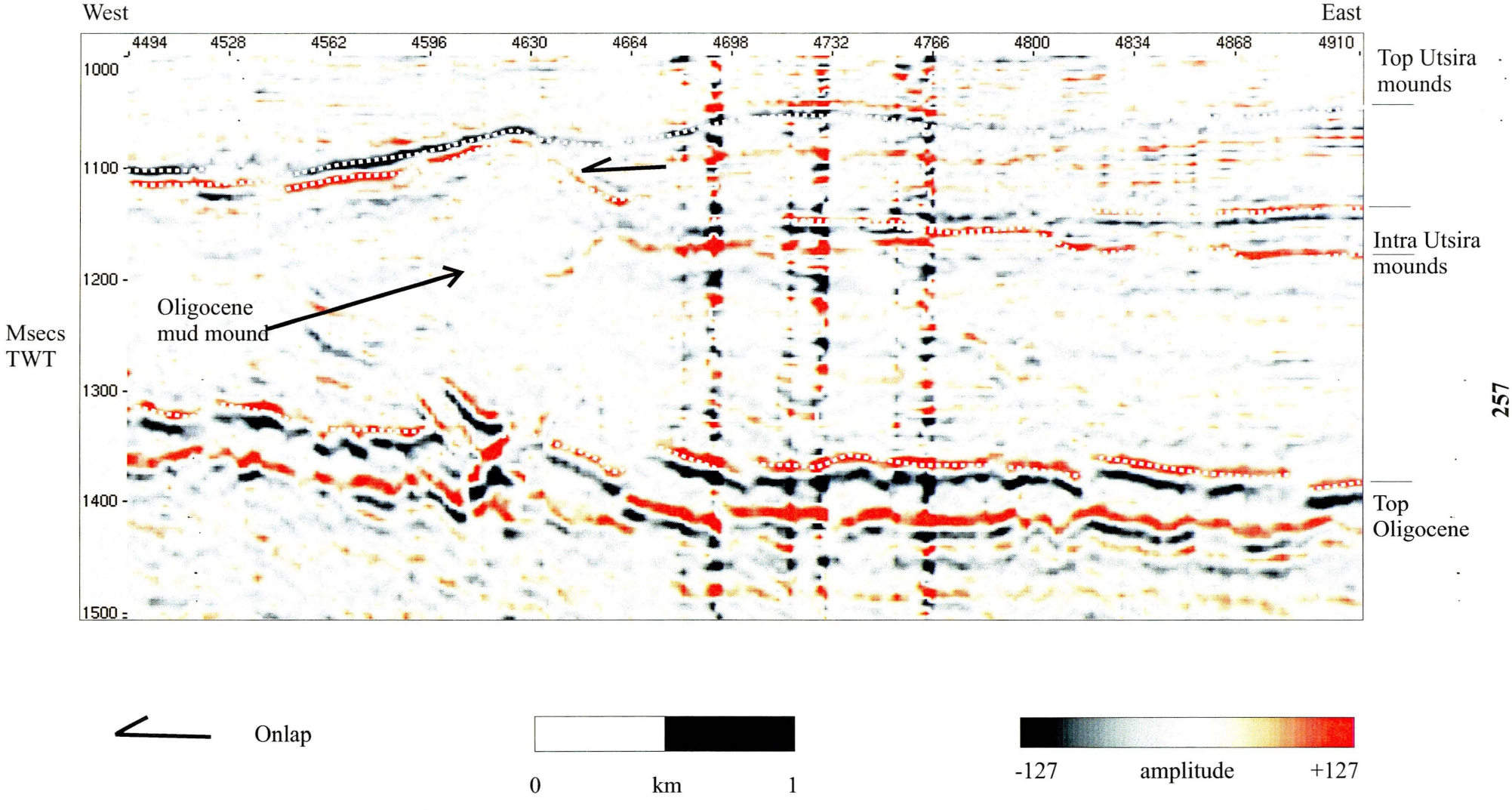


Figure 6.12. UK Block 16/27 - Utsira mounds - crossline 2200

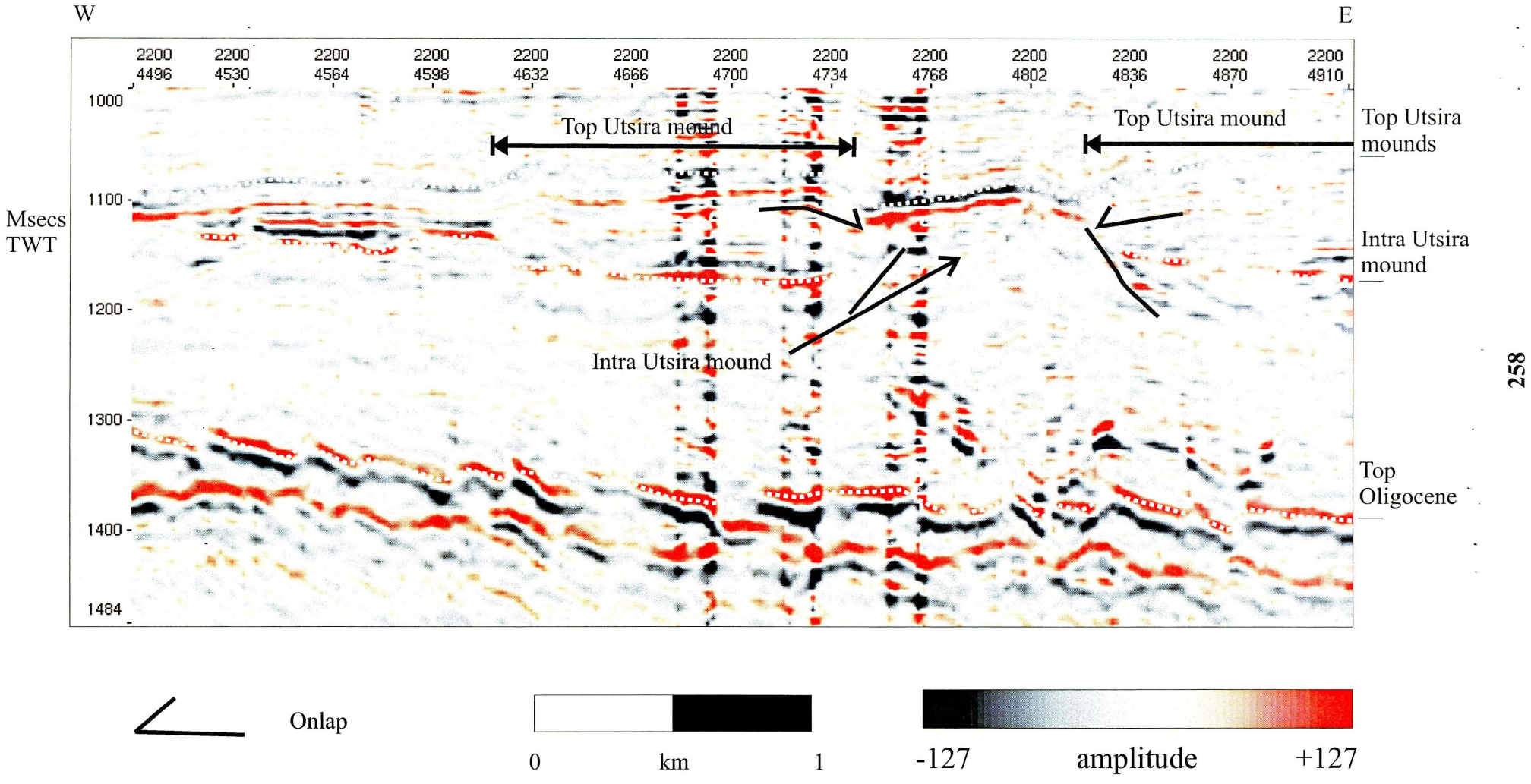


Figure 6.13. UK Block 16/27 - Utsira mounds - crossline 2300

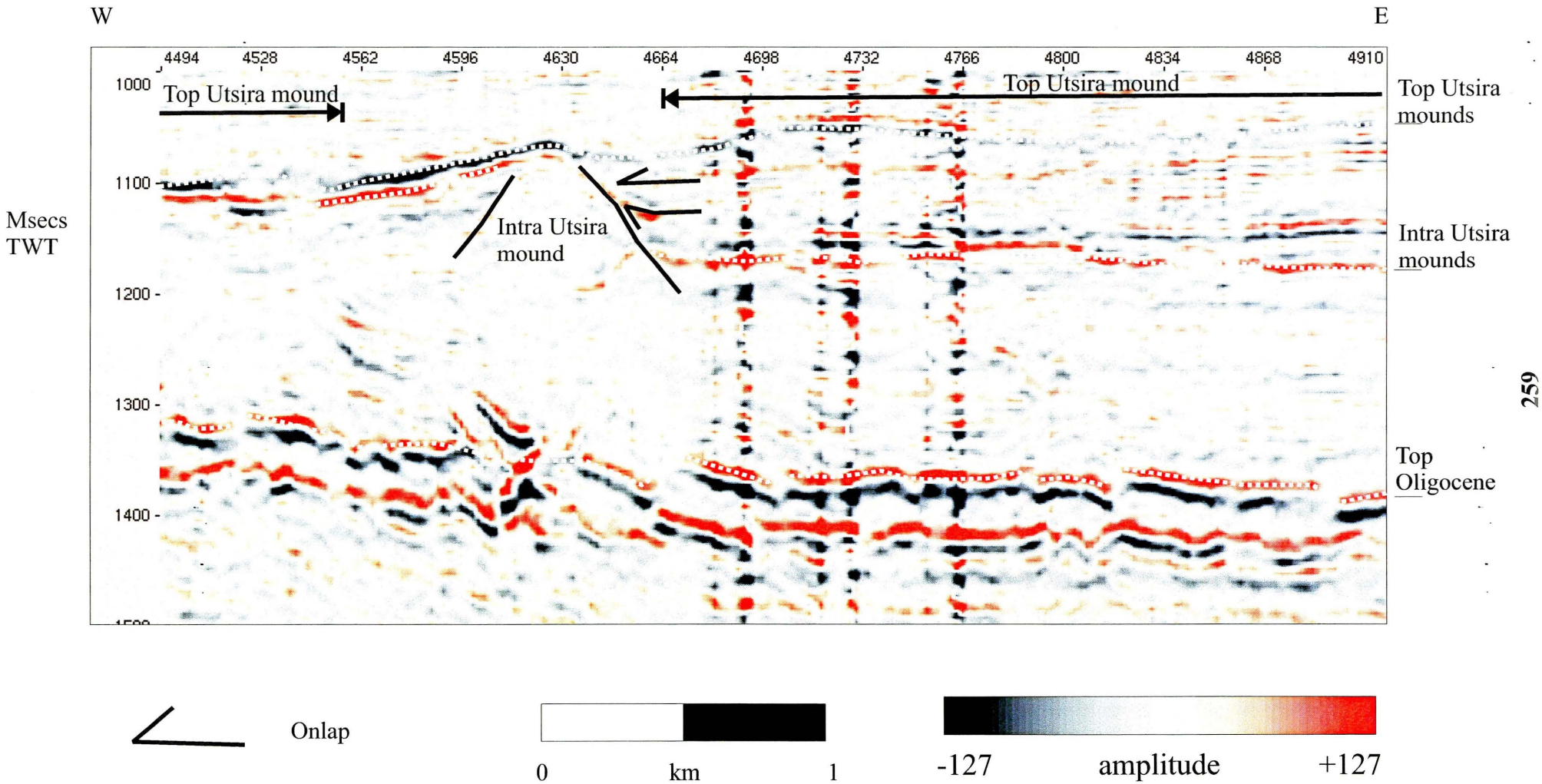


Figure 6.14. UK Block 16/27 - Utsira mounds - crossline 2400

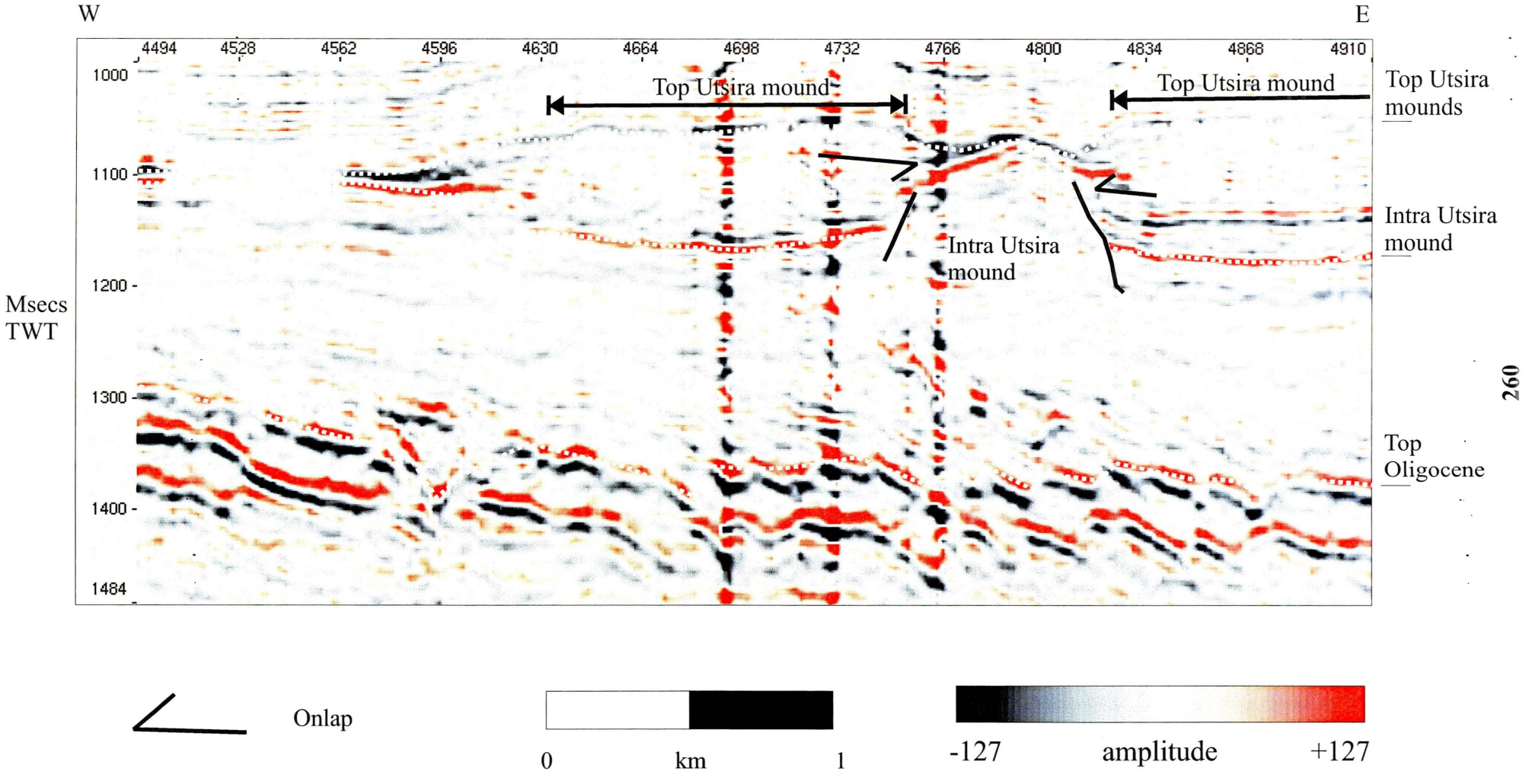


Figure 6.15. UK Block 16/27 - Utsira mounds - crossline 2500

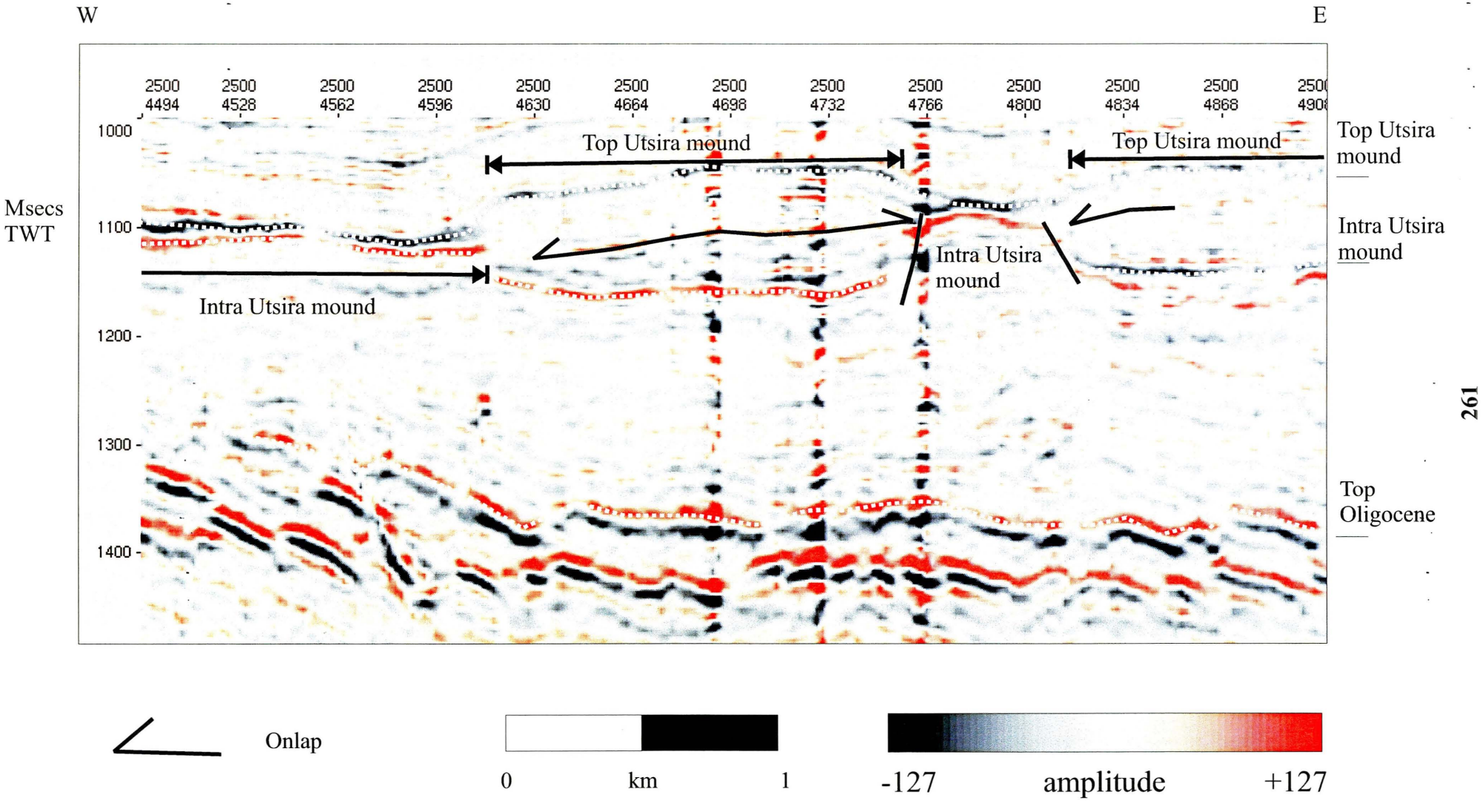


Figure 6.16. UK Block 16/27 - Utsira mounds - crossline 2600

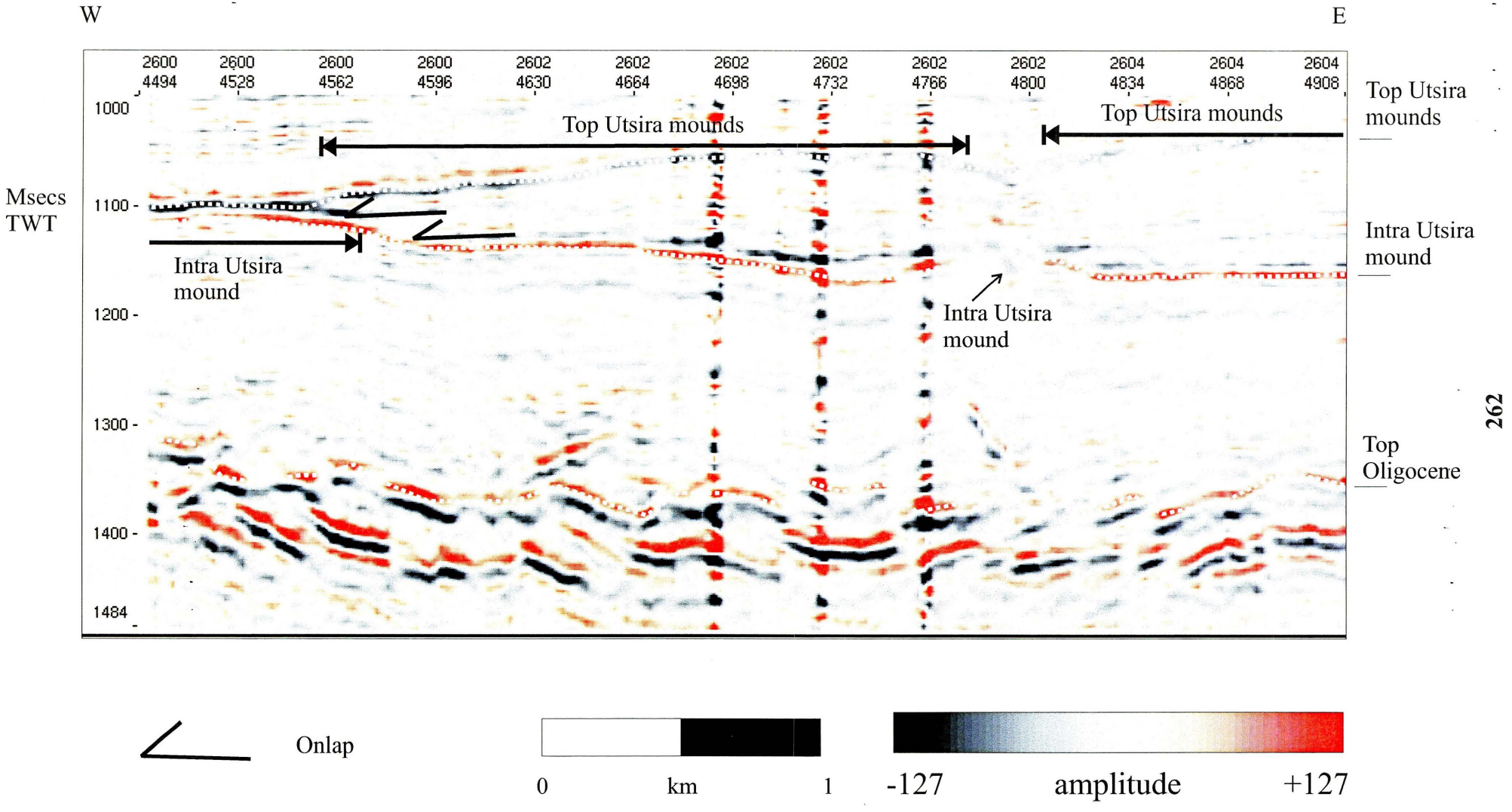


Figure 6.17. UK Block 16/27 - Utsira mounds - inline 4800

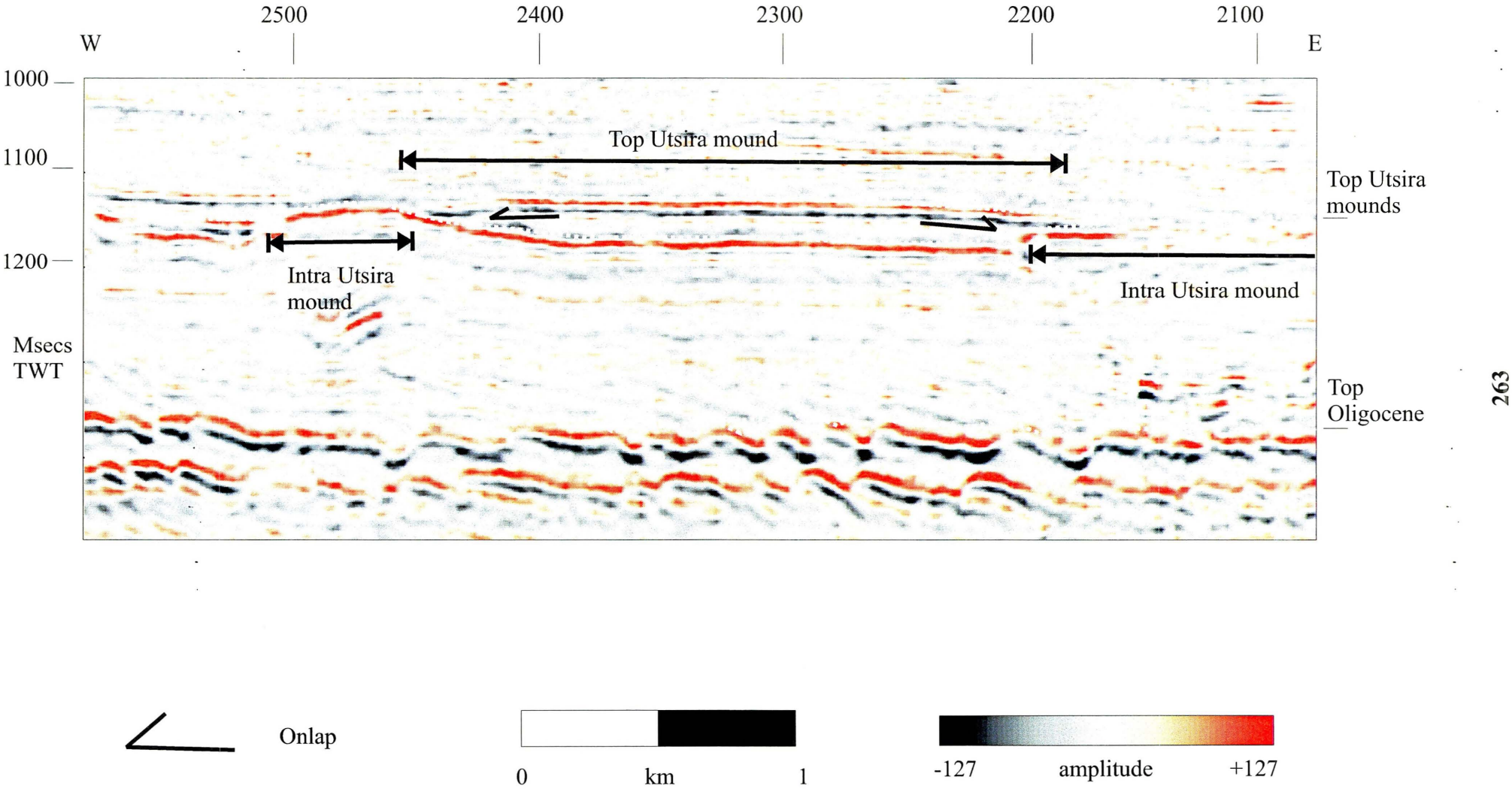


Figure 6.18. Structure contour map of Top Utsira mound surface with pinchout to the west of this surface against the Fladen Ground Spur over UK North Sea Block 16/27.

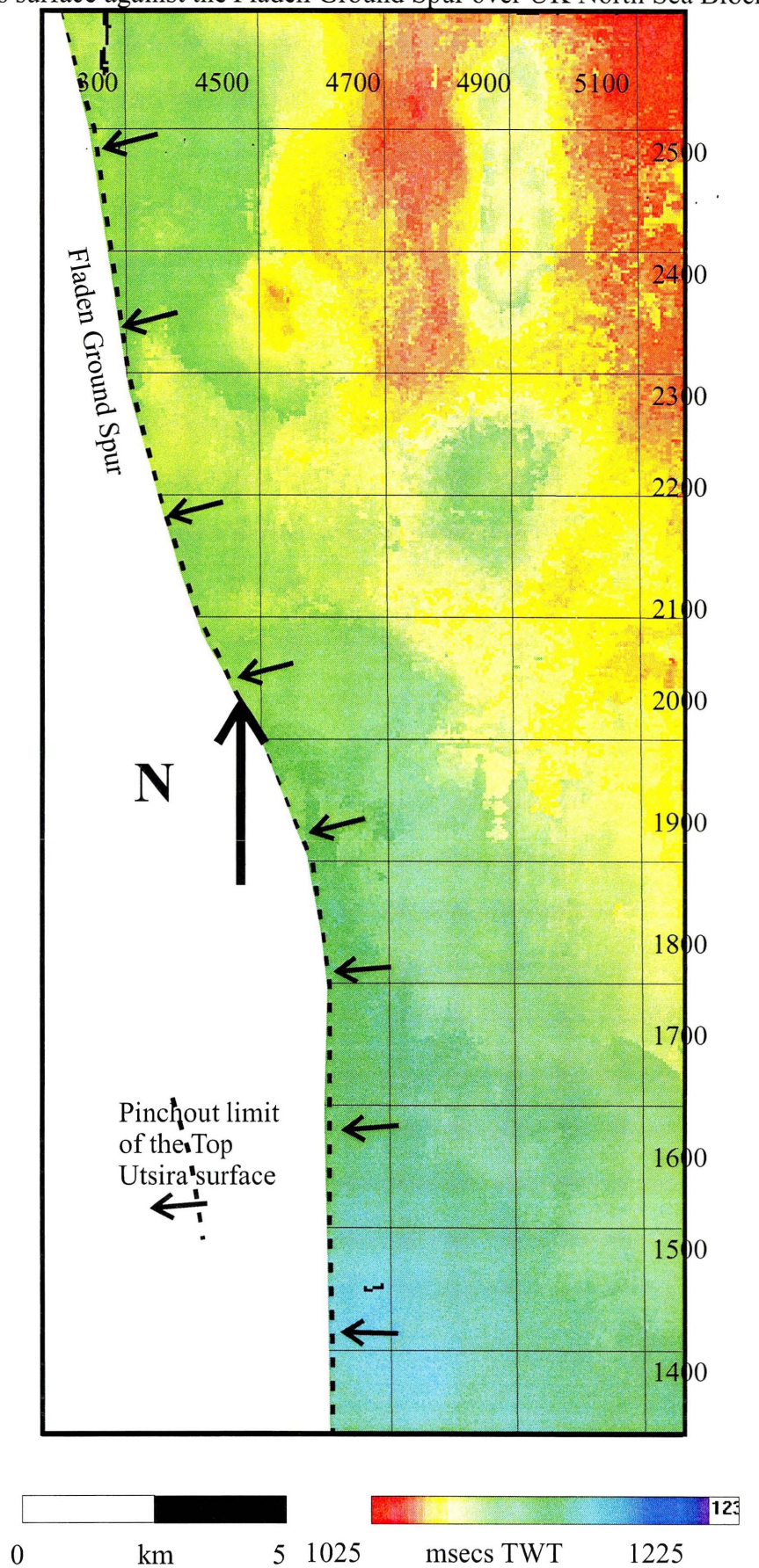


Figure 6.19. Model of Middle Miocene Utsira mound Formation over UK Central North Sea Blocks 16/27

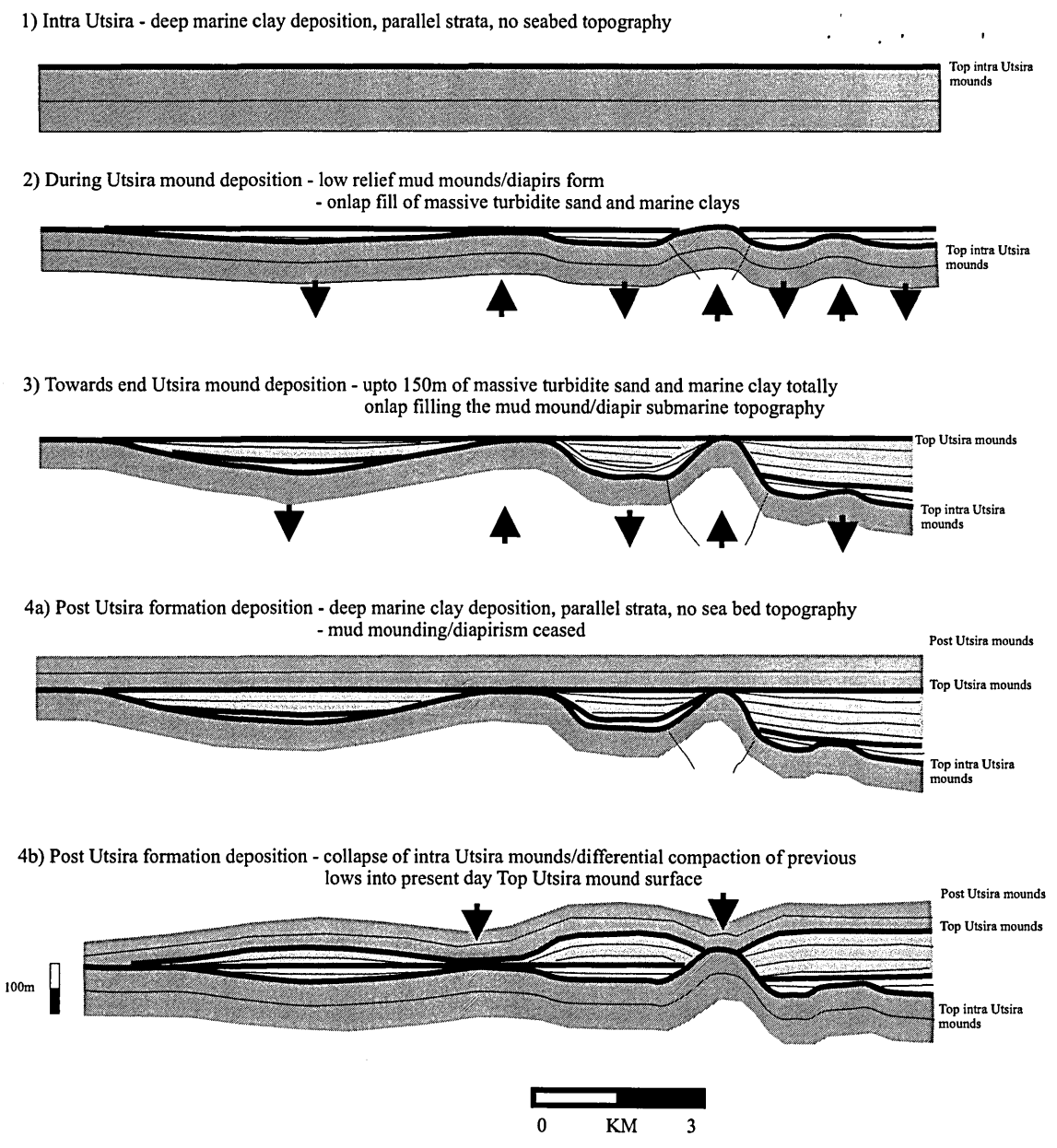


Figure 6.20(i). Base Cretaceous structure contour map over UK Central North Sea Blocks 16/28 and 16/29

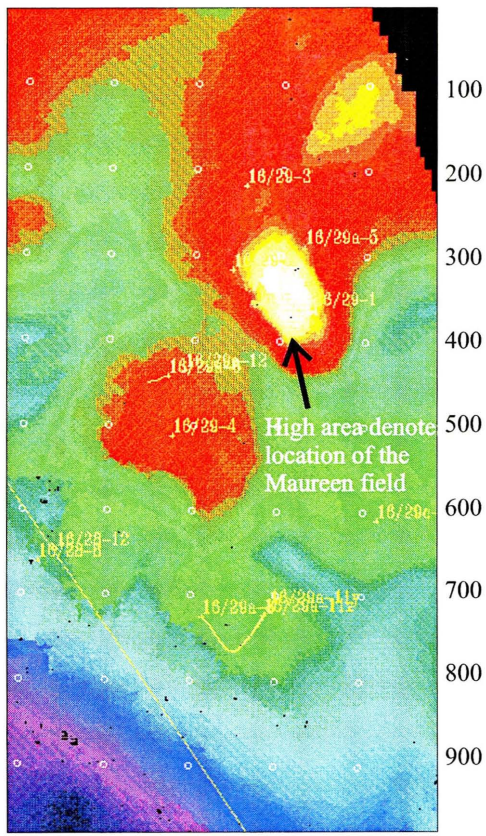


Figure 6.20(iii). Top Sele structure contour two way time map over UK Central North Sea Blocks 16/28 and 16/29

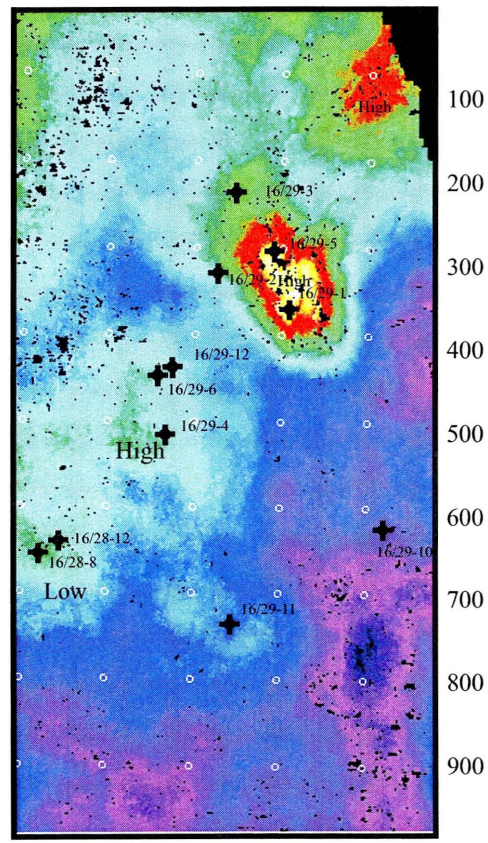
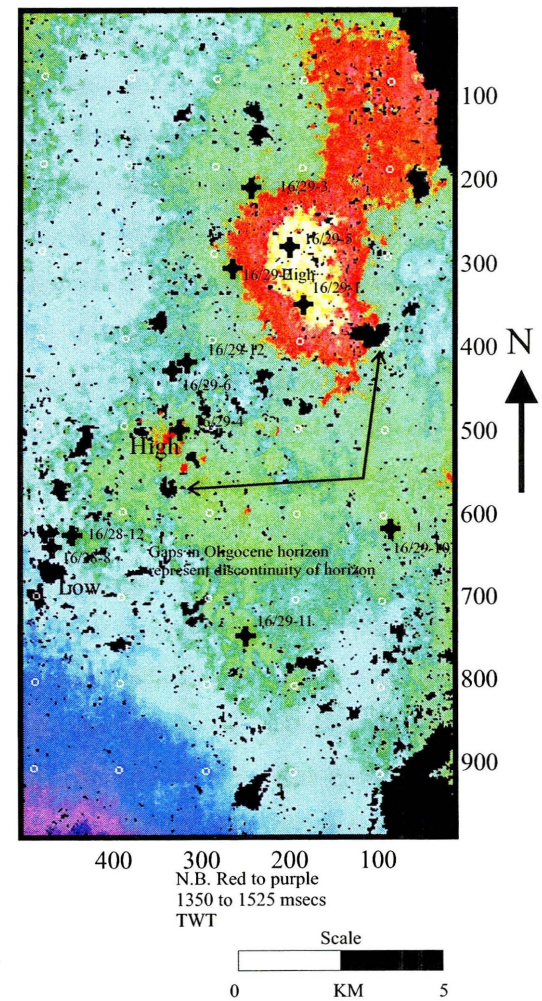


Figure 6.20(ii). Top Oligocene structure contour two way time map over UK Central North Sea Blocks 16/28 and 16/29



Note : Highs of the Top Utsira mound surface mirror highs at the Top Oligocene level and Top Sele level. Gaps in Top Oligocene structure map also occur approximately above highs on the Top Sele map.

Figure 6.21. Seismic cross section, northeast/southwest oriented through Utsira mounds and location of Jurassic fault blocks below these mounds in UK Central North Sea Blocks 16/28 and 16/29

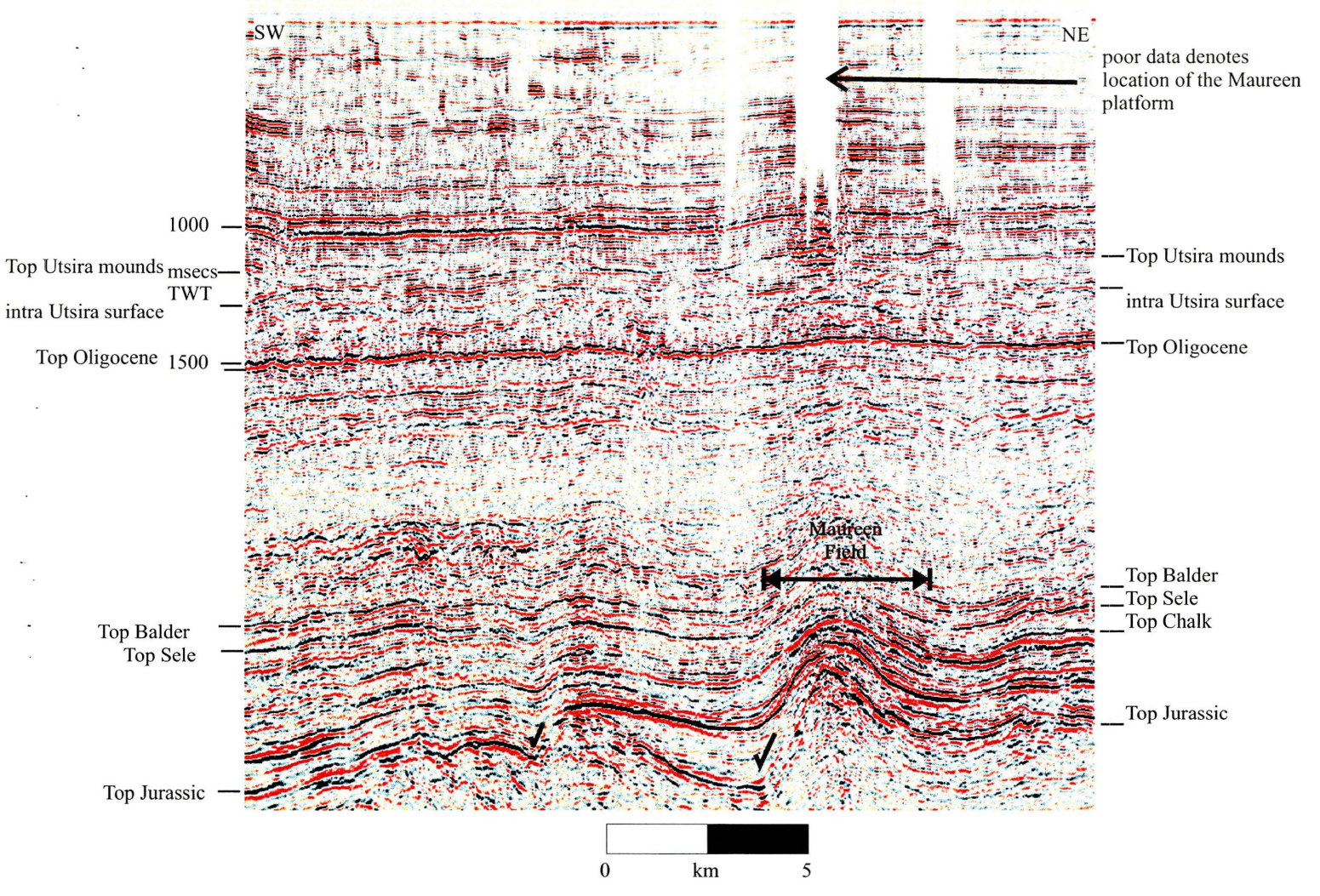


Figure 6.22. Time structure contour map of Top Utsira mounds over UK North Sea Blocks 16/28 and 16/29

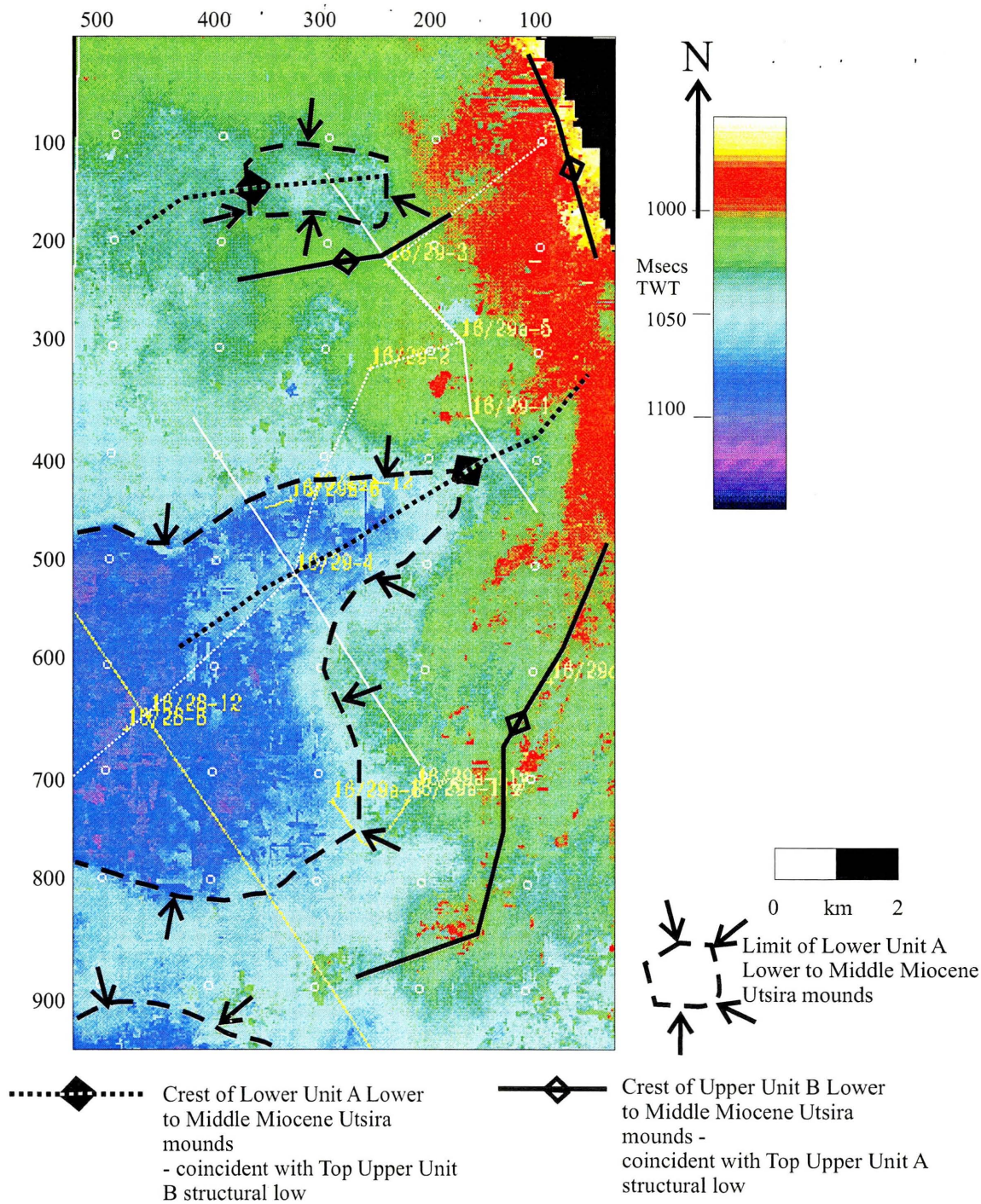


Figure 6.23. Seismic/well calibration through UK North Sea well 16/29-4 over the Lower to Middle Miocene Utsira Formation

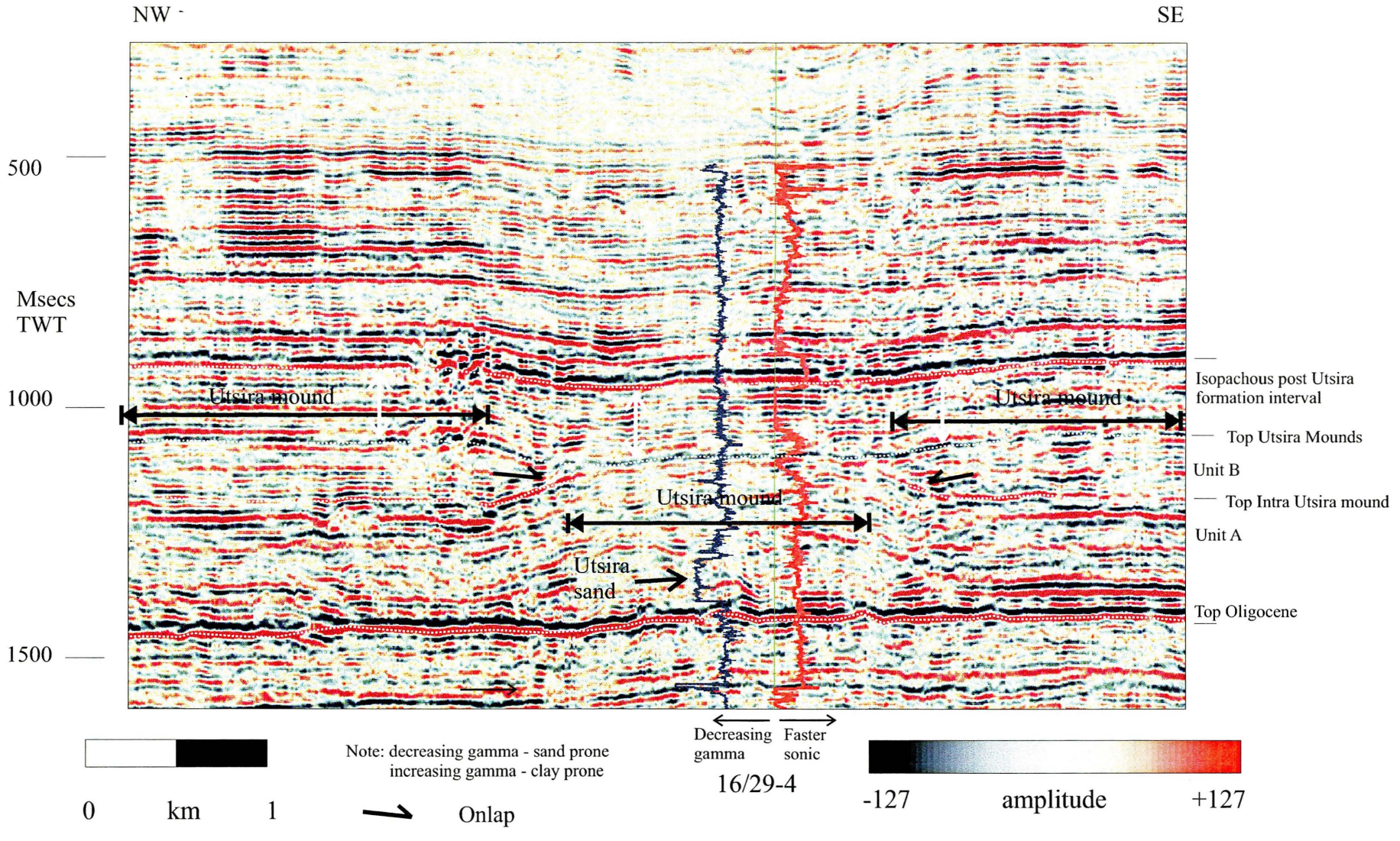


Figure 6.24. Composite log of UK North Sea well 16/29-4 over the Miocene Utsira Formation

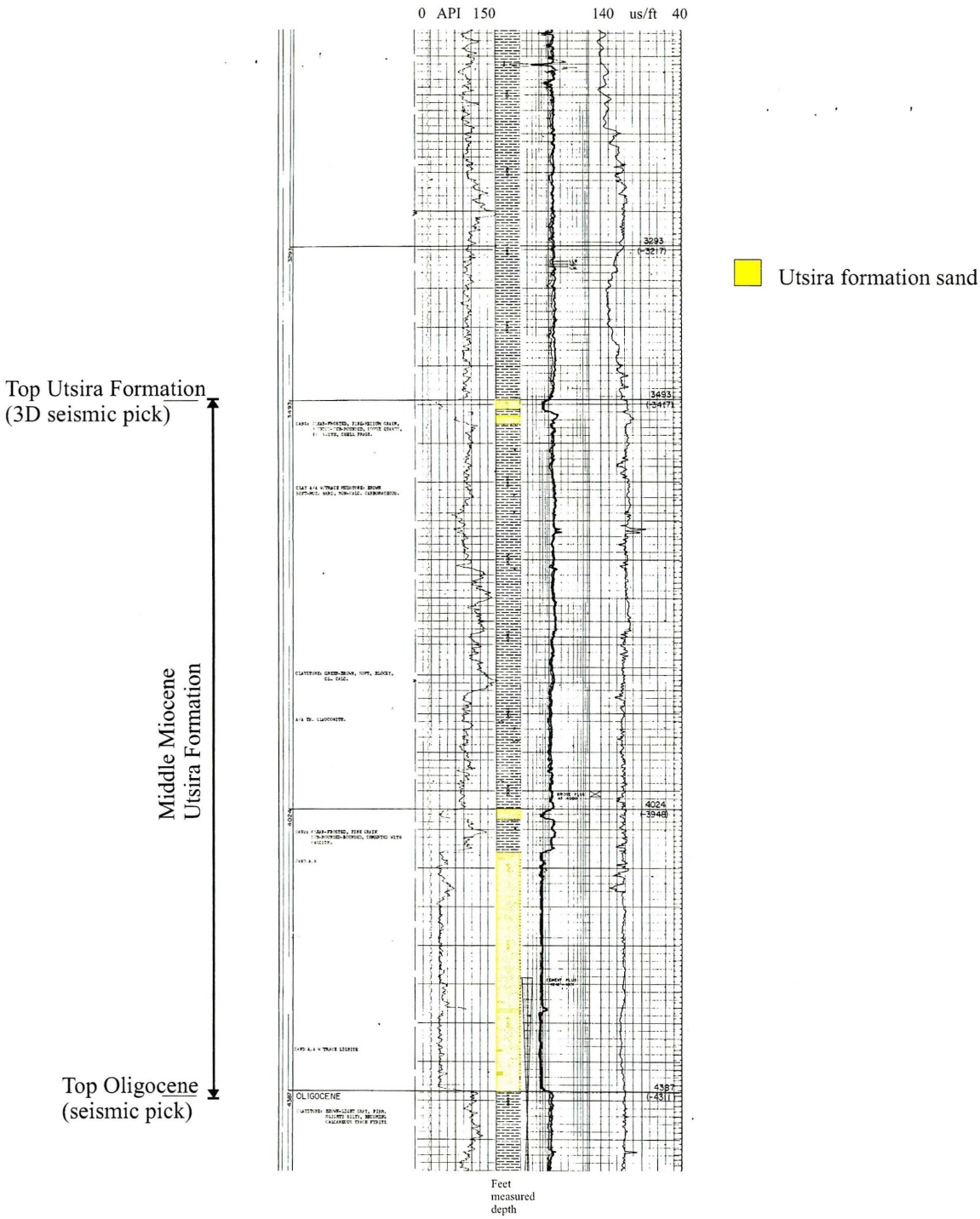


Figure 6.25. Seismic/well calibration through UK North Sea well 16/29-3, 5 and 1 over the Lower to Middle Miocene Utsira Formation

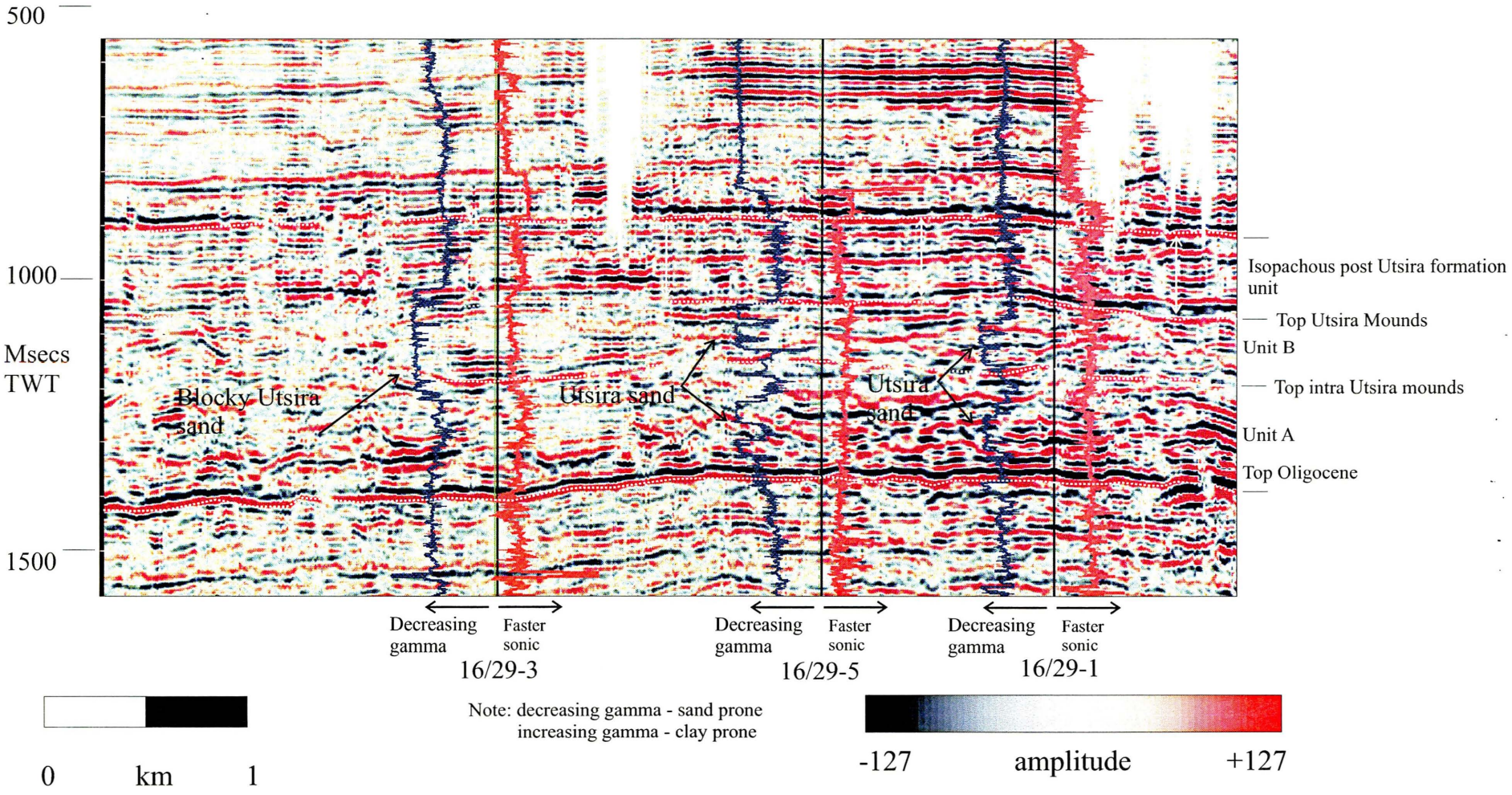


Figure 6.26. Composite log of UK North Sea well 16/29-1 over the Miocene Utsira Formation

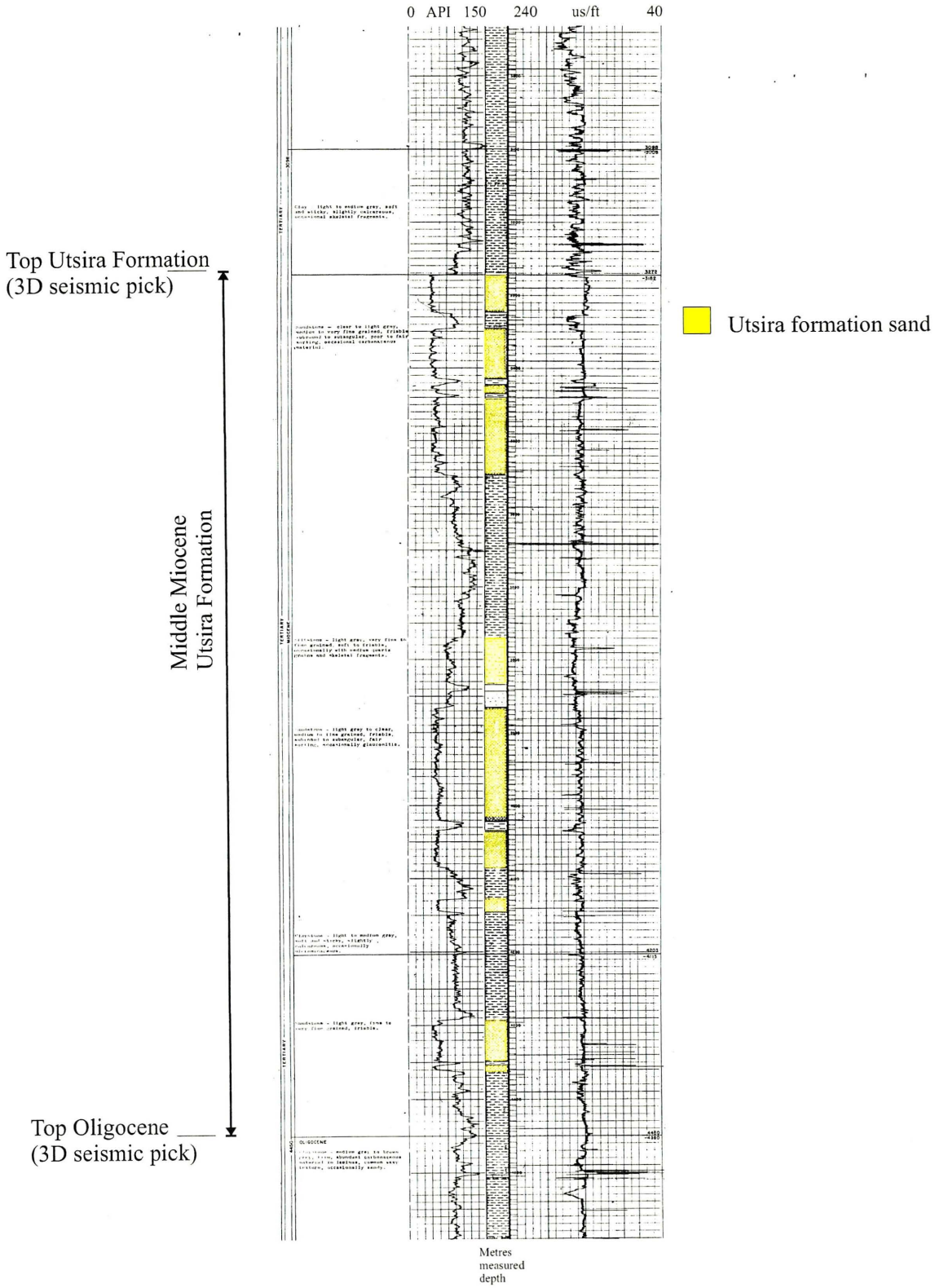


Figure 6.27. Composite log of UK North Sea well 16/29-5 over the Miocene Utsira Formation

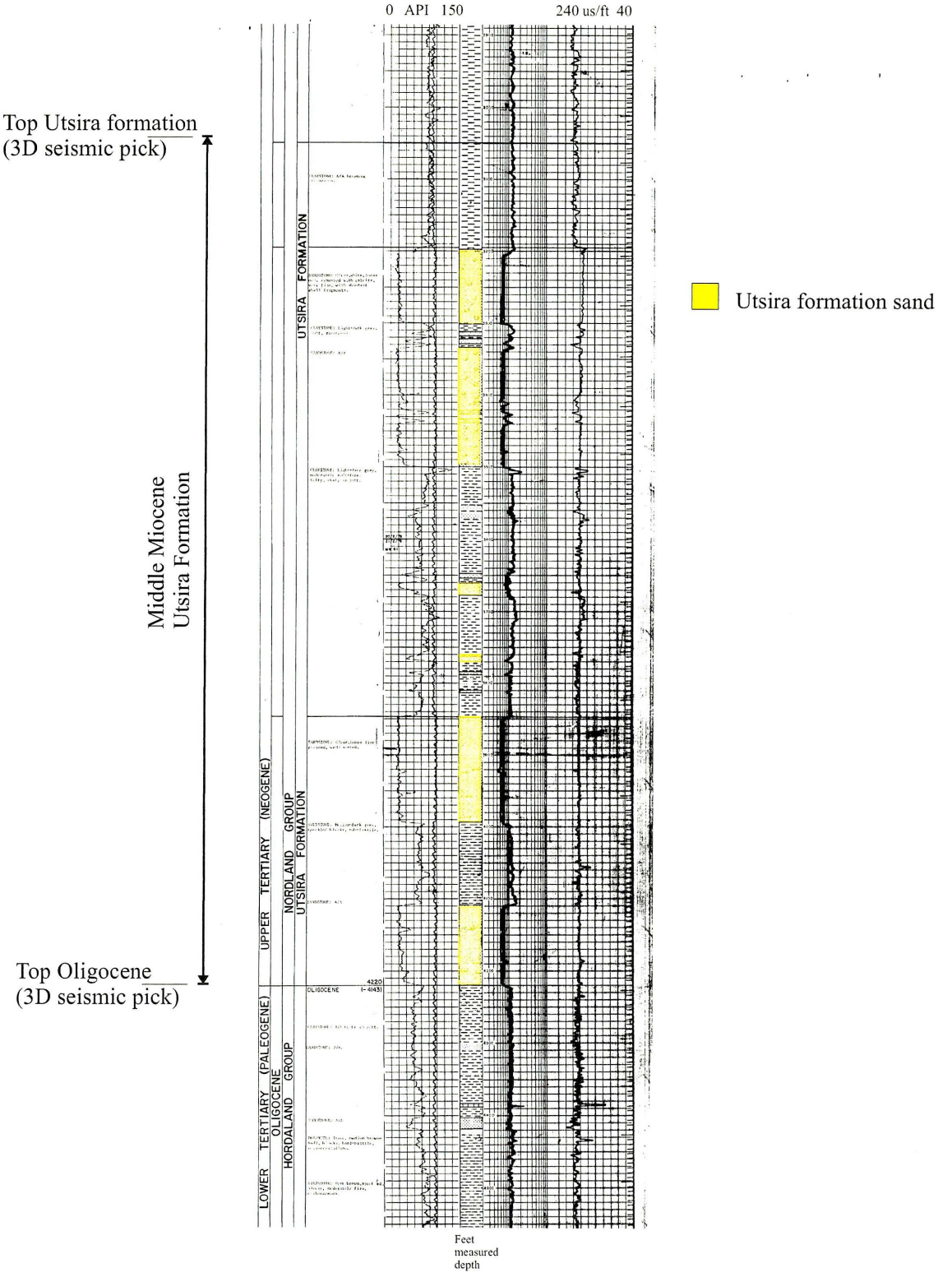


Figure 6.28. Composite log of UK North Sea well 16/29-3 over the Miocene Utsira Formation

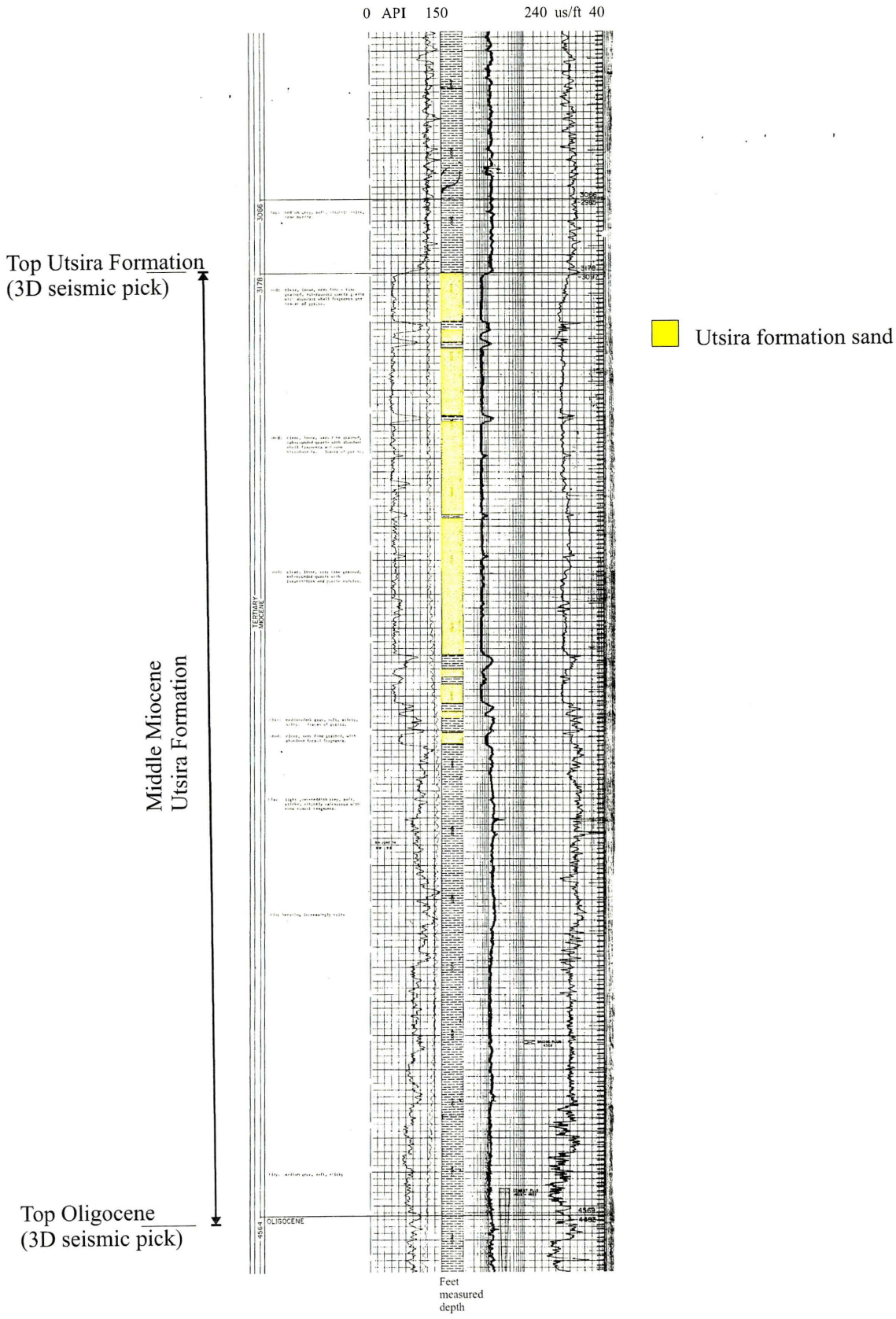


Figure 6.28. Composite log of UK North Sea well 16/29-3 over the Miocene Utsira Formation

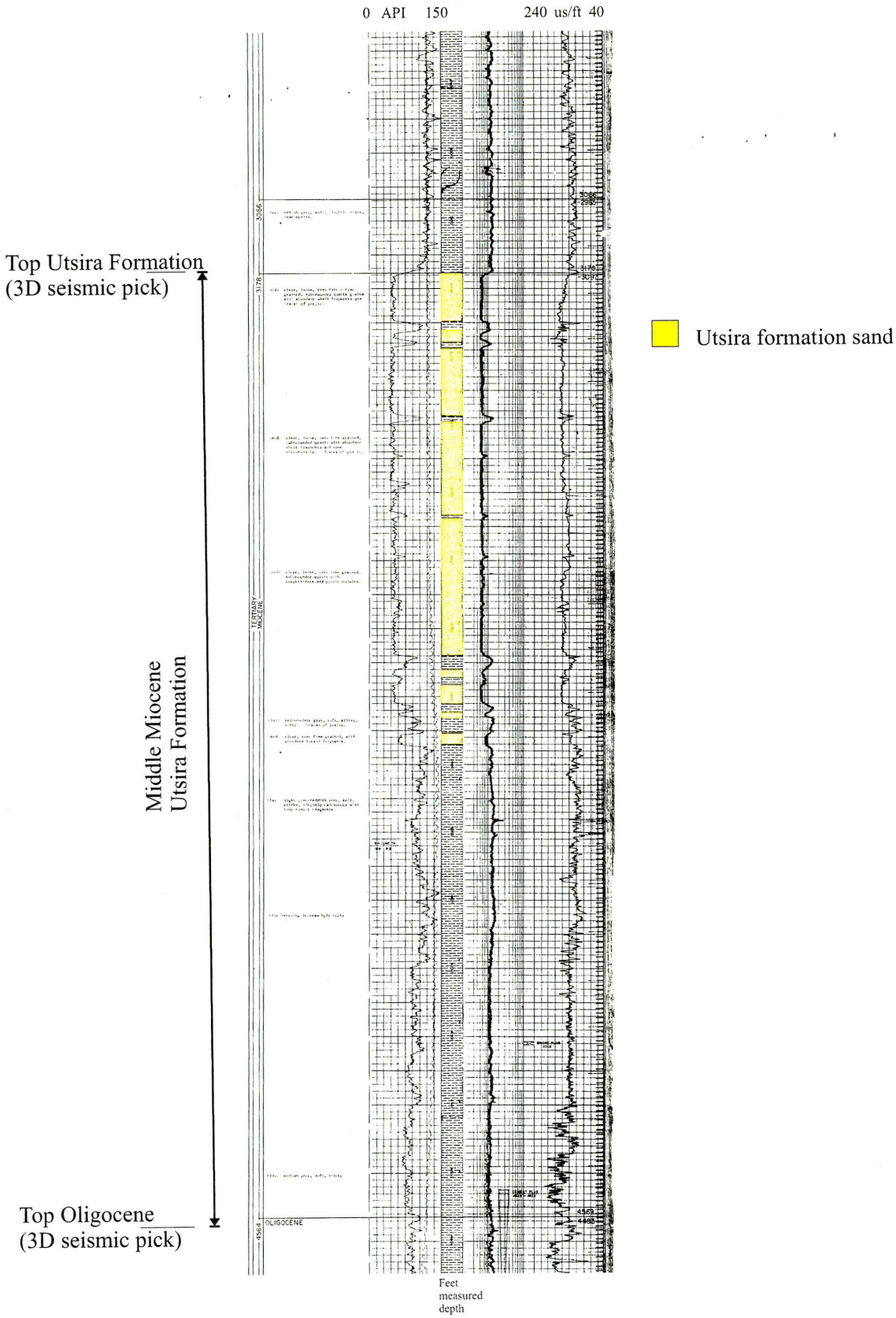


Figure 6.29. Seismic/well calibration over UK North Sea well 16/29-2 through Lower to Middle Miocene Utsira Formation

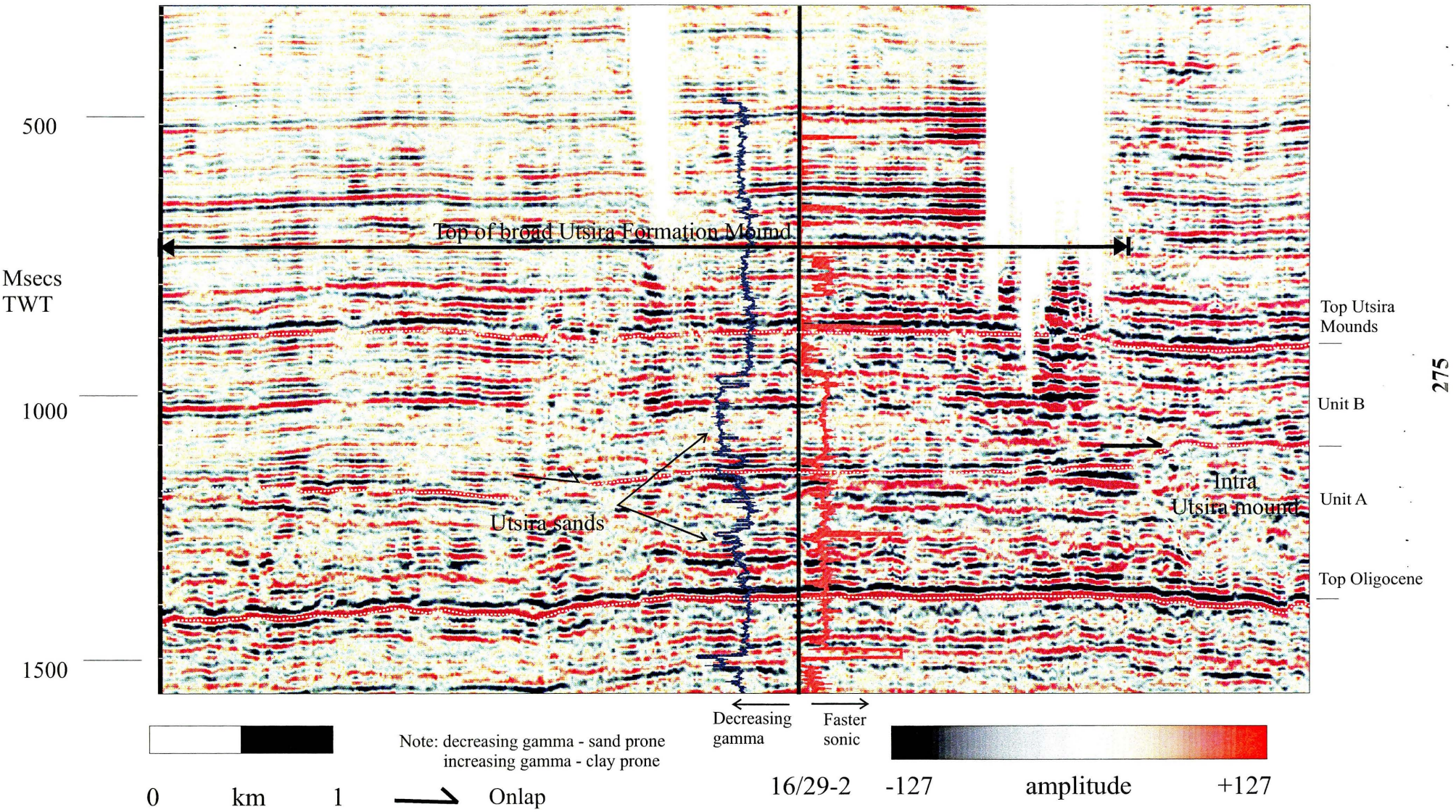


Figure 6.30. Composite log of UK North Sea well 16/29-2 over the Miocene Utsira Formation

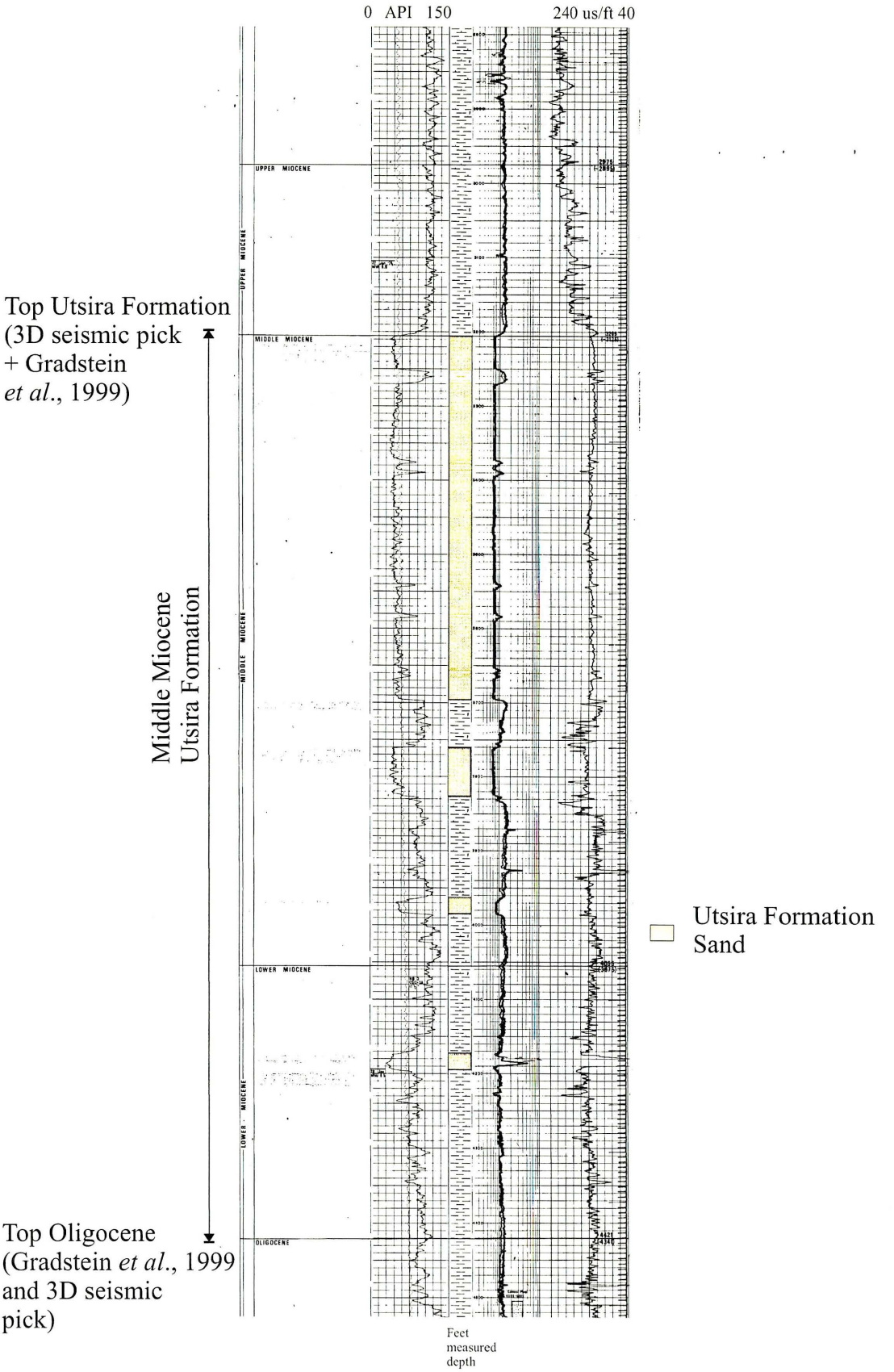


Figure 6.31. Seismic/well calibration over UK North Sea well 16/28-12 through Lower to Middle Miocene Utsira Formation

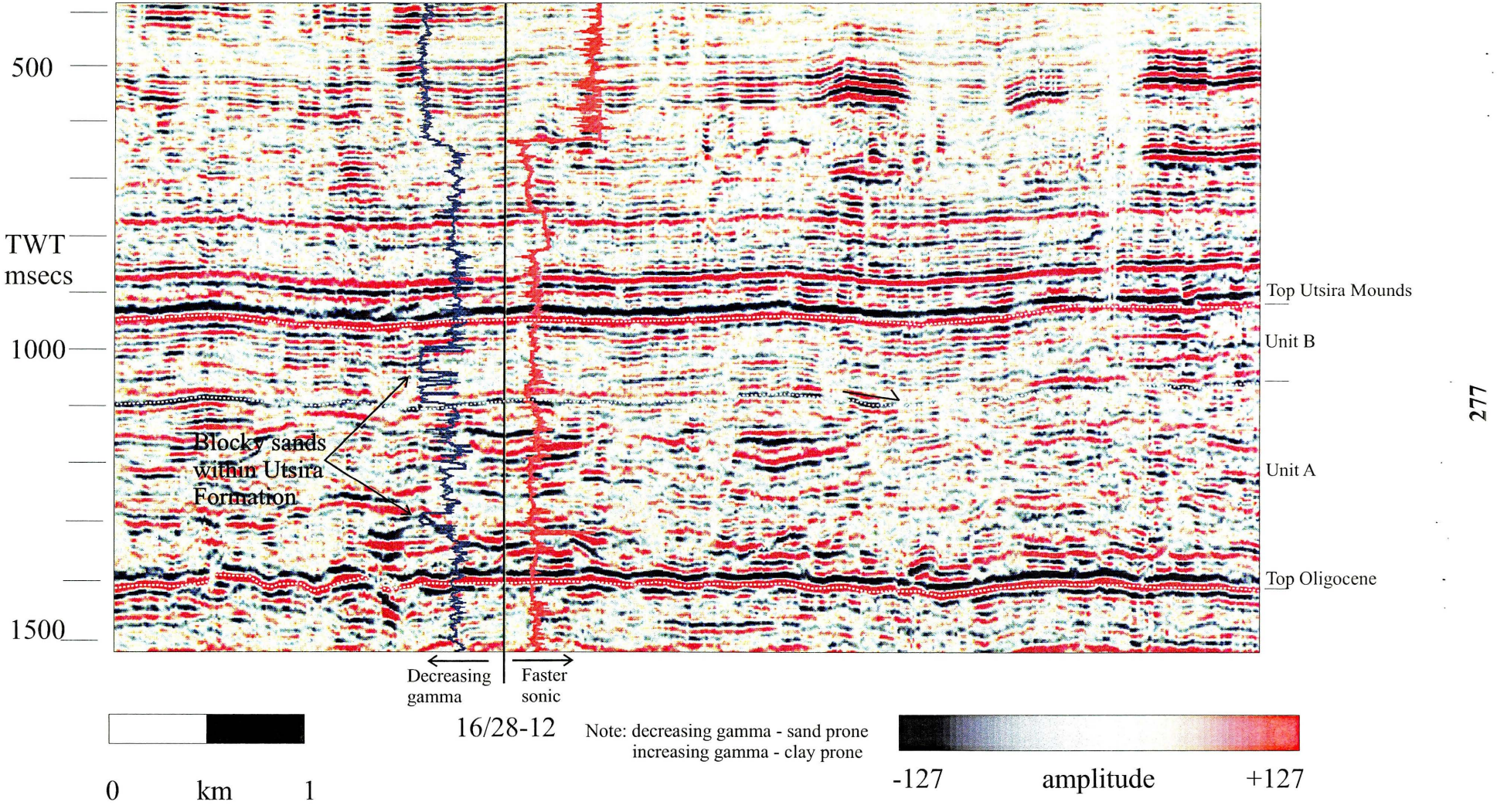


Figure 6.32. Composite log of UK North Sea well 16/28-12 over the Utsira Formation interval

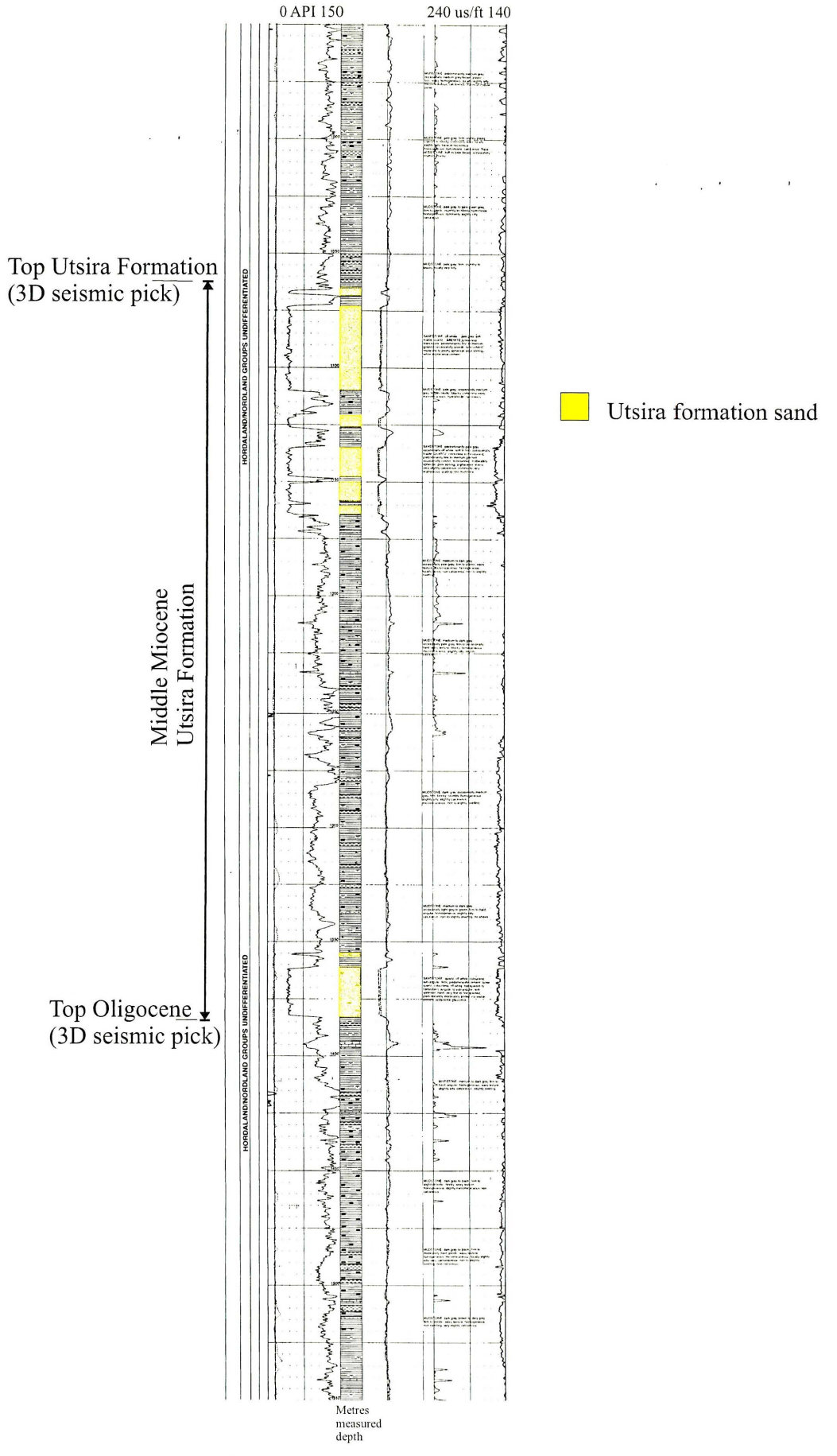


Figure 6.33. Seismic cross section with generalised well calibration of Utsira mounds over UK Central North Sea Blocks 16/28 and 16/29

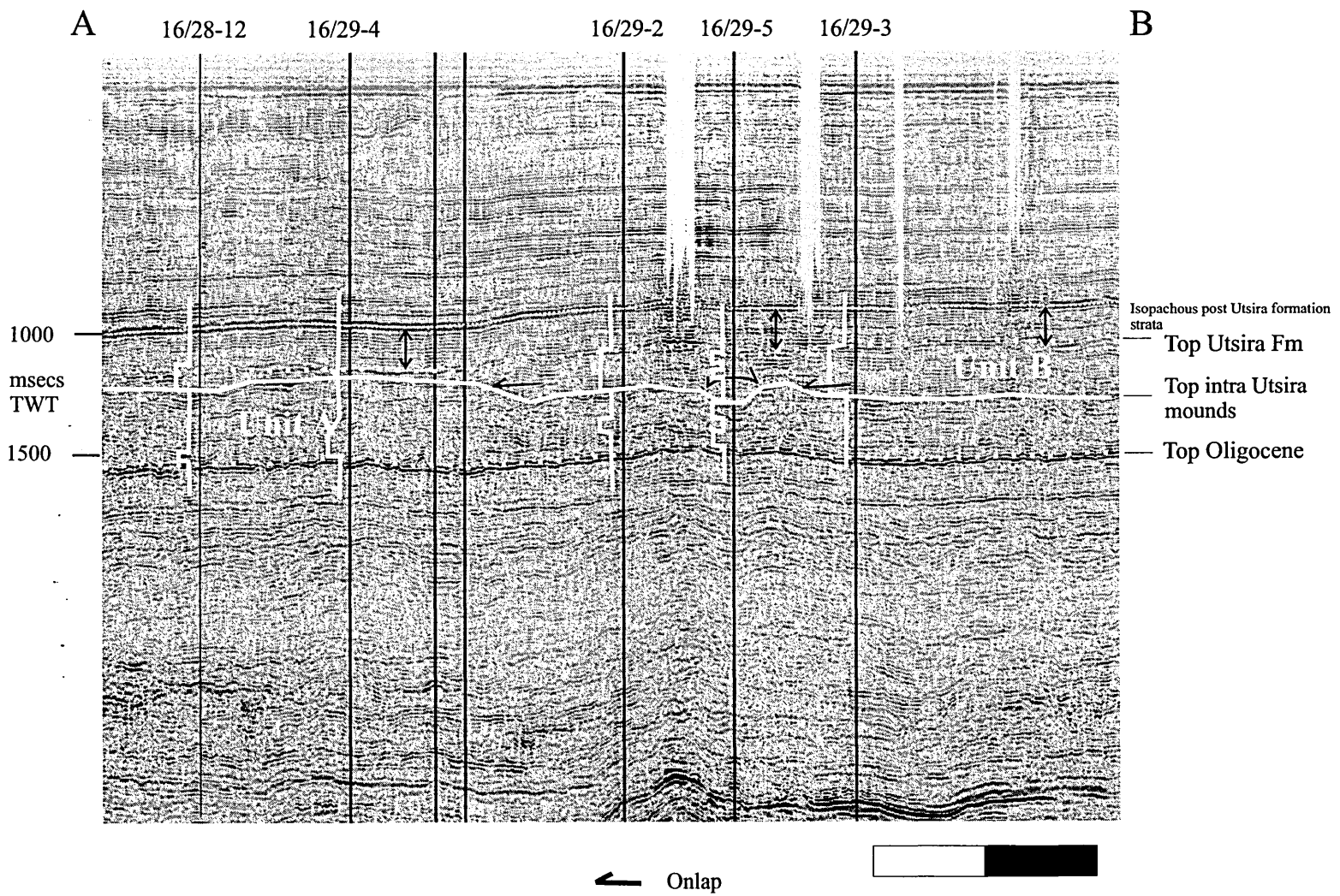
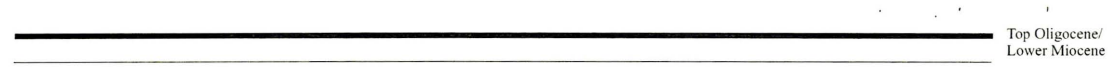


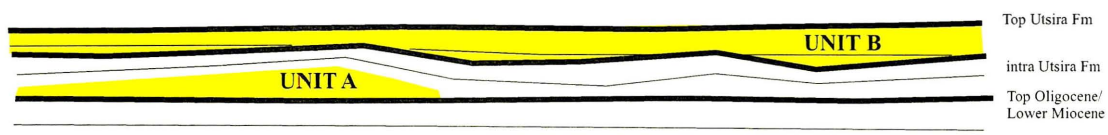
Figure 6.34. Model of Middle Miocene Utsira mound formation over UK Central North Sea Blocks 16/28 and 16/29



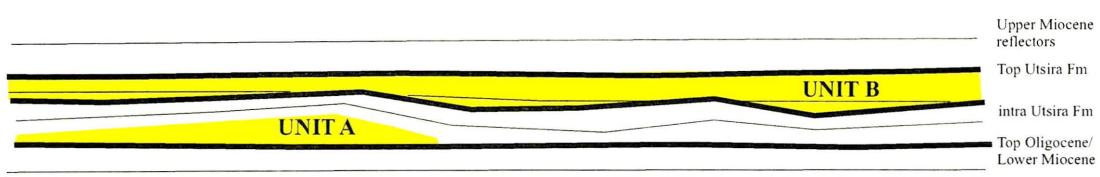
1. End Oligocene/Lower Miocene - deep marine clay deposition, parallel strata, no seabed topography



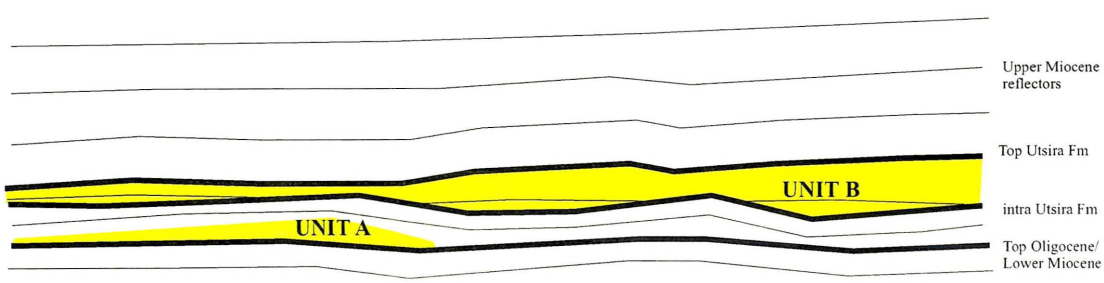
2. Unit A deepwater sands deposit onto Top Oligocene/Lower Miocene muddy seabed. Sands may have been deposited into lows within the seabed topography or form as topographic depositional features



3. Unit B deepwater sands deposit into topographic lows set up by Unit A sands



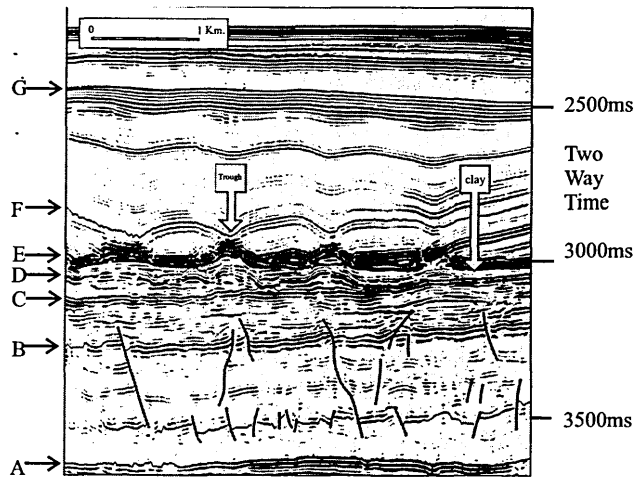
4. Intra Upper Miocene - deep marine clay deposition, parallel bedded indicating no seabed topography



5. post intra Upper Miocene - differential compaction over sand thicks forming Utsira mounds

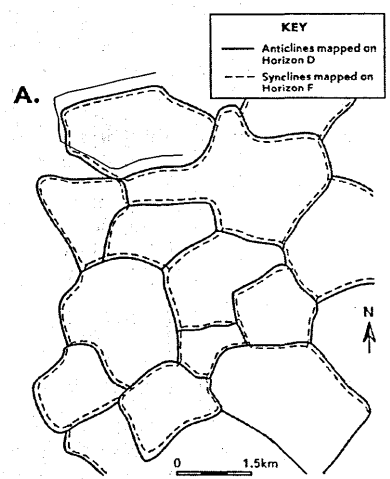
Sand prone

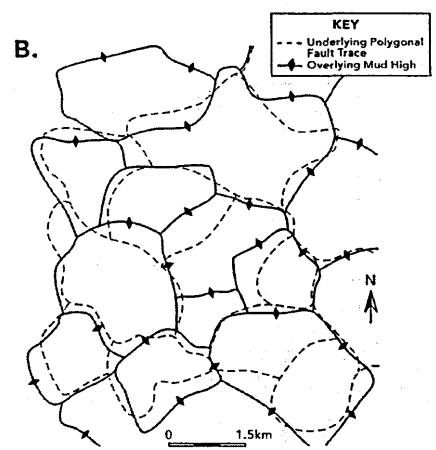
Figure 6.35. Model of giant scale differential compaction/density inversion pillows in fine grained sediments in the Oligo-Miocene in the Faeroe-Shetland Trough (Davies *et al.*, 1999)



"large scale domal features (pillows) from an Oligo-Miocene succession in the Faeroe-Shetland Trough, off the northern coast of the UK. These pillows have a wavelength of 1-2km, an amplitude of about 50m, and are characterised by a polygonal planform geometry. Two successive depositional packages in this probably pelagic-dominated interval have this form of structural, expression, but troughs of the younger set are directly superposed on crests of the older set. This extraordinary structural configuration is attributed to a protracted depositional/deformational history in which a density inversion is established, pillows form in response to a possible fault trigger, and then subsequently collapse, to produce syn-depositional troughs in the overlying units. These structures are similar in geomtry to hummocks described from near-surface sediments in the Norway Basin by Vogt (1997), and are probably the largest type of density inversion-related deformation structure yet described."

Davies *et al.* (1999)





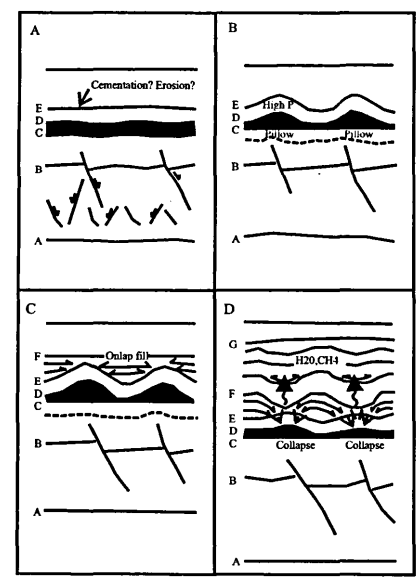
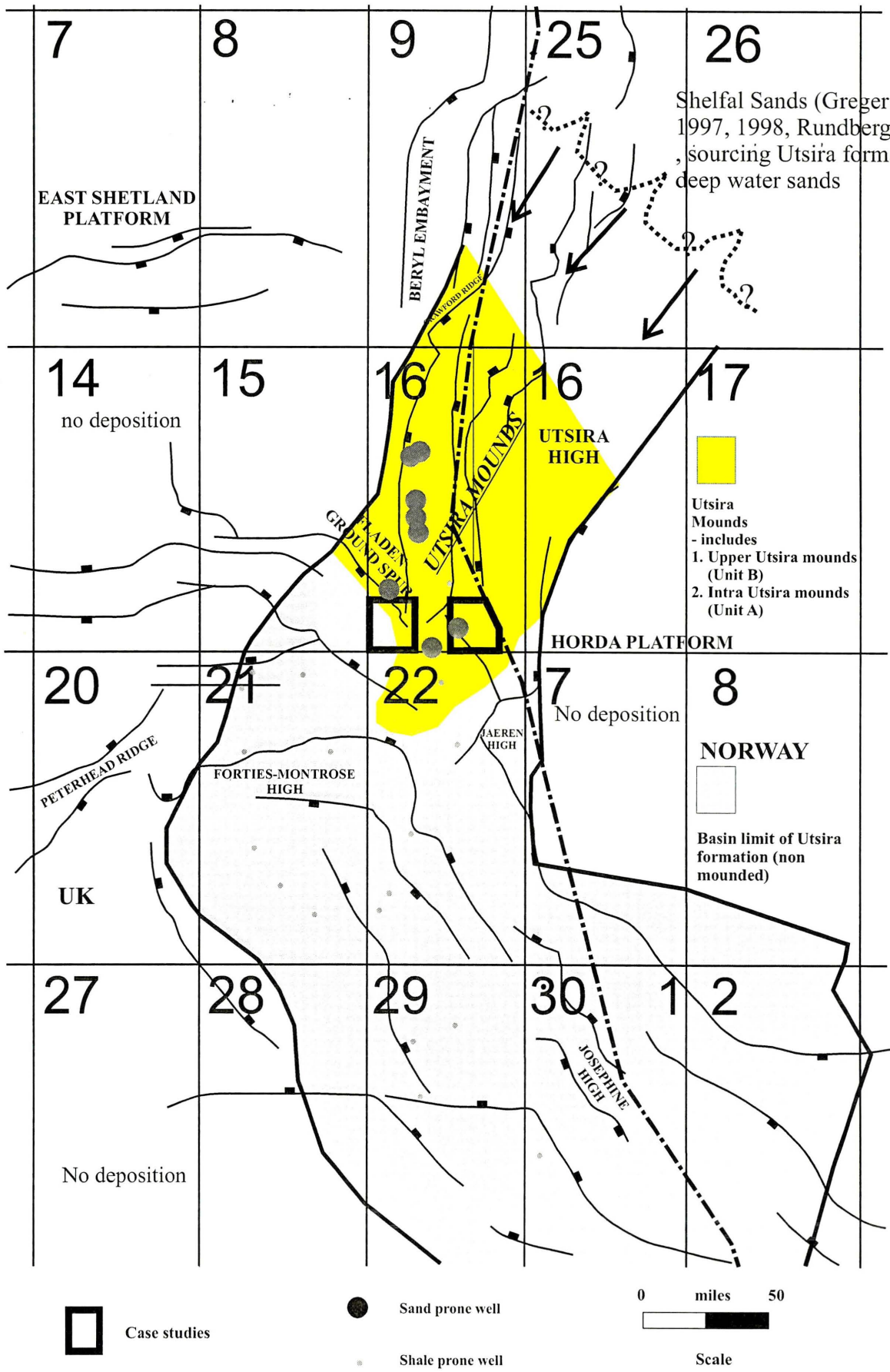


Figure 6.36. Middle Miocene Utsira formation palaeogeography over the North Sea



CHAPTER 7. GENETIC MECHANISMS OF LARGE SCALE POST DEPOSITIONAL SANDSTONE REMOBILISATION

7.1. Introduction

Large scale post depositional sandstone remobilisation has been a rarely documented phenomena in the literature, largely due to the size of outcrop exposure that allows the investigator only a limited scale of view. With the advent in the 1980's and 1990's of 3D seismic techniques, detailed observations of kilometre scale features have now been observed in the subsurface. The documented examples in this thesis of a Lower Eocene kilometre-scale sandstone intrusion complex (chapter 3); Lower Eocene kilometre scale low angle cone shaped amplitude anomalies (chapter 4); Lower Eocene Balder age kilometre-scale pockmarks (Cole 1996, chapter 4); Upper Eocene Belton Member syn- to post-depositional faulting (chapter 5) and Middle Miocene seabed mounding (chapter 6) illustrate large scale remobilisation phenomena that occur within the deepwater sediments of the Eocene to Miocene of the North Sea. These large scale remobilisation features are interpreted to have been caused by specific processes, which are highlighted below. By identifying and understanding the processes involved a model containing all the possible features acsribed to these processes can be formed.

7.2. End members of large scale remobilisation

A three part classification scheme is proposed for features related to large scale remobilisation in the Eocene to Miocene deepwater sediments of the North Sea as illucidated from examples described in this thesis and the literature. This is represented by figure 7.1 and below:

(i.) Clastic intrusion and seabed blow out (e.g. Norwegian 24/9 giant scale intrusive complex, the cone shaped anomalies of UK Blocks 21/3, 4 and 5 and pockmarks of Cole (1998)

(ii.) Seafloor Mounding (e.g. Utsira mounds of UK Blocks 16/27, 28, 29 and Norwegian Block 15/9 (Zweigler *et al.*, 1999)

(iii.) Faulting (Belton member faulting of Norwegian Block 24/9)

Each category will be reviewed and related processes outlined below.

7.2.1. Large scale clastic intrusion and pockmarks

7.2.1.1. Large scale clastic intrusions

Small scale sandstone intrusions have been documented in outcrop since the 1800's (Strangeways, 1821). Since then, sheet-like sedimentary bodies of secondary origin have been described from a broad range of sedimentary environments (see Allen 1982 for review). Most work has emphasised the genetic controls and kinematics of sedimentary emplacement.

Allen (1982) believed that sedimentary intrusions arose only where three conditions are met: (1) a state of horizontal tension (allowing vertical fractures to form), (2) the presence nearby of suitable source material (e.g. plastic clays or poorly cemented sands or gravels), and (3) in the case of sand or gravel source, a pore pressure temporarily in excess of lithostatic so that liquefaction and fluidisation can occur allowing mobilisation of sediment and fluid into dilating fractures. Allen (1982) states these conditions are satisfied under two broad and only partially separable circumstances: (1) penecontemporaneously with deposition, often in association with sediment slumping and sliding, seismically induced liquefactions or with the movement of growth faults, and (2) during tectonic events that occur significantly after sediment deposition, but before lithification is completed. Allen (1982) further states:

(I) **Penecontemporaneous clastic intrusion** has been attributed to the following mechanisms: earthquake-induced fracturing and shaking (Hobbs, 1917; Reimnitz and Marshall, 1965; Eisbacher, 1970; Hesse and Reading, 1981); early jointing/infilled growth faults (Cook and Johnson, 1970); slumping (including earthquake-induced slumps) (Smith and Rast, 1958; Truswell, 1972; Hiscott, 1979; Pickering, 1983; Archer, 1984). Evidence supporting the penecontemporaneous origin for intrusive sedimentary dykes and sills is their close spatial association with mobilized strata (slumps, slides and soft sediment deformation) and a lack of a directional relationship to tectonic structures and the

existence of ptygmatic folding which can indicate an early emplacement of an intrusion and subsequent differential compaction of sand intrusions compared to the mud country rock (Kuenen, 1938).

(II) **Tectonic clastic intrusion** has occurred with a spatial association with faults and an orientation that is closely related to that of joints, folds or faults (Diller, 1889; Newsom, 1903; Jenkins, 1930; Harms, 1965; Peterson, 1966, 1968; Marschalko, 1965; Spencer, 1971; Brandon, 1972; Truswell, 1972).

Allen (1982) has attempted to outline the general parameters required for clastic intrusion to occur and the potential settings in which intrusion has been documented. Allen (1982) did not address the reason for the range in scales of intrusion, sometimes upto 100's of metres (Harms 1965; Thompson, 1995, 1996, 1999, Nilsen *et al.*, 1998). The subsequent explanation of the North Sea seismic examples attempts to address the difference between small scale and large scale clastic intrusions.

7.2.1.2.Why are some intrusions small scale and some large scale?

Clastic intrusion within deepwater sediments of the Eocene to Miocene of the North Sea have special characteristics that favour remobilisation:

(1) Originally rapidly deposited deepwater sands, often formed as discrete sand channels/bodies, encased within basinal shales.

(2) Tectonic activity at the time of deposition or soon after (Eocene).

(3) Maturation of Jurassic age organic rich source rocks during the Eocene to Recent, directly below the Eocene to Miocene deepwater sediments (Barnard and Bastow 1996; Mason *et al.* (1995).

Clastic intrusion within these deepwater sediments varies between the small scale dykes and sills conclusively seen in core within field reservoirs of this age (Alba, Gryphon, Forth, Harding, Balder) and much larger scale intrusion which may have associated smaller scale intrusions (Norwegian 24/9 large scale intrusion of chapter 3 and UK blocks 21/3, 4, 5 cone shaped intrusions of chapter 4). Conclusions within these chapters indicate the discordant relationships observed in core and upon the seismic that an intrusive nature is ascribed to these large scale seismic amplitude anomalies well calibrated to 10 to 50 metre thick

sand. These observations of the process of clastic intrusion are based upon seismic and well description and calibration. Quantifying the forces at work to create such large scale intrusions has never been undertaken in the literature, though within the group of small-scale intrusions, Allen (1982) ascribed many small scale dykes to synsedimentary deposition. As this loading is invariably local in extent, potential pressure build up in the sediment would be short lived and be of a small magnitude (Allen, 1982). Overpressure would build up and be released where pore pressure became greater than lithostatic, hydrofracturing the encasing sediment. Entrainment of sand and intrusion would occur into pre-existing weaknesses (i.e. faults, polygonal or tectonic) or into fractures created by the overpressure. The size of the clastic intrusions is inferred to be directly related to the amount of overpressure generated within such a set of parameters. As such, intrusions would be small as pressures are inferred to be small. Small scale clastic intrusions can also be related to shallow burial. Here dewatering of the clays in the first 1000 metres expels 50% of the rock volume of water (Barron *et al.* 1985). Overpressure would build up in compartmentalised sand bodies and eventually lead to liquifaction/fluidization of sand as small scale intrusions.

Conversely, the large scale clastic intrusions would have to be related to much greater absolute magnitude of overpressures in order to explain the increased scale of the intrusions. From the explanations given in chapters 3 and 4 for the origin of these large scale intrusive features, fluid for the injection process is inferred to have been generated from a Jurassic source kitchen from Eocene times and migrated through Cretaceous sediments. This fluid reached and pressure built up within Eocene/Paleocene deepwater sands which were sealed by Eocene shales. In these areas overpressure bleeding is postulated to occur along tectonic trends. During fault movement it is postulated that large volumes of fluid expelled during fault movement, with subsequent pressure build up until the next fault movement and release of pressure. This process is known as seismic pumping and has been documented by Sibson (1975, 1994) and Muir Wood (1994) (see figure 7.2). The model is based on the concept that prior to shear failure along the fault, the region about the fault dilates in response to the rising tectonic shear stresses by the development of extensional fractures. It was indicated that these fractures would be oriented normal to the direction of least

principal compressive stress. The development of this fracture porosity causes fluid pressure within the dilatant zone to decrease. The decrease in fluid pressure around the fault causes a rise in the frictional resistance to shear along the fault and at the same time the reduction in fluid pressure induces a slow migration of fluid towards the fault zone. This inward migration of fluid gradually reverses the tendency for fluid pressure decrease. As this pressure climbs back to its original value there is a concomitant decrease in the frictional resistance to shear along the fault. When the increasing shear stress equals the frictional resistance failure will occur. At failure there is a rapid partial relief of shear stress which allows the cracks within the dilatant zone to relax, expelling the fluids they contain in the direction of easiest pressure relief.

Such a process involves large volumes of fluid which may indeed be able to form intrusions tens of metres across and kilometres in length. Several documented examples of high rates of fluid flow have been documented with earthquake activity, in the USA. The Borah Peaks earthquake, Idaho occurred on October 28th 1983 and was measured with a magnitude of 7.3 on the Richter scale. The earthquake caused a 34 km rupture at the surface with several hydrological effects recorded by Whitehead (1985) and Wood (1986). Fluid discharge of nearby rivers dramatically increased during the actual earthquake with several warm springs in the area doubling flow, one increasing volume ten fold from the original flow. Temperatures of ejected fluids (i.e. warm springs) increased from 16 degrees celsius to 30 degrees celsius. On August 17th, 1959 a magnitude 7.1 earthqauke on the Richter scale occurred. Hydrological effects were recorded on several rivers by Swenson (1964). Several river discharges doubled during the earthquake and with flow staying above normal levels for several months later. Many sand spouts were observed in the region during the earthquake. These examples indicate increased volumes of fluid are associated with fault activity and may act as areas of cyclical pressure build up.

Examples of large scale intrusions are either related to the presence of hydrocarbons (e.g. Yellow Bank Creek Intrusion, Santa Cruz (Thompson 1995, 1999; Molyneux 1998, 1999; Block 24/9 offshore Norway Intrusion complex (Lawrence *et al.* 1999)) and large scale clastic intrusion in the Miocene deepwater sands of the Sunset Midway Oilfield, California (Nilsen *et al.*, 1998)

which are all related to wrench faulting) and/or tectonism (Laramide large scale clastic intrusions of Colorado, Harms 1965). Pressure differential between source and sites of intrusions involving large scale intrusions must have been immense. For instance Kugler (1933, 1938) documents the presence of fauna within Tertiary sediments within clastic intrusions of Trinidad which can only have come from stratigraphy several thousands of feet below. Several Precambrian sandstone dykes exist within the Canadian shield which contain igneous boulders some 5 metres plus in diameter (H.G.Reading pers.comm. 1997). Pressure gradients necessary to move sediment these distances or to move material of this size must have been very substantial. The high pressure in the source unit may have been created in these two latter cases by the sediment being buried to a great depth allowing the sediment to be greatly compacted and to be able to withstand a high pore pressure. When the overpressure was released the force of injection would have been much greater than at shallow depths, as pressure had been allowed to build up to very high levels and thus allow injection of large particles/ or material long distances. In the case of the North Sea examples, several dykes and sills exhibit ptygmatic folding, indicating the intrusion to have occurred soon after sediment deposition at shallow depths of burial.

In all these Tertiary North Sea cases and within the literature, pore fluid is generally regarded as the overpressured medium. It is well documented that gas is present in clay rich sediments (Hovland and Judd 1988; Sims 1995) and may come from both biogenic and abiogenic sources. If the large scale intrusions of the Tertiary of the North Sea are related to hydrocarbon generation and expulsion, then gas may be associated with the intrusion. If this assumption is taken as reasonable, then very high pressures and volume changes could be generated with gas, as gas expands dramatically upwards (figure 7.3; Dake, 1978 and Eddy, pers.comm. 2000) as a consequence of pressure reduction on the gas as it passes upwards (Sims, 1995). The relationship of hydrocarbon generation to clastic intrusions has been documented by Jenkins (1930) and Kruegler (1930) in the early literature. Both authors note that in outcrops from California and Trinidad outcrops respectively of hydrocarbon stained clastic intrusions and the location of these intrusions is near the crest of local oilfields. Analysis of the cement phase within intrusive complexes such as Norwegian North Sea Block

24/9 and the Yellow Bank Creek intrusions has highlighted the variable delta C13 PDB values from -15 to +30 O/oo, indicate the presence of hydrocarbons during cementation of the carbonate cement (Irwin, 1977). These cements may have been related to the intrusion phase and as such may contain a fingerprint of the fluid phase at the time of intrusion. To further understand the origin of the cement fluid (and thus the intruding fluid) screening for fluid inclusions of these carbonate cements was attempted by the author, though none were found. It is hoped in the future that other carbonates in intrusive complexes may contain fluid inclusions so approximations of paleotemperature can be made and the presence of a hydrocarbon phase observed, which would confirm the relationship of hydrocarbons to large scale clastic intrusion.

7.2.1.3 Summary

Lonergan *et al.* (1999), have attempted to summarise the process of post depositional intrusion of sands. Lonergan *et al.*(1999) notes that the scale, style and geometry of clastic intrusions are controlled by:

(i) stress state of the country rock

(ii) burial depth

(iii) fluid pressure

(iv) rheology of the sediment host rock

(v) presence of pre-existing or contemporaneous fracturing

Lonergan *et al.* (1999) proposed that the process of intrusion occurs due to three main processes outlined in figure 7.4;

(1) tectonic activity/seismic shaking

(2) addition of fluid e.g. basinally expelled/hydrocarbons

(3) build up of insitu pore pressure due to depositional events, e.g. channel loading, slumping

Formation of clastic intrusions occur by sealing of a sand prone unit, into which fluid moves. Overpressure develops which causes failure of the cap rock that seals the sand prone unit. The pressure differential generated allows rapid fluid flow, thus fluidising the sand grains.

When the pore pressure within the sand (Pf) exceeds the minimum principal stress (h1) and the tensile strength (T), of the host sediment, then a sandstone dyke can propogate by brittle failure (Lonergan *et al.*, 1999). In a basin with no tectonic influence on the stress system, the minimum principal stress (h1) is typically horizontal with the maximum principal stress being vertical. In such a case vertical dykes will form (figure 7.5a).

In the case of pre-existing fractures already existing (figure 7.5b) in the host sediment, then the fluid pore pressure (Pf) only needs to exceed the normal stress (N) acting on the fracture walls, for them to dilate and oblique dykes can propogate (Lonergan *et al.*, 1999). Elevation of the fluid pressures can cause either shear failure or dilation on pre-existing fractures depending on the orientation of the fractures relative to the stress field.

7.2.1.4 Pockmarks

A reliable indicator of gas being a contributor to sediment remobilisation is the occurrence of pockmarks. The only ancient documented example of pockmarks is reported within this volume - North Sea Eocene age pockmarks (Cole 1998) which indicate expulsion of fluid at the seabed within the Eocene deepwater system. Present day examples of pockmarks are much more commonly reported with examples from the British Isles, the North Sea, Adriatic Sea and Arabian Gulf (Hovland and Judd, 1988) and the Aegean Sea (Papatheodorou, *et al.*, 1993). Pockmarks occur in a diverse range of environments, from estuarine to deep ocean, but are mainly found in fine grained sediments. If underlain by petroleum source rocks, gas in surficial sediments is normally of thermogenic or mixed origin (Hovland and Judd, 1988).

Based on many works, Hovland and Judd (1988) proposed a generalised model for pockmarks formation (see figure 7.6) as outlined in Sims (1995):

(i) Fluid (most commonly methane), not trapped in lower layers, progressively migrates from porous layer to porous layer, using each as a temporary reservoir. As each reservoir fills, pore pressure increases until gas overflows into a higher reservoir. The pressure required decreases as gas encounters younger and less compacted sediments.

(ii) Due to an increased pore pressure in near surface gas charged sediments, a dome like swelling occurs, representing a zone of tension. Many small fractures will form centrally and on the flanks of the dome.

(iii) As gas establishes a route through these fractures, and a hydraulic connection is established, the pressure drop results in a "violent" burst of seeping gas. The gas will expand and surrounding sediment will fall by fluidization, becoming entrained with the gas and forming a gas/sediment plume. The resulting freshly-formed pockmark will be rugged, with smaller pockmarks clustered around the site of the former dome. Their number will be greatest where the fracture intensity was highest at the centre of the dome.

(iv) The finest sediment may drift with the water current before settling, whereas silt and sand will settle within the vicinity of the pockmark. The scale of emission, the particle size distribution and the strength of the current will determine the precise sediment distribution

(v) Whereas the initial escape of gas will be violent, subsequent escapes will be less so, as the resistance to migration will be lower and there will be no seabed doming. Once established, an adjacent gas will be routed through the pockmark, which will serve as a gas drainage pathway.

(vi) Unless there is a continuous supply of gas and a permanent pathway, it is unlikely that seepage will be constant (cycles of activity are more likely). Hovland and Judd (1988) believe that once a new pathway has been set up, most of the gas will dissipate in a single event, rapidly at first and then more gradually. The resulting reduction in pore pressure will increase the pressure gradient between this and deeper reservoirs, initiating a new cycle.

7.2.2. Sea Floor Mounding – overpressure related

Many origins exist for large scale deepwater mounds not related to primary turbidite deposition, and are listed below. These mound processes all involve an increase in pore pressure. The possible origin of large scale mounds are highlighted below and places the intra Utsira mounds of UK Blocks 16/27, 28 and 29 into a broader context of the processes capable of forming large scale mounds:

7.2.2.1 Gas hydrate mounds

Gas hydrates form in muddy marine sediments under conditions of low temperature and high pressure (greater than 400 metres water depth, Kayen 1991). Methane gas is then trapped in a complex ice lattice at far greater concentrations than at the same temperature and pressure in free space. When sea level falls during a lowstand, gas at the base of a gas hydrate layer is released from the ice lattice and increases in volume. This gas becomes overpressured as it is unable to escape upwards due to the sealing effect of the gas hydrate preserved above. This free gas may pool into circular or elongate domes, pushing up the surrounding sediment (Brooks *et al.*, 1984, 1985). If the gas in the domes reached the surface the domes would collapse partially thus causing the sediment in the low to partially invert and form structures similar to the Middle Miocene Utsira Mounds. It is possible that the Utsira mounds formed in this manner as they occurred within at least 500 to 1000 metres water depth. This has been noted from large scale 2D seismic lines and comparing the postulated shelf edge to the mound depths. Cold water circulating from the Arctic at this time (Gradstein, 1994) , combined with water depth pressures, may have allowed the formation of gas hydrates (Kayen and Lee, 1991).

Further examples of gas hydrate mounds have been documented on the Gulf of Mexico slope at depths of between 600 to 2400 metres, and produced features called "giant gas mounds" (Brooks *et al.*, 1984, 1985). These large gas-exhaling features range from large domes, collapsed structures and diapiric crests to deep faults on the flanks of diapirs. Some measure 2 km across and rise over 100 metres above sea bed. The occurrence of nodules and blocks of gas hydrates on the seabed indicates that the diapirism has broken through layers of hydrates interbedded with the sediments. When gas hydrates are brought into contact with the relatively warm water at the seabed, they will start to decompose (melt) and large volumes of light hydrocarbon gases will be released. The giant gas mounds themselves were probably formed when excessive pore-fluid pressure caused the sediments to expand and well-up towards the seabed. The following mode of formation of the giant gas mounds and associated features (figures 7.8 and 7.9) is

put forward by Brooks *et al.* (1984, 1985) in Hovland and Judd (1988), for these Gulf Coast Mexico examples:

(1) A continuous deep source of hydrocarbon gases, liquids and solids is assumed to feed the structures from below, possibly by seepage above a buried salt diapir.

(2) These hydrocarbons rise owing to their buoyancy. As the gas rises it expands, increasing the pore pressure in the unconsolidated muddy sediments. These fail, become mobilized by gas entrainment and rise owing to the lowering of their bulk density. As the sediment-oil-gas mixture rises further it may pierce through and mobilize thin layers of gas hydrates. Gas hydrates may even form by adiabatic cooling when the gases rise and expand in the sediments.

(3) The buoyant mass breaks the seabed surface and flows out over the soft seabed.

(4) As more and more buoyant mud flow over the surface, continually releasing gases, the dome shaped diapir crest builds up and attains a complex and irregular morphology.

(5) Low-density hydrocarbon gases and liquids mix and dissolve in the seawater and rise through the water column.

(6.) The domes probably still contain interstitial gases trapped inside the mixture of clay and gas hydrates. After the gas has been released from the gas mounds they will probably deflate and a large collapse structure may be the result.

The relationship of migrating hydrocarbons being trapped below a layer of gas hydrate is difficult to prove for the intra Utsira mounds over UK Blocks 16/27, 29 and 30. However, it should be noted that (1) these mounds exist over a series of Jurassic fault blocks at a time in the Oligocene when hydrocarbons may have been generated and migrated through this section (Cooper, 2000) and (2) that they formed in a water depth which was sufficiently deep for gas hydrate development. A similar process to Brookes et.al.(1994, 1995) may have caused these intra Utsira mounds.

Hovland and Judd (1988) have noted that gas hydrate mounds can and have occurred over large parts of the ocean floors. They often create mounded sea bed topography, but are not the only phenomenon capable of explaining

large-scale deep marine seafloor mounds. Mud diapirs and volcanoes are also a well documented contributor to this form of syn-depositional topography.

7.2.2.2 Mud volcanoes/diapirs

Diapirism occurs where a plastically deforming body of sediment rises through another medium due to buoyancy (Judd and Hovland, 1992). Mud diapirs have been recognised in numerous places around the world. Barber and Brown (1988) describe diapirs within accretionary complexes. In the Barbados Accretionary Complex, mud diapirs occur in association with accretion of rapidly deposited turbidites, and the authors propose that mud diapirism is an adequate mechanism to produce ancient melange deposits. Other well described examples of mud diapirism within accretionary complexes include the Makran (Platt *et al.*, 1985) and the Shimanto accretionary prisms (Taira and Ogawa, 1988). During accretion wet sediments often become liquefied and fluidized to produce mud diapirs, ridges and volcanoes. The largest injections comprise of a fine grained matrix with incorporated blocks of rock, raise the sea floor hundreds of metres, even to the point of forming islands. In ancient successions, with limited exposures, such chaotic layers could easily be misinterpreted as debris flows or even "tectonic" melanges.

Hovland (1990) proposes that clay diapirism has caused ridges on the seabed off mid Norway, similar features subsequently described by Vogt (1997) in the same area. Hovland and Curzi (1989), described mud diapirism from the Italian Central Adriatic, where the mounds are underlain by hydrocarbon bearing strata, which are interpreted to have leaked upsection, increasing the buoyancy of near surface muds and creating gas charged diapiric masses. Mud diapirs or shale ridges are also found at or near the shelf edge in the Fraser, Magdelena, Niger and Orinoco deltas (Nota, 1958; Matthews and Shepard, 1962; Shepard, Dill and Heezen, 1968; Shepard, 1973; Weber and Daukoru, 1975). In the Niger Delta, for example, shale ridges that occur along the continental slope in front of the extensively growth-faulted depocentre, are a surface expression of overpressured clays that flowed away from the depocentre.

The intra Utsira mounds exist within passive margin deepmarine clays, so it is unlikely that these mounds are caused by accretionary prism processes. These sediments may be at the base of slope and it is possible that the mounding could be ascribed to toe-of-slope contractional deformation as in the Niger Delta example above or to density inversion/loading of the seabed during deepwater sedimentation as in Vogt (1997).

7.2.2.3. Sand gas mounds

North Sea Pliocene circular to ovoid mounded plan view geometries have been noted by Brooke *et al.* (1995)(figure 7.10 and 7.11) with spacing from crest to crest of 500 to 1000 metres, and peripheral dips of 15 degrees. Onlap and isopach changes above the mounds suggest that although they formed relatively early, at shallow depths of burial, their development was not coeval. In addition, radial, often listric fractures occur above the mounds, analogous to fault patterns modelled from salt dome intrusion (Withjack and Scheiner, 1982). Brooke *et al.*, (1995), also noted that fault zones extend from deep in the section where Upper Jurassic source rocks are gas mature and that this might suggest a possible mechanism for mound formation (figure 7.12). Brooke *et al.* (1995) proposes that gas has migrated to shallow levels along fault conduits into these deepwater Tertiary sands, and resulted in sediment liquefaction. The movement of gas results in entrainment of sand grains and the creation of a mound by withdrawal of sand from the flank areas and redeposition towards the centre of the feature (figure 7.12).

7.2.2.4. Summary

This short review of gas hydrate mounds and mud diapirs serves the purpose of outlining the common occurrence of these phenomena within deep marine settings and the possibility that the intra Utsira mounds which confined the deposition of the Top Utsira mounds, may be formed by one or more of these processes. Though origins may vary, the scale of mounds may reach tens of metres in height and hundreds of metres in wavelength. The intra-Utsira mounds

occur within a muddy substrate, and they may have formed due to differential loading by depositing sediment, leakage of gas from hydrocarbon reservoirs, gas hydrate formation, or diapirism of a lower density medium according to the models of Anketell *et al.* (1970). As noted chapter 6, the Top Utsira mounds are formed by differential compaction, though their original depositional character was controlled by the intra-Utsira mounding as seen from onlap relationships of the Top Utsira onto the intra-Utsira mounds.

7.2.3. Syn- to early post-depositional faulting and structures in Block 24/9

7.2.3.1. Examples

Growth faulting during sedimentation and post deposition have been described from the subsurface of the Gulf of Mexico, the Mackenzie delta and the Niger Delta (Ocamb, 1961; Weber, 1971; Evamy, *et al.*, 1978; Coleman, Prior and Lindsay, 1983). This type of faulting is created by the interaction of slip movement inside a brittle layer, located above a ductile layer (i.e. fault decollement) and deposition of sediment during the fault displacement.

The location and description of these synsedimentary faults has been generally described from delta slope settings, where normal faulting is a consequence of slope failure and extension. Spectacular synsedimentary faulting on the western coast of Edgeoya (Svalbard archipelago; Edwards, 1976; Nemec *et al.*, 1988) consists of ten growth faults exposed in a 500 metre high cliff exposure. These faults occur within upper Triassic deltaic deposits. Throws are about 50 to 75 metres which is comparable to the Belton Member polygonal faults of Norwegian Block 24/9 described in this volume. Other synsedimentary faulting includes areas of the Namurian of the west coast of county Clare, Ireland (Rider, 1978; Gill, 1979; Crans *et al.*, 1980; Martinsen, 1989). The scale of these structures is tens of metres with fault geometries related to large slump events. Recent observations of synsedimentary faults discovered in the Gres d'Annot of South East France within the slope facies of turbidites, further illustrates metric scale faulting within a 600 metre high cliff section, that has influenced the thickness and facies of deepwater sediments (Bouroullec, 2000).

A more detailed example of synsedimentary faulting affecting deepwater sediments exists within the Kimmeridgian of Helmsdale, NE Scotland (Crowell, 1961; Neves and Selley, 1975; Pickering, 1984). The approximate 1000 metre thick Kimmeridgian succession outcrops along the shore as a narrow strip between the sea and the footwall scarp of the Helmsdale Fault. The sediments consist of estaurine, shallow to deep marine sediments. Within the deepwater sediments, soft sediment deformation is ubiquitous and includes syn-sedimentary faults, sediment slides, clastic dykes and convolute bedding, all indicating fault activity syn- to early post-deposition, prior to significant lithification.

Cartwright *et. al.*(1999) (figure 7.14) outlines unpublished seismic examples of the affects of polygonal faults on North Sea Tertiary sediments. The polygonal faults may act as growth faults in the interpreted case of the Upper Eocene Belton Member of Norwegian block 24/9. Syn and postdepositional polygonal faulting either controls deepwater deposition or significantly reorganises reservoir geometry by injection/smearing of sediment along polygonal fault planes and/or bed length shortening.

7.2.3.2. Summary

In conclusion, examples of synsedimentary faulting occur in the literature of a comparable scale (tens of metres high faults) and depositional location (base of slope - either of a delta or ramp) to the Belton Member base of slope deepwater turbidite sands of the Norwegian offshore North Sea block 24/9 which are interpreted to be deposited onto a polygonally faulted seafloor. At present only examples in two dimensions exist to date when comparing the three dimensional Belton Member example of the North Sea. Most significant in the case of Block 24/9 is the interpretation that these faults developed with essentially polygonal geometries, and it is suggested in this thesis that they may represent a class of polygonal fault system whose displacement characteristics have been modified (enlarged for a given length) by sediment loading.

7.2.4 Large scale remobilisation model for the Eocene to Miocene of the North Sea

Figure 7.13 is a composite model of the large remobilisation phenomena that have been documented and recognized by the author that occur in the Eocene to Miocene of the North Sea. Migrating fluids either from burial expulsion of fluids or actively migrating hydrocarbons are interpreted to have caused many remobilisation phenomena such as:

(i) Lower Eocene Pockmarks (Cole 1998)

During the Lower Eocene about UK North Sea Block 15/18 active migrating fluids and hydrocarbons from Jurassic organic rich source rocks were trapped and migrated updip at the base of the Lower Eocene basinal clays. As these fluids reached the palaeoshelf and more permeable sands, fluids/gas blew out at this palaeoseabed position, forming kilometre scale seabed pockmarks

(ii) Lower Eocene large scale conical intrusions (chapter 4)

The above fluids also were focused over intra basinal highs, such as the Renee Ridge and created overpressure within isolated Palaeocene deepwater sands, which explosively injected into the overlying polygonally faulted Lower Eocene shales as around UK Blocks 21/4, 5. These intrusions form the conical amplitude anomalies in these blocks. Similar seismic geometries, well calibration and the same intrusion process are described by MacLeod *et al.* (1999) as "wings" along the edges of the Alba field in UK North Sea Block 16/26.

(iii) Balder age kilometre scale intrusion complex (chapter 3)

These migrating fluids also created overpressure within Balder age sediments (Upper Palaeocene). Sands injected a ring dyke complex tens of metres wide, over hundreds of metres to a few kilometres, from around the edge of an isolated, base of slope deepwater sand pod in Norwegian offshore North Sea Block 24/9. The overpressured fluids migrated up along a set of cross trending wrench faults.

(iv) Upper Eocene Belton Member polygonal fault controlled deepwater sands (chapter 5)

Polygonal faulting of the seabed during the Upper Eocene, focused deepwater sand deposition in the downfaulted lows of Norwegian North Sea blocks 24/9.

(v) Middle Miocene and Mio-Pliocene kilometre scale mounding (chapter 6)

Kilometre scale mounding of the Middle Miocene muddy sea floor (intra Utsira mound - chapter 6) and mounding of the Mio-Pliocene sands post deposition (Brookes *et al.*, 1995).

The affect on primary reservoir geometry is variable, but in some cases leads to wholly different sand bodies. As these Tertiary sands of the North Sea make up an important hydrocarbon reservoir, it is important to highlight these features and the geometries they create. Figures 7.14 and 7.15 further outline possible geometrical consequences of large scale sediment remobilisation. Polygonal faults and mud mounding as shown by the author can affect palaeo seafloor and hence deepwater deposition. Polygonal faults may subsequently acts as sights along which sand intrusion can occur along. Polygonal faulting may in addition fault offset or fold beds.

7.3. The impact of reservoir remobilisation to the reservoir geology of deepwater sediments

Modelling of productive North Sea Palaeogene deepwater sandstone reservoirs is normally based on the interpretation of reservoir geometry that has a primary depositional origin. But seismic and core evidence from isolated sandbodies in the Balder, Forth/Harding, Gryphon, Alba fields of the North Sea and field analogues studies by the author shows that original depositional geometries can be significantly modified by sub-surface remobilisation of sands by processes related to elevated pore fluid pressures which may involve hydrocarbons including gas (see also Newman *et al.*, 1991; Dixon *et al.*, 1995).

Reconfiguration of primary depositional geometries by various remobilisation processes has been discussed in the preceeding chapters. Well and seismic evidence, plus field analogue data has been presented. In the light of this data, it is now considered how the recognition of remobilisation could be applied to the analysis of relevant reservoir geometries.

7.3.1. Reservoir remobilisation : impact on reservoir geometries/properties (figure 7.15)

Sediment remobilisation affects reservoirs in the following manner:

(i) Remobilisation can occur almost immediately after deposition or much later in the burial history.

(ii) Remobilisation can be small scale (centimetres) or potentially can be large scale, affecting the entire volume of a reservoir sandbody.

(iii) Remobilisation can involve changes in geometry and physical properties of the reservoir.

Post-depositional geometrical changes can involve steepening of original depositional geometries , differential compaction of Utsira mounds or Balder Field (Jenssen *et al.*, 1993), development of pod-like sandbodies, intrusion of clastic dykes and sills above top reservoir and laterally along the reservoir (e.g. Alba, Gryphon, Forth, Harding, Balder, Norwegian 24/9 intrusive complex and UK 21/3, 4, 5 cone shaped intrusions).

(iv) Remobilisation can often homogenise reservoir properties and eliminates original sedimentary structures e.g. leading to massive sandstone facies. These facies can often be misinterpreted as an original depositional facies such as a grainflow. For example cores in the main sand bodies in Alba, Gryphon, Forth etc all share the common property of almost homogenous structureless, massive sand facies.

The entrainment of sand during the remobilisation process has been shown to homogenise (producing massive sands) and remove clay from the intruded sand (Hurst and Buller, 1984; Hurst pers.comm. 1999) improving vertical permeability and porosity. Clay removed often forms at the top of remobilised beds (dish structures; Hurst and Buller, 1984) or at the end of intrusions (Hurst pers.comm. 1999). This causes a reduction in effective porosity and development but is volumetrically less than the increased porosity and permeability caused by fluidisation and liquefaction.

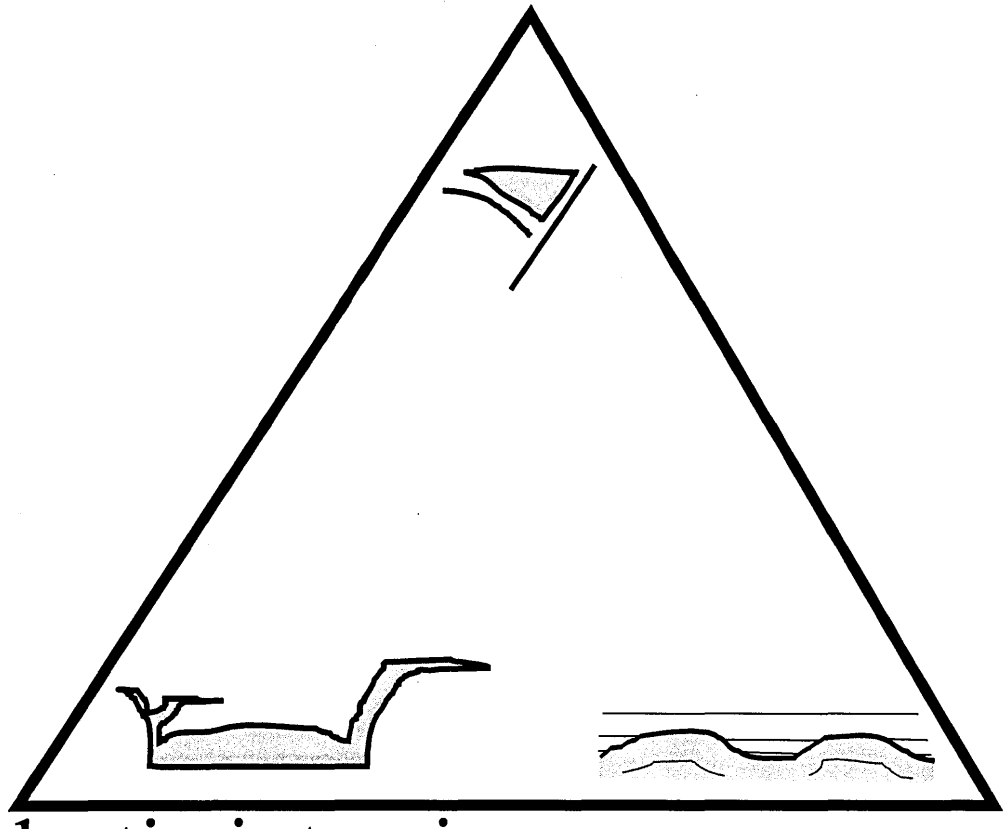
(v) Clastic intrusions can alter the transmissivity of the reservoir. They may be productive but can also lead to (a) breaching of top seals or (b) improved connectivity between isolated reservoir units within a field complex (see figure 7.15). This last point is highlighted by Cossey (1994). He noted how in a Cretaceous North Sea deepwater clastic reservoir that by building into a poorly connected turbidite reservoir model small scale clastic intrusions (below the

resolution of seismic data) that the vertical connectivity increased by 100 fold and increased the "accessible" oil by 50%. The reduced importance placed on these small scale intrusion in a field development could lead to the planning for a production facility with capacity too small for the "real" production capacity.

Figure 7.1. Three part classification scheme for large scale remobilisation in Eocene to Mio-Pliocene sediments of the North Sea

- Upper Eocene polygonally faulted Belton Member Norway 24/9
- Eocene polygonal faulting UK 16/29 (Whitbread and Anderton, 1997)

faulting



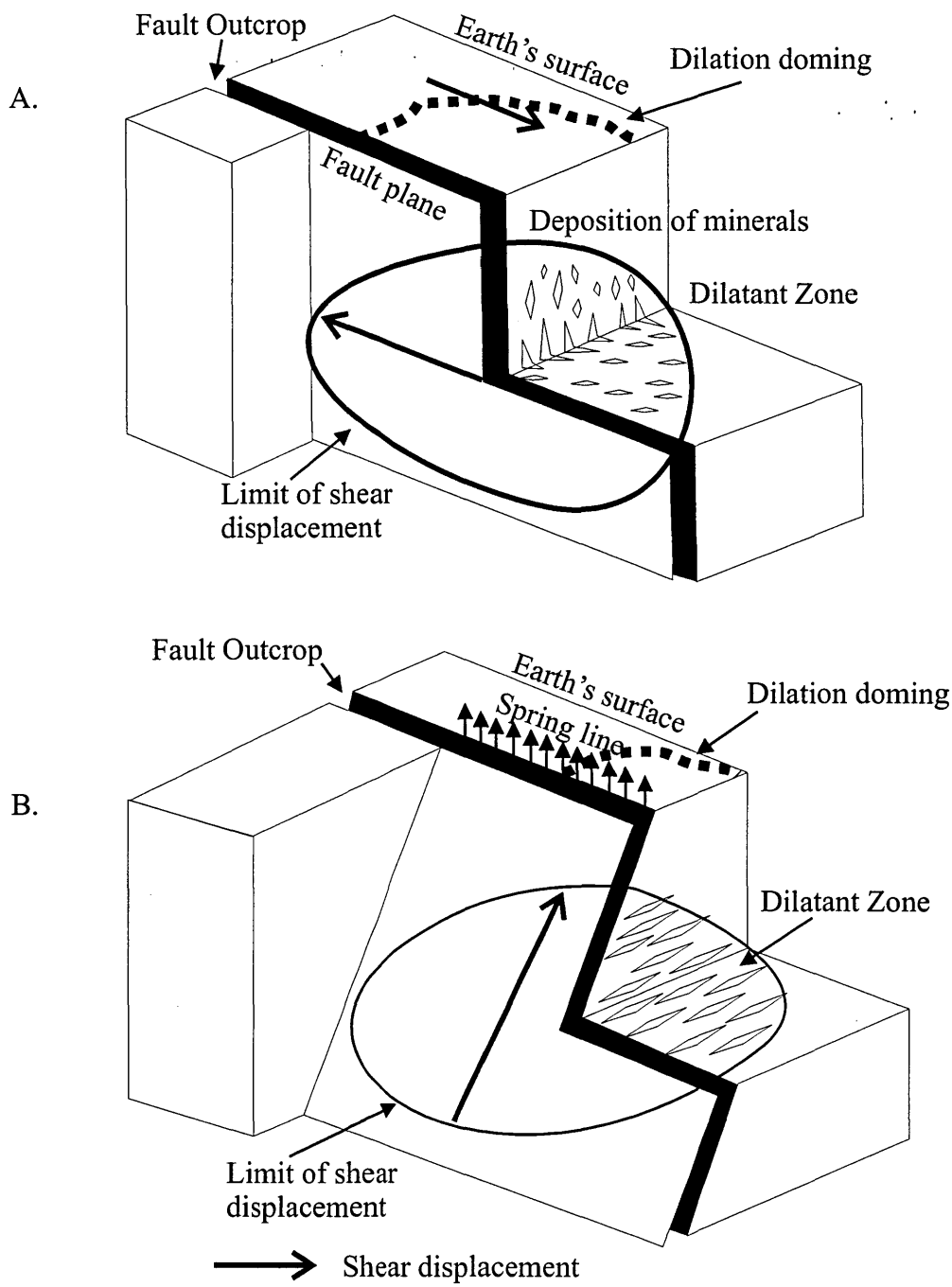
clastic intrusion

- small and large scale dykes and sills Norway 24/9 Eocene intrusion and Yellow Bank Creek Giant Sandstone Intrusion, California
- pockmarks e.g. Cole (1998) and Hovland (1988)

mounding

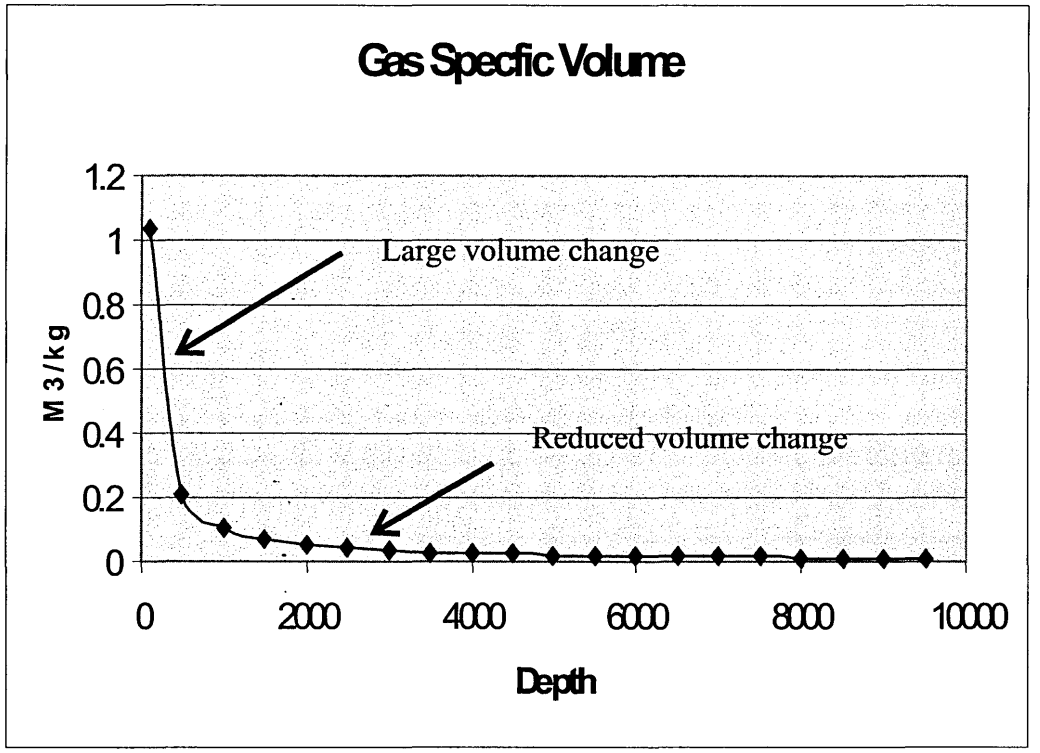
- diapirs,gas hydrate mounds
- Miocene Utsira mounds of UK 16/27, 28 and 29
- Mio-Pliocene gas mounds Brookes *et al.*, 1995
- Oligo-Miocene mounds Davies *et al.*, 1999
- Miocene diapirs Vogt, 1997

Figure 7.2 Model of seismic pumping (from Muir Wood, 1994)



Schematic diagrams showing the dilatancy models for fluid transport, assuming displacement is along a spherical dilation zone;
A - the seismic pumping mechanism for a strike-slip fault (after Sibson *et al.*, 1975)
B - the seismic valving mechanism for reverse shear on a steeply dipping fault. (after Jaffri, 1993)

Figure 7.3. Graph of gas and water expansion with depth (partly from Dake, 1978 and Eddy pers. comm., 2000)



Using the "real gas law" below, and assuming certain values for the gas gradient (0.1 psi/ft), water gradient (0.45 psi/ft) and a temperature gradient, the change in the volumes and therefore equated to relative changes in pressures of gas and water with decreasing depth, can be calculated.

The table below and graphs opposite show how the water volume progressively increases very little with decreasing depth. This is due to the relatively incompressible nature of water. In contrast, gas volumes increase dramatically with decreasing depths, doubling between 8000 to 4000 metres, 4000 to 2000 metres and 2000 to 1000 metres. Between 1000 to 100 metres gas expands in volume ten times.

"Real gas law"

V = ZRT/P

V= volume
Z= compressibilty
T= temperature
P= pressure

Depth(metres)	Volume (m3/kg)	
	gas	water
0	1.04	0.000999
	(x10)	*(<1%)*
1000	0.1	0.000999
	(x2)	*(<1%)*
2000	0.05	0.000998
	(x2)	*(<1%)*
4000	0.25	0.000996
	(x2)	*(<1%)*
8000	0.13	0.000992

Figure 7.4. Three main processes contributing to clastic intrusion (partially from Lonergan *et al.*, 1999)

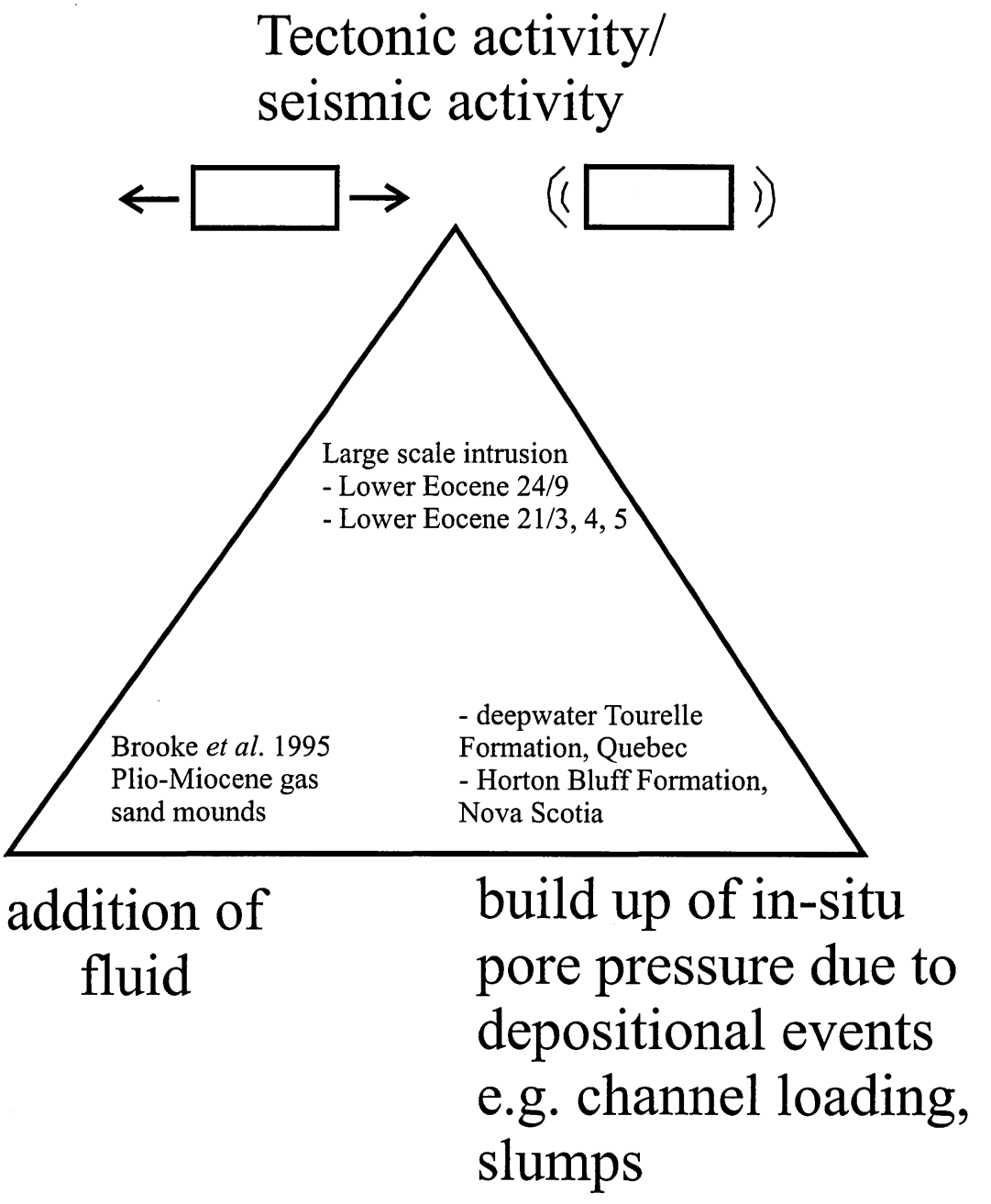
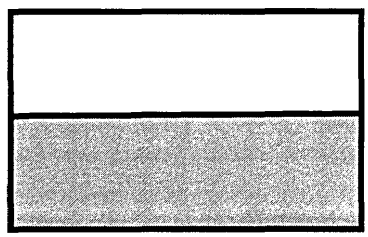
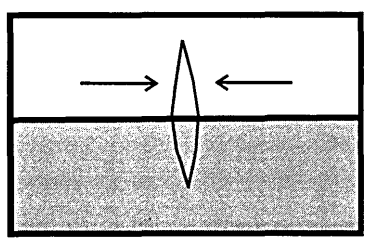


Figure 7.5. Clastic intrusion development with : (a) no pre-existing weaknesses; (b) with pre-existing weaknesses (from Lonergan *et al.*, 1999)

A. no pre-existing weaknesses



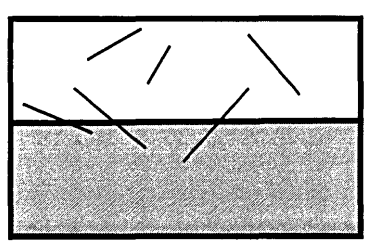
h1



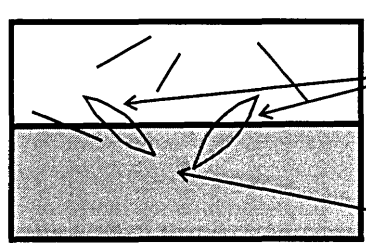
Pf > h1 + T

When the pore pressure within the sand (Pf) exceeds the minimum principal stress and the tensile strength , T , of the host sediment, then a dyke can propogate by brittle failure. In a basin with no tectonic influence on the stress system, the minimum principal (h1) is typically horizontal with the maximum principal stress being vertical. In such a case vertical dykes will form.

B. pre-existing weaknesses



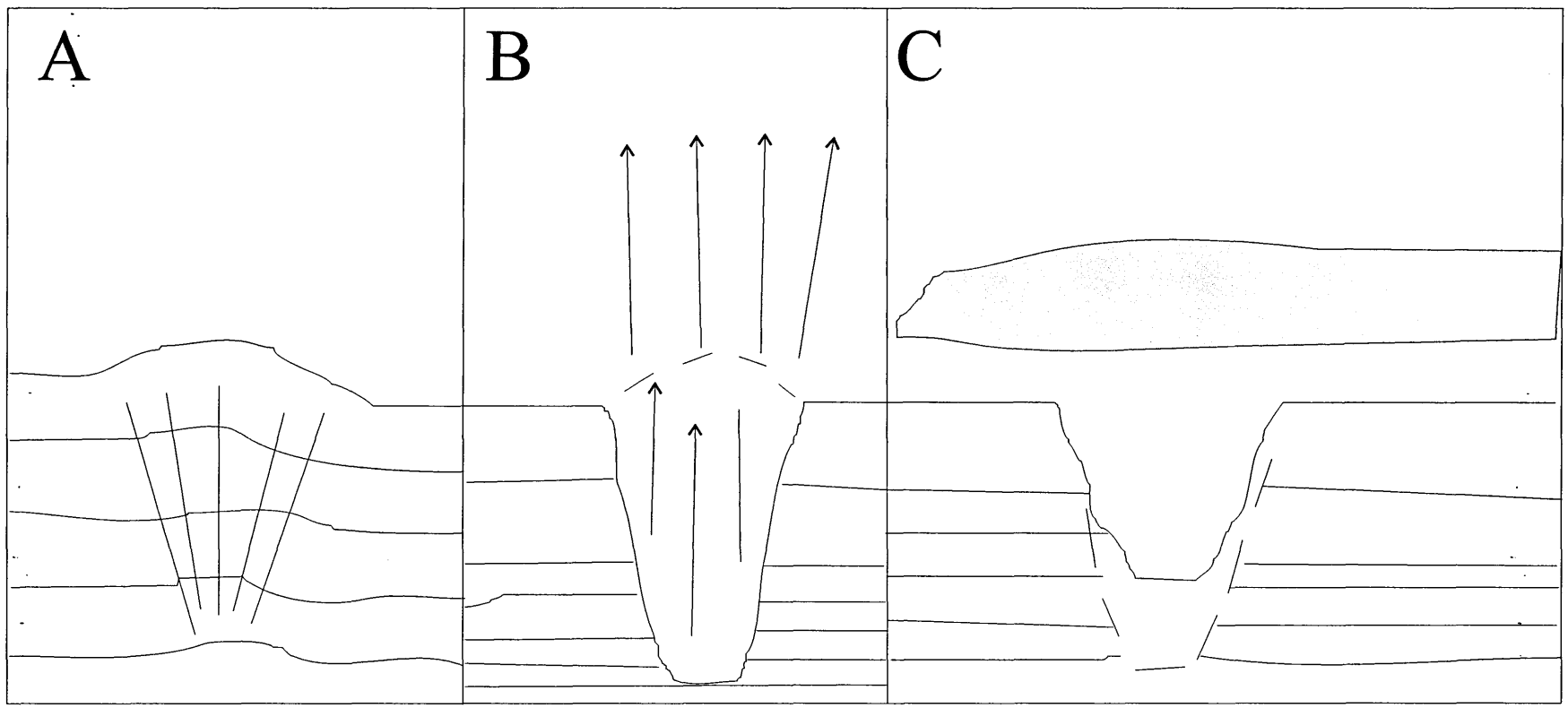
Pf < h1



If faults already exist in the host sediment then the fluid pore pressure (Pf) only needs to exceed the normal stress (h1) acting on the fracture walls, for them to dilate and oblique dykes can propogate. Elevation of the fluid pressures can cause either shear failure or dilation on pre existing fractures depending on the orientation of the fractures relative to the stress field.



Figure 7.6. Generalised formation of pockmarks (from Hovland and Judd, 1988)



A. Mounding of the sea bed by fluid/gas build up

B. Expulsion of fluid/gas build up explosively

C. Pockmark at seabed signifies expulsion phase with a plume of sediment from the expulsion dispersing sediment

Figure 7.7. Giant gas mounds from the Gulf Coast of Mexico (Brooks *et al.*, 1984)
(a) a low relief gas mound on the Texas - Louisiana slope, Gulf of Mexico
(b) a high relief "giant gas mound" on the Texas - Louisiana slopes, Gulf of Mexico

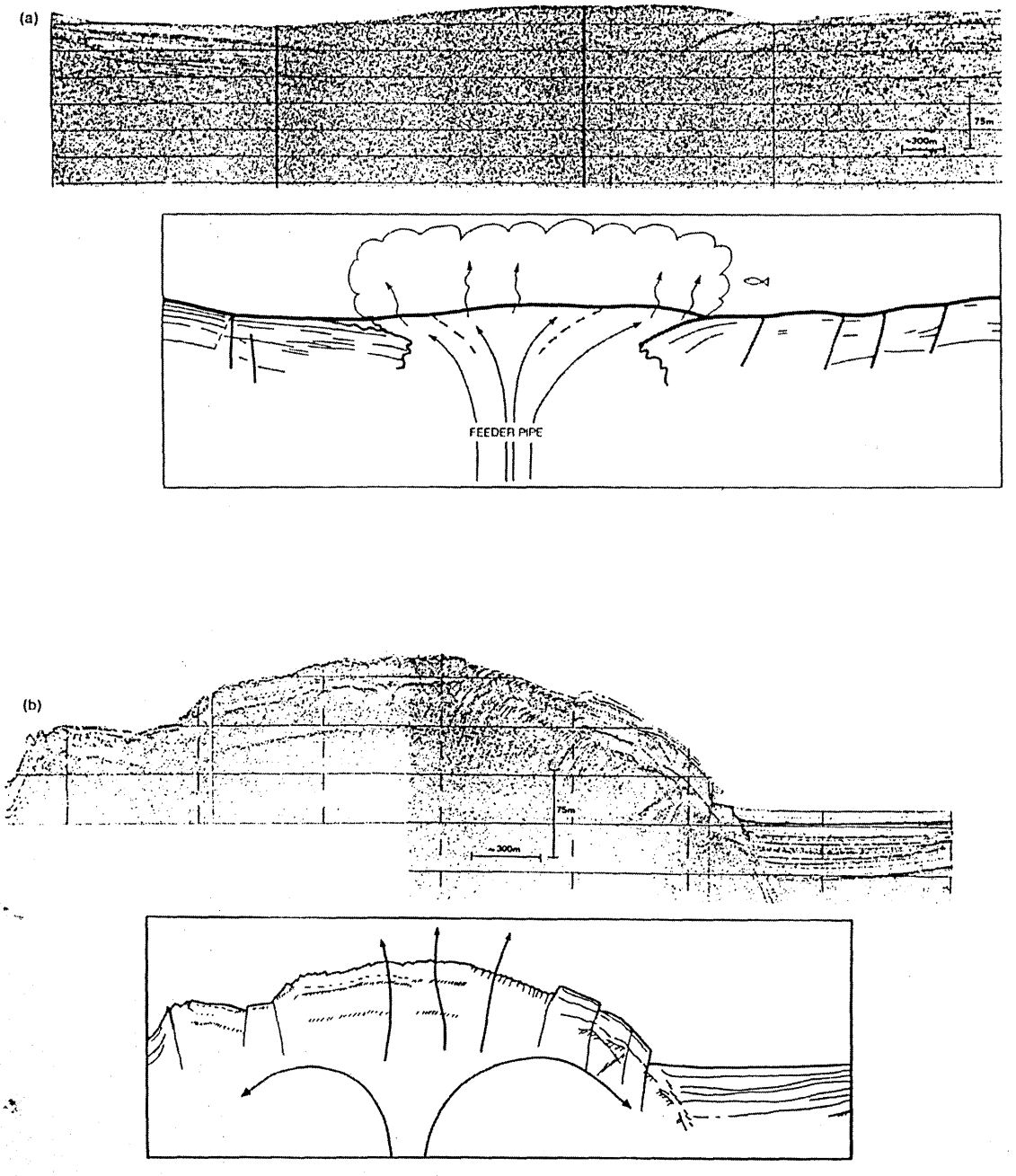


Figure 7.8. Giant gas mound formation model from the Gulf Coast of Mexico (Brooks *et al.*, 1984)

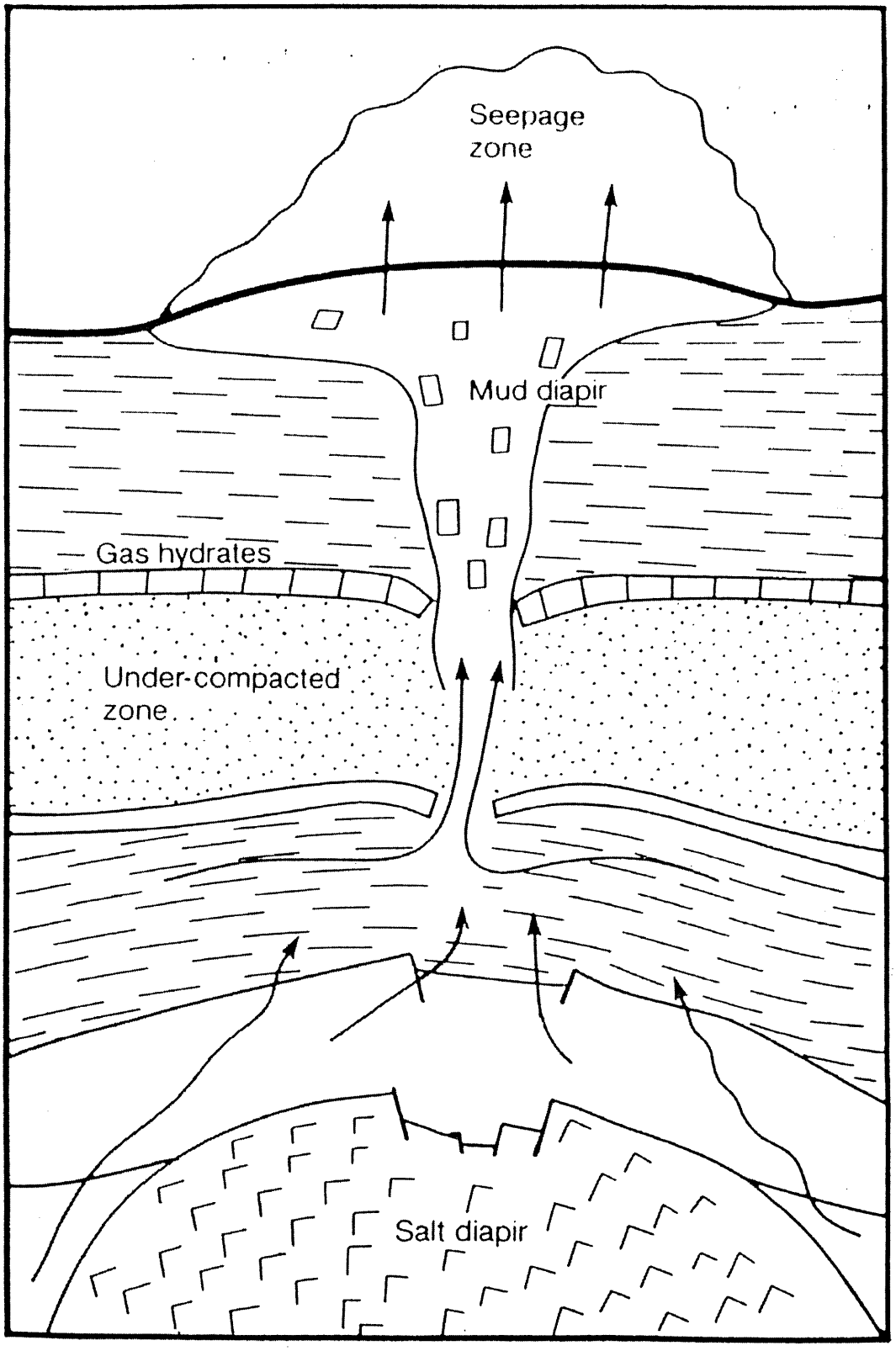
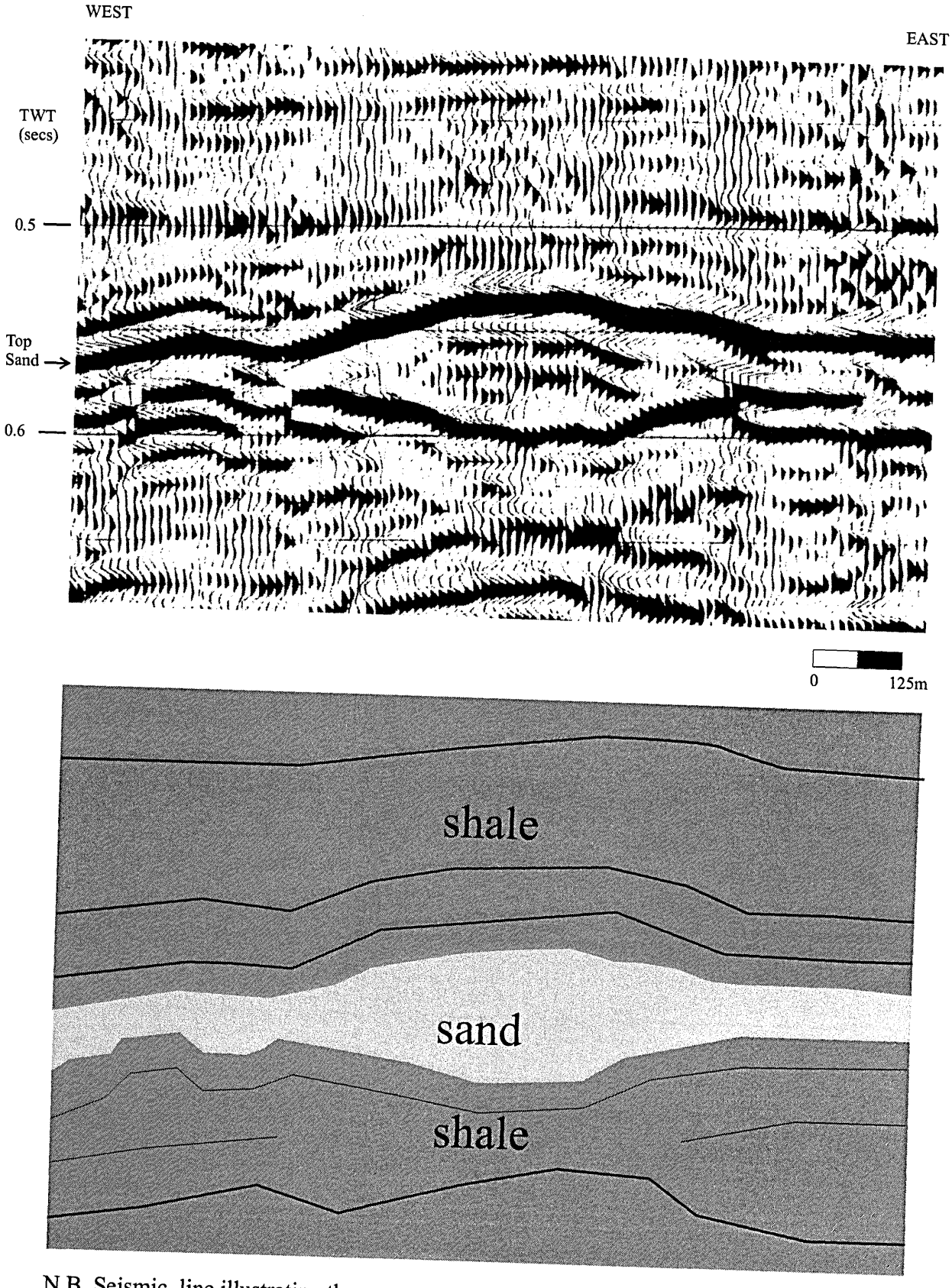


Figure 7.9. Seismic cross section through Mio-Pliocene gas mounds (Brooke *et al.*, 1995)



N.B. Seismic line illustrating the goemetry of a typical sand mound in cross section. Note conformity of reflectors immediately overlying high amplitude reflections at the top of the mound. Sand thickness is up to 45 metres.

Figure 7.10. Timeslice display through the crest of the sand mounds highlighting the circular to ovoid shape in plan view (Brooke *et al.*, 1995)

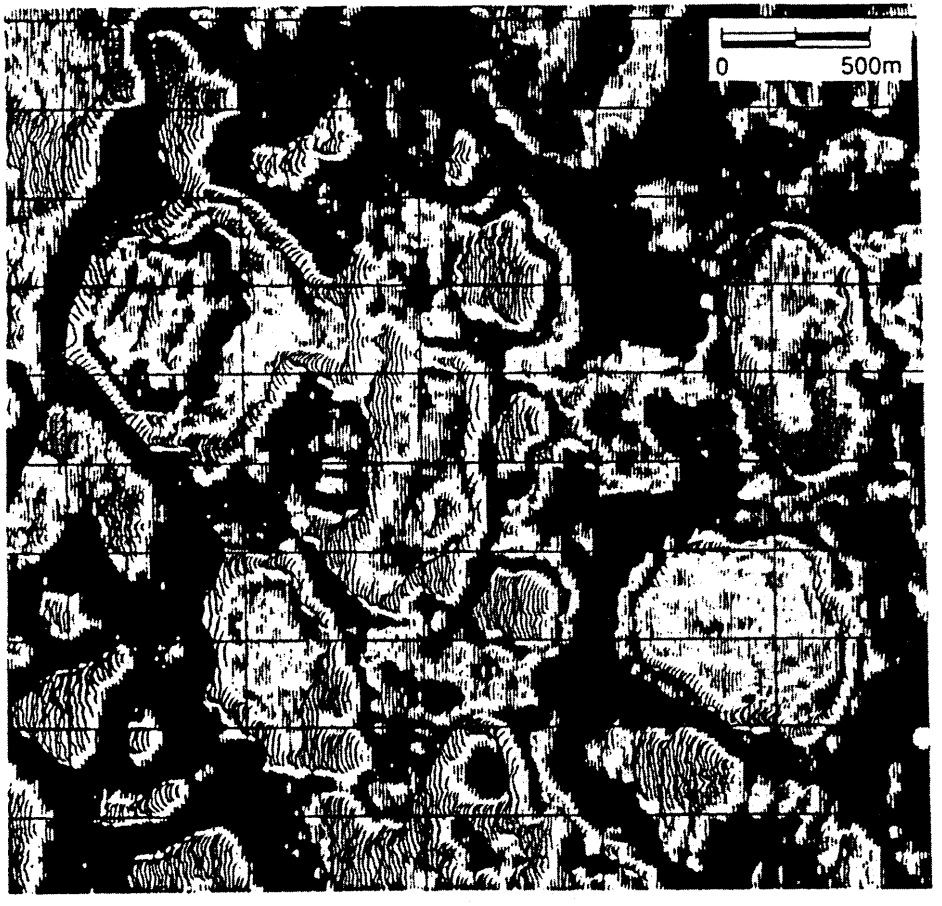


Figure 7.11. Vertical time section showing possible gas conduits extending from deeply buried high at 3.5 s to the mounded shallow gas level at 0.55 s. Gas movement is believed to have taken place along discrete, small offset faults at depth, but high intensity of small-scale faulting in the post-Palaeocene section allows migration over much wider areas, giving diffractive (diffuse) appearance to the younger section (Brooke *et al.*, 1995)

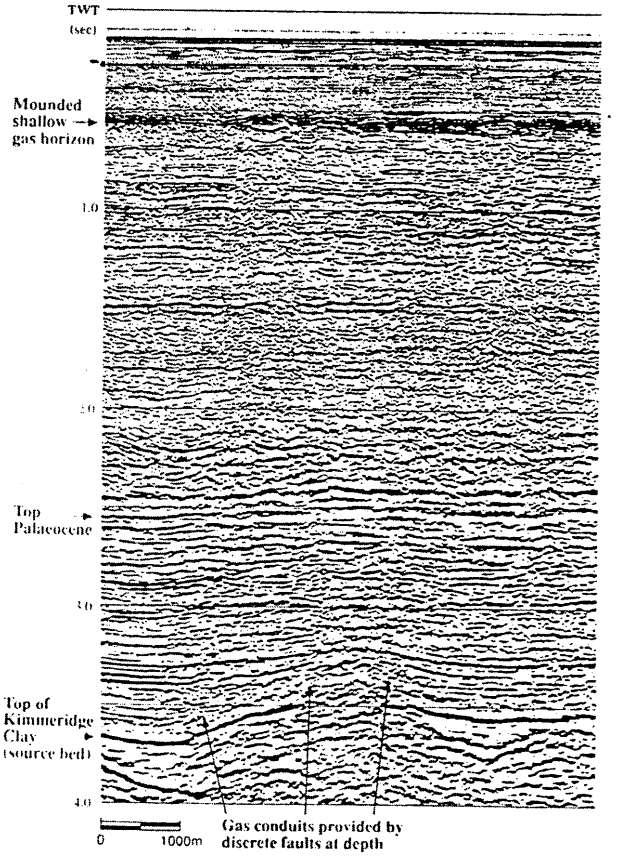


Figure 7.12. Conceptual model for the formation of mounded sands by liquification (from Brooke *et al.*,1995).
(a) Gas fed by fault conduits into a poorly consolidated sand.
(b) sand liquefies and is transported towards a subtle high in the bed surface

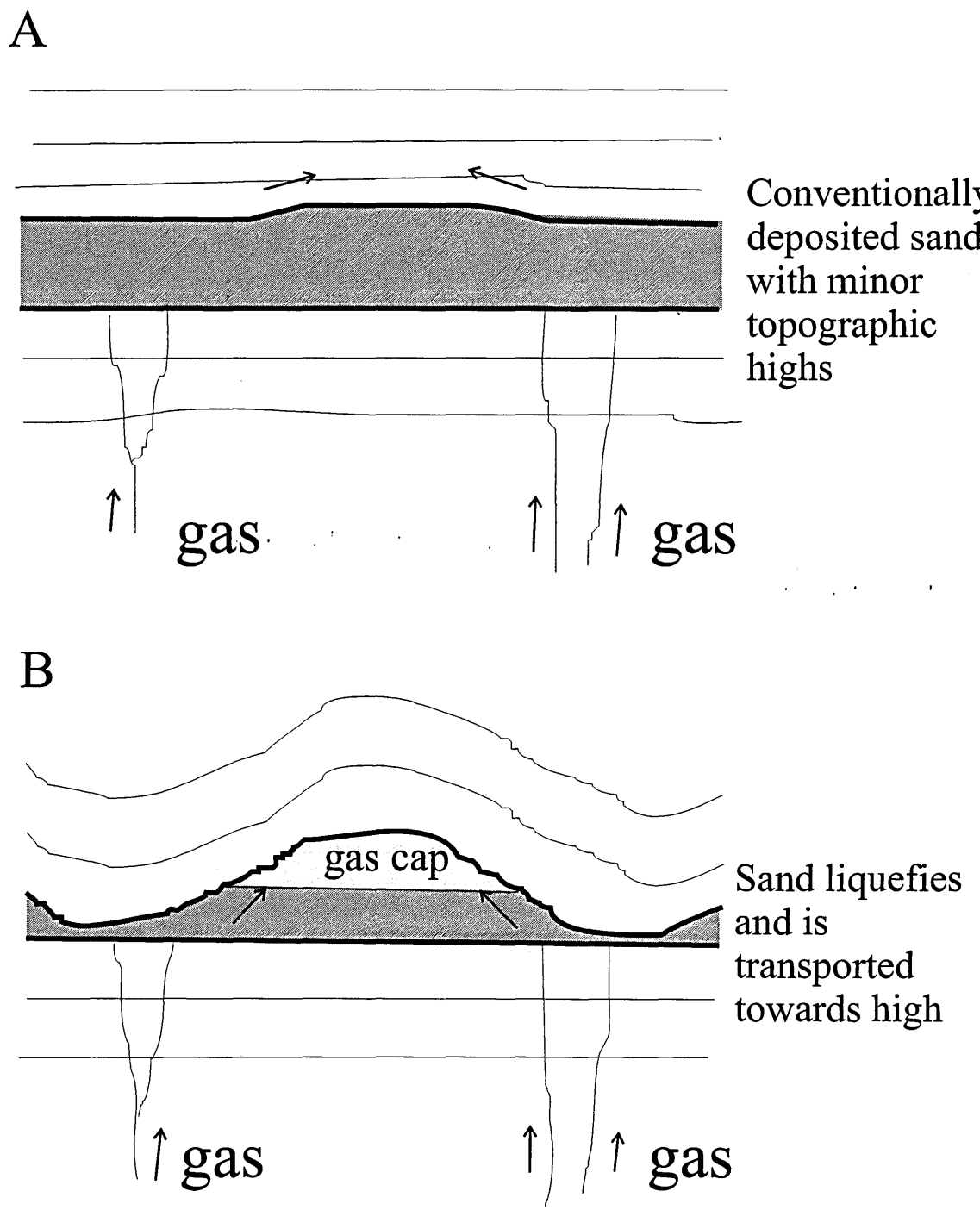


Figure 7.13. Model of large scale remobilisation features in the Eocene to Miocene of the North Sea

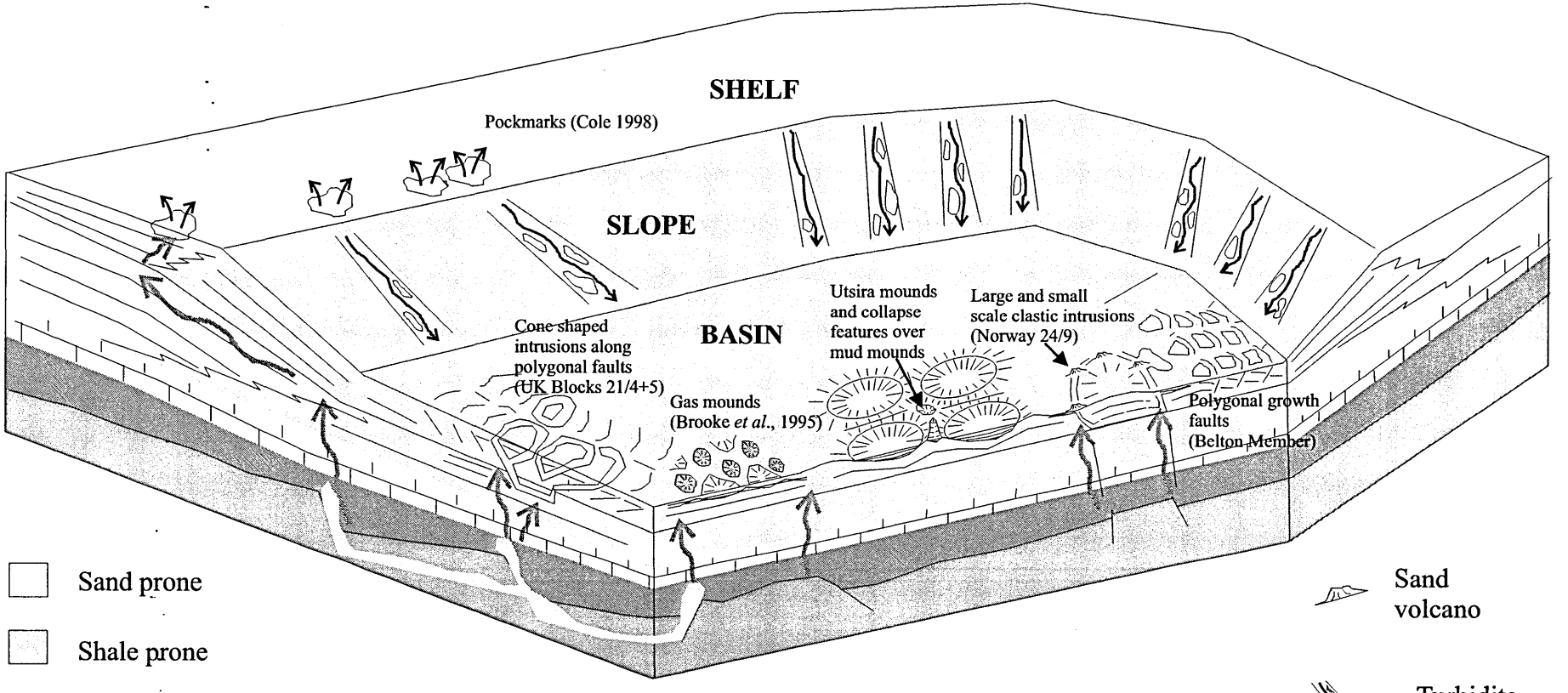


Figure 7.14. Impact of polygonal faulting on reservoir geometry (Cartwright *et al.*, 1999)

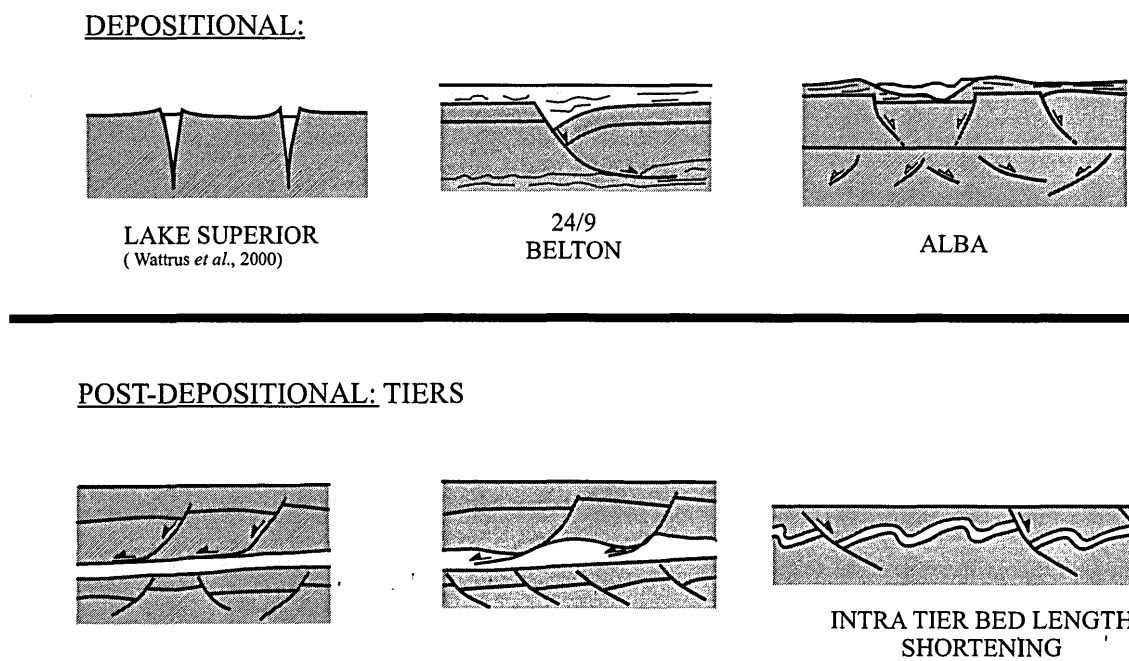
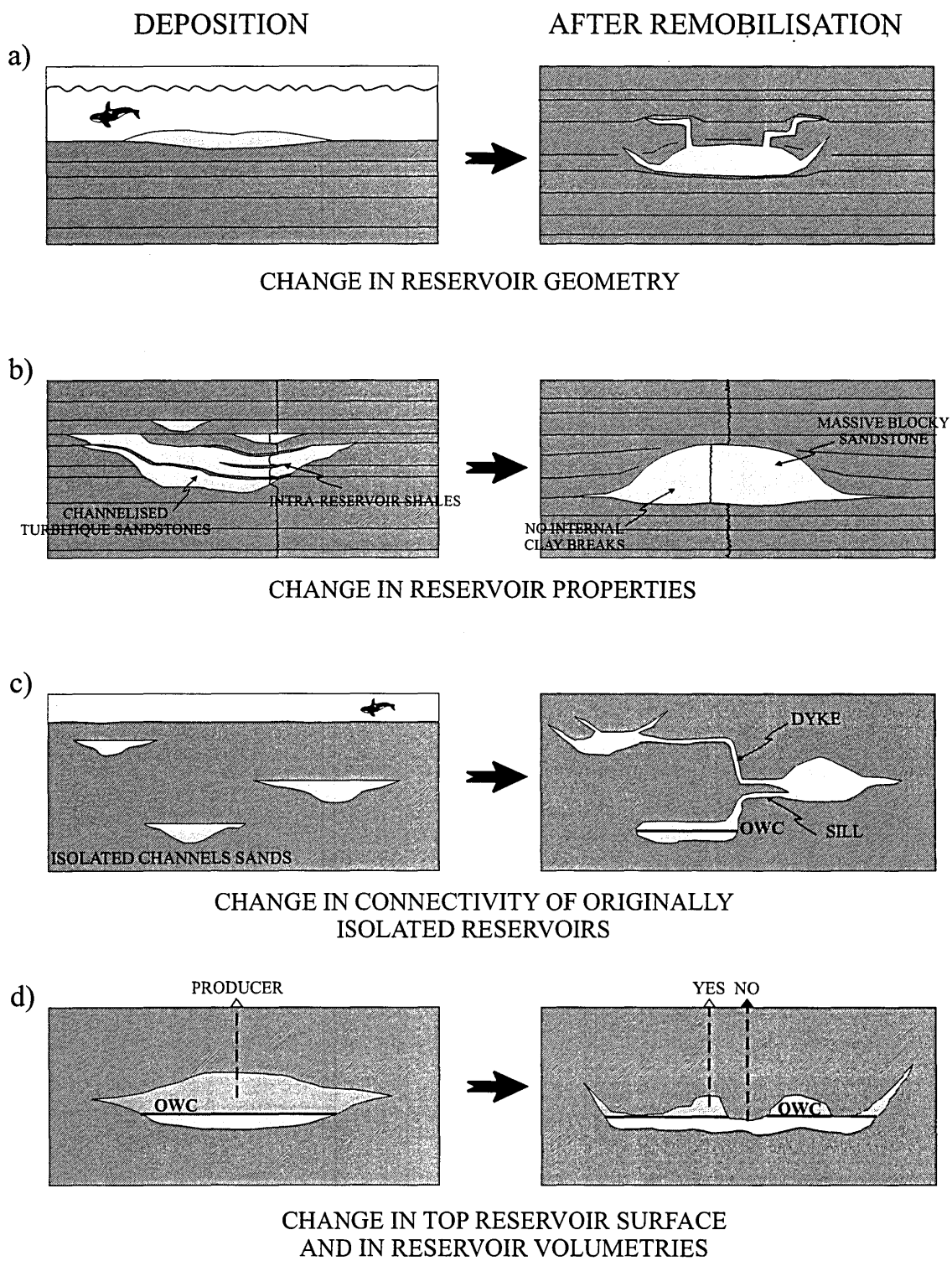


Figure 7.15. Examples of remobilisation affects on deepwater reservoirs



CHAPTER 8. CONCLUSIONS AND FUTURE RESEARCH RECOMMENDATIONS

8.1 Conclusions

The authors work highlights the occurrence of large scale remobilisation within deepwater sediments from seismic examples in the Tertiary of the North Sea and a few rarely documented outcrop analogues in the East Coast of Canada and California. Below are the main conclusions of the authors work:

(1) Post depositional remobilisation of deepwater sandstone reservoirs is an important element in reservoir description/modelling for North Sea Tertiary clastic reservoirs.

(2) Remobilisation involves in situ, higher pore pressure related processes such as fluidization and liquifaction of porous, poorly cemented sandstones at some stage during burial and the reconfiguration of the original depositional geometry.

(3) Remobilisation changes reservoir properties and geometry. Reservoir characterisation must be approached with this in mind.

(4) Failure to identify remobilised reservoirs prior to completion of the reservoir model will lead to unexpected results during development drilling (figure 7.15) as for instance disparate sand bodies may be connected by below seismic resolution sandstone intrusions.

(5) Large scale intrusion complexes may be related to tectonic activity and related fluid flow which may also be associated with the migration of hydrocarbons from basinal kitchen areas. The presence of gas may be a large factor in heightened pore pressures associated with intrusions and such explain the large scale of seismically observable sediment intrusions.

(6) Large scale sand mounds confined by palaeoseafloor mud mounds may act as significant future reservoir targets.

(7) Relationship to active faulting and folding such as large scale polygonal faulting of clay dominant systems may affect primary deposition of deepwater sand reservoirs and significantly change final reservoir geometry.

(8) Geometry of typical dyke-sill complexes

Wide varieties of geometries exist, from simple vertical dykes and

horizontal sills to more complex sill-dyke geomtries with conical, rectilinear or radial patterns. The factors controlling specific geometries are still poorly understood, hence further research is required to constrain the detailed processes of remobilisation.

Interpretation of deepwater sandstone reservoirs is normally based on the modelling of reservoir geometry that has a primary depositional origin. However, seismic and core evidence from isolated deepwater sandbodies in the Palaeocene and Eocene of the North Sea and the field analogues, as shown in this thesis, shows that original depositional geometries can be significantly modified by sub-surface remobilisation of sands by processes related to elevated pore fluid pressures which may involve hydrocarbons including gas. A lack of understanding of these reservoirs by the geoscientist can lead to exploration and production drilling "surprises" as highlighted in figure 8.1.

8.2 Future work

Continued research of large scale remobilisation should involve:

(1) Integrated 3D seismic and well calibrated case studies

Continuing availabilty of more 3D seismic datasets will lead to remobilisation features being recognized. Documentation and subsequent comparison to previous studies will further constrain the processes of large scale remobilisation.

(2) Comparison with field analogues

The reappraisal of previously described exposures as being not wholly depositional massive sands but partly or wholly remobilised, may explain some large scale sands and their discontinuity/continuity in the field e.g. Hareelv Formation of Greenland (Surlyk, 1987). Re-visiting previously described large scale intrusions has confirmed the scale of intrusion of these features. Re-examination of these exposures will explain in more detail the relationship local stress regimes may have exerted on the intrusion geometry.

(3) Cement/fluid studies

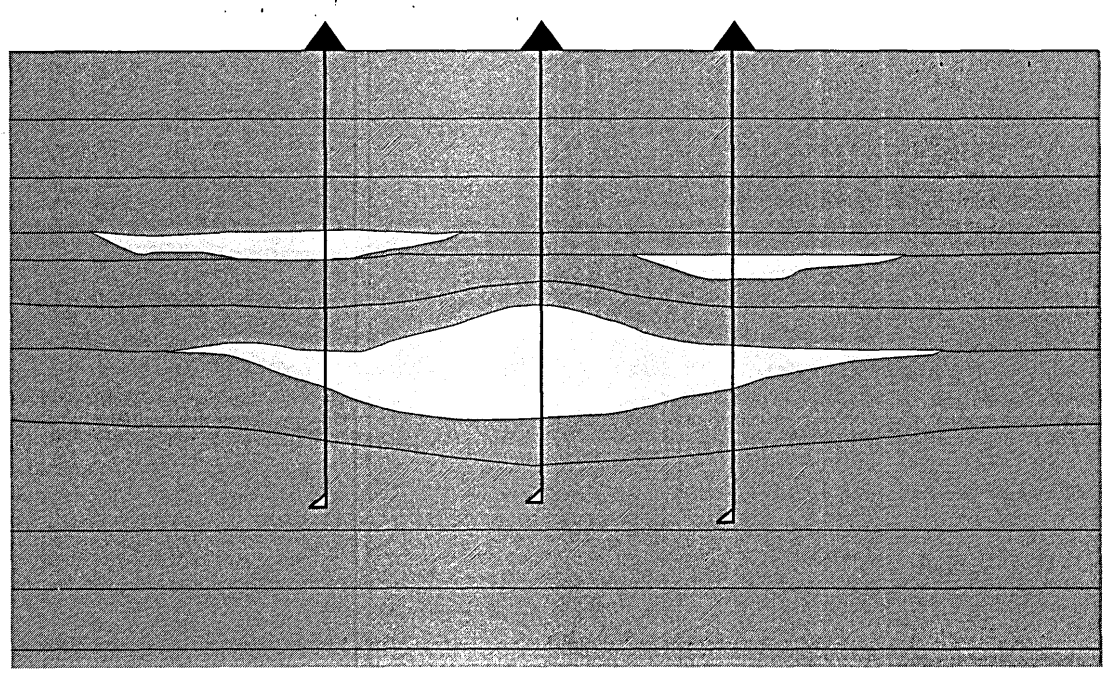
In the North Sea and outcrop examples a comparison of the cements involved (predominantly carbonate) would be very important. These cements may represent the fluid that was involved with the intrusion. By analysing both cement samples from the North Sea and outcrop remobilised sands a common geochemistry may occur. A link to a hydrocarbon phase by observing fluid inclusions and isotope geochemistry on these cements is envisaged.

(4) Theoretical/Experimental studies of remobilisation

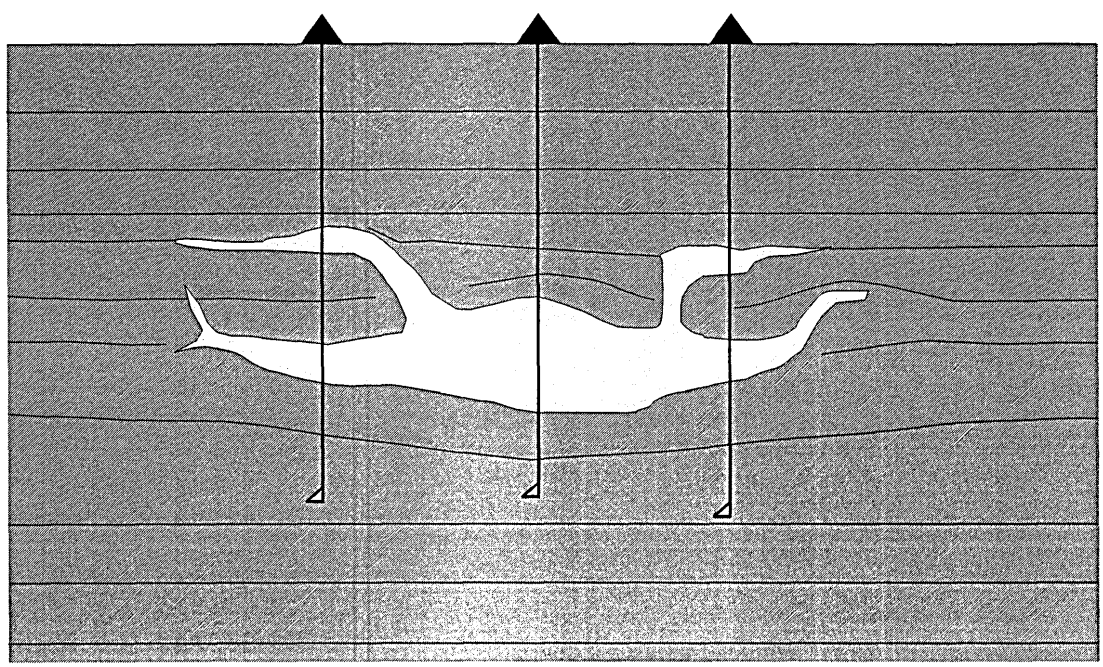
This could take the form of computer generated modelling or physical scaled models. Both approaches would be invaluable in recreating primary to post-depositional changes. An understanding and quantification of the actual process involved that can generate these large scale remobilisation phenomena is required.

Figure 8.1. Contrasting interpretations of reservoir geometry from the same well calibration

(A) DEPOSITIONAL MODEL



(B) REMOBILISATION MODEL



REFERENCES

ALLEN, J.R.L. 1982. *Developments in Sedimentology*. Elsevier. p 663

ALEXANDER, R.W.S., SCHOFIELD, K. & WILLIAMS, M. C. 1992. Understanding the Eocene Reservoirs of the Forth Field, UKCS Block 9/23b. *In: Spencer, A.M. (ed) Generation, Accumulation and Production of Europe's Hydrocarbons III. Special Publication of the European Association of Petroleum Geoscientists*, **3**.

ANDERSON, R.A. and MENKING, K.M. 1994. The Quaternary marine terraces of Santa Cruz, California: Evidence for coseismic uplift on two faults: *Geologic Society of America Bulletin*, vol.**106**, pp.649-664.

ANKETELL, J.M.,CEGLA, J. & DZULYNSKI, S. 1970. On the deformational structures in systems with reversed density gradients. *Rocznik Polsk. Towarz. Geol.*, **40**, pp3-30.

ARCHER, J.B. 1984. Clastic intrusions in deep-sea fan deposits of the Rosroe Formation, Lower Ordovician, Western Ireland. *J.Sediment. Petrol.*, **54**, 1197-1205.

ATWATER, T. and STOCK, J. 1998. Pacific-North America Plate Tectonics of the Neogene Southwestern United States – An Update. International Geological Review, April 1998, Hall Symposium Volume, ed; G.Ernst.

BAGNOLD, R.A. 1956. The flow of cohesionless grains in fluids. *Phil.Trans.Royal Soc.*, **A249**. 235-297.

BARBER, A.J. and BROWN, K.M. 1988. Mud Diapirs: The origin of melanges in accretionary complexes. Geology Today, May-June 1988, 89-94.

BARNARD, P.C. and BASTOW, M.A. 1996. Hydrocarbon generation, migration, alteration, entrapment and mixing in the Central and Northern North Sea. From: England, W.A. and Fleet, A.J. (eds), Petroleum Migration. Geological Society Special Publication No. 59, pp. 167-190.

BELL, W.A. 1929. Horton-Windsor district, Nova Scotia. *Geol. Surv.Can., Mem.* **155**, 269 pp.

BELL, W.A. 1960. Mississippian Horton Group of type Windsor-Horton district, Nova Scotia. *Geol. Surv. Can., Mem.* **314**, 58 pp.

BERGGREN, W.A. and GRADSTEIN, F.M. 1981. Agglutinated benthonic assemblages. *In: the Palaeogene of the Central North Sea: their biostratigraphic and depositional environmental significance. In: Illing, L.V. and Hobson, G.D. (eds.), Petroleum geology of continental shelf of Northwest Europe. Proceedings of the 2nd Conference., Institute of Petroleum.*, Heyden and Son Ltd., London, p.282-285.

BOUROULLEC, R. 2000. Kinematics of synsedimentary normal growth faults. Unpublished PhD thesis, Imperial College, London.

BOUMA, A.M. 1962. *Sedimentology of some flysch deposits; a graphic approach to facies interpretation.* 264p. Elsevier.

BOWMAN, M.B.J. 1998. Cenozoic; in: *Petroleum Geology of the North Sea, ed. by K.W. Glennie.* Blackwell Science.

BRANDON, A. 1972. Clastic dykes in the Namurian shales of County Leitrim, Republic of Ireland. *Geological Magazine*, **109**: 361-367.

BROOKE, C.M., TRIMBLE, T.J. and MACKAY, T.A. 1995. Mounded shallow gas sands from the Quaternary of the North Sea: analogues for the formation of sand mounds in deep water Tertiary sediments. From: *Hartley, A.J. and Prosser,*

D.J. (eds), Characterization of Deep Marine Clastic Systems, Geological Society Special Publication, **94**, pp. 95-101.

BROOKS, J. M., KENNICUTT, M. C II, FAY, R. R., MCDONALD, T. J. AND SASSEN, R. 1984. Thermogenic gas hydrates in the Gulf of Mexico. *Science*, **225**, p409 - 411.

BROOKS, J. M., COX, H. B., BRYANT, W. R., KENNICUTT, M. C. II., MANN, R. G. AND MACDONALD, T. J. 1985. Association of gas hydrates and oil seepages in the Gulf of Mexico. In: *Leytheauser, D. and Rullkotter, J. (eds), Advances in Organic Geochemistry, 1985; Part I, Petroleum Geochemistry*, pp.221-234.

CARL, J. D. + AMSTUTZ, G.L. 1958. Three dimensional rings in a colloidal matrix and their significance for the interpretation of geological phenomena. *Geological Society of America Bulletin.* **69**; 11, p.1467-1468.

CARROLL, R.L., BELT, E.S., DINELY, D.L., BAIRD, D. and McGREGOR, D.C. 1972. Vertebrate palaeontology of Eastern Canada. *XXIV Int. Geol. Congr.*, Montreal, Quebec, Excursion A59.

CARTWRIGHT, J.A. 1989. The kinematics of inversion in the Danish Central Graben. In :*Cooper, M.A. and Williams, G.D. (eds) Inversion Tectonics. Geological Society, London, Special Publications*, **44**, 153-175.

CARTWRIGHT, J.A. 1990. The structural evolution of the Ringkobing-Fyn High. In *: Blundell, D.J. and Gibbs, A.D. (eds) The Tectonic Evolution of the North Sea Rifts*. Oxford Science Publications, 200-216.

CARTWRIGHT, J.A. 1994a. Episodic basin-wide fluid expulsion from geopressured shale sequence in the North Sea basin. *Geology*, **22**, pp.447-450.

CARTWRIGHT, J.A. 1994b. Episodic basin-wide hydrofracturing of overpressured Early Cenozoic mudrock sequences in the North Sea basin. *Mar. Petrol. Geol.*, **11**, pp.587-607.

CARTWRIGHT, J.A. & LONERGAN, L. 1996. Volumetric contraction during the compaction of mudrocks: a mechanism for the development of regional-scale polygonal fault systems, *Basin Research*, **8**, pp.183-193.

CLARK, J. C. 1981. Stratigraphy, Paleontology and Geology of the Central Santa Cruz Mountains, California Coast Ranges*: U.S. Geological Survey Professional Paper*, **1168**, 51p.

CLARK, J.C. & BABB, E.E. 1978. Stratigraphic contrasts across the San Gregorio fault, Santa Cruz Mountains, west central California*: California Division of Mines and Geology*. No. 137, p.3-12.

CLIFT, P.D., CARTER, A. and HURFORD, A.J. 1998. The erosional and uplift history of NE Atlantic passive margins:constraints on a passing plume. *Journal of the Geological Society, London*, Vol. **155**, pp. 787- 800.

COLE, M. 1998. Large crater-like structures in the Palaeogene sediments of Block 15/18, Outer Moray Firth, UK North Sea. Unpublished MSc thesis, Imperial College, London.

COLEMAN, M.L. and RAISWELL, R. 1981. Carbon, oxygen and sulphur isotope variations in carbonate concretions from the Upper Lias of NE England. *Geochim. Cosmochim. Acta*, **45**, 329-340.

COLEMAN, J.M., PRIOR, D.B. and LINDSAY, J.F. 1983. Deltaic influences on shelf edge instability processes. In*: The Shelfbreak: Critical Interface on Continental Margins (Ed. by D.J.Stanley and G.T. Moore)*, pp 121-137. *Spec. Publ. Soc. Econ. Palaeont. Miner.*, **33**, Tulsa.

COLEMAN, M.L. 1985. Geochemistry of diagenetic non-silicate minerals; kinetic considerations. *In: Geochemistry of buried sediments, (edited by) Eglington, G., Curtis, C.D., McKenzie, D.P., Murchison, D.G., Philisophical Transactions of the Royal Society of London, Series A: Mathematical and Physical Sciences.* **315**; 1531, p.39-56.

COLLINSON, J.D. and READING, H.G. 1997. *Deepwater Clastic Depositional Systems. JAPEC Course Notes* No. **165**.

COOK, A.C. and JOHNSON, K.R. 1970. Early joint formation in sediments. *Geological Magazine.* **107**, 4, p.361-368.

CONNAN, J. 1984. Biodegradation of crude oils in reservoirs. *In: advances in petroleum geochemistry (ed.) Brooks, J. and Dietrich, W.H.* **Vol.1.** p.298-335.

COOPER, M.C. 2001. Shallow gas migration. Unpublished PhD thesis, University of London.

CONEYBEARE, D.M. 1996. Diagenesis and Reservoir Quality in the Everest Complex, North Sea. Unpublished PhD thesis, Imperial College, UK.

COOK, A.C. and JOHNSON, A.R., 1970. *Geol. Mag.*, **107**:361-368.

CORNFORD, C. 1990. Source rocks and hydrocarbons of the North Sea. In: *Glennie, K.W. (ed.) Introduction to the Petroleum Geology of the North Sea.* JAPEC, Blackwell Scientific Publications, Oxford, pp.294-361.

CORNFORD, C. 1998. Source Rocks and Hydrocarbons of the North Sea. In *: Petroleum Geology of the North Sea, basic concepts and recent advances (ed.) Glennie, K.W.* p.636.

COSSEY, S.P.J., BYRD, T.M. and HOWARTH, R.J. 1994. Producibility and characteristics of oil and gas fields with deepwater clastic reservoirs. *AAPG and SEPM abstract.* p.126.

COWARD, M.P. 1993. The affect of Late Caledonian and Variscan continental escape tectonics on basement structure, Palaeozoic basin kinematics and subsequent Mesozoic basin development in NW Europe. In: *Parker, J.R. (ed.) Petroleum Geology of Northwest Europe : Proceedings of the 4th Conference.* Geological Society, London, 1095-1108.

CRANS, W., MANDL, G. and HAREMBOURE, J. 1980. On the theory of growth faulting: a geomechanical delta model based on gravity sliding. *J.petrol.Geol.*, **2**, 265-307.

CROWELL, J.C. 1961. Depositional structures from Jurassic Boulder Beds; *East Sutherland. Trans. Edinburgh geol. Soc.*, **18**, 202-219.

CURTIS, C.D. 1977. Sedimentary geochemistry: Environments and processes dominated by involvement of an aqueous phase. *Phil.Trans.Royal Soc., Lond.*, **137**. 189-194.

CURTIS, C.D. 1978. Possible links between sandstone diagenesis and depth related geochemical reactions occurring in enclosing mudstones. *In: Sandstone diagenesis. Journal of the Geological Society,* **vol.1,** p.107-117.

CURTIS, C.D. and COLEMAN, M.L. 1986. Controls on the precipitation of early diagenetic calcite, dolomite and siderite concretions in complex deposition. In*: Roles of organic matter in sediment diagenesis (ed. by D.L.Gautier). Soc.Econ.Miner.Palaeont.Spec.Publ.* **38**. 375-386.

DAVIES, R.J., O'DONNELL, D., BENTHAM, P.N., GIBSON, J.P.C., CURRY, M.R. and DUNAY, R.E. 1999. The origin and genesis of major Jurassic unconformities within the triple junction area of the North Sea, UK. In : *Fleet,*

A.J. and Boldy, S.A.R. (eds) Petroleum Geology of the Northwest Europe : Proceedings of the 5th Conference. Geological Society, London, 117-131.

DAVIES, R., CARTWRIGHT, J. and RANA, J. 1999. Giant (km) scale differential compaction/density inversion pillows in fine grained sediments. *Geology*. 711-716.

DEEGAN, C.E. and SCULL, B.J., 1977. *A Standard Lithostratigraphic Nomenclature for the Central and Northern North Sea. Institute of Geological Science Report No. 77/25*, HMSO, 36 pp.

DEN HARTOG JAGER, D., GILES, M.R, & GRIFFITHS, G.R. 1993. Evolution of Paleogene submarine fans of the North Sea in space and time. In: *Parker, J.R. (ed) Petroleum Geology of Northwest Europe: Proceedings of the 4th Conference. Geological Society, London*, pp59-72.

DICKINSON, J.A.D. 1966. Carbonate identification and genesis as revealed by staining. *J.sedim.Petrol.*, **36**. 491-505.

DILLER, J.S. 1889. Sandstone Dykes. *Bulletin Geoogical Society Am*erica, **1**: 411-442.

DIXON, R. J. & PEARCE, J. 1995. Tertiary sequence stratigraphy and play fairway definition, Bruce-Beryl Embayment, Quadrant 9, UKCS. In: Steel, R. (ed.) Sequence Stratigraphy of the North West European Margin. Norsk Petroleumsforening, Oslo.

DIXON, R.J., SCHOFIELD, K., ANDERTON, R., REYNOLDS, A.D., ALEXANDER, R.W.S., WILLIAMS, M.C. & DAVIES, K.G. 1995. Sandstone diapirism and clastic intrusion in the Tertiary Submarine fans of the Bruce-Beryl Embayment, Quadrant 9, UKCS. In: *Hartley, A.J. & Prosser, D.J. (eds), 1995, Characterization of Deep Marine Clastic Systems, Geological Society Special Publication No. 94*, pp. 77-94.

DONOVAN, T. J. 1974. Petroleum microseepage at Cement, Oklahoma: evidence and mechanism. *Bulletin of the American Association of Petroleum Geologists*, **58**, p 429-446.

DONOVAN, T. J., FRIEDMAN, I. And GLEASON, J.D. 1974. Recognition of petroleum-bearing traps by unusual isotopic compositions of carbonate cemented surface rocks. *Geology*, **2**, p.351-354.

DOTT, R.H., Jr and BOURGEOIS, J. 1982. Hummocky stratification : significance of its variable bedding sequences. Bull.Geol.Soc.Am., 93:663-680

EDWARDS, M.B. 1976. Growth faults in Upper Triassic deltaic sediments, Svalbard. *Bull.Am.Assoc.petrol.Geol.*, **60**, 341-355.

EGGINK, J.W., RIEGSTRA, D.E and SUZANNE, P. 1996. Using 3D seismic to understand the structural evolution of the UK Central North Sea. *Petroleum Gescience* **2(1)**, 83-96.

EIDVIN, T., RIIS, F. and RUNDBERG, Y., 1999 : Upper Cainozoic stratigraphy in the central North Sea (Ekofisk and Sleipner fields). *Norsk Geologisk Tiddskrift*, **79**, 97-128.

EISBACHER, G.H., 1970. Contemporaneous faulting and clastic intrusions in the Quirke Lake group, Elliot Lake, Ontario. *Canadian Journal Earth Sciences.*, **7**: 215-225.

ELDRIDGE, G.M. 1901. The asphalt and bituminous rock deposits of the United States : *US Geol.Survey 22nd Annual Report*, pt2, pp.381-407.

EMERY, D. & MYER, K.J. 1996. *Sequence Stratigraphy*, Blackwell Science, Oxford.

ERICKSON, C.L., MOORE, J.C. and GARRISON, R.E. 1994. The influence of changing tectonic styles on petroleum migration in a small, Pacific rim basin : the Majors tar sand deposits, Santa Cruz County, California . *A study for the University wide Energy Research Group, University of California, Berkely*, unpublished.

EVAMY, B.D., HAREMBOURE, J., KAMERLING, P., KNAAP, W.A., MOLLOY, F.A. and ROWLANDS, P.H. 1978. Hydrocarbon habitat of Tertiary Niger delta. *Bull.Am.Ass.petrol.Geol.*, **62**, 1-39.

FINA NORGE. 1990. *PL 150 - Block 24/9 Prospectivity Evaluation.* Internal Report.

FINA NORGE. 1998. PL 150 - Block 24/9 Geological and Geophysical Review. Internal Report.

FISHER, M.J. and MILES, J.A. 1983. Kerogen types, organic maturation and hydrocarbon occurences in the Moray Firth and South Viking Graben, North Sea Basin. *In: Petroleum geochemistry and exploration of Europe; International congress (ed. By Brooks, J.). Special Publication of the Geological Society of London.* **12**, p.195-201.

FISHER, M.J. and MUDGE, D.C. 1998. Triassic; *In: Petroleum Geology of the North Sea; basic concepts and recent advances (edited by Glennie, K.W.).* p.212-244.

FRIEDMAN, I. 1959. Deuterium content of natural water and other substances. *Geochim. Cosmochim. Acta.* **4**. 89-103.

FRIEDMAN, I. and O'NEIL, J.R. 1977. Compilation of stable isotope fractionation factors of geochemical interest. In: *Data of Geochemistry, Sixth Edition (Ed. by H. Fleischer). United States Geol. Surv. Prof. Paper*, 440-KK.

GALLOWAY, W.E., GARBER, J.L., XIJIN, LIU & SLOAN, B.J. 1993. Sequence stratigraphic and depositional framework of the Cenozoic fill, central and northern North Sea Basin. In: *Parker, J. R. (ed.) Petroleum Geology of NorthWest Europe: Proceedings of the 4th Conference. Geological Society, London*, pp.33-44.

GIBBONS, A. M. 1978. Liesegang rings and agate banding. *The Journal of the Colorado – Wyoming Academy of Science*. **10**; 1, p.60-61.

GILES, M.R., STEVENSON, S., MARTIN, S.V., CANNON, S.J.C., HAMILTON, P.J., MARSHALL, J.D. and SAMWAYS, G.M. 1992. The reservoir properties and diagenesis of the Brent Group: a regional perspective. From: *Morton, A.C., Haszeldine, R.S., Giles, M.R. and Brown, S.(eds), Geology of the Brent Group. Geological Society Special Publication No **61***, pp. 289-327.

GILL, W.D. 1979. Syndepositional sliding and slumping in the West Clare Namurian basin, Ireland. *Special Paper – Geological Survey of Ireland.* **4**.

GLENNIE, K.W (ed.). 1998. *Petroleum Geology of the North Sea, basic concepts and recent advances (fourth edition).* p.636.

GLENNIE, K.W. 1998. Permian. In : *Petroleum Geology of the North Sea, basic concepts and recent advances (fourth edition) (ed.) Glennie, K.W.* p.636.

GOFF, J.C. 1983. Hydrocarbon generation and migration from the East Shetland Basin and Viking Graben of the Northern North Sea. *Journal of the Geological Society*. **140**, 445-74.

GOULD, K. W. + SMITH, J. W. 1978. Isotopic evidence of microbiologic role in genesis of crude oil from Barrow Island, Western Australia. *Bulletin of the American Association of Petroleum Geologists*, **62**, 455-462.

GRADSTEIN, F.M., KAMINSKI, M.A., BERGGREN, W.A., KRISTIANSEN, I.L. AND D'IORIO, M.A. 1994. Cenozoic biostratigraphy of the North Sea and Labrador Shelf. *Micropalaeontology*, vol.**40**, pp. 1-152.

GREEN, P. F. 1986. On the thermo-tectonic evolution of Northern England: evidence from fission track analysis. *Geological Magazine*, **123**, pp.493-506.

GREEN, P. F. 1989. Thermal and tectonic history of the East Midlands shelf (onshore U.K.) and surrounding regions assessed by apatite fission track analysis. *Journal of the Geological Society, London*, **146**, pp.755-773.

GREGERSEN, U., MICHELSEN, O. AND SORENSEN, J.C. 1997. Stratigraphy and facies distribution of the Utsira Formation and the Pliocene sequences in the northern North Sea. *Marine and Petroleum Geology*, Vol. **14**, No 7/8, pp.893-914.

GREGERSEN, U. 1998. Upper Cenozoic channels and fans on 3D seismic data in the northern Norwegian North Sea. *Petroleum Geoscience*, Vol.**4**, pp 67-80.

HALL, M. G. & LLOYD, G. E. 1981. The SEM examination of geological samples with a semi-conductor backscattered electron detector. *Am.Miner.* **66**, 362-368.

HAMPTON, M.A. 1972. The role of subaqueous debris flow in generating turbidity currents. *J.sedim.Petrol.*, 42. 775-793.

HARMS, J. C. 1965. Sandstone Dikes in relation to Laramide Faults and Stress Distribution in the Southern Front Range, Colorado. *Geological Society of America Bulletin*, v. **76**, September 1965, pp. 981 - 1002.

HATHAWAY, J. C. & DYERS, E. T. 1969. Methane derived carbonates of Pleistocene age. *Science*, **165**, 691-692.

HESSE, R. & READING, A. G. 1981. *Special Publications Int. Association Sedimentology*, **2**, p.241-257.

HISCOTT, R. N. 1979. Clastic sills and dykes associated with deep-water sandstones, Tourelle Formation, Ordovician, Quebec. *Journal of Sedimentary Petrology*, **49**, pp1-10.

HOBBS, W.H., 1917. The erosional and degradational processes of desserts, with especial reference to the origin of desert depressions. *Annals of the Association of American Geographers.*, **7**: 25-60.

HOEFS, J. 1987. *Stable Isotope Geochemistry*. 241p. Springer-Verlag, Berlin.

HOVLAND, M. and CURZI, P.V. 1989. Gas seepages and assumed mud diapirism in the Italian Central Adriatic Sea. *Marine and Petroleum Geology*, **6**, 161-169.

HOVLAND, M., & JUDD, A.G. 1988. *Seabed pockmarks and seepages: London, Graham and Trotman*, 293p.

HURST, A. and BULLER, A.T. 1984. Dish structures in some Palaeocene deep-sea sandstones (Norwegian sector, North Sea): Origin of the dish-forming clays and their effect on reservoir quality. *Journal of Sedimentary Petrology*, Vol.**54**, No.4, p.1206-1211.

IRWIN, H., CURTIS, C. and COLEMAN, M. 1977. Isotopic evidence for source of diagenetic carbonate fromed during burial of organic-rich sediments. *Nature*, **269**, 209-213.

ISAKSEN, D. and TONSTAD, K. 1989. A revised Cretaceous and Tertiary lithostratigraphic nomenclature for the Norwegian North Sea. *NPD Bull.* **5**, 1-59.

JAFFRI, F. 1993. Cross-cutting sand bodies of the Tertiary, Beryl Embayment, North Sea. Unpublished PhD thesis, University of London, UK.

JENKINS, O. P. 1930. Sandstone dikes as conduits for oil migration through shales. *Bulletin of the American Association of Petroleum Geologists.* Vol. **14.** pp 411 - 421.

JENSSEN, A.I., BERGSLIEN, M. RYE-LARSEN, M. and LINDHOLM, R.M. 1993. Origin of complex mound geometry of Paleocene submarine-fan sandstone reservoirs, Balder field, Norway. From: *Petroleum Geology of Northwest Europe Proceedings of the 4th Conference (edited by J.R.Parker)*, p.135-143.

JOHNSON, H. 1987. Seismic expression of major chalk reworking events in the Palaeocene of the central North Sea. In : *Brooks, J. and Glennie, K. (ed) Petroleum Geology of Northwest Europe. Graham and Trotman, London*, 591-598.

JONES, R. W. and MILTON, N.J. 1994. Sequence development during uplift: Palaeogene stratigraphy and relative sea-level history of the Outer Moray Firth, UK North Sea. *Marine and Petroleum Geology*, vol. **11**, No.2, pp 157-165.

JONES, G., RORISON, P., FROST, R., KNIPE, R and COLLERAN, J. 1999. Tectonostratigraphic development of the southern part of UKCS Quadrant 15(eastern Witch Ground Graben) : implications for the Mesozoic-Tertiary evolution of the Central North Sea. In : *Fleet, A.J. and Boldy, S.A.R (eds) Petroleum of Northwest Europe. Proceedings of the 5th Conference*, 133-151

JORDT, H., FALEIDE, J.J., BJORLYKKE, K. AND IBRAHIM, M.T. 1995. Cenozoic sequence stratigraphy of the central and northern North Sea Basin: tectonic development, sediment distribution and provenance areas. *Marine and Petroleum Geology*, vol. **12**, No.8, pp.845-879.

JOY, A.M. 1993. An Analysis of the post-rift subsidence history of the North Sea Basin. Unpublished PhD thesis of the University of London.

KAYEN, R. E. & LEE, H. J. 1991. Pleistocene Slope Instability of Gas Hydrate-Laden Sediment on the Beaufort Sea Margin. *Marine Geotechnology*. Vol. **10**, pp 125-141.

KOOI, H., CLOETINGH, S. and REMNELTS, G. 1989. Intraplate stresses and the stratigraphic evolution of the North Sea Central Graben. *Geol. Mijnbouw* , **68**, 49-72.

KNOX, R.W.O'B and MORTON, A.C. 1988. The record of early Tertiary N. Atlantic volcanism in sediments of the North Sea Basin. From: *Morton, A.C. and Parson, L.M.(eds), Early Tertiary volcanism and the Opening of the NE Atlantic, Geological Society Special Publication No 39*, pp 407-419.

KNOX, R.W.O'B. and HOLLOWAY, S. 1992. Paleogene of the Central and Northern North Sea. In: *KNOX, R.W.O'B. and CORDEY, W.G. (eds) Lithostratigraphic Nomenclature of the UK North Sea.* BGS, Nottingham, 133 pp.

KROUSE, H. R. 1977. Sulphur isotope studies and their role in petroleum exploration. *Journal of Geochemical Exploration*, **7**, 189-211.

KUGLER, H. G. 1933. Contributions to the knowledge of sedimentary volcanism. In: *Trinidad Journal of the Institution of the Petroleum Technologists.* **19**; 119, p. 743-772.

KUGLER, H. G. 1938. Nature and significance of sedimentary volcanism. In: Science of Petroleum. 1, p.297-299. Oxford University Press.

KUENEN, P.H. 1937. Experiments in connection with Daly's hypothesis on the formation of submarine canyons. *Leidsche.Geol.Med.* D1. **7**. 327-351.

KUENEN, P.H. 1938. *Bull.Comm. Geol. Finl.*, No. **123**; 11-28

KUENEN, P.H. and MIGGLIORINI, L.J. 1950. Turbidity currents as a cause of graded bedding. *J.Geol.*, **58**. 91-127.

LAWRENCE, D. A., BERAT SANCAR AND MOLYNEUX, S.J.M. 1999. Large-scale sandstone remobilisation in the Tertiary of Block 24/9, Norwegian North Sea: Origin, timing and implications for reservoir continuity. AAPG Birmingham Conference, UK.

LE PICHON, X, BERGERAT, F. and ROULET, M-J. 1988. Plate kinematics and tectonics leading to the Alpine belt formation; a new analysis. *In: Processes in continental lithospheric deformation (edited by Clark, S.P., Clark, B.B., Suppe, J.) Special Paper – Geological Society of America.* **218**, p.111-131.

LISTER, D. 2000. Computer applications to characterising polygonal faults. Unpublished PhD thesis, Imperial College, London, UK.

LONERGAN, L., CARTWRIGHT, J.A. and JOLLY, R. 1998. The geometry of polygonal fault systems in Tertiary mudrocks of the North Sea. *Journal of Structural Geology*, Vol.**20**, No.5, pp.529-548.

LONERGAN, L. and CARTWRIGHT, J.A. 1999. Polygonal faults and their influence on deepwater sandstone reservoir geometries, Alba field, UK Central North Sea. *AAPG Bulletin.* **83**. 410-432.

LONERGAN, L., CARTWIGHT, J.A., MOLYNEUX, S.J.M., LEE, N., JOHNSON, H.D., JOLLY, R., and COPE, M. 1999. Post depositional remobilisation of deepwater massive sandstone reservoirs : impact on reservoir modelling and prediction (abstract). AAPG Birmingham Conference, UK.

LONGSTAFFE, F.J. 1986. Oxygen isotope studies of diagenesis in the basal Billy River Sandstone. *J.sedim.Petrol.* 56. 78-88.

LOVELL, J.P.B. 1990. The Cenozoic. In: *Glennie, K.W. (ed.) Introduction to the Petroleum Geology of the North Sea. Blackwell Scientific Publications, Oxford,* pp.273-293.

LOWE, D. R. 1975. Water escape structures in coarse grained sediments. *Sedimentology*, **222**, p.157-204.

LOWE, D.R. 1976. Subaqueous liquefied and fluidized sediment flows and their deposits. *Sedimentology*, **23**, 285-308.

LOWE, D.R. 1979. Sediment gravity flows : Their classification and some problems of application to natural flows and deposits. In: *The Geology of Continental Slope. (ed. by M.R.S. Doyle and O.H.Pilkey). Soc.Econ.Palaeont.Miner.Spec.Publ.* **27**. 75-82.

LOWE, D.R 1982. Sediment gravity flows : II. Depositional models with special reference to the deposits of high density turbidite currents. *J.sedim.Petrol.*, **52**. 279-297.

LOWE, D.R. and LaPICCOLO, R.D. 1974. The characteristics and origin of Dish and Pillar structures. *Journal of Sedimentary Petrology.*, **44**. p. 484-501.

MACLEOD, M. K., HANSON, R. A., BELL, C. R. & MCHUGO, S. 1999. The Alba Field ocean bottom cable seismic survey : Impact on development. *Leading Edge*, November, p.1306-1312.

MARSCHALKO, R., 1965. *Geol. Pr.*, **36**: p.139-148.

MARTEL, T.A. and GIBLING, M.R. 1993. Clastic dykes of the Devono-Carboniferous Horton Bluff Formation, Nova Scotia: storm-related structures in shallow lakes. *Sedimentary Geology*, **87**, p.103-119.

MARTINSEN, O.J. 1989. Styles of soft-sediment deformation on a Namurian (Carboniferous) delta slope, western Irish Namurian Basin, Ireland. In*: Deltas: Sites and Traps for Fossil Fuels (Ed. by M.K.G. Whateley and K.T.Pickering)*, pp. 167-177. Spec.Publ.geol. Soc.Lond., **41**.

MARTINSEN, O.J., BOEN, F., CHARNOCK, M.A., MANGERUND, G and NOTTVEDT, A. 1999. Cenozoic development of the Norwegian margin 60-64 degrees N : sequences and sedimentary response to variable basin physiography and tectonic setting. In : *Fleet, A.J. and Boldy, S.A.R. (eds) Petroleum Geology of Northwest Europe : Proceedings of the 5th Conference*, 293-304.

MASON, P.C., BURWOOD, R. and MYCKE, B. (1995). The reservoir geochemistry and petroleum charging histories of Palaeogene reservoired fields in the Outer Witch Ground Graben. In: *Cubitt, J.M. and England, W.A. (eds). The Geochemistry of Reservoirs. Special Publication No86. Geological Society of London*, pp 281-302.

MATTHEWS, W.H. and SHEPARD, F.P. 1962. Sedimentation of Fraser River delta: British Colombia. *Bull. Am. Ass. Petrol. Geol.*, **46**, 1416-1446.

MICHELSON, O., DANIELSEN, M., HEILMANN-CLAUSEN, C., JORDT, H., LAURSEN, G.V. and THOMSEN, E. 1995. Occurrence of major sequence stratigraphic boundaries in relation to basin development in Cenozoic deposits of the southeastern North Sea. In: *Sequence Stratigraphy on the Northwest European margin edited by R.J.Steel et.al. NPF Special Publication 5*, pp. 415-427.

MIDDLETON, G.V. 1966a. Experiments on density and turbidity currents, II. Uniform flow of density current. *Can.J.Earth Sci.*, **3**. 627-637.

MIDDLETON, G.V. 1966b. Experiments on density and turbidity currents, III. Deposition of sediment. *Can.J.Earth Sci.*, **4**. 475-506.

MIDDLETON, G.V. 1967. Experiments on density and turbidity currents; [part 3], Deposition of sediment. Canadian Journal of Earth Sciences. **3**, p.475-505.

MIDDLETON, G.V. and HAMPTON, M.A. 1973. Sediment gravity flows: Mechanics of flow and deposition. In: *Turbidites and deep water sedimentation (ed. by G.V.Middleton and A.H.Bouma). Soc.Econ.Palaeont.Miner. Short Course*. 1-38.

MIDDLETON, G.V. and HAMPTON, M.A. 1976. Subaqueous sediment transport and deposition by sediment gravity flows. (In: *Marine Sediment Transport and Environmental Management by D.J.Stanley and D.J.P.Swift*). 197-217.

MOLYNEUX, S. J. M. 1999. Giant Clastic Dykes and Sills of Santa Cruz, Coastal California. Petroleum Exploration Society of Great Britain Newsletter.

MOZLEY, P.S. and BURNS, S.J. 1993. Oxygen and carbon isotope composition of marine carbonate concretions : an overview. *Journal of Sedimentary Petrology*. **63.** p. 73-83.

MUDGE, D.C. and BUJAK, J.P. 1999. NorthEast Atlantic Margin Lower Tertiary Stratigraphy and Plays – proprietary report.

MUIR WOOD, R. 1994. Earthquakes, strain cycling and the mobilization of fluids. In: Geofluids: Origin, migration and Evolution of Fluids in Sedimentary Basins; *Ed: Parnall, J. Special Publication of the Geological Society London*, **78**, p.85-98.

NADIN, P.A and KUSZNIR, N.J. 1995. Palaeocene uplift and Eocene subsidence in the northern North Sea Basin from 2D forward and reverse stratigraphic modelling. *Journal of the Geological Society*, London, **152**, 833-848.

NEMEC, W., STEEL, R.J., GJELBERG, J., COLLINSON, J.D., PRESTHOLM, E. and OXNEVAD, I.E. 1988. Anatomy of collapsed and re-established delta front in Lower Cretaceous of eastern Spitsbergen:gravitational sliding and sedimentation processes. *Bull.Am.Ass.petrol.Geol.*, **72**, 454-476.

NEVES, R. and SELLEY, R.C. 1975. A review of the Jurassic rocks of North-east Scotland. *In: Proceedings of the Northern North Sea Symposium (Ed. by K.G.Finstad and R.C. Selley), Norwegian Petroleum Society.*

NEWMAN, M.St.J., REEDER, M.L., WOODRUFF, A.H.W. and HATTON, I.R. 1993. The geology of the Gryphon Oil Field. From: *Petroleum Geology of Northwest Europe: Proceedings of the 4th Conference (edited by J.R.Parker)*, pp.123-133.

NEWSOM, J. F. 1903. Clastic Dikes. *Bulletin of the Geological Society of America.* Vol. **14**, pp.227 - 268.

NICHOLS, R.J. 1995. The liquefaction and remobilization of sandy sediments. From*: Hartley, A.J. and Prosser, D.J. (eds), Characterization of Deep Marine Clastics Systems, Geological Society Special Publication, No.94*, pp.63-76.

NICHOLS, R.J., SPARKS, R.S.J. and WILSON, C.J.N. 1994. Experimental studies of the fluidization of layered sediments and the formation of fluid escape structures. *Sedimentology.* **41**, p. 233-253.

NILSEN, T. 1998, Geology of the Midway Sunset field and Temblor Ranges – AAPG Pacific Field Guide.

NOTA, D.J.G. 1958. Reports of the Orinoco Shelf Expedition, **2**, 98 pp. H. Veenman en Zonen, Wageningen.

OAKMAN and PARTINGTON. 1998. Cretaceous; *In: Petroleum Geology of the North Sea, basic concepts and recent advances (4th edition).*

OCAMB, R.D. 1961. Growth faults of south Louisiana. *Trans. Gulf Coast. Ass. Geol. Soc.*,11, 139-175

PAPATHEDOROU, G., HASIOTIS, T. and FERENTINOS, G. 1993. Gas-charged sediments in the Aegean and Ionian Seas, Greece. *Marine Geology*, **112**, 171-184.

PEGRUM, R.M. and SPENCER, A.M. (eds.) 1990. Hydrocarbon plays in the North Sea. In: Brooks, J. (ed.) Classic Petroleum Provinces. Special Publication No. 50, Geological Society, London, pp.441-70.

PESGB. 1997. *Structural Framework of the North Sea and Atlantic Margin - map.*

PETERSON, G.L., 1966. Structural interpretation of sandstone dikes, northwest Sacremento Valley, California. *Geological Society American Bull*etin, **77**: **8**, p. 833-842.

PETERSON, G.L. 1968. Flow structures in Sandstone Dikes. *Sedimentary Geology*, **2**, p.177-190.

PETTIJOHN, F.J., POTTER, P.E. and SIEVER, R. 1972. *Sand and Sandstone.* 618p. Springer-Verlag, New York.

PETTIJOHN, F.J. 1975. *Sedimentary Rocks (3rd edition).* 628p. Harper and Row, London.

PHILLIPS, R.L. 1981. Depositional and structural controls on the distribution of tar sands in the Santa Cruz Mountains, California: in *Garrison, R.E., Greene H.G., and Weber, G.E., eds., Geology of the Santa Cruz Mountains and adjacent coastal regions: Pacific Section, Society of Economic Paleontologists and Mineralogists Publication*, p. 105-122.

PHILLIPS, R.L. 1990. Depositional and structural controls on the distribution of tar sands in the Santa Cruz Mountains, California : *in Garrison, R.E., Greene, H.G., Hicks, K.R., Weber, G.E. and Wright, T.C. (eds.). Geology of the Santa Cruz Mountains and adjacent coastal region : Pacific Section, Society of Economic Palaeontologists and Mineralogists. Volume and Guidebook Gb 67*, p 105-122.

PICKERING, K.T. 1983. Transitional submarine fan deposits from the late Precambrian Kongsfjord Formation submarine fan, NE Finnmark, N.Norway. *Sedimentology*, **30**, 181-199.

PICKERING, K.T. 1984. The Upper Jurassic "Boulder Beds" and related deposits: a fault controlled submarine slope, NE Scotland. *Journal of the Geological Society.*, **141**, 357-374.

PICKERING, K.T., SMITH, R.D.A., HISCOTT, R.N., RICCI LUCCHI, F. and KENYON, N.H. 1995. Atlas of Deepwater Environments : Architectural style in turbidite systems.

PLATT, J.P., LEGGETT, J.K., YOUNG, J., RAZA, H. and ALAM, S. (1985). Large-scale sediment underplating in the Makran accretionary prism, southwest Pakistan. *Geology*, **13**, 507-511.

PLATT, N.H. 1995. Structure and tectonics of the northern North Sea : new insights from deep regional seismic data. In : *Lambaise, J.J (ed.) Hydrocarbon Habitat in Rift Basins. Geological Society, London, Special Publications*, **80**, 103-113.

POWERS, M.C. 1953. A new roundness scale for sedimentary particles. *J.sedim.Petrol.*, **23**. 117-119.

PRIOR, D.B., DOYLE, E.H., and KALUZA, M.J., 1989, Evidence for sediment eruption on deep sea floor, Gulf of Mexico, *Science*, **v.243**, p.517-519.

RAISWELL, R. 1987. Non-steady state microbiological diagenesis and the origin of concretions and nodular limestones. In: *Marshall, J. D. (ed.) Diagenesis of sedimentary sequences. Geological Society, London, Special Publication*, **36**, 41-54.

REIMNITZ, E. & MARSHALL, N.F. 1965. Effects of the Alaska earthquake and tsunami on Recent deltaic sediments. *J. Geophys. Res.* **70**, pp. 2363-2376.

RIDING, J.B. 1993. Jurassic of the Central and Northern North Sea. In*: Knox, R.W.O.B. and Cordey, W.G. (eds) Lithostratigraphic Nomenclature of the UK North Sea. BGS, Nottingham.*

RIDER, M.H. 1978. Growth faults in the Carboniferous of western Ireland. Bull.Am.Assoc.petrol.Geol., **62**, 2191-2213.

ROBERTS, H. H., SARSEN, R., CARNEY, R. & AHARON, P. 1989. 13C depleted authigenic carbonate buildups from hydrocarbon seeps, Louisiana continental slope. *Transactions of the Gulf Coast Association of the Geological Societies*, **39**, 523-530.

ROBERTSON RESEARCH. 1998. Norwegian offshore wells 24/9-5 and 24/9-6 clay clast biostratigraphic proprietary report.

RUNDBERG, Y. 1989. Tertiary sedimentary history and basin evolution of the Norwegian North Sea between 60-62 degrees - an integrated approach. Doktor

ingenioravhandling 1989: 33, Institut for Geologi og Bergteknikk, Universitet I Trondheim, Norges Tekniske Hogskole.

RUNDBERG, Y. and SMALLEY, P.C. (1989). High Resolution dating of Cenozoic sediments from Northern North Sea using 87Sr/86Sr stratigraphy. *AAPG Bulletin.* **73 (3)**, 298-308.

RUSSEL, K. L., DEFFEYES, K. S. & GOWLER, G. A. 1967. Marine dolomite of unusual isotopic composition. *Science*, **155**, 190-191.

ST-JULIEN, P. and HUBERT, C. 1975. Evolution of the Taconic orogen in the Quebec Appalachians : *Am.Jour.Sci.*, **v.275-A**, 337-362.

SARJEANT, W.A.S. and MOSSMAN, D.J. 1978. Vertebrate footprinys from the Carboniferous sediments of Nova Scotia : a historical review and description of newly discovered forms. *Palaeogeogr., Palaeoclimatol., Palaeoecol.*, **23** : 270-306.

SHACKLETON, N. J. & KENNETT, J. P. 1975. Palaeotemperature history of the Cenozoic and the initiation of the Antarctic glaciation: oxygen and carbon isotope analysis in DSDP sites 277, 279 and 281. *Initial Reports of the Deep Sea Drilling Project*, **24**, p.743-755.

SHEPARD, F.P., DILL, R.F. and HEEZEN, B.C. 1968. Diapiric intrusions in foreset slope sediments off Magdalena delta, Colombia. *Bull.Am. Ass. Petrol. Geol.*, **52**, 2197-2207.

SHEPARD, F.P. 1973. Sea floor off Magdalena delta and Santa Marta area, Colombia. *Bull.geol.Soc.Am.*, **84**, 1955-1972.

SIBSON, R.H. 1974. Frictional constraints on thrust, wrench and normal faults. *Nature*. **249**, p.542-544.

SIBSON, R.H., MOORE, J.M. and RANKIN, A.H. 1975. Seismic pumping - a hydrothermal fluid transport mechanism. *Journal of the Geological Society of London*, **131**, 653-659.

SIBSON, R.H. (1990). Conditions of Fault-valve behaviour. In: Rheology and *Tectonics(Eds. Knipe, J.R. and Rutter, E.H.). Special publication of the Geological Society London*, **54**, 15-28.

SIBSON, R.H. 1994. Crustal stress, faulting and fluid flow. From: *Parnell, J.(ed.), Geofluids: Origin, migration and evolution of fluids in Sedimentary Basins, Geological Society Special Publication*, No **78**, p. 69-84.

SIMS, R. 1995. The migration of gas through shallow marine sediments. MPhil-PhD Transfer Report, School of the Environment, University of Sunderland, UK.

SMITH, A.J. and RAST, N., 1958. Sedimentary dykes in the Dalradian of Scotland. *Geological Magazine.*, **95**:p.234-240.

SMITH, K and RITCHIE, J.D. 1993. Jurassic volcanic centres in the Central North Sea. In : *Parker, J.R. (ed.) Petroleum Geology of Northwest Europe : Proceedings of the 4th Conference. Geological Society, London*, 519-532.

SPENCER, A.M., 1971. Late PreCambrian glaciation in Scotland. *Memoir Geological Society London*, No.6. pages 98.

STRANGEWAYS, T.H.F. 1821. Description of strata in the Brook Pulcovea near the village of Great Pucovea in the neighbourhood of St.Petersburg. *Transactions of the Geological Society of London*, **5**: p.382-458.

SURLYK, F. 1987. Slope and deep shelf gully sandstones, Upper Jurassic, East Greenland. *AAPG Bulletin.* **71**; **4**, p.464-475.

SWENSON, F.A. 1964. Groundwater phenomena associated with the Hebgen Lake earthquake. *USGS. Professional Paper. 435*, 159-165.

TERVOORT, E. 2000. Polygonal fault characterisation. Unpublished PhD thesis, Imperial College, London, UK.

TAIRA, A. and OGAWA, Y. 1988. The Shimanto Belt, Southwest Japan - Studies on the Evolution of an Accretionary Prism. *Modern Geol.*, **12**, 542 pp.

THOMPSON, B.J., 1995. Geometry and fluid flow mechanisms of the bituminous sandstone intrusion at Yellow Bank Creek, western Santa Cruz County, California : Thesis for Masters Degree, University of California, Santa Cruz, unpublished.

THOMPSON, B. J. 1996. Geometry and fluid flow mechanisms of the bituminous sandstone intrusion at Yellow Bank Creek, northern Santa Cruz County, California. Annual Meeting. Abstracts - AAPG and SEPM. **5**. P.139.

THOMPSON, B.J., GARRISON, R.E. and MOORE, J.C. 1999. A late Cenozoic intrusion west of Santa Cruz, California : fluidized flow of water and hydrocarbon-saturated sediments. In : *Late Cenozoic fluid seeps and tectonics along the San Gregorio fault zone in the Monterey Bay region, California (eds) Garrison, R.E., Aiello, I.W. and Moore, J.C, Annual Meeting of the Pacific Section AAPG, Monterey, California, April, 1999.*

THOMSON, K., UNDERHILL, J.R., GREEN, BRAY, R.J. and GIBSON, H.J.1999. Evidence from apatite fission track analysis for the post-Devonian burial and exhumation history of the northern Highlands, Scotland. *Marine and Petroleum Geology*. **16**. pp. 27-39.

TIMBRELL, G. 1993. Sandstone architecture of the Balder Formation depositional system, UK Quadrant 9 and adjacent areas. From*: Petroleum*

Geology of Northwest Europe: Proceedings of the 4th Conference (edited by J.R. Parker), p. 107-121.

TISSOT, B.P., DURAND, B., ESPITALE, J. and COMBAX, A. 1974. Influence of nature and diagenesis of organic matter in formation of petroleum. *Bull.Ass.Am.petrol.Geol.*, **58**. 499-506.

TRUSWELL, J.F., 1972. *J.Sediment. Petrol.*, **42**: 578-583.

TUCKER, M.E. 1981. *Sedimentary Petrology : an introduction*, pp.252. Blackwell, Oxford.

UNDERHILL, J.R. and PARTINGTON, M.A. 1993. Jurassic thermal doming and deflation in the North Sea: implications of the sequence stratigraphic evidence. In: *Parker, J.R. (ed.) Petroleum Geology of NorthWest Europe : Proceedings of the 4th Conference. Geological Society, London*, 337-346.

UTTING, J., KEPPIE, J.D. and GILES, P.S. 1989. Palynology and stratigraphy of the Lower Carboniferous Horton Group, Nova Scotia. Contributions to Canadian Palaeontology, *Geol.Surv.Can.Bull.*, **396** : 117-143.

VOGT, P.R. 1997. Hummock fields in the Norway Basin and Eastern Iceland Plateau: Rayleigh - Taylor instabilities? *Geology*, June 1997, **v. 25**, no.6, pp. 531-534.

WALKER, G. 1985. Mineralogical applications of luminescence techniques. In: *Chemical Bonding and Spectroscopy in Mineral Chemistry*, pp 103-140. Chapman and Hall, London.

WATSON, R.S., TREWIN, N.H. and FALLICK, A.E. 1995. The formation of carbonate cements in the Forth cements in the Forth and Balmoral Fields, northern North Sea: a case for biodegradation, carbonate cementation and oil leakage during early burial. From: *Hartley, A.J. and Prosser, D.J.(eds).*

Characterization of Deep Marine Clastic Systems, Geological Society Special Publication, **No 94**, pp. 177-200.

WEBER, K.J. 1971. Sedimentological aspects of oilfields of the Niger delta. *Geol.Mijnbouw*, **50**, 559-576.

WEBER, K.J. and DAUKORU, E. 1975. Petroleum Geology of the Niger delta. *Proc. 9th World Petrol. Conf.*, 209-221.

WHITBREAD, T. & ANDERTON, P. W. 1997. Blocks 16/24 and 16/29 Eocene, Volume 1, Regional Evaluation, FINA Exploration Ltd.

WHITE, N and LATIN, D.M. 1993. Subsidence analysis from the North Sea triple junction. *Journal of the Geological Society London.* **150**. 473-488.

WHITEHEAD, R.I. 1985. Hydrologic changes following the Idaho Borah Peak earthquake. *USGS. Proc. Workshop XXVIII on the Borah Peak Idaho Earthquake*. A, 556-572.

WILLS, J.M. 1991. The Forties Field, Block 21/10, 22/6a, UK North Sea. In: Abbotts, I.L. (ed.) UK North Sea United Kingdom Oil and Gas Fields : 25 , UK North Sea. In: Abbotts, I.L. (ed.) UK North Sea United Kingdom Oil and Gas Fields : 25 Years Commemorative Volume. Memoir No14, Geological Society, London, pp.301-308.

WILLS, J.M. and PEATTIE, D.K. 1990. The Forties field and the evolution of a reservoir management strategy. In: *Buller, A.T., Berg, E., Hjelmeland, O., Kleppe, J., Torsueter, O. and Aasen, J.O. (eds) North Sea Oil and Gas Reservoirs. Norwegian Inst. Tech., Graham and Trotman, London.*

WITHJACK, M.O. and SCHEINER, C. 1982. Fault patterns associated with domes - an experimental and analytical study. *American Association Petroleum Geologists Bulletin*, **66**, 302-316

WOOD, S.H. 1985. Regional increase in groundwater discharge after the 1983 Idaho earthquake: coseismic strain release, tectonic and natural hydraulic fracturing. *USGS. Proc. Workshop XXVIII on the Borah Peak Idaho earthquake.* A, 573-592.

WOOD, R.M. 1986. North Sea neotectonics. *In: Neotectonics, edited by Hancock, P.L. and Williams, G.D., Journal of the Geological Society of London. 143; 2*, p.326.

ZIEGLER, P.A. 1982. *Geological Atlas of Western and Central Europe. Elsevier, Amsterdam.*

ZIEGLER, P.A. 1990a. *Geological Atlas of Western and Central Europe. 2nd Ed., Elsevier, Amsterdam*, 239pp.

ZIEGLER, P.A. 1990b. Tectonic and palaeogeographic development of the North Sea rift system. *In: Blundell, D.J. and Gibbs, A.D. (eds) Tectonic Evolution of the North Sea Rifts.* pp. 1-36.

ZOBACK, M. 1992. First and second order patterns of stress in the lthophere : the world stress map project. *Journal of Geophysical Research*, **97** (B8), 11708-11728.

ZWEIGLER, P., LOTHE, A.E and LUNDBERG, E. 1999. Offshore underground carbon dioxide disposal - "Reservoir geology" of the Neogene Utsira Formation, Sleipner Field, North Sea (abstract). AAPG Birmingham Conference, UK.

... it is now!"

(Kenneth Woolstenholme of the BBC commentating on the Geoff Hurst goal that sealed beating the Germans in the 1966 World Cup Final)